IAEA-TECDOC-CD-1693

Hot Cell Post-irradiation Examination and Poolside Inspection of Nuclear Fuel

Proceedings of the IAEA–HOTLAB
Technical Meeting held in
Smolenice, Slovakia, 23–27 May 2011

IAEA
International Atomic Energy Agency

April 2013

For further information on this publication, please contact:

Nuclear Fuel Cycle and Materials Section
International Atomic Energy Agency
Vienna International Centre
PO Box 100
1400 Vienna, Austria
email: Official.Mail@iaea.org

EDITORIAL NOTE

This CD-ROM has been prepared from the original material as submitted by contributors. Neither the IAEA nor its Member States assume any responsibility for the information contained on this CD-ROM.

The use of particular designations of countries or territories does not imply any judgement by the publisher, the IAEA, as to the legal status of such countries or territories, of their authorities and institutions or of the delimitation of their boundaries.

The mention of names of specific companies or products (whether or not indicated as registered) does not imply any intention to infringe proprietary rights, nor should it be construed as an endorsement or recommendation on the part of the IAEA.

HOT CELL POST-IRRADIATION EXAMINATION AND POOLSIDE INSPECTION OF NUCLEAR FUEL
IAEA, VIENNA, 2013
IAEA-TECDOC-CD-1693
ISBN 978–92–0–191210–7
ISSN 1684–2073

Produced by the IAEA in Austria
April 2013

HOT CELL POST-IRRADIATION EXAMINATION AND POOLSIDE INSPECTION OF NUCLEAR FUEL

The following States are Members of the International Atomic Energy Agency:

AFGHANISTAN
ALBANIA
ALGERIA
ANGOLA
ARGENTINA
ARMENIA
AUSTRALIA
AUSTRIA
AZERBAIJAN
BAHRAIN
BANGLADESH
BELARUS
BELGIUM
BELIZE
BENIN
BOLIVIA
BOSNIA AND HERZEGOVINA
BOTSWANA
BRAZIL
BULGARIA
BURKINA FASO
BURUNDI
CAMBODIA
CAMEROON
CANADA
CENTRAL AFRICAN REPUBLIC
CHAD
CHILE
CHINA
COLOMBIA
CONGO
COSTA RICA
CÔTE D'IVOIRE
CROATIA
CUBA
CYPRUS
CZECH REPUBLIC
DEMOCRATIC REPUBLIC OF THE CONGO
DENMARK
DOMINICA
DOMINICAN REPUBLIC
ECUADOR
EGYPT
EL SALVADOR
ERITREA
ESTONIA
ETHIOPIA
FIJI
FINLAND
FRANCE
GABON
GEORGIA
GERMANY
GHANA
GREECE
GUATEMALA
HAITI
HOLY SEE
HONDURAS
HUNGARY
ICELAND
INDIA
INDONESIA
IRAN, ISLAMIC REPUBLIC OF
IRAQ
IRELAND
ISRAEL
ITALY
JAMAICA
JAPAN
JORDAN
KAZAKHSTAN
KENYA
KOREA, REPUBLIC OF
KUWAIT
KYRGYZSTAN
LAO PEOPLE'S DEMOCRATIC REPUBLIC
LATVIA
LEBANON
LESOTHO
LIBERIA
LIBYA
LIECHTENSTEIN
LITHUANIA
LUXEMBOURG
MADAGASCAR
MALAWI
MALAYSIA
MALI
MALTA
MARSHALL ISLANDS
MAURITANIA
MAURITIUS
MEXICO
MONACO
MONGOLIA
MONTENEGRO
MOROCCO
MOZAMBIQUE
MYANMAR
NAMIBIA
NEPAL
NETHERLANDS
NEW ZEALAND
NICARAGUA
NIGER
NIGERIA
NORWAY
OMAN
PAKISTAN
PALAU
PANAMA
PAPUA NEW GUINEA
PARAGUAY
PERU
PHILIPPINES
POLAND
PORTUGAL
QATAR
REPUBLIC OF MOLDOVA
ROMANIA
RUSSIAN FEDERATION
RWANDA
SAUDI ARABIA
SENEGAL
SERBIA
SEYCHELLES
SIERRA LEONE
SINGAPORE
SLOVAKIA
SLOVENIA
SOUTH AFRICA
SPAIN
SRI LANKA
SUDAN
SWAZILAND
SWEDEN
SWITZERLAND
SYRIAN ARAB REPUBLIC
TAJIKISTAN
THAILAND
THE FORMER YUGOSLAV REPUBLIC OF MACEDONIA
TOGO
TRINIDAD AND TOBAGO
TUNISIA
TURKEY
UGANDA
UKRAINE
UNITED ARAB EMIRATES
UNITED KINGDOM OF GREAT BRITAIN AND NORTHERN IRELAND
UNITED REPUBLIC OF TANZANIA
UNITED STATES OF AMERICA
URUGUAY
UZBEKISTAN
VENEZUELA
VIETNAM
YEMEN
ZAMBIA
ZIMBABWE

The Agency's Statute was approved on 23 October 1956 by the Conference on the Statute of the IAEA held at United Nations Headquarters, New York; it entered into force on 29 July 1957. The Headquarters of the Agency are situated in Vienna. Its principal objective is "to accelerate and enlarge the contribution of atomic energy to peace, health and prosperity throughout the world''.

IAEA-TECDOC-CD-1693

HOT CELL POST-IRRADIATION EXAMINATION AND POOLSIDE INSPECTION OF NUCLEAR FUEL

PROCEEDINGS OF THE IAEA–HOTLAB
TECHNICAL MEETING HELD IN
SMOLENICE, SLOVAKIA, 23–27 MAY 2011

INTERNATIONAL ATOMIC ENERGY AGENCY
VIENNA, 2013

For further information on this publication, please contact:

Nuclear Fuel Cycle and Materials Section
International Atomic Energy Agency
Vienna International Centre
PO Box 100
1400 Vienna, Austria
Email: Official.Mail@iaea.org

Printed by the IAEA in Austria
April 2013

IAEA Library Cataloguing in Publication Data

Hot cell post-irradiation examination and poolside inspection of nuclear fuel : proceedings of the IAEA-HOTLAB technical meeting held in Smolenice, Slovakia, 23–27 May 2011. – Vienna : International Atomic Energy Agency, 2013.
CD-ROM. – (IAEA-TECDOC-CD series, ISSN 1684-2073; no. 1693)
ISBN 978-92-0-191210-7
Includes bibliographical references.

1. Spent reactor fuels – Storage – Congresses. 2. Nuclear fuels – Testing – Congresses. 3. Hot laboratories (Radioactive substances) – Congresses. I. International Atomic Energy Agency. II. Series.

IAEAL 13-00801

FOREWORD

The growing operational requirements for nuclear fuel, such as longer fuel cycles, higher burnups and wider use of transient regimes, require more robust fuel designs and more radiation resistant materials. Development of such advanced fuels is only possible with testing and analysis of their performance and application of adequate post-irradiation examination (PIE) methods and techniques. In addition, operational feedback data from poolside and PIE facilities are absolutely necessary for verification of fuel modelling codes and analysis of fuel failure mechanisms. For these reasons, the International Atomic Energy Agency (IAEA) has supported the international exchange of knowledge and sharing of best practices in the application of modern destructive and non-destructive methods of investigation of highly radioactive materials through a series of technical meetings (TMs), the last of which was held in 2006 in Buenos Aires.

Since 1963, similar meetings, initially at the European level, have been organized by the Hot Laboratories and Remote Handling Working Group (HOTLAB), a partner in the development of the IAEA's Post Irradiation Examination Facilities Database (PIEDB), part of the IAEA's Integrated Nuclear Fuel Cycle Information System.

With this successful partnership in mind, in 2010 the IAEA Technical Working Group on Fuel Performance and Technology recommended that a joint IAEA–HOTLAB TM be held on "Hot Cell Post-Irradiation Examination and Pool-Side Inspection of Nuclear Fuel", covering questions relevant to the IAEA sub-programmes on "Nuclear Power Reactor Fuel Engineering" and "Management of Spent Fuel from Nuclear Power Reactors". The TM was held on 23–27 May 2011, in Smolenice, Slovakia, with the participation of a large number of interested organizations and comprehensive coverage of major PIE and poolside inspection issues relating to both operation and storage of fuel for nuclear power reactors. The proceedings, summaries and conclusions of that joint TM are included in this publication and have been reviewed by both IAEA staff and members of the HOTLAB steering committee, the latter acting as co-chairs of the meeting sessions.

The IAEA wishes to thank the hosts and all the participants for their contributions to the meeting, particularly V. Chrapčiak and A. Leenaers. The IAEA officers responsible for this publication were A. Bevilacqua and V. Inozemtsev of the Division of Nuclear Fuel Cycle and Waste Technology.

EDITORIAL NOTE

The papers in these proceedings are reproduced as submitted by the authors and have not undergone rigorous editorial review by the IAEA.

The views expressed do not necessarily reflect those of the IAEA, the governments of the nominating Member States or the nominating organizations.

The use of particular designations of countries or territories does not imply any judgment by the publisher, the IAEA, as to the legal status of such countries or territories, of their authorities and institutions or of the delimitation of their boundaries.

The mention of names of specific companies or products (whether or not indicated as registered) does not imply any intention to infringe proprietary rights, nor should it be construed as an endorsement or recommendation on the part of the IAEA.

The authors are responsible for having obtained the necessary permission for the IAEA to reproduce, translate or use material from sources already protected by copyrights.

CONTENTS

PAPERS TO THE POSTER SESSION

SUMMARY

Session 1: Inspection

Chairmen: F. Flachet (ELECTRABEL) and R. Zajac (VUJE)

1. BACKGROUND

Poolside inspections can give a lot of information on the behaviour of a fuel assembly without the need to withdraw and transport fuel pins to a hot lab. This makes the inspection quicker and can reduce the costs of the investigations. Some operators have installed the equipment in their own pools, while other operators have independent companies performing the inspections at their plant.

The inspection of a fuel assembly can be the initial step to defining the cause of a leaking fuel assembly. On the other hand regular inspections can be used in the frame of a surveillance program. The inspections can also give information on the reliability and the performance of a fuel assembly.

Poolside inspections have a strong advantage compared to hot cell examinations because the number of the high fuel rods that can be examined, i.e. a whole assembly can be checked, whereas hot cell post-irradiation examintaion (PIE) is only undertaken on few, most relevant fuel rods.

Different techniques are being used at the power plants around the world; the most common are visual inspection, ultrasonic testing (UT) measurement and corrosion layer measurements. Burnup measures seem to be used by many operators for different purposes. The measurements can be used to check the core calculations, or reduce the margins used in the safety evaluations.

2. SUMMARIES AND COMMENTS

Presentation: Gamma spectrometric measurement of burnup, V. Chrapčiak, VUJE, Slovakia.

An inspection stand is under construction at the wet pool for interim storage of Bohunice. This inspection stand will make it possible to inspect VVER 440 assemblies and control rods. It is of a modular design and capable of different methods of inspection: visual inspection, UT inspection, cleaning brushes and sampling of oxides, gamma spectrometry and clad to fuel gap measurement.

On the other hand burnup (BU) measurements are also performed by gamma spectrometry. The ratio of caesium-134 and caesium-137 activity is measured. This ratio has a linear dependence on BU. It works best for spent fuel which has cooled down for 1–4 years. For longer cooling times the caesium-134 signal gets very weak. The analysed assembly has a radial profile of enrichment, average enrichment is 3.82%. In the case of Bohunice this measurement is also used to find the spacer grid positions. Comparisons were made with calculated BU by the 3D pin wise PERMAK 3D Code.

Presentation: Studies on the sintering behaviour of UO_2–Gd_2O_3 fuel pellets, G. Ruggirello, CNEA, Argentina.

At the PHWR of Atucha-1 inspections are performed on the cooling channels. This is needed since irradiation growth has caused the coolant channels (CCs) to bend in the past. The Zr channels have been replaced with Zr-4 with different structure and lower tin for better dimensional and corrosion behaviour but the results are still not as good as was hoped for.

First a remote visual inspection of the cooling channels was performed in the core. Then a dimensional control was executed in the SFP. Finally destructive testing was carried out in a hot cell.

A laser distance meter is mounted on the mast of the refuelling machine to measure the height of the assemblies and hence the elongation of the fuel assemblies.

Not only the cooling channels were modified, Atucha NPP also made changes to their fuel assemblies. The enrichment of the fuel has been increased to increase the discharge BU. By an increase to 0.85% of the enrichment the BU could be doubled from 5.8 $MW \cdot d \cdot kg^{-1}$ to 11.1 $MW \cdot d \cdot kg^{-1}$ U. Underwater inspection and metrology techniques are being applied for the monitoring of cooling channels, as useful tools to assure the operational safety of Atucha-1 NPP.

Presentation: Gamma spectrometry for burnup determination of spent fuel assemblies at the Paks NPP, I. Almási, KFKI, Hungary.

At Paks NPP BU measures are performed: to decrease of the BU margins in the safety studies, to check for anomalies in the core and for safeguards.

By taking the ratio of caesium-134 and caesium-137 activity the geometry dependence disappears from the measurement. Activity ratios were evaluated by intrinsic efficiency calibration. In total 28 fuel assemblies were measured with a coaxial germanium detector. Burnup differences were clearly observable between assembly sides looking at the centre and in opposite directions. The uncertainty was found to be 4%. This could be decreased by longer measuring time. The best results were obtained for decay times of 2–4 years.

Presentation: The role of CVR (Research Centre Řež) in the fuel inspection at Temelín NPP, M. Mikloš, NRI Řež, Czech Republic.

Different problems which were encountered at Temelín were presented. These included incomplete rod insertion due to fuel assembly bow and twist, elongation of the fuel assemblies and leaking fuel rods. From 63 leaking fuel assemblies only 23 were repaired, however the effectiveness of the leaking fuel rod extraction from the fuel assembly is quite high, 93%.

Fuel inspections and repair were performed to find the root cause. The causes of different leakers were identified as being due to grid to rod fretting, secondary hydriding, and upper weld leakers. Design changes have been made to the fuel as a consequence. The most drastic solution was changing the full core with fuel from a new vendor. This new vendor will also perform inspections of the fuel.

The fuel repair and inspection equipment (FRIE) designed by Westinghouse was presented. This tool makes it possible to do a visual inspection, an ultrasound and eddy current inspection. NPP Temelín is a first VVER-1000 reactor, where the Russian reactor design meets the US fuel inspection design.

A fuel rod was broken during an inspection. This was probably caused by secondary hydriding. No fuel pellets were lost.

The research centre Řež has a research reactor that can simulate loops of PWR, BWR, and VVER for corrosion research. The measurements of Temelín will also be used to compare the results.

Presentation: Spent fuel attribute tester realization and application, Z. Hlavathy, KFKI, Hungary.

The spent fuel attribute tester was developed in a programme for the IAEA. This tool allows the fissile material to be identified. It consists of a CdZnTe medium resolution detector which is used to detect the 662 keV peak of caesium-137. This detector can be mounted on the railings of the refuelling machine. A measurement takes around five minutes and can also detect fissile material in the lower layer when two layers of assemblies are present. The cobalt-60 sources method for revealing undeclared irradiation was also verified.

This technique can be used when Cherenkov light viewing device would be difficult due to use geometry

Presentation: The poolside inspection of post-irradiation fuel assembly in Qinshan NPP, S. Wang, Qinshan Nuclear Power Company Ltd., China.

Qinshan NPP (QNPP) is the second generation Chinese nuclear power plant with capacity of 310 MW(e), which came into operation in 1991. All of the spent FAs are stored in the pool and will start transportation to the reprocessing factory in the near future. At Qinshan different inspections are performed in the pools. These include the sipping of the fuel assemblies, visual testing and dimensional measurement (verticality, twist, rod spacers, growth).

When a fuel rod is disassembled it can also be used to perform eddy current testing and oxidation film thickness measurements.

Different reasons were mentioned for the use of these inspections. The first reason was to confirm the integrity and the reliability of the fuel assemblies. They can also be used to perform a root cause analysis. If it can be done and it is considered of interest Qinshan will perform a repair of the fuel assembly.

PIE is also performed on the fuel assemblies of Qinshan to inspect the structures, performance and reliability. The non-destructive techniques used are gamma spectrometry, visual inspection, UT inspection and dimensional measurements. The determination of absolute BU of fuel rods by precise analysis of the concentration of caesium-137 and neodymium-148 is also performed. In-core behaviour analysis and performance evaluation of fuel rods is done by comparing the results of hot cell examination with computer code calculation. Destructive measurements performed are the release rate of fission gas, axial tension of the cladding, followed by microstructure and scanning electron microscope (SEM) of the tensile samples as well as macro and micro structure determination of the UO_2 pellets.

A new device allows performing an ultrasonic measurement of deformation in the pools. It has a high accuracy (0.3 mm) and low measurement time (5 min/FA). The information from this measurement is used as guide to fuel loading.

3. PROBLEMS, CHALLENGES AND PERSPECTIVES

The different burnup measurement devices described in the presentations were difficult to move. They used fixed collimators and needed cooling. Therefore it would be useful to look into techniques that are easier to move.

The accuracy of the measurements is also important, especially when the BU measurements are used to check core calculations or to reduce margins in the safety evaluations. Therefore some effort should be put in reducing the uncertainty of the measurements.

Growth of irradiated materials also seems to be a concern for the operators. On the one hand the fuel assemblies tend to grow, but it was also seen that coolant channels at Atucha-1 showed significant growth after irradiation. Therefore investigations should be performed to look into the material characteristics which cause this growth and look for adequate materials to minimize the effects.

4. RECOMMENDATIONS FOR FUTURE WORK

Burnup measurements seem to be used quite often, for safeguard purposes but also for the core monitoring. Therefore it might be worthwhile to give special attention to this kind of measurement. The burnup measurements is very important and useful for calibration, validation of operational and

scientific computer codes and also for verification of the United States of America (ENDF/B-VII.0), the European Union (JEFF-3.1), Japan (JENDL) and the Russian Federation (ROSFOND) data files.

Some recommendations could also be made on the content of a surveillance programme for the fuel. This could include the measurements to perform and the frequency to do this.

Session 2: Hot laboratories' experience and capacity (Overviews)

Chairwoman and Chairman: A. Leenaers (SCK·CEN) and M. Wade (Merrick Company)

1. BACKGROUND

To keep up with the growing demands from the industry, regulators and safety authorities, it is necessary for the hot laboratories to continuously upgrade, refurbish and even reorientate their activities.

The five papers in the session are dedicated to overviews and status updates of hot laboratories, including their capacity, current experience and activities, or future activities. The papers focused primarily on PIE activities in the NNL Windscale facility (UK), JRC-ITU (Germany); IGCAR (India), NPIC (China), as well as the refurbishment status of semi-hot cells at NRI Řež (Czech Republic).

The session was opened with an IAEA address by A. Bychkov, IAEA Deputy Director General and Head of the Department of Nuclear Energy.

2. SUMMARIES AND COMMENTS

A. Bychkov talked about the Fukushima incident and how important it would be if coalitions between hot laboratories would be formed when PIE on the Fukushima fuel is requested. Such extensive PIE would give great input for the safety studies on fuel performance under accidental conditions. He furthermore emphasized the importance of educating a new generation of nuclear scientists and engineers.

Presentation: Treatment and disposal of problematic and poorly characterized nuclear fuels in a post-irradiation examination facility, D. Wright, NNL Sellafield, UK, presented by D. Wright NNL Sellafield, UK.

The paper by D.M. Willey focuses on the role of the Windscale PIE facility operated by the National Nuclear Laboratory (NNL). These facilities are well equipped for the treatment and disposal of problematic fuel. A flexible flasking, material handling and PIE systems combined with lots of experience, allows them to handle larger quantities of historic fuel.

Historic material is often degraded and without treatment, one is often left with pessimistic assumptions. A typical procedure to handle problematic fuel is to first assay the type of fuel (enrichment), analyse the material and try to confirm the assumption. The facility can assay various types/quantities of isotopes; sample and analyse wastes; perform size reduction, segregation, and packaging of wastes; decontaminate items and treat stable waste.

Presentation: Current status of the refurbishment of five semi-hot cells at NRI Řež, R. Kopriva, NRI Řež, Czech Republic.

R. Kopriva presented the current status of the refurbishment of five semi-hot cells at NRI Řež, Czech Republic, and also focused on safety lessons learned. The goal of the recent refurbishment was to increase the mechanical testing capacity in the scope of testing for the surveillance programs of Czech

and Slovak commercial nuclear reactors. Considerable attention was paid to planning and continuous photo documentation. For each work, a detailed assignment procedure was prepared.
The refurbishment started in 2009 with a feasibility study and obtaining safety approval. The activities started with the construction of a sealed area for dismantling works, removing the old glove boxes and their supports as well as dismantling of the shielding concrete wall of the transport system. The reconstruction phase included the construction of a new supporting structure, mounting of shielding steel plates and constructing a welded inner SS layer. The inner surfaces were sanded and the shielded wall was painted.

The current status of the refurbishment project is to install manipulators and the test equipment. The facility is on schedule for October 2011 start up.

Presentation: Hot cells post-irradiation examination at JRC-ITU, V. Rondinella, JRC-ITU, EC.

The paper of V. Rondinella highlights the main PIE capabilities of the ITU hot cells. These primarily revolve around the safety of nuclear fuels and cycles from conventional to advanced concepts. For the hot cell facility it is a big technical challenge to be able to cover such a wide range of fuel concepts, which are characterized by having different compositions, physico-chemical properties, geometries and configurations. In addition to basic techniques for non-destructive and destructive examination of fuel rods and other configurations, more "in-depth" examination tools are needed for the measurement and analysis of specific physical, thermomechanical and micro-analytical properties. In many cases additional information can be gained by combining different techniques. The challenge thus lies in having suitable facilities, measurement techniques, irradiation facilities, suitable analytical and modelling tools and continuous renovation of equipment and facilities.

Presentation: Post-irradiation examination of fuel and core structural materials irradiated in FBTR, N.G. Muralidharan, presented by C.N. Venkiteswaran, IGCAR, India.

C.N. Venkiteswaran presented the PIE capabilities of the hot cell facility in the radiometallurgy laboratory at IGCAR. Performance assessment of various in-core materials of the Fast Breeder Test Reactor (FBTR) at Kalpakkam has been carried out. FBTR uses mixed uranium–plutonium carbide (U0.3 Pu0.7)C as fuel and 20% CW 316 stainless steel as the material for clad and wrapper. Performance evaluation of carbide driver fuel subassemblies through PIE at various burnup levels lead to extending the fuel burnup safety margin from the initial design burnup limit of 50–165 $GW \cdot d \cdot t^{-1}$. The irradiation behaviour of various other core materials like the control rod (B4C pellets with stainless steel clad) and the Nickel reflectors were also presented. Mechanical properties of the cladding were obtained as well as the microstructure evolution at different DPA levels by TEM.

Presentation: Status and activities and status of PIE on nuclear fuel in NPIC, M. Feng, Nuclear Power Institute of China, China.

M. Feng presented the activities and status of PIE for nuclear fuel in the Nuclear Power Institute of China (NPIC). Two research reactors are operated by NPIC, one of which is the High Flux Engineering Test Reactor (HFETR). Since 1980 various kinds of testing fuel assemblies had been irradiated in HFETR and subsequently examined in the hot laboratory. The purpose of the PIE is the qualification of new fuel assembly design technology and demonstration of properties to finally obtain permission from the safety authorities.

The facilities are recently refurbished and NPIC also provides the poolside inspection of the HFETR.

3. PROBLEMS, CHALLENGES AND PERSPECTIVES

The Windscale laboratory shows that a post-irradiation examination facility can be used to support decommissioning projects. However the characterization, treatment and disposal of problematic and poorly documented experimental fuels located in storage ponds characterized nuclear fuels remains a challenge. For the refurbishment of the five semi hot cell at Nuclear Research Institute (NRI) Řež, one has profited from the experiences from previous campaigns. The modular design and the used of an inner stainless steel layer will simplify future decommissioning. Precise preparation of the work

assignments and documentation has shown to be crucial in this project. The activities at the Institute for Transuranium (ITU) show that one not only needs suitable facilities to perform thorough PIE in nuclear materials, but also suitable measurement techniques should be available as well as suitable irradiation facilities.

PIE is needed to evaluate the stability of materials under irradiation. This has led to lifetime extension of the FBTR structural materials or higher burnup of the nuclear fuel.

NPIC is in the process of renewing some of the hot cells, to keep up with the growing demand for PIE. As a PIE facility, they are also reorienting towards becoming NPP poolside inspection experts.

5. **RECOMMENDATIONS FOR FUTURE WORK**

The TM highlights the growing deficiency of trained professional staff and irradiation/PIE facilities able to carry out research on nuclear fuel and materials at the necessary level of detail. That is why it is recommended that IAEA facilitates collaboration of national research and development (R&D) centres in possible forms of coalitions, centres of excellence and user facilities, aiming at more efficient utilization of facilities and harmonization of material testing, material irradiation, PIE methodologies and practices.

Session 3: Hot laboratories' experience and capacity (advanced technologies)

Chairmen: D. Bottomley (JRC-ITU) and P. Thijssen (NRG)

1. BACKGROUND

This session included various examples — installing new equipment in old facilities, constructing new cells and also whole new installations. In all cases, the main problems remain the same. New installations need to be designed both for specific research requirements at the same time the restraints of the (particularly older) facilities limit the possibilities.

2. SUMMARIES AND COMMENTS

Presentation: Post-irradiation capabilities at the Idaho National Laboratories (INL), A.B. Robinson for K.E. Rosenberg, INL, USA.

This was a short presentation that consisted of a video showing the new post-irradiation examination laboratories under construction at INL. The facilities being installed have been the subject of a thorough reflection on the future PIE needs of the US nuclear research and technology. In particular the example was given of the new SEM and specifications of the associated EDS and WDS systems adapted to those future requirements.

Presentation: Mechanistic fuel failure examination system (MFFES), A.B. Robinson, INL, USA.

Robinson gave a second presentation of behalf of a colleague. This reviewed the construction of a new facility to examine the degradation and fission product release during annealing tests, and indicated how research requirements had directed the construction details This consisted of a water cooled vertical tube furnace with direct electrical heating by graphite rods of a gas-tight system containing the sample under vacuum conditions up to 2000°C or inert gas (argon) conditions up to 2200°C. The tube was 10 cm diameter by 30 cm long and had a large crucible to contain the fuel pieces. Alternatively there was an open sample holder, to allow sample photography.

The facility was also equipped with a collimated HPGe detector aimed at the sample position to monitor the loss of total and of individual fission product activities. There was also a thermal gradient

tube directly above the furnace and an enclosing 6 heating zone furnace to control the temperature gradient.

Two shielded video cameras could be placed on supports of the main furnace to monitor the sample in the open crucible up to 550°C. Beyond this temperature it was necessary to stop the furnace, dismount the cameras and restart the test with the samples in a closed crucible continuing up to 2000°C (maximum). The annealing could be with either a ramp or a step-wise temperature profile. The thermal gradient tubes will also be scanned with a CdZrTe detector and so can offer a real time deposition profile of the volatilized fission products. The samples will be either plate-like or monolithic samples of research reactor fuel (such as U–Al or U–Si metallic fuels). The test will go in a first ramp to 550°C to monitor blistering on the surface of the fuel plates in replication of older work in this field. There was a second ramp of these samples beyond 550°C to see the fission product release from these fuels up to their melting point and the fission product deposition on the thermal gradient tubes.

The final part of this presentation looked at the lessons learned from the construction in the hot cell. Particularly the positioning of the equipment off-centre from a window and its manipulators in the facility caused a lot of problems (because of an existing immobile piece of equipment). This required design improvements with associated time delays and increased costs; however they could also draw on existing experience from other constructions. The facility should go into operation in 2012.

Presentation: Installation of a scanning electron microscope in the hot cell laboratory of NRG Petten, J.A. Vreeling, NRG, Netherlands.

NRG in Petten have a hot cell chain where the final hot cell has an SEM. The challenge was to fit the SEM into the existing hot cell. The hot cell was a Pb-shielded α-tight glove box. This had already been decontaminated and the Pb-shielding removed for installation of a new glove box containing the new SEM. The SEM purchased was a high resolution (3 nm) JEOL 6490 with a W-filament (W was considered as more robust) working under low vacuum with adapted shielding and 5-axis motorised stage (3-axes, inclination and rotation). Energy and wavelength dispersive units were from Oxford Instruments and an EBSD (electron backscattered diffraction) unit was from HKL Nordlyss.

The first consideration was to ensure the microscope fitted within the existing dimensions of the glove box (a mock-up of the glove box was used), the next was the removal of all non-essential electronics to the outside. The 10 m cable connections to the operator required testing both after fabrication and finally when in position (the design of the Pb-shielding feedthrough was difficult). The essential electronics especially the emitted electron and EDS detectors needed shielding from irradiation by specially-made dense W-based alloy components. Some irradiation-testing of the electronic components to failure was carried out up to a 25 000 Gray limit. Further design modifications were necessary to ensure replacement or repair of key components (eg. specific positioning of extra glove rings to enable changing the W-filament). The SEM door was redesigned to facilitate the sample insertion/removal using the simple tong manipulators of the glove box. Further features included angled lead glass windows to permit easier viewing of the sample.

Presentation: Development and design considerations for a suite of new post-irradiation examination hot cells to be constructed at McMaster University, J. Luxat, McMaster University, Canada.

McMaster has obtained a grant to examine non-fuel containing irradiated materials for basic materials research and applications to support McMaster's 5 MW pool reactor which would be part of the Centre for Advanced Nuclear Reactor Systems (principally involving SCWR). A building with excellent shielding was found on an existing nuclear research site that had previously housed an accelerator. The requirement was for mechanical properties, optical and micro-analytical examination (OM, FIB, SEM, TEM). A design and cost estimate from the Merrick&Co was obtained. This was for 6 cells with 12 inches of steel protection which had to be organiszed (for reasons of space) in two zones; this was designed for operating limits of 2.5 $\mu Sv \cdot h^{-1}$ for operating staff and 2.5 $\mu Sv \cdot yr^{-1}$ for non-operating staff. The design has a shipping and receiving cell at the entrance to be able to take an

AECL flask. Small transport flasks will be handled by a fork-lift truck. The receiving cell will be attached to a machining cell for sample preparation; there was a transfer cell for movement between the 2 zones of the facility. The SEM/TEM cell was positioned in a corner of the cells which posed particular design problems. Cameras were needed to overcome the problem of dead zones and an additional manipulator in the receiving /isolation zone was added to allow for major hot cell intervention. There was an extra cell for additional equipment in the future. The final design has been submitted for approval.

3. PROBLEMS, CHALLENGES AND PERSPECTIVES

It is important that some flexibility in equipment operation is maintained (for repair/renovation) and additional space (or the possibility for extra space) is planned in the facility, to allow for future needs and optimise the current investment by prolonging the facility's lifetime. In practically every case whether it is a single cell or piece of equipment or a complete new facility, each case has some specific aspect that requires individual attention and sometimes requires a novel solution. For example, ultra-high purity dry argon atmospheres result in unexpected material failures (e.g. seals) and metal specimen stains after etching. Other problems can be resolved with new techniques or simple innovations. Thus the use of reliable flexibly mounted lighting and angled windows are simple, effective improvements; while the appearance of cheap video cameras requiring less shielding offer more possibilities for its use.

4. RECOMMENDATIONS FOR FUTURE WORK

Typical for renovation projects of cells (such as a new SEM in an old cell) is the requirement for the highest possible performance that the old cell can physically allow, and to mount the best possible combination of detectors to maximise the analytical techniques. Robustness of design and sensitivity of a technique are often contrary aspects. For example, electron backscattered diffraction (EBSD) is a very useful technique offering crystallographic information on a sample but the closeness of the detector to the sample and hence the high dose rate results in low detector performance or lifetimes.

Session 4: PIE methods and results (Methods)

Chairmen: D. Gavillet (PSI) and V.V. Rondinella (ITU)

1. BACKGROUND

During the last decade, the research community and the nuclear industry have requested more and more detailed experimental characterization of radioactive materials. One major goal is to answer the increasing demand for validation data for computer models and predictive tools. Mostly detailed knowledge of the material structure but also crystallography and chemical state were requested. The hot lab community has then started to adapt or develop new specific methods for radioactive materials.

The five papers of the session were dedicated to advanced PIE techniques for the analysis of fuel and other radioactive materials in hot laboratories. These techniques are new developments or adaptation of well known methods for specific analyses of nuclear materials. They are mostly foreseen as additional source of information for the detailed analysis of irradiated material properties. These methods have been developed to answer specific question but will offer the possibility to improve our understanding of nuclear materials.

2. SUMMARIES AND COMMENTS

Presentation: Eddy current detection of cladding defects due to fuel pellet imperfections, D. Papaioannou, JRC-ITU, EC.

D. Papaioannou from JRC-ITU, EC presented a new small eddy current apparatus for the detection and analysis of small defects in fuel rods.

The system allows a local measurement at high resolution that brings a notable improvement in comparison with the standard eddy current systems available in many laboratories. Tests made with dummy specimens demonstrated the capability of the method to reveal small defects on the fuel rod with a size resolution of about 0.1 mm. The acquisition and treatment software allow a holographic presentation of the surface of the specimen.

The instrument was successfully used in the hot cell for the investigation of suspected defective rods. Defects not detected by standard visual inspection were clearly revealed with this method. It could define precisely the fuel rod zone to be further analysed by destructive methods (metallography, electron microscopy analysis). Another application of this technique is for detection and analysis of the onset of defects in the cladding during creep tests.

Further development and improvement of the technique could lead to a better characterization of the defects and possibly the detection of defect under the surface of the cladding (at the fuel pellet–clad interface).

Presentation: Scanning acoustic microscope: An advanced technique for the mechanical characterization of irradiated nuclear fuel, W. De Weerd, JRC-ITU, EC.

W. de Weerd from JRC-ITU, EC presented the applications of an acoustic probe microscope adapted to the hot cell. This development is a collaboration between ITU, an industrial partner and a university. Acoustic microscopy has been developed to determine the elastic moduli (mainly Young's modulus) of irradiated fuel, but allows also the detection of defects, such as cracks, voids and large precipitation phase in the subsurface layers of thick materials.

The acoustic microscope had to be modified for the use in the hot cell, removing as far as possible all electronic parts (control and acquisition) from the "hot" areas. All sensors are interchangeable and sustain irradiation quite well. This insures a reliable service in the hot cell. Best results are obtained on a polished flat specimen. Usually, the fuel pieces mounted on specimen holder for ceramography and so can be analysed using the acoustic probe. They are immersed in methanol that provides the coupling of the ultrasonic lenses with the specimens.

UO_2 fuel at burnups ranging from ~(35–100) $GW \cdot d \cdot t^{-1}$ U has been analysed with the instrument. Young's modulus has been determined with a precision of about 4%. The capability of the instrument to detect cracks under the surface enabled suitable areas to be chosen for the determination of the elastic modulus in defect free zones. This feature is also important to select sampling zones for other measurements requiring a defect-free volume.

This technique is sensitive to the surface quality of the specimen. Great care must then be taken during the specimen preparation to insure a stress free flat surface if high resolution is requested (down to 1 micro-meter). The audience showed a great interest for the different capabilities of the instrument, particularly subsurface defect detection (pores, cracks, precipitation) in fuel but also in cladding.

Presentation: Non-destructive fission gas release determination of irradiated experimental fuel rods using gamma spectrometry, H. Jenssen, OECD Halden Reactor Project, Norway.

The third paper was a presentation of the non-destructive determination of fission gas release (FGR) in irradiated experimental fuel rods using gamma spectrometry by H. Jenssen from the OECD Halden Reactor Project.

Detailed gamma spectrometric measurements of the krypton-85 emission in the plenum of the rod coupled with collimated measurements in the fuel stack and complex theoretical analyses of the absorption and efficiency coefficients allow a precise determination of the FGR ratio.

Measurements on test fuel rods with long acquisition time were carried out. The agreement with standard (mass spectrometry) method is about 0.1–0.2%. The accuracy of the method is linked to the long acquisition time, the precise geometrical characterization of the rod (spring position that determines the signal attenuation by the spring itself). This method has the advantage of being very cheap, but requires a very good characterization of the fuel rod.

Presentation: Pulsed eddy current defectoscopy of irradiated WWER fuel rods, S.S. Sagalov, SCC-RIAR, Russian Federation.

S.S. Sagalov from SCC-RIAR presented post-irradiation examination of 5–75 $MW \cdot d \cdot kg^{-1}$ U burnup VVER fuel rods by pulsed eddy current method.

In this case eddy current is used as a first screening tool for detecting defects in fuel rods and to identify those that must be sent to hot cell for further PIE analyses. The technique used in RIAR allows not only the detection of the defect, but also the determination of its nature, for example fretting, bulging, cracks, or missing pellet surface (MPS). This is obtained by use of an annular sensor connected to dedicated analysis software. The software produces a phase/amplitude plot (A-scan) that is characteristic for the type of defect. Also inner defects such as strong corrosion of the inner cladding surface or MPS can be detected.

Presentation: Possibilities and features of electron backscatter diffraction for reactor materials investigation, Y. Goncharenko, SCC-RIAR, Russian Federation.

The last presentation of the session was given by Y. Goncharenko from SCC-RIAR. He reported on the commissioning of a high resolution analytical SEM for irradiated material. In particular the use of the EBSD technique was presented in detail. This technique allows the detailed characterization of the grain orientation at the surface of a specimen. This is very effective for deformation analysis in structural material.

As an example, steel deformation including the formation of sub-grains and change in phase crystallography was presented in details. Observations of irradiated material have already been made, but were not presented. The first experience gained with this method stresses the need of an extremely well prepared specimen surface, which is the main difficulty for its use with radioactive materials. In particular, the sensitivity of the detector to gamma irradiation requires preparing very small and thin irradiated specimens. Nevertheless this is an effective method for the characterization of the deformed materials.

3. PROBLEMS, CHALLENGES AND PERSPECTIVES

The five presentations of the session led to lively discussion showing the interest for the methods presented. The questions and discussions stressed the need for new investigation tools, but also clearly pointed out the need of cross-checking and validation of any new methods.

For any new analytical method that is developed in the investigation of nuclear material a validation program, if possible at international level must be planned. This is the most efficient way to increase the acceptance of these techniques or methods and assists their further development in particular for the analysis of materials from power plants.

Another point that clearly appeared during the discussion is the need of dedicated specimen preparation methods. In future it will be essential to have the capability to prepare small specimens that allow the detailed analysis of the material properties. A key factor will be the capacity to extract micro-specimens at well chosen locations from the bulk of strongly radiating material.

4. RECOMMENDATIONS FOR FUTURE WORK

The rather empiric approach of the past, based on the analysis of extensive, parametric irradiation campaigns of fuels and materials, is not sustainable today due to lack of resources and of irradiation and infrastructure facilities. Thus it is necessary to focus on the scientific understanding of fundamental mechanisms underpinning the behaviour and properties of fuels and materials under irradiation. Moreover, the experimental outcome must be targeted and coordinated for the validation of suitable predictive tools, modelling and codes. The development of new experimental and modelling techniques opens the way to better understanding and prediction of particular nuclear fuel and irradiated materials. The ultimate goal of these activities is to ensure the safe application of existing and future nuclear energy concepts.

Two important areas can be singled out for further development with respect to experimental methods for the characterization of irradiated fuels and materials: the improvement of the spatial resolution (particularly relevant in the case of highly heterogeneous fuels and materials) and the capability of analysing bulk properties of a sample using non-destructive methods (thus avoiding artefacts induced by sample preparation techniques). In addition to the measurement techniques (and their adaptation to hot lab environments) this trend requires also the development of dedicated specimen preparation methods that will allow the most effective use of these complex new analytical methods.

Session 5: PIE methods and results (Results)

Chairmen: J.Y. Blanc (CEA) and Y. Goncharenko (SCC-RIAR)

1. BACKGROUND

This session was a continuation of the preceding session on PIE methods and results (Methods). Seven papers were presented, all of them with the global objective of a better knowledge of fuel after irradiation. However, some papers were focusing on the examination of spent fuel bundles or assemblies in normal conditions for a leakage (Chalk River, Canada and NSC KIPT, Ukraine) or a defect (PSI, Switzerland), whereas other papers were presenting developments of new fuels (BARC, India and RIAR, Russian Federation). One paper (Institute for Nuclear Research (INR) Piteşti, Romania) looked at an irradiated fuel for safety purposes and the last paper (KAERI, Republic of Korea) gave improvements in fuel models.

2. SUMMARIES AND COMMENTS

Presentation: Defective fuel examination using coulometric titration and analytical electron microscopy at Chalk River laboratories, Z. He, AECL, Canada.

Z. He from AECL Chalk River described some examinations on defective CANDU fuel rods. This work was performed in order to quantify the extra oxidation on UO_2 after a leakage of the cladding and water ingress. This would give results for safety purposes (to model how many uranium can be found in the primary circuit due to pellet oxidation and leeching) and to improve fuel modelling. Two different methods were applied: (i) coulometric titration, i.e. extra oxidation by H_2 to quantify the quantity of oxide that has been formed on a macroscopic scale and (ii) SEM with WDS analysis to quantify the same oxidation on a microscopic scale. Both methods gave converging results on the O/M ratio.

Presentation: Post-irradiation examination of thoria–plutonia mixed oxide fuel in Indian hot cells, J.L. Singh, BARC, India.

J.L. Singh from BARC, presented a whole set of PIE on a cluster of irradiated experimental pins. These analyses were performed to qualify a new fuel (Th + 4% Pu)O_2 in the frame of developing thorium fuels. India possesses a lot of thorium reserves and its national nuclear programme is targeted around three steps: (1) burning uranium in PHWR to create plutonium, (2) burning plutonium in FBR with thorium blankets to produce uranium-233 and (3) burning uranium-233, thorium and plutonium in AHWR. The cluster of pins was irradiated to 18.5 $GW \cdot d \cdot t^{-1}$ in a pressurized water loop inside the CIRUS reactor. The micrographic structure after irradiation was investigated. Results for two of the experimental pins were given and considered satisfactory for further irradiation.

Presentation: Destructive examination of experimental CANDU fuel elements irradiated in TRIGA-SSR reactor, S.I. Ionescu, INR Pitesti, Romania.

S.I. Ionescu from INR Piteşti, presented the results of non-destructive and destructive PIE on a CANDU fuel rod. The bundle was irradiated in the steady state TRIGA reactor in Piteşti and submitted to PIE in the adjacent hot laboratory. With the support of IAEA, this laboratory has recently installed a new tensile machine and a new SEM, and so was able to complete previous optical microscopic examinations. The tensile test was performed on rings after mechanical defueling and the new SEM was employed for examining the rupture surface. The results were considered typical for a CANDU 6 fuel.

Presentation: The main results of investigation of modified dispersion LEU U–Mo fuel tested in the MIR reactor, V.V. Iakovlev, SCC-RIAR, Russian Federation.

V.V. Iakovlev from RIAR in Dimitrovgrad described some results on the improvement of the U–Mo fuel. The RERTR programme aims at developing a new fuel with a higher density of uranium atoms to compensate for poorer uranium-235 enrichment in order to stay below the enrichment limit of 20%, for non-proliferation purposes. The UMo is a good candidate for a uranium high density fuel for experimental reactors. Unfortunately, there is some interaction between UMo and the aluminium matrix. PIE on experimental rods by SEM and EPMA showed that two technical solutions have significantly reduced this interaction: either adding silicon to the aluminium matrix (Al + 13% Si was better than Al + 5% Si) or by using a ZrN coating prepared by the Bochvar Institute in Moscow. Rod BUs were around 60–84%.

Presentation: Examination of an irradiated fuel pin segment by laser scanning profilometry, gamma spectrometry and neutron radiography, H. Wiese, PSI, Switzerland.

H. Wiese from PSI in Switzerland showed some investigations performed during the classical surveillance programme on a BWR fuel rod. Some diameter reduction was detected on a rod and tracked using three complementary techniques: laser profilometry using a new device, gamma spectrometry and finally neutron radiography at SINQ neutron spallation source. These techniques enable the best position for a metallographic cutting to be chosen. The reduction of diameter was attributed to a bad rectification (ellipsoidal shape) of one pellet during its manufacturing process.

Presentation: Post-irradiation examination of the fuel rods operated in WWER-1000 mixed cores, M.V. Tretyakov, NSC KIPT, Ukraine.

M.V. Tretyakov from NSC KIPT in Ukraine presented in-pool non-destructive examination results. Ukraine VVER-1000 units are supplied with Russian fuel assemblies manufactured by TVEL. In 2005, six lead test assemblies, provided by Westinghouse, were inserted in South Ukraine 3 and examined in 2007, 2008 and after 4 cycles (49 $GW \cdot d \cdot t^{-1}U$). Visual inspections were satisfactory. Sipping test showed 5 leaktight assemblies and a minor leakage in the 6^{th} but below the operational limit. Consequently Westinghouse will provide fuel loadings for three Ukrainian units.

Presentation: The development of xenon diffusivity measurement for irradiated ceramic fuels with low burnup, H.-M. Kim, KAERI, Republic of Korea.

H.-M. Kim from KAERI presented a study on the release of xenon in small samples irradiated for a short time (16–20 minutes) in the HANARO reactor. These samples were submitted to a heat treatment and release of xenon-133 was measured and so the diffusivity coefficient of xenon was acquired. Samples included UO_2, UO_2 with additives such as Nd_2O_3, CeO_2 and Nb_2O_5, SIMFUEL, UN and $(Th,U)O_2$. Physical forms included powders and disks as well as single-grained or polycrystalline materials. This study will give data for improved modelling of the fuel.

3. PROBLEMS, CHALLENGES AND PERSPECTIVES

Concerning the objectives of these papers, they showed the continuous need for surveillance programs for fuel vendors as Westinghouse in Ukraine, or to check the quality of fuel (for BWR in PSI or for CANDU in Piteşti). Non-destructive investigations on complete fuel assemblies can be performed in the reactor pool, but also on a few rods in hot cells. They give data to the regulatory bodies concerning limits that can be accepted or not in case of leakage (Chalk River) or after experimental irradiation (Piteşti). More comprehensive investigations in hot cells are indispensable in the case of development of new fuels, such as U–Mo or thorium fuels. They give also data to theoretical models to improve code qualification (KAERI).

Concerning the techniques, all the papers showed classical techniques (sometimes with clever improvements, such as image analysis on neutron radiography), with emphasis on leakage detection methods and SEM examinations. SEM is a rather basic tool for a hot laboratory (see also the paper from NRG, Netherlands in session III). The use of laser diameter measurement in PSI is rather new, although EDF Chinon has already used this technique. Another rather uncommon technique described during this TCM was the acoustic microscopy by ITU (D. Papaioannou) in the preceding session. Coulometric titration is also a rather unconventional technique although some similar studies have been performed by CEA (ADAGIO experiments).

As usual, the combination of several techniques on the same object is very powerful as demonstrated in the papers from Piteşti, PSI, Chalk River, RIAR Dimitrovgrad and BARC Mumbai.

It is interesting to note both development programs for new fuels: (a) UMo for non-proliferation purpose and (b) thorium fuels for using this alternative fertile material.

4. RECOMMENDATIONS FOR FUTURE WORK

PIEs represent a constant need for fuel surveillance programs and also provide data to ensure the safety of current and advanced fuels. It is then recommended to go on with specialists' meetings, either under IAEA TCM form or under HOTLAB annual conferences, to provide a forum where:

- Specialists can share their experience on current PIE techniques and about the technical implementation of PIE devices;
- Specialists can acquaint themselves either with new techniques or new developments on conventional techniques, e.g. such as the acoustic microscopy presented in this TCM.

These discussion forums are also a place where hot laboratory staff can set up small workshops on specific matters. For instance, PSI has organized in 2010 a small workshop on the "analysis of small incidents in hot laboratories" using the return of experience in foreign hot labs in order to elaborate a common response to the safety.

Session 6: Irradiated fuel and radwaste management

Chairmen: A. Bevilacqua (IAEA) and P. Marty (CEA)

1. BACKGROUND

For more than three decades hot cell examination and poolside inspection play the key role for assessing the performance of spent fuel particularly as burnup and storage time increase. The safe management of spent fuel heavily rely on the results of examinations and inspections determining the physicochemical properties which define the behaviour during storage and transport.

As an unavoidable by-product of the hot cell post-irradiation examinations some quantities of radioactive waste is generated once the integrity of the spent fuel rod is lost e.g. by chopping, cutting or puncturing. Furthermore, the use of organic materials e.g. resins for allowing the metallographic preparation of spent fuel or corium samples for analysis originates a more complex radioactive waste which generates hydrogen as a result of the interaction of the gamma, neutron, beta and alpha radiation from the spent fuel or corium with the organic material.

The presentations of Session 6 provide results and analysis directly related with the above mentioned subjects.

2. SUMMARIES AND COMMENTS

Presentation: Estimation of hydrogen production rates from radiolysable material in contact with various irradiated fuels, D. Bottomley, JRC-ITU, European Commission.

This paper deals with the estimation of hydrogen (detected by gas chromatography) production rates from radiolysable material (composites and epoxides resins). It shows that total activity (with the burnup of UO_2 fuel) of the spent fuel and more precisely the gamma activity is responsible of the H_2 production. Typically gamma power appears to be the main source deposited in resin at about 80% and shows a slow exponential growth with burnup at a cooling period of 5 years; alpha and beta radiation are then the next major source at ~20%, but are the most poorly characterized. Finally, the proposed rate is approximately 0.00217 cm^3 H_2/day/cm^3 resin for a 23 $GW{\cdot}d{\cdot}t^{-1}UO_2$ sample and is linked with the burnup (within a factor 1 up to 3.3 for a burnup from 23 $GW{\cdot}d{\cdot}t^{-1}U$ up to 60 $GW{\cdot}d{\cdot}t^{-1}U$). This allows having calculations before transportation and/or storage. These can assist in transport licensing and design considerations of storage for irradiated radiolysable material. It could be interesting for further works to increase the universality of such equation.

Presentation: CEA strategy for civil spent fuels, J.-Y. Blanc, CEA, France.

The French strategy for the spent fuel discharged from the experimental reactors and samples from post-irradiation examinations in its hot laboratories is presented. For significant spent fuel quantities discharged from Osiris MTR and Orphées, the priority solution is reprocessing to value their energetic content. Further contracts should be negotiated with AREVA for Phénix FBR and Phébus. However, some specific spent fuel assemblies are not easily reprocessed, because quantities are too small for an economic treatment, or because they are embedded in epoxy. CEA manages spent fuel storage facilities, such as PEGASE and CASCAD in Cadarache and other facilities (ISAI, STAR) for putting spent fuel assemblies inside welded canisters. However, wet storage in PEGASE does not comply with current seismic standards. So the spent fuel assemblies are sent to STAR for new containerization before dry storage in wells at CASCAD or wet storage in RES canal. Other old spent fuel types are stored in INB 72 Saclay facility. Phénix spent fuel should be sent to La Hague inside canisters to be welded in ISAI in Marcoule. Retrieving old spent fuel canisters requires safety demonstrations and sometimes R&D too. One problem is to demonstrate that no water has penetrated inside the canister. Another is to find a way to remove the epoxy embedding of former metallographic samples or to deal with potential hydrogen due to radiolysis of epoxy. Moreover, a stabilization treatment should be

performed on metallic spent fuel from graphite reactors to avoid a pyrophoric reaction. For very old spent fuel surveillance of canisters inside dry wells or finding all necessary data before a new containerization is not easy. The shipment of small quantities of PWR spent fuel remnants to La Hague has been recently investigated. If this way is opened, it can be extended to other laboratory spent fuel. Summarizing, the CEA currently manages a quite large quantity of spent fuel with many different physicochemical characteristics.

Presentation: BEFAST and SPAR from 1981 to present: Thirty years of spent fuel behaviour, performance and research, A. Bevilacqua, IAEA.

The paper presents a complete overview of two IAEA Coordinated Research Projects (CRPs) and associated publications related to the spent fuel behaviour, performance and research in the past 30 years. Presenting the main results of all completed phases of both CRPs: Behaviour of Spent Fuel and Storage Facility Components during Long Term Storage (BEFAST–I, II and III) and Spent fuel Performance Assessment and Research (SPAR-I, II and III ongoing), the paper shows the considerable work done by all the participating countries (up to 12). The conclusions of the last phase of BEFAST (BEFAST-III (1991–1996)) evidence that PWR and BWR burnup was steadily increasing in the last decade from 40–50 GWd/tU resulting in: increased fuel rod internal pressure, higher Zr alloy corrosion from longer residence time and increased cladding hydrogen concentration from higher Zr alloy corrosion. Furthermore, after 14 years cooperation the fundamental R&D questions had been answered so that licensing of both wet and dry spent fuel storage is possible in most countries. On the other hand the effects of extended burnup needed to be assessed and the extrapolation to very long storage times (> 50 years, exceeding the periods covered by the CRP) had to be confirmed. The subsequent SPAR CRP — currently in its third phase — encompassed the higher burnup and longer time in its main objectives as: Develop a technical knowledge base on long term storage of spent fuel from nuclear power reactors through evaluation of operating experience and research, and extrapolate predictions of spent fuel behaviour over long periods of time.

Presentation: Development of a set-up for the detection of failed fuels in TAPS BWR spent fuels storage bay, J.L. Singh, BARC, India.

It describes a technique tested at the laboratory to demonstrate its technical feasibility and reliability for detecting failed fuel rods in leaky fuel assemblies during poolside examination and discusses the issues associated with the test and approaches to enhance the reliability for detecting failed fuel. Based on the measurement of the water entered the fuel pin through the breach in the zircaloy clad, that indicates or confirms clad/weld failure of a fuel pin. A non-destructive (ultrasonic testing technique) method helps in identifying the failed fuel pin without dismantling the fuel assembly. It was found that the pitch-catch technique has higher signal to noise ratio. Different positions on the detectors have been tested and the results, obtained within 3 hours, enable to determine the incriminated fuel pin. The next step will be to test a real assembly and results are expected next year.

Presentation: Establishment of the disassembling technique of the driver fuel assembly irradiated in JOYO, S. Ichikawa, JAEA, Japan.

In order to increase the final burnup and neutron fluence of fuel rods of the experimental fast reactor JOYO it is presented a new approach for the establishment of the disassembling technique of its driver fuel assembly. This technique made it possible to remove the fuel pins from the driver fuel assembly without fuel pin sectioning. After disassembling, some selected fuel pins can be reassembled into a new irradiation vehicle for continuous irradiation in JOYO. This technique allows the irradiation data of high burnup fuel and high neutron fluence material to be obtained like power to melt (PTM) examinations using previously irradiated pins.

Presentation: Reassembling procedure of the fuel assemblies for the nuclear power ship “Mutsu”, H. Matsui, JAEA, Japan.

It presents the reassembling procedure of the fuel assemblies for the nuclear power ship “Mutsu”. The Japan’s first voyage utilized by nuclear power was made by nuclear power ship "Mutsu" in 1990. After the research voyage in 1992, decommissioning work of the nuclear reactor for “Mutsu” was started to change it from the nuclear power ship to an ordinary power ship. The presentation deals with the removal fuel assemblies from the reactor, transportation to the Reactor Fuel Examination Facility (RFEF) in Nuclear Science Research Institute (NSRI) (JAEA). To avoid contamination of the pool, the “Mutsu” fuel assemblies were loaded directly into a hot cell of RFEF using the roof-gate as the top loading procedure. Finally after separation the 34 fuel assemblies were reassembled as six PWR type fuel assemblies in order to adjust the acceptable specifications of the reprocessing plant in JAEA: the shape of fuel assembly is the same as the PWR type commercial reactor fuel and the average enrichment of uranium in the assembly is under 4.0%.

3. PROBLEMS, CHALLENGES AND PERSPECTIVES

Because of the typical timeframe for managing spent fuel which last for several decades the potential problem of aging of facilities and human capital should be timely addressed. The knowledge should particularly be carefully managed in order to transfer it between the more experienced generation of professionals and technicians who approach their retirement and the younger generations that will fill their vacancies.

As spent fuel storage time extends more assemblies approach a condition that could well be virtually characterized as ancient spent fuel. In this context, the hot cell post-irradiation examination and poolside inspection community is challenged by two key issues: spent fuel integrity during long term wet storage and spent fuel transportability after long term dry storage.

4. RECOMMENDATIONS FOR FUTURE WORK

As a consequence of the Fukushima Dai-ichi accident the immediate and medium term future will be dominated by the need of a remarkable effort on corium characterization and management at the Units 1–3 as well as spent fuel characterization and management at the Units 1–4. Certainly all currently available hot cell post-irradiation examination and poolside inspection techniques and methodologies will sooner or later, in greater or lesser extent, have the chance to contribute to this end. Last, but not least, methods, techniques, devices, instruments, etc., either novel or adapted ad hoc could be needed to cope with this unprecedented challenge.

INSPECTION

(Session 1)

Chairpersons

F. FLACHET
Electrabel

R. ZAJAC
Vuje

GAMMA SPECTROMETRIC MEASUREMENT OF BURNUP

V. CHRAPČIAK, M. LISTJAK, V. FRIDRICH, P. ŠIMON
VUJE, a.s.,
Trnava, Slovakia
Email: chrapciak@vuje.sk

Abstract

The gamma spectrometric measurement of burnup is based on measurement of activity Cs-134 and Cs-137. The ratio activity Cs-134/activity Cs-137 is linear in dependence on burnup. Fuel assemblies VVER-440 were in ISFSF Jaslovske Bohunice measured. The analysed assembly has radial profile of enrichment, average enrichment is 3.82%. The burnup was calculated with the PERMAK-3D code. The activity was calculated with the SCALE 5.1 system (the TRITON module).

1. INTRODUCTION

The gamma spectrometric measurement of burnup is based on measurement of activity Cs-134 and Cs-137. The ratio activity Cs-134/activity Cs-137 is linear in dependence on burnup.

Fuel assemblies VVER-440 were in ISFSF Jaslovske Bohunice measured. The analysed assembly has radial profile of enrichment, average enrichment is 3.82%. The assembly is hexagonal.

The measurement of burnup has several steps:

(1) Measurement of activity Cs-134 and Cs-137:
  (a) Spectrum acquisition on specific positions;
  (b) Analysis and quantification activity of Cs-134 and Cs-137 from spectrums of specific "cuts" of fuel assembly.
(2) Calculation ratio activity Cs-134/activity Cs-137 in dependence on burnup;
(3) Determine ratio activity Cs-134/activity Cs-137 by the SCALE 5.1 code system;
(4) Determine experimental burnup according measured activity Cs-134 and Cs-137;
(5) Comparison experimental and calculated (3D pinwise PERMAK-3D code) burnup.

2. MEASUREMENT OF ACTIVITY Cs-134 AND Cs-137

Gamma spectrometric measurement of burnup has been carried out in inspection stand SVYP-440 in ISFSF Jaslovske Bohunice. Measurement of ^{134,137}Cs was performed by HPGe GC2018 detector. Scheme of measurement is shown in Fig. 2.1. Positioning of fuel rod in front of collimator was performed by manipulator MAPP-440.

Spectroscopic software Genie2000 was used for acquirement and analysis of spectra. Photon energy interval from 20–2000 keV was recorded. Dead time of measurement varied from 5% up to 25% according to measurement point (count rate 9000–48 000 cps). Example of the spectrum is shown in Fig. 2.2.

Each position (radial and axial) of fuel rod was measured via 1.5 m thick steel rectangular collimator. Position of measurement was controlled by particular device with appropriate software. This position was recorded to the spectrum description to meet QA requirements (e.g. traceability). Time of measurement was set up according to the aim of the measurement from 20 s up to 3600 s. Efficiency calibration of HPGe detector was done by ISOCS software (generic characterization). For efficiency calculation some simplifications were accepted like homogeneous material of fuel rod.

After measurement device was calibrated, there were measured more than 200 spectrums in various positions. It was necessary to decrease the dead time because of high input count rate. The original

project included the measurement of construction properties like spacer grid position (and its comparison with documentation). For declaration of spacer grid position, 20 seconds measurements were sufficient. Activities of ^{137}Cs round 3rd spacer grid are in Table 2.1 and Fig. 2.3.

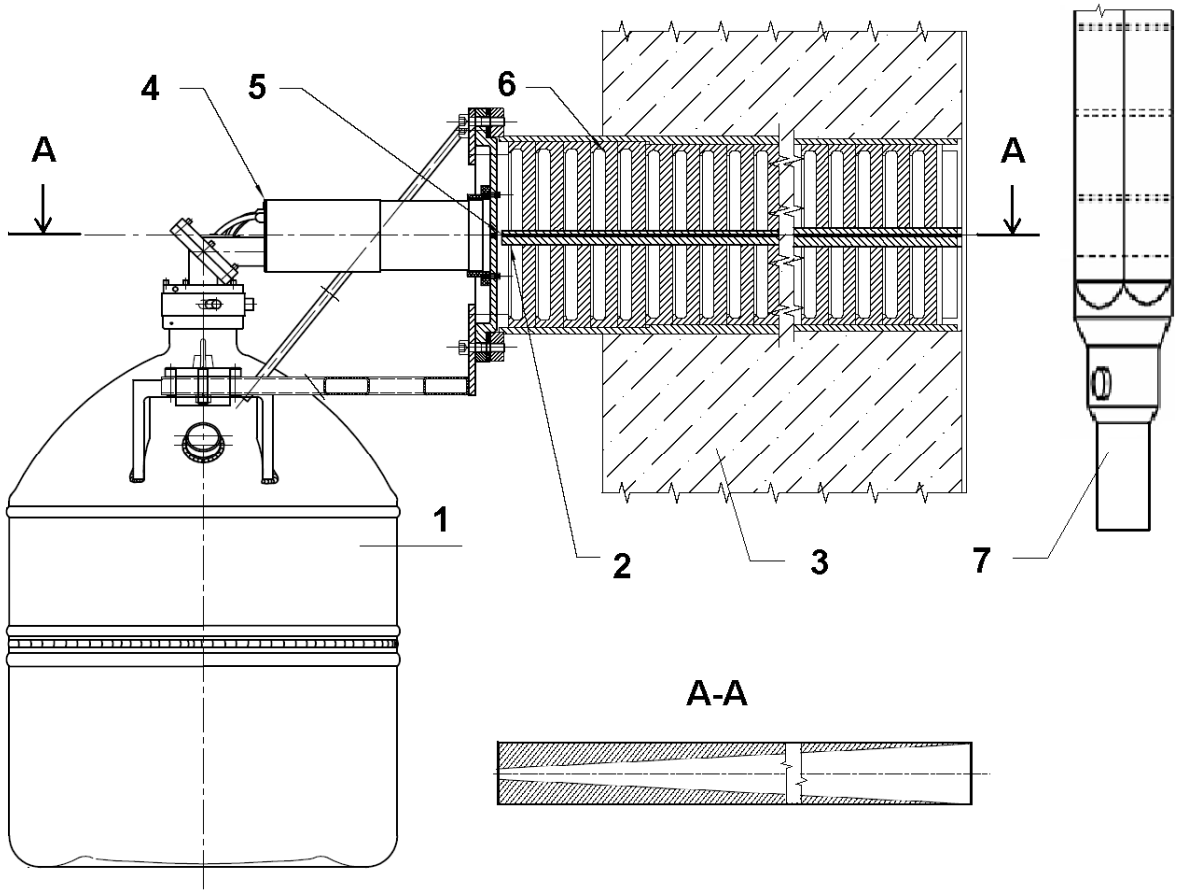

1. Cryostat
2. Lath of collimator
3. Wall between shaft 02 and room No. 113 — pool wall
4. HPGe detector
5. Colimator
6. Shielding rings
7. Fuel rod in pool of shaft No. 02

A-A Profile of colimator

FIG. 2.1. Scheme of measurement.

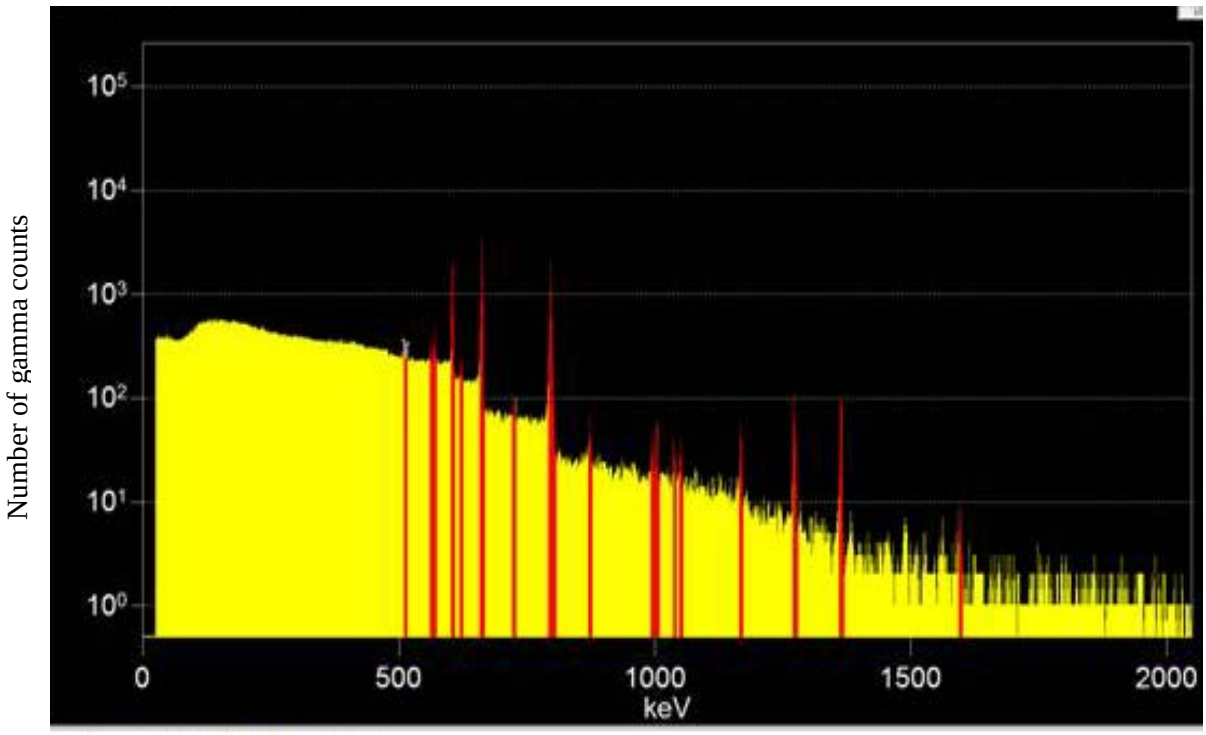

FIG. 2.2. Example of measurement spectrum.

TABLE 2.1. SUMMARY OF SPACER GRID MEASUREMENTS

Order	Rotation [°]	Height coordinate [mm]	File name	A (^{134}Cs) [Bq/section]	A (^{137}Cs) [Bq/section]	Time [s] /live/	Time [s] /real/	Date and time
1	27	1125.00	6211.cnf	1.21E+11	2.46E+11	20.00	25.73	18.2.2010 9:58
2	27	1127.00	6213.cnf	1.25E+11	2.48E+11	20.00	25.68	18.2.2010 9:59
3	27	1129.00	6215.cnf	1.20E+11	2.48E+11	20.00	25.69	18.2.2010 9:59
4	27	1131.00	6217.cnf	1.23E+11	2.46E+11	20.00	25.71	18.2.2010 10:00
5	27	1133.00	6219.cnf	1.12E+11	2.40E+11	20.00	25.66	18.2.2010 10:00
6	27	1135.00	6221.cnf	1.10E+11	2.27E+11	20.00	25.61	18.2.2010 10:01
7	27	1137.00	6223.cnf	1.11E+11	2.26E+11	20.00	25.59	18.2.2010 10:02
8	27	1139.00	6225.cnf	1.13E+11	2.28E+11	20.00	25.57	18.2.2010 10:02
9	27	1141.00	6227.cnf	1.17E+11	2.27E+11	20.00	25.61	18.2.2010 10:03
10	27	1143.00	6229.cnf	1.19E+11	2.40E+11	20.00	25.67	18.2.2010 10:03
11	27	1145.00	6231.cnf	1.19E+11	2.47E+11	20.00	25.73	18.2.2010 10:04
12	27	1147.00	6233.cnf	1.20E+11	2.48E+11	20.00	25.71	18.2.2010 10:05
13	27	1149.00	6235.cnf	1.26E+11	2.47E+11	20.00	25.77	18.2.2010 10:05
14	27	1151.00	6237.cnf	1.21E+11	2.51E+11	20.00	25.77	18.2.2010 10:06

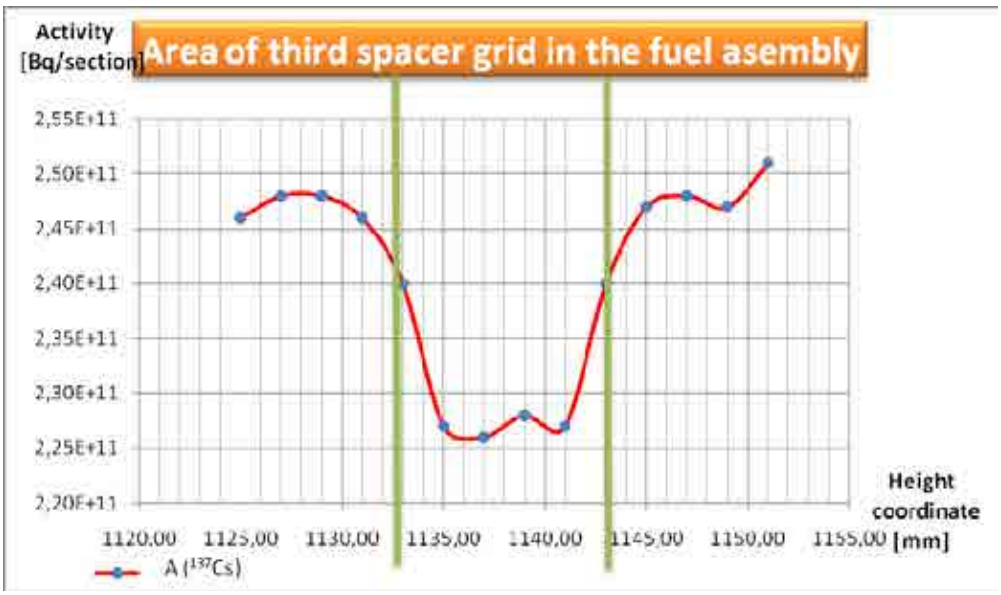

FIG. 2.3. Spacer grid in the fuel assembly.

3. CALCULATION RATIO ACTIVITY Cs-134/ACTIVITY Cs-137 IN DEPENDENCE ON BURNUP

The measured assembly 138 62894 has profiled enrichment, average enrichment is 3.82%. The average burnup is 46 206 MW·d·t^{-1} U. The cooling time was 1328 days. The ratio activity Cs-134/activity Cs-137 was calculated with the TRITON module (the SCALE 5.1 system)[1]. By the shroud are pins with enrichment 3.3% and 3.6%, inside with 4.0%. The ratio for pins 3.3%, 3.6% and 4.0% is in Fig. 3.1 shown.

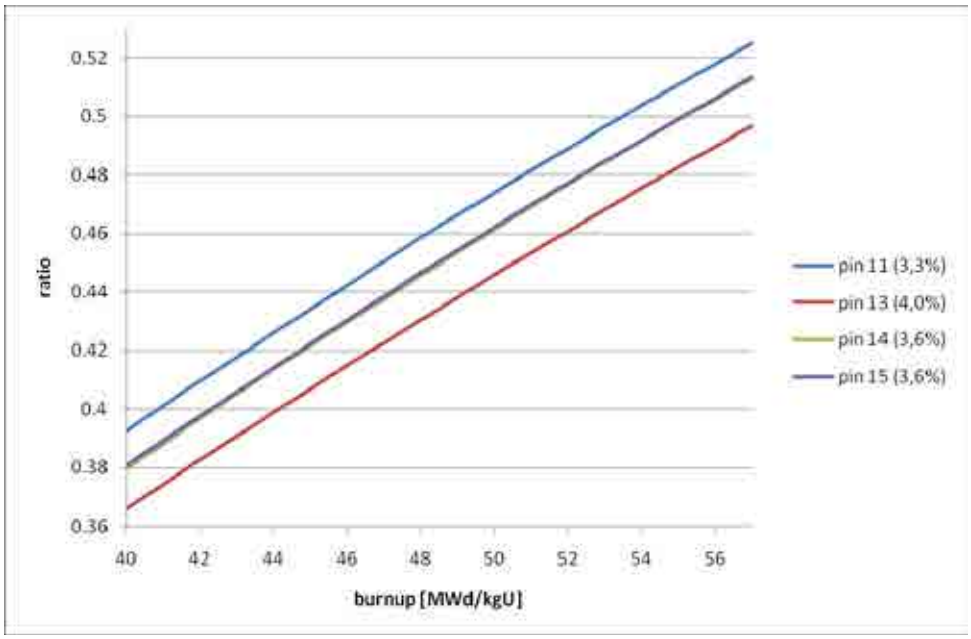

FIG. 3.1. Assembly 138 62894, ratio activity Cs-134/activity Cs-137 calculated with the TRITON module for different pins.

4. DETERMINE EXPERIMENTAL BURNUP ACCORDING MEASURED ACTIVITY Cs-134 AND Cs-137

The calibration measurement has been carried out as first step and later measurement of activity Cs-137 (see Section 2). For calibration measurement we have:

– Ratio measured activity Cs-134/measured activity Cs-137;
– Ratio calculated activity Cs-134/calculated activity Cs-137 for burnup (calculation TRITON).

For measured activity Cs-137 we have "measured" burnup: $B = k \cdot$activity Cs-137

The measured burnup is shown in Table 4.1. We see that for position Z = 90 cm is strong decreasing. Here is a space grid.

TABLE 4.1. ASSEMBLY 138 62894, MEASURED BURNUP [MW·d·kg^{-1} U]

Z [cm]	0°	60°	120°	180°	240°	300°
30	49.68	49.17	50.07	51.9	51.58	51.11
60	56.29	55.09	56.24	58.36	58.55	56.85
90	51.78	51.42	52.01	54.62	53.81	52.78
120	55.97	55.27	57.51	59.66	60.09	58.88
150	55.46	54.8	56.63	59.36	59.59	59.29
180	53.26	52.42	54.69	57.53	57.79	57.23
210	42.28	40.45	43.03	45.9	46.34	44.8

5. COMPARISON EXPERIMENTAL AND CALCULATED (3D PINWISE PERMAK-3D CODE) BURNUP

The PERMAK-3D code [2] is diffusion, 4 group and three dimensional pinwise code. With the PERMAK-3D code is possible to calculate power and burnup distribution in pins (radial and axial). In Fig. 5.1 is comparison of axial burnup distribution, in Table 5.1 is comparison of radial burnup distribution (relative value). We see that for position Z = 90 cm is strong decreasing. Here is a space grid.

The difference between measured and calculated power distribution are less than 5%.

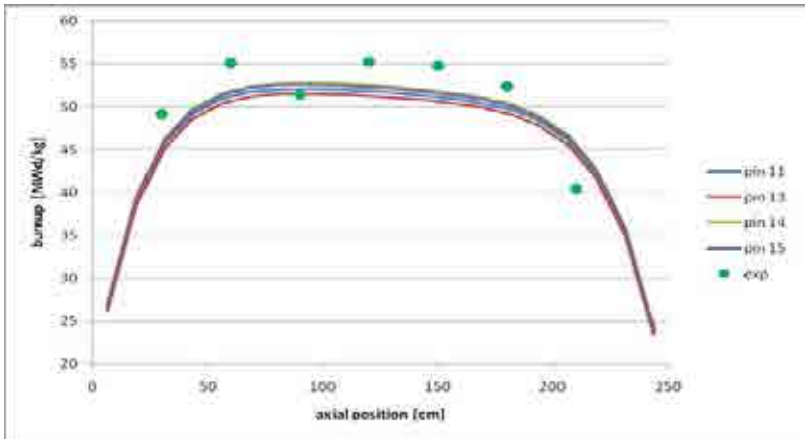

FIG. 5.1. Assembly 138 62894, axial profile of burnup for different pins. Calculated value is from the PERMAK-3D code.

TABLE 5.1. ASSEMBLY 138 62894, RADIAL PROFILE OF BURNUP (RELATIVE VALUE), Z = 120 CM

Angle	0°	60°	120°	180°	240°	300°
PERMAK-3D	0.99	0.98	0.99	1.01	1.02	1.00
Measurement	0.97	0.95	0.99	1.03	1.04	1.02

6. CONCLUSION

Gamma spectrometric measurement has wide utilization by checking of spent fuel assemblies:

– To find top and bottom of fuel pin;
– To find space grid;
– To measure burnup.

For burnup measurement gamma spectrometric measurement need theoretical calculation of activity Cs-134 and activity Cs-137 for some burnup interval and for specific cooling time. The half time of Cs-134 is $T_{1/2}$ = 2.065 y, therefore the cooling time between end of irradiation in reactor and measurement should be no longer than four years.

Other very important point is how pins are by shroud. If they have very different enrichment (or Gd content) the ratio calculated activity Cs-134/calculated activity Cs-137 is very different and is problem to define calibration constant.

REFERENCES

[1] OAK RIDGE NATIONAL LABORATORY, SCALE 5.1, Oak Ridge National Laboratory, Oak Ridge (2006).
[2] LIZORKIN, M.P., SAPRYKIN, V.V., Programma PERMAK, Kurchatov Institute of Atomic Energy, Moscow (1989).

STUDIES ON THE SINTERING BEHAVIOUR OF UO_2–GD_2O_3 FUEL PELLETS

G. RUGGIRELLO, R. MIZRAHI, H. CALABRONI,
Ciclo Combustible Nuclear,
Comisión Nacional Energía Atómica (CNEA),
Buenos Aires

R. PEREZ, J.M. FREDIANI
Atucha-1 NPP,
Nucleoeléctrica Argentina SA,
Lima, Buenos Aires

Argentina

Abstract

Atucha-1 NPP is a Siemens-KWU designed PHWR which started its operation in June 1974 and has accumulated up to December 2010 around 26 fpy, that mean a load factor of above 72%. It began its operation with natural uranium fuel and since 1995 the core has been converted to SEU (0.85% enriched). Moreover, in the recent years CNEA Fuel Engineering Branch has developed a programme to increase the U mass, involving a new structural design of the fuel element (FE), in order to achieve a higher burnup and to reduce the frequency of daily on-line refueling.On the other hand, this type of reactor design involves the use of coolant channels (CC) which interact strongly with the FEs. The original CCs had to be replaced when signs of degradation were noticed at about 10.4 fpy. The new CCs have an improved design and are made of zircaloy-4 with enhanced oxidation and mechanical properties. According to these needs a number of activities were planned for the follow-up and periodic control of the FEs and CCs in service. This presentation describes the poolside facilities used to perform visual inspection and dimensional measurements as well as the contribution of these results to both programs.

1. INTRODUCTION

NA-SA and CNEA have performed different activities regarding the follow-up and periodic control of the behaviour of the FE and their interaction with the CCs under operational conditions. The CCs are structural components which are characteristic of these type of reactors moderated and cooled by heavy water.

Being originally a natural uranium prototype reactor, Atucha-1 has undergone constant improvements in order to get a better efficiency in the utilization of the FEs, as well as concerning safety in operation. Improved fuel management implies that the FEs are now working at a lower linear power and reach a higher burnup.

In the recent years, our Fuel Engineering Branch has implemented a programme to increase U mass in the FE. Also, NA-SA has replaced all original CCs by ones with an improved new design. The effects of these modifications were monitored through visual inspection and PIE activities.

2. ATUCHA-1 REACTOR, MAIN CHARACTERISTICS

Atucha-1 is Argentina's first NPP and began its commercial operation in 1974. It is a PHWR designed by Siemens, with a gross electrical power of 360 MW(e). The reactor core has 250 vertical coolant channels which contain the FE and separate the coolant from the moderator. Refueling is made periodically during operation.

Power regulation is made through three absorber rods made of stainless steel for coarse control, three rods made of Hf for fine control, and additional rods of both types for shutdown. All rods are inserted

at different angles, thus allowing on-line fuel shuffling by the refueling machine. Up-to-date the plant has operated with a 72% load factor (26 fpy).

Figure 2.1 shows a schematic view of the pressure vessel which contains the moderator tank and structural components defined as reactor internals, such as: guide tubes for detector probes, control rod guide tubes, and coolant channels inside which the FE dwell.

All internals are fixed to the reactor lid and slide into the moderator tank bottom to allow for axial displacements due to different temperatures and materials. Also dimensional changes such as irradiation growth have to be considered and continuously monitored.

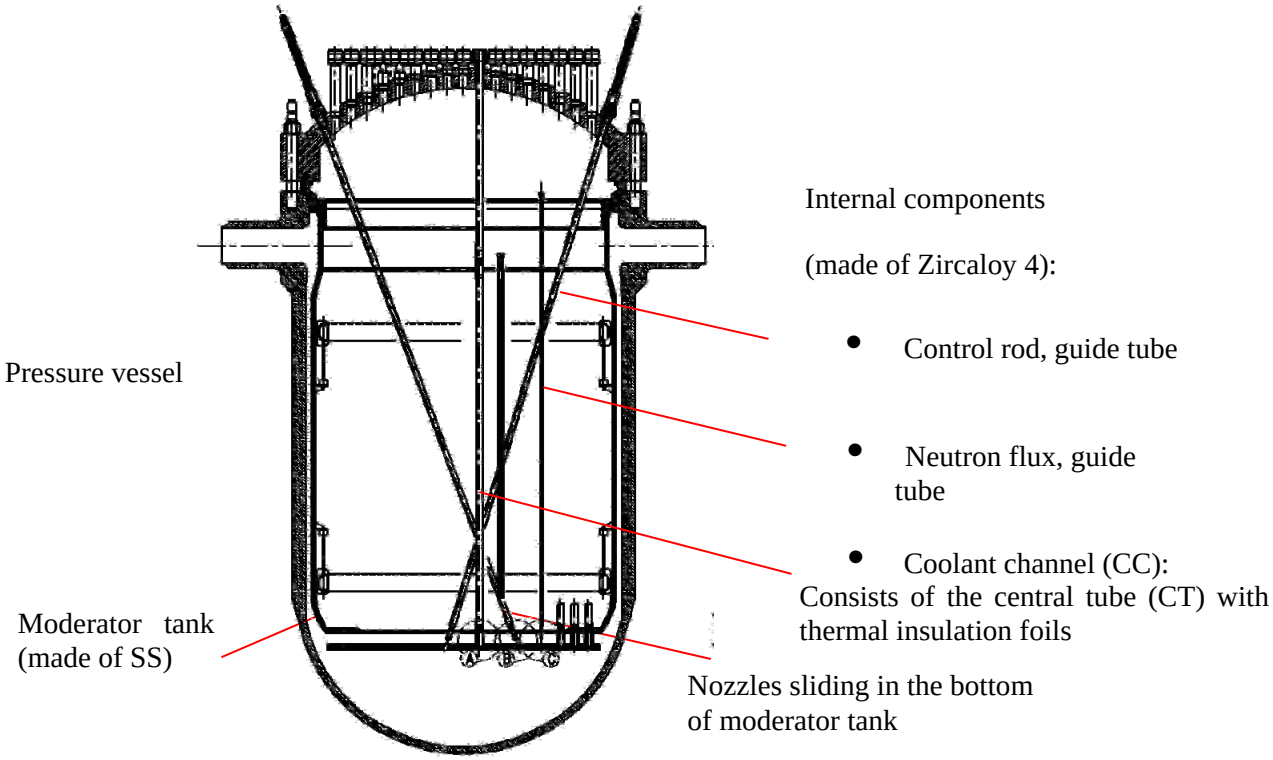

FIG. 2.1. Simplified cut view of Atucha-1 reactor.

The central tube (CT) of CC (also called shroud tube of FE) is made of zircaloy 4 of 1.73 mm thick; it bears major temperature gradients and undergoes mechanical interactions with the FE. Operating conditions involve:

– Temperatures above 300°C on its inner surface. The outer surface is in contact with the moderator water at about 180°C, and an insulation foil is used to minimize heat flux through the CT wall;
– Fast neutron flux ($f \approx 10^{13}$ n·cm^{-2}·seg^{-1}; E>1 Mev);
– D_2O with controlled chemistry.

Microstructural changes undergone by the CT during service bring about macroscopic effects such us:

– Axial elongation;
– Diameter expansion or shrinking;
– Growth of zirconium oxide layer;
– Increase of hydrogen/deuterium concentration;
– Degradation of mechanical properties (mainly a decrease in ductility).

In fact, in 1988 (at about 10.4 fpy of reactor operation), signs of degradation were observed on those CC with the highest fluences [1]. The main features were an excessive axial growth of CT (exceeding in some cases the design limit), and a high degree of oxidation and embrittlement of the insulation foils which led to their breaking into pieces. Both phenomena (high axial growth and the presence of debris) resulted in the restriction of sliding of CC guidance nozzle at the bottom of the moderator tank; some of them got stuck and underwent bending [1].

Original CCs and guide tubes were then gradually replaced by ones of a new design. The main modifications introduced in the improved new CC design were:

– The gap of the CC nozzle at the bottom of the moderator tank was increased and a special piece was added to avoid dirt accumulation above the nozzle;
– The original two-foil insulation was replaced by only one foil of 0.4 mm thick;
– The manufacturing process of CT and insulation foil was improved. A modified zircaloy-4 (PCA-S) with a different texture and lower tin content was used to obtain better properties regarding dimensional changes and oxidation resistance.

All CCs were replaced by those with the new design between 1996 and 2005. The operator of the plant (NA-SA) developed consequently a strict surveillance plan of continuous monitoring of reactor internal components as part of an "Early Alert Program" (early warning failure detection).

3. CONTROL METHODOLOGY OF THE CC

The surveillance plan consists of the following actions, which are being taken during planned outage:

– Remote visual inspection (RVI), inner and outer surfaces;
– Dimensional control of the CT, internal diameter and length;
– Metallurgical evaluation by destructive testing in hot cell.

3.1. Remote visual inspection inside the reactor

During each planned outage about 5% of resident CCs are inspected in situ with an underwater radiation resistant TV camera mounted on a column with a LED lighting system.

In the first place, the inner surface is scanned in its entire length with an axial lens; any signs of fretting, wearing or scratches are then further inspected using a radial lens. Documentation is recorded by image digitalization. A screen editor is used to annotate the position of the feature and other useful information. Special care is taken in the observation of marks left by interaction of the FE and the oxidation layer appearance of the surface (see Fig. 3.1).

3.2. Metrology and inspection in the SFP

During each planned outage about 4 resident CCs are taken out form the reactor and sent to the SFP for a complete inspection (inner and outer surfaces) and the measurement of the internal diameter (ID) and length of the CT.

The criteria to choose the CCs for inspection and metrology in the SFP are:

(1) To get data from CC with different fluence;
(2) To allow a remote visual inspection of different internal zones of the moderator tank with a TV camera inserted through the opening left when the CC is taken out;
(3) To follow the evolution of the macroscopic changes, the same CCs are inspected every four planned outages (approx. 6 years).

Up-to-date, the CCs of the following positions are being measured:

– Eight CC of central zone (without water flow throttle);
– Two CC of maximum dose (throttle #7);

– One CC of medium dose (throttle #6);
– One CC of peripheral zone (throttle #1).

Figure 3.2 shows the plan view of reactor lattice, the position pointed in black are the CC under follow-up. For the inspection, the CC is hung vertically from a shelf at the water level of the pool. Figure 3.3 shows the inspection bay. The remote visual inspection procedure is the same than that used inside the reactor, but also the outer surface of CC is inspected to check the state of the thermal insulating foil.

Axial length Measurement of the CT is obtained by direct comparison with a calibrated ruler made of a zircaloy cladding FE skeleton (a column so-called squirrel cage) which have three millimeter rulers at a 120° angular distance in both ends. The observation of the end position of the CT respect to the ruler is done by the same TV column used in the inspection. As the ruler column has the same thermal dilatation coefficient than the CT, the measurement can be done at any temperature condition (including thermal gradients) and also on a CC inside the reactor.

Figure 3.4 shows the ruler during its introduction into the CC and Fig. 3.5 shows an image captured from the TV screen showing the upper end position of the CT relative to the ruler.

Internal diameter (ID) measurement is performed using an ad hoc gauging head consisting of an underwater LVDT sensor which self centers on the CT through a roller pad guide. Calibration of the head is done with a centesimal micrometer and verified using a reference calibrated tube. Figure 3.6 shows the gauging head during calibration. Axial scans are performed and the maximum and minimum ID at each 50 cm of length are recorded; in this way the ID profile along the CT is obtained. Figure 3.7 shows the comparison of measured ID growth with the theoretical profile predicted by code calculation.

3.3. Metallurgical evaluation by destructive testing in hot cells

In order to perform metallurgical analysis, it was necessary to extract samples from different zones of the CT and insulation foil. A practical method was designed and implemented in the SFP to obtain the desired pieces of both materials by mechanical cutting, without affecting the integrity of the CC needed for its handling during storage maneuvers.

The device for the extraction of samples consists of a grey H-column supported by underwater shelves, where the CC is positioned horizontally (see Fig. 3.8). A pneumatic low speed motor driven by a trolley and sliding over the grey performs the cutting and extraction of the sample of CT and insulation foil at any desired axial position (see Fig. 3.9). The cutting tool is a diamond disk which performs a clean cut leaving a “window” of approx. 10 × 30 cm on the CT wall and insulation foil.

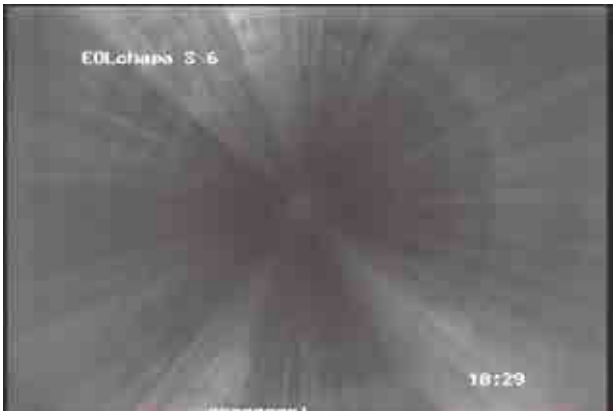

FIG. 3.1. CC internal visual inspection. Contact marks left by interaction of the FE shoes.

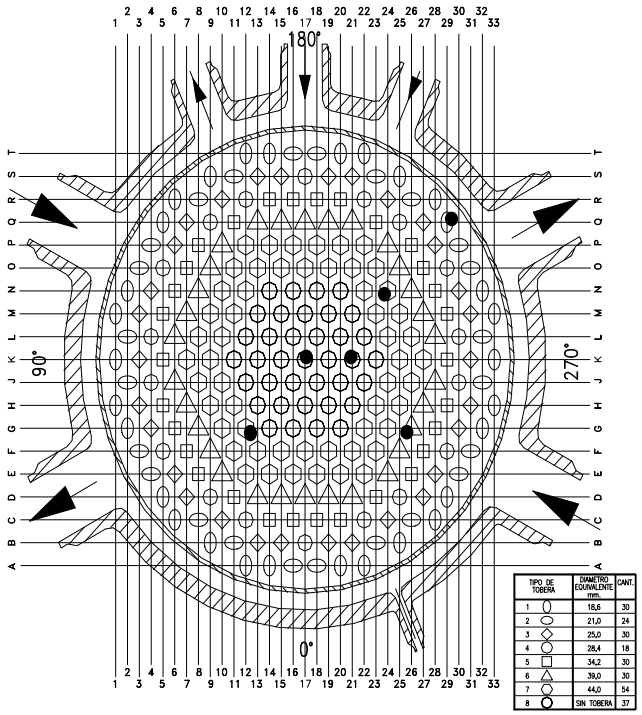

FIG. 3.2. Plan view of reactor lattice, the position pointed in black are the CC under follow-up.

FIG. 3.3. Shows the inspection bay for the CC in the SFP.

FIG. 3.4. Shows the ruler during the introduction in the CC for the length measurement.

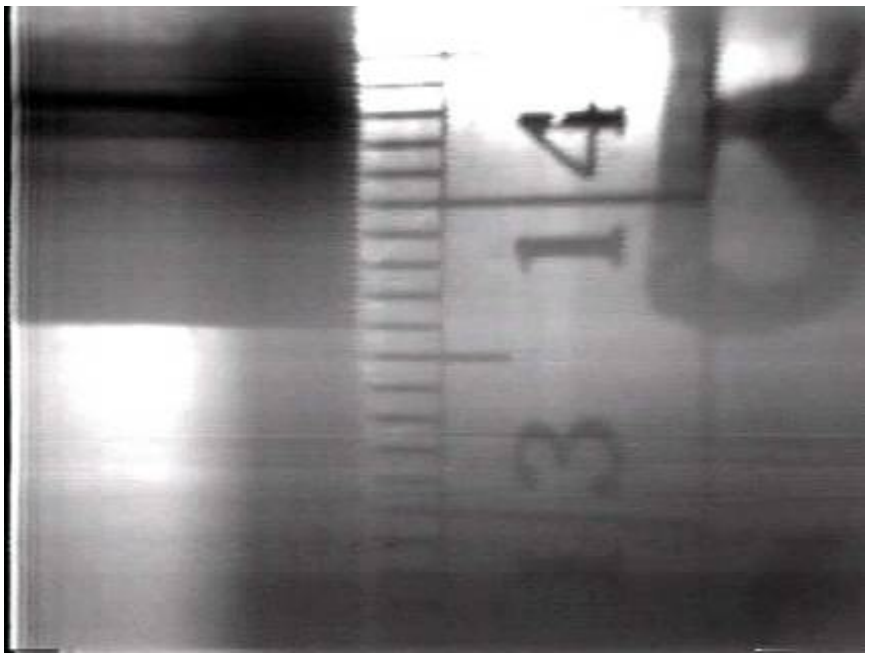

FIG. 3.5. Image captured from the TV screen showing upper end position of the CT respect to the ruler (resolution 0.5 mm).

FIG. 3.6. Self centered ID gauging head, during calibration.

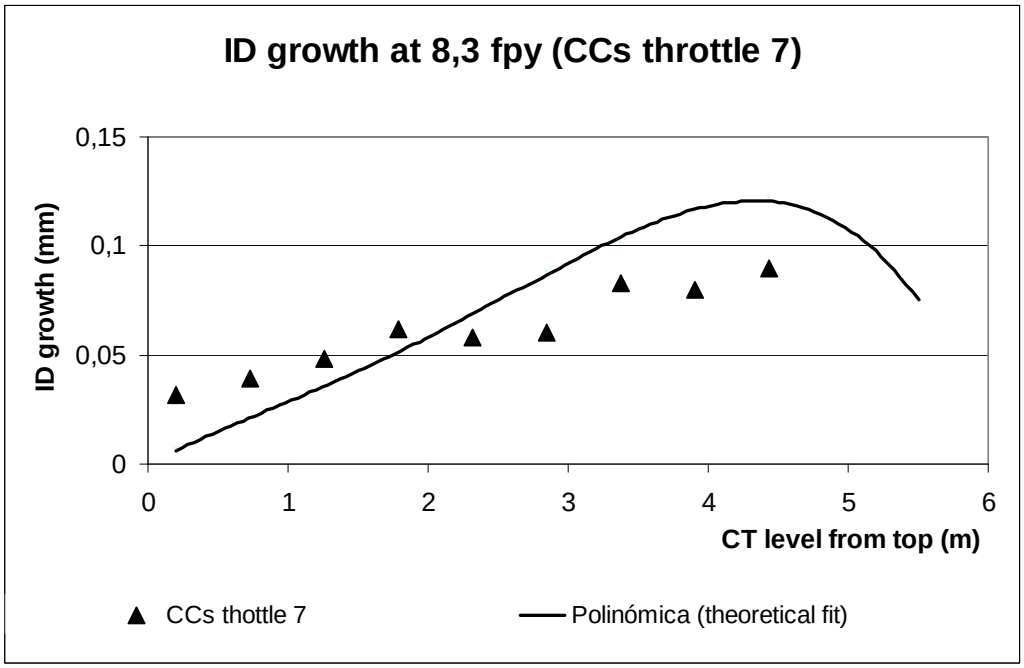

FIG. 3.7. Comparison of measured ID growth with the theoretical profile predicted by code calculation. (Values are the average of two CCs with throttle 7, maximum dose).

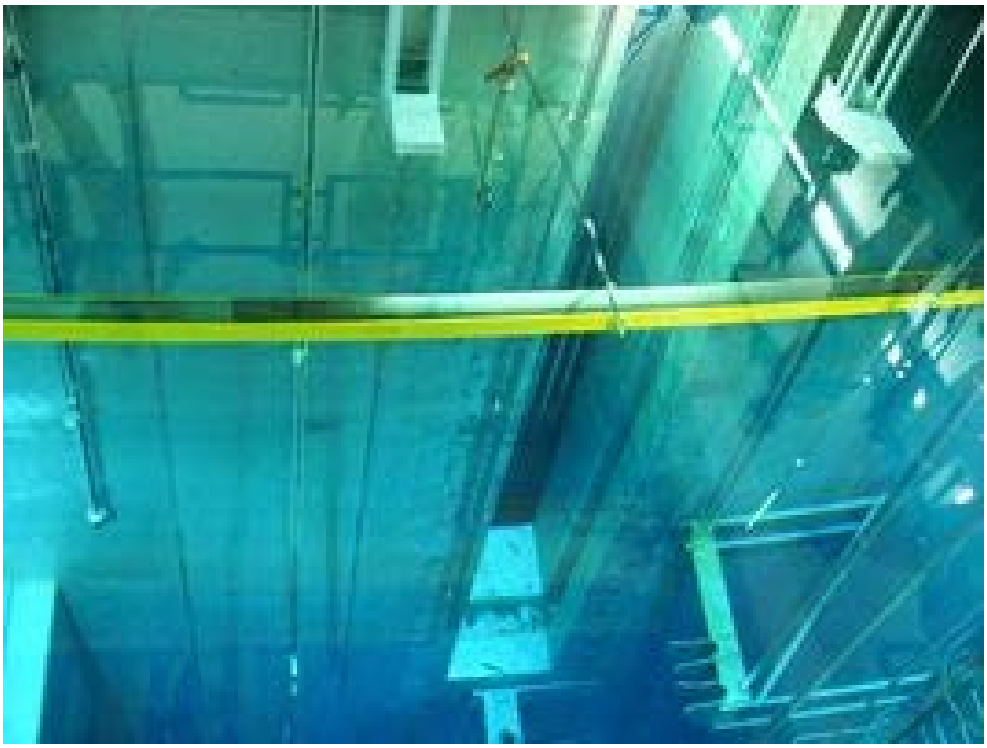

FIG. 3.8. Allocation of the CC in the grey H beam supported on underwater shelves.

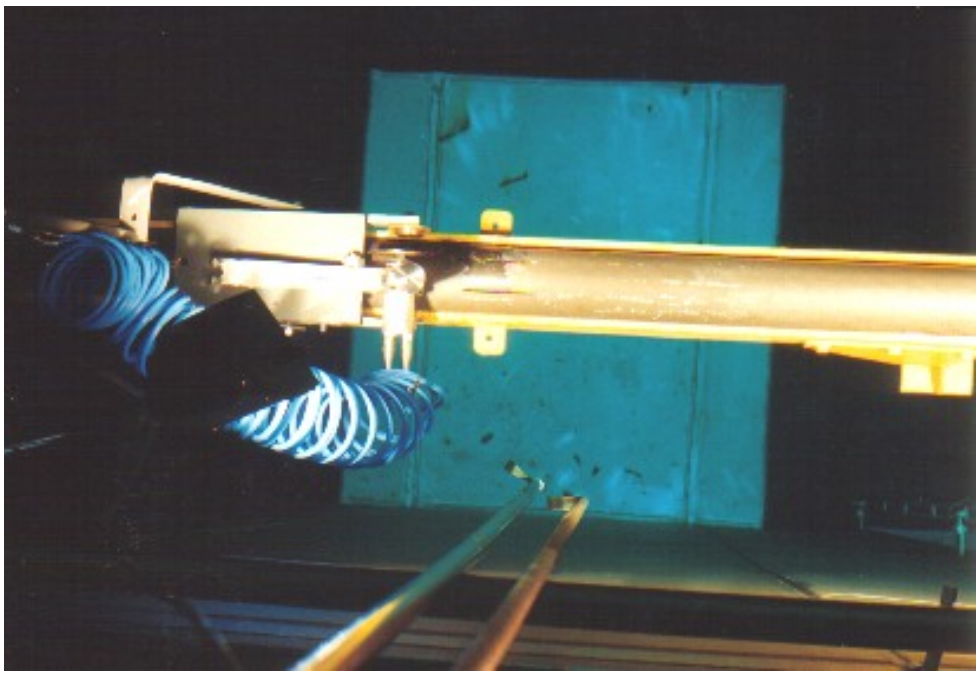

FIG. 3.9. A pneumatic motor driven by a trolley and sliding over the grey is cutting and extracting the sample of CT and insulation foil.

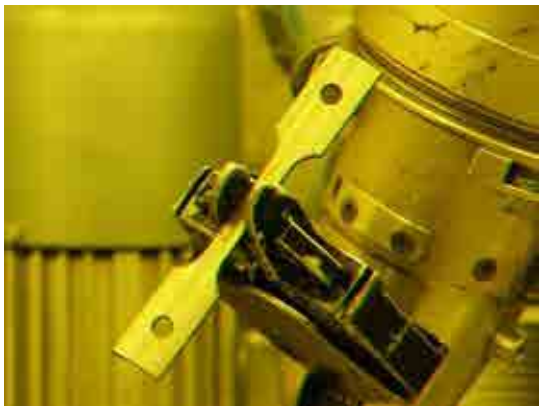

FIG. 3.10. Tensile specimen is obtained by machining in CAD-CNC mill.

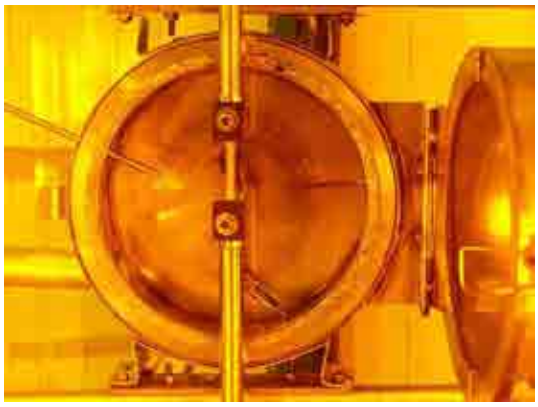

FIG. 3.11. Tensile testing in an environmental furnace at room temperature and 250°C.

The samples are sent to the hot cells facility at Ezeiza Atomic Center (CELCA) [2]. The following tests are performed sequentially:

– Visual inspection, characterization and measurement of oxide layer by an eddy current technique on both inner and outer sides;
– Machining of the normalized tensile specimen with a numeric control mill assisted by computer (CAD-CNC) (see Fig. 3.10);
– Tensile testing is performed with a universal testing machine (see Fig. 3.11);
– The remaining parts of the sample are cut in an appropriate size to perform destructive analysis, metallographic studies (by optical microscope and SEM) and the measurement of hydrogen and deuterium content by hot vacuum extraction (LECO equipment).

TABLE 3.1. CHANGES INTRODUCED IN FUEL ELEMENTS

	Changes introduced in fuel elements	
	Original design	New design
Assembly geometry	Circular array	
Fuel rods	36	37
Structural rod	1	none
Enrichment	natural	0.85% (SEU)
Uranium mass [kg·FE^{-1}]	152.5	160.5
Tie plate	1	
Rigid spacer grids	15	
Active length [mm]	5300	
Cladding material	Zircaloy-4	
Outside diameter [mm]	10.90 mm	
Cladding wall thickness [mm]	0.55 mm	
UO_2 pellet density [g·cm^{-3}]	10.60	
Elastic pad for adjusting to the CC	In structural rod	In spacer
Discharge burnup [MW·d·kg^{-1} U]	5.8	11.1
Refuelling frequency [FE·fpd^{-1}]	1.4	0.7

4. INSPECTION AND METROLOGY OF THE FUEL ELEMENT

Atucha-1, initially designed for natural uranium fuel, has gradually performed improvements in fuel discharge BU and consequently in the fuel economy. The first action taken was to increase the enrichment to 0.85 wt% U235, this programme began during 1993 and concluded when the core was fully converted to SEU in 2000 [3]. At the same time, a second programme to increase U mass was implemented through a modification in the design of pellet geometry and a reduction in the inner free volume of the rod. The result of this programme was an increase of 2.5 wt% in U mass.

The last action in the U mass increase programme is the replacement of the structural rod by an active one which adds up to 5.3 wt% of U mass to the original design. This modification involved the redesign of the elastic pad which adjusts the FE to the CC; this pad was originally fixed to the structural tube and now it is fixed to the spacer grid. Then, this new FE design consists of a circumferential array of 37 rods with an active length of 530 cm, assembled by fifteen rigid spacers. The rod adjusts to each spacer through three rigid pads welded to the rod at specific axial positions. Figure 4.1 shows the main features and obtained Bu of the new design FE in comparison with the original one.

For the follow-up of the behaviour of this modification, visual inspection and metrology control of the rods was implemented at the SFP. Visual inspection is done by viewing directly through a diagonal mirror inverted periscope installed at a bay of the reception pool [4]. This equipment has been working since the beginning of the operation of the plant and its upgraded version now gives an excellent image quality. A digital camera can be attached to the telescope for displaying images on the TV screen and taking pictures. Visual inspection is normally used to check the surface condition of the rod (oxide layer appearance and crud deposits), and to identify defects or secondary degradation signs.

Regarding the new 37 active rod FE design the main interest is to evaluate the wear condition of the structural part, the interaction of the elastic pad and rigid pad that are fixed in each spacer with the CC and any fretting mark induced by vibration. The evaluation of the loosening or relaxation of the elastic pad fixed to the spacer is done by comparison of its curvature with a reference image taken during pre-irradiation inspection. Figure 4.2 shows a side view of the elastic pad fixed in the spacer.

The measurement of total and partial elongation along the rod is of interest to assess the possible effects of U mass increase. Elongation data give information about differential growth caused by any

hard pellet—cladding interaction at sections of the rod with different linear power. Partial elongation is obtained measuring the change in length (pre- and post-irradiation) in four sections of one outer rod. Each section is defined between the sharp edges of the rigid pads of the rod corresponding to spacers 1–4, 4–7, 7–10 and 10–15. Total length is considered between the rigid pads of the rod corresponding to the spacers 1–15. Length measurements are performed observing the displacement of the mast of the crane bridge, when the FE is lifted in front of the periscope. A laser distance meter (precision 0.1 mm) attached to the mast measures the displacement while the pad edge level is observed on the TV screen from the periscope view. Figure 4.3 shows edge levels corresponding to spacers 1 and 15, between which Δ length is measured.

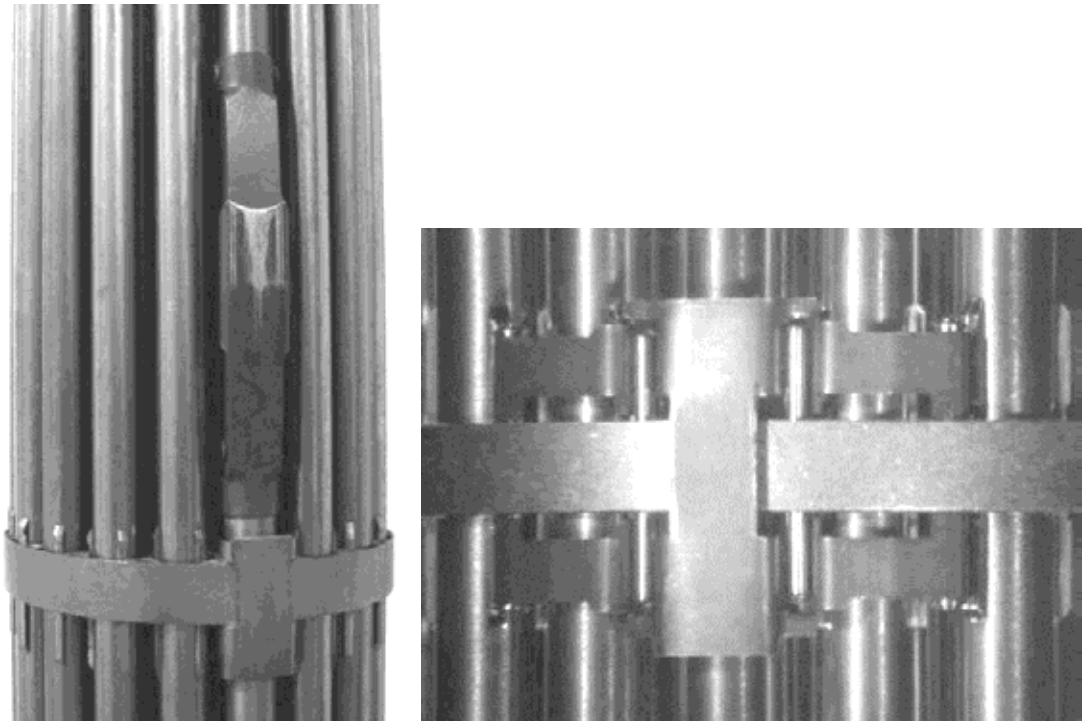

FIG. 4.1. Main characteristic of the Atucha 1 FE.

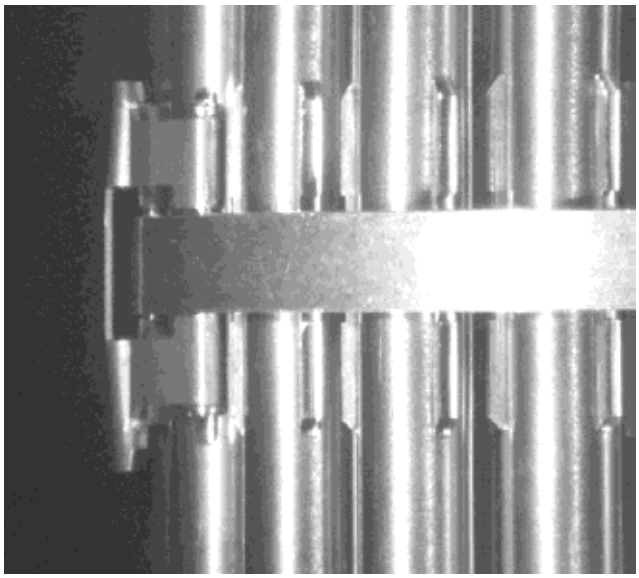

FIG. 4.2. Evaluation of relaxation and wearing from the visual inspection of the side view of elastic shoes.

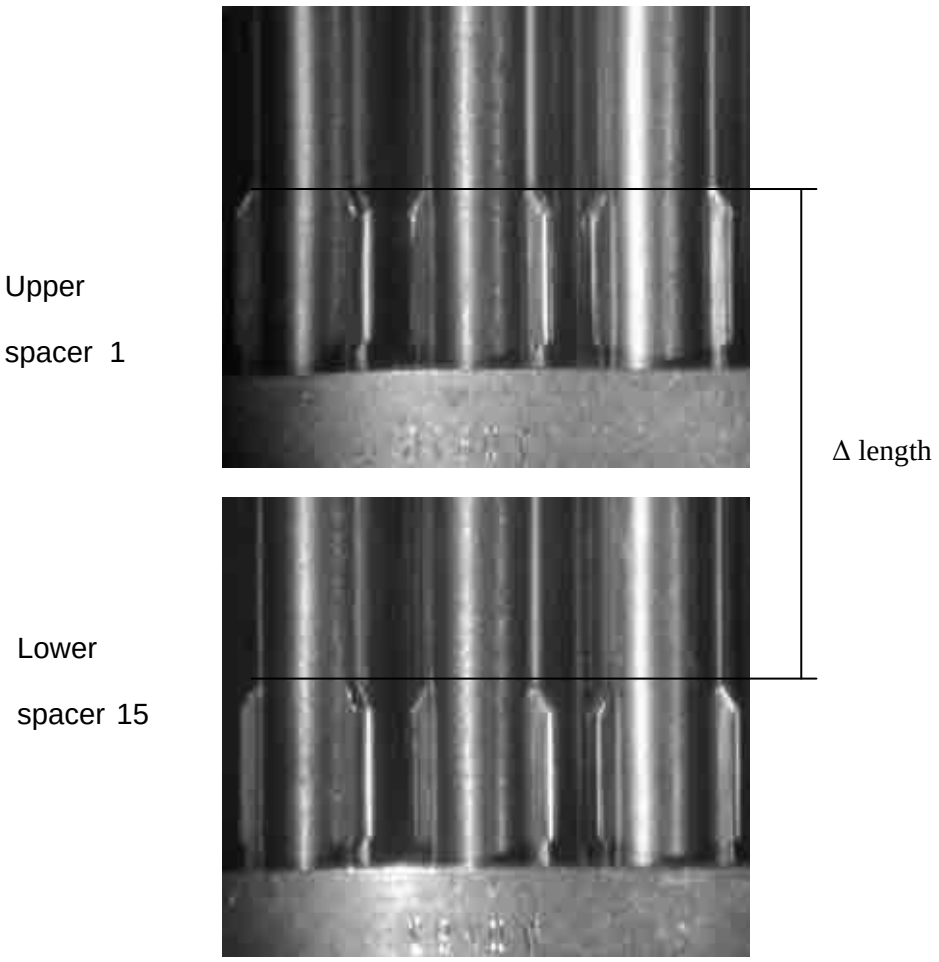

FIG. 4.3. Reference level taken at the rigid pads (central rod) from an image of the periscope to measure the rod length. Resolution 0.5 mm.

5. FINAL REMARKS

Underwater inspection and metrology techniques are being applied for the monitoring of cooling channels and fuel elements behaviour, as useful tools to assure the safety in operation of Atucha-1 NPP.

Regarding cooling channels, the inspection methodology provides enough data about the state of irradiation-induced degradation and consequently preventive actions can be taken in advance of any incident. The length and internal diameter measurements on the central tube allow the assessment of the dimensional stability of the CC of new design. The tools and instruments used in the measurements show a good precision and are easy to operate. Also a novel underwater technique was developed for the extraction of samples of the central tube, minimizing the costs and risks of material handling. The samples were then sent to the hot cells for metallurgical analysis.

Concerning fuel element, visual inspection and metrology controls assured the progressive implementation of the U mass increase program. As a result of this, nowadays a fuel discharge burnup of about twice the original value has been achieved and the refueling frequency has been reduced to one half of the previous one, which means a huge improvement in fuel economy.

REFERENCES

[1] MOLITERNO, G., RUGGIRELLO, G., MIZRAHI, R., et al., Methods for detection and monitoring of age-related degradation of reactor internal in Atucha-1 NPP, IAEA Specialists Meeting on Age Degradation in NPP, Bariloche (1995).

[2] RUGGIRELLO, G., et al., Status of the activities of examination water cooled reactor fuel in Argentina, Co-ordinated research project on examination and documentation methodology for water reactor fuel (ED-WARF-II), Dimitrovgrad (1995).

[3] RUGGIRELLO, G., "PIE in hot cells and poolside: Facilities and techniques applied in Argentina — A brief overview", Post-Irradiation Examination and In-Pile Measurement Techniques for Water Reactor Fuels, IAEA-TECDOC-1635, IAEA, Vienna (2009).

[4] FINK, J.M., et al., "Overview of the SEU project for extended burnup at the Atucha-1 NPP: Four years of operating experience", Technical and Economic Limits to Fuel Burnup Extension, IAEA-TECDOC-1299, IAEA, Vienna (2002).

GAMMA SPECTROMETRY FOR BURNUP DETERMINATION OF SPENT FUEL ASSEMBLIES AT THE PAKS NPP

I. ALMÁSI, Z. HLAVATHY, C.T. NGUYEN, P. NAGY, L. LAKOSI, T. PARKO, I. POS
Institute of Isotopes,
Hungarian Academy of Sciences
Budapest, Hungary
Email: hlavathy@iki.kfki.hu

Abstract

VVER-440 fuel assemblies sunk in the loading pit were measured by gamma spectrometry. The assemblies were moved to the front of a 1.6 m long collimator built in the concrete wall of the pit in the reactor block and lifted down and up under water for scanning by the refuelling machine. The HPGe detector was placed behind the collimator in an outside staircase. The measurements involved scanning of the assemblies along their length of all the 6 sides, at 5–12 measurement positions side by side. Axial an azimuthal burnup profiles were taken up in this way. Assembly groups for measurements were selected according to their burnup (10–45 GW·d·t^{-1}U) and special positions (e. g. control assembly, neighbor of control assembly). The ratio of the activities of Cs-134 to Cs-137 was found to be proportional to the burnup. Activity ratios were evaluated by intrinsic efficiency calibration. Burnup differences were well observable between assembly sides looking at center and opposite directions. Also, burnup profiles are different for control assemblies and normal fuel assemblies. Uncertainty is around 3%. Taking into account irradiation history and cooling time, the ratio Cs-134/Cs-137 shows good correlation with declared burnup.

1. INTRODUCTION

To validate the calculation of burnup from the reactor parameters an independent measurement method would be useful. If the results of the measurement correspond with calculated values, the safety margin could be decreased in the calculation, thus the assemblies could be used for higher power output. In Paks NPP, each reactor block has a collimator built in the wall of the loading pit. So a high resolution detector placed behind the collimator and by hanging up a spent fuel assembly in front of the collimator, gamma spectra can be taken.

2. THEORETICAL BASIS

Production of Cs-137 is linearly proportional to the neutron fluence, i.e. the number of U-235 nuclides undergoing fission. Cs-134 is produced in two steps: first the fission product Cs-133 is produced, then Cs-134, by neutron capture. The alternative way (direct Cs-134 production from fission of U-235) is of lower probability by orders of magnitude. The production of Cs-134 is almost proportional to the square of neutron flux. If the activity of Cs-134 and Cs-137 is known, the burnup can be calculated as:

$$BU = k(A_{\text{Cs-134}}/A_{\text{Cs-137}})$$

Why is it useful to follow this complicated way of determining burnup instead of the simpler way of determining the activity of Cs-137?

Count rate measured by the detector coming from Cs-137 content in the assembly depends on many coefficients. These are as follows: the gamma yield (I_g factor), self absorption in the loading material (enriched uranium), absorption of construction materials (zircon tubes, assembly wall), gamma absorption by the water from the assembly to the wall of the loading pit and by the collimator, distance coefficient, efficiency of the detector. Some of them are well known or measurable (I_g factor, distance coefficient, efficiency of detector), others can be calculated with acceptable precision and some of them can be only estimated.

Cs-134 has two strong peaks at 605 keV, I_g=97.6%, and at 796 keV, I_g=85.5%. Cs-137 has one peak at 662 keV, I_g=85.1%. From the two peeks of Cs-134 one can determine the relative efficiency of detection of the of 662 keV line gamma line by intrinsic calibration. In this way the geometry dependent parameters will be eliminated. For dependence of the activity ratio on the distance see Fig. 2.1.

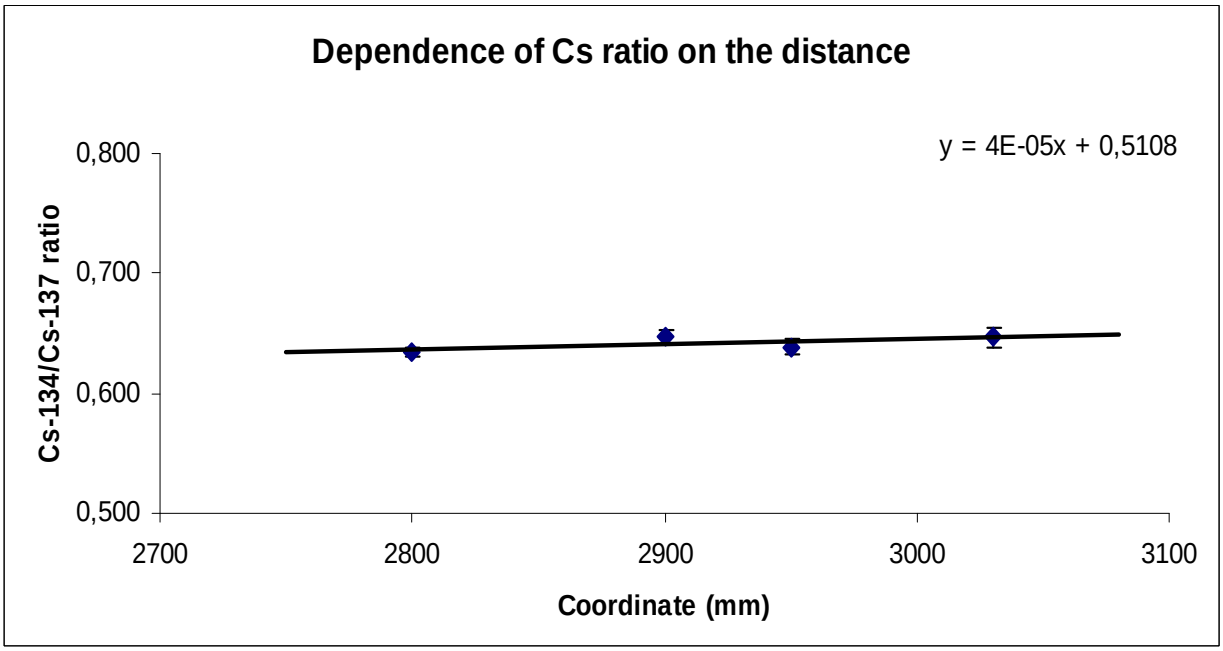

FIG. 2.1. Cs-134/Cs-137 activity ratio vs. distance.

This method can be used with linear, logarithmic, or polynomial fitting. The polynomial fitting would be the best, but more peaks of the same isotope would be needed. Unfortunately, other peaks of Cs-134 come with much lower yields, so their uncertainties are higher. Thus they do not improve but reduce the trustiness of the fitting. The remained two methods differ from each other by 3% in calculating the activity ratio Cs-134/Cs-137. Considering the uncertainty around 1% of the peak areas, this uncertainty is acceptable now.

3. MEASUREMENTS

The collimator built into the south wall of the loading pit is looking to the centre, its axis is almost parallel with the axis of the “carriage” of the refuelling machine The field of vision of the collimator at the measuring distance is about 200 mm horizontal and 15–20 mm vertical. The distance coordinate does not represent the real distance of the assembly to the detector, but the “carriage” coordinate of the refuelling machine does it. The real distance was 1800–2000 mm, depending on the gamma activity of the assembly. “Bridge” and “carriage” coordinates of the refuelling machine were measured from a base point (south-west corner of the podium). The vertical coordinate was given by the length of the refuelling machine’s “rope”, which lowers the assembly down. To match this coordinate to the assembly, the endpoints of uranium loaded into the pin was determined first, by measuring the peak of Cs-137. The ends of the loading were where it decreased hardly. The average value of the two endpoints was the vertical coordinate of the pin’s centre. The code, (C-porka developed by the Reactor Physics Departement of Paks NPP) which calculates the burnup and production of isotopes for pins, divides each pin in 48 nodes by assembly length, 41 among them contain fuel. If there had been enough time, each node would be measured. Mainly 9 nodes (5–12) measurement were used to characterize the typical burnup profile. Two from the bottom end of the pin to the plateau, 5 from the

plateau and 2 from the plateau to the top end of the pin. A typical burnup profile with measured values is shown in Fig. 3.1.

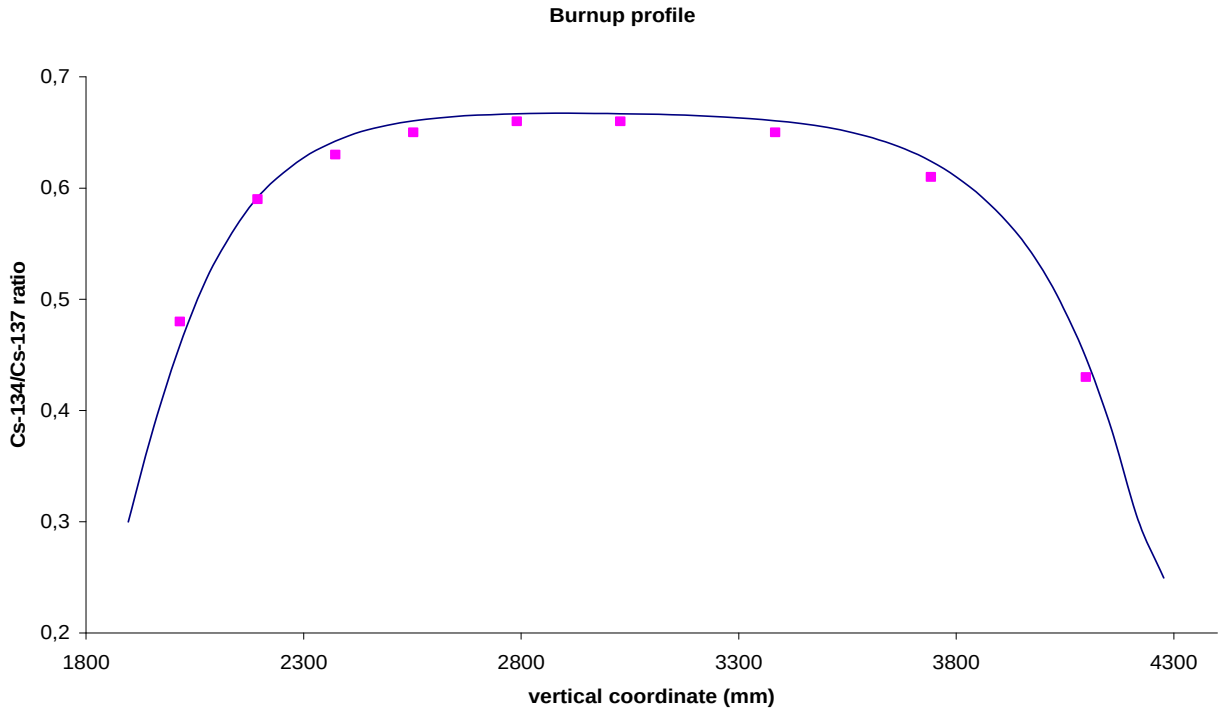

FIG. 3.1. A typical burnup profile with measured values.

Six assembly groups were selected for the measurements, one of high burnup (44 GW·d·t^{-1}U) and the second of low burnup (10 GW·d·t^{-1}U). The third one was of normal burnup (39 GW·d·t^{-1}U) and 3.8% initial enrichment, the fourth one was of 26 GW·d·t^{-1}U burnup and 2.4% initial enrichment. The above groups consist of 6 assemblies, as the core is divided into 6 sectors. Their positions in each sector were the same. Two control assemblies and two of the neighbor of control assemblies were taken. Altogether 28 assemblies were measured. The measurements involved scanning of the assemblies along their length of all the 6 sides. To collect spectra, there are two methods: one is continuously moves the assembly and periodically save the data, and the other one measures determined positions, and fits a curve to the measured values. The first method is better for the unknown distribution of the material in the measured region. The precision of this method in each region is less, but the sum of the regions determines a not continuous distribution well. The second method gives more precise values for each measured position, but gives no information on between the positions. This method is better to measure the continuous distribution of material. In this case the second method was chosen with 5–12 measurement positions side by side. Around 1200 spectra were collected. Axial and azimuthal burnup profiles were taken in this way. Measuring time was 300 or 600 s by position. Spectra were evaluated automatically by a computer code including the intrinsic calibration method. Considering the short half-life of Cs-134 (2.06 years), all the calculated values from the measurements were corrected for the first day of the measurements. Measurements took five weeks.

The different cooling time and burnup of assembly groups give different measurement distance and time. The evaluation spectra of low cooling time assemblies are complicated because of the short half-life isotopes, mainly Zr-95 (724.2 keV and 756.7 keV $T_{1/2}$=64.02d). After 1.5 year it is decayed. Long cooling time (six years or more) decreases the amount of Cs-134, increasing the uncertainty.

The isotope activity ratio values, calculated for the pins from the burnup, needs to be averaged for the whole assembly. It is not a simple average of course, because of the distance correction (smaller part) and self-absorption correction of the other pins (main part). This calculation was performed by the

code MCNP at Paks NPP. The calculation gives different values side by side, depending on the surroundings of the assembly (i.e. working/control assembly and its situation to the centre of the core). In the calculation of the decay of isotopes was corrected to the first day's measurement.

4. RESULTS

Upon representing the ratios by sides and matching the core sector and turning degrees, burnup differences were well observable between assembly sides looking at the centre of core and opposite to it. Azimuthal profiles of the 39 GW·d·t^{-1}U burnup group at the centre of pins are seen in Fig. 4.1.

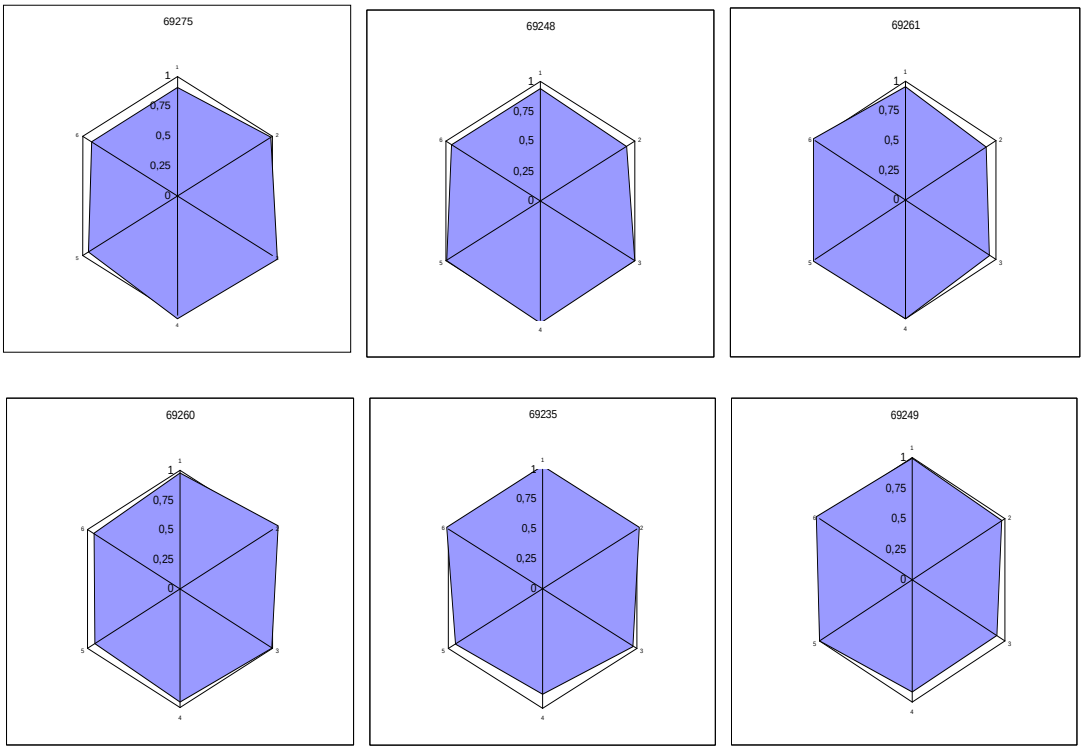

FIG. 4.1. Azimuthal profiles of the 39 GW·d·t^{-1}U burnup group at the centre of pins.

Also, burnup profiles are different for control and normal “working” fuel assemblies, see Figs 4.2–4.3.

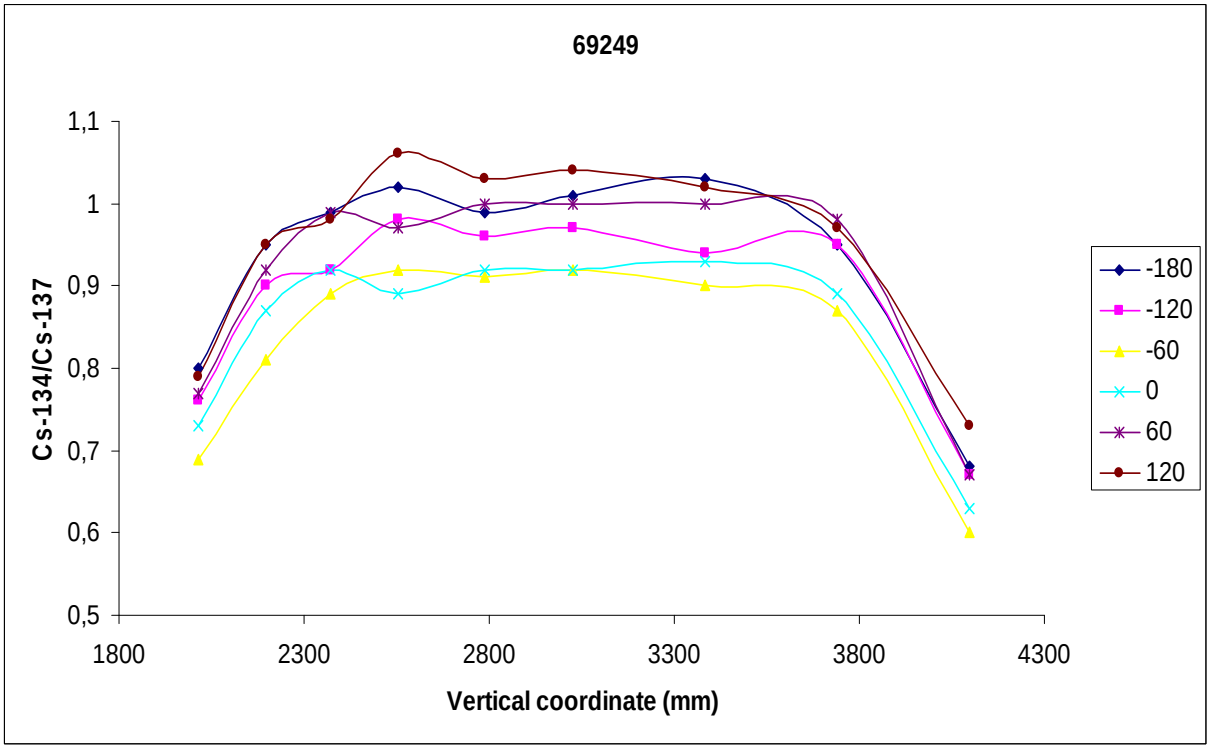

FIG. 4.2. Burnup profile of a working fuel assembly.

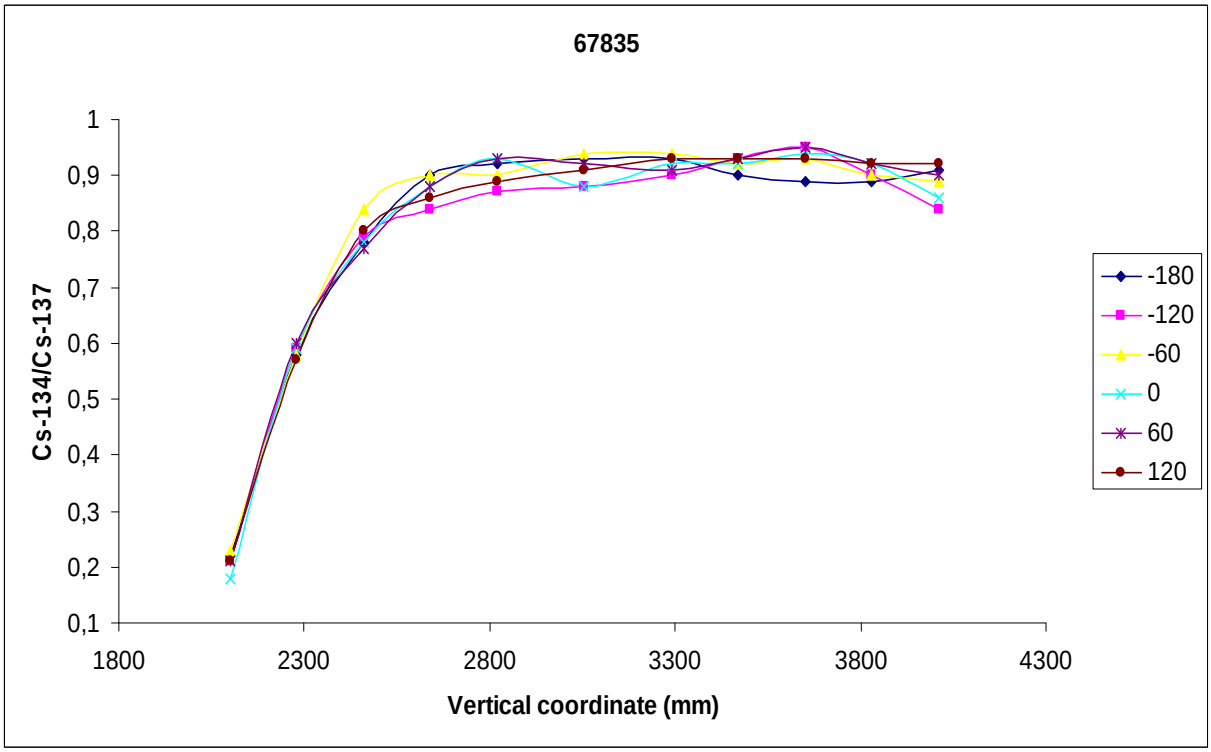

FIG. 4.3. Burnup profile of a control fuel assembly.

To compare calculated results based on the measurements and the burnup, the ratio Cs-134/Cs-137 shows good correlation see Fig. 4.4.

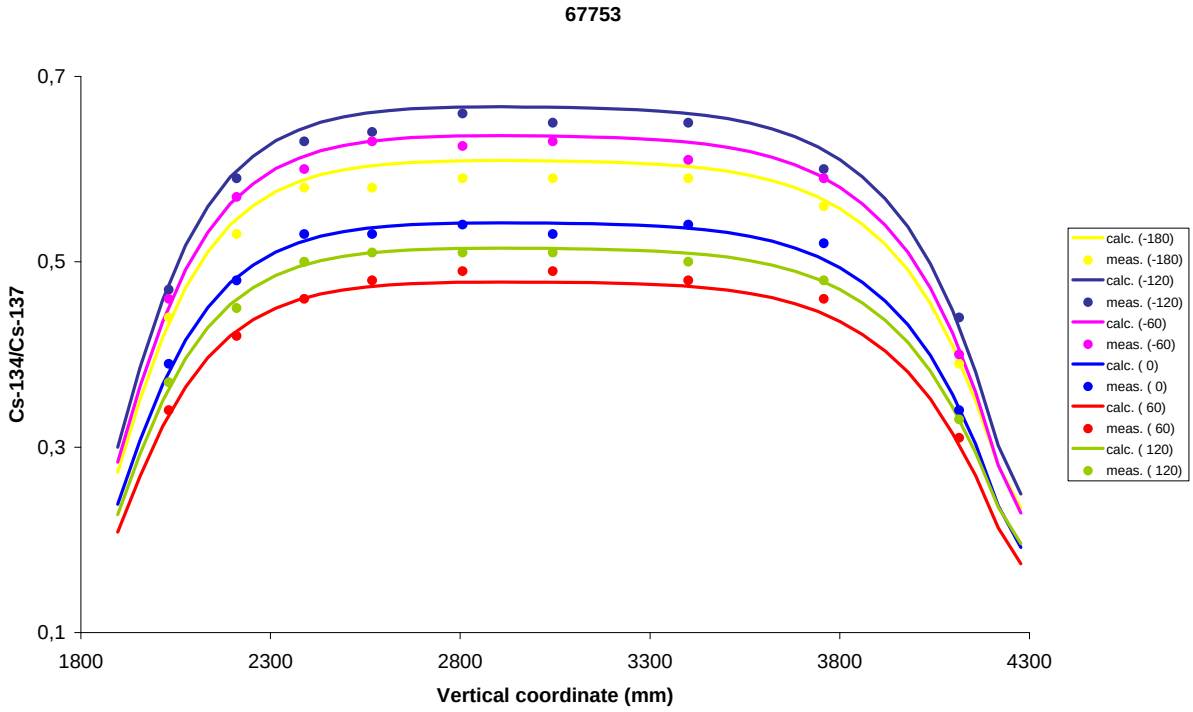

FIG. 4.4. The Cs-134/Cs-137 ratio from measurements and calculation.

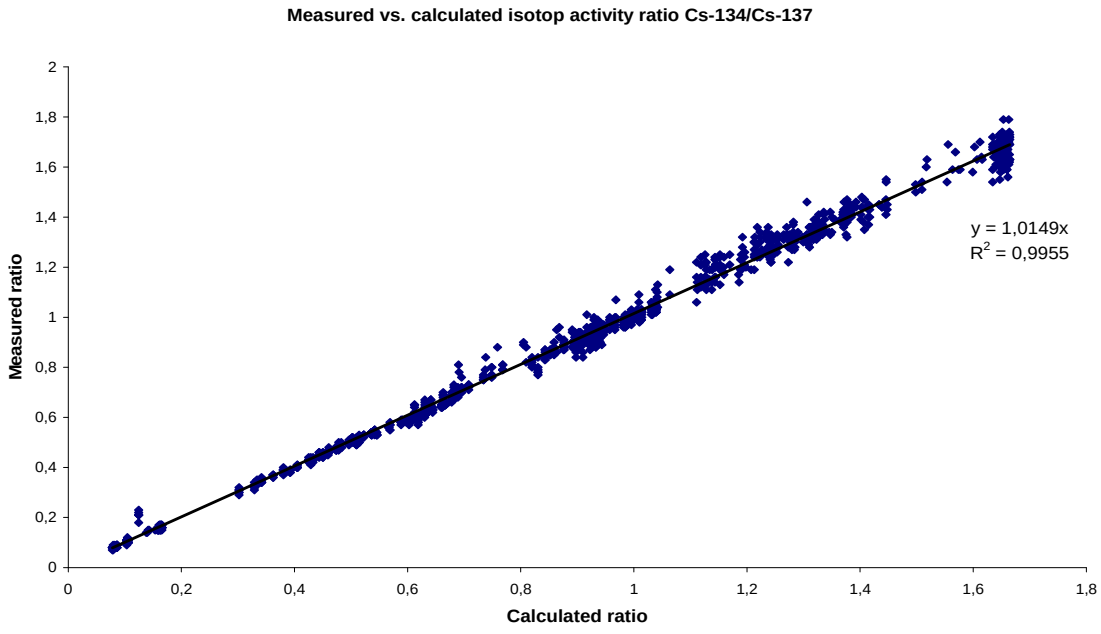

FIG. 4.5. Measured vs. calculated activity ratio Cs-134/Cs-137.

When representing the measured Cs-134/Cs-137 ratio as a function of the ratio calculated from the reactor parameters for the whole data sets, the correlation is significant, see Fig. 4.5.

5. SUMMARY

By this method the burnup of assemblies can be determined. Uncertainty of the method is around 4%. To decrease the uncertainty the measurement time should be increased by decreasing the number of measured positions and/or assemblies. For the best results 2–4 years old assemblies are to be measured.

The method should be checked at other ponds in Paks NPP first. It is also planned to modify the detector system to measure ponds without built-in collimator, to be able to use the method for other reactors too.

BIBLIOGRAPHY

[1] NUCLEOELECTRICA ARGENTINA, S.A, CNA–2 Historias de irradiación de las barras combustible en las condiciones más desfavorables esperables durante la operación normal (2009).

[2] U.S. NATIONAL REGULATION COMMISSION, “Chapter 4.2: Fuel system design”, Standard Review Plan, NUREG–0800 (2007).

[3] CNEA, Análisis del diseño de la barra combustibles para incremento de la masa de uranio de la BC CNAl, Internal Report (1999).

[4] NOTARI, C., A PHWR with slightly enriched uranium, Annals of Nuclear Energy 31, Issue 3 (2003) 303–309.

THE ROLE OF CVR IN THE FUEL INSPECTION AT TEMELÍN NPP

M. MIKLOŠA, M. MALÁ,
Research Centre Řež Ltd.,
Řež
Email: mkl@cvrez.cz

D. ERNST
NPP Temelín,
Temelín

Czech Republic

Abstract

Since first reload, NPP Temelín together with the fuel vendor (Westinghouse Electric Company LLC) is performing post-irradiation inspection on the fuel assemblies as additional proof of PWR material compatibility in VVER water chemistry. However, after ten years of successful operation the fuel vendor is changing and new plans for the fuel inspection are ready. Paper describes the past experiences with the fuel inspections and repairs at the NPP Temelín and the role of Research Centre Řež, Ltd. (CVR) in the cooperation with the new fuel vendor.In addition, Research Centre Řež Ltd. is a non-profit organization devoted to activities that require research reactors LR-0, LVR-15 and several experimental loops and devices. The Centre was founded in 2003 by the Czech Ministry of Education that fully endorsed a research proposal for all scientific and R&D activities. It is a unique institution providing a sophisticated infrastructure for research and development focused on advancement of analytical methods. The main purpose of the Research Reactors Division in CVR with aim of the fuel on-site post-irradiation inspection and water chemistry research are also presented in paper.

1. INTRODUCTION

Reliability of nuclear fuel and radiation fields surrounding primary systems are important aspects of overall nuclear reactor safety. In recent years, the management of nuclear fuel operation has been faced with new challenges. The extension of nuclear reactor lifetimes beyond their initial design values, a higher level of fuel utilization (higher fuel burnup, extension of fuel cycles, higher power), shortening of outages, etc., are present requirements in evolution of nuclear energy. Along with these requirements, other circumstances that impose increased demands on chemistry management are also taken into account. However, new changes and design modifications of fuel assemblies are still needed.

Nuclear fuel failures in PWR/VVER reactors caused by mechanical and physical–chemical aspects are quite often and were studied and described in late 70s. Although the zirconium cladding alloys are showing high reliability and operational stability, the probability of their failure is not so low (Fig. 1.1, [1]). According to the IAEA studies, the fuel failure rate in the world is around 10^{-5}, which means 1–3 failed fuel rods from 100 000 fuel rods in operation (in average for VVER-440 1–2 failed fuel rod, for VVER-1000 2–4 failed fuel rods). However, with use of better alloys, different fuel design, advanced water chemistry, etc., the fuel failure rate is decreasing.

There are different types of fuel failures which are characteristic for all type of reactors like fretting (debris, grid-to-rod), pellet cladding interaction, hydration of fuel rod cladding, corrosion and CRUD at the fuel rod cladding, which can also lead to the problem with axial offset (AOA), failures during fuel handling, manufacturing defects (weld contamination), cross-flow/baffle jetting; as well as anomalies leading to deterioration in fuel operation like fuel assembly/rod bow, leading to the problems with incomplete rod insertion (IRI), fuel assembly twist, unexpected fuel assembly/rod elongation; and the combinations of all these fuel problems. However, only few of these problems are still occurred and these are the most dominant for:

– PWR/VVER: grid-to-rod/debris fretting;

– BWR: crud and corrosion.

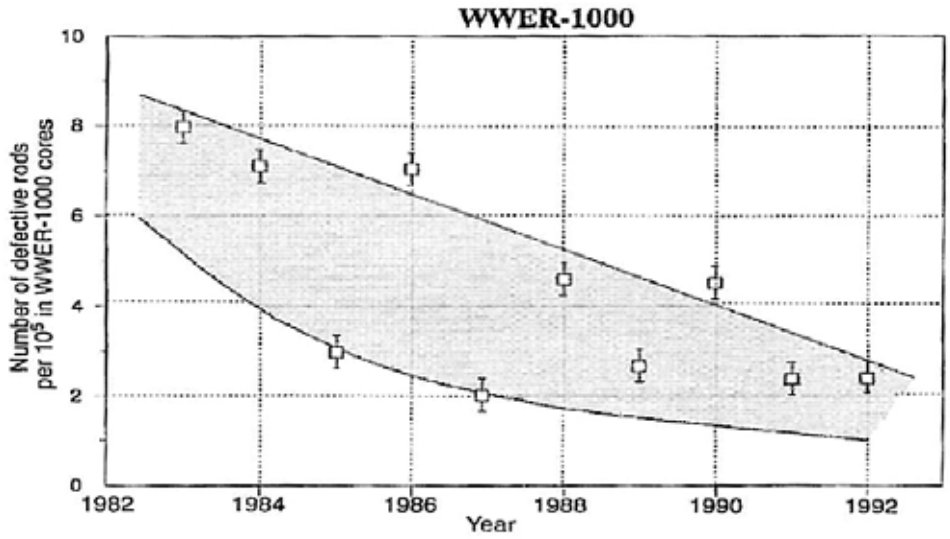

FIG. 1.1. The number of defective rods in WWER-1000 reactors in 1983–1992.

2. TEN YEARS OF TEMELÍN NPP

In December 2010 ten years have passed since the first unit of the Temelín NPP has been build. Test operation of the first unit started 10 June 2002, and the second unit started 18 April 2003. The operation on 100% power started in the years 2002–2003. Temelín NPP finally allowed replacing obsolete and gradually shut units at the North Bohemian coal power plants. The total quantity of electric production made in the Temelín NPP since its start is 100 billion kW·h. This would cover nearly seven years in consumption of all Czech households.

The Temelín nuclear power plant is situated about 24 km away from České Budějovice. Electricity is generated in two production units with VVER-1000 type V-320 pressurized water reactors. Technological scheme of the power plant corresponds to the latest world parameters. The reactor core contains 163 fuel assemblies, each with 312 fuel rods, and 61 regulating rods. Fuel rods are fuelled by UO_2, uranium dioxide enriched by an average of 3.5% of the fission isotope ^{235}U (maximum allowed enrichment is (4.95±0.05)%). Since the beginning, the fuel for the Temelín NPP is supplied by the Westinghouse Electric Company LLC, which also supplied the new instrumentation and control system.

NPP Temelín is operated on a modified water chemistry optimized for minimization of the level of transport activities and the reduction of radiation field creation via the creation and maintenance of constant chemical conditions in primary coolant. Optimal pH at 300°C is set at 7.1±0.1, initial concentration of alkali about 20 $mg \cdot kg^{-1}$. Dosing of ammonia is used for hydrogen generation.

2.1. Fuel description

Since first reload in 2002 at unit 1 and 2003 at unit 2, fuel assemblies from US fuel vendor Westinghouse VVantage-6 are used (at unit 1 until August 2010, at unit 2 until May 2011, [2]). VVantage-6 design is Westinghouse pilot assembly with hexagonal shape, which became from the square design VVantage-5 (Fig. 2.1). Westinghouse fuel assemblies for PWR reactors have undergone significant evolutionary changes, from the early standard fuel assembly with Inconel spacer grids to

the VVantage-5. VVantage-5 PWR fuel already included state-of-the-art features such as removable top nozzle (RTN), debris filter bottom nozzles, low pressure

rop zircaloy structural grids, zircaloy intermediate flow mixing grids, optimized fuel rods, in-fuel burnable absorbers (IFBAs) and increased burnup capability to region average values of 48 000 $MW \cdot d \cdot Mt^{-1}$ U. These advanced product features have been adapted for the VVER reactors in order to update VVER fuel and provide increased fuel reliability, more efficient uranium utilization, and enhanced performance margins, and the VVANTAGE-6 fuel assembly was designed.

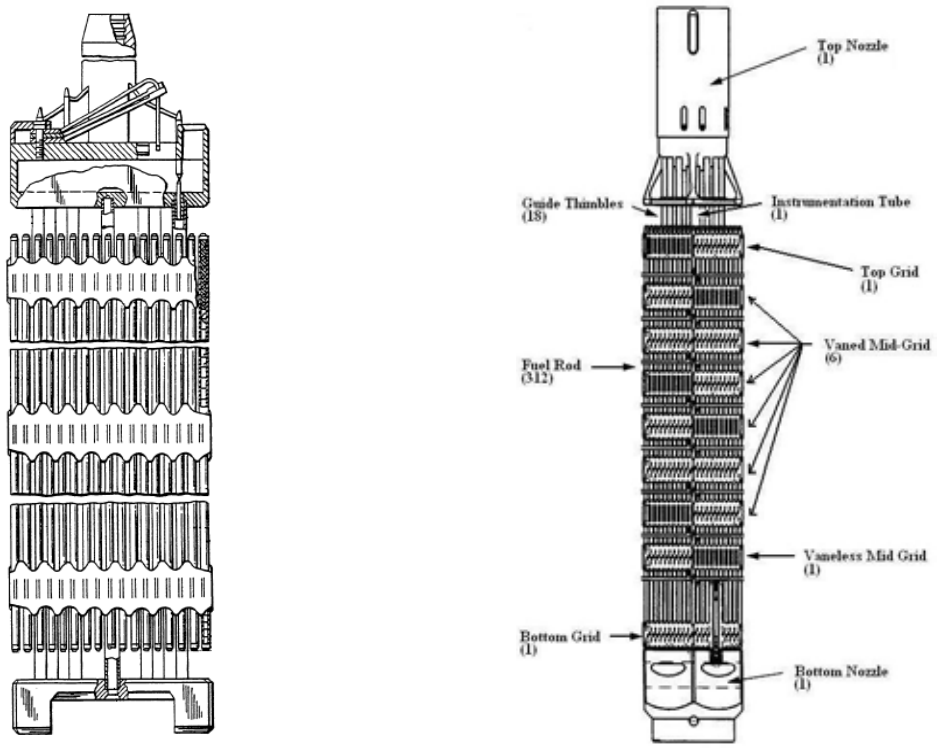

(a) (b)

FIG. 2.1. Illustration of Westinghouse fuel assemblies, (a) VVantage-5, (b) VVantage-6.

2.2. Fuel operational experiences

Although the VVantage-6 as a pilot design of the fuel assembly for VVER-1000 promised successful operation, the late experience showed several problems with this design. Flexibility in the fuel designs (different types of enrichment) and in fuel batch design allowed to absorb important and dynamic changes in the cycle length, especially cycle shortening, mostly caused by unexpected fuel failures. In several cases the fuel failures was so high, that the cycle needed to be shut down with the unburned fuel. Due to these unexpected problems, very often during fuel reloading (when the number of leakers was found) redesign of whole core was needed. Although all of these problems, the effectiveness of ^{235}U utilization in individual cycles has gradually stabilized on the very favourable values fully comparable with other VVER-1000 reactors. Average BU of spent fuel loaded out of the core was approximately 37800 $MW \cdot d \cdot t^{-1}$ U. The maximum achieved average BU of fuel assembly was then around 44500 $MW \cdot d \cdot t^{-1}$ U.

2.3. Fuel failures at Temelín NPP

Mechanical deformation of fuel assemblies and rods, as bow and twist, growth, dynamic vibrations, etc., are already under consideration during fuel designing. However, some deformations are very unpredictable, especially the progress of deformations, and fuel failures and anomalies are occurred

during unit operation. The situation at Temelín is similar, and several about mentioned fuel problems were occurred as well.

Some RCCAs (on both units) do not drop fully to the bottom position (incomplete rod insertion), which is quite large problem from the nuclear safety point of view. The worst case was at unit 1 in June 2007, where the test showed that two RCCAs stopped above the level of the hydraulic dashpot. In other words, they failed to meet the limit condition and caused unscheduled outage for refuelling. Due to large post-irradiation inspection programme (PIIP) and very precise fuel inspections, the root cause was found —— fuel assembly bow and twist [3].

Some fuel rods which were visually inspected had the *leaker in the upper weld connection* (mostly occurred at fuel assemblies, used in first several cycles). This type of defect was in that times quite common, and it was primary problem due to manufacturing of the fuel rods (incorrect weld between upper end-seal and the cladding tube). This type of fuel failure was occurred only several times at Temelín site, and was solved with manufacturing improvements.

Most common fuel failure for the Temelín unit 1 and 2 was and unfortunately still is, grid-to-rod fretting (Fig. 2.2, [3]). Grid-to-rod fretting failures are due to rod/assembly vibrations induced by turbulence and flow heterogeneities which are always present, particularly in the inlet range up through the bottom grid. Failure occurs if either turbulence is higher than anticipated in design, or fuel rod support in the spacer grid is not sufficient. This type of fuel failure is still present on the Temelín site. However, it was minimize due to several design changes of the fuel assembly. At US PWRs, this issue was also minimized due to grid design change (grid springs in 45 degree angle were change into vertical position).

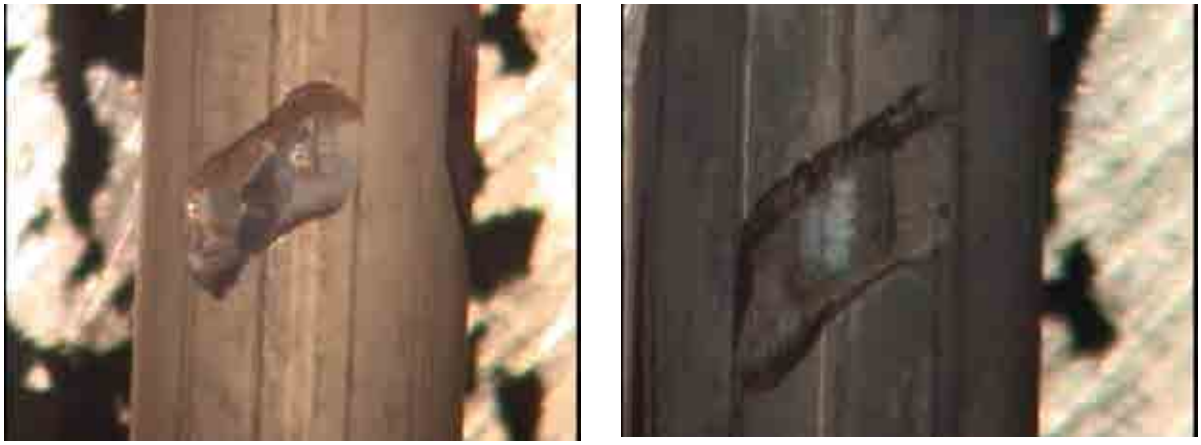

FIG. 2.2. Grid-to-rod fretting failure on several fuel rods at Temelín site.

Even due to the leakers in the core, maximal total activities in the coolant through all cycles was in the range from 2.4–8.5 $MBq \cdot l^{-1}$, which is by 3 orders less than a limiting value for the emergency conditions 3700 $MBq \cdot l^{-1}$. Therefore, this activity is negligible from the nuclear safety point of view and there was no reason of any restricts changes and remedies for fuel operation from the site of the Czech Nuclear Regulatory Body (SUJB).

2.4. Fuel inspections and repairs at Temelín NPP

Since first reload, fuel operator (CEZ) together with the fuel vendor (Westinghouse Electric Company LCC) is performing post-irradiation inspection on the fuel assemblies with the use of fuel repair inspection equipment (FRIE). There were several reasons for using this equipment like additional proof of PWR materials compatibility in VVER water chemistry, analytical method support and verification, overall thermomechanical performance demonstration, independent check of the fuel

system in-core behaviour, root causes examination of an eventual fuel rod and fuel assembly failure or unexpected deformation; and fuel assembly repair.

FRIE is mobile equipment, which means that it can be used at both units. This equipment is stored in several boxes in the fresh fuel storage during reactor operation, and during outage is transported to the reactor hall where is assembled and placed into the spent fuel pool next to the reactor. After the fuel assembly is placed into the FRIE, several procedures can be done:

– FA measurement (Visual inspection, bow and twist measurements, overall FA length measurements, peripheral FR corrosion inspection, grid cell geometry measurements);
– Single FR measurements (Visual inspection, corrosion measurements, profilometry measurements);
– RCCA inspections (The measurements of total wear of the tube cross-section, the distribution of the wear around the circumference of the rodlet).

With use of these inspections, the root causes of fuel deformation and failures were identified and minimized by the changes in fuel assembly design. Since first startup four different types of fuel assemblies were used at Temelín site. The first one called, VVantage6 T1 design, was the first prototype of VVantage6 fuel assembly for VVER-1000 reactors and was used only for the first batch at the unit 1. The second design VVantage6 T2 was used at both units till 2006 and according to T1 design only small changes in the fuel assembly design were made. The bigger changes were made in 2005–2006, where the VVantage6-Phase 0 and in 2007 VVantage-Phase 1X were designed. The main design changes were [3, 4]:

– Tube-in-tube dashpot design and top nozzle modifications (Phase 0);
– Fuel rod loading equipment alignments;
– New structural materials of FR cladding and other FA components (Phase 1X).

After these design changes the problem with Incomplete Rod Insertion was solved, as well as the fuel assembly bow and twist and the grid-to-rod fretting was minimized on the as low as achievable level. The unit 1 is a proof of these successes, where no leakers were occurred during the last cycle with Westinghouse fuel.

2.5. New fuel for Temelín NPP

Unfortunately due to large problems with fuel operation at Temelín NPP in 2003, ČEZ started a tender (bid) for new fuel supplier and two main companies were involved — US Westinghouse Electric Company LLC and Russian TVEL. After two years, the new supplier was nominated and the contract for the period 2010–2020 was signed in May 2006 with the Russian company TVEL.

According to the contract between ČEZ and TVEL, the first load of whole core was in August 2010 at unit 1, and in May 2011 at unit 2. The fuel assemblies TVSA-T was designed and assembled by MSZ Elektrostal. The main differences between VVantage6 fuel assembly and TVSA-T fuel assembly are:

– Different construction of the top nozzle (also removable, but under different processes);
– Sox corner plates (for better stiffness of whole assembly);
– Different grids design (to minimize grid-to-rod fretting,);
– Debris filter in the bottom nozzle (to avoid any debris fretting);
  Main materials of the whole fuel assembly are E110 and E635;

3. THE ROLE OF CVR

Research Centre Řež, Ltd. (CVR) is a non-profit organization and its activities are restricted only to fundamental research and development. The centre was established in 2003 for R&D in areas, where the research reactors and experimental devices can be used. The overviewed research programme was supported by the Ministry of Education of the Czech Republic. The main activities are:

– Fundamental research in natural sciences using neutrons;
– R&D in nuclear energy related fields as corrosion processes, radiation induced damages in reactor construction materials, as well as in innovative neutron sources;
– R&D of radio-pharmaceuticals prepared by using nuclear reactors, design of new treatment procedures using neutrons.

CVR plays an important role in the Czech nuclear research market. Division of research reactors besides the material irradiation and radioisotopes research is involved in the water chemistry research for PWR, BWR and VVER reactors and its impact on the crud deposition and fuel cladding reliability. For this purpose light water research reactor LVR-15 and several experimental loops are used.

The research reactor LVR-15 is a tank type and currently uses two types of fuel manufactured by the NZCHK company in Novosibirsk with 36% (IRT-2M) and <20% enrichment (IRT-4M). The reactor's systems permit an output up to 10 MW. The reactor's design and active zone permit the usage of various diameters of irradiation channels and thus flexibility from the standpoint of optimal neutron usage in the core (Fig. 3.3).

Experimental loops are used to study the effect of environment on materials in the active zone of power reactors. Phenomena under study include corrosion, the influence of physical and radiation stresses on the rate of crack propagation, the interaction of fuel and coolant coverage, including cladding corrosion and the deposition of corrosion products on the surface of the fuel elements, further for the research of water chemistry of PWR, BWR and VVER reactors, including the development and testing of special measurement technology such as, for example ECP measurement. The main goal of the reactor's facilities is to model conditions that are as close as possible to real conditions, and thus secure the reproducibility and utilization of measured values.

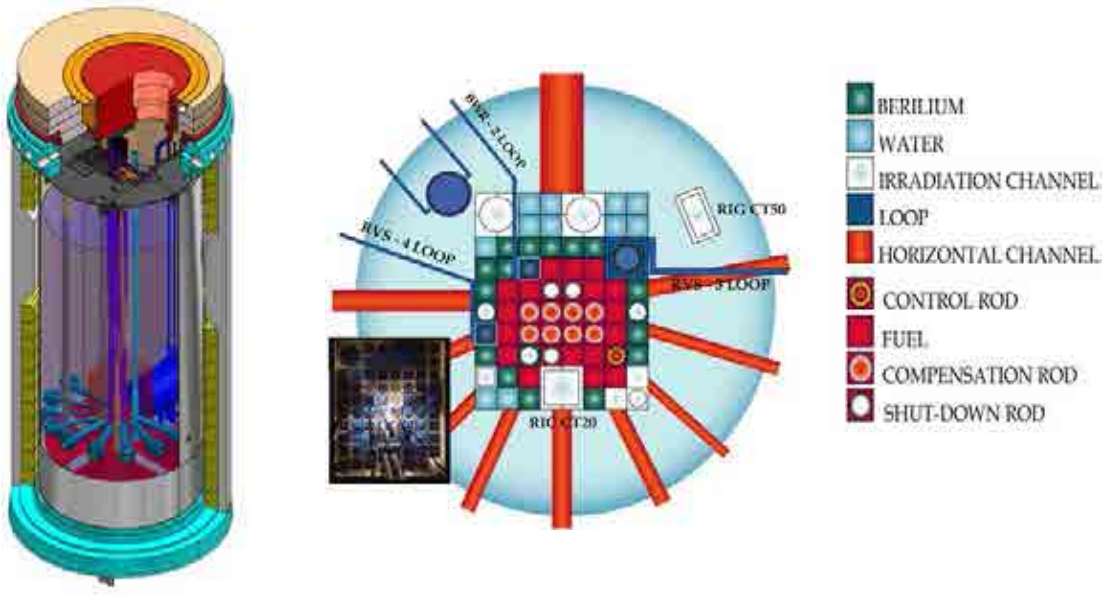

FIG. 3.3. Research reactor LVR-15, loops and rings.

Besides, CVR together with NPP Temelín and Westinghouse Electric Company LLC is cooperating on the fuel inspection and repair since 2009. Due to the fuel vendor change at Temelín, new PIIP will be implemented to avoid any fuel problems in the future operation. During the unit outage several fuel assemblies will be chosen and inspected on the FRIE. The main operations, which were set up to present, with the fuel assemblies at FRIE are:

– Inspections:
    - Visual inspection of fuel assemblies, extracted fuel rods, and RCCA;
    - Ultrasound inspection (to detect leaking fuel rod).
– Measurements:
    - Fuel assembly and rod bow and twist;
    - Fuel assembly and rod length measurement (growth).
– Fuel assemblies repair.

All activities at FRIE will be covered by present fuel vendor — TVEL. However, CVR will participate on the fuel inspections and measurements to support the independent long term monitoring and evaluation of fuel behaviour at Temelín NPP. These measurements will be used for the codes validation (for better understanding of fuel failure processes to make more realistic models) and as a main basis for the future experiments for fuel failure behaviour study under normal and abnormal conditions.

4. CONCLUSIONS

NPP Temelín is a first VVER-1000 reactor, where the Russian reactor design meets the US fuel design. Since first load, VVantage-6 fuel assemblies from Westinghouse Electric Company LLC were used at both units. During past ten years, Temelín gets lot of operational experiences with Westinghouse fuel. Besides successful operation, several fuel problems were occurred too, like incomplete rod insertion due to strong bow and twist of the fuel assemblies and fission product release into the primary coolant due to primary cladding failures by grid-to-rod fretting. Since first startup of Temelín NPP, 63 leaking fuel assemblies at both units were found and 27 of them were repaired and successfully reused in next cycles.

PIIP was specified, and different inspections were done to get large amount of data from the bow, twist and growth measurement. In several years many data were measured, root causes were found and many recommendations for new fuel design were applied.

All these changes led to the successful operation with Westinghouse fuel assemblies. The problem with IRI, as well as the fuel assembly bow and twist was removed in 2005, and the leaking fuel due to grid-to-rod fretting was minimized. From 63 leaking fuel assemblies only 23 were repaired, however the effectiveness of the leaking fuel rod extraction from the fuel assembly is quite high, 93% [2]. From these fuel operational problems, the fuel vendor (ČEZ) as well as their subcontractors (NRI, CVR, ŠJS, etc.) made a big lesson and these experiences are now fully prepared to use on the new Russian fuel TVSA-T in fuel operation as well as fuel inspection and repair.

REFERENCES

[1] INTERNATIONAL ATOMIC ENERGY AGENCY, Fuel failures in water cooled reactors, TM meeting, IAEA (1998) 180.

[2] ERNST, R., ERNST, D., MILISDORFER, L., Palivo Westinghouse — r.2000 až 2010, Bezpečnost jaderné energie, Vol. 18 (2010) 349–356.

[3] ERNST, D., MILISDORFER, L., 10 Years of experience with Westinghouse fuel at NPP Temelin, Proccedings of VVER 2010, Prague (2010) 30.

[4] HLAVINKA, V., International cooperation in development and supply of nuclear fuel for Czech NPPs, Atomexpo 2009 (2009) 16.

SPENT FUEL ATTRIBUTE TESTER REALIZATION AND APPLICATION

Z. HLAVATHY, I. ALMASI, C. T. NGUYEN, L. LAKOSI, N. BUGLYÓ, M. BEIER

* Institute of Isotopes,
Hungarian Academy of Sciences
Budapest
Email: hlavathy@iki.kfki.hu

** Paks Nuclear Power Plant Ltd.
Paks

Hungary

Abstract

Presently 19-element natural uranium fuel bundles are used in 220 MW(e) Indian PHWRs. The core average design discharge burnup for these bundles is 7000 MW·d·Te^{-1}U and maximum burnup for assembly goes upto of 15 000 MW·d·Te^{-1}U. Use of fuel materials like MOX, Thorium, slightly enriched uranium, etc., in place of natural uranium in 19-element fuel bundles, in 220 MW(e) PHWRs is being investigated to achieve higher burnups. The maximum burnup investigated with these bundles is 30 000 MW·d·Te^{-1}U. In PHWR fuel elements no plenum space is available and the cladding is of collapsible type. Studies have been carried out for different fuel element target burnups with different alternative concepts. Modification in pellet shape and pellet parameters are considered. These studies for the PHWR fuel elements/assemblies have been elaborated in this paper.

1. INTRODUCTION

The most widespread method for verifying the presence of the fissile material is the viewing of Cherenkov light. However it cannot be applied if the water is not clean enough and it does not identify the source of radiation. A more sophisticated method of verification is the SFAT where a medium resolution gamma detector identifies the source of radiation through a collimator tube. Such a device was designed and built in our Institute and it was tested in a series of verification problems.

2. SETTING UP THE DEVICE

Our apparatus consists of a detector house, which provides place for a 500 mm^3 CZT detector and a lead collimator shielding the detector from side directions and a set of closed end (watertight) steel collimator tubes of 1 m length and 50 mm diameter, containing air (Fig. 2.1). The collimation itself is provided by the surrounding water.

The number of the tubes applied depends on the task. The maximum number of 6–8 tubes can be applied when the assemblies are stored in two levels and the assemblies in the lower level have to be verified. In most cases use of 2–4 collimator tubes is suitable while for assemblies cooled for a long time, use of 1 or 2 tubes provides good results. A part of the system is a stand for holding and positioning the detector and collimator tube system, which can be installed on the railings of the refuelling machine, or on a service bridge (Fig. 2.2). By the aid of the stand the mounted system can be moved above the assembly to be examined and sunk under water by the winch. A rough positioning can be done by moving the refuelling machine or substituting bridge, and by shifting the stand perpendicularly to the railing by the aid of rollers. Fine positioning goes by screws on the stand in two directions. The system can be mounted up to 4 collimator tubes laid just on the platform in advance and can be let down as a whole to the pond, while in the case of a longer collimator the individual tubes can be joined step by step and let the mounted part moving down. Detector house is connected at last.

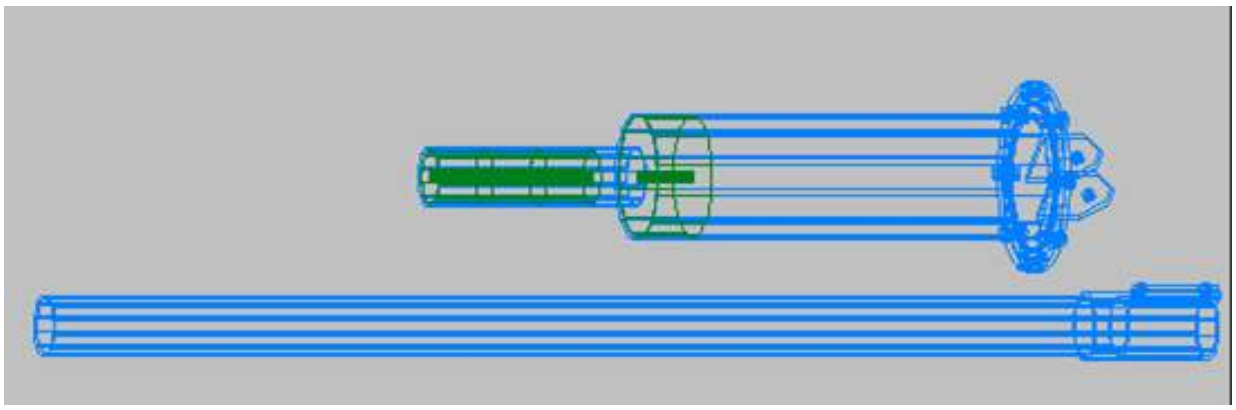

FIG. 2.1. Detector house and collimator tubes. The thick green line shows the volume inside the lead collimator.

FIG. 2.2. The stand with the winch.

For performing verification, the lower end of the collimator tube enters into the headpiece of an assembly until it neither impacts on the upper grid nor leans against the interior of assembly head, ensuring that the spent fuel and the detector are in line of sight through the collimator tube (Fig. 2.3).

Positioning is supported by a TV camera and monitor as a surveying system. A camera mounted to the detector house may promote a more compact design.

FIG. 2.3. End of the collimator tube above the fuel assembly.

Although it was developed for verifying VVER-440 assemblies, and also the positioning stand was designed to the refuelling machine established in the Paks NPP, the system can be used, with a minor change and transformation of the stand, in other plants as well.

The signal from the detector comes to the mini MCA analyser through a watertight insulated cable controlled by a laptop computer.

3. APPLICATIONS

Assemblies and other objects stored in the spent fuel pond were examined by the SFAT. The spent fuel assemblies produce a 662 keV peak from the fission product Cs-137 as well as 1173 keV and 1332 keV peaks from Co-60, an activation product originating from the headpiece of the assemblies. If the cooling time of the assembly is less then 6 years, the 794 keV peak of the Cs-134 (2 y half-life) can be observed as well. However, for very fresh assemblies (CT<1 y) the Compton-tail of the peaks of Zr-95 (half-life 64 d) and other short lived activation products can cover the Cs peaks (Fig. 3.1).

With medium cooling times both Cs-134 and Cs-137 (Figs 3.2–3.3) peaks can be clearly observed. As the intensity of the Cs-134 peaks is proportional to the square of the burnup, so the burnup can be assessed from the extrapolated initial value of the intensity.

Due to the 30 y half-life of Cs-137, the 662 keV peak can even be revealed after an extreme long ((>14 y) cooling time (Fig. 3.4) or very low burnup (order of a few $GW{\cdot}d{\cdot}t^{-1}U$) up to 6–7 y cooling time, when the Cherenkov viewing device (ICVD) is not suitable for verification. The measuring time needed for a relyable spectrum lies between 300–1200 s.

With the same method, we verified the fissile material content of those canisters which contained damaged spent fuel originating from the 2004 incident, and demonstrated the absence of the fissile

material in canisters containing only the head and foot parts of the assemblies. In addition we demonstrated the absence of fissile material in the containers of irradiated Co-60 sources.

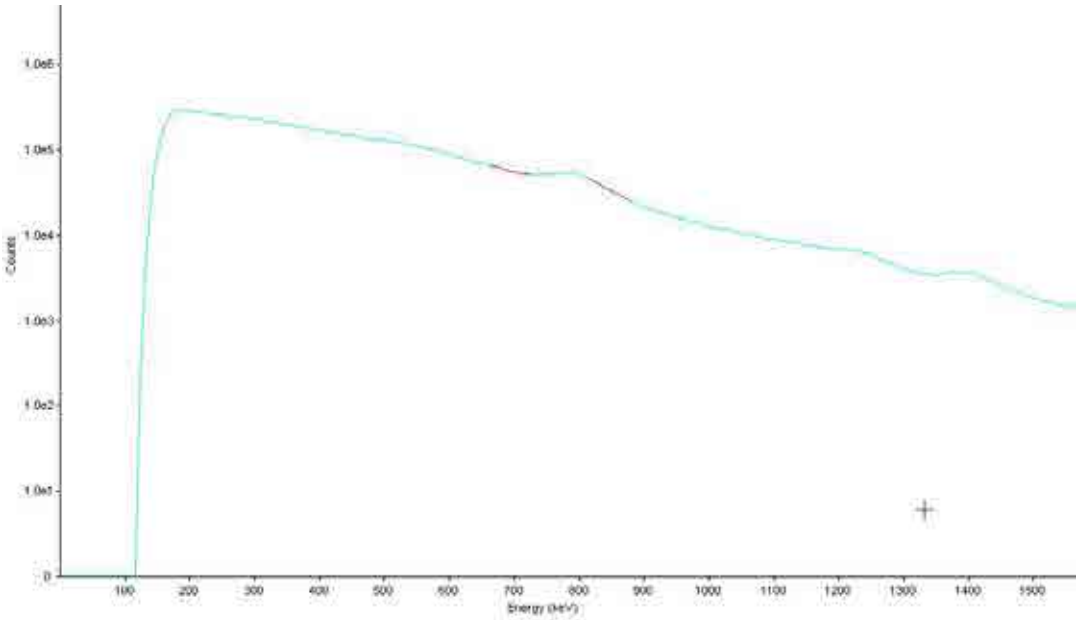

FIG. 3.1. Spectrum from the spent fuel assembly with CT=8 months.

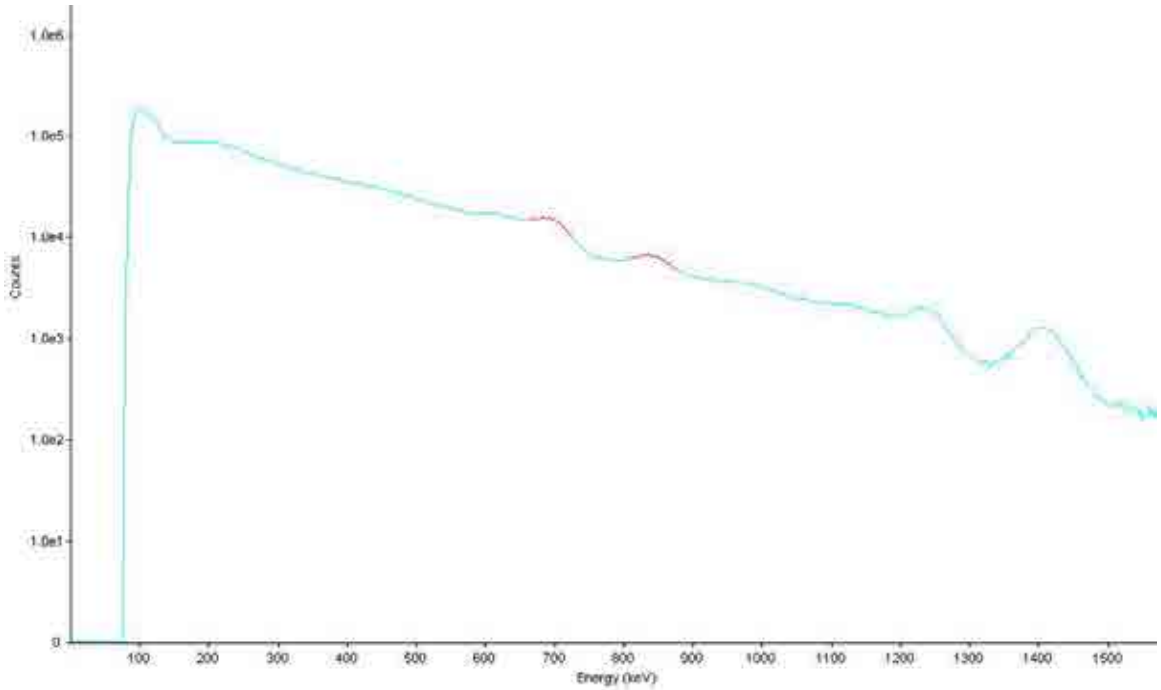

FIG. 3.2. Spectrum from the spent fuel assembly with CT=2.7 y, BU=22.6 GW·d·t^{-1}U.

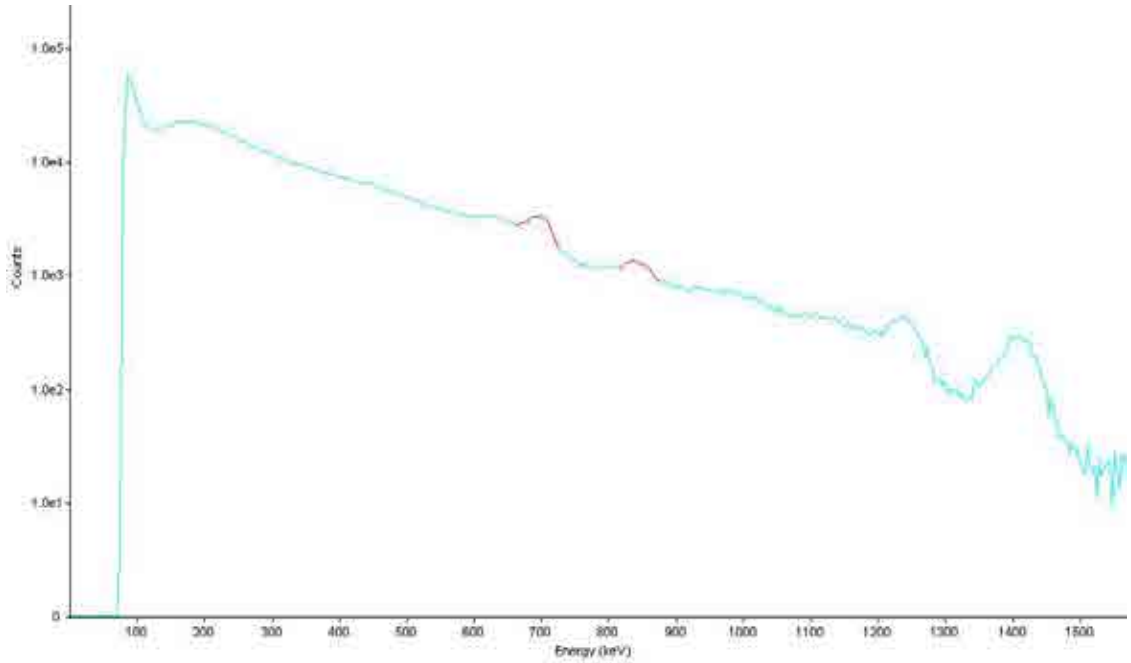

FIG. 3.3. Spectrum from the spent fuel assembly with CT=3.7 y, BU=41 GW·d·t^{-1}U.

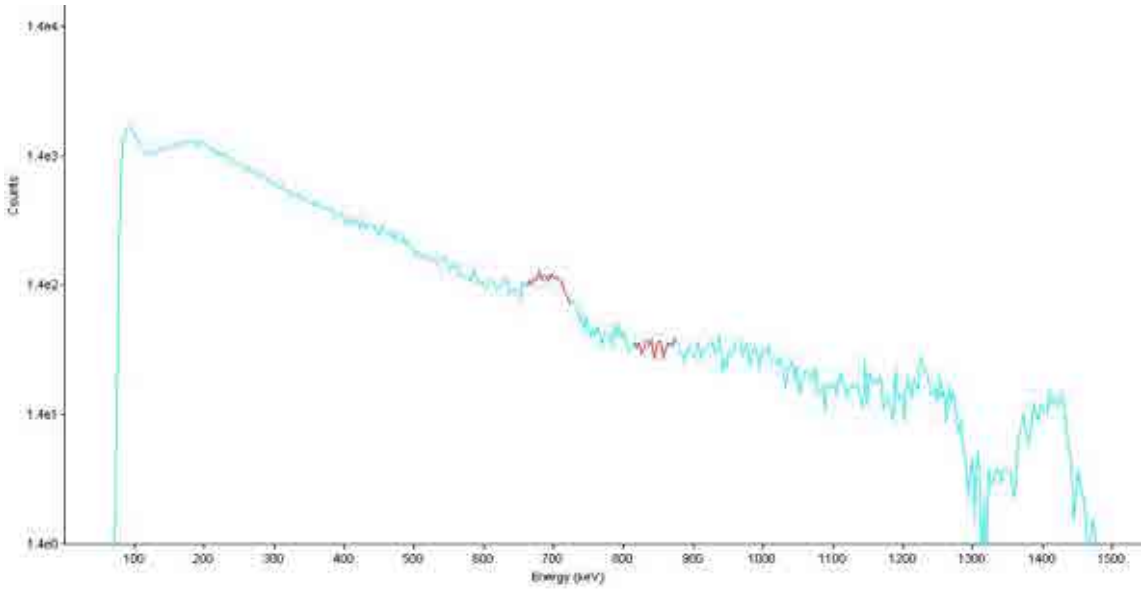

FIG. 3.4. Spectrum from the spent fuel assembly with CT >14 y.

4. SUMMARY

SFAT is useful, whereas acknowledging its limits, for verifying fissile material in fuel assemblies, containers and other objects. Detection of undeclared irradiation is also possible, even in the presence of Co-60. Necessary measurement time is 300–1200 s pro assembly/object, depending on its parameters.

Even if it cannot be a rival of ICVD in comfortable employment and easy evaluation, in cases where the water in the pond is of too high level or bad quality, burnup is very low or cooling time is too long, as well as if the task is to verify an assembly in the lower rack, it may be a good alternative for substituting ICVD.

BIBLIOGRAPHY

[1] LAKOSI, L., TAM, N.C., ZSIGRAI, J., SÁFÁR, J., A NDA method for revealing unreported irradiation using a CdTe-based PSFAT, Proceedings of 21st ESRADA Annual Symposium on Safeguards and Nuclear Material Management, Sevilla, (Foggi, C., Petraglia, E., Eds) (1999) 369–374.

[2] LAKOSI, L., TAM, N.C., ZSIGRAI, J., BÍRÓ, T., SÁFÁR, J., Recent developments and experience with a CdZnTe-based PSFAT, Proceedings of 23rd ESARDA Annual Symposium on Safeguards and Nuclear Material Management, Brugges (2001) (Foggi, C., Ed.) 688–692.

THE POOLSIDE INSPECTION OF POST-IRRADIATION FUEL ASSEMBLY IN QINSHAN NPP

Shiwei WANG
Qinshan Nuclear Power Company Ltd.,
Haiyan, China

Abstract

Poolside inspection of post-irradiative fuel assembly is used to evaluate the integrity and reliability of reloaded FAs in Qinshan NPP during reloading outage, and find out the failure assemblies and locate the position of failure rods before repair. And the poolside inspections also play a significant role in burnup increment test in Qinshan NPP. Main results of poolside inspections testify that the relevant requirement of performance of FAs can be satisfied as the burnup increment within the range of test. Some others examinations and poolside inspections of post-irradiative fuel assembly are introduced briefly also.

1. INTRODUCTION

In these years the prosperity of nuclear power development in China is just beginning. There are 13 nuclear power units in operation now. There are 24 units under construction with construction permit (CP) issued by National Nuclear Safety Administration (NNSA). And 8 units whose PSARs are being reviewed by NNSA are waiting for CP. And the nuclear power development has been confirmed as the important policy for China's national energy in 21st century. According to the scenario the total installed nuclear power capacity will be 70–80 GW(e) until 2020.

But since the accident of Fukushima nuclear power plant in Japan, every country reconsidered their nuclear policy and plan, and China is included certainly. Many measures were forced to implement. A series of comprehensive inspections and reviews are obliged to execute in nuclear power plants throughout country and in the near future there may be some significant modifications in plant such as movable diesel generator, passive containment hydrogen recombining system, etc. To the nuclear power plants under construction, it is required to evaluate and review its safety standard based on the most advanced standards. New issues of CP have already been suspended until the adjusted and improved nuclear power development programming is unveiled.

As the second generation of nuclear power plant, Qinshan nuclear power plant (QNPP) with capacity of 310 MW(e) came into operation in 1991, the current cycle is C13 just at the ending part of its 30 years design life. QNPP is the first nuclear plant which is designed and constructed by ourselves in China mainland.

The core of QNPP 310 MW(e) unit consists of 121 FAs designed by Shanghai Nuclear Engineering Research and Design Institute and supplied by China Jianzhong Nuclear Fuel Co., Ltd (CJNF). Any FA comprises 204 fuel rods, 20 guide thimbles and 1 instrument thimble arrayed in a matrix of 15 × 15 and the enrichment of U-235 is 3.4% since balance cycle. The cladding material is Zr-4. The 8 grid spacers Inconel (GH4169) and the top and bottom nozzles are stainless steel (0Cr18Ni10Ti). There are two main modifications after cycle 7, the bottom nozzle filter and dish chamfers of pellet are added. Now all of the spent FAs store in the pool in FX and will transport to the reprocess factory in future.

2. METHOD AND APPLICATION OF POOLSIDE INSPECTION IN QNPP

Method of poolside inspection in QNPP included: sipping inspection, VT inspection, and dimension measurement for example: verticality, twist, variation of rod spacer and irradiative growth, etc., and disassembly inspection such as ET and oxidation film thickness for rods.

2.1 The welding joint form

The poolside inspection methods are used to evaluate and check whether a FA is failure or not. Based on daily operational monitoring on Fuel Reliability Index and Iodine Equivalent Value, there will be a preliminary judgment of fuel integrity. If no FA failure happens, inspection of VT and dimension measurement will be arranged at a specified ratio of fuel assembles to evaluate the reliability and integrity of reloaded FAs during reloading outage. But if judgment goes to the contrary, sipping inspection for all FAs need to reload will be arranged in order to find out the damaged FAs. If success, there will be a comprehensive inspection include VT, dimension measurement inspection, and disassembly inspection by ET before repair it by take the place of failure rods with intact rods, if necessary.

In cycle 4, many FAs damaged due to the loose of bolt of the barrel. After that only a few FA failures happened during fuel handling. QNPP has device and skills to repair the damaged FAs. Evidence proves that the repaired FAs have the same performance with the intact assemblies. The failure history of FAs in QNPP are shown in Table 2.1.

TABLE 2.1. FAILURE HISTORY OF FAS IN QNPP

Cycle	FAs failure history
C1–C3	No FA failure monitored
C4	9 FAs breakage, 2FAs have grid spacers deformation, and 6 FAs have mix wing damage
C5–C6	1 FAs damage
C7–C12	No FA failure monitored

2.2 In-core burnup increment test of FAs in QNPP

As fuel management developed, the burnup of the FA is requested to increase properly in order to prolong the cycle life [1]. The poolside inspection in QNPP also gives the method to verify the fuel property after burnup increment test in core. Restricted by level of design, technology and verification test at that time, QNPP 310 MW(e) FAs' burnup limit was only 30 000 MW·d·t^{-1}U initially, large margin was reserved. Under the precondition that safety of the FAs and reactor must be guaranteed, many tests were performed aim to increase the burnup step by step. After more than 7 cycles effort, the test was complete successfully till the ending of cycle 11. After this fuel management improvement, average burnup of assembly is nearly to 32 000–3000 MW·d·t^{-1}U, max burnup of FA achieve to 40 000 MW·d·t^{-1}U, and max rod burnup is 44 000 MW·d·t^{-1}U.

Main test items and results can be found at [2].

Irradiative growth: no irradiative growth of FAs is occurring. Nevertheless irradiative growth of fuel rods was observed. The distribution of irradiative growth value versus burnup is shown in Fig. 2.1. The relevant results of 3 × 3 FA during the design verification test are also shown in Fig. 2.1.

Measurement of oxidation film of rod: Maximum thickness of oxidation film is 49 μm much lower than the requirements of regulation and guideline [3–4] that corrosion thickness at the end of life should be less than 10% (0.7 mm) of cladding wall. That means the anti-corrosion performance of fuel cladding is sufficient in the range of burnup test, and the fuel rod is safe.

As shown in Fig. 2.2, it is obvious that the oxidation film thickness of rod is linearity with its endured cycle number. That is corresponding with the results of relevant compute code.

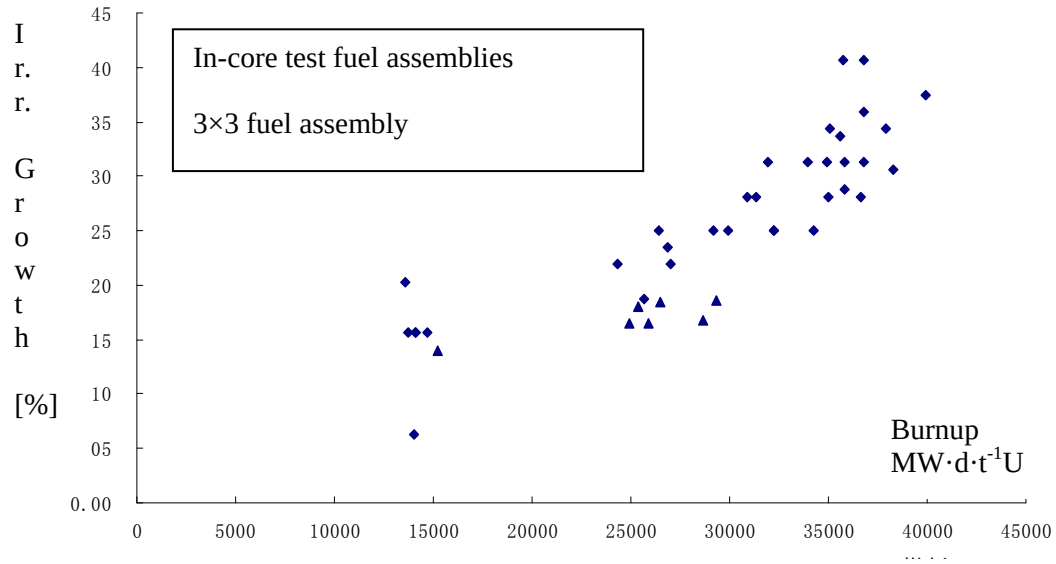

FIG. 2.1. Irradiative growth effects in fuel rods.

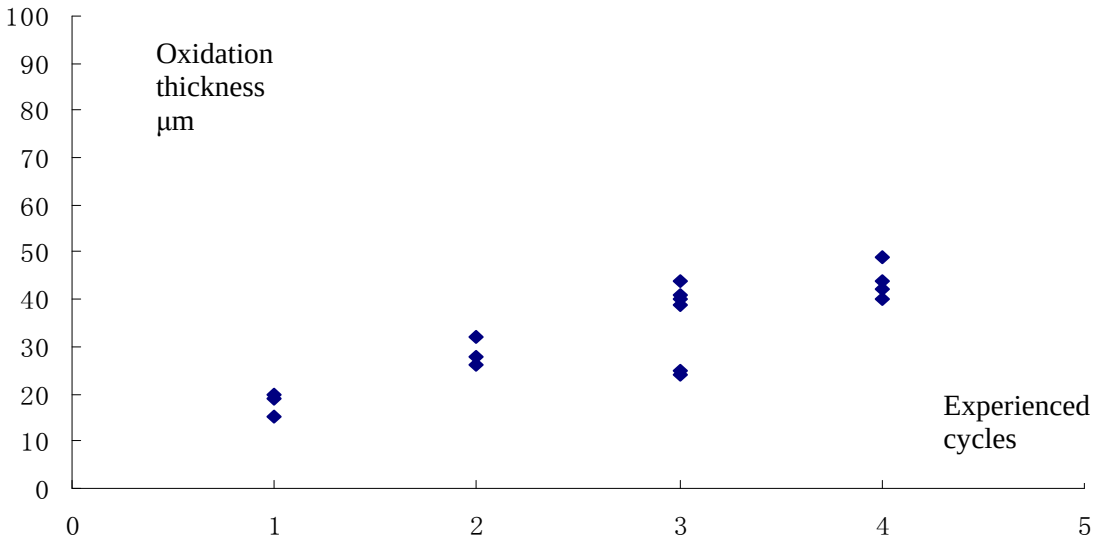

FIG. 2.2. The effect of oxidation film in fuel rod.

ET inspection on fuel rod: ET results shown that no inner and outer wall defects, holes, ring ridges happened. That means no occurrence of PCI, abrasion, hydrogen brittleness.

Through the poolside inspection of post-irradiative FAs, the conclusion can be made that after 4 cycles, up to 40 000 MW·d·t^{-1}U BU, no obvious irradiative growth happened, and the thickness of oxidation film still fulfils requirement of the regulations, and no PCI effect occurred. Combined with some other necessary tests such as rod drop test and many calculation results of computer codes, the following conclusion can be made. The high performance of FAs of QNPP can be guaranteed within the burnup test range, and are capable to satisfy the operation safety after 4 cycles, and 40 000 MW·d·t^{-1}U BU.

3. OTHER METHODS AND APPLICATIONS IN CHINA

3.1. Hot cell inspection of post-irradiative FAs

China Institute of Atomic Energy undertakes a nuclear energy science and technology research subject, post-irradiative inspection of FAs of PWRs. By means of the post-irradiative inspection on the FAs of QNPP, CIAE will obtain the data such as structures, performance, and stability, and verify the rationality and dependability of domestic FAs, and then evaluate the in-core behaviours of FAs, meanwhile accumulate the behaviour data of PWRs.

In fact, the inspection methods of FAs in QNPP site are no more than poolside inspection, so to understand the entire nature performance of the post-irradiative FAs by hot cell examination, especial to the FAs after burnup increment test, is very attractive. All of these can be preparations for further burnup increments. According to this subject, 8 rods were extracted from specified FAs. The selected rods are shown in Table 3.1.

TABLE 3.1. THE EXTRACTED RODS INFORMATION

Operation cycles	Enrichment	Burnup [$MW \cdot d \cdot t^{-1}U$]	Unload date	Position of rod
4	3.4%	39 922.18	2006-6-25	A-15, K-08, N-04
3	3.4%	36 006.96	2006-6-25	A-15, K-08, N-04
4	3.0%	33 956.02	2002-4-14	K-08, N-04

The hot cell examination in of CIAE will consist of four parts mainly. The non-destructive will include VT, ET, dimensions measurement and Gamma spectrometry of fuel rod, and the destructive inspection will involve release rate of fission gas, axial tension test of cladding, observation, measurement and analysis of macro and micro structure of UO_2 pellets, micro-structure analysis and SEM of section of tension sample of cladding. Determination of absolute burnup of fuel rods by precise analysis of the concentration of Cs-137 and Nd-148, and in-core behaviour analysis and performance evaluation of fuel rods by compare the results of hot cell examination and calculation results of computer code are also involved. But for many reasons the examination was postponed many times. No more information can be acquired now.

3.2. Poolside inspection of FAs [5]

Since 2003, Qinshan nuclear power plant phase 2 and Research Institute of Nuclear Power Operation researched and developed cooperatively the ultrasonic measurement system of deformation of post-irradiative FAs. Calibrated with a standard FA, the system can measure the deformations of FA rapidly during outage. Now this set of system has already been put into use and do help greatly. This system has its advantage in technical such as less measurement time (less than 5 mins per assembly), higher accuracy (less than 0.3 mm of system errors), etc., so that any bending and twist of FAs can be detected precisely and rapidly. The measurement results can be a very useful guide to fuel loading in order to mitigate the difficulty due to deformation of post-irradiative FAs. And at the same time data of measurement can be accumulated for FAs design institute and manufacture plant.

4. SUMMARY

(1) Poolside inspection in QNPP is an efficient way to evaluate the reliability and integrity of FAs;
(2) The results of poolside inspection and analysis support the conclusion sufficiently that the integrity of FAs can be guaranteed in in-core test of burnup increments in QNPP, and then improve the fuel management level and the economy of plant;

(3) Specialization, integration and high technology of poolside inspection increase the work efficiency, save the human resource cost significantly, shorten the time of outage, and then improve the economy of plants in general.

The post-irradiative examination and poolside inspection of FAs are playing more and more important role in nuclear power plants.

REFERENCES

[1] KONG, D., LIAO Z., WU X., Improvement of in-core fuel management in qinshan npp. Nuclear Power Engineering, Vol. 27, No. **2** (2006) 5–8.

[2] LIAO, Z., KONG D., LI, Z., et al., The in-core burnup test and evaluation of Qinshan 310 MW(e) FA, Academic Annual Meeting of Chinese Nuclear Society (2009).

[3] EJ/T 1029-1996, Regulation For Design Limits of Fuel System in PWR Nuclear Power Plant [S] (1996).

[4] EJ/T 323-1998, Design Guideline of Fuel Assembly in PWR Nuclear Power Plant [S] (1998).

[5] QINGSHAN, B., Deformation management of fuel assembly in Qinshan NPP phase 2, Meeting on Communication of Technical Field in Six Nuclear Plants in China (2010).

HOT LABORATORIES' EXPERIENCE AND CAPACITY (OVERVIEWS)

(Session 2)

Chairpersons

A. LEENAERS
SCK·CEN

M. WADE
Merrick Company

TREATMENT AND DISPOSAL OF PROBLEMATIC AND POORLY CHARACTERIZED NUCLEAR FUELS IN A POST-IRRADIATION EXAMINATION FACILITY

D.M. WILLEY
National Nuclear Laboratory
Windscale, Seascale, United Kingdom

Presented by D. WRIGHT

Abstract

The hot cells at the Windscale Laboratories of the UK National Nuclear Laboratory are a particularly flexible facility, capable of characterizing and co-processing a variety of irradiated fuels and other radioactive materials on a semi-industrial scale in addition to performing 'traditional' Post-irradiation Examination for reactor component monitoring and fuel development. The use of the Windscale PIE Laboratory for work of this type is summarised and two examples are discussed. Decommissioning of two early Windscale site reactors resulted in the recovery of unrecorded fuel and isotope cartridges of various types. The process by which these were identified by non-destructive methods is described. Magnox fuel elements (uranium metal bar clad in magnesium alloy) had been stored within nominally dry sealed canisters under water for >20 years. Leaks had resulted in production of prophetic uranium hydride. The process applied to safely open these canisters to recover the remaining uranium and segregate the various waste streams is outlined.

1. INTRODUCTION

The Windscale facilities of the UK National Nuclear Laboratory were developed over many years to co-process large PIE programs on a variety of fuel and reactor core components; they are complementary to other NNL analytical and test laboratories at Sellafield and Springfields in the UK.

Windscale adjoins the Sellafield fuel reprocessing plant site in the NW of England, which has a variety of problematic legacy fuel types and other radiological wastes to dispose of before decommissioning can be completed. This paper describes how the Windscale PIE laboratory has been able to support some of the Sellafield and Windscale sites decommissioning projects.

2. WINDSCALE FACILITIES

The core facilities of the Windscale laboratory comprises of 60 heavily radiation shielded workstations, each equipped with a viewing window and a pair of master–slave manipulators (MSMs), distributed between 13 interlinked hot cells termed 'caves', plus 2 satellite cells. In addition, there are a number of other integrated laboratory areas and workshops capable of handling materials of lower activity. There are three separate shielded cask/flask receipt crane halls (Fig. 2.1).

Most of the hot cells measure approximately 11 × 2.5 × 4 m internally and have an installed 0.5te or 1te capacity hoist, plus one or more horizontal or vertical cask ports; some have heavy-duty powered manipulators (Fig. 2.2). At either end of the facility the cells are capable of receiving large top opening casks of up to 55te. The roof of each cave is constructed of removable interlocking concrete blocks allowing access to the cave for introduction of large items of equipment. The caves are linked together by a shared shielded transport corridor from which each cave can be separately isolated and shielded by insertion of bulkheads from the roof, to allow refitting or refurbishment without affecting the operation of the remainder of the plant.

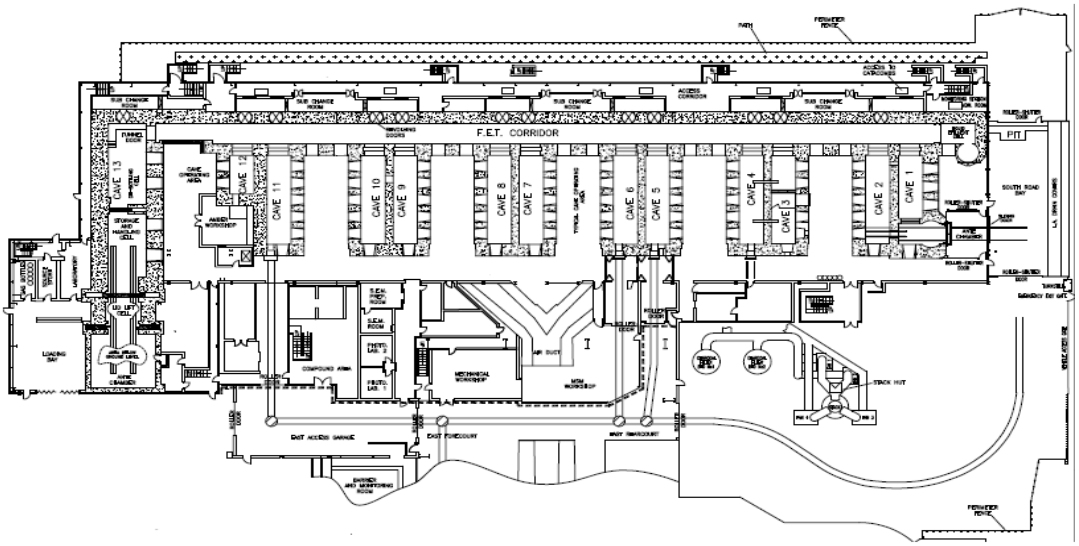

FIG. 2.1. Hot cells layout.

FIG. 2.2. Typical Windscale hot cell operating face.

This layout has resulted in a particularly flexible and adaptable plant capable of co-processing several different work streams delivered in a wide range of casks. Within the facility individual cave areas can be dedicated to very different types of work enabling effective segregation of PIE work from activities such as those described here.

3. DECOMMISSIONING SUPPORT

Most aged plants undergoing decommissioning generally have limited capability for the treatment and disposal of problematic or poorly characterised nuclear fuels and wastes. In some cases they cannot readily interface directly with waste storage facilities.

As such, in addition to ‘traditional’ PIE for reactor component monitoring and fuel development, the handling and analysis capabilities of the Windscale facilities and staff have been used for:

– Assaying type and/or quantity of radioactive isotopes present in waste to define and justify an appropriate disposal route;

– Sampling of waste to confirm the activity assumed or calculated to be present in waste;
– Breakdown of waste items, with segregation of low and intermediate level waste components from fissile materials, followed by appropriate disposal routes;
– Cutting, compaction and efficient packing to minimise waste volumes;
– Repacking of wastes into standard disposal configurations;
– Decontamination of items, where economic, to a lower level waste category;
– Consolidation of small quantities of different waste types into standard/economic waste packages;
– Stabilisation and treatment of special wastes (e.g. chemically reactive, prophetic, mobile) into a form suitable for final disposal or safe long term storage;
– Preparation of non-standard nuclear fuels for reprocessing in existing plant, removing requirement for disposal, or build of new plant which eventually would itself become radioactive waste;
– Preparation of packages from a form necessary for export, or public road transport, to that suitable for transfer to long term storage/disposal.

The experience gained at Windscale Laboratories in use of simple, quick and low-cost methods to infer identity has proven applicable, in combination with manufacturing records and archived unirradiated samples, to a number of projects requiring disposal of large quantities of problematic materials. In the absence of such assay, sorting and segregation, pessimistic assumptions have to be made which have significant cost penalties for subsequent storage and disposal.

The benefits resulting from use of a PIE Laboratory for work of this type are many. The workforce is highly experienced in remote handling and investigative examination of a variety of fuel types, and readily identify unexpected items which can then be segregated and dealt with accordingly. High standards of data quality assurance can readily be achieved. The facility is tolerant of a wide range of materials and configurations, and the existing flask handling capability allows import of a wide variety of transport package designs.

Task analyses show that, when the lead time before operation is factored, a new purpose-built industrial plant to perform similar waste characterisation, sentencing and processing, is unlikely to be attractive, both in terms of in time-averaged tonnage processed and cumulative workforce/public radiation dose uptake. A new dedicated waste handling plant of similar capability and flexibility would also be prohibitively expensive to build, plus result in additional decommissioning liability at end of life.

Example 1: ‘Piles’ fuel and isotope cartridges.

During the early stages of decommissioning two early air cooled reactors (termed ‘piles’), hundreds of unrecorded fuel plus various isotope cartridges were retrieved from adjacent air and water ducts; all fuel and isotope types were externally similar. It was not possible to segregate fuel from isotopes at source, and the degraded state of much of the fuel did not permit it to be directly reprocessed.

Destructive examination techniques for identification and assay were deliberately excluded due to the potential effect on plant discharges. However it was possible to devise an examination regime, consisting of a simple combination of X radiography at a fixed geometry together with weighing, to allow determination of the internal structure and individual component densities, from which positive identification could be made cheaply and rapidly. As an example: a lithium–magnesium alloy has a significantly different density to one of aluminium nitride; the densities of bismuth oxide and cobalt are similar, but the internal structure of cartridges containing these were very different.

FIG. 3.1. CAGR fuel element dismantling.

The work performed included (Fig. 3.1):

– Segregation and identification of isotope cartridges, then consignment to appropriate waste streams;
– Removal of aluminium cladding from broken and corroded uranium metal fuel bars;
– Cleaning and volume minimisation of this cladding prior to transfer as intermediate level waste;
– Transfer of intact fuel elements, plus cleaned uranium bar pieces, to reprocessing.

The identification of a number of undamaged fuel elements gave the opportunity for work to be conducted for the benefit of an additional decommissioning project:

– Exact duplication of the historical fuel de-cladding technique followed by measurement of fissile carryover in that cladding, of interest to the project emptying the original waste disposal silo.

Example 2: 'Debottling' of Magnox fuel.

Around 1000 Magnox fuel elements (uranium metal bar clad in magnesium alloy (Fig. 3.2)) totalling nearly 10 t of uranium, were individually stored in nominally dry sealed canisters ('bottles') within a pond for more than 20 years. The majority of these had subsequently leaked, severely degrading the fuel by corrosion and frequently resulting in large accumulations of prophetic uranium hydride and hydrogen gas.

Opening the canisters in pond would have resulted in a high operator dose penalty in comparison to performing the task within the Windscale laboratory. A simple process was developed, based on in-canister conditioning to allow the fuel to be removed safely into an air-filled hot cell and to be returned the fuel ponds for consolidation with fuel for reprocessing (Fig. 3.3). The technical strategy minimised the equipment required for this work, thus minimising capital costs and the generation of secondary wastes [1].

FIG. 3.2. Pile isotope cartridge (upper) and fuel element (lower).

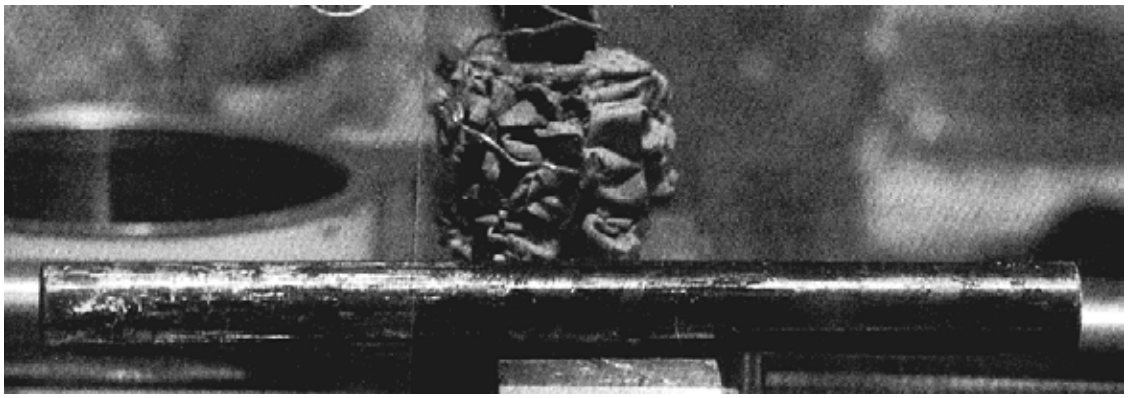

FIG. 3.3. Compacted aluminium cladding removed from the now bare uranium fuel bar below. X rays of these allowed estimation of fissile material carryover to the original waste silos.

After X radiography to provide an initial estimate of fuel type and quantity, and corrosion extent, a low percentage O_2/argon gas mixture gas was injected into the canisters at a low flow rate to purge the gaseous hydrogen content and 'passivate' the exposed corrosion product surfaces within, so that air could be admitted without risk of fire or explosion. The fuel could then be removed from the canisters after which the fuel pieces were subjected to detailed inventory assessment and identified by various minor unique design characteristics, then despatched for reprocessing. Unexpected objects were segregated. High fissile content sludge was sent for encapsulation, and empty canisters together with non-fissile fuel element components were volume reduced and sent for waste disposal by standard routes.

The process made extensive use of existing facility infrastructure and technical equipment, minimising the need for capital investment. Process-specific equipment was designed in-house to optimise the interface with existing plant infrastructure and to enable remote installation and decommissioning.

During the early processing of the canisters, operating experience was reviewed and this, combined with small scale experimental work and theoretical modelling, substantiated the safety case and reaffirmed the selected strategy. The experience gained was recently deployed to assist AB SVAFO in

the development of their process to deal with a similar problem with container stored metallic uranium fuel at Studsvik, Sweden (Figs 3.4–3.7).

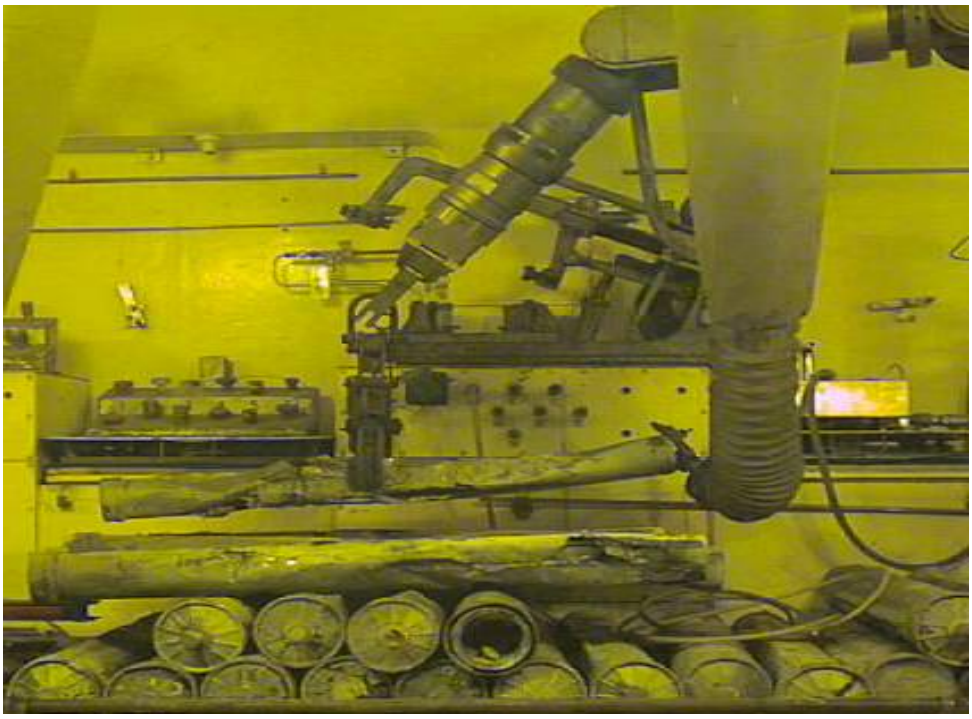

FIG. 3.4. Processing of fuelled canisters.

FIG. 3.5. Degraded Magnox fuel element after removal from canister.

FIG. 3.6. Radiograph of corroded Magnox element end section, taken when within canister.

FIG. 3.7. Cleaned uranium bar piece after removal of Magnox cladding.

4. NEXT

The next major challenge of this type is the removal and sentencing of a wide variety of poorly documented experimental fuels from another legacy storage pond, where identification of fuel enrichment will perhaps be the greatest problem. Three levels of identification ambiguity after any examination must be anticipated:

– items whose identity is positively known;
– items which cannot be fully identified, but it is positively known what they are not;
– items whose identity is effectively unknown.

Positive identification of enrichment by simple indirect methods for all the fuel types known to be present will not be possible; the complexity and timescale of some existing direct measurement techniques will however not be cost effective. The key objective will be to segregate out the higher enrichment fuel, and limit the remaining pessimistic assumptions applied to the 'uncertain' material.

An experienced operator, with access to manufacturing records, will be able to positively identify the majority of fuel types from a simple visual examination where viewing and handling conditions are adequate. Initially it should be possible to read inscribed manufacturing identification numbers, at least on the oxide fuel types and bulk containers. Where these numbers been lost or rendered illegible due to corrosion much can be made of readily visible external features such as component form and materials, number and type of fins/ribs, etc. Where this is insufficient then relatively cheap and fast non-destructive techniques such as mass, dimensional measurement and X radiography for internal configuration, (number of pellets, pellet or rod dimensions) is be capable of providing sufficient information to make the identification in a large proportion of the remainder. Laser induced breakdown spectroscopy (LIBS) has previously been successfully deployed within the Windscale cells to aid material identification and the technique may be capable of some refinement. Only where necessary will more expensive and time consuming techniques be applied.

REFERENCES

[1] HAMBLEY, D., WILLEY, D.M., STRIDSMAN, H., Conditioning and unloading of a canister of corroded uranium fuel, Proceedings of Global 2009, Paris (2009) Paper 9511.

CURRENT STATUS OF THE REFURBISHMENT OF FIVE SEMI-HOT CELLS AT NRI ŘEŽ

R. KOPRIVA, M. KYTKA
Nuclear Research Institute Řež
Řež, Czech Republic
Email: kor@ujv.cz

Abstract

The paper presents the procedure and current status of refurbishment of five semi-hot cells at Nuclear Research Institute Řež (NRI Řež). Reconstruction is carried out at the Mechanical Testing Department of Integrity and Technical Engineering Division. The whole procedure from the start of the project (feasibility study, work schedule) to the current status of refurbishment is depicted in this paper.

1. INTRODUCTION

Semi-hot cells are used at NRI Řež for mechanical testing of irradiated structural materials, usually from reactor pressure vessels within the frame of surveillance programs of Czech and Slovak commercial nuclear power stations. The system of semi-hot and hot cells at NRI Řež consists of 51 cells situated in 3 floors, from which 5 cells are at the present time in reconstruction.

The design of semi-hot cells differs significantly from hot cell facility. Hot cells, where the preparatory activities as unloading of irradiation containers and testing specimen machining are performed, are shielded by 1.25 m thick layer of heavy concrete, while standard NRI Řež semi-hot cells are shielded by 100–150 mm of lead.

The hot cells facility was constructed in NRI Řež at the end of 1970. In the first period of service until 1978, considerable attention was paid in hot cells to verifying the operational ability of fuel elements. In connection with introducing the manufacture of WWER-440 type light water reactor pressure vessels in former Czechoslovakia, hot cells were used since 1978 for an extensive programme of verification tests of the technology of 15KCh2MFA steel production. In 1984 the programme was extended to 15KCh2NMFA steel for the WWER-1000 type reactors.

In 1980–1985, extensive reconstruction of semi-hot laboratory was carried out to enable to study experimentally the change of mechanical properties of surveillance specimens of VVER reactors. Besides the surveillance program, the main task solved in hot cells in NRI Řež is the problem of the effects of recovery heating on mechanical properties of material after the irradiation.

2. REFURBISHMENT PROJECT

Starting point for the refurbishment was the strong need for enlargement of the testing capacity of Mechanical Testing Department (Fig. 2.1) in the scope of testing for the surveillance programs of Czech and Slovak commercial nuclear reactors. In the year 2009 was decided to refurbish five semi-hot cells from former radiochemistry facility. Preparatory activities included feasibility study of reconstruction, project work plan and obligatory approval of State Office for Nuclear Safety of the Czech Republic.

Considerable attention was paid within the project to planning and continuous photo documentation. For each work was prepared detailed assignment procedure. Former radiochemistry facility consisted of five glove boxes with several rod manipulators, connected with belt conveyer transport system. Significant advantage that has been taken to account in the preparatory phase was the absence of α contamination in the former facility. This fact contributed to simplification of work procedures prepared for the dismantling phase of the refurbishment. In the year 2010 reconstruction works started with the dismantling phase. Facility is accessible from two sides — from operator area and from active

maintenance corridor. From both sides was constructed sealed area from modular plastic panels to prevent the possible contamination outside the work place. After that, glove boxes and its support construction were dismantled. Also, according to the new design of planned semi-hot cells, the shielding concrete wall of the transport system was dismantled.

FIG. 2.1. The Mechanical Testing Department's semi-hot facility.

Construction phase of the project started in the beginning of year 2011 with the assembly of the support system for modular steel shielding. Shielding consists of several layers of 50 mm thick steel plates connected with bolts. After assembly of the steel shielding, cells were equipped with the welded inner layer of stainless steel, which was sanded after the installation. Subsequently, construction works continued with the installation of inner lighting system, painting of the front wall in the operator area and assembly of the shielding windows (Figs 2.2–2.3).

FIG. 2.2. Welding of inner stainless steel layer.

FIG. 2.3. Inner surface of the cell after sanding.

3. CONCLUSION

Next steps in the refurbishment project are the installation of supply systems for water, air, liquid nitrogen, etc., installation of manipulators and testing equipment. Start of the operation of the facility is scheduled on October 2011 — refurbishment works are carried out according to the project schedule.

Reconstruction of the former radiochemistry facility was projected on the basis of successful previous construction projects and the whole project was unique opportunity for the transfer of knowledge from experienced personnel to young colleagues.

Successful previous projects:

(a) Construction of the hot cell for unloading of surveillance irradiation containers from Temélin NPP.
(b) Construction of the hot cell for repacking of spent nuclear fuel from NRI Řež LVR-15 research reactor.

A significant advantage of the project is the new modular system (steel shielding plates and inner stainless steel layer) of the semi-hot cells, designed taking into account the future decommissioning of the facility.

HOT CELLS POST-IRRADIATION EXAMINATION AT JRC-ITU

V.V. RONDINELLA, C.T. WALKER, P.D.W. BOTTOMLEY, D. PAPAIOANNOU, S. BREMIER
European Commission
Joint Research Center – Institute for Transuranium Elements
Karlsruhe, Germany
Email: vincenzo.rondinella@ec.europa.eu

Abstract

This contribution provides some highlights on the main post-irradiation examination capabilities and on recent and ongoing effort aimed at developing advanced tools for the study of relevant properties of irradiated nuclear fuels at ITU. The scope of application covers conventional, evolutionary and advanced fuel concepts for today's commercial reactors and for future generations of nuclear power plant. It is a big technical challenge for a hot cell facility to be able to cover effectively a broad variety of fuel concepts, characterized by different compositions, physico-chemical properties, geometries and configurations. In addition to basic techniques for non-destructive and destructive examination of nuclear fuel rods (covering both fuel and cladding) and other configurations, "in-depth" investigation tools are applied for the measurement and analysis of specific physical, thermomechanical and micro-analytical properties of irradiated fuel. In many cases additional information can be gained by combining different techniques. As an example, the quantitative information obtained using electron probe microanalysis (EPMA), e.g. on the chemical behaviour of fission products in the fuel matrix, is effectively complemented by the capabilities of the secondary ion mass spectrometry (SIMS), e.g. for detection of low yield fission products, or for the analysis of the fission gas contained in bubbles and pores, independent of their size. Some indications concerning the main lines of development for upgrading the scientific equipment and the infrastructure will be provided.

1. INTRODUCTION

The Institute for Transuranium Elements (ITU) [1] is one of seven institutes of the Joint Research Centre (JRC) [2] of the European Commission [3]. The JRC provides customer-driven scientific and technical support for the conception, development, implementation and monitoring of European Union (EU) policies, functioning as an independent reference for science and technology. The mission of ITU, which started operation in 1963, is to provide the scientific foundation for the protection of the European citizen against risks associated with the handling and storage of highly radioactive material. ITU's prime objectives are to serve as a reference centre for basic actinide research, to contribute to an effective safety and safeguards system for the nuclear fuel cycle, and to study technological and medical applications of radionuclides/actinides.

The studies on the safety of the nuclear fuel cycle constitute an important fraction of the activities carried out in ITU. Essentially all aspects of the fuel cycle, except the front end and reactor irradiation, are covered. This includes: laboratory scale fuel fabrication, characterization and preparation for test-irradiation; post-irradiation examination (PIE); fuel behaviour in severe accident scenarios; back end studies including open and closed cycle options. The scope of the studies covers the safety of current, evolutionary and advanced nuclear fuel cycle concepts. This includes fuel compositions and configurations encompassing essentially all major thermal and fast rector concepts. In particular, oxide fuels for LWR (UO_2, MOX, Th–MOX), mixed oxides, carbides, nitrides, metal alloy and composites for sodium fast reactors, and fuel elements for High Temperature Reactor (HTR) are object of dedicated PIE. Particular mention is due to safety studies on minor actinide (Np, Am, Cm) fuels and/or targets envisaged for partitioning and transmutation concepts. The fuel pins come from commercial or test-reactor irradiation campaigns (in many cases performed on fuel samples fabricated in ITU).

The experimental programs are complemented by modelling and theoretical multi-scale studies ranging from ab initio calculations to thermomechanical fuel code applications (TRANSURANUS [4]).

The experimental research infrastructure and facilities at ITU include 24 hot cells, with different configurations and shielding, and a maximum allowed total activity level of 1 MCi (3.76×10^{16} Bq). Additionally, approximately 400 glove boxes are available in the different laboratories. PIE and the other studies on irradiated fuel are performed in hot cell (Fig. 1.1) or in dedicated facilities based on glove box systems (Fig. 1.2) equipped with heavy shielding and, in some cases, telemanipulators. All the irradiated fuel transported to ITU is received, handled and tested in the hot cell facilities, which also act as hub for the preparation and transport of small samples to shielded facilities in other laboratories. These internal transports are limited to perform specific "in-depth" measurements, after which the irradiated material is returned to the hot cells. The shielded glove box option is adopted for complex measuring devices which require frequent manual intervention by the operator for maintenance and/or fine tuning/upgrade. The measurements either involve specimens of very small size (a few mg or less), or consist of non-destructive tests which allow the effective and complete removal of the fuel sample after the measurement (hence the minimization of the activity level inside the glove box when no measurement is carried out).

FIG. 1.1. View of the PIE hot cells at ITU.

Figure 1.3 summarizes competences, scope and techniques available and adopted in ITU for PIE and other studies on irradiated fuels and materials. The following sections will show examples related to some of the PIE techniques in bold in Fig. 1.3, highlighting the variety of fuels and concepts investigated.

FIG. 1.2. Glove box used for fission products revaporisation tests simulating the behaviour of nuclear fuel components in case of severe reactor accident involving core melting. This is an example of a shielded glove box which allows for testing of small amounts of irradiated material outside the hot cells. Differently from the typical layout for this type of facility, here the Pb shielding is inside the box.

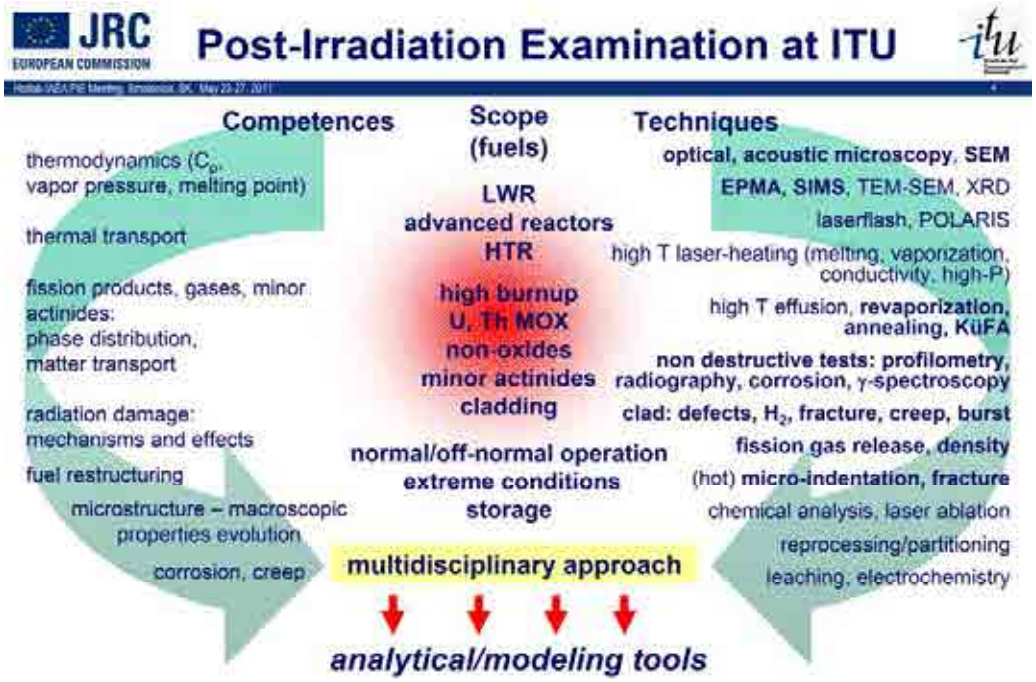

FIG. 1.3. Synoptic scheme summarizing scientific aspects investigated, fuels/materials considered and tools available in ITU for PIE and other irradiated fuel studies.

2. INSTALLED POST-IRRADIATION EXAMINATION CAPABILITIES

2.1. Non-destructive testing (NDT)

A γ-shielded cell allows for reception of full length light water reactor (LWR) fuel rods (ITU is not equipped to receive LWR fuel assemblies; only individual rods can be accepted). The cell contains the facilities to perform determination of the variation of the fuel rod diameter (profilometry) as a function of the axial position, visual inspection, outer oxide layer thickness and defects determination using eddy current method, x ray radiography, γ spectroscopy (axial and circumferential scanning). These measurements aim at determining the effects on the fuel rod (cladding and fuel) properties of the specific irradiation history.

Figure 2.1 shows the axial configuration of a fuel pin and the axial γ-scanning profile for a metal alloy, minor actinide fuel pin irradiated in the Phenix reactor to a burnup of ~7 at% as part of the METAPHIX program, a collaboration between the Central Research Institute of Electric Power Industry (CRIEPI, Japan) and ITU devoted to the study of MA-containing fast reactor metal fuels [5]. The total γ ray intensity for the complete wavelength range is measured to determine the axial distribution of γ emitters. Isotopic analysis of different species allows to evaluate distribution and, in some cases, relocation of the γ emitters.

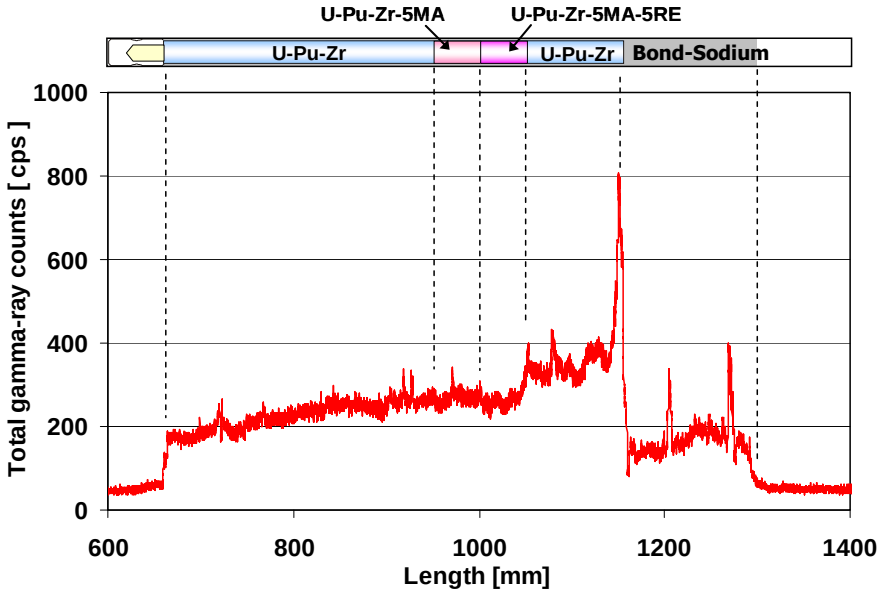

FIG. 2.1. Axial γ–ray scanning on a pin containing metallic alloy fuel U-19Pu-10Zr-5MA-5RE irradiated in the Phenix reactor (CEA) to a burnup ~7 at.% (MA=Np, Am, Cm; RE=Y, Ce, Nd, Gd). METAPHIX project (collaboration ITU-CREPI, with the contribution of CEA). From [5].

In addition to the NDT, in this γ-shielded cell the measurement of fission gas release during irradiation from the fuel to the fuel rod plenum is also performed. Through a tiny hole drilled in the plenum zone, a small aliquot of gas is transferred to a mass spectrometer (situated in a glove box adjacent to the hot cell) for the determination of the isotopic composition of the fission gas.

Finally, in this hot cell are located capabilities for the conditioning of fuel rod remnants in ad hoc sealed capsules that can be transferred back to the reactor storage pool, including TIG-welding and He-leak testing.

2.2. Optical and scanning electron microscopy

Ceramography and microindentation (Vickers) are performed in a shielded glove box connected to a hot cell for sample polishing by a remotely operated transfer tunnel. Figure 2.2(a) and (b) show the cross-sections of a LWR and a fast reactor fuel rod, respectively. The macrographs highlight the main

features characterizing the behaviour of the fuel in the thermal reactor (cracking, gap closure, formation of the high burnup structure at the pellet rim) and those, much more "dramatic", induced in a fast reactor by the high linear power rating and steeper thermal gradients along the pellet radius (pore migration and formation of central hole, columnar, equiaxed and unaltered grain morphology).

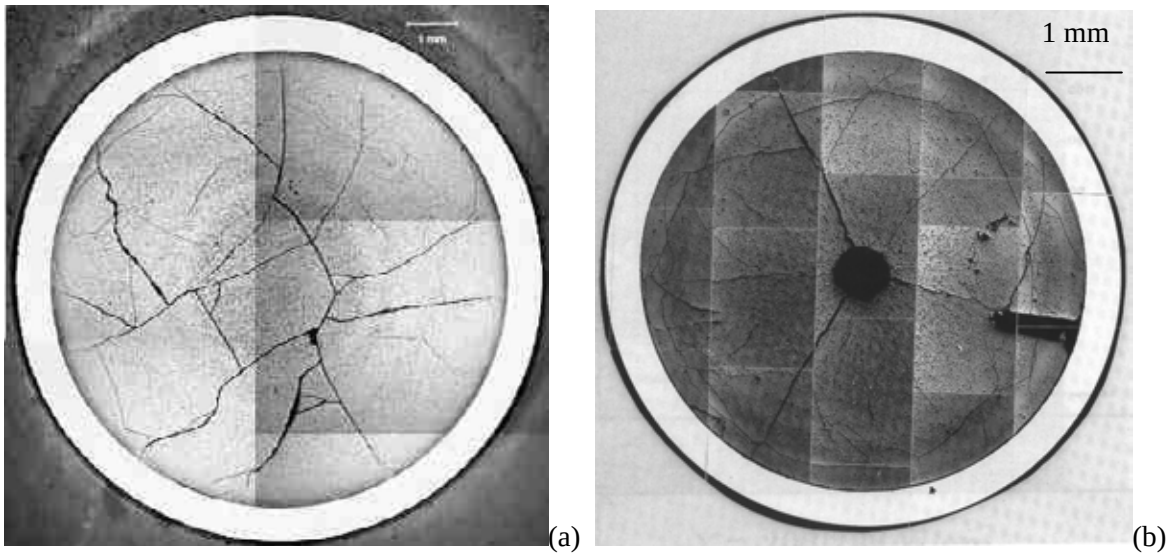

FIG. 2.2. Ceramography of irradiated fuel. Cross-section macrographs of (a) commercial LWR UO_2 with a burnup of ~65 GW·d·t^{-1}; (b) fast reactor minor actinide homogeneous recycling MOX ($U_{0.74}Pu_{0.24}Am_{0.02}$)$O_2$ irradiated to a 6.5% burnup in the Phenix reactor (SUPERFACT program).

Figure 2.3 illustrates aspects of the LWR fuel morphology investigated using SEM. In particular, examples of the occurrence of the high burnup structure [6] in correspondence with the Pu-rich islands in the fuel in MOX (Fig. 2.3(a)), and at the pellet rim in UO_2 (Fig. 2.3(b)) are shown.

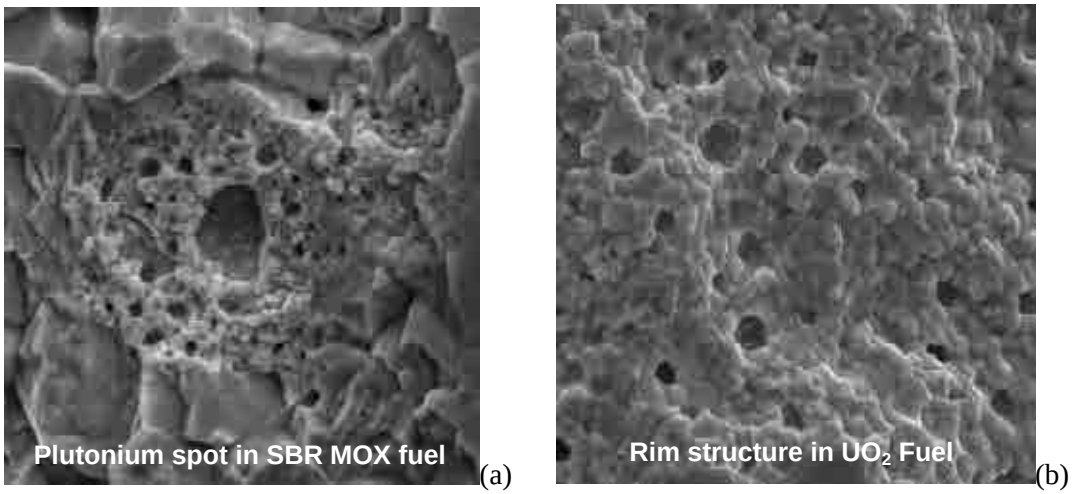

FIG. 2.3. SEM images showing the high burnup structure occurring in commercial LWR fuel: (a) at the Pu-rich areas in MOX fuel; (b) at the radial periphery of the pellet in UO_2 fuel.

The microscopy capability for PIE in hot cell is complemented by an acoustic probe device, which can be used for the quantitative determination of the elastic properties of irradiated fuel and for qualitative bulk characterization of fuel samples. This technique is described in detail in the paper by de Weerd et al. in the present volume [7].

2.3. Density

Irradiated fuel density to characterize the swelling behaviour of fuel as a function of burnup and irradiation conditions is measured by the Archimedes, or immersion, method using calibrated volume samples for the determination of the liquid density and a Mo-standard (nominal density 10.223 $g \cdot cm^{-3}$) for overall calibration of the system; the weight of the immersed specimen is determined in tetrabromo-1,1,2,2-ethane of density 2.963 $g \cdot cm^{-3}$. Figure 2.4 shows the density evolution as a function of burnup and irradiation temperature for UO_2 and $(U,Gd)O_2$ fuel discs irradiated in the Halden reactor in the frame of the High Burnup Rim Project (HBRP) [8–9].

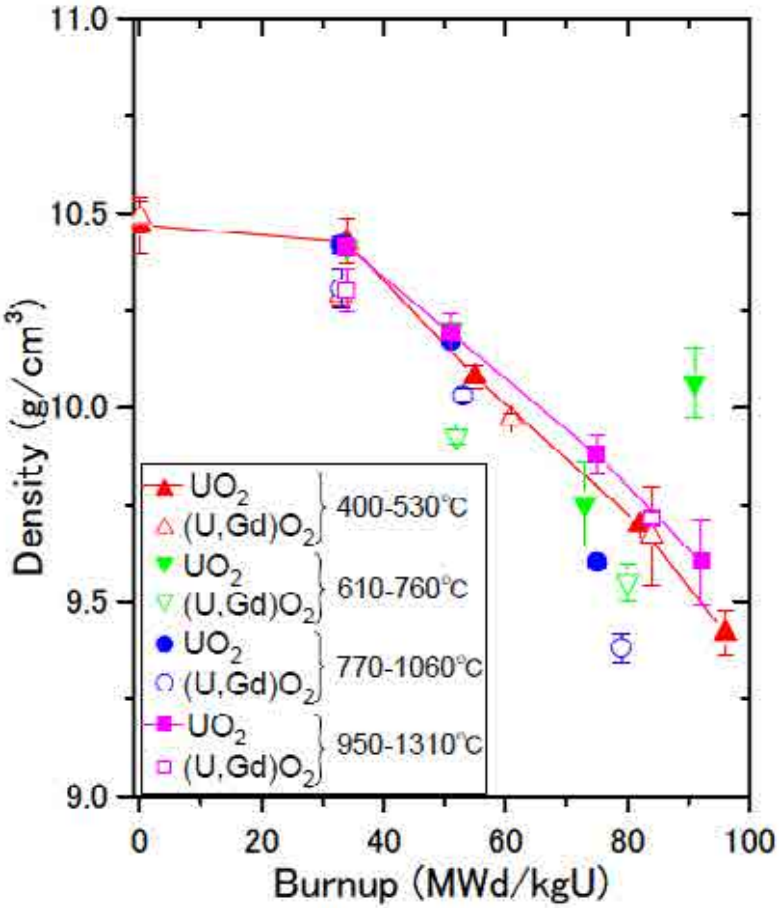

FIG. 2.4. Density of HBRP UO_2 and $(U,Gd)O_2$ fuel disks irradiated in the Halden reactor as a function of burnup and irradiation temperature. From [9].

2.4. Simulated (severe) accident conditions: high temperature release of fission gas and volatiles

The objective of the nuclear fuel safety research is to ensure that under normal operating conditions the fuel operates within relevant safety margins. A fundamental understanding of off-normal, transient and severe accident response of the nuclear fuel is necessary to improve the reactor safety and to minimise probability and extent of any release of radioactive inventory. Experimental data collected in ITU is used to improve computer simulation codes and their predictive capacity and ultimately the design of the nuclear facilities.

The amount and composition of fission gases released to the plenum of the fuel rod during in-pile operation is measured by performing puncture test and mass spectrometry on the released gas. Furnace systems are available for examining the release of fission gas retained in the fuel under different temperature profiles and in various atmospheres. Hot cell thermal annealing up to 1500°C is used to investigate amount and stability of the gaseous fission products under conditions corresponding to transient regimes. High temperature treatments up to 2500°C (either staircase profiles, or rapid ramps)

of irradiated fuel segments (up to 4 cm long) are used to assess the reactions occurring between the fuel, cladding and the structural materials of the reactor during severe accidents. A special furnace operating under inert or reducing atmospheres and combined with mass spectrometer is available for this purpose.

A revaporisation device (see Fig. 1.2) is used to reheat real (irradiated) fission product deposits for determining how easily they can be revolatilised and further transported in various conditions. The samples are heated up to 1000°C in flowing steam and their volatilisation into the steam flow is measured as a decrease of activity by a gamma spectrometer located above the sample in the furnace. After cooling down, the spectrometer can be driven along rails to measure the deposition profile of the revolatilised fission products (mainly Cs) along the condensation tube and how it is distributed along the end filter.

Very valuable high temperature devices and techniques, complementary to he hot cell testing capabilities, are in operation at the materials research laboratories of ITU. In particular, a shielded glove box hosting a Knudsen cell combined with a mass spectrometer constitutes a very effective facility for fission gas release and for vaporization tests of small fragments of irradiated fuel [10]. In addition to samples thermally treated in our facilities, it is worth mentioning that comprehensive analysis and characterization has been performed in ITU on samples coming from real accidents (e.g. Three Miles Island) [11] or from international projects dedicated to this type of events (e.g. the Phebus [12] and COLOSS [13]).

A worldwide unique facility available in ITU is the Kühl Finger Apparat (Küfa), or cold finger apparatus. This is a special furnace designed to host a graphite pebble, i.e. the fuel element of a pebble bed high temperature reactor (HTR) originally developed at the FZA, Jülich (Germany) and subsequently transferred to ITU, where it was installed in hot cell (with some modifications) for testing irradiated fuel pebbles. The furnace can simulate temperature conditions corresponding to loss of coolant accidents in HTR, and is equipped with cold traps to measure the release of fission gases. The name of the device comes from the 'cooling finger', i.e. a condensation plate located just above the fuel element in the furnace. The cold finger is water cooled, and provides a condensation surface for volatile species released from the fuel at high temperature. The cold finger can be replaced during the heating schedule. The loaded plates are then examined by gamma spectroscopy and microscopy. This allows obtaining volatiles and fission gas release curves as a function of temperature and time during the test. Figure 2.5(a) and (b) show an image of the Küfa inside the hot cell and its schematic layout, respectively.

Figure 2.6 illustrates the results of an annealing test performed on a pebble irradiated at the High Flux Reactor (HFR) in Petten (Netherlands) to 9.7% burnup during the K6 irradiation campaign [14]. The results confirm the excellent coated particle retention capability under loss of coolant accident conditions. In fact, the heating schedule applied here represents a conservative case with respect to any possible accident scenario. The first coated particle failure was observed only during the second heating step at 1800°C whereas a small Cs release occurred up to 1700°C (10^{-6} fractional release).

2.5. Mechanical properties determination, testing on irradiated cladding materials

The study of mechanical properties is an expanding field of interest in ITU. Traditionally, most of the mechanical testing performed in hot cell concerns cladding studies, consisting of indentation (see Section 2.2), burst tests under temperature regimes corresponding to operating conditions and creep tests (both short and long term, see e.g. [15]) at temperatures of relevance for dry storage of spent fuel rods. The creep tests are combined and complemented by an eddy current device that can be used on fuel rod segments to detect and characterize the onset of defects in the cladding. This technique is described in detail in the paper by Papaioannou et al. in this publication [16]. The mechanical properties of the cladding are strongly affected by the behaviour of hydrogen picked up by the zircaloy from the water during irradiation, especially the formation and orientation of precipitated hydride phase. Therefore, specific microscopy examination of presence and configuration of the hydride phase

is often performed on irradiated cladding samples. The amount of hydrogen present in the irradiated cladding is measured by hot inert gas extraction.

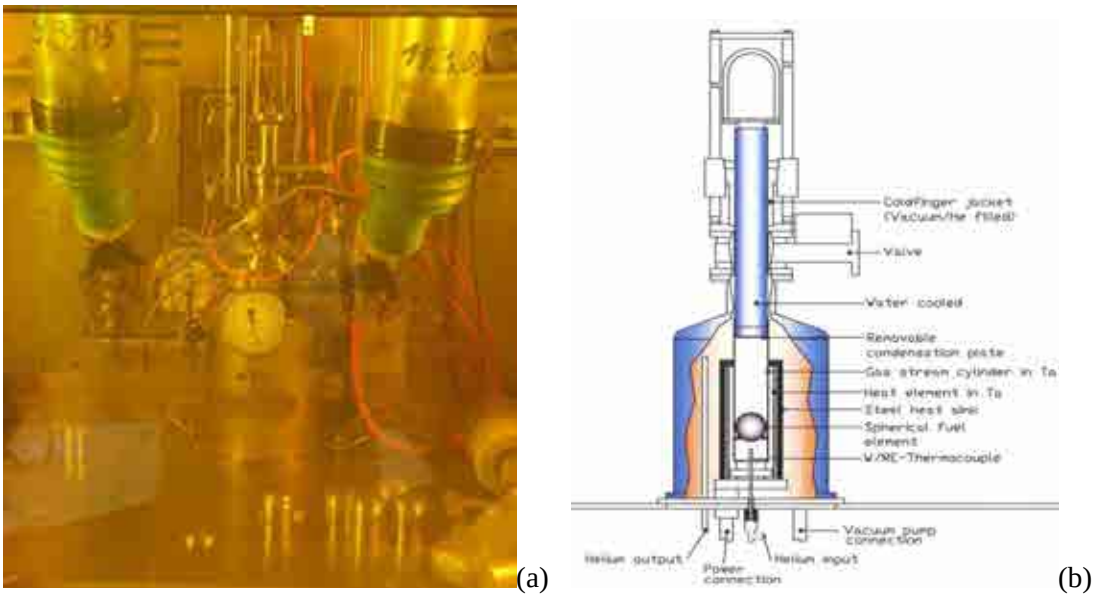

(a) (b)

FIG. 2.5. (a) Image of the Küfa (cold finger apparatus) inside the hot cell; (b) Schematic of the Küfa layout.

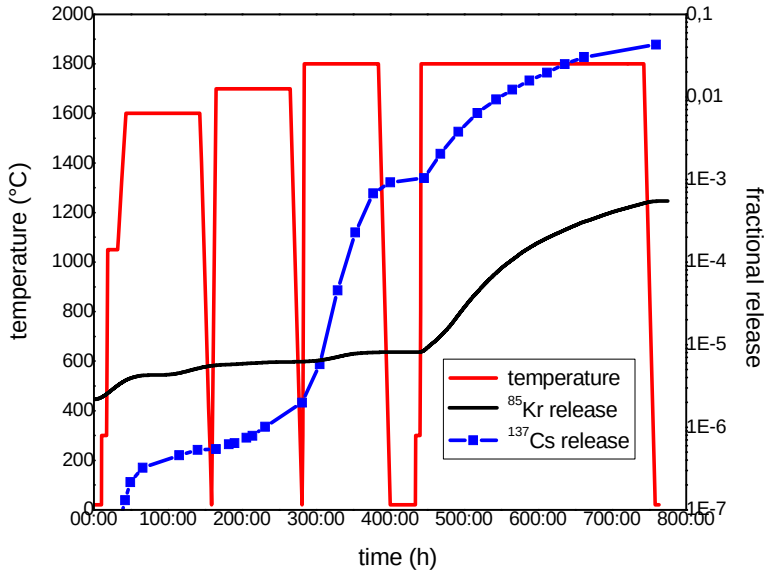

FIG. 2.6. Küfa testing of the HTR fuel element K6/3, irradiated in the HFR to a nominal burnup of 9.7% FIMA. The first Kr-85 release is observed during the second heating plateau at 1800°C, well above the operating temperature of an HTR and also above the maximum temperature normally expected in case of loss of coolant accident. The release of Cs occurs at the same temperature, but during the first plateau, indicating higher mobility of this species through the material. From [14].

The mechanical properties of irradiated fuel are studied with respect of their dependence and evolution as a function of burnup. Since commercial LWR fuels are characterized by strong property gradients across small (radial) distances, a significant part of the activities is related also to the development of appropriated micro-gauge techniques for local property determinations. Most of the data are obtained by micro-indentation and by acoustic determination of the elastic constants of the fuel [7]. The

swelling behaviour and the high burnup fuel properties are important because they govern, together with the mechanical properties of the cladding an in-pile conditions, the pellet–cladding mechanical interaction. Microindentation allowed determining radial hardness and fracture toughness profiles in high burnup fuel, and showed that the formation of the high burnup structure corresponds to a softening of the fuel. This has a beneficial effect on relieving local stresses and allows longer operating times for LWR fuel [17].

The behaviour of the spent fuel rod during dry storage is rapidly becoming a very hot topic. All the countries that have not yet defined a clear disposal/back end strategy for the fuel cycle will have to extend the dry storage duration well beyond the few decades considered so far. This stresses the necessity of producing a robust base of experimental data to predict the behaviour of spent fuel during extended storage (up to a few hundred years), and in particular, the capacity of the spent fuel rod to retain sufficient mechanical strength and stability to allow for handling and transportation after the extended storage time. ITU has developed a set-up to simulate impact accidents during transportation of spent fuel rods. Figure 2.7(a), (b) and (c) illustrates the outcome of this type of tests. The images show photograms collected by a high speed camera which describe the impact and consequent fracture mode of a high burnup fuel rodlet. The experiments performed so far in the frame of collaboration with GNS and AREVA provide a relatively benign picture of this type of events, indicating that the fuel released during an impact failure corresponds only to the volume directly affected by the fracture [18]. Future tests will analyse more in detail the fuel release modes and amounts; it is also foreseen to combine impact tests with accelerated ageing treatment simulating extended storage.

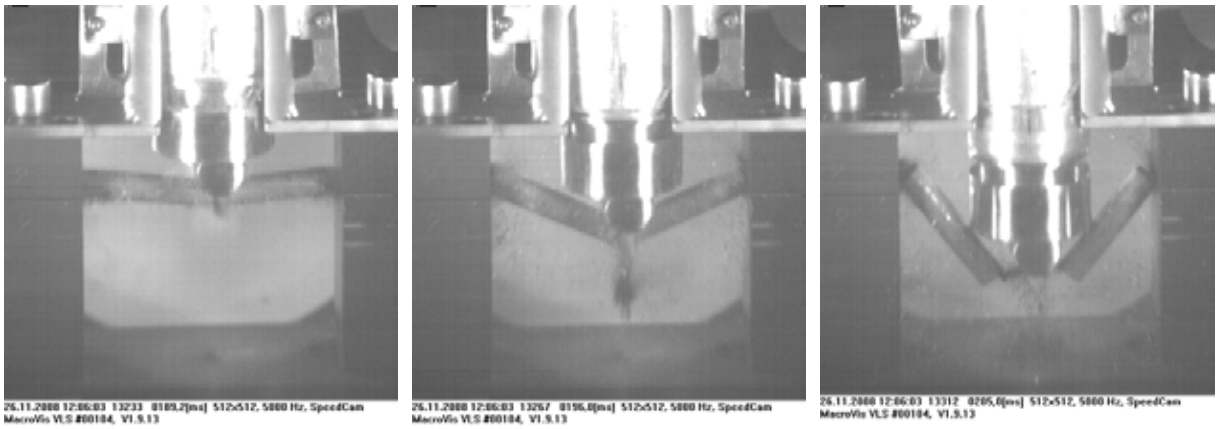

FIG. 2.7. Hammer impacting on a ~74 GW·d·t^{-1} PWR rod (high speed camera sequence). Collaboration ITU-GNS-AREVA. From [18].

2.6. Microanalysis studies on irradiated fuel

A shielded electron probe micro-analysis (EPMA) and a shielded secondary ion mass spectrometry (SIMS) provide extended micro characterisation of irradiated nuclear fuels and materials studied at ITU. The microanalyses are performed on embedded samples prepared for ceramography. Taking advantage of the complementary nature of the two techniques the investigations carried out on irradiated materials provide deeper insight as demanded by modern fuel performance research programs. The quantitative information obtained using EPMA is effectively complemented by the capabilities of the SIMS. Figure 2.8 illustrates the synergy obtainable by combining the two techniques, in this case for the determination of fission gas release retained in the high burnup structure [19]. In the outer radial interval r/r_o is in the range of 0.95–1, where the HBS is present, SIMS measures a steep increase in the concentration of Xe as it detects the gas in the pores (EPMA does not). The fact that the increase in gas concentration measured at the fuel rim by SIMS is greater than the increase in the local burnup suggests that almost all the gas missing from the UO_2 matrix is contained in the pores of the high burnup structure.

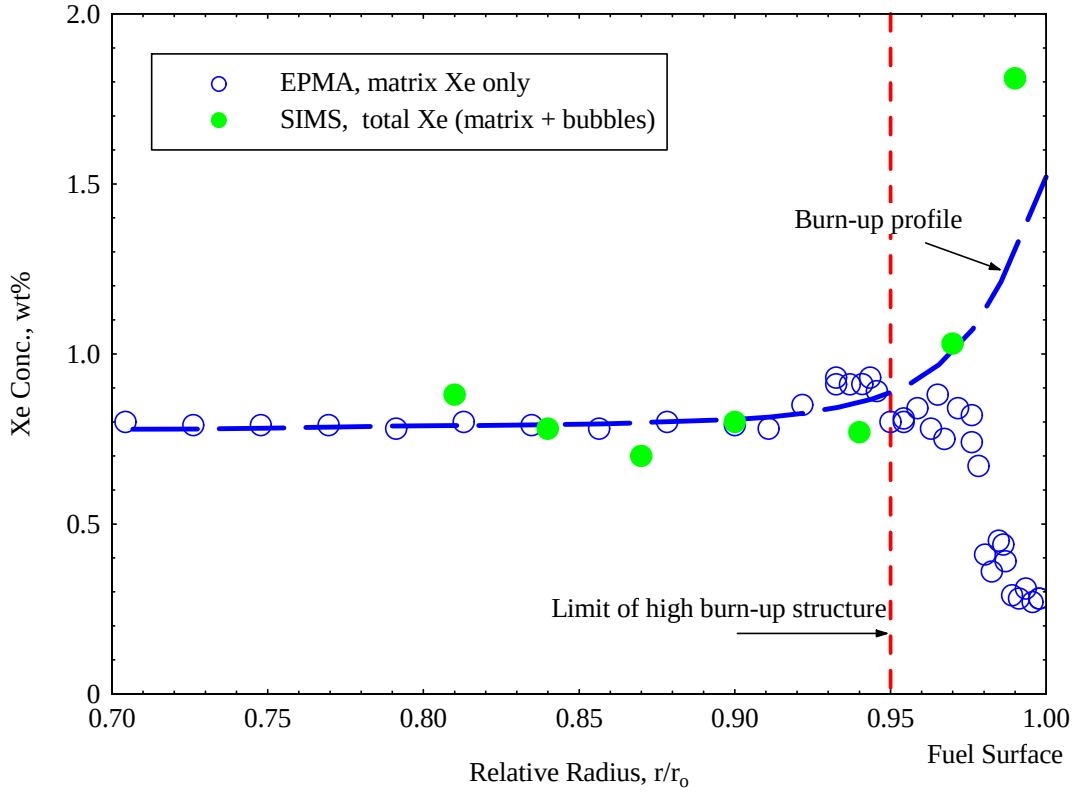

FIG. 2.8. Local concentration of Xe retained in the outer region of a high burnup fuel pellet as measured by SIMS and EPMA. The burnup profile determined from the local concentration of neodymium measured by EPMA is included for the purposes of comparison. From [19].

2.7. Other shielded facilities outside hot cells

For a complete picture of the PIE capabilities in ITU, two additional installations for irradiated fuel studies operating as shielded glove box outside the hot cells have to be mentioned: a shielded laserflash apparatus for thermal diffusivity and heat capacity measurements [20–21] and a transmission electron microscope for microstructure analysis (see e.g. [22]). The combined operation of these with all the above described techniques enables significant synergies and allows producing a full characterization of all major aspects relevant to assess the safety of nuclear fuel concepts under various configurations.

3. OUTLOOK

In order to be able to fulfil ITU's mission with respect to the safety of the nuclear fuel cycle a continuous process of renovation/upgrade/innovation has to be applied to the scientific infrastructures. In parallel, similar effort has to be put in the renovation of the technical/radioprotection support infrastructure, to ensure a continuous, reliable and efficient operation of the facilities in full compliance with relevant, ever developing safety regulation. In particular, a significant degree of flexibility in experimental conditions in hot cell must be achieved to be able to cover effectively fuel compounds and materials with unconventional properties or configurations (e.g. atmosphere control, handling tools and equipment adapted to different geometries, etc.). In the medium term, major renovation has to be planned on the whole half-century old hot cell infrastructure.

With respect to scientific equipment, in addition to the ever improving possibilities offered by new devices and techniques, two main lines of development are worth singling out: on one hand, improving the local resolution of the measurement is necessary to be able to attribute measured property values to a specific region and/or phase occurring in the highly heterogeneous irradiated fuel

system; on the other hand, techniques providing information on the bulk conditions in the fuel are necessary to remove artefacts created by surface preparation procedures necessary for most examination techniques presently available.

Several tools are being installed, planned or under discussion for possible PIE applications in ITU. Among others:

– Universal materials testing device;
– Cone-mandrel set-up for mechanical testing;
– Hot indentation apparatus;
– Focused ion beam;
– Digital microscopy;
– X ray densitometry/tomography applications;
– Furnace system for high temperature corrosion studies (Kora);
– Laser heating based system for melting and vaporization of irradiated fuel in hot cell;
– Raman probe for phase analysis.

4. ACKNOWLEDGEMENTS

The authors are indebted with many colleagues in ITU. In particular, we would like to thank all colleagues in the hot cells unit and also D. Staicu, T. Wiss, J.-Y. Colle, J. Spino, E.H. Toscano. We acknowledge also the contribution of customers and partners that provide the fuel materials for the examinations, in particular W. Goll (AREVA), the High Burnup Rim Project and M. Kinoshita, T. Sonoda, A. Sasahara (CRIEPI).

REFERENCES

[1] JOINT RESEARCH CENTRE, Institute for Transuranium Elements, http://itu.jrc.ec.europa.eu/
[2] EUROPEAN COMMISSION, Joint Research Centre, The European Commission's in-house science service, http://ec.europa.eu/dgs/jrc/index.cfm
[3] EUROPEAN COMMISSION, http://ec.europa.eu
[4] LASSMANN, K., TRANSURANUS. A fuel rod analysis code ready for use, J. Nucl. Mater. **188** (1992) 295–302.
[5] RONDINELLA, V.V., OHTA, H., PAPAIOANNOU, D., OGATA, T., NASYROW, R., KOYAMA, T., GLATZ, J.-P., Characterization of metallic fuel for the transmutation of minor actinides in fast reactor, Proc. ANS Winter Conf. 2009, Washington (2009) Paper 210565, CD-ROM. Trans. ANS **101** (2009) 353–354.
[6] RONDINELLA, V.V., WISS, T., The high burnup structure in nuclear fuel, Materials Today **13** (2010) 24–32.
[7] DE WEERD, W., DESPAUX, G., LAUX, D., KELLERBAUER, A., RONDINELLA, V.V., WALKER, C.T., PAPAIOANNOU, D., AUGEREAU, F., Scanning acoustic microscope: advanced technique for the mechanical characterization of irradiated nuclear fuel, this volume.
[8] KINOSHITA, M., SONODA, T., KITAJIMA, S., SASAHARA, A., KAMEYAMA, T., MATSUMURA, T., KOLSTAD, E., RONDINELLA, V.V., RONCHI, C., HIERNAUT, J.-P., WISS, T., KINNART, F., EJTON, J., PAPAIOANNOU, D., MATZKE, H.J., High burnup Rim project (III). Completed scope and results, Proc. Int. Conf. on LWR Fuel Performance, ANS, Orlando, Fl (2004) 207–213, Paper 1102.
[9] SONODA, T., KAMEYAMA, T., SASAHARA, A., KITAJIMA, A., NAUCHI, Y., KINOSHITA, M., RONDINELLA, V.V., WISS, T., HIERNAUT, J.-P., PAPAIOANNOU, D., SHEINDLIN, M., STAICU, D., et al., Clarification of rim structure effects on properties and behaviour of LWR UO_2 fuels and gadolinia doped fuels, Proc. Int. LWR Fuel Performance Meeting, ANS, San Francisco, CA (2007) 340–346, paper 1026.

[10] CAPONE, F., HIERNAUT, J.-P., MARTELLENGHI, C., RONCHI, C., Mass spectrometric measurements of fission product effusion from irradiated light water reactor fuel, Nucl. Sci. Eng. **124** (1996) 436–454.
[11] BOTTOMLEY, P.D.W., COQUERELLE, M., Metallurgical examination of bore samples from the Three Mile Island, Nucl. Tech. **87** (1989) 120–136.
[12] BOTTOMLEY, P.D.W., BRÉMIER, S., PAPAIOANNOU, D., WALKER, C.T., Microprobe analysis and X-ray diffraction analysis of a degraded fuel bundle: Phebus FPT1, Mikrochimica Acta **139** (2002) 27–38.
[13] BOTTOMLEY, P.D.W., KNOCHE, D., Zircaloy-fuel interactions at high temperatures — preliminary results from the COLOSS program, 8th International Quench Workshop, FZK Karlsruhe, (2002).
[14] FREIS, D., BOTTOMLEY, P.D.W., EJTON, J., DE WEERD, W., KOSTECKA, H., TOSCANO, E.H., Post-irradiation testing of high temperature reactor spherical fuel elements under accident conditions, J. Eng. Gas Turbines Power **132** (2010) 042901.
[15] GOLL, W., SPILKER, H., TOSCANO, E.H., Short-time creep and rupture tests on high burnup fuel rod cladding, J. Nucl. Mater. **289** (2001) 247–253.
[16] PAPAIOANNOU, D., NASYROW, R., NIAGOLOVA, Y., RONDINELLA, V.V., GOLL, W., Eddy current detection of cladding defects due to fuel pellet imperfections, this volume.
[17] SPINO, J., COBOS-SABATE, J., ROUSSEAU, F., Room-temperature microindentation behaviour of LWR-Fuels. Part 1: fuel microhardness, J. Nucl. Mater. **322** (2003) 204–216.
[18] PAPAIOANNOU, D., NASYROW, R., RONDINELLA, V.V., GOLL, W., WINKLER, H.-P., LIEDTKE, R., HOFFMANN, D., Fuel release experiments on irradiated fuel rodlets under transient impact conditions, Proc. Jahrestagung Kerntechnik 2009, Dresden (2009).
[19] WALKER, C.T., BRÉMIER, S., PORTIER, S., HASNAOUI, E., GOLL, W., SIMS analysis of an UO_2 fuel irradiated at low temperature to 65 $MW \cdot d \cdot kg^{-1}$ HM, J. Nucl. Mater. **393** (2009) 212–223.
[20] RONCHI, C., SHEINDLIN, M., STAICU, D., KINOSHITA, M., Effect of burnup on the thermal conductivity of uranium dioxide up to 100000 $MW \cdot d \cdot t^{-1}$, J. Nucl. Mater. **327** (2004) 58–76.
[21] STAICU, D., COZZO, C., PAGLIOSA, G., PAPAIOANNOU, D., BREMIER, S., RONDINELLA, V.V., WALKER, C.T., SASAHARA, A., Thermal conductivity of homogeneous and heterogeneous MOX fuel with up to 44 $MW \cdot d \cdot kg^{-1}$ HM burnup, J. Nucl. Mater. **412** (2011) 129–137.
[22] SONODA, T., KINOSHITA, M., RAY, I.L.F., WISS, T., THIELE, H., PELLOTTIERO, D., RONDINELLA, V.V., MATZKE, H.J., TEM observation on irradiation-induced microstructural evolution in high burnup UO_2 disk fuel, Nucl. Instr. and Meth. in Phys. Res. B, **191** (2002) 622–628.

POST-IRRADIATION EXAMINATION OF FUEL AND CORE STRUCTURAL MATERIALS IRRADIATED IN FAST BREEDER TEST REACTORS

N.G. MURALIDHARAN, C.N. VENKITESWARAN, V. KARTHIK, V. ANANDRAJ, J. JOSEPH, K.V. KASIVSWANATHAN, S. VENUGOPAL, T. JAYAKUMAR, B. RAJ
Indira Gandhi Centre for Atomic Research
Kalpakkam, Republic of India
Email: cnv@igcar.gov.in

Abstract

Performance assessment of various in-core materials of Fast Breeder Test Reactor (FBTR) at Kalpakkam has been carried out in the hot cell facility of Radiometallurgy Laboratory at IGCAR. FBTR uses a unique, indigenously developed mixed uranium–plutonium carbide (U0.3 Pu0.7)C as the fuel and 20% CW SS316 as the material for clad and wrapper. Performance evaluation of carbide driver fuel subassemblies through post-irradiation examination (PIE) at various burnup levels was instrumental in extending the fuel burnup safely to 165 $GW{\cdot}d{\cdot}t^{-1}$ from the initial design burnup limit of 50 $GW{\cdot}d{\cdot}t^{-1}$. Besides the carbide driver fuel assemblies, the irradiation behaviour of various other core materials like the control rod (B4C pellets with stainless steel clad) and the Nickel reflectors have also been investigated. FBTR finds application as a test bed for irradiation experiments of 500 MW(e) Prototype Fast Breeder Reactor (PFBR) fuel and structural materials. Experimental pin with MOX fuel composition of PFBR has been irradiated in FBTR and examined in the hot cells for assessing the evolution of fuelclad gap evolution in the beginning-of-life and optimizing the duration of pre-conditioning of the fuel in PFBR. As a part of life extension studies of FBTR, an irradiation experiment was carried out to study the changes in mechanical properties of grid plate material at low dose irradiation. This paper will discuss the results of PIE carried out for performance assessment of the unique FBTR mixed carbide fuel and structural materials, control rod, nickel reflector subassembly and test irradiations of grid plate specimens and MOX fuel.

1. INTRODUCTION

The Fast Breeder Test Reactor at Indira Gandhi Centre for Atomic Research (IGCAR), Kalpakkam has been in operation since 1985 with a unique high plutonium content carbide fuel ($U_{0.3}Pu_{0.7)}C$ as the driver fuel. The core has been progressively expanded by adding Mark II fuel ($U_{0.45}Pu_{0.55)}C$ and MOX fuel making the core a hybrid one. Performance evaluation of all the in-core materials had been envisaged during the design of FBTR and a series of α-tight hot cells with inert nitrogen atmosphere ventilation was established in the Radio Metallurgy Laboratory (RML) to carry out the post-irradiation examination (PIE) [1]. The concrete shielded hot cells having 1200 mm thick high density concrete wall are designed to handle radioactivity up to 3.7 × 107 GBq. The hot cells have state-of-art equipment for carrying out a wide spectrum of non-destructive as well as destructive metallurgical examinations. The non-destructive techniques employed include visual examination, dimensional measurements, X ray and neutron radiographic examinations, eddy current testing, leak testing and gamma scanning. The destructive examinations include metallography, fission gas extraction and analysis, high temperature tensile tests, micro-hardness, swelling measurements, small specimen test techniques and electron microscopy. Mixed carbide driver fuel and other core structural materials such as the control rod assembly, nickel reflector assembly, etc., discharged from FBTR have been examined in the hot cells. Since FBTR is being used for irradiation testing of advanced fuel and structural materials for the future fast reactors, PIE has an increasing role to play in characterizing their irradiation behaviour and in providing feedback to the designers.

2. PIE OF FBTR MIXED CARBIDE FUEL

2.1. Beginning-of-life performance assessment of carbide fuel

One of the initial concerns of the designers in limiting the linear heat rating and burnup of the FBTR fuel to 250 $W{\cdot}cm^{-1}$ and 50 $GW{\cdot}d{\cdot}t^{-1}$, was the high swelling rate anticipated for the high plutonium content carbide fuel based on the literature data available for carbide fuels up to 30% plutonium.

Hence a series of irradiation tests were done on experimental fuel pins having Mark I & Mark II fuel compositions irradiated to low burnups from 1.6–10 GW·d·t^{-1} (16–100 effective full power days (EFPD)). The aim of the experimental irradiation was to study the fuel swelling and cracking behaviour in the beginning-of-life period.

The fuel pins were subjected to radiographic and ceramographic examinations during PIE. The examinations revealed that the swelling and cracking of the carbide fuel occurs within a few days of irradiation thus reducing the fuel—clad gap and enhancing the gap conductance. Swelling rate was found to be lower for Mark II fuel as compared to Mark I fuel. The feedback from PIE gave confidence to optimize the conditioning period at lower linear power and to increase the linear heat rating of the fuel progressively to 400 W·cm^{-1}.

2.2. PIE of FBTR driver fuel subassemblies

Systematic performance evaluation of fuel and structural materials was carried out at different peak burnups of (25, 50, 100 and 155) GW·d·t^{-1} to understand the irradiation behaviour. FBTR fuel burnup was progressively increased to 165 GW·d·t^{-1} after considering the implications of extending the burnup at each stage. The salient results of the PIE are presented in this section.

2.2.1. Evaluation of fuel performance

Radiographic examination

X radiography of fuel pins were done at different burnup levels to obtain data on the increase in fuel stack length, reduction in pellet-to-pellet gap and pellet-to-clad gap and fuel pellet integrity. In general, evaluation of the radiographs of fuel pins after 25 GW·d·t^{-1} and 50 GW·d·t^{-1}, revealed presence of pellet-to-pellet gaps and pellet-to-clad gaps at the ends of the fuel column. In the case of fuel pins of 100 GW·d·t^{-1} burnup, the pellet-to-pellet gaps and pellet-to-clad gaps were not discernible at the centre of the fuel column, while pellet-to-pellet gap was still observed at the end of the fuel column. The radiography of 155 GW·d·t^{-1} fuel pins indicated the closure of pellet-to-pellet gap and pellet-to-clad gap almost throughout the length of the fuel column. Figure 2.1 shows the X radiographs of the fuel pin of 155 GW·d·t^{-1} burnup. Figure 2.2 shows the trend in the increase in fuel stack length as a function of burnup, expressed in terms of the percentage of the initial fuel stack length (320 mm).

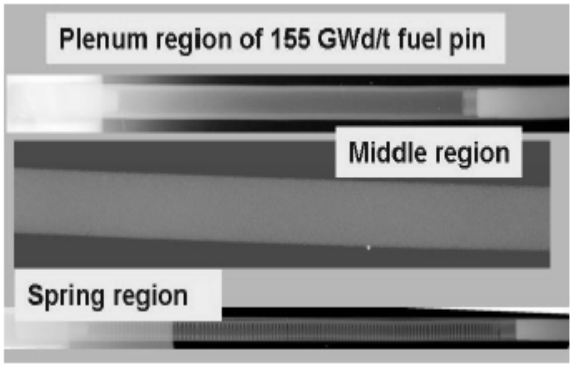

FIG. 2.1. X radiographs of fuel pins after 155 GW·d·t^{-1} burnup.

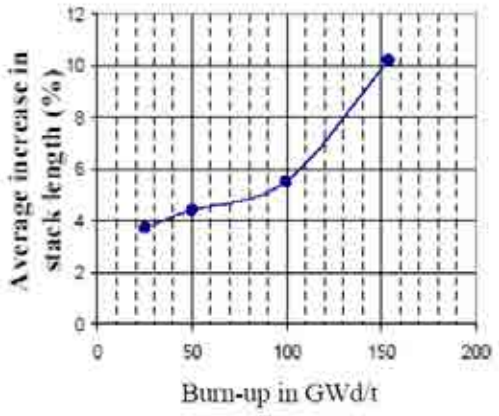

FIG. 2.2. Fuel swelling as a function of burnup.

Neutron radiography of fuel pins [2] at different burnups did not indicate any evidence of actinide redistribution. The fuel stack lengths measured from neutron radiographs compared well with that of the measurements from X radiographs.

Gamma scanning

Gamma scanning has been carried out on FBTR fuel pins which have seen a peak burnup of 100 $GW{\cdot}d{\cdot}t^{-1}$ and 155 $GW{\cdot}d{\cdot}t^{-1}$, to assess the axial fission product distribution. Gamma scanning system inside the hot cell has a precision scanning bench with four axis motorized stages for precise movement of fuel pins with software for automated movement and acquisition of gamma spectrum. Collimators of four different dimensions in the turret assembly established in the hot cell wall facilitate a well defined region of the fuel pin to be seen by the detector. High purity germanium (HpGe) based gamma spectroscopy system was used for gamma scanning.

Axial distribution profile of different fission products was obtained by acquiring gamma spectrum from various locations along the length of the fuel pin. Gamma scanning clearly revealed migration of caesium from the centre of the fuel column. Plenum regions also indicated the presence of caesium. Axial distribution of ruthenium (Ru-106) indicated a smooth profile. Figure 2.3 shows the axial profile of caesium and Ruthenium. Axial flux profile was estimated from the gamma count rates for Ruthenium at various locations of the fuel column and the form factor is around 0.6 which compares well with the reactor physics estimates.

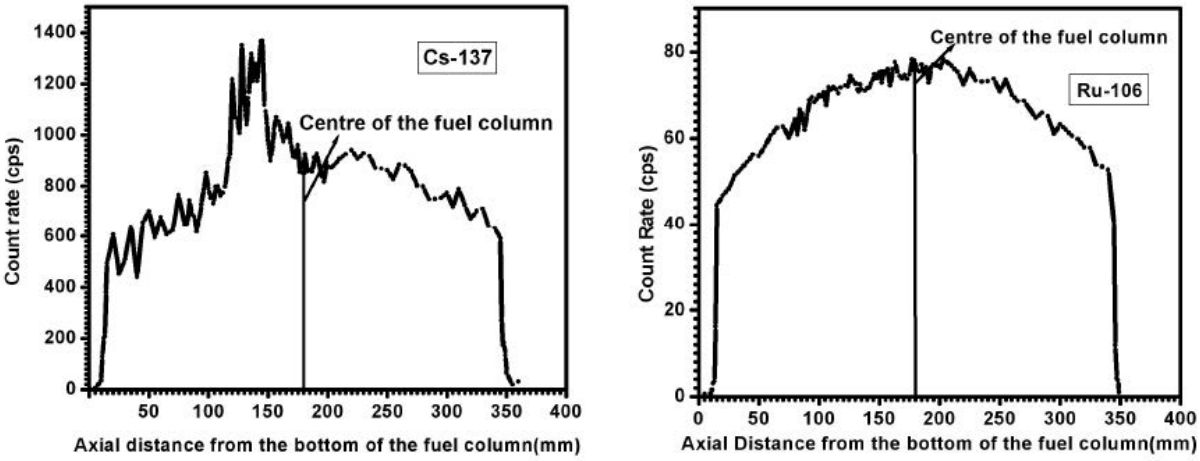

FIG. 2.3. Axial distribution of ruthenium and caesium in the fuel pins.

Fission gas release

Fission gas was extracted by puncturing the fuel pins and the samples were analysed using gas chromatograph. An improved double end fuel pin puncture chamber was used for extraction of fission gas from high burnup fuel pins to facilitate puncturing and collection of fission gas from the top and bottom plenums simultaneously. This was necessitated due to fuel—clad gap closure significantly reducing the communication between the plenum regions.

In 25 $GW{\cdot}d{\cdot}t^{-1}$ burnup fuel pins, fission gas release was found to be less than 1%. In 50 $GW{\cdot}d{\cdot}t^{-1}$ burnup fuel pins, fission gas release varied from 8–18%. Fission gas release measurements after 100 $GW{\cdot}d{\cdot}t^{-1}$ burnup indicated that the gas release is in the range of 4–14% [3]. The lower fission gas release in 100 $GW{\cdot}d{\cdot}t^{-1}$ burnup fuel pins is attributed to the reduction in fuel operating temperatures due to closure of fuel—clad gap. Maximum fission gas release estimated on 155 $GW{\cdot}d{\cdot}t^{-1}$ burnup fuel pins was 16% and the corresponding internal pressure in the fuel pin was measured to be 2.1 MPa. The ratio of xenon to krypton was estimated to be around 13. The helium content in the fuel pins at different burnups indicated that most of the helium produced due to alpha decay is released from the fuel matrix to the gas plenum. Figure 2.4 shows the volume of fission gases released and maximum plenum pressure as a function of burnup.

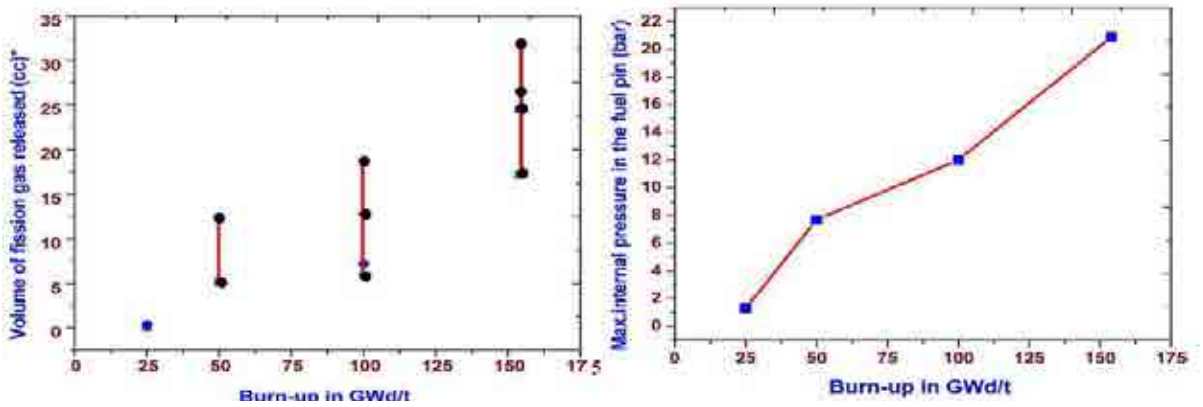

FIG. 2.4. Volume of fission gas released and plenum pressure as a function of burnup.

Ceramography of fuel—clad cross-section

Metallographic examinations of the fuel pin cross-sections at various stages of burnups has provided valuable information on the fuel—clad gap and microstructural evolution of the carbide fuel. Figure 2.5 shows the photomosaics of fuel pin cross-sections at the centre of the fuel column after (25, 50, 100 and 155) GW·d·t^{-1} burnups. Progressive reduction in the fuel—clad gap and radial cracks were observed in 25 GW·d·t^{-1} and 50 GW·d·t^{-1} burnup fuel pins. The fuel—clad cross-section of 100 GW·d·t^{-1} burnup fuel pin revealed absence of the gap at the centre of the fuel column with circumferential cracks whereas the cross-section at the end of the fuel column indicated presence of fuel—clad gap of a few micrometers with radial cracks.

In 155 GW·d·t^{-1} burnup fuel pins, the fuel—clad gap had closed completely along the entire length of fuel column with circumferential cracks in the centre and end of the fuel region indicating initiation of fuel clad mechanical interaction (FCMI). The steep increase in the axial stack length of the fuel column beyond 100 GW·d·t^{-1} burnup measured from X radiographs (Fig. 2.2) is also indicative of the restrained swelling in the radial direction. Exhaustion of porosities was noticed in the outer rim in 155 burnup fuel pin at the centre of the fuel column indicating that the fuel is undergoing hot pressing/creep deformation due to fuel swelling under clad restraint. From the pellet diameters measured by image analysis of photomosaics, the volumetric free swelling rate of fuel was estimated to be around 1.2 at.% burnup at 25 GW·d·t^{-1} and 1 at.% burnup at 50 GW·d·t^{-1} [4].

Microstructural examination of the clad did not indicate any evidence of carburization on the inner diameter of the clad tube. Microhardness measurements across the clad wall thickness also did not indicate any significant change in hardness values. Clad inner and outer diameters were measured from the ceramographs. The maximum increase in cross-sectional area was estimated to be around 6.9% which is in good agreement with swelling measurements carried out on the clad.

2.2.2. Performance assessment of structural materials

Neutron irradiation of core structural materials induces two types of phenomena (i) changes in dimensions associated with swelling and irradiation creep and (ii) degradation of mechanical properties and embrittlement associated with microstructural evolution [5]. The irradiation induced changes in mechanical properties is a function of neutron fluence (dpa) and the irradiation temperature. The typical axial profile of dpa and irradiation temperature along the core length of the fuel pins in FBTR for 155 GW·d·t^{-1} burnup fuel subassembly is shown in Fig. 2.6.

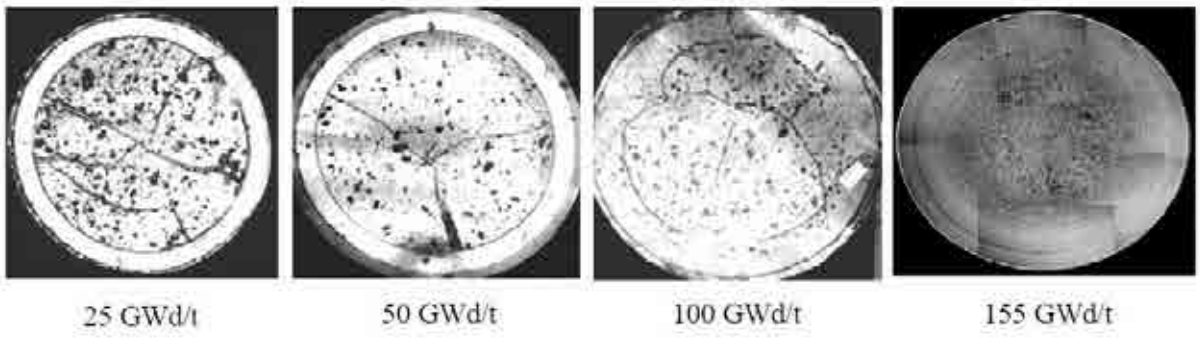

FIG. 2.5. Micrographs of fuel pin cross-sections at the centre of fuel column at various burnup.

2.2.3. Metrology of hexagonal wrapper and cladding

The maximum increase in the dimensions of hexagonal wrapper and fuel pin was seen to occur in the region of peak dpa close to the centre of the fuel column. The trends in the changes in corner-to-corner distance (CCD) and flat-flat distance (FFD) of the wrapper and diametral strain of the fuel pin with dpa are shown in Fig. 2.7. The hexagonal wrapper and the fuel pin did not indicate any increase in their dimensions at low dpa irradiation corresponding to 25 $GW{\cdot}d{\cdot}t^{-1}$ and 50 $GW{\cdot}d{\cdot}t^{-1}$ burnups. Beyond about 30 dpa, the dimensions of both the wrapper and fuel pin were seen to progressively increase with increasing dpa. The rate of increase in the dimensions was higher beyond 100 $GW{\cdot}d{\cdot}t^{-1}$ burnup as compared to that at lower burnups. The maximum percentage increase in the fuel pin dimensions was significantly higher than that of hexagonal wrapper dimensions on account of the higher temperatures of the cladding (Fig. 2.6) close to the peak swelling temperatures of 20% cold worked SS316. Similar trends were also observed in the void swelling estimates of clad and wrapper samples determined from density measurements (Fig. 2.7).

Considering a nominal gap of 0.7 mm between adjacent fuel subassemblies in the FBTR core, the dilation of 0.65 mm of the 155 $GW{\cdot}d{\cdot}t^{-1}$ burnup wrapper is one of the factors of concern, from fuel handling considerations, for further increasing the residence time of the fuel subassemblies.

Mechanical properties of cladding and wrapper

The mechanical properties of irradiated SS316 cladding were determined by remote tensile tests carried out on tube specimens sectioned from various locations along the length of the fuel pins corresponding to a combination of dpa (0–83) and irradiation temperature (430–500°C). The tests were conducted at temperatures corresponding to (i) reactor operation conditions (ii) fuel handling operations (180ºC) and (ii) ambient conditions (25ºC). It was seen that the ultimate tensile strength (UTS) of the cladding shows a significant decrease at displacement damages >60 dpa both in high temperature and room temperature tests, while the uniform elongation was around 3–4.5% (Fig. 2.8). Similar trends of decreasing UTS with increasing dpa have been reported in the literature [6].

The tensile properties of the hexagonal wrapper were evaluated by shear punch tests involving blanking a 1.0 mm thick and 8.0 mm diameter specimen in a test fixture using a flat cylindrical punch. The load displacement plot obtained during the punching operation was analysed and correlated with the conventional tensile test data. Tensile-to-shear punch property correlation was established from standardization experiments on various cold rolled and solution annealed specimens of SS316. Shear punch tests were carried out at room temperature and irradiation temperature on the specimens extracted from wrapper. The results indicate that there is an increase in the yield strength (YS) and the UTS with increasing dpa (Figs 2.9–2.10) and a decrease in the ductility. The tensile properties of the wrapper showed a hardening behaviour as its irradiation temperature is around 400–430ºC.

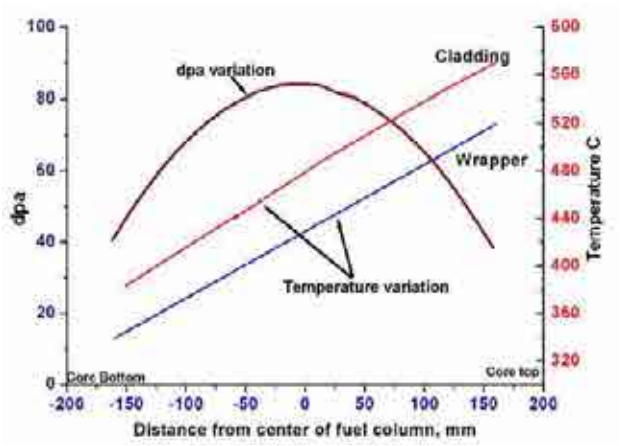

FIG. 2.6. Typical axial profile of dpa and irradiation temperature along the core for the 155 GW·d·t^{-1} burnup fuel subassembly.

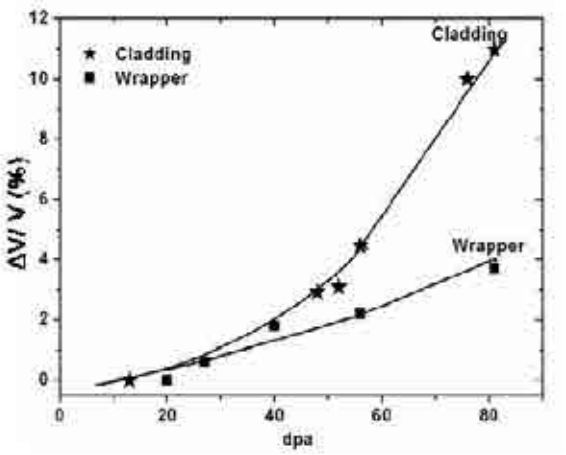

FIG. 2.7. Trends in void swelling of FBTR clad and wrapper with dpa from density measurements.

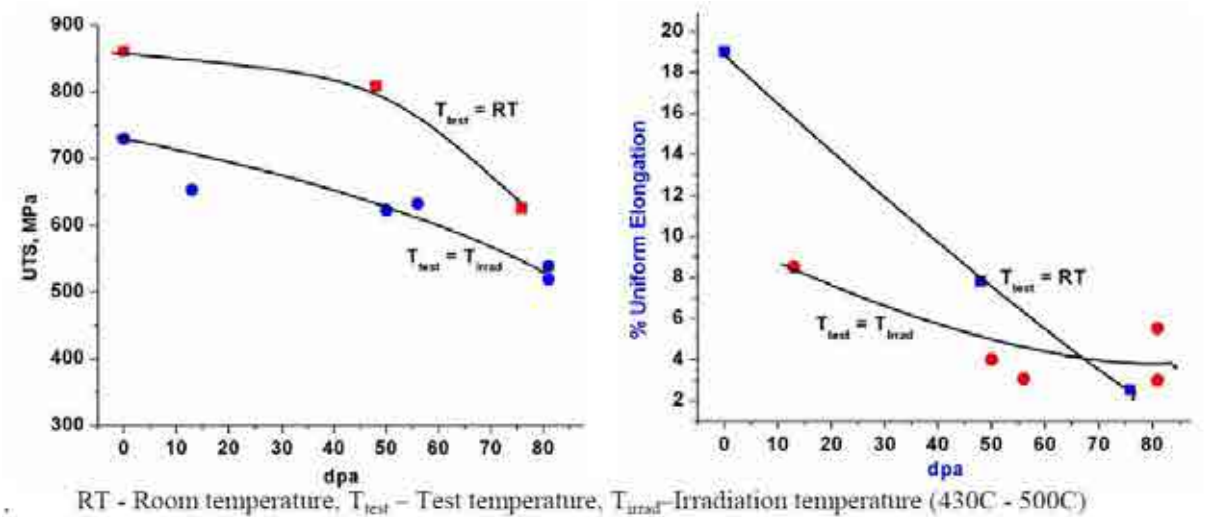

FIG. 2.8. Trends in the UTS and per cent uniform elongation of SS 316 cladding with dpa.

Electron microscopic studies of SS316 cladding and wrapper

Transmission electron microscopy (TEM) studies of hexagonal wrapper showed extensive void formation beyond 40 dpa in addition to precipitation and dislocation loops. Figure 2.11 shows the TEM micrographs at different dpa superimposed on the swelling curve. The void density showed a progressive increase with displacement damage. The precipitates were identified to be mainly of nickel and silicon enriched M6C type of η phase, whereas radiation induced G phase was also observed at 83 dpa. The precipitates were found to be associated with the voids possibly due to the growth of precipitates by diffusion of solutes along with surplus vacancies. The retention of cold worked structure was unambiguously seen even after 83 dpa which suggests that no recrystallisation has taken place and irradiation hardening is more prominent than the softening effects as indicated in tensile properties [7].

To characterize the fracture surfaces of the tensile tested specimens, fractography of the irradiated clad specimens was carried out by extracting the fractured region of the sample and subsequent examination in SEM. Three fracture specimens have been extracted from the tensile tested clad tubes corresponding to dpa levels of 13 dpa, 56 dpa and 83 dpa. Examination of the clad sample exposed to 13 dpa showed features similar to that of un-irradiated cladding. Fracture mode was found to be

ductile with numerous dimples on the fracture surface. Examination of 56 dpa sample showed mixed mode of fracture with predominantly brittle fracture. Faceted surfaces typical of channel fracture reported in irradiated austenitic stainless steel, were observed [8]. Fractography of 83 dpa sample shows completely brittle faceted surfaces. No indication of ductile fracture was observed in 83 dpa sample. Figure 2.12 shows the SEM fractographs of 56 dpa and 83 dpa clad samples. The above observations correlate well with the measured tensile properties of the irradiated clad at different 'dpa' levels.

PIE of FBTR mixed carbide fuel at different burnup levels has indicated excellent performance of the fuel. The burnup limits arising out of various factors such as fuel swelling, porosity exhaustion, metal phase formation, fuel—clad chemical interaction, etc., were thoroughly analysed and it was found that fuel performance is not a life limiting factor. The main limiting factors for further enhancing the burnup were (i) dilation of wrapper and its impact on the fuel handling operations and (ii) loss of cladding mechanical properties. The thermomechanical analysis of the fuel subassembly based on the PIE results indicated possibility of a marginal increase in the fuel burnup beyond 155 $GW \cdot d \cdot t^{-1}$. The burnup of a one representative subassembly has been increased to 165 $GW \cdot d \cdot t^{-1}$.

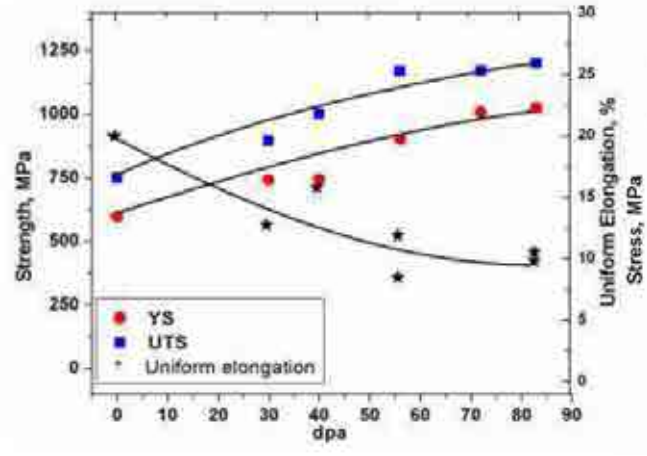

FIG. 2.9. Trends in the room temp. mechanical properties of SS316 wrapper as a function of 'dpa'.

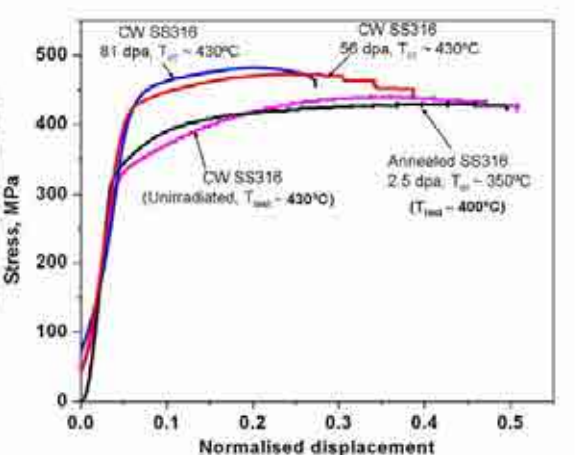

FIG. 2.10. Stress-normalised displacement plots of high temperature shear punch tests on wrapper.

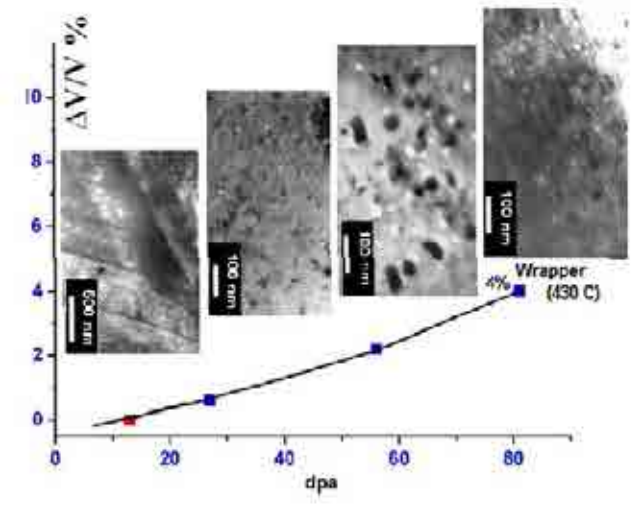

FIG. 2.11. TEM micrographs of SS316 wrapper at various dpa superimposed on swelling curve.

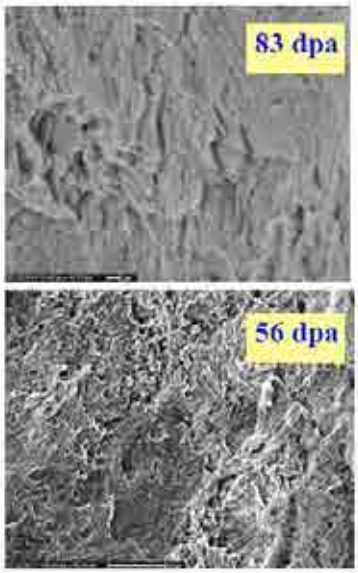

FIG. 2.12. SEM fractographs of irradiated cladding after 56 dpa and 83 dpa.

3. POST-IRRADIATION EXAMINATION OF CONTROL ROD ASSEMBLY OF FBTR

FBTR has six control rod assemblies with sintered boron carbide pellets (90% enriched in ^{10}B isotope) inside SS316 cladding. One of the control rods was discharged after subjecting to a fluence level of 7.0×10^{22} n·cm^{-2} to assess its irradiation behaviour and to investigate the cause of excessive load encountered during raising of control rod beyond a particular axial position. It was also required to assess the swelling behaviour of boron carbide (B_4C) pellets since volumetric expansion is one of the life limiting factors of the control rod [9]. The control rod is of vented type design having nine boron carbide pellets stacked to a length of 430 mm inside the cladding. It moves axially inside an hexagonal sheath made of SS316 during raising/lowering and the interfaces have stellite coating/tracks. The design fluence limit of FBTR control rod is 1.14×10^{23} n·cm^{-2}.

Examinations carried out on the control rod assembly include precise dimensional measurements to investigate the possibility of interference between the control rod and the outer sheath which can result in excessive load, neutron radiography and X radiography to assess the integrity of the boron carbide pellets and other internals of the control rod, density measurements to assess the swelling behaviour of boron carbide pellets and metallographic examinations to study the cracking behaviour and microstructural changes in the pellet and the clad. Laser ablation mass spectrometry was done to estimate the depletion of ^{10}B in the pellets.

Dimensional measurements did not indicate any significant changes in the outside diameters of the control rod or the inner diameters of the stellite tracks of outer sheath. Minor misalignments of the order of 1.01 mm and 0.83 mm were observed in the axes of the control rod and the outer sheath. This could have led to the interference between them during raising of power when the shoulder region of the control rod begins to enter the top stellite track of the outer sheath.

Neutron radiography revealed that control rod internals are intact without any blockages which can restrict coolant flow (Fig. 3.1). No gross depletion of ^{10}B was observed. Extensive cracking and fragmentation were observed in the X radiographs particularly in the bottom pellets which have been exposed to higher neutron fluence. Figure 3.2 shows the X radiographs of the boron carbide pellets inside the control rod. X radiographs did not indicate any significant change in dimensions of the pellets.

FIG. 3.1. Neutron radiographs of the bottom portion of control rod showing support sleeve, insulation pellet and boron carbide pellet.

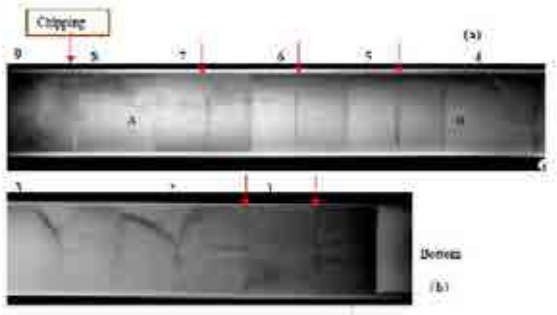

FIG. 3.2. X radiographs of B4C pellets in the control rod (a) top portion, (b) bottom portion.

The control rod was cut using laser beam on a dismantling bench to retrieve the pellets from the clad. Infiltration of sodium was observed within the fragmented pellets in the bottom region. Extraction of bottom pellets was difficult due to the expansion of the pellet by the presence of frozen sodium within the fragments.

Maximum volumetric swelling of around 2% was estimated from the density measurements of the pellets. Ceramographic examination of three pellets each from the top, middle and bottom regions of

the pellet column showed extensive cracking of the bottom pellet. No significant change in the microstructure was observed in the three pellets examined. Metallographic examination of the control rod cladding was carried out to study the interaction of boron carbide pellet and the cladding. The microstructure of the clad cross-section did not indicate any significant interaction between the boron carbide pellet and stainless steel cladding, revealing absence of absorber-clad chemical interaction as observed by optical microscopy.

The isotopic ratio of $^{10}B/^{11}B$ was determined using Laser ablation mass spectrometer. The mass spectrum clearly revealed the presence of ^{7}Li in the irradiated pellets confirming the consumption of ^{10}B. However, ^{10}B depletion in all the pellets was found to be less than 1%.

PIE of control rod assembly has provided valuable information regarding the dimensional changes in the control rod, pellet integrity, swelling behaviour and B10 depletion in B4C pellets. It has been concluded that the excessive load encountered during raising of the control rod could be due to the marginal interference between control rod and outer sheath. Pellet integrity assessment indicated that due to extensive cracking and fragmentation, it may not be possible to reuse most of the pellets. The PIE has clearly indicated that the boron carbide pellets and the structural materials have not reached life limiting conditions.

4. PIE OF FBTR NICKEL REFLECTOR SUBASSEMBLY

One nickel reflector subassembly was discharged from the 4th ring of FBTR core after attaining a fluence level of 1.09×10^{23} n·cm^{-2}. The design fluence limit for nickel subassembly is 1.14×10^{23} n·cm^{-2}. Nickel subassembly was subjected to PIE to assess the swelling of the nickel blocks, condition of the collapsible tube inside the nickel subassembly and the radial gap between the nickel blocks and he hexagonal wrapper. It is well known that neutron induced swelling is higher in high purity nickel than that of nickel with impurity content [10]. Nickel blocks used in FBTR reflector subassembly have an impurity content of 0.6%.

PIEs carried out on the nickel subassembly include non-destructive examinations such as neutron radiography and gamma autoradiography to examine the internals of the nickel subassembly such as the collapsible tube and the spacing between the hexagonal wrapper and the nickel blocks. Dimensional measurements were done on the hexagonal wrapper and the nickel blocks after dismantling the subassembly and retrieving them from the wrapper. Volume and density of the nickel blocks were measured to estimate the irradiation induced swelling.

Neutron radiography has indicated that the collapsible tube has undergone deformation due to axial expansion of the nickel blocks (Fig. 4.1). Interior of the subassembly was found to be free of sodium and the nickel blocks could be retrieved without any difficulty. Dimensional measurements on the nickel blocks have revealed that the radial gap between the blocks and the hexagonal wrapper has reduced from 3–2 mm. Total axial expansion of the nickel blocks has been measured to be 7 mm. This has been confirmed from gamma autoradiography of the head portion of the subassembly. Density measurements carried out on the nickel blocks have indicated that the maximum volumetric swelling is of the order of 3.6%. This correlates well with the dimensional measurements. Figure 4.2 shows the density variation in the nickel blocks.

PIE of the nickel reflector subassembly has indicated that radial gap is still available between the nickel blocks and the hexagonal wrapper and enough margin is available for accommodating axial expansion of the nickel blocks. The life of other nickel reflector subassemblies in the core can be extended further without any concern regarding the mechanical interaction between the nickel blocks and the wrapper.

FIG. 4.1. Neutron radiograph of nickel subassembly showing the collapsible tube.

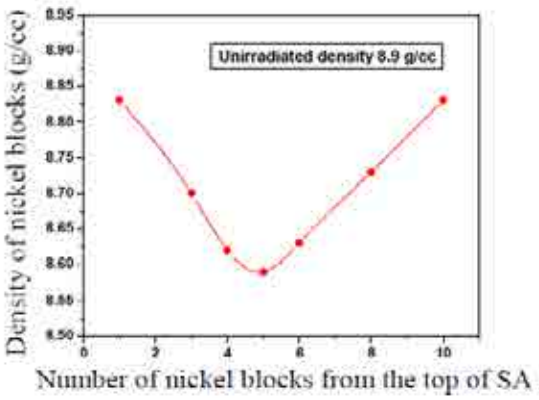

FIG. 4.2. Density variation in the nickel blocks.

5. BEGINNING-OF-LIFE GAP CLOSURE BEHAVIOUR OF EXPERIMENTAL PFBR MOX FUEL PIN

The Protoype Fast Breeder Reactor (PFBR) will use mixed oxide fuel with two different PuO_2 compositions, 21±1% and 28±1% for the two enrichment zones. The fuel pellets are of annular type designed to operate at a peak linear heat rating (LHR) of 450 $W \cdot cm^{-1}$. However, the fabrication tolerances in the fuel pellet dimensions may result in higher fuel—clad gap resulting in lower gap conductance. To limit the central line temperature within the permissible limits, linear heat rating of fresh fuel will be limited to 400 $W \cdot cm^{-1}$ in the initial phase. Subsequent to the restructuring of the pellet by swelling and cracking and resulting improvement in the gap conductance, LHR will be enhanced to the rated power of 450 $W \cdot cm^{-1}$.

To evaluate the beginning-of-life gap-closure behaviour and to arrive at the optimum duration of preconditioning of fresh fuel, an experimental MOX fuel pin of PFBR fuel composition $(U_{0.71}\ Pu_{0.29})O_2$ was irradiated in FBTR for a duration of 13 days in an irradiation capsule at a maximum linear power of 400 $W \cdot cm^{-1}$. This fuel pin has a fissile column length of 240 mm. The fuel pin was extracted from the capsule in the hot cells, sectioned at five axial locations along the length of the fuel column and remote metallography was carried out on these sections.

Fuel-clad radial gap was estimated from the metallographic images at six circumferential locations in the fuel—clad cross-sections. The average radial gap was calculated and compared with that of the unirradiated fuel pin. The typical photomosaic of the fuel pin cross-section at the centre of the fuel column (120 mm from the top of the fuel column) is shown in Fig. 5.1. The photomicrograph shows the presence of a few radial cracks. Polished fuel cross-section was chemically etched for microstructural examination. Fig. 5.2 shows the microstructure having evidence of grain growth in the intermediate zone of the pellet.

PIE has revealed that the fuel—clad gap has reduced considerably from the pre-irradiation radial gap of around 75–110 micrometers to around 13 micrometers throughout the fuel column length after irradiation for 13 days. Cracking of the pellets and relocation of the fuel has resulted in reduction of the fuel—clad gap. The early closure of the fuel—clad gap is a valuable feedback indicative of the optimum preconditioning period required for the fresh fuel before enhancing the LHR to the design value.

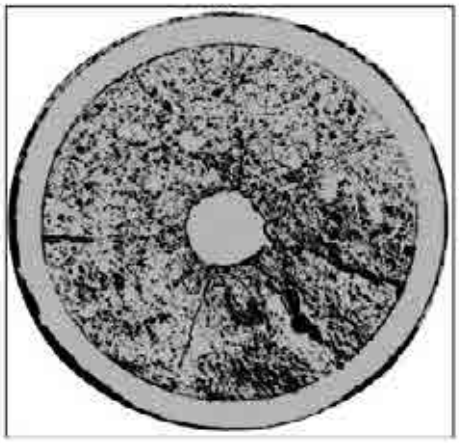

FIG. 5.1. Photomosaic of MOX fuel pin cross-section at the centre of the fuel column.

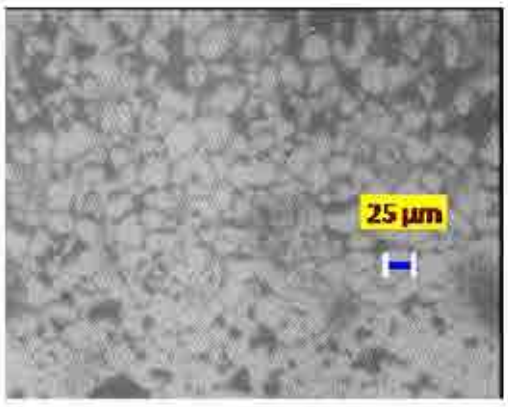

FIG. 5.2. Microstructure of MOX fuel pin.

6. MECHANICAL PROPERTY EVALUATION OF FBTR GRID PLATE MATERIAL

FBTR has been in operation for more than 25 years. As a part of the life extension programme of the FBTR, an assessment of the irradiation induced degradation of FBTR grid plate was undertaken. The performance of the grid plate which supports the core subassemblies is one of the factors considered for extending the life of FBTR. The grid plate of FBTR (SS316) operating at a temperature of about 350°C experiences a cumulative neutron dose of a few dpa over its lifetime. An accelerated rradiation experiment was performed in FBTR to characterize the mechanical property changes of the SS316 grid plate material subjected to low dose irradiation.

The experimental subassembly used for this test consisted of an irradiation capsule with five compartments in which prefabricated miniature tensile and disc specimens of FBTR grid plate material (SS316) were stacked. The experimental assembly was irradiated in the 4th ring of FBTR for a duration of 58.18 EPFD. The temperature of the irradiation was around 350°C and the accumulated displacement damage ranged from about 1.08 dpa (displacement per atom) to a maximum of 2.57 dpa at the center of the capsule.

The irradiated experimental subassembly was received in hot laboratory (RML) and dismantled using laser cutting to retrieve the irradiated tensile and disc specimens. Remote tensile tests were carried out on the irradiated tensile specimens at temperatures of 25°C, 350°C and 400°C using a universal testing machine installed in the hot cells. As conventional or readily available grips did not exist for ambient/elevated temperature tests of miniaturized tensile specimen (12.7 mm gage length, 3 mm gage width, 1 mm thick), considerable efforts went into development of miniaturized wedge type grips and accessories for carrying out the remote tensile tests.

The stress–strain curves of the irradiated SS316 tested at 350°C are shown in Fig. 6.1. It can be seen that the irradiated SS316 undergoes an increase in YS and UTS with respect to the unirradiated values for all the dpa conditions. Up to 1.08 dpa, this hardening results in negligible changes in uniform elongation (UE). Above 1.08 dpa, the increase in YS is considerably higher than the increase in UTS. The narrowing of the difference between YS and UTS with increase in dpa results in the reduction of uniform elongation to about 20% for the specimen irradiated to 2.57 dpa. The trends in the YS, UTS and per cent UE of irradiated SS316 tested at 350°C are shown in Fig. 6.2. These results are consistent with the results of irradiated SS316 reported in the literature [11]. The effect of low dose neutron irradiation on the material properties is considered in the design standard of FBR structural materials by limiting the accumulated neutron irradiation to maintain ductility above 10%. A uniform elongation of above 20% at test temperatures of 28°C, 350°C and 400°C of SS316 indicates retention of adequate ductility in SS316 grid plate of FBTR for an accumulated fast neutron dose of 2.57 dpa.

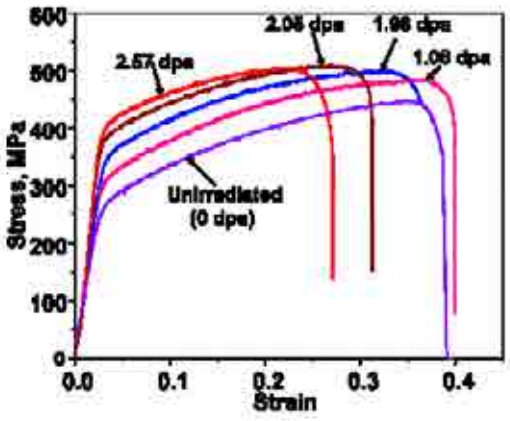

FIG. 6.1. Stress–strain curves of SS316 irradiated to various displacement damages and tested at 350°C.

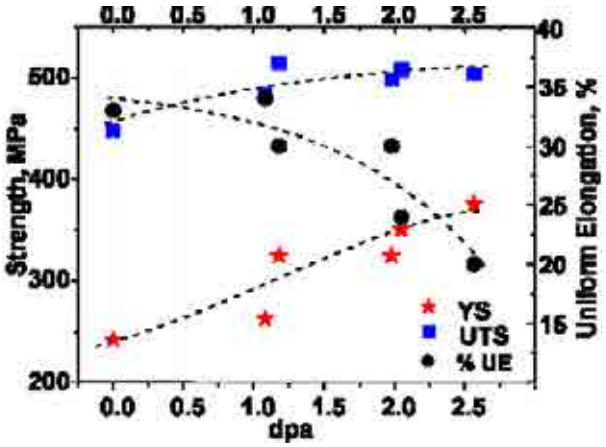

FIG. 6.2. Trends in YS, UTS and per cent UE of irradiated SS 316 tested at 350°C as a function of dpa.

7. SUMMARY

The stage wise performance assessment of the plutonium rich mixed carbide fuel of the Fast Breeder Test Reactor (FBTR), starting from beginning-of-life performance studies and subsequently at various stages of burnup has led to a comprehensive understanding of the fuel and structural material irradiation behaviour. Compared to the initial design limit of 50 $GW{\cdot}d{\cdot}t^{-1}$, the burnup reached 165 $GW{\cdot}d{\cdot}t^{-1}$ for the plutonium rich mixed carbide fuel. PIE has thus played a crucial role in validating the design and choice of the unique fuel material of FBTR, thereby increasing its in-reactor life. Besides the driver fuel assembly, the performance evaluation of various other core materials like the control rod subassembly and nickel reflector subassembly has provided valuable information on swelling and dimensional changes under fast neutron irradiation. Mechanical property evaluation of grid plate material has provided crucial feedback for the life extension programme of FBTR. PIE inputs from the examination of PFBR MOX fuel will be significant for the economical operation of PFBR.

8. ACKNOWLEDGEMENTS

Authors gratefully acknowledge the guidance and support of S.C. Chetal, Director, IGCAR, during the course of the reported work. The contributions of the colleagues from various groups such as reactor design, reactor operations, physical metallurgy and the chemistry group of IGCAR and Radiometallurgy Division, BARC are also acknowledged.

REFERENCES

[1] BALDEV, R., et al., ”Post-irradiation examination of mixed (Pu, U)C fuels irradiated in the fast breeder reactor”, Influence of High Dose Irradiation on Core Structural and Fuel Materials in Advanced Reactors, IAEA-TECDOC-1039, IAEA, Vienna (1998) 57–68.

[2] KASIVISWANATHAN, K.V., VENKATRAMAN, B., RAJ, B., Neutron radiographic facilities available with KAMINI, Proceedings of 6th World Conference on Neutron Radiography, (Ed. Shigenori Fujine, Hisao Kobayashi and Keiji Kanda, Gordon) Breach Science Publishers, Tokyo (1999) 117.

[3] KASIVISWANATHAN, K.V., MURALIDHARAN, N.G., VIJAYARAGHAVAN, A., JOSEPH, J., VENUGOPAL, V., KASIVISWANATHAN, K.V., Estimation of fission gas release in FBTR fuel pins, Int. Journal of Nuclear Energy Science and Technology. **2** (2006) 352.

[4] MURALIDHARAN, N.G., VENKITESWARAN, C.N., KARTHIK, V., MANOJKUMAR, P.A., SOSAMMA, S., RAO, S.B., VENUGOPAL, V., KASIVISWANATHAN, K.V., Remote metallographic examination of mixed carbide fuel of Fast Breeder Test Reactor at Radio Metallurgy Laboratory, Int. Journal of Nuclear Energy Science and Technology, **1** (2005) 191.

[5] GARNER, F.A., Irradiation performance of cladding and structural steels in liquid metal reactors, in Nuclear Materials, Part 1, Materials Science and Technology, Vol. 10A, (Eds. Frost B.R.T), VCH Publishers (1993) 420.

[6] POROLLO, S.I., KONOBEEV, Yu.V., GARNER, F.A., Swelling and microstructure of austenitic stainless steel ChS-68 CW after high dose neutron irradiation, J. Nucl. Mat. **393** (2009) 61.

[7] VENKITESWARAN, C.N., KARTHIK, V., PARAMESWARAN, P., MURALIDHARAN, N.G., RAJ, V.A., SAROJA, S., VENUGOPAL, V., VIJAYALAKSHMI, M., KASIVISWANATHAN, K.V., RAJ, B., Study of microstructure and property changes in irradiated SS316 wrapper of Fast Breeder Test Reactor, ASTM STP 1513 (2010) 196–209.

[8] HUANG, F.H., The fracture characterization of highly irradiated type 316 stainless steel, International Journal of Fracture **25** (1984) 181–193.

[9] INTERNATIONAL ATOMIC ENERGY AGENCY, Absorber Materials, Control Rods and Designs of Shutdown Systems for Advanced Liquid Metal Fast Reactors, IAEA-TECDOC-884, IAEA,Vienna (1995).

[10] HOLMES, J.J., Irradiation induced swelling in nickel alloys, Transaction of American Nuclear Society, Vol. 12 (1969) 117.

[11] TAVASSOLI, A.A., PICKER, C., WAREING, J., Data collection on the effect of irradiation on the mechanical properties of austenitic stainless steels and weld metals, Effect of Radiation on Materials, ASTM STP 1270 (1996) 995.

STATUS AND ACTIVITIES OF POST-IRRADIATION EXAMINATIONS ON NUCLEAR FUEL IN THE NUCLEAR POWER INSTITUTE OF CHINA

G. LI, M. FENG, F. WANG
Hot Laboratory
Nuclear Power Institute of China,
China
Email: fengmq1@163.com

Abstract

Development and status of hot laboratory in Nuclear Power Institute of China was presented. Main activities of post-irradiation examination on nuclear fuels, including testing fuel bundles for PWRs and dispersion fuels for research reactors were also generally described.

1. INTRODUCTION

Nuclear Power Institute of China (NPIC) was a research center for PWRs in China. Two research reactors were operated by NPIC, one of which, was the High Flux Engineering Test Reactor (HFETR, Figs 1.1–1.2). Since 1980, HFETR was in operation for more than 30 years. Various kinds of testing fuel assemblies have been irradiated, and, then examined in hot laboratory. An overview of activities and an status of those post-irradiation examinations (PIEs) is briefly presented in this paper.

FIG. 1.1. Main building of HFETR.

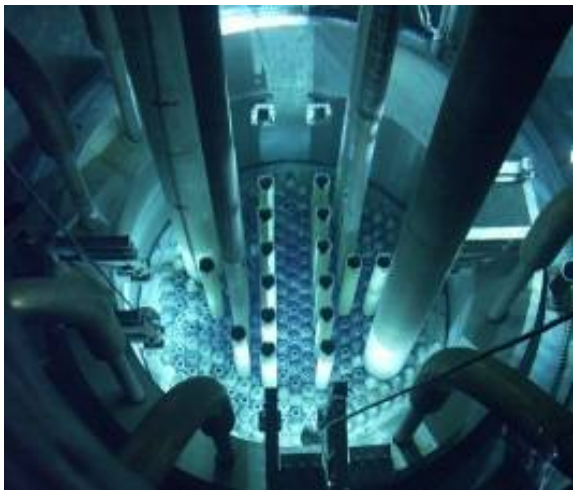

FIG. 1.2. Reactor core of HFETR.

2. HOT LABORATORY

A complex of hot cells was built just aside the HFETR during same period of construction. Two lines on the second floor were used for PIE of fuels (Fig. 2.1), which is connected with the spent fuel pool of HFETR by an underwater transfer channel. A line of semi hot cell on the first floor (Fig. 2.2) was used for mechanical testing of reactor structure material. From 2006–2011, two rounds of refurbishments and upgrading of hot cell facilities were performed. The main capacity of the hot laboratory is listed in Table 2.1.

FIG. 2.1 Hot cells for dismantling and NDT.

FIG. 2.2. Semi-hot cells for mechanical testing.

TABLE 2.1. MAIN CAPACITY OF THE HOT LABORATORY

Majority	Items
Physical analysis	Metallurgical analysis（OM), SEM, EDS, corrosion, differential scanning calorimeter (DSC), high temperature annealing, density measurement.
Mechanical testing	Tensile testing, pendulum impact testing, drop-weight impact testing, compression testing, low cycle fatigue, fracture toughness, bend testing, microhardness testin, burst testing.
Non destructive testing	Visual inspection（VT), X ray and γ ray testing（RT), ultrasonic testing (UT), leakage testing (LT), penetration testing（PT), eddy current testing（ET), profilometry measurement.
Radiochemical analysis	Water chemistry analysis, burnup determination, isotope separation.

3. POST-IRRADIATION EXAMINATIONS ON FUELS

3.1 Disassembly of fuel elements

For the disassembly of irradiated fuel assemblies, 2 miller and 1 laser cutting machines were deployed in 3 hot cells respectively. A small cutting saw was also used for precious sampling.

3.2 Visual examination

Visual examination was performed in the spent fuel pool and hot cell respectively. Surface conditions, such as obvious deformation, defects, damage could be determined (Fig. 3.1). Water proof and radiation resistance cameras were used in most occasions.

3.3 Profilometry measurement

Deformation and curvature of fuel elements were measured in hot cell with a remote controlled 3-D coordinator machine. Also a LVDT apparatus and a laser beam device were used to measure the variation of fuel rod diameter (Fig. 3.2).

3.4 X ray radiography

X ray radiography was used as a non-destructive testing to inspect the defects, uniformity and structural integrety of fuel elements (Fig. 3.3). The X ray generator can reach high voltages up to 450 kV.

3.5 Γ profilometry scanning

Relative burnup distribution of fuel elements was measured by γ profilometry scanning. ^{137}Cs was used as the monitoring isotope for counting. Axial distribution of burnup of a HFETR fuel elements is shown in Fig. 3.4. Due to tubular structure and core loading of HFETR, the outer fuel tube reached high burnup, and lowest burnup corresponding to 3rd tube which was in the middle layer.

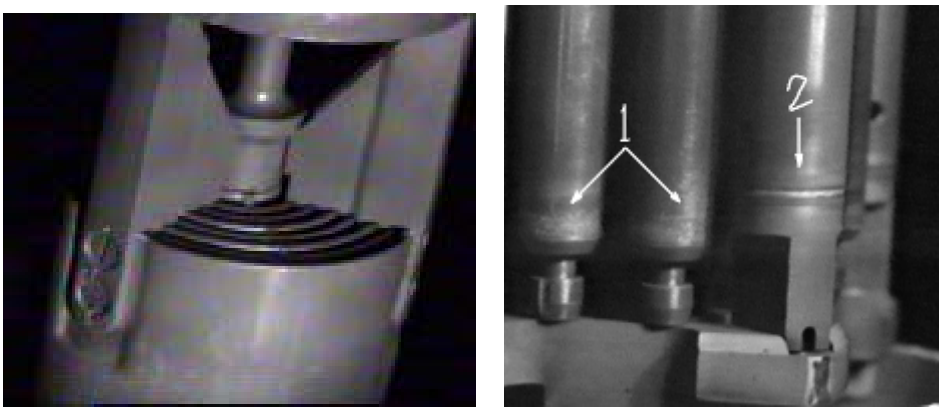

FIG. 3.1. Underwater visual inspection of fuel element (left: top end of HFETR fuel element; right: bottom end of a testing PWR fuel bundle).

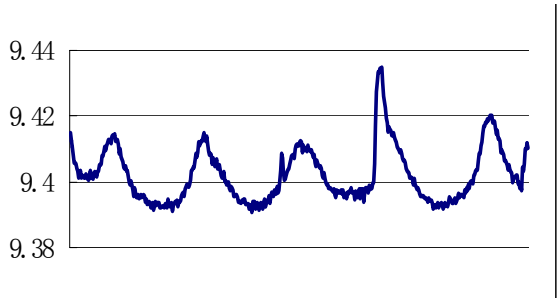

FIG. 3.2. Fuel rod diameter variation (mm).

FIG. 3.3. HFETR fuel element X ray radiography.

3.6 Burnup determination

Fuel elements could be dismantled and sampled to absolute burnup determination. The uranium isotope was separated and measured by mass spectrometer. Averaged burnup of HFETR fuel tube and axial distribution were in good accordance with the γ profilometry results (Fig. 3.5).

3.7 Microstructure analysis

The evolution of microstructure was a big concern during irradiation. Microstructure was examinated by a remote controlled optical microscopy (OM, LeikaMef4A, Fig. 3.6) in hot cell. Conjunction between cladding and fuel meat (Fig. 3.7), cracks and microvoids in pellets can be examinined.

Further more, a customized scanning electron microscopy (SEM) was used for fractograghy of irradiated materials. Figure 3.8 showes microviods and porosity of a PWR fuel pellet.

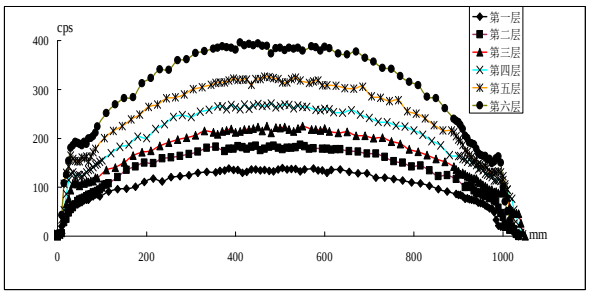

FIG. 3.4. Γ profilometry of fuel tubes.

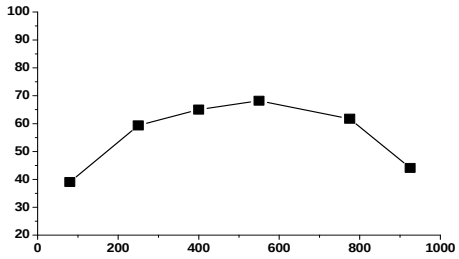

FIG. 3.5. Burnup distribution of fuel tube (axial position (mm) vs. burnup (at.%)).

FIG. 3.6. OM in hot cell.

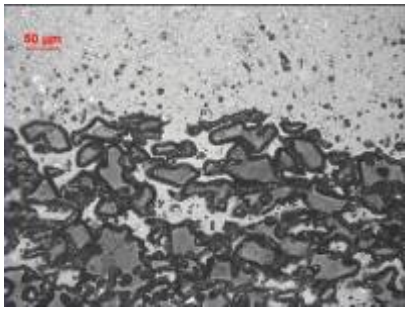

FIG. 3.7. Conjunction of fuel meat and cladding.

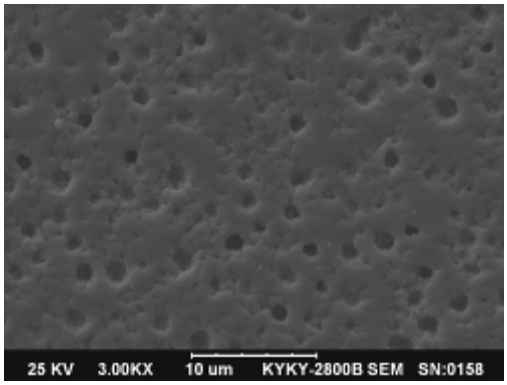

FIG. 3.8. SEM of irradiated UO_2.

3.8 Blistering testing

For dispersion fuel elements, high temperature blistering can lead to fuel failure. So it was important to determine the initial threshold temperature at which blistering occurs. A high temperature furnace was installed in hot cell to perform blistering testing for fuel tubes in full length. A blistering test for a HFETR fuel tube showed that threshold temperature was more than 500°C. Results are shown in Figs 3.9–3.10.

3.9 Burst testing

Burst testing of cladding tube for PWR fuel, could be performed in hot laboratory, both at ambient temperature and 350°C. A failed tube and strain vs. inner pressure relationship of burst testing is shown in Figs 3.11–3.12.

FIG. 3.9. Blistering of fuel tube.

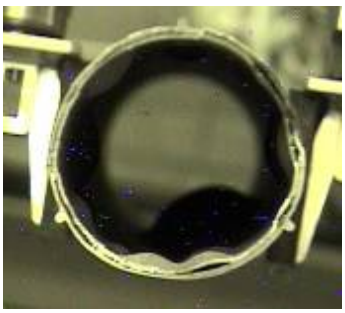

FIG. 3.10. Separation of cladding and fuel matrix.

FIG. 3.11. Failed tube.

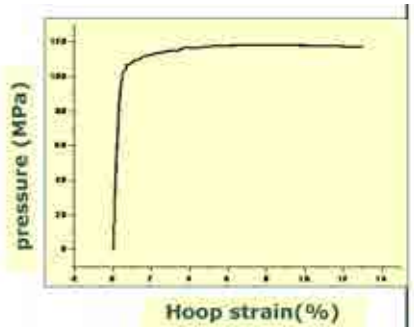

FIG. 3.12. Strain vs. inner pressure relationship.

4. CONCLUSIONS

NPIC hot laboratory plays a very important role in PIE of nuclear fuel in China. With the reconstruction of several hot cells and a renewal of instruments and facilities, more PIE work will be performed in the NPIC hot laboratory in the next decade.

BIBLIOGRAPHY

[1] SHIBIN, Y., Designing of HFETR hot laboratory, Symposium of 10th anniversary of HFETR operation, Bejing (1991).

[2] XIAOYONG, W., Status and refurbishment of HFETR hot laboratory, Symposium of 30th anniversary of HFETR operation, Bejing (2011).

[3] LI, G., Post-irradiation examination of a 4 × 4 testing fuel assembly, Symposium of 30th anniversary of HFETR operation, Bejing (2011).

[4] FENG, M., Post-irradiation examination of LEU fuel element of HFETR, The 13th International Conference on Nuclear Engineering Abstracts (ICONE13), Bejing (2005).

HOT LABORATORIES' EXPERIENCE AND CAPACITY (ADVANCED TECHNOLOGIES)

(Session 3)

Chairpersons

D. BOTTOMLEY
JRC-ITU

P. THIJSSEN
NRG

POST-IRRADIATION CAPABILITIES AT THE IDAHO NATIONAL LABORATORY

J.L. SCHULTHESS, K.E. ROSENBERG
Idaho National Laboratory (INL)
Idaho Falls, United States of America
Email: kenneth.rosenberg@inl.gov

Presented by A. Robinson

Abstract

The US Department of Energy (DOE), Office of Nuclear Energy (NE) oversees the efforts to ensure nuclear energy remains a viable option for the United States of America. A significant portion of these efforts are related to post-irradiation examinations (PIE) of highly activated fuel and materials that are subject to the extreme environment inside a nuclear reactor. As the lead national laboratory for nuclear energy, Idaho National Laboratory (INL) has a rich history, experience, workforce, and capabilities for performing PIE. However, new advances in tools and techniques for performing PIE now enable understanding the performance of fuels and materials at the nano-scale and smaller level. Examination at this level is critical since this is the scale at which irradiation damage occurs. The INL is on course to adopt advanced tools and techniques to develop a comprehensive nuclear fuels and materials characterization capability that is unique in the world. Because INL has extensive PIE capabilities currently in place, a strong foundation exist to build upon as new capabilities are implemented and workload increases. In the recent past, INL has adopted significant capability to perform advanced PIE characterization. Looking forward, INL is planning for the addition of two facilities that will be built to meet the stringent demands of advanced tools and techniques for highly activated fuels and materials characterization. Dubbed the Irradiated Materials Characterization Laboratory (IMCL) and advanced post-irradiation examination capability, these facilities are next generation PIE laboratories designed to perform the PIE work that cannot be performed in current DOE facilities. In addition to physical capabilities, INL has recently added two significant contributors to the Advanced Test Reactor-National Scientific User Facility (ATR-NSUF), Oak Ridge National Laboratory and University of California Berkeley.

1. INTRODUCTION [1–3]

The US Department of Energy (DOE) Office of Nuclear Energy (NE) oversees the research, development, and demonstration activities that will ensure nuclear energy remains a viable energy option for the United States of America. Fuel and material development through fabrication, irradiation, and characterization play a significant role in accomplishing the research needed to support nuclear energy. All fuel and material development requires the understanding of irradiation effects on the fuel performance and relies on irradiation experiments ranging from tests aimed at targeted scientific questions to integral effects under representative and prototypic conditions.

The DOE recently emphasized a solution driven, goal oriented, science based approach to nuclear energy development. Nuclear power systems and materials were initially developed during the latter half of the 20th century and greatly facilitated by the United States of America's ability and willingness to conduct large scale experiments. Fiftytwo research and test reactors were constructed at what is now Idaho National Laboratory (INL), another 14 at Oak Ridge National Laboratory (ORNL), and a few more at other national laboratory sites. During this time, the United States of America embraced a regulatory process that relied, and still relies, heavily on the use of experiments to confirm the ultimate safety of nuclear power systems and materials.

Building on the scientific advances of the last two decades, our understanding of fundamental nuclear science, improvements in computational platforms, and other tools can now enable technological advancements with less reliance on large scale experimentation.

Advanced tools and techniques enable the science based approach to emphasize an understanding of the behaviour of fuels and materials in a nuclear reactor irradiation environment at the nano-scale and smaller. Understanding of nuclear fuel and material performance in the nuclear environment at this scale is critical to the development of the innovative fuels and materials required for tomorrow's nuclear energy systems since this is the scale at which irradiation damage occurs. This of course is the driving need for establishing an advanced PIE capability at INL that can perform PIE on highly activated fuels and materials at ever increasing levels of sophistication.

2. GOALS [2]

Idaho National Laboratory has a vision to develop a consolidated PIE complex at the INL Materials and Fuels Complex (MFC), which is unique in the world in terms of comprehensive characterization and analytical capabilities applied to nuclear fuels and materials and efficient operations. In some cases, new capabilities beyond the current state-of-the-art need to be developed and implemented to perform detailed measurements. Such detailed measurements were not necessary in the more traditional empirically based approach that was used in previous fuel development and qualification programs.

3. CHALLENGES [3,9]

Traditional PIE capabilities at US DOE laboratories, universities, and in the private sector are widely distributed and lack the state-of-the-art capability necessary to meet the US nuclear energy mission need. Current PIE capabilities will continue to be necessary to serve basic needs for fuel examination, material handling, and waste disposal but are limited in their ability to function on the micro, nano, and atomic scale. The DOE-NE mission will be difficult to achieve without establishing a suitable nuclear facility environment that can accommodate these capabilities for research on highly radioactive fuels and materials. In addition, DOE seeks to make these capabilities available to the broader nuclear energy research community as a user facility concept, similar to the INL Advanced Test Reactor-National Scientific User Facility (ATR-NSUF), to enable the United States of America to effectively harness the intellectual capital of the country to advance US research and development (R&D) goals and objectives.

4. CURRENT CORE CAPABILITIES [2, 4, 10]

Idaho National Laboratory is the United State of America's only DOE laboratory with a core mission of supporting the development of nuclear energy. INL has a long history of performing PIE to support various DOE programs and has an existing trained workforce, with considerable expertise in fuels and materials technology. This expertise forms a foundation to build upon as new capabilities are implemented and workload increases.

At INL, the core nuclear and radiological facilities needed to support PIE R&D capabilities already exist, e.g.:

(a) Hot Fuel Examination Facility (HFEF) with neutron radiography capability, a large inert environment hot cell facility with the ability to receive and process large material and fuel components;
(b) Analytical Laboratory (AL), focused on analysis of irradiated and radioactive materials;
(c) Electron Microscopy Laboratory (EML), radiological facility containing optical, scanning, and analytical microscopes;
(d) Fuels and Applied Science Building (FASB), used for fuel development, materials characterization and irradiated materials testing;
(e) Carbon Characterization Laboratory (CCL), used to conduct both pre-irradiation and post-irradiation material property measurements of carbon/graphite materials;
(f) Center for Advanced Energy Studies (CAES), by design, the CAES research facility operates in the same manner as universities do; in the case of low risk radiological research, this approach

provides a cost-effective, innovative, and productive environment for exploring fundamental science questions and executing basic research complementary to research at INL site facilities.

The majority of these facilities exist at MFC while CCL and CAES are located at the INL Research and Education Campus (REC). INL also has close proximity to irradiation facilities like ATR and the Transient Reactor Experiment and Test (TREAT) facility. INL's current capabilities are outlined in more specific detail in Tables 4.1–4.7. Recently many of these current capabilities, particularly the macroscopic examination capabilities, have undergone or been scheduled for refurbishment. Collectively, the combined capabilities at INL now provide the most comprehensive capability in the United States of America.

TABLE 4.1. NON-DESTRUCTIVE EXAMINATION CAPABILITIES

Capability	Description
Neutron radiography	250 kW TRIGA reactor, two beam tubes and two separate radiography stations.
Precision gamma scanning	Measures fission and activation–product activity distribution.
Dimensional inspection	Continuous contact profilometer. Measures diameter profiles.
Element/capsule bow and length examination	Measures distortion (bow) and length of fuel elements.
Visual exam	Dedicated workstation, and in-cell exam stage.
Eddy current examination	Measures material defects
High precision specific gravity measurements	Pycnometer and immersion scales

TABLE 4.2. SAMPLE PREPARATION CAPABILITIES

Preparation type	Preparation
Solid metallography	Sectioned and cut
	Mounted into metallographic bases
	ground and polished
Gas sampling	Laser puncture and gas collection

TABLE 4.3. CHEMICAL, ISOTOPE, AND RADIOLOGICAL ANALYSIS CAPABILITIES

Elemental / chemical mass concentration and isotopic analyses
Inductively coupled plasma mass spectrometry (ICP-MS) with dynamic reaction cell (DRC)
Inductively coupled plasma atomic emission spectroscopy (ICP-AES)
Carbon, oxygen, and nitrogen analysis
Atomic absorption analysis
Thermal ionization mass spectrometry (TIMS)

TABLE 4.3. CHEMICAL, ISOTOPE, AND RADIOLOGICAL ANALYSIS CAPABILITIES (cont.)

Isotope mass separator
Gross and isotopic radiological analysis
Gross alpha/beta analysis
Gamma spectroscopy analysis
Alpha spectroscopy analysis
Micro-gamma analysis
Beta spectroscopy analysis

TABLE 4.4. MECHANICAL PROPERTY EXAMINATION CAPABILITIES

Capability	Equipment
Metallography	Leitz metallograph or Olympus IX70 optical microscope (up to × 1500) at EML
Microhardness testing	LECO AMH43 microhardness tester
Tensile testing	FASB or HFEF Instron tensile tester w/ furnace (1600°C)
Shear punch testing	FASB or HFEF Instron tensile tester w/ furnace (1600°C)

TABLE 4.5. THERMAL PROPERTY EXAMINATION CAPABILITIES

Capability
Thermal diffusivity (laser flash method and scanning diffusivity analysis)
Differential scanning calorimitry (DSC)
High temperature accident testing of HTGR fuel

TABLE 4.6. MICROSTRUCTURE PROPERTY ANALYSIS CAPABILITIES

Capability	Equipment
Scanning transmission electron microscope (STEM)	JEOL 2010, 200 kV, 2000–1 500 000 ×, equipped with energy dispersive X ray spectrometer
Scanning electron microscope (SEM) with energy dispersive (EDS) and wavelength dispersive X ray spectrometers (WDS) and electron back scatter diffraction detector (EBSD)	JEOL JSM 7000F FEG SEM, up to 30 kV and 600 000 ×.
	Zeiss DSM 960a SEM, up to 30 kV
	LEO 1455 VP SEM, up to 30 kV, operates at higher pressures
Dual beam focused ion beam (FIB)	FEI Quanta 3D FEG, up to 1 280 000 ×, ion source enables site specific sectioning of materials for 3D analysis or high resolution TEM characterization

TABLE 4.6. MICROSTRUCTURE PROPERTY ANALYSIS CAPABILITIES (cont.)

Shielded electron microprobe	Capable of analysing elements from Be through Cm with full matrix correction, including fission gases on samples
X ray diffractometer	Micro diffractometer performs micro-scale phase identification, small-sample powder diffraction and texture determination

TABLE 4.7. RECENT CAPABILITY ADDITIONS

Capability	Equipment
Nano indentation	CAES — Hysitron Tribo Indenter (TI-950) yields relation of mechanical properties on a very small length scale
Dual beam focused ion beam (FIB)	CAES — FEI Quanta 3D Field Effect Gun enables site specific micro sampling for use in TEM characterization
Field effect gun-scanning transmission electron microscope (FEG-STEM)	CAES — Tecnai TF30 Field Effect Gun Super Twin (STwin) with scanning transmission electron microscope, 300 kV provides better penetration of heavy element nuclear fuels and better resolution with ferritic/martensitic materials
Local electrode atom probe (LEAP)	CAES — Imago LEAP 4000X HR, creates atom-by-atom maps by extracting atoms from a needle shaped sample tip then using time of flight spectroscopy to determine the specific atom type. 3D reconstruction of up to hundreds of millions of atoms
Scanning electron microscope (SEM)	CAES — JEOL JSM-6610LV/TMP SEM with EDX and EBSD systems,
Scanning thermal diffusivity microscope (STDM)	AL – Shielded in-cell thermal properties measurements
Electron probe micro analyser (EPMA)	AL — Elemental redistribution, coupled with FIB gives atomic scale elemental redistribution analysis
Carbon oxygen nitrogen analyser	AL — LECO — provides elemental analysis

5. FUTURE CAPABILITIES [3, 5–7, 9, 10]

Idaho National Laboratory hosts a large variety of PIE capabilities and is upgrading and adding more. For example, INL currently has plans to stand up an irradiation assisted stress corrosion cracking rig (IASCC) in FASB to provide valid crack growth data on unirradiated benchmark material specimens. INL also plans to stand up a hot cell electron discharge machine (EDM) for use in sample preparation.

Feedback from potential users was recently solicited via the US National PIE Workshop to ensure any new capability is optimized for customer needs. The workshop helped identify many needs that are

currently unfilled as well as capabilities that otherwise do not meet current needs due to capacity, configuration, etc. The top four needs identified in the workshop are as follows:

(a) Instrumentation that supports analysis of materials at the nano-scale to support increasing knowledge of mechanisms that causes material degradation at the nano-scale. As such, an advanced PIE facility designed and constructed to support analysis on highly activated fuels and materials that incorporates strict environmental controls (vibration, electro-magnetic interference, temperature, etc.) and can also support environmental testing of materials (e.g. high temperature testing) with sample storage and preparation that is adjacent to other irradiation and PIE capabilities to support the advanced characterization tools is critical.

(b) Coupling the advanced characterization capabilities with advanced modelling so that better and more predictive models can be developed, thus reducing the need for extensive empirical integral effects testing.

(c) Accessibility and infrastructure that support sharing of data and creating administrative systems that facilitate collaborations with entities that are subject to different constraints than national laboratories. This need includes the physical infrastructure to perform PIE and the non-physical needs of creating systems that are flexible to deal with entities (i.e. national laboratory, industry, university) and projects (e.g. experiment, project and reactor timeline vs. career scale) that have different time cycles and support the development, hiring, and retention of nuclear material R&D talent.

(d) Pursued development of in situ techniques, analysis, and instrumentation that supports real time data acquisition for deformation mechanics, damage development, and other time resolved measurements. In situ characterization shows the development of material characteristics with time compared to traditional static PIE work.

The reinvigoration of nuclear fuels and materials research is bringing new and different tools to PIE and nuclear and radioactive materials characterization. These new tools, and the research materials examined with them, require unique, reconfigurable, accessible, modularized support facilities that are not presently available at INL. To support the INL's customers, the CAES will house many of these new instruments that focus on nano-scale and atomic-level characterization, where examinations can be completed using micrograms or nanograms of irradiated specimens prepared at the MFC. As new capability is created by the scientific community, the CAES will be the entry point for bringing new analysis technologies to the INL.

The rapid evolution of analytical electron microscopes and the advent of high performance computer interfaces with instruments were not envisioned when many of the existing facilities were constructed at INL. A new laboratory operational model will promote and support continual implementation of state-of-the-art tools and technologies.

To meet the needs of the future, INL is standing up new capabilities that have the sophistication and refinement to house next generation PIE characterization equipment. The near term capability is the Irradiated Materials Characterization Laboratory (IMCL); the subsequent longer term facility will be an Advanced Post-Irradiation Examination capability.

5.1. Irradiated Materials Characterization Laboratory (IMCL)

The IMCL (see Fig. 5.1) will be the first facility of its type in the United States of America designed specifically for advanced instrumentation and equipment. The IMCL will contain space for installation of instruments and equipment within shielding structures that can be redesigned and refitted whenever necessary. The IMCL will also have mechanical systems that tightly control temperature, electrical and magnetic noise, and vibration to the standards required for advanced analytical equipment. Although some of the advanced characterization equipment is already in use in other industries, IMCL will be unique in the United States of America because the equipment will be housed in a nuclear facility and dedicated to the examination of irradiated fuels and materials.

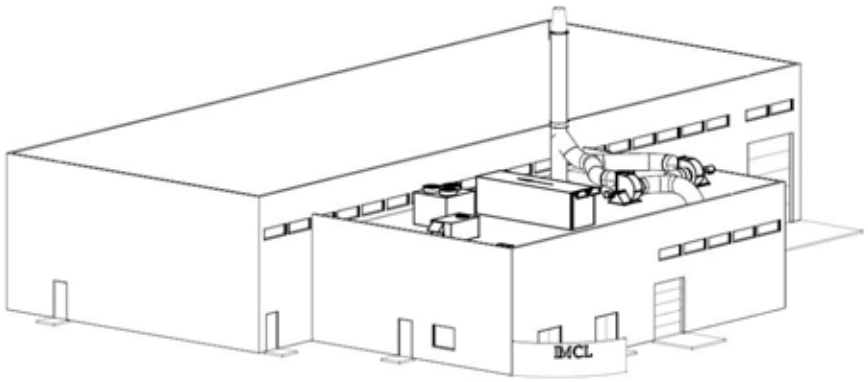

FIG. 5.1. Irradiated Materials Characterization Laboratory.

Designed as a multipurpose facility suitable for many different missions over its projected 40 year life, the IMCL will have as its first mission the task of housing modern, state-of-the-art PIE instrumentation. The IMCL will be used to routinely perform micro- and nano-scale characterization of material specimens and irradiated fuel samples in the mass range of tens of grams down to micro-grams. The facility will also be designed to allow easy routine maintenance of the instruments. The initial suite of equipment planned for installation into IMCL includes:

(a) Electron probe micro analyser (EPMA);
(b) Focused ion beam (FIB);
(c) Micro-X ray diffractometer (MXRD);
(d) Field effect gun-scanning transmission electron microscope (FEG-STEM);
(e) Mechanical testing;
(f) Sample preparation.

5.2. Advanced post-irradiation examination facility

Although the IMCL represents a significant advancement over current US nuclear energy R&D capabilities, DOE has approved the mission to significantly expand the PIE and full-spectrum nuclear research capabilities of the United States of America through various alternatives, primary among them is a new multi-programme facility called the Advanced Post-Irradiation Examination capability (see Fig. 5.2). This capability will handle considerably more sample and examination equipment than current facilities, both in types and quantities. The individual equipment and capabilities added will be based on an evaluation of need benefit and cost. As the project matures and the anticipated facility is built, some of the capability demonstrated in IMCL will transition to the new facility, freeing up IMCL to take on a key role of developing and deploying the next generation of “state-of-the-art” examination equipment. This would be consistent with the useful lifetime of such research equipment and would provide the newer facility with demonstrated state-of-the-art instrumentation.

The process for achieving advanced PIE capabilities in the United States of America, inclusive of standing up the advanced post-irradiation examination capability, recently marked a major milestone with the approval of the Mission Need Statement in January 2011. The Advanced Post-Irradiation Examination facility alternative is anticipated to be a modular design to facilitate equipment specific shielding and flexibility for future equipment development, configuration alteration, and ease of replacement. The initial suite of equipment anticipated for installation includes:

(a) Cask receipt;
(b) Comprehensive sample preparation;
(c) Expanded mechanical testing;
(d) Focused ion beam (FIB);

(e) High temperature X ray diffractometer (HT-XRD);
(f) Local electrode atom probe (LEAP);
(g) Secondary ion mass spectrometer (SIMS);
(h) Full suite of thermal property characterization: laser flash thermal diffusimeter (LFD), STDM, differential scanning calorimeter (DSC), thermogravimetry (TGA)
(i) Knudsen cell;
(j) Auger electron microprobe (AEM);
(k) Positron annihilation spectrometer (PAS);
(l) Advanced transmission electron microscope (TEM);
(m) Atomic force microscope (AFM);
(n) Laser resonant ultrasound spectrometer (LRUS);
(o) Nuclear magnetic resonance using Raman spectroscopy;
(p) Anklylography.

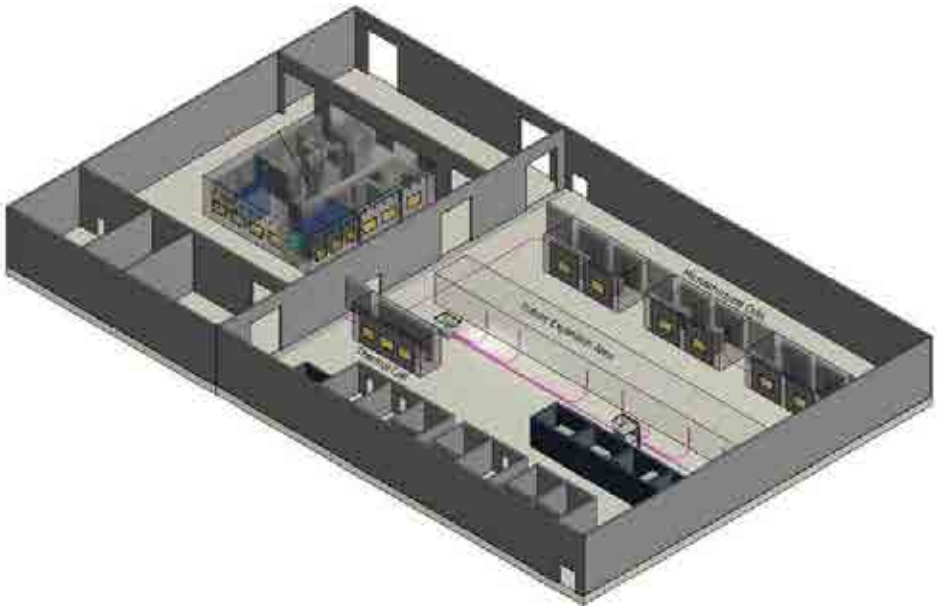

FIG. 5.2. Advanced post-irradiation examination.

6. PARTNERSHIPS/ATR-NSUF [8]

In addition to increasing physical capabilities through equipment and facilities, INL is expanding its partnerships and collaborations. Recently the ART-NSUF added ORNL and the University of California Berkeley as facility partners. Such partnerships increase access to national irradiation and testing capabilities and provide greater flexibility to respond to user needs.

The new partnerships will make ORNL's High Flux Isotope Reactor (HFIR) and its associated capabilities available to the ATR-NSUF users. The HFIR is a versatile, 85 megawatt isotope and test reactor that provides one of the highest steady state neutron fluxes of any reactor in the world. Irradiation experiment facilities include a wide variety of test positions, a hydraulic shuttle, and the capability for multiple instrumented target positions. Target fabrication, hot cell facilities for the examination of nuclear fuels and irradiated materials, the Radiochemical Engineering Development Center, and a set of special radiological laboratories at ORNL will also join the partnership. HFIR is operated by DOE, Basic Energy Sciences.

University of California Berkeley will bring several capabilities for examining irradiated material samples. Its facilities include a nano-indentation system for nano- and microscale hardness testing at

ambient and elevated temperature and inert environments, positron annihilation spectroscopy, and warm sample preparation.

7. CONCLUSIONS [3]

The DOE's ability to build a technical foundation to sustain the long term contribution of nuclear generation to meet US energy needs will be significantly hampered without obtaining a fundamental understanding of irradiation behaviour at the nano-scale and below. All significant advances in nuclear energy technology will rely on the development of improved performance of fuels and more durable materials. Development of improved fuels and materials relies on the fundamental understanding of the effects of irradiation, which in turn relies on a programme that couples experimental investigation with modelling and simulation. Current PIE capability does not provide the information required to obtain the fundamental understanding to continue to advance nuclear technology as an economical and sustainable energy source.

For this reason, INL has embarked on a significant effort to expand its already extensive capability to perform PIE through the addition of physical capabilities to the addition of partnerships. These capabilities will be expanding with the installation of state-of-the-art nano- and atomic-scale characterization equipment and the addition of two new facilities, IMCL and Advanced Post-irradiation Examination Facility, which will follow a reconfigurable and flexible design plan to ensure compatibility for performing advanced PIE on highly activated fuels and materials along with flexibility for future capabilities.

The INL incorporates all the necessary elements for successfully performing PIE and meeting the research needs to enable the advancement of nuclear energy. It allows parties interested in the advancement of scientific knowledge access to the powerful and versatile irradiation capabilities of the ATR and provides them with the diverse equipment and methods needed to analyse their experiment after irradiation. The quality of the programme will only improve with time as the INL adds equipment and facilities to what is already available.

REFERENCES

[1] UNITED STATES DEPARTMENT OF ENERGY OFFICE OF NUCLEAR ENERGY, Nuclear Energy Research and Development Roadmap, Report to Congress (2010). http://nuclear.energy.gov/pdfFiles/NuclearEnergy_Roadmap_Final.pdf

[2] IDAHO NATIONAL LABORATORY, Consolidated World-Class Post-Irradiation Examination Capabilities Strategic Plan, INL/EXT-09-16831, Idaho National Laboratory (2009).

[3] UNITED STATES DEPARTMENT OF ENERGY OFFICE OF NUCLEAR ENERGY, Mission Need Statement for Advanced Post-Irradiation Examination Capability: A Non-Major Systems Acquisition Project, US Department of Energy (2011).

[4] CARMACK, J., Post-Irradiation Examination Capabilities at the Idaho National Laboratory, INL/MIS-11-21996, Idaho National Laboratory (2011).

[5] AUSTED, S., Conceptual Design Report for the Irradiated Materials Characterization Laboratory (IMCL), INL/EXT-10-17562, Idaho National Laboratory (2010).

[6] SCHULTHESS, J.L., DRAFT: National Post-irradiation Examination Workshop Report, INL/EXT-11-21922, Idaho National Laboratory (2011).

[7] LANDMAN, W.H., Jr., Preconceptual Design Report for Post-irradiation Examination Line Item building, INL/EXT-10-19923, Idaho National Laboratory (2010).

[8] IDAHO NATIONAL LABORATORY NEWS RELEASE, Two new partners join Advanced Test Reactor National Scientific User Facility (2011) https://inlportal.inl.gov/portal/server.pt?open=514&objID=1555&mode=2&featurestory=DA_574357.

[9] ROSENBERG, K.E., ALLEN, T.R., HALEY, J.C., MEYER, M.D., National Science User Facility purpose and capabilities, Proceedings of HOTLAB 2010 Conference, Dimitrovgrad (2010) Session 5, Paper 34.
[10] IDAHO NATIONAL LABORATORY, Ten-year Plan for Implementation of Advanced Post-irradiation Examination Capability at the Idaho National Laboratory (FY 2011 to FY 2020), INL/EXT-10-20022, Idaho National Laboratory (2010).

MECHANISTIC FUEL FAILURE EVALUATION SYSTEM (MFFES)

F. RICE
Idaho National Laboratory (INL)
Idaho Falls, United States of America
Email: francine.rice@inl.gov

Presented by A. Robinson

Abstract

Failure thresholds and fission product releases will be used to define the allowable safety margins for U–Mo monolithic and dispersion fuel plates. These margins can be improved through high fidelity testing. Failure points will be defined at clad blistering, clad failure, then diffusion barrier (as applicable) failure, and finally at fuel failure. In order to characterize these failure points, mechanistic behaviours, and the fission product release, a robust state of the art, multipurpose furnace and fission product analysis system must be developed.

1. INTRODUCTION

Previous studies performed on metal and oxide fuels demonstrate sound methodologies that can be applied to characterize these emerging fuel types. Literature from 1966 [1] and 1970 [2] discuss gas retention properties studied under meltdown conditions for UAlx and U_3O_8 dispersion plates. More recent literature, from 1993 [3] and 1994 [4], reports both fission gas behaviours in metallic fuels in addition to fuel/cladding chemical and mechanical interactions. An additional report from 1994 [5], discusses the deposition of fission product volatiles on the reactor coolant system. Work to characterize these behaviours in fuels developed in the last fifteen years has not been conducted. Therefore it is important that a system be developed to define the mechanistic behaviours of the monolithic fuels, new dispersion fuels, and transmutation fuels.

1.1. Hypothesis

Mechanistic fission product behaviour of monolithic, dispersion, and transmutation fuels can be evaluated as released fission products are measured in solid and gaseous states, if a stepped approached to fuel failure is followed. Once these techniques are developed for the specific fuel type, a more comprehensive understanding of in-pile fission product mechanistic behaviour can be formulated as they affect the material failure thresholds. As these failure parameters are determined and empirical data is gathered, the safety basis for new fuel types can then be established. Further development of the system and experimental methods can be initiated so that the furnace can mimic reactor over power thermal conditions to form eutectic and chemical interactions between clad and fuel. Fuel can be sectioned and examined to characterize these layers and interactions to define how they affect fuel performance.

2. SYSTEM DEVELOPMENT

A furnace will be placed in HFEF main hot cell at MFC. Irradiated fuel and cladding specimens will be put in the furnace for thermal degradation of materials so that fission products will be liberated at established failure points. As the temperature of the furnace is increased step wise or ramped, to follow known failure points and the fission products, both gases and volatized solids, will be measured using gamma spectroscopy (online), gas mass spectroscopy (grab sample) and chemical dissolution examinations (sectioned samples). Attached to the furnace port, in series, will be a thermal gradient tube, a HEPA filter, a gas expansion segment and a port for the gas grab sample. The gases collected in bottle will then be analysed by gas mass spectroscopy.

The HEPA filter gradient tube sections can be further analysed using a gamma detection system located in the AL hot cells. Additionally, the HEPA filter can then be dissolved in the hot cells and

dilutions made for transfer out of the hot cells for further analysis of other solid fission products as well as solid activation products. A combination of chemical separations and analytical instrumentation for quantitative and qualitative measurements will be used. Some of these techniques will include anion exchange separations (both gravimetric and automized separation methods), inductively coupled plasma mass spectrometry and atomic emission spectroscopy (ICP-MS, and ICP-AES).

Analysis approach will be broken up into four stages and applied to each irradiated plate. The first will be to initiate blisters on the plate and measure any fission gas release. The second will be to ramp up the temperature at a rate yet to be determined, to breach and then completely melt the plate clad. Thirdly, the temperature of the furnace will continue to increase until the entire sample is melted and fission gases and volatilized solids measured by on-line gamma detectors. Stage four is comprised of three grab samples to be further analysed for non-gamma emitters in the thermal gradient tube and the melted sample, and gases using gas mass spectroscopy.

3. BLISTERING

Blistering thresholds are the standard by which the safety margin for reactor operation is established. The assumption is that once blistered, the plates are presumed to be at the point of failure and total release of fission product is imminent. What has not been determined is the following:

Are blisters really indicative of imminent plate failure?

(1) Are the blisters created by fission gases?

(2) Is there is fission gas release at the point of blistering?

(3) If not, how long at blister temperature before a release might occur?
   (a) Can a blistered plate safely remain in the reactor for any period of time before a breach can be expected?
   (b) How is the clad corrosion rate at the blister point increased?

(4) If clad still remains intact following a hold period at blister temperature, at what temperature do the fission gases begin to escape?

(5) If fission gases do not initiate blisters what does?

Several studies were reviewed to evaluate some of what is known about clad blistering behaviours. Development work for ATR fuel [6] observed that while gases do not contribute to creep or yielding behaviours but do fill in those voids that remained after fabrication and those created during the U_3O_8–Al reaction. Fission gases are credited (by calculation) with volumetric void expansion increase of 2.8% which is almost that of the 3 vol% voids increase measured during irradiation. If there is an interconnection mechanism of these voids the volume is claimed to be sufficient to cause blistering.

An Olander authored [7] article suggests otherwise. He argues that the pressure of the fission gases contained within the measured volume is not sufficient to deform the cladding and that mechanical failure of the clad can be attributed to the tensile stress normal to the plate. A journal paper [8] on non-fueled aluminum was also explored for any non fission gas contributions to blistering behaviours that might be better understood. While this article did not point to anything specific within our current systems, the blistering documented, was a function of the presence of hydrogen introduced during the fabrication processes. As most of RERTR fuels are clad with aluminum in addition to being in the matrix material for dispersions, it is important to be cognizant of the fact that gases, to some small degree are already present with the clad and matrix materials.

4. PROJECTED DATA

Expected fission product inventories following a forty day cooling in the ATR canal are:

- Plate blistering temperatures for given fuel type, clad type and clad bonding method.
    - Initial blistering temperature;
    - Video capture of blister propagation.
- Detection of fission gas release via HpGe detector during clad blistering phase of plate thermal degradation.
    - Xe, Kr and Br.
- Fission gas release as a function of temperature, clad degradation and fuel degradation.
    - Xe, Kr and Br.
- Total fission gas release collected as a grab sample (gas mass spectroscopy analysis) following completed fuel failure.
    - Xe, Kr and Br.
- Temperature dependent volatilized solids deposition behaviour.
    - Real time measurement using CZT gamma detectors of volatilized solids.
    - I, Cs, Sb, Ag, Te, Mo, Ba, Rh, Eu, Ru, Ce, Pr, La Nb and Zr.
- Type and quantity of deposited volatiles.
    - Mass balance for determination of weight of solids deposition;
    - Chemical dissolutions of thermal gradient tube sections for determination of presence of non-gamma emitters.
- Waste plate material will be sampled and chemically analysed for any retained fission gases and isotopic elements (some may not be present due to decay).
    - H, Be, C, Co, Ni, Cu, Zn, Ga, Ge, As, Se, Br, Kr, Rb, Sr, Y, Zr, Nb, Mo, Tc, Ru, Rh, Pd, Ag, Cd, In, Sn, Sb, Te, I, Xe, Cs, Ba, La, Ce, Pr, Nd, Pm, Sm, Eu, Gd, Tb, Dy, Ho, Er and Tm.
- Re-irradiated future samples for reactivation of decayed fission products for a more comprehensive analysis of inventories while in reactor.

5. MECHANISTIC FUEL FAILURE EXAMINATION SYSTEM COMPONENT SPECIFICATIONS

The furnace components are front access (see Fig. 5.1). This furnace is engineered and fabricated for high temperature operation in a controlled atmosphere, the hot zone, in the shape of a cylinder, is resistance heated and is insulated from the cold wall by fibrous graphite shields. Access to the furnace for loading and unloading is manual via remote operated manipulators with sample melt contained within a retort as shown in Fig. 5.2. Door clamps are provided for operation to slightly positive pressure. The entire inside of the vacuum chamber is designed to conform to the best high vacuum practices with particular attention given to surface finishes and choice of materials. Visual observation of the specimen is provided for by a sight port with a rotatable viewing glass. Ports are also provided for inert gas inlet, thermocouples and pertinent instrumentation. All controls and instrumentation are positioned to optimize monitoring and control. Furnace temperature is controlled by closed-loop circuit between the temperature sensor, the control instrument, and the power supply. System protection is provided by water-flow interlock. Components are readily accessible for inspection and maintenance.

5.1. Thermal gradient tube and furnace

Movement of volatilized fission product solids will be facilitated along the length of the Inconel or stainless steel gradient tube using the thermal gradient furnace shown on top of main furnace in Figs 5.1 and 5.3 with 6 discreet temperature zones.

FIG. 5.1. Main furnace and thermal gradient furnace at the bottom and top respectively.

FIG. 5.2. Retort (sample holder) mounted inside main furnace.

FIG. 5.3. Thermal gradient furnace with deposition tube in place.

5.2. Camera system

In order to capture blister formation with removing plate from the furnace, the system will be equipped with 2 cameras and 4 lights located at view ports with quartz windows. The configuration can be seen in Fig. 5.4.

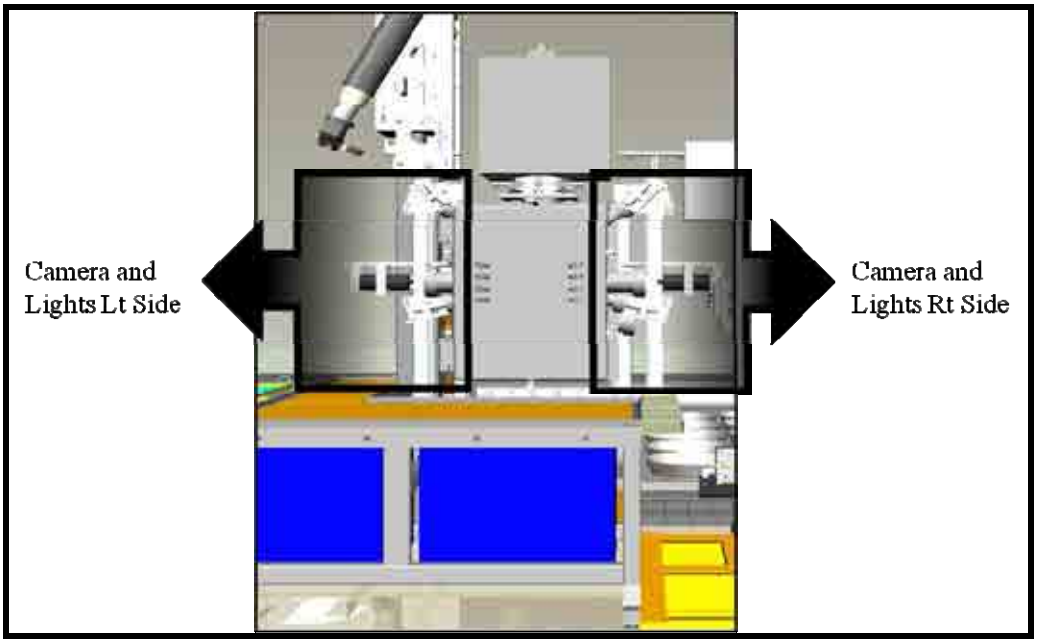

FIG. 5.4. Camera and light configuration.

5.3. Fission gas loop

The fission gas line will be placed in series with the thermal gradient tube. Gas line will pass through hot cell feed to the detection system located at the expansion segment of the system. Gases will loop back into the furnace for a measure of total fission gas accumulation attributed to the fuel plate failure

during the thermal degradation regime. A grab sample of the accumulated fission gases will be collected at a port outside the hot cell following completion of test.

5.4. Fission product detection system

In-cell detectors will be cadmium zinc telluride spear gamma detectors provided by eV products. The SPEARS will be shielded and non-stationary to facilitate optimal resolution. The out of cell for system will be the fission gas detection component will be an ORTEC HpGe detector.

5.5 In-cell SPEAR gamma detector system specifications

CdZnTe detector dimensions (example shown in Fig. 5.5):

1. 5 × 5 × 5 mm with CAPture® contacts;
2. Measurement capabilities;
3. Energy range: 1–10 MeV;
4. Energy resolution: <4% FWHM @ 122 keV @ 25ºC;
5. Operating temperature;
6. Range: -10–50ºC standard.

FIG. 5.5 Example SPEAR detectors.

SPEAR™ dimensions:

1. 13 mm diameter × 89 mm length (without cable);
2. Total length of SHV HV output cable is 3’;
3. Total length of lemo connector cable is 6’;
4. Total length of BNC output cable is 3’.

SPEAR detector input requirements:

1. 9 PIN sub D connector: +12 VDC, ground;
2. SHV connector: HV bias (typically +500 to +1000 VDC).

Signal output:

1. BNC connector and preamplifier output;
2. As assembled, all input/output connectors will interface directly with any standard spectroscopy or counting system.

SPEAR performance:

1. + 7 to 12 VDC operation;
2. Input capacitance: 6.6pF;
3. Risetime @ C source: 1pF, 35nS;

4. Falltime @ C source: 1 pF, 725 μS;
5. Noise @ C source: 0 pF, ~160 e — (Si);
6. Sensitivity: 3.2 mV/fCoul;
7. Power dissipation: 130 mW (+ 12 VDC supply).

ORTEC GEM series coaxial HpGe detector specifications:

1. Energy resolution at 1.33 MeV photons from 60Co at optimum shaping time;
2. Relative photopeak efficiency for a 60Co 1.33 MeV peak;
3. Peak-to-compton ratio for a 60Co 1.33 MeV peak;
4. Peak shape ratio for the full-width tenth maximum to the full-width half-maximum for a 60Co 1.33 MeV peak;
5. Energy resolution at 122 keV photons from 57Co at optimum shaping time.

6. ACKNOWLEDGEMENTS

D.M. Wachs, D. Sell, J. Berg, J. Fonnesbeck, D. Akers, C. Shull, C. Baily, G. Preslar, L. Roybal and J Blaylok.

REFERENCES

[1] FRANCIS, W.C., MOEN, R.A., Annual Progress Report on Reactor Fuels and Materials Development for FY 1966, IDO-17218 (1966).
[2] BRUGGER, R. M., Metallurgy and Materials Science Branch Annual Report Fiscal Year 1970, Idaho Nuclear Corporation (1970).
[3] KRAMER, J.M., et al., Modeling the behaviour of metallic fast reactor fuels during extended transients, The Journal of Nuclear Materials **204** (1993) 203–211.
[4] HOFMAN, G.L., WALTERS, L.C., Materials science and technology, Nuclear Material Part 1, Section 1, **10A**, Publisher: VCH Verlagsgesellschaft mbH, Weinheim (Federal Republic of Germany) and VCH Publishers Inc., New York (1994).
[5] LE MARIOS, G., MEGNIN, M., Assessment of fission product deposits in the reactor coolant system: the DEVAP program, Nuclear Safety **35**, No. 2 (1994).
[6] WALKER, V.A., GRABER, M.J., GIBSON, W., ATR fuel materials development irradiation results – part II, IDO-17157 (1966).
[7] OLANDER, D., Growth of the interaction layer around fuel particles in dispersion fuel, Journal of Nuclear Materials **383** (2009) 201–208.
[8] O'DETTE, J.H., Blister formation in rolled aluminum, Journal of Metals **924 (**1957).

INSTALLATION OF A SCANNING ELECTRON MICROSCOPE IN THE HOT CELL LABORATORY OF NRG PETTEN

J.A. VREELING, F.A. VAN DEN BERG, P. VAN DEN IDSERT, T.V. PHAM, O. WOUTERS
Nuclear Research and Consultancy Group
Petten, The Netherlands
Email: vreeling@nrg.eu

Abstract

In 2010 a new scanning electron microscope (SEM), equipped with several detectors (EDS, WDS and EBSD) is installed in a new hot cell. The SEM is modified for use in a radioactive environment. Therefore the irradiation sensitive parts are removed or protected. In addition changes have been made to the SEM to allow remote handling and to allow maintenance of the important parts. This paper describes the new facility at the NRG Hot Cell Laboratories and gives some examples of the first microscopy results.

1. INTRODUCTION

The Hot Cell Laboratories (HCL) of the Nuclear Research and Consultancy Group (NRG) are equipped with both glove boxes and hot cells to perform research on structural materials and nuclear fuels. This research covers non-destructive testing, testing of physical and mechanical properties and microstructural investigations. This complete package of pre- and post-irradiation testing in combination with the high flux reactor (HFR) allows irradiation testing at one location, avoiding complex and costly transports. Recently NRG improved the microscopy facilities by installing a new scanning electron microscope (SEM). Besides the standard secondary electron (SE) and Backscatter Electron detectors, this SEM is equipped with additional detectors for energy dispersive spectrometry (EDS), wavelength dispersive spectrometry (WDS) and electron backscatter diffraction (EBSD). The equipment is placed in alpha tight hot cell to allow analysing radioactive samples emitting α, γ and β radiation, therefore both nuclear structural materials and nuclear fuels can be analysed. The new equipment did not fit in the existing hot cell of the previous SEM. As a result the hot cell is dismantled, the old SEM removed and a new hot cell engineered and built. This paper describes the equipment, modifications for using the SEM in a radioactive environment, the installation of this equipment and gives some examples of the first results.

2. EQUIPMENT

2.1. Microscope and detectors

In 2005 and 2006 several SEM suppliers were contacted to have discussions on specifications, possibilities of adding extra detectors and possibilities to install the equipment in hot cell to allow analysing radioactive samples.

In 2007 it was decided to buy a Jeol JSM-6490 SEM, equipped with Oxford EDS/WDS/EBSD detectors. The SEM has a Tungsten filament and an acceleration voltage between 0.3–30 keV. It can be operated in both low and high vacuum mode. Low vacuum mode is useful for bad conducting samples, the resolution of 3.0 nm is reached in the high vacuum mode at 30 keV. Figure 2.1 gives of summary of the equipment.

2.2. Modifications to the SEM for use in radioactive environment

The purpose of this SEM is to analyse radioactive samples, emitting γ/β radiation, as well as α radiation. To protect the operators and environment the SEM is placed in alpha tight box that itself is placed in a hot cell with lead walls. During operation the pressure in the box is lower than the surrounding, to keep the radioactive material in the box.

Besides the operators and environment, the SEM has to be protected as well. The parts of the equipment that are sensitive for radiation damage (electronics) were positioned outside the hot cell, if possible. This means that most cables are extended to allow separation of electronics and vacuum chamber. Vacuum tight connectors are used to lead the cables through the glove box wall to prevent leakage of potential radioactive air.

	JEOL 6490 LV SEM • Placed in hot cell for radioactive specimens. • High resolution (3.0 nm). • Possibility of low vacuum mode for badly conducting surfaces. • Enhanced SE and BSE detection. • Five-axis motorised stage. • Equipped with EDS, WDS and EBSD detectors.
	Oxford Instruments energy-dispersive spectrometer (EDS) • Able to operate with high count rates. • Accurate element identification. • Accurate element quantification. • Superior light element analysis. • Fast mapping.
	Oxford Instruments wavelength dispersive spectrometer (WDS) • Trace analysis possible due to high sensitivity (0.01 wt%). • Excellent energy resolution. • Quantitative elemental analysis. • Five crystals (detection from Be to Pu). • Extra shielding for radioactive specimens.
	HKL Nordlyss electron backscatter diffraction (EBSD) • Phase analysis and identification. • Texture analysis. • Can be combined with EDS. • Indexed mapping at speeds up to 100 Hz.

FIG. 2.1. Summary of description of the scanning electron microscope with the installed detectors.

The vacuum chamber is placed, together with the detectors, inside the hot cell. Electronics and equipment that was possible to separate was placed outside the hot cell. This concerns electronics of the SEM (placed under the hot cell), controllers and vacuum pumps (placed next the hot cell) and operating equipment (placed at some distance from the SEM). Figure 2.2 shows a drawing of the SEM and hot cell. The green unit below the cell contains the electronics that is separated from the cell.

Some sensitive parts could not be placed outside the hot cell, for instance the detectors and motor stage. Therefore local shielding by Tungsten is applied near the sample or near the sensitive equipment, considering the limited space available for shielding, and without compromising the functionality of the microscope.

The electronics of the motor stage is very close to the sample position and in this region of the SEM limited volume is available to add tungsten shielding. These parts are unavoidably exposed to γ radiation, in spite of the Tungsten shielding that is applied where possible. To investigate the sensitivity of the electronics of the motor stage parts of the same type are deliberately exposed to gamma radiation in the HFR. The results showed that the electronics can withstand enough γ radiation (at 250 Gy no degradation in resistance values, at 2500 Gy minor degradation in resistance values), to be operated for a significant period. However, because only one device is tested, we anticipated that during the lifetime of the SEM it may happen that this motor stage may fail. A plan is in place to repair or exchange the motor stage when this will happen.

Besides the radiological protective measures, a lot of effort is taken on the handling of the sample in the hot cell. This handling is limited by the fact that the cell is equipped with tong manipulators (manoeuvrable rods with a handle outside the hot cell, that the operator can use to position and tweak the grips at the end of the rod in the hot cell). These tongs are restricted in their movements with respect to the more common master/slave power manipulators. The hot cell has two tong manipulators (Fig. 2.2). One tong is positioned opposite to the posting port that is located between the hot cell of the SEM and the adjacent hot cell (in this second cell the sample is placed in the sample holder). This tong is used for getting the sample holder (including the sample) from that cell to the SEM hot cell.

The second tong is positioned in front of the door of the vacuum chamber. The door of the SEM vacuum chamber is redesigned to be able to open and close the door by using this tong. Opening and closing is done vertically, by using a counterweight. The same tong manipulator is used for placing the sample holder in the vacuum chamber by a specially engineered loading system.

Another limitation is the lack of space in the hot cell, because the SEM and its detectors are filling up most of the workspace. To ensure good visibility the windows are therefore placed under an angle.
Another important item is accessibility of the system in case of servicing, replacing the filament and repairing or removing detectors, etc. The glove box is equipped with openings for gloves on all necessary locations (Fig. 2.2). The access to the electronics is provided by the relocation of parts that need to be serviced to the side of the electronics unit that can easily be reached.

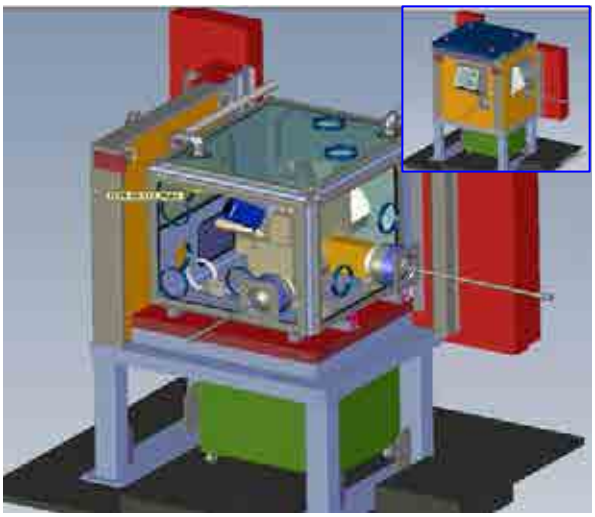

FIG. 2.2. Drawing of the hot cell (without two lead walls and roof), showing the part of the SEM inside the glove box and the separated electronics unit under the cell (green). The positions of the openings for gloves are visible in this figure as well. The insert shows the complete hot cell with special lead windows and two tong manipulators.

3. BUILDING THE FACILITY

The situation at the start of the project was a contaminated hot cell (F6 cell) with the old SEM. This hot cell was connected to a contaminated cell (F5 cell) that was connected to the other cells used for sample preparation. Building of the new facility was carried out in different phases:

– Phase 1: Removing old SEM and hot cell:
All activity from the old hot cell was removed. When the activity in the hot cell was low enough, a lead wall was removed to have better access to the glove box. The glove box is further decontaminated by using the gloves. After this the lead walls were dismantled (Fig. 3.1). The glove box and SEM were transported to the decontamination facilities of NRG, where the box and equipment is decontaminated. Parts that could not be decontaminated were treated as waste. The old F6 cell was placed on a concrete block. For the new set-up this space is needed for the electronics, as a result this block was removed. A maquette of the SEM and detectors was made, at the same size of the original SEM. After the old hot cell was removed this maquette was placed in the same position of the new SEM. This maquette was used for the design of the new hot cell (determining sizes, position of tongs, windows, openings for gloves and position of posting port).

– Phase 2: Modification of F5 hot cell:
The new F6 cell is connected to the existing F5 cell. To achieve this in the new situation a posting lock needed to be designed and build. Therefore the F5 cell needed to be decontaminated and modified as well. This opportunity is taken to remove old equipment (that is not being used anymore) from this hot cell. Size and position of the lead window and tong positions of this cell were optimised for the new situation as well.

– Phase 3: Building the new hot cell:
During the manufacturing of the hot cell the modified SEM is tested in another lab at NRG. Due to the modifications of the electronics some measures had to be taken to reach the specifications of the microscope. This time was also used to train the operators and to develop the final modifications in local shielding and handling tools.

The hot cell was built in the HCL after all its parts were available, initially without equipment. After acceptance test of the hot cell the SEM is placed (Fig. 3.2) and tested. After a period of optimising the performance of the SEM a final acceptance test was performed. After this milestone the hot cell was connected to the other cells, off-gas system and HCL alarm system. In August 2010 the SEM was ready for analyses on radioactive samples (Fig. 3.3).

FIG. 3.1. Dismantling the old hot cell.

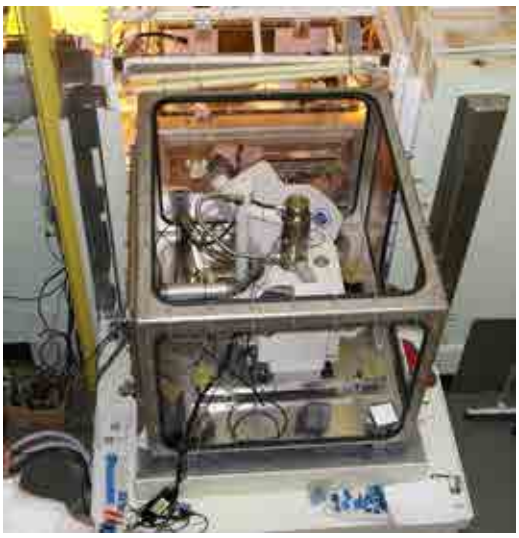

FIG. 3.2. Installation of the SEM in the hot cell.

FIG. 3.3. Hot cell with SEM. One lead wall and the roof is removed to show the equipment.

4. EXAMPLES OF FIRST RESULTS

Since August 2010 several projects on irradiated samples are carried out. The section gives some examples.

– Irradiated fuel pebbles:
In the European HTR (High Temperature Reactor) programs HTR-F and RAPHAEL-IP an irradiation experiment (HFREU1BIS) is carried out on HTR fuel pebbles [1, 2]. In the post-irradiation examinations the pebbles are analysed with the new SEM. Figure 4.1 gives an overview and detail by SEM-imaging of one HTR TRISO fuel particle from an HTR fuel pebble, after irradiation. UO_2 kernel, buffer, inner Pyrocarbon, SiC and outer Pyrocarbon layers and surrounding graphite matrix can be clearly distinguished. The images show fission gas bubble formation at the grain boundaries, metallic fission product precipitates, and a peculiar kernel surface, indicating fission gas release. On these samples many WDS measurements are performed to get information on the present elements. Figure 4.2 shows an example of a Cs mapping in the layers around UO_2 kernel. The red dots indicate presence of Cs.

– Irradiated SiC/SiC composites:
Different material types were irradiated in the HFR within the EXTREMAT Integrated Project (6th Framework programme of the EU). The aim of this project was to investigate materials in extreme environments like intense neutron fields. Carbon Fibre Reinforced Ceramics (SiC/SiC, SiC/C, C/C) are envisaged to be used as structural or functional materials in high temperature applications, i.e. up to about 1100–2000°C in fusion reactors and up to about 850–1500°C in advanced fission reactors, respectively. These materials were, among other materials, investigated in the EXTREMAT project. The SEM is an excellent good tool to study fracture surfaces and this is valuable information to the strength test results. Figs 4.3–4.4 show two examples of fracture surfaces of SiC/SiC samples, fractured in four point bending tests, after irradiation in the HFR.

– EBSD:
In the first period of the SEM the EDS and WDS detectors were successfully used on irradiated samples. In this half year no experience is gained with the EBSD detector. This detector gives crystallographic information, like crystal structure and orientation [3]. This can be used for example for phase identification, texture, orientation relationships or grain boundary definition. Figure 4.5 gives an example of EBSD result on unirradiated Si samples. The Kikuchi lines on the image are detected and identified by the software. The plan is to test the EBSD technique on irradiated samples this year.

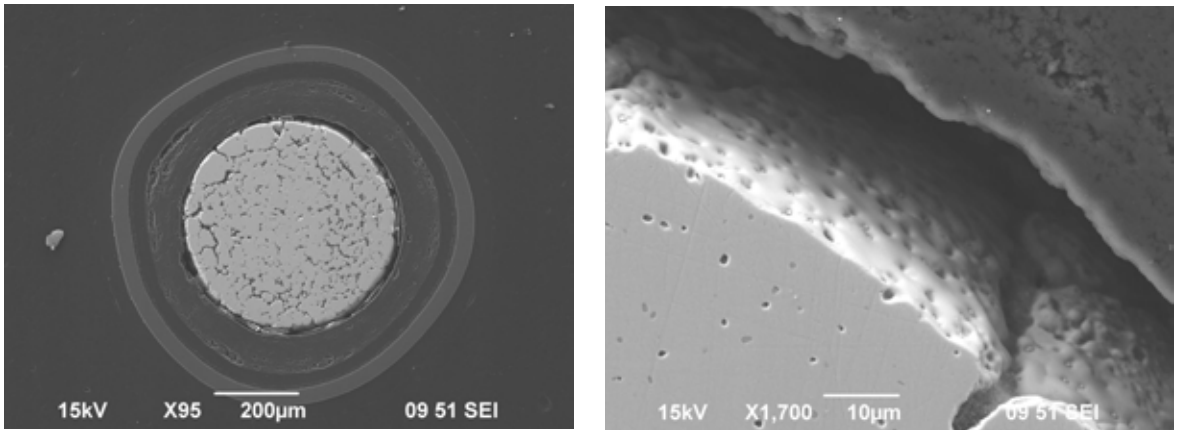

FIG. 4.1. SEM images of HTR TRISO fuel particle (left: overview, right: detail between UO_2 kernel and buffer layer).

FIG. 4.2. Example of element mapping (Cs) in the layers around the UO_2 kernel. Red dots indicate presence of C.

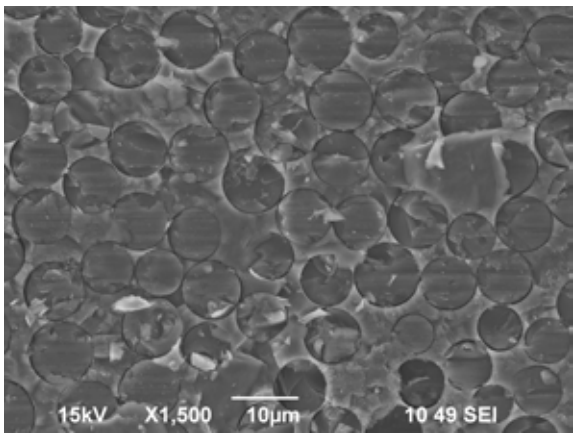

FIG. 4.3. Fracture surface of SiC/SiC bonded type 1, irradiated to 2.4 dpa (steel) at 600ºC.

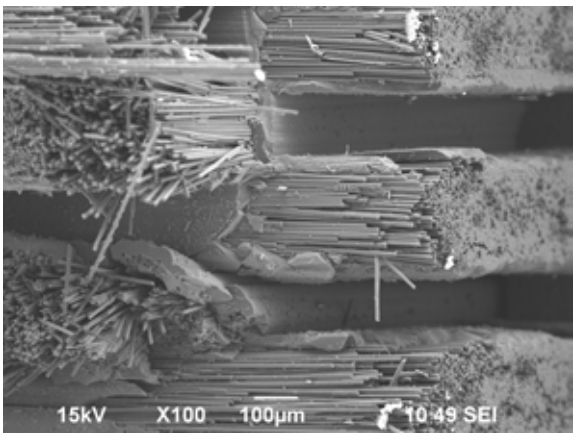

FIG. 4.4. Fracture surface of SiC/SiC 3D woven type 1, to 4.5 dpa (steel) between 800–900ºC.

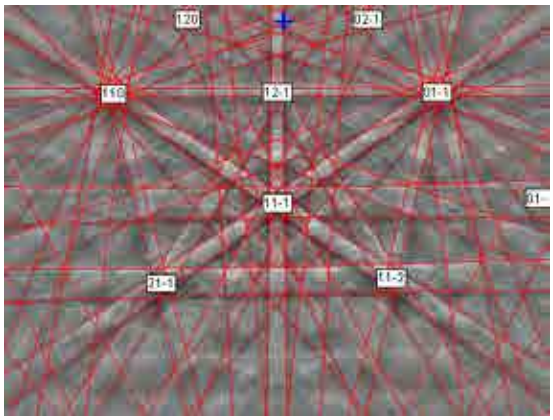

FIG. 4.5. EBSD pattern of a Si sample (unirradiated).

5. CONCLUSIONS

A Jeol JSM-6490 SEM, equipped with Oxford EDS/WDS/EBSD detectors, was successfully installed in a new hot cell at the NRG Hot Cell Laboratory. The first radioactive samples were investigated by this equipment in August 2010.

EDS and WDS detectors were successfully used to analyse irradiated fuel and structural materials.

The EBSD detector is not used on irradiated materials yet.

REFERENCES

[1] FÜTTERER, M.A., et al., Irradiation results of AVR fuel pebbles at increased temperature and burnup in the HFR Petten, Proc. HTR2006, Johannesburg (2006).
[2] DE GROOT, S., et al., Fission product behaviour during irradiation of TRISO-coated particles in the HFREU1bis experiment, Proc. HTR2008, Washington DC (2008).
[3] DINGLEY, D.J., RANDLE, V., Microtexture determination by electron backscatter diffraction, Journal of Materials Science **27** (1992) 4545–4566.

DEVELOPMENT AND DESIGN CONSIDERATIONS FOR A SUITE OF NEW POST-IRRADIATION EXAMINATION HOT CELLS TO BE CONSTRUCTED AT MCMASTER UNIVERSITY

J. LUXAT, D. NOVOG
Department of Engineering Physics
McMaster University
Ontario, Canada
Email: mailto:luxatj@mcmaster.ca

G. BOTTON
Department of Materials Science and Engineering
McMaster University
Ontario, Canada

V. WALKER, S. SHAW, G. PIERCE, W. GRANGER, M. WADE
Merrick and Company
Aurora, CO, United States of America

Abstract

McMaster University, Hamilton, Ontario, houses the McMaster Nuclear Reactor (MNR), the highest flux university research reactor in Canada. MNR is a 5 MW(th), light water cooled and moderated, LEU fuelled, pool-type reactor. A single support hot cell also exists but is not suited for PIE. A suite of new PIE cells will be designed, constructed, and installed in room 105 of the Tandem Accelerator Building (TAB). The objective of the capability is materials characterization research at the atomistic level. This paper presents planning, design, and construction considerations associated with the new cells. The project poses a three way contest among limited available space, maximum desired PIE capabilities, and funding (the Canada Foundation for Innovation and the Ontario Ministry for Research and Innovation are jointly funding the project). Maintaining other tenants' use of the TAB complicates design and construction. The concept includes initial sizing of large specimens, such as entire CANDU pressure tubes, elsewhere, plus six new cells in the TAB to perform: receipt and shipping, non-destructive examination, waste management; machining; preparation of mechanical test specimens; mechanical testing; preparation of microscopy specimens/light microscopy; long term mechanical testing; and specimen archives. The first cell is highly shielded, to allow handling of maximum size and activity specimens. The remaining cells will handle smaller specimens, typical of PIE microscopy, and the cells are modular of all steel construction. In-cell capabilities and equipment include: material transfers — input and output; one pair of manipulators; in-cell lifting equipment; in-cell lighting, utilities, fire protection; heating, ventilation, and air conditioning (HVAC) connections; work tables or equipment stands, and specimen preparation and testing equipment (including focused ion beam (FIB) apparatus. A transmission electron microscope (TEM) and scanning electron microscope (SEM) are also located in the same TAB room, with both pneumatic and manual shielded container transfer capabilities.

1. INTRODUCTION

The McMaster Nuclear Reactor (MNR) is a low enriched uranium (LEU) fuelled, light water cooled and moderated, 5 MW(th) pool type reactor located at McMaster University, Hamilton, Ontario, Canada. The MNR is the highest flux university research reactor in Canada. A recent major infrastructure grant has been awarded to McMaster by the Canada Foundation for Innovation and the Ontario Ministry for Research and Innovation to establish the Centre for Advanced Nuclear Systems (CANS). This centre will have new facilities for post-irradiation examination, a 3-D atom probe, SEM/FIB and TEM facilities for both irradiated and un-irradiated material, all of which will support materials characterization research at the atomistic level. Additionally, CANS will have facilities for new alloy development and supercritical water mechanical testing of materials supporting research on Gen IV nuclear reactors and a new facility for safety thermal hydraulics experiments.

The University has the faculty expertise, instrumentation, and research support to conduct materials characterization (i.e. post-irradiation examination (PIE)) of irradiated materials at the atomistic level, but does not have the shielded facilities required to perform sample preparation and testing. CANS will establish that capability.

Beginning with the first exploratory discussions between the university and the facility designer, it was clear that the space available for construction of the PIE facility was limited, but that compensating limits to the scope of PIE operations were possible.

Consideration of existing permits and licenses, as well as adjacent support facilities (such as change rooms) led to the decision to locate the hot cells in room 105 of the TAB. Figure 2.1 shows the location of room 105 within the TAB.

Design bases, space limitations, and the resultant conceptual design are described in subsequent sections (design, construction, and operating costs are also an overall consideration, but costs are not within the scope of this paper except as discussed with regard to specific design decisions).

2. DESIGN BASES

The essential design bases for the PIE facility are:

– The design will meet requirements and guidance of Canadian Nuclear Safety Commission (CNSC) guide-52 [1];

FIG. 2.1. Existing ground level floor of McMaster University tandem accelerator building, with exposure rate zones shown.

– The design basis flasks for receipt of specimens from off-site are not yet determined (although several flask configurations are expected);
  - Flasks will be brought to the receipt cell on a forklift.
  - The flask transit path is from the parking lot south of the TAB, northward in the corridor.
  - The design basis specimen is a segment of zircaloy 4 CANDU reactor pressure tube, maximum length of 50 cm, nominal diameter of 104 mm, a maximum source (i.e. zircaloy) weight of 10 kg, and maximum additional weight from non-zircaloy items, such as inner packaging, of 10 kg, for a total design basis specimen weight of 20 kg.

- The radiological source term is based on initial material composed of zircaloy 4, assumed to be 98.2 weight per cent Zr-94, 1.8 weight per cent tin, with a cobalt (Co-59) content of 20 parts per million by weight, irradiated in a flux of 1×10^{14} neutrons $cm^{-2} \cdot sec$, for a period long enough to be at saturation with Zr-95 and its decay products Nb-95m and Nb-95, with Co-60 also at saturation, followed by a post-irradiation cooling time of 3 years.
- No actinides are present in the specimens, except as incidental trace contamination.
- The nominal shielding performance requirement is that allowable dose rates shall be <0.25 $mrem \cdot h^{-1}$ (2.5 $\mu Sv \cdot h^{-1}$) in areas restricted to occupancy by qualified radiation workers, and <5 $mrem \cdot y^{-1}$ (50 $\mu Sv \cdot y^{-1}$) in unrestricted areas, as designated in Fig. 2.1.
- The sample receipt and examination throughput rate is 1 per week, based on five shifts per week.

3. SPACE CONSIDERATIONS

At the project inception, it was apparent from informal and qualitative considerations, along with order-of-magnitude cost estimates, that the only realistic option for locating the PIE facility was within the existing TAB. A green field location was deemed more expensive (for land acquisition). Both a green field location and a campus location not presently associated with the MNR were considered more expensive and time consuming to license, whereas zones within the TAB are already licensed and operated as radiological areas. The space available for construction of the suite of cells, previously shown in plan view in Fig. 1.1, is designated room 105, and is 60 feet (18.3 m) wide by 24 feet (7.2 m) deep by approximately 20 feet (6.1 m) tall. The existing side walls are 3–5 feet (0.9–1.5 m) thick normal density (approximately 2.3 $g \cdot cm^{-3}$) concrete. The areas south and east of the existing side walls are not accessible for this project. The area north of the existing side wall is not accessible for routine operations and maintenance, but the existing doorway in the northeast corner is available as an emergency personnel exit. The area west of the existing side wall is an 8 foot wide corridor connecting directly to an outdoor receiving area. The corridor is periodically available to bring shielded casks (flasks) containing irradiated specimens from the outdoor receiving area to the (new) transfer port in the existing west wall of room 105. Forklifts will be used for cask movements. The existing doorway between the corridor and room 105 will be relocated.

The room 105 floor is concrete slab-on-grade. The floor will be evaluated during detailed design to confirm loading capacity and vibration response; necessary modifications will be determined.

The overhead space in room 105 is more than necessary for the new cells. The existing bridge crane will be evaluated and modified or replaced as necessary. No modifications to the room 105 ceiling are planned at this time.

4. DESIGN CONCEPT

The design concept is comprised of a suite of six steel-, or steel and concrete-walled hot cells and an adjacent enclosed space for electron microscopy, plus ancillary spaces and equipment for sample handling, waste management, equipment maintenance and transfers, and heating, ventilation, and air conditioning (HVAC) equipment, all to be installed and operated within the existing footprint of room 105 in the Tandem Accelerator Building at McMaster University. Isometric views of the general arrangement of cells and support spaces in room 105 are shown in Figs 4.1–4.2.

The six cells are:

– The receipt, shipping, and machining cell, in which:
  - Specimens are received, in shielded shipment and transfer flasks, from off–site;
  - Specimens are removed from any packaging internal to the flask that was needed for shipment;

    - Unpackaged specimens are visually examined;
    - Specimens are machined (with in-cell equipment including a cut-off saw, a band saw, and a three way (i.e. mill, drill press, and lathe combination) machine) into smaller samples as required for subsequent destructive PIE;
    - Unused segments of the original specimens are repackaged as required and loaded into a shielded shipment flask for return to the specimen originator.
- The waste management cell, in which radioactive wastes generated in the PIE facility are packaged and characterized as required for subsequent storage, transport, and disposal as directed by the university;
- The mechanical test cell, in which mechanical test apparatus, such as tensile strength racks, are installed and used;
- The microscopy sample preparation cell, in which equipment used to prepare samples for light or electron microscopy, such as polishing wheels or sputter coaters, are installed and used;
- The light microscopy cell, in which light-based microscopy equipment is installed and used;
- The support cell, in which temporary and non-routine tests and test in apparatus can be deployed, or active equipment can be repaired and maintained.

Other features of the PIE suite in room 105 include:

- The sample transfer glove box (off-the-shelf design), connected to the support cell, from which microscopy samples, or samples for laboratory analyses performed elsewhere, or miscellaneous small contaminated items, can be transferred. The principal transfer routes out of the sample transfer glove box are either into the pneumatic transfer system (with connections to the electron microscopy annex, or into a shielded transfer "pig" for manual transfer as needed.
- The electron microscopy annex, which houses the scanning electron microscope/focused ion beam (SEM/FIB) and the transmission electron microscope (TEM). The electron microscopy annex also houses a small shielded glove box (off the shelf design) for receiving microscopy samples from the sample preparation cell (via the pneumatic transfer system) or the sample transfer glove box (via manually transferred pigs).
- Isolated foundation(s) for the SEM and TEM that will provide vibration free mounting recommended for instrument use.
- The sample storage archives, which are shielded spaces adjacent to the electron microscopy annex, dedicated to shielded retrievable storage of previously examined samples.
- A pneumatic transfer system, connecting the PIE cells to the electron microscopy annex.
- An isolation room, which continuously spans the "back" (i.e. the north) side of the PIE cells (except the receipt, shipping, and machining cell), and provides a shielded (but potentially contaminated) maintenance and repair area, and a transfer corridor, in which personnel can perform operations and maintenance activities.

Operations and maintenance approach: the operations approach is that any radioactive material with a contact dose rate >10 mrem·h^{-1} (0.1 mSv·h^{-1}) will be exclusively handled remotely, regardless of the duration of material handling operations. Hands-on operations with materials having dose rates <10 mrem·h^{-1} (0.1 mSv·h^{-1}) will be evaluated during preliminary design, with consideration given for brief or infrequent operations. Contamination confinement will be conducted in accordance with established university procedures. Design provisions will be made to ensure temporary shielding and contamination confinement during material transfers.

The principal equipment for in-cell material handling is a pair of through-the-wall master–slave manipulators at each cell window. The manipulator model number(s) are not yet determined. However, sealed thru-tube models will not be required, since the expected specimens do not include irradiated fuel. Manipulators are augmented by in-cell hoists where required to lift components that exceed the lifting capacity of the manipulators. Manipulators cannot be installed in the north end of the receipt cell, since there is not room for an operator to stand nor for manipulator removal. Consequently, a robot arm will be provided for material handling in that region.

The preferred maintenance approach for major equipment is to disconnect the failed component in-cell, remotely decontaminate (with manipulator-borne wipes and foam-type cleaning agents) to the extent practicable, then remove the component to a suitable location for either hands-on repair or appropriate packaging as waste. This approach allows for prompt replacement of a failed component and minimizes downtime. Accordingly, design provisions are made to remove the largest equipment items from each individual cell, either through doors in the cell backs or removable plugs in the cell roofs.

Only gaseous and solid wastes are generated within the PIE facility. Gaseous wastes are discharged through HEPA filters, into the existing building contaminated off-gas system. Access for testing and replacement of the HEPA filters is via the isolation room.

No significant volumes of liquid wastes are generated within the facility. No liquid based processes are conducted within the facility. Small (i.e. <2 litres) amounts of liquids such as cutting liquids or decontamination solutions will be absorbed onto suitable media or evaporated to dryness in the waste management cell and packaged there with other solid wastes for subsequent handling and disposal.

Health physics instrumentation (personnel monitors, air monitors, and area monitors) is included in cost estimates, but specific locations are not yet determined.

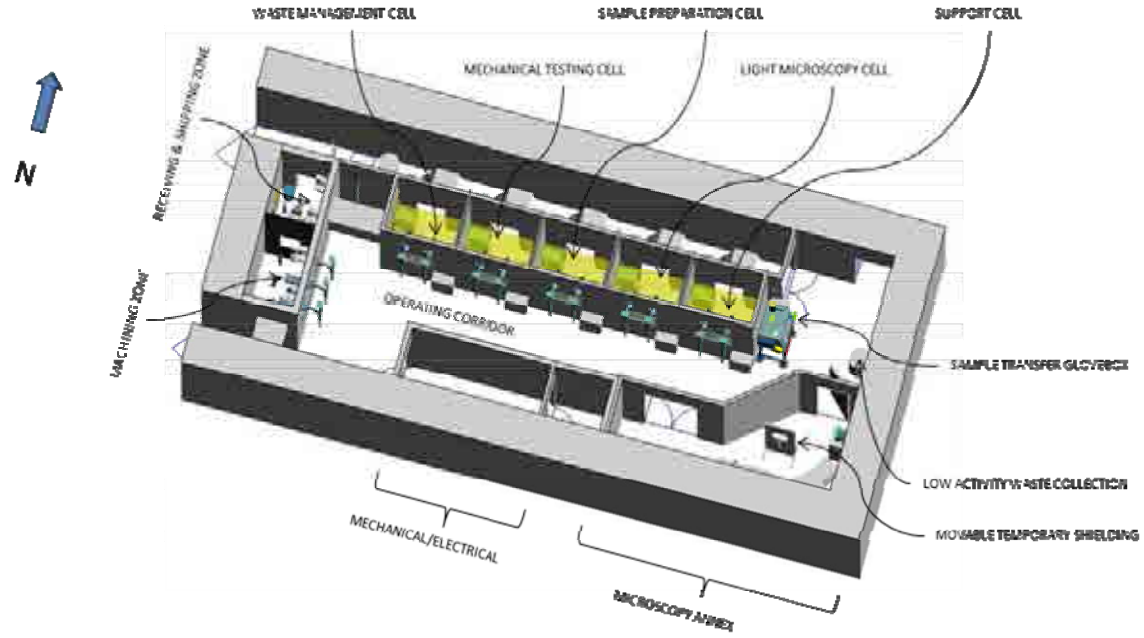

FIG. 4.1. McMaster University PIE cells; overall arrangement.

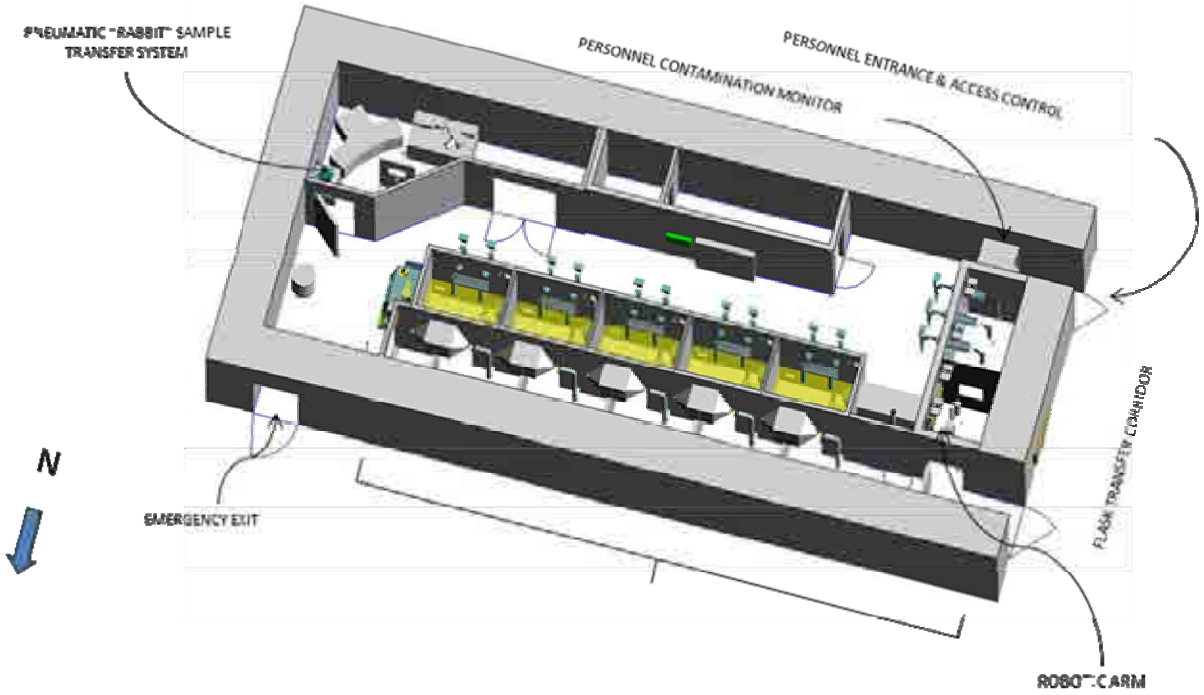

FIG. 4.2. McMaster University PIE cells, view of rear of cells from within isolation room.

REFERENCES

[1] CANADIAN NUCLEAR SAFETY COMMISSION, Design Guide for Nuclear Substance Laboratories and Nuclear Medicine Rooms, GD-52 (2010).

PIE METHODS AND RESULTS (METHODS)

(Session 4)

Chairpersons

D. GAVILLET
PSI

V.V. RONDINELLA
ITU

EDDY CURRENT DETECTION OF CLADDING DEFECTS DUE TO FUEL PELLET IMPERFECTIONS

D. PAPAIOANNOU, R. NASYROW, N. NIAGOLOVA, V.V. RONDINELLA
European Commission
Joint Research Centre
Institute for Transuranium Elements
Karlsruhe
Email: dimitrios.papaioannou@ec.europa.eu

W. GOLL
AREVA NP GmbH
Erlangen

Germany

Abstract

An eddy current device has been used to localise cladding defects on irradiated fuel rods. The system has been initially tested with cold specimens, providing very good results and is now in regular operation in a hot cell at the Institute for Transuranium Elements (ITU). In this paper we demonstrate the system's performance and present recent results on a series of irradiated fuel rods with PCI failures and partly long splits (secondary failures). The rods were delivered in tight capsules and only gamma scans could be done in the β and γ reception cell. Big defects were well visible through distortions in the gamma profile, whereas the smaller ones were very hardly detectable. They could be precisely localised later on, as soon as we cut the fuel rod and examined the individual segments with the eddy current device in an α cell. Careful sampling around the defect location, specimen preparation and detailed microscopic analysis confirmed cladding cracks driven by fuel pellet imperfections or, more specifically, by missing chips from the pellet surface (MPS). MPS in fuel rods increases the probability of cladding failures caused during power changes. In addition to uniform stresses engendered by pellet expansion, local strains are applied onto the cladding at regions where a piece of pellet is missing. In the examined rods the MPS meniscus sizes varied between 26° and 44°.

1. INTRODUCTION

One of the primary non-destructive tests (NDT) of the post-irradiation examinations (PIE) performed on irradiated fuel rods is to control the cladding integrity and search for cladding cracks, deformations or other anomalies that could permit escape of volatile fission products or even spent fuel particles and therefore cause risks of contamination. In nuclear research eddy current techniques are routinely used in examinations related to defect or failure in the cladding material. The corresponding eddy current equipments are in the most cases utilised to study the complete rod length in a reasonable time with properly adapted sensitivity. However, very small clad defects can be sometimes either not detectable, or must be precisely localised in order to proceed with further examinations. At ITU, fuel rod testing equipment is available and installed in a non-alpha contaminated hot cell, where the spent fuel rods are received and studied as a whole. After completion of the NDT the fuel rod is segmented; another small eddy current device has been installed in a hot cell in order to perform in-depth analysis at a level allowing a precise localisation of cladding defects.

2. EDDY CURRENT DEVICE AND COLD TEST

The photos and the drawing of Fig. 2.1 show the small eddy current device and the sensor, respectively. The sensor, connected with the controlling hardware, is positioned inside a bronze holder and its nose tip is softly touching the fuel segment, which can be rotated. The sensor can be axially moved along the segment and the data acquisition can be performed on the complete specimen outer surface. The distortions of the sensor's magnetic field are then presented through proper software in holographic format, as shown in Fig. 2.2.

(a)

(b)

(c)

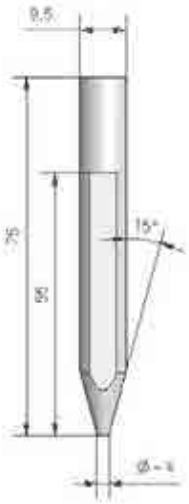

FIG. 2.1. (a), (b) The eddy current device for segment analysis. The sensor shown in the drawing (c) is placed inside the bronze holder, H.

(a)

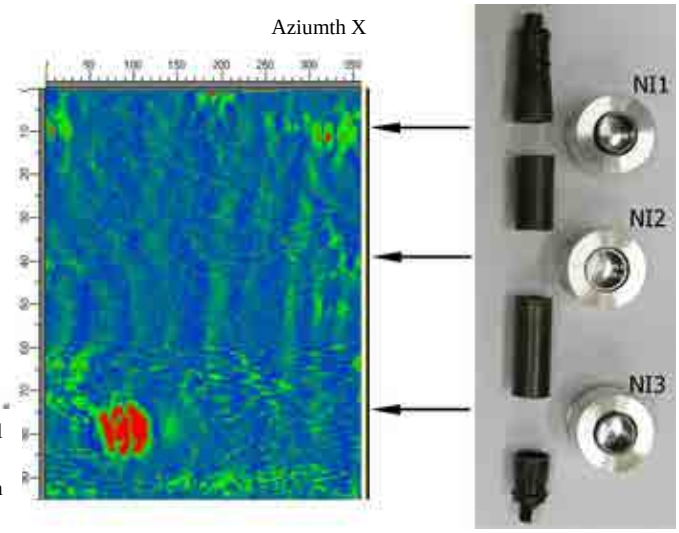

(b)

FIG. 2.2. (a) Eddy current hologram of a non-irradiated creep test cladding specimen; (b) The green colour on the hologram represents small, and the red colour bigger defects.

The hologram in Fig. 2.2(a) has been recorded on the surface of a cladding tube after creep test. In this graph the X-abscissa-axis gives the azimuth and the Y-ordinate-axis the axial position of the sensor. The colour variation from the blue background (corresponding to surface level) denotes presence of small (green colour) or bigger (red colour) cladding defects. In order to confirm this, three small pieces of the tube specimen were cut at the positions of interest, embedded in proper holders, polished

and observed with an optical microscope (Fig. 2.3). In all cases the observed defects are in very good agreement with the hologram result.

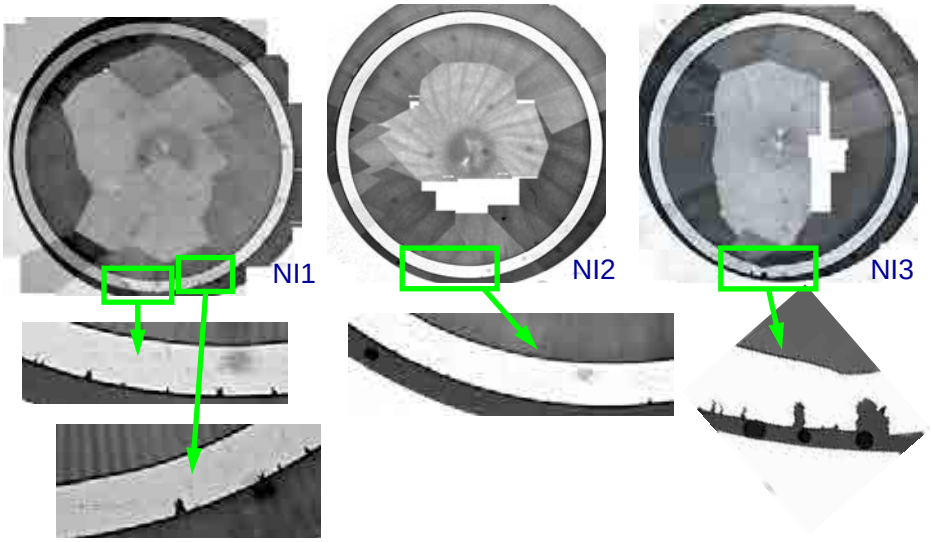

FIG. 2.3. Macrographs and detailed cladding photographs of the cross-sections of the three specimens cut as shown in Fig. 2.2.

3. EXAMINATION OF ACTIVE SAMPLES

After some additional cold tests confirming the system's good performance, the device has been installed in hot cell and used to examine 4 irradiated fuel rods. Due to strong suspicion of clad defects, at the reactor site the rods were already packed in welded outer capsules and delivered to ITU for post-irradiation examinations. The rods, just referred as No.1, 2, 3 and 4, were burnt up to 51.7 $GW \cdot d \cdot t^{-1}$ U, 58.4 $GW \cdot d \cdot t^{-1}$ U, 56.3 $GW \cdot d \cdot t^{-1}$ U and 55.7 $GW \cdot d \cdot t^{-1}$ U, respectively. The only non-destructive control that could be performed outside the tight capsules was γ spectrometry.

The obtained spectra, shown in Fig. 3.1, did not provide unequivocal information about the suspected positions of cladding failures. The fuel rods were then cut in 480 mm long segments and the segment eddy current device was used to identify and precisely localise the defects. The obtained EC hologram around the interesting rod axial region helped successfully to identify and localise the cladding defect, as can be seen in Fig. 3.2.

The assumption of the power plant experts was that the defects could be due to pellet imperfections, such as missing chips from the pellet edge, usually called MPS [1–2]. In such a case, stress-corrosion cracking caused by iodine (ZrI_4 is brittle) can take place in the cladding.

It was expected therefore that the tips of the initiating cladding defects in the delivered fuel rods would be close to a pellet–pellet interface. For this purpose, cuts were implemented just before the corresponding pellet of interest, whose position had been located by finding a dishing position at the beginning of the segment and counting the pellets up to the desired position. Such a cut from fuel rod No. 4, as well as the prepared specimen and photographs of the identified cladding defects are presented in Fig. 3.3, whereas Fig. 3.4 shows photographs of the MPS areas with the cracked cladding from all examined fuel rods.

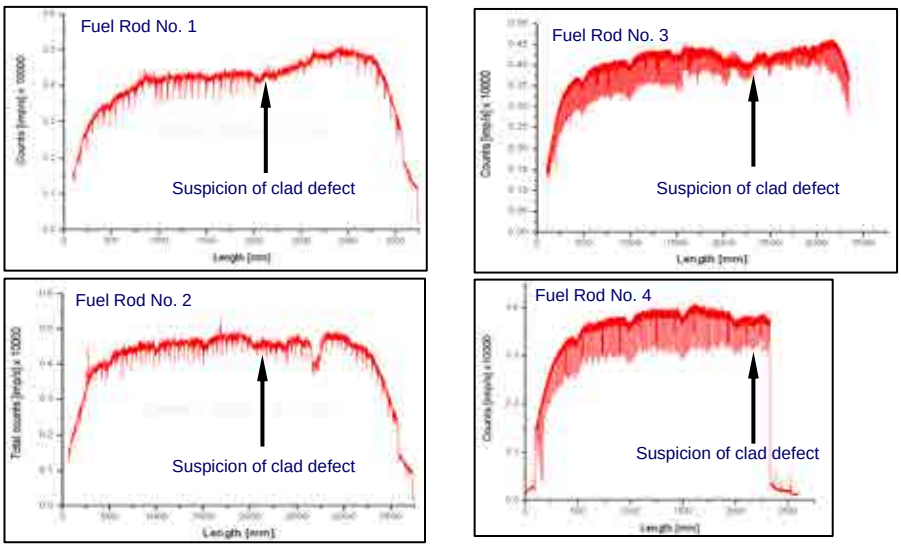

FIG. 3.1. The γ spectra of the 4 irradiated fuel rods; the suspected position of cladding defects are indicated.

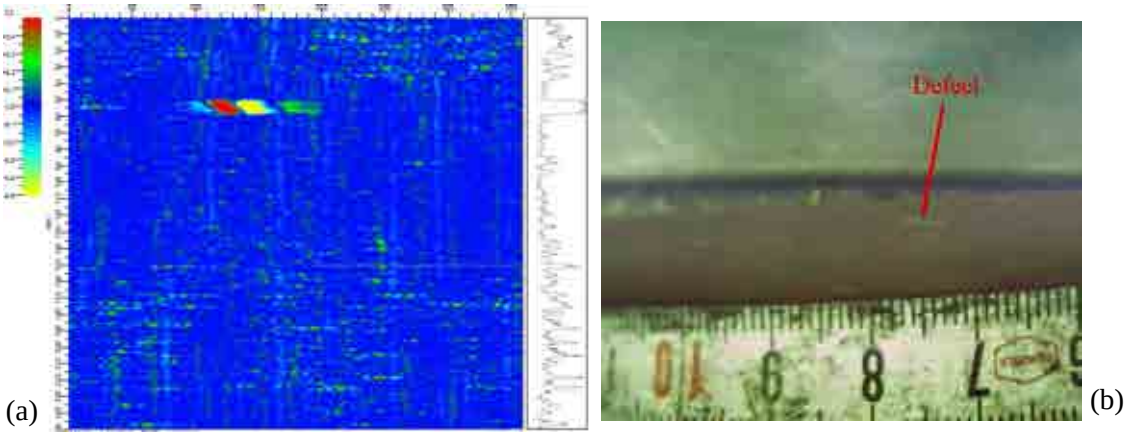

(a) (b)

FIG. 3.2. The EC hologram (a) and the cladding defect visually identified (b).

FIG. 3.3. (a) Sections from which the metallographic sample was prepared; (b) Overview of the metallographic sample with the MPS defect; (c) Close up of the defect area at the beginning of the fuel pellet; (d) Defect area at an axial location ca. 0.8 deeper (after grinding) than in (c).

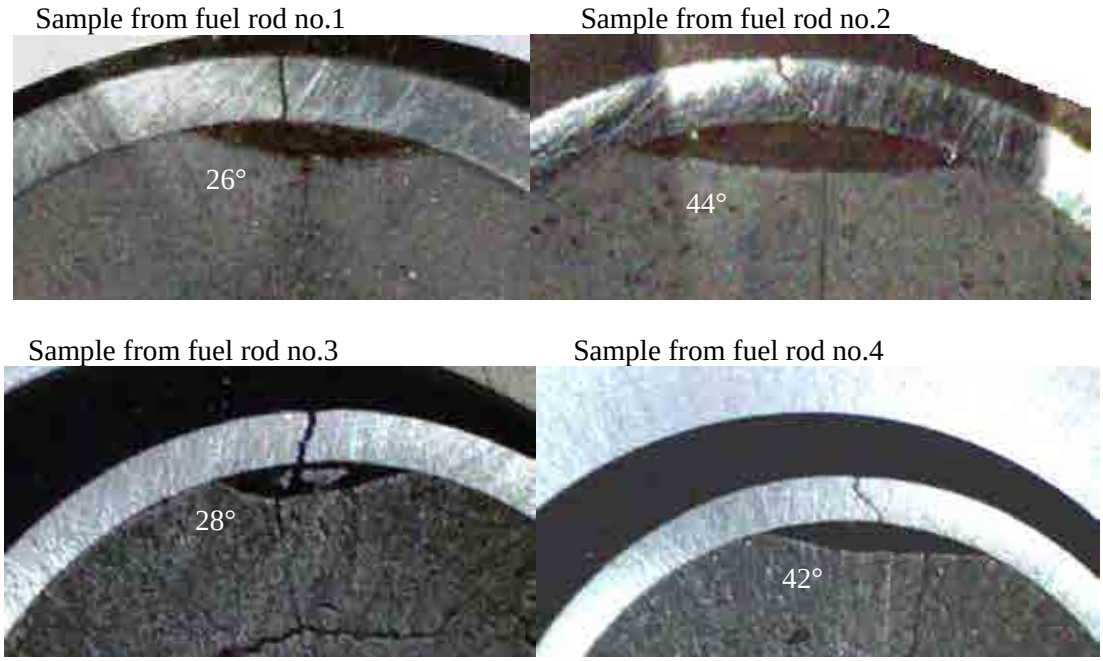

FIG. 3.4. Photographs of all confirmed MPS and corresponding cladding defects in the four rods analysed.

4. CONCLUSION

Using a small EC device assembled and installed at ITU, cladding material defects due to pellet imperfections (MPS) could be successfully identified and precisely localised. MPS areas are endangering the cladding integrity because of the local strains that can be generated in these areas. The holograms of the data obtained on a series of spent fuel rods confirmed the expectations of clad failures and permitted the preparation of exact and proper specimens to study cladding crack growth and MPS meniscus sizes.

5. ACKNOWLEDGMENTS

The authors would like to thank RWE Power AG for the support of this work.

REFERENCES

[1] OLANDER, D., Nuclear fuels – present and future, J. Nucl. Mater. **389**, 1 (2009) 1–22.

[2] LEE, J.S., YOO, J.S., KIM, H.K., MITCHELL, D., ALESIN, Y., Proceedings of the 2007 Int. LWR Fuel Performance Meeting, San Francisco (2007) Paper 1022.

SCANNING ACOUSTIC MICROSCOPE: AN ADVANCED TECHNIQUE FOR THE MECHANICAL CHARACTERIZATION OF IRRADIATED NUCLEAR FUEL

W. DE WEERD, A. KELLERBAUER, V.V. RONDINELLA, C.T. WALKER, D. PAPAIOANNOU
European Commission
Joint Research Centre
Institute for Transuranium Elements
Karlsruhe, Germany
Email: wim.de-weerd@ec.europa.eu

G. DESPAUX, D. LAUX, F. AUGEREAU
Université Montpellier II
CEDEX 5
Montpellier, France

Abstract

The characterization of mechanical properties constitutes a key challenge for the study of nuclear fuel behaviour under conditions relevant for safe in-pile operation. This applies to both conventional and advanced fuel concepts. At JRC-ITU new tools are being developed to extend the knowledge on the thermomechanical behaviour of the fuel during irradiation. In particular, a scanning acoustic microscope was recently tested in hot cell for the measurements of elastic constants of irradiated fuel (in the frame of collaboration with EdF). The technique has been adapted to the conditions characterizing the hot cell environment and the configuration of typical irradiated fuel samples. The results obtained so far are very promising and indicate that this could become a very useful tool not only for the measurement of elastic properties, but also as complementary method to assess bulk properties and initial conditions of fuel samples destined to various types of analysis.

1. WORKING PRINCIPLE

Elastic properties of UO_2 have been studied for a long time. Their determination is relevant particularly to reactor transients for which creep relaxation is unlikely to happen. This type of situation produces pellet–cladding mechanical interaction (PCMI) and possibly cladding failure. This has been a subject of concern for all reactor types using UO_2 or mixed oxide fuel. Elastic properties, combined with thermal expansion, determine the level of stress in the fuel and consequently in the cladding when interaction occurs. The pellet stiffness evolves with burnup because of the pellet cracking (macro and micro cracks) and also with the bulk intrinsic elastic moduli. Under this situation Young's modulus, E, is the most important parameter to assess for code calculations.

It was found that the elastic modulus in oxide fuel decreases both with increasing temperature and porosity volume fraction. The fractional porosity in UO_2 has been extensively studied at room temperature and in the range 90–100% of theoretical density. Although data on mixed oxides are scarce, it was found that the elastic modulus versus temperature followed the same pattern as for UO_2, but increased with the plutonium content. The most reliable estimate seems to be 3% increase for a 20% PuO_2 fuel.
The influence of the O/M ratio on Young's modulus was studied, suggesting that Young's modulus is higher for stoichiometric fuel, but decreases with hyper- or hypo-stoichiometric shifts. The influence of stoichiometry is difficult to quantify, because other parameters (e.g. the fabrication route, grain size, etc.) interfere.

1.1. Acoustic waves for elastic modulus of nuclear fuel evaluation

Because of the fractured pattern of irradiated pellets and the variation of mechanical properties along the radius, classical methods (e.g. mechanical traction, global echography) are not applicable and only

novel non-destructive and non-invasive methods, applied on a very small area of the sample, such as high frequency acoustic microscopy or indentation, can give useful results.

The theory of elasticity in an isotropic material such as sintered UO_2 shows that only two ultrasonic velocities are needed to assess the elastic constants. Usually the longitudinal (V_L) and the transverse (V_T) velocities are measured. To perform local measurements, frequencies between 50–200 MHz have to be used. In this range of frequencies, the transverse attenuation in irradiated fuel is very high and the transverse velocity cannot be measured. Furthermore, for transverse waves the coupling between the ultrasonic sensor and the sample has to be made with a viscous liquid. Working on irradiated samples in hot cells with such liquids seems difficult. An alternative possibility is to use another ultrasonic wave, which is the Rayleigh surface wave. Its velocity will be called V_R. With the measurement of V_L and V_R, the transverse velocity V_T is deduced using the Eq. (1),

$$V_T^{\,8} - (V_L^{\,2} + V_R^{\,2})V_T^{\,6} + \frac{3}{2}V_L^{\,2}V_R^{\,2}V_T^{\,4} - \frac{1}{2}V_L^{\,2}V_R^{\,4}V_T^{\,2} + \frac{1}{16}V_L^{\,2}V_R^{\,6} = 0 \tag{1}$$

Available in the range

$$0 \le V_T \le \frac{V_L}{\sqrt{2}} \tag{2}$$

The elastic moduli (E and G) and the Poisson's ratio ν are then calculated as follows:

$$E = \rho V_T^{\,2}\,\frac{3V_L^{\,2} - 4V_T^{\,2}}{V_L^{\,2} - V_T^{\,2}} \tag{3}$$

$$G = \rho V_T^{\,2} \tag{4}$$

$$\nu = \frac{1 - 2\left(\frac{V_T}{V_L}\right)^2}{2\left(1 - \left(\frac{V_T}{V_L}\right)^2\right)} \tag{5}$$

Where ρ is the mass density of the material.

For measurements on nuclear fuel oxide, the Rayleigh surface wave velocity is obtained from the acoustic signature (see Section 1.2). Even if theoretically the longitudinal wave velocity can also be assessed with the acoustic signature, in most cases the wave attenuation is too large to permit the detection of the longitudinal velocity in the signature. Therefore, this last velocity has to be measured using a classical echographic technique on a fuel slice about 1 mm thick: with the knowledge of thickness and thanks to the measurement of the propagation time of the ultrasonic wave in the sample, the velocity is simply deduced.

1.2. Rayleigh wave velocity assessment

An ultrasonic focused transducer made of a piezoelectric crystal excited with a sinusoidal voltage, settled on a silica rod in which a spherical lens has been designed is gradually defocused towards the sample surface along the z axis. Thanks to piezoelectric effect, mechanical (ultrasonic) waves are generated and interferences then created between the specular wave (normal ray) and the Rayleigh wave (which propagates on the surface). The ultrasonic signal received by the piezoelectric crystal

versus z and reconverted in voltage is then pseudo-periodic and is called the acoustic signature $V(z)$. From the measurement of the pseudo-periodicity Δz, V_R is deduced using the following relation:

$$V_R = \frac{V_{fluid}}{\sqrt{1-\left(1-\frac{V_{fluid}}{2.f.\Delta z_i}\right)^2}} \tag{6}$$

Where V_{fluid} is the ultrasonic velocity in the coupling fluid and f is the operating frequency. We recall that the coupling fluid (water, ethanol or methanol for $V(z)$ experiments) ensures the propagation between the sensor and the sample. Using high frequency ultrasonic waves (around 100 MHz), the zone investigated is less than 100 μm, assuming special signal processing is used.

An acoustic image can also be obtained by recording the amplitude of the signal during an x–y scan and transforming it to false colours. It reveals variations of mechanical properties and subsurface micro-cracks. Such pictures are used to identify adequate zones for $V(z)$ measurements.

1.3. Adaptation of the method to irradiated fuel

When samples are already embedded, echographic measurements are impossible as only one free surface is available. Then we have tried to find a way to assess E and G with V_R alone. Indeed for V_R evaluation, only one free surface is needed. Regarding Eqs (1–5) and assuming that the Poisson's ratio is not very different from 0.3, the elastic moduli E and G can be directly related to V_R as follows:

$$\nu \approx 0.3 \Rightarrow \begin{cases} E \approx 3.000 \rho V_R^{\,2} \\ G \approx 1.162 \rho V_R^{\,2} \end{cases} \tag{7}$$

In isotropic materials, such as sintered UO_2, the elastic constants can be determined by measuring only two ultrasonic velocities. Usually, the longitudinal velocity V_L and the transverse velocity V_T are measured. At the frequencies used for local measurements (between 50–200 MHz), the strong transverse signal attenuation makes the transverse velocity measurement impossible. Instead, the Rayleigh surface wave can be considered. The transverse velocity can then be trivially calculated from the longitudinal velocity and the Rayleigh velocity V_R. The elastic moduli E and G and Poisson's ratio ν are then calculated from the relations

$$E = \rho V_T^2 \frac{3V_L^2 - 4V_T^2}{V_L^2 - V_T^2} \tag{8}$$

$$G = \rho V_T^2 \tag{9}$$

$$\nu = \frac{1-2\left(\frac{V_T}{V_L}\right)^2}{2\left(1-\left(\frac{V_T}{V_L}\right)^2\right)}, \tag{10}$$

where ρ is the density of the sample.

The operating principle of the acoustic microscope is shown in Fig. 1.1.

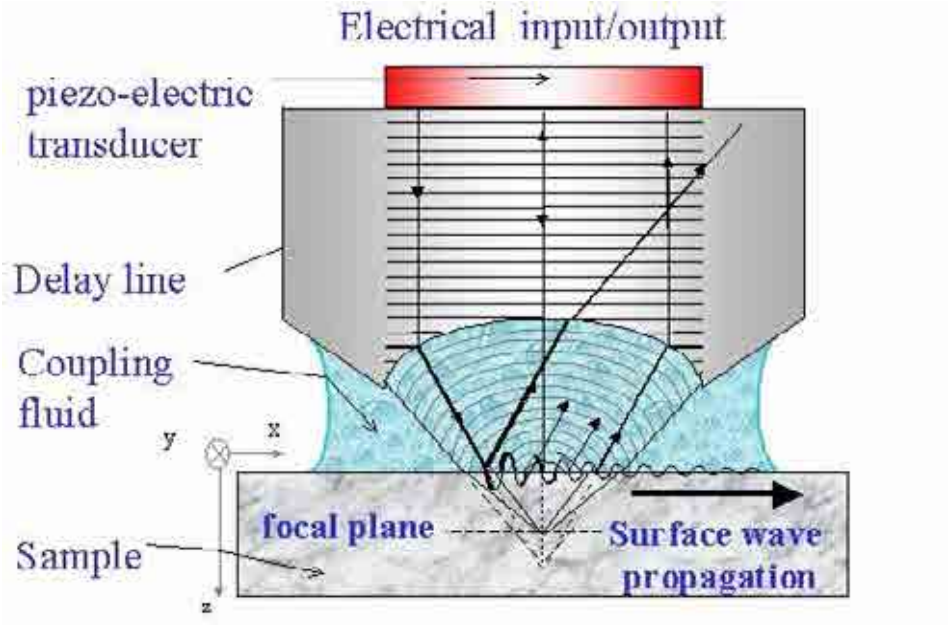

FIG. 1.1 Principle of the acoustic microscope.

The acoustic signal from a transducer is focused by a spherical lens and coupled to the sample by a coupling fluid. A so-called “acoustic signature” is acquired by gradually de-focusing the focused wave of the ultrasonic transducer towards the sample surface. Interference is created between the specular wave (normal ray in the coupling fluid) and the Rayleigh wave which propagates along the surface. The acoustic signature is the pseudo-periodic signal received by the piezoelectric crystal versus the *z* coordinate. The Rayleigh velocity is then obtained by Eq. (6), where Δz is the pseudo-periodicity of the signal, V_{fl} is the ultrasonic velocity in the coupling fluid, and f is the operating frequency.

2. SCANNING ACOUSTIC MICROSCOPE IN HOT CELL

2.1. Device installed at ITU

In 2000, an acoustic microscope was built and introduced into ITU’s hot cell facilities as part of a collaboration with IES (Institut d’Electronique du Sud) at University of Montpellier and EDF. Figure 2.1 shows a photograph of the device in a hot cell. Inside the cell are the sensor heads, translation stage, micrometer motors and acoustic sensors. Outside the cell are the complex electronics which consist of remote triple axis sample movement control electronics, RF amplifiers, acquisition boards, computer for data processing are located outside the hot cell (see Fig. 2.2).

The acoustic sensor is connected with a coaxial cable and fixed in the lower part of the z-axis translation stage. Sensors are easily interchangeable and very rigid in order to withstand high doses of gamma radiation for an extended period of time, as normally the case in hot cells. The x–y–z translation stages are each connected with cables and are remotely controlled (see Fig. 2.2). Micrometric adjustment screws are used to level out the sample platform to ensure an equal distance between sensor and sample in the plane of the scanned area during imaging. The focus distance is based on the direct signal from the sensor which gives a feedback to the z translation stage. The size of the sample platform is restricted by the hot cell layout limitations. In this case a 90 mm large coupling liquid holder is used which gives an effective sample imaging area of approximately 50 × 50 mm which is enough to select an appropriate spot for measuring acoustic velocities. Due to the fact that each sensor gives a different resolution one can select a sensor suitable for the application, as illustrated in Fig. 2.3. In this case 140 MHz was found to give satisfactory results for UO_2 irradiated fuel samples. For each operating frequency a separate sensor head needs to be used (see Fig. 2.3).

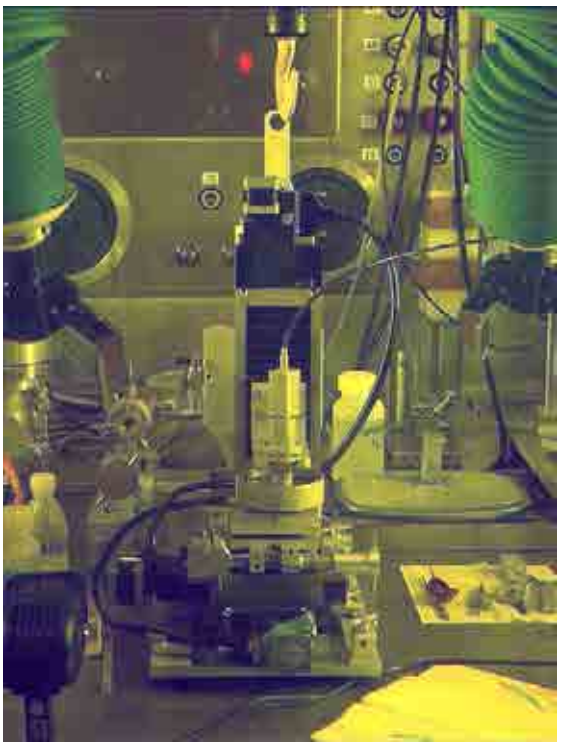

FIG. 2.1. Acoustic microscope installed in hot cell.

Samples with a thickness of about 1 mm are placed in an aluminium sample holder which can hold up to 3 different samples at a time, as shown in Fig. 2.4. After embedding with resin the sample holder is polished to obtain a smooth surface area ready for measurement. Figure 2.5 shows a SEM image of three embedded samples illustrating that this sample preparation can be used for both SEM and acoustic microscopy. The methanol coupling liquid is poured in the basket so the sample holder is completely submerged. After horizontal alignment with two adjusting screws the acoustic sensor is lowered in such a way that no air bubble is trapped which could lead to false readings. The sensor is then further lowered until a few µm distance from the sample and defocusing is started in order to get an acoustic image. The signal from the sensor is converted to an optical signal to be displayed on a computer screen. Figure 2.6(a), (b) shows acoustic and optical images of a UO_2 sample. Micro-cracks can be clearly seen in the subsurface acoustic picture making it helpful to select a suitable area for quantitative measurement.

FIG. 2.2. Overview of the device showing acoustic sensors, coupling liquid holder, sample platform, translation stages.

Frequency	Resolution
1 GHz	1 µm
100 MHz	10 µm
10 MHz	100 µm
1 Mhz	1 mm

FIG. 2.3. On the left, acoustics sensors (from left to right 10 MHz, 80 MHz and 100 MHz). On the right, frequency/resolution correlation.

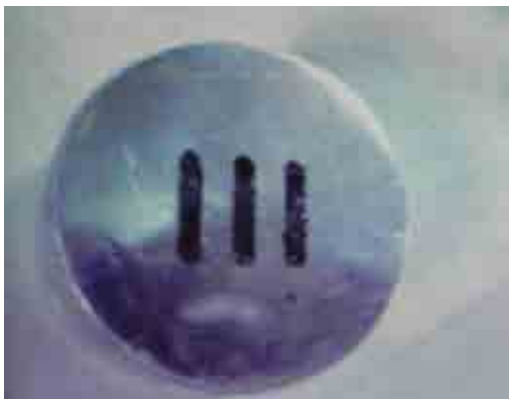

FIG. 2.4. Sample holder containing 3 samples.

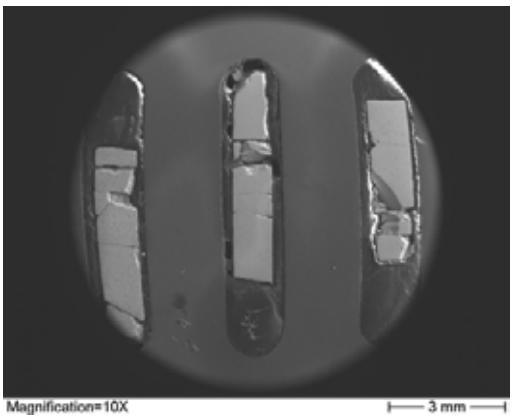

FIG. 2.5. SEM image of 3 samples ready for measurement.

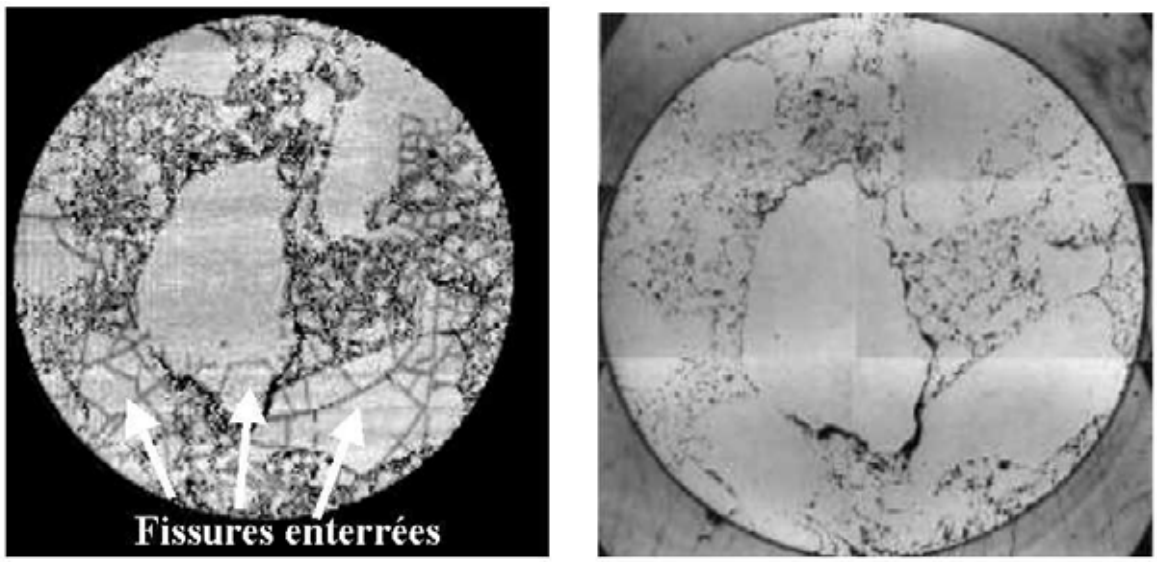

FIG. 2.6. (a) Acoustical image of a UO_2 high burnup sample showing subsurface micro cracks. (b) Optical image of the same sample.

3. RESULTS AND CONCLUSIONS

The acoustic microscope was successfully tested at ITU on samples from the High Burnup Rim Project (HBRP). The experimental results were found to be in agreement with those obtained with a microindenter, also deployed at ITU. Since 2000, the apparatus has been preserved in one of the hot cells. In 2010, with the support of EDF it was decided to install a new acquisition hardware at ITU with a view to integrating acoustic microscopy as a standard characterization technique for spent fuel. In addition to the device in the hot cell, a "cold" acoustic microscope is provided to allow easy calibration of the acquisition electronics. By analysing the available hot cell samples, it was learned how even in the case of well polished specimens some particles could come under the acoustic lens and render the acoustic signature unusable. A specific procedure was developed to eliminate this nuisance. The consistency obtained when measuring at high frequency, obtaining good quality signals indicates that the scanning acoustic microscope is a valid alternative for the evaluation of local elastic properties of irradiated nuclear material. The measurements are local enough to be carried out on pellet fragments. The choice of the acoustic frequency depends on the heterogeneity scale of the material investigated. It is a non-invasive method for material characterisation, which has shown very good accuracy and reproducibility.

The set of results obtained so far using this technique includes simulated fuel samples manufactured at ITU, two sets of irradiated UO_2 and UO_2+ 5% Gd samples from the High Burnup Rim Project with irradiation temperatures ranging from 500–1200°C and burnup ranging from 35–100 $GW{\cdot}d{\cdot}t^{-1}M$, and a N118 BR3 irradiated fuel sample with an average pellet burnup of 68 $GW{\cdot}d{\cdot}t^{-1}M$. For all measurements Young's modulus has been deduced from the V_R value. Despite some scatter in the results, Young's modulus after porosity correction was:

– Almost constant between 0–30 $GW{\cdot}d{\cdot}t^{-1}M$;
– Decreasing by about 25% between 30–80 $GW{\cdot}d{\cdot}t^{-1}M$;
– Stabilized above 80 $GW{\cdot}d{\cdot}t^{-1}M$ and consistent with SIMFUEL analogues;
– Similar observations were made for $(U,Gd)O_2$ fuels.

The whole body of data showed a general decrease of the elastic modulus with burnup (pure UO_2 taken as reference), particularly in the burnup range 0–50 $GW{\cdot}d{\cdot}t^{-1}M$ where in irradiated fuels still no high burnup transformation has occurred, with an apparent stabilisation above 100 $GW{\cdot}d{\cdot}t^{-1}M$ (to be confirmed by future measurements). New sets of fuel samples will be identified for the next measurement campaigns; ongoing and new projects will ensure the need for measurements in the coming years.

BIBLIOGRAPHY

[1] DESPAUX, G., LAUX, D., KELLERBAUER, A.I., WALKER, C.T., Installation of a scanning acoustic microscope in hot cell. Measurement campaign on irradiated fuel. JRC-ITU-TN-UM2-IES (2010)/13, European Commission, Joint Research Centre, Institute for Transuranium Elements, Karlsruhe (2010).

[2] LAUX, D., DESPAUX, G., SAUREL, J.M., CROS, D., Caracterisation du comportement mecanique du combustible nucleaire par methodes microacoustiques; Bilan de la campagne de mesures au TUI, Internal report of the Université Montpellier, II. Sciences et techniques du Langedoc, Laboratoire d´analyse des interfaces et de nanophysique (1999).

[3] LAUX, D., DESPAUX, G., SAUREL, GLATZ, J.P., SPINO, J., RONDINELLA, V., BARON, D., TUI second campaign on HBRP samples, European Commission, DG Joint Research Centre – Institute for Transuranium Internal Technical Report (2002).

[4] BARON, D., MASSON, R., GATT, J.M., SPINO, J., LAUX, D., Evolution of the nuclear fuel mechanical properties with burnup an extensive European experimental program, 2005 Water Reactor Fuel Performance JNS-ENS-ANS meeting, Kyoto (2005).

[5] LAUX, D., Caracterisation mecanique de combustibles nucleaires a fort taux de combustion par methods micro-acoustiques, University Montpellier, Montpellier (2002).
[6] INSTITUTE FOR TRANSURANIUM ELEMENTS, Activity report (2005).
[7] LAUX, D., BARON, D., DESPAUX, G., Projet international HBRP. Mesure des constantes elastiques sur UO_2 et UO_2+5% Gd du materiau non irradie jusqu'a 100 GWJ/TU, Technical note EDF HT-25/02/053/A, Électricité de France (2003).
[8] LAUX, D., BARON, D., DESPAUX, G., KINOSHITA, M., Determination of high burnup nuclear fuel elastic properties by micro acoustic method, Journal of Nuclear Materials **420** (1–3) (2012) 94–100.

NON-DESTRUCTIVE FISSION GAS RELEASE DETERMINATION OF IRRADIATED EXPERIMENTAL FUEL RODS USING GAMMA SPECTROMETRY

H.K. JENSSEN, B.C. OBERLÄNDER
OECD Halden Reactor Project
Institutt for Energiteknikk
Halden, Norway
Email: haakonj@ife.no

Abstract

The trend towards higher burnup of commercial nuclear fuel enhances the fission gas release (FGR) and related phenomena like high burnup rim structure. Rod internal pressure may exceed the reactor system pressure resulting in clad creep-out which can disturb normal reactor operation. A high purity germanium (HPGe) Ortec detector system was utilized for acquisition of gamma photons characterizing disintegration of Cs-137 and Kr-85 fission products in nuclear fuel rods irradiated in the OECD Halden Reactor in Norway. The main purpose of the technique is to estimate the released fission gas krypton and xenon of UO_2 and MOX fuel rods without performing destructive puncturing and subsequent mass spectrometer analysis. The gamma spectrometry was performed at the Institute for Energy Technology's hot laboratory at Kjeller located in the Oslo area.

1. INTRODUCTION

A high-purity germanium (HPGe) Ortec detector system was utilized for acquisition of gamma photons characterizing disintegration of Cs-137 and Kr-85 fission products in nuclear fuel rods irradiated in the OECD Halden Reactor in Norway. The main purpose of the technique is to estimate the released fission gas krypton and xenon of UO_2 and MOX fuel rods without performing destructive puncturing and subsequent mass spectrometer analysis.

Kr-85 is the only radioactive isotope of the fission gases that is produced under nuclear fission with a half-life that is high enough (10.78 year) for estimation of the total fission gas release. The main gamma peak of Kr-85 is located at 514 keV. This is a somewhat troublesome energy, since it is very near to the electron–positron annihilation peak at 511 keV and the 512 KeV gamma peak of Ru-106 / Rh-106. Deconvolution of the Kr-85 peak is performed with the ORTEC software "gammaVision" from Advanced Measurement Technology, Inc.

Another complicating factor is the understanding of gamma ray interaction with matter and to calculate the gamma rays absorption / transmission of the nuclear fuel rod itself and for eventual extra lead shield set-ups utilized in the measurement configurations. The gamma ray self-absorption is calculated with the software "microShield" from Groove. This simplifies the amount of work relative to the normal way of manual calculations involving the modified Bessel and Struve functions [1].

From the quantum mechanical point of view, a scattering event is a collision of two particles, e.g. a photon and an electron or a photon and an atom. From the laws of conservation of energy and momentum it follows that due to scattering by electrons, the photon energy must decrease.
This effect, which was first described in 1922 by the US physicist Arthur H. Compton, became one of the cornerstones of quantum mechanics. When photon energy is of the order of 10 keV or more, Compton scattering is the dominant scattering mechanism when gamma radiation interact with matter.

The irradiation history must be known to calculate the effect of Kr-85 and Cs-137 isotopes production and decay until the gamma scanning is performed. This is a rather straightforward calculation based on the solution of a first order differential equation assuming negligible absorption cross-section of the Kr-85 and Cs-137 isotopes [3].

There are several ways to obtain the efficiency calibration of the measurement set-up for gamma radiation from Kr-85 and Cs-137 isotopes. An irradiated fuel rod with known Cs-137 activity was selected when the absolute efficiency is needed.

2. EXPERIMENTAL AND RESULTS

2.1. Kr-85 methods

Two different non-destructive methods are discussed for estimation of released fission gases in irradiated fuel rods. One method is based on gamma spectrum measurements of Kr-85 in the plenum and of Cs-137 of the fuel stack column (method 1). This method is first explained. The other method is based only of gamma spectrum measurement of Kr-85 in the plenum (method 2). These methods were originally developed at Studsvik and at SCK-SCN institutes. Nowadays, it is interesting to use the methods because new software (e.g. microshield) makes the interpretations and measurements easier.

Method 1:
(1) Measurement of Kr-85 in the plenum

Assuming the release rate of fission gas is equal for all gas atoms and isotopes, the number of Kr-85 gas atom in the plenum is given by,

$$N_{Kr85} = F_{tot} \times \gamma_{Kr85} \times FGR \times D_{Kr85}$$

F_{tot} is the total number of fission and γ_{Kr85} is the fission yield of Kr-85. FGR is the fission gas release rate and D_{Kr85} is the effect of decay, which means the ratio of residual Kr-85 which has not been decayed at the day of gamma spectrometry performance.

When the number of detected Kr-85 in the plenum by gamma spectrometry is R_{Kr85}, a correlation between R_{Kr85} and N_{Kr85} is as follows,

$$R_{Kr85} \times V_{free-volume} = N_{Kr85} \times \lambda_{Kr85} \times A_{Kr85} \times B_{Kr85} \times E_{Kr85}$$

$V_{free\text{-}volume}$ is the free volume of the fuel rod and λ_{Kr85} is the decay constant of Kr-85. A_{Kr85} is the γ ray abundance (emission probability through disintegration of γ ray emission) of Kr-85 which is defined as number of photon emitted per decay and its value is 0.434%. B_{Kr85} is the effect of absorption, which means a ratio of Kr-85 escaping from absorption by plenum spring, cladding (escape probability). E_{Kr85} is the detector and set-up efficiency.

$$R_{Kr85} \times V_{free-volume} = F_{tot} \times \gamma_{Kr85} \times FGR \times D_{Kr85} \times \lambda_{Kr85} \times A_{Kr85} \times B_{Kr85} \times E_{Kr85}$$

$$\Leftrightarrow F_{tot} = R_{Kr85} \times \frac{V_{free-volume}}{\gamma_{Kr85} \times D_{Kr85} \times \lambda_{Kr85} \times A_{Kr85} \times B_{Kr85} \times E_{Kr85}} \times \frac{1}{FGR}$$

(2) Measurement of Cs-137 in the fuel stack

Following the same way as for Kr-85, the number of detected Cs-137 in the fuel stack $R_{Cs\text{-}137}$ is given by,

$$R_{Cs137} \times V_{fuel} = F_{tot} \times \gamma_{Cs137} \times D_{Cs137} \times \lambda_{Cs137} \times A_{Cs137} \times B_{Cs137} \times E_{Cs137}$$

$$\Leftrightarrow F_{tot} = R_{Cs137} \times \frac{V_{fuel}}{\gamma_{Cs137} \times D_{Cs137} \times \lambda_{Cs137} \times A_{Cs137} \times B_{Cs137} \times E_{Cs137}}$$

Relating the two expressions for F_{tot} we get,

$$FGR = \frac{R_{Kr85} \times V_{free-volume} \times \gamma_{Cs137} \times D_{Cs137} \times \lambda_{Cs137} \times A_{Cs137} \times B_{Cs137} \times E_{Cs137}}{R_{Cs137} \times V_{fuel} \times \gamma_{Kr85} \times D_{Kr85} \times \lambda_{Kr85} \times A_{Kr85} \times B_{Kr85} \times E_{Kr85}}$$

Method 2:

$$n_i = \frac{C_i^{decay} \times C_i^{shielding}}{E_{i,Kr85} \times VA_{Kr85} \times A_{Kr85}} \times I_i$$

n_i equals the volume of Kr-85 per unit length at STP conditions of fuel rod i at the end of irradiation (EOI), i.e. [cm^3/mm]. I_i is the γ-ray peak intensity (cps) of Kr-85 of the fuel rod i. C_i^{decay} is the compensation coefficient of the decay of Kr-85 of the fuel rod i from the end of irradiation (EOI) to the day of measurements. A_{Kr85} is defined under method 1.

$$C_i^{decay} = e^{\frac{ln2}{T_{0.5}}(t_{spec}-t_{EOI})}$$

where $T_{0.5}$ is the half-life period of Kr-85 (10.78 years) and (t_{spec}-t_{EOI}) is the time period from end of irradiation to the day of gamma scanning.

$C_i^{shielding}$ (B_{Kr85i}^{-1}) is the compensation coefficient (escape propability^{-1}) of the γ ray shielding of the fuel rod i and E_i is the detector efficiency of Kr-85 at 514 keV[$\frac{cps}{Bq/mm_{plenum}}$]. VA_{Kr85} is the Kr-85 intensity per volume at STP, i.e. 0.55×10^{11} Bq·cm^{-3}.

$V(^{85}Kr_{i,EOI}^{released}) = n_i \times \frac{V_i^{free}}{S_i}$ I.e. gas emission volume (cm3 of Kr-85 at STP) of the fuel rod i at EOI. S_i is the cross section area of the fuel rod (interior) for fuel rod i. V_i^{free} is the free-volume of the fuel rod i at the time of EOI.

When calculating the total gas volume from the volume of Kr-85, the Kr-85/Kr ratio as well as the Xe/Kr ratio is necessary to know. The experiences from earlier chemical analysis of fission gasses are used for estimation of these parameters.

The total gas volume of [Xe and Kr] at STP is calculated using the following equation.

$$V(Xe+Kr)_{i,EOI}^{released} = [1 + \ Xe/Kr\ _{i,EOI}] \times \frac{V(^{85}Kr_{i,EOI}^{released})}{(^{85}Kr/Kr)_{i,EOI}}$$

$V(Xe+Kr)_{i,EOI}^{released}$ is equal to gas emission volume at EOI of the fuel rod i and

$Xe/Kr\ _{i,EOI}$ is the Xe/Kr ratio at EOI of the fuel rod i and $(^{85}Kr/Kr)_{i,EOI}$ is the Kr-85/Kr ratio at EOI of the fuel rod i.

The fission gas release (FGR) is expressed as the total fission gas released to the total fission gas produced in the fuel.

$$FGR_i = \frac{(Xe+Kr)_{i,EOI}^{released}}{(Xe+Kr)_{i,EOI}^{produced}} \times 100\ [\%]$$

The total amount of produced Xe+Kr (cm^3 at STP) is given by the following
$V\ Xe+Kr\ _{i,EOI}^{produced} = 0.030/0.031 \times (BU)_i \times (ifhm)_i$ where 0.030 is utilized for UO_2 fuels and 0.031 is utilized for MOX fuels.

2.2. Production and decay calculations

The general solution for the irradiation/decay problem includes solution of the following differential equation,

$$\frac{dN_i}{dt} = \gamma_i \times F - \lambda_i \times N_i$$

The index i represent the isotope. N is the isotope density and λ is the disintegration constant. γ is the fission yield and F is the fission rate. If we assume the fission yield and rate to be constant, the following solution gives the isotope density during the j'th irradiation and decay cycle

$$N_{j,i}\ t\ = \frac{\gamma_i F_j}{\lambda_i}\ 1 - e^{-\lambda_i t}\ + N_{j-1,i} e^{-\lambda_i t}$$

This expression must be used several time when many irradiation cycles are performed and t equals the irradiation time or cooling time when only decay takes place. $N_{j-1,\,i}$ equals the isotope density just before the j'th irradiation and decay cycle starts, i.e. $N_{j,i}(0) = N_{j-1,i}$. The index j represents the various irradiation and decay cycle. The total number of produces atoms is $F_j \times T_{irradiation}$. This number is used for normalisation of the irradiation/decay result $N_{j,i}(t)$.

2.3. Gamma ray absorption with matter

Calculations of absorption effects (escape probabilities) for gamma rays traversing the fuel sample itself (self-absorption) and other shielding materials (lead) utilized in the set-up for Kr-85 measurements is performed with "microShield" radiation software from Grove. This software can handle many sources and shields configurations and thereby making the calculation possible in an easy way. Cylindrical source and clad with various lead shields is the configuration normally utilized in the simulations performed for Kr-85 measurements of fuel rods. The calculation results (i.e. exposure $mR \cdot h^{-1}$) are compared to similar results obtained from transmission of the actual gamma rays in air. The end results from the calculations give the escape probabilities for the gamma rays, i.e. the fraction reaching the detector area.

2.4. Efficiency calculations

For utilization of method 1, it is only necessary to know the relative efficiency ($E_{Cs\text{-}137}/E_{Kr85}$) between the gamma signals of Cs-137 (661.66 keV) in the fuel stack and for Kr-85 (514 keV) in the plenum. This can be achieved by acquisition of gamma spectrum from the actual fuel rod itself. By relating the Cs-134 peak signals in the fuel spectrum, it is possible to estimate the linear relative efficiencies for the fission gas release estimations. It is no need for any other calibration sources. The definition for the set-up efficiency is given by

$$E_i = \frac{I_i}{Activity_i \times B_i \times A_i}$$

Where the index i represents the different energy peaks belonging to the specific source isotopes. The B_i is calculated by using the radiation software from Grove. By comparing the fractions of various energy peaks in a specific isotope the activity is the same and is thereby not needed. However, for absolute efficiency calculations, a calibration fuel rod is suitable. Cs-137 peak activity is first measured and utilized in the absolute efficiency calculations. The assumption of a linear efficiency behaviour is a good approximation in the energy area of interests. The accuracy in the results will increase with utilization of relatively long acquisition times for the gamma spectra (e.g. 2–5 days) and for larger activity in thei fuel rod.

2.5. Example of Kr-85 method applied on two UO_2 fuel rods

Two 16% enriched UO_2 fuel rods (A and B) irradiated simultaneously in the Halden Boiling Water Reactor were selected to demonstrate the application of the Kr-85 methods. The irradiation was performed in 4 cycles accumulated up to 5.5 years with decay times of several months in between the in-pile reactor services. The burnup for the two rods was 58 $MW \cdot d \cdot kg^{-1}$ oxide. The diameter of fuel and cladding tube was 8.36 mm and 9.5 mm respectively with a clad thickness of 0.57 mm. The initial fuel oxide weight was 163.6 g for both rods. The dimensional data was used to calculate the escape probabilities from "microshield". In addition to the self-absorption of the source an extra lead shielding was located just in front of the gamma acquisition HPGe detector. The escape probabilities were 0.133 for the Kr-85 and 0.194 for the Cs-gamma radiation. It should be emphasized that the escape probability is strongly influenced by the extra shielding layers introduced in the measurement set-ups.

The equation of isotope densities given under Section 2.2 is utilized for calculations of the effect of irradiation and decay or in other words the fractions which is not yet decayed at the time of measurements. The calculation results for the Kr-85 and Cs-137 appearances at the day of gamma measurements were 0.7824 and 0.9143 respectively.

The gamma spectrum measurements were performed in the plenum and fuel stack regions with several days of acquisition time to ensure high accuracy in the collected data, especially for the Kr-85 peak. The count rates for Kr-85 in the plenum were 0.030 cps (rod A) and 0.036 cps (rod B) and 25.25 cps (rod A) and 25.08 cps (rod B) from the Cs-137 accumulated in the fuel stack. The linear coefficient of efficiency ($\Delta E_i/\Delta$keV) was estimated from measurements performed in the fuel stack regions and it was $-\text{konst} \times 1.188 \times 10^{-3}$ per keV for both rods.

Figures 2.1–2.3 show the gamma scanning results acquired from the fuel stack region and plenum of two rods. The fission gas release was 11.3% and 13.5% for rod A and B respectively. These values agree quite well with the results obtained from puncturing and free volume measurements performed after the Kr-85 methods were applied.

The gamma scanning bench is outlined in Fig. 2.4. This is a quite new system with possibilities for x, y and z movements in addition to rotation of the sample under gamma scanning and spectrum acquisitions. The bench was built at the hot laboratory with the assistance of the electronics department at the institute.

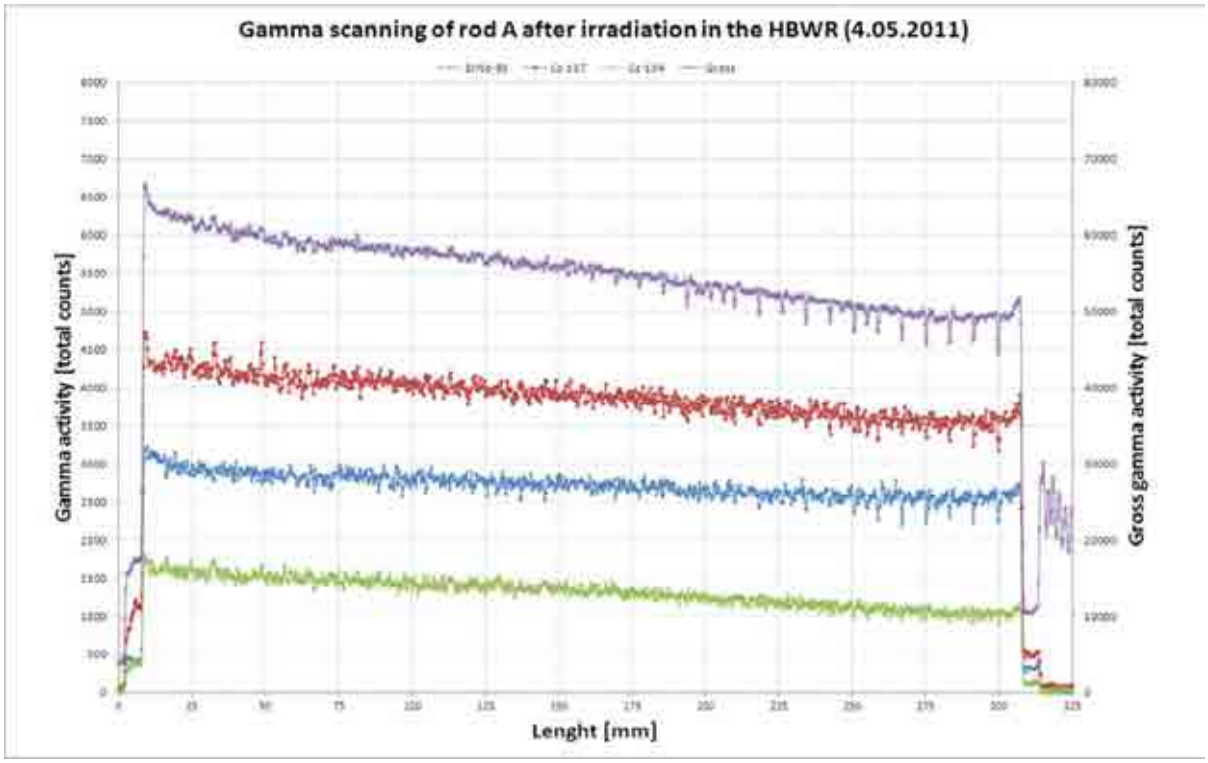

FIG. 2.1. Gamma scanning results obtained from rod A after 5.5 years of irradiation in the HBWR.

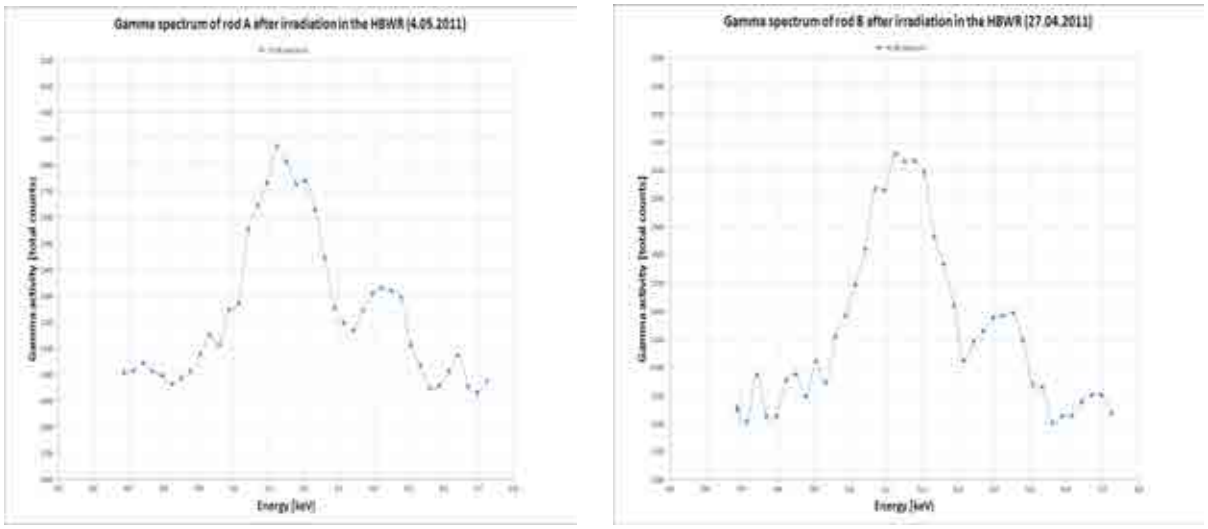

FIG. 2.2. Gamma spectrum of Kr-85 (514 keV) results obtained over the plenum of rods A and B performed after 5.5 years of irradiation in the HBWR.

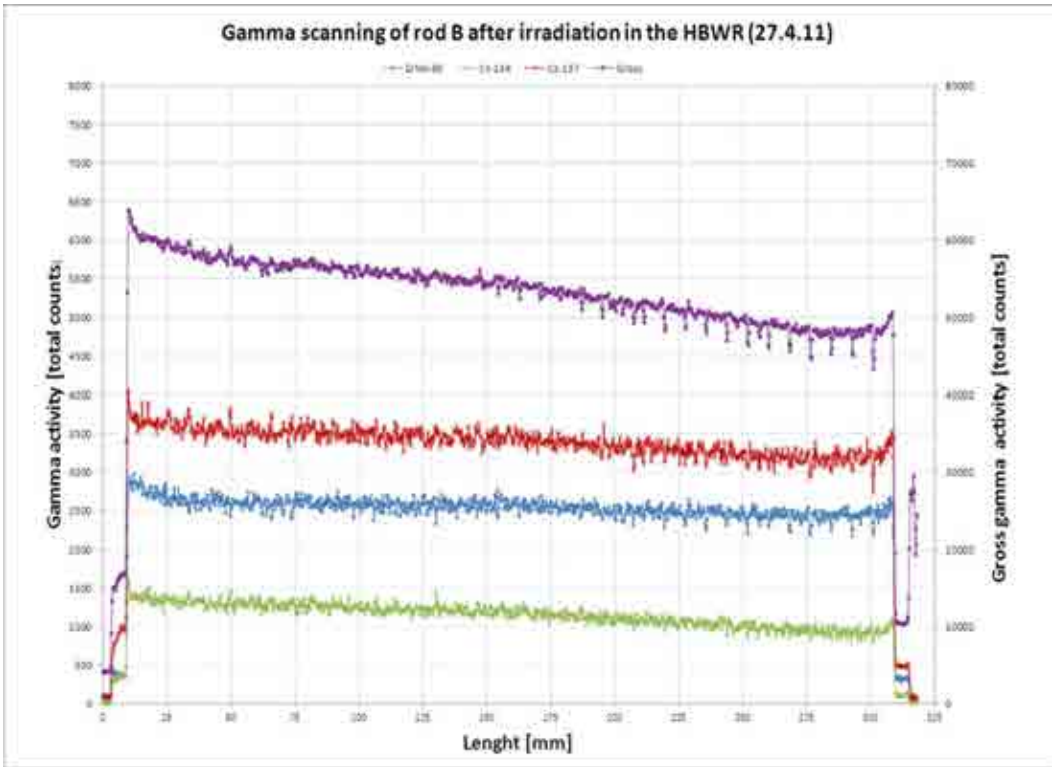

FIG. 2.3. Gamma scanning results obtained from rod B after 5.5 years of irradiation in the HBWR.

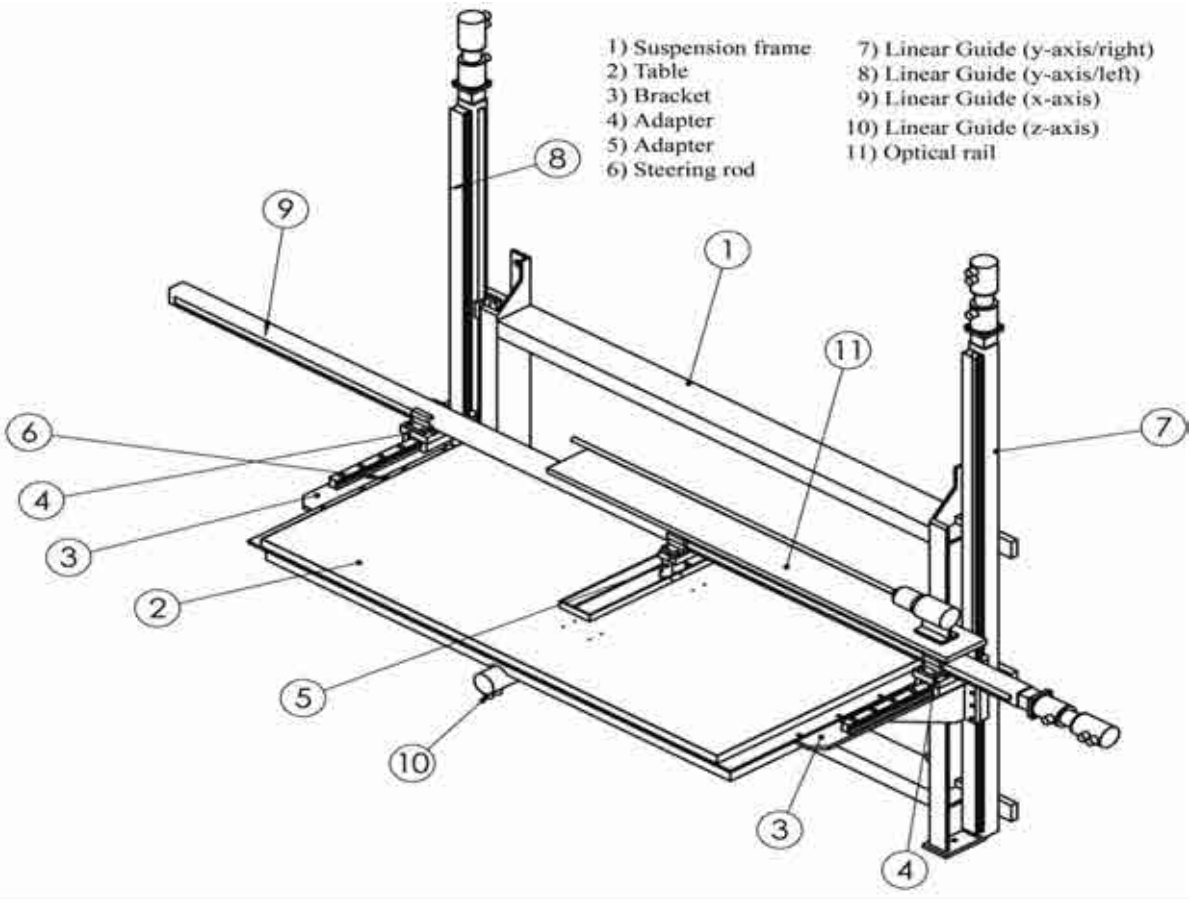

FIG. 2.4. Gamma scanning bench outlines with 3-axis system and sample rotation possibilities.

3. SUMMARY

The main purpose of the technique is to estimate the released fission gas krypton and xenon of UO_2 and MOX fuel rods without performing destructive puncturing and subsequent mass spectrometer analysis. Sometimes it is also impossible to do destructive puncturing and fission gas analysis on the fuel rods, e.g. when further irradiation is demanded.

The utilization of “microShield” software makes any need of complicated standards unnecessary. This situation simplifies the Kr-85 measurements and decreases the acquisition times needed for measurements of fission gas release. Also, the price of radioactive standards has increased enormously the last few years.

The Kr-85 method 1 is based on a relative comparison of Kr-85 and Cs-137 measurements and the calibration data or efficiency is acquired from the fuel rod itself. This simplifies the measurements and the final results are achieved easy and fast. The results for the FGR based on the Kr-85 method is in good agreement to the results obtained from puncturing and free volume measurements of the two rods.

For utilization of method 2 it is necessary to know the Kr-85/Kr amount and the Xe/Kr relations for the actual rods. These data is normally well known from other types of measurements performed earlier e.g. mass spectrometer and puncturing data on similar rods. This method also requires a calibration fuel rod for simultaneous measurements of the Kr-85 efficiency determination for the various set-ups in use.

REFERENCES

[1] PARKER, J.L., The use of calibration standards and the correction for sample self-attenuation in gamma-ray non-destructive assay, Los Alamos National Laboratory report 10045 (1986).

[2] TERREMOTO, L., Gamma-ray spectroscopy on irradiated fuel rods, 2009 International Nuclear Atlantic Conference, Rio de Janeiro (2009).

[3] SOBIESKA, M., HVAL, S., Karakterisering av lavaktivt restavfall fra betongcellene på Metlab2, IFE/I-2004/06 (2004).

PULSED EDDY CURRENT DEFECTOSCOPY OF IRRADIATED WWER FUEL RODS

S.S. SAGALOV, E.A. ZVIR, D.V. MARKOV, S.V. PAVLOV, A.V. SUKHIKH
JSC “SSC RIAR”
Dimitrovgrad, Russian Federation
Email: adm@niiar.ru

Abstract

Defectoscopy of irradiated WWER fuel rods in the RIAR hot cells is performed by means of pulsed eddy current method. Uniformity defects, local geometry anomalies can be formed during the operation of fuel rods. For failed fuel rods, appearance of secondary defects related to water ingress, oxidation and hydrogenation of ZR alloy cladding is typical. The defectoscope consists of two modules built in the industrial computer-pulse generator and analog-to-digital converter (ADC). To reveal and identify anomalies, A-, D-scans, envelope curves and hodograph curves of pulse signal are used. The EC-method makes it possible to reveal damaged fuel rods in failed WWER fuel assemblies (FAs), determine location and identify primary through defects and secondary anomalies. Totally 49 WWER FAs, including 18 failed FAs, were examined by means of this method.

1. INTRODUCTION

Eddy current (EC) defectoscopy is one of the main methods for non-destructive control of irradiated fuel elements in the hot cells of the RIAR Material Testing Complex [1]. This method is applied at one of the initial stages of PIEs for fuel elements: presence of anomalies in fuel rod claddings is revealed when passing the fuel rods discharged from the fuel assemblies through the EC-sensor. Abnormal fuel rods are then sent for further NDEs and DEs needed for evaluation of their state.

2. OBJECTS OF DEFECTOSCOPY

Figure 2.1 presents the design of the researched WWER-440 and WWER-1000 fuel rods. Initial outer diameter of the fuel rod cladding is 9.1 mm, wall thickness — 0.69 mm, material — alloy E110 (Zr-1%Nb).

Defects typical for the irradiated WWER fuel rod claddings can be divided into two categories: uniformity defects and local changes in diameter. Among the uniformity defects of the cladding outer surface there are:

– Fretting wear resulting from interaction of the fuel rod cladding with the spacer grids of FAs;
– Debris defects – traces of interaction of the claddings with foreign objects in the coolant;
– Local (nodular) corrosion;
– Cracks.

Development of outer and inner defects across the entire thickness of the cladding results in through defects.

As a rule, local changes in the fuel rod diameter are induced by thermal–mechanical interaction of fuel and cladding or penetration of moisture inside the fuel rod with further cladding hydrogenation.

In the claddings of failed fuel rods, super positions of defects in various combinations are formed together with single defects.

Figure 2.2 presents various uniformity defects observed for the irradiated WWER fuel rod claddings.

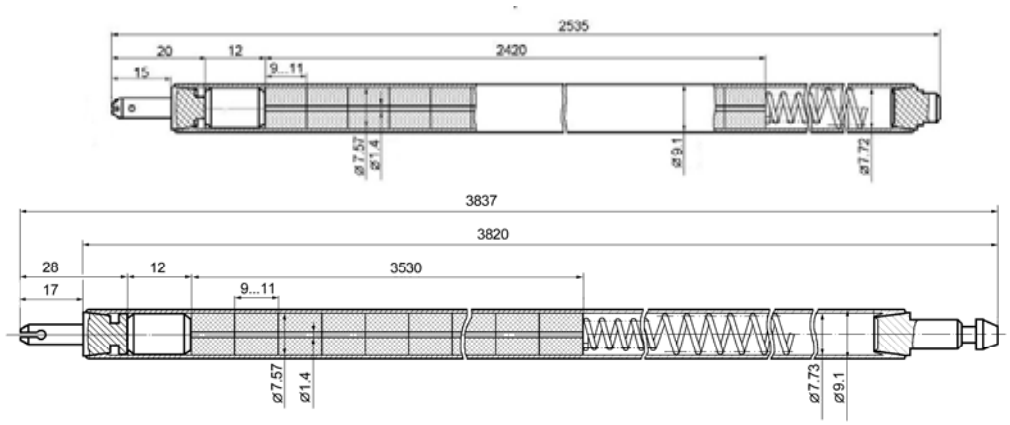

FIG. 2.1. Design of WWER-440 (top) and WWER-1000 (bottom) fuel rods.

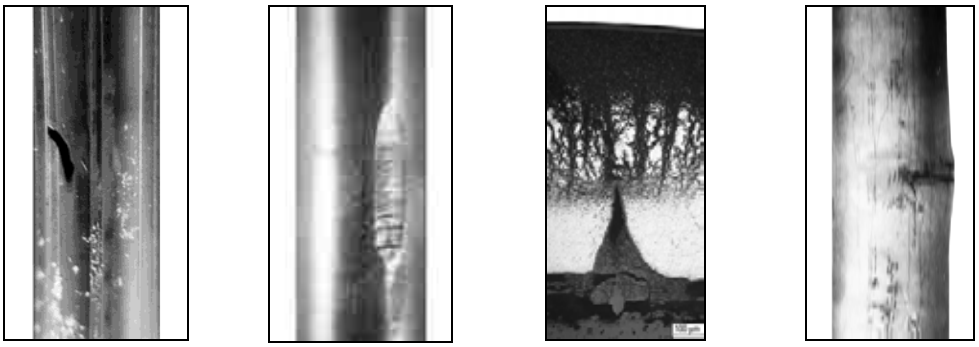

a b c d

FIG. 2.2. Defects of the irradiated WWER fuel rod claddings: (a) debris-defect; (b) fretting-wear; (c) internal hydrogenation; (d) superposition of the through crack and local change in diameter.

Data on the state of spent WWER fuel rod claddings are used for development of reference samples with artificially applied defects simulating actual anomalies. Identification features of defects revealed by scanning of reference samples make it possible to analyse the state of irradiated fuel rod claddings.

3. DEFECTOSCOPY TECHNIQUE AND METHODS

The developed on-line EC control system is based on the pulsed eddy current defectoscope [2]. It consists of a pulse generator and 12-bit analog-to-digital converter (ADC) built in the industrial PC (Fig. 3.1). The main advantages of the pulsed eddy current method are simple hardware design, high self-descriptiveness due to generation of a wide frequency spectrum and high sensitivity to defects. Basic parameters of the EC equipment are as follows: length of fuel rods under inspection, up to 4 m, cladding diameter, 6–15 mm, scanning step, 1 mm, scanning rate, 35 mm·s^{-1}.

Induction coils are used as sensor elements of the EC probe. Measuring coils are switched by differential circuit. They register changes of the electromagnetic field of eddy currents induced in the fuel rod cladding with a transmitting coil to which the generator feeds current pulses. Such probes meet the requirements of the on-line EC control of irradiated fuel rods in hot cells and inspection stands to a sufficient extent. They feature high radiation resistance, low cost, ease of fabrication, possible leaktight execution and high sensitivity to changes of the electromagnetic field within a range of 50–1000 kHz.

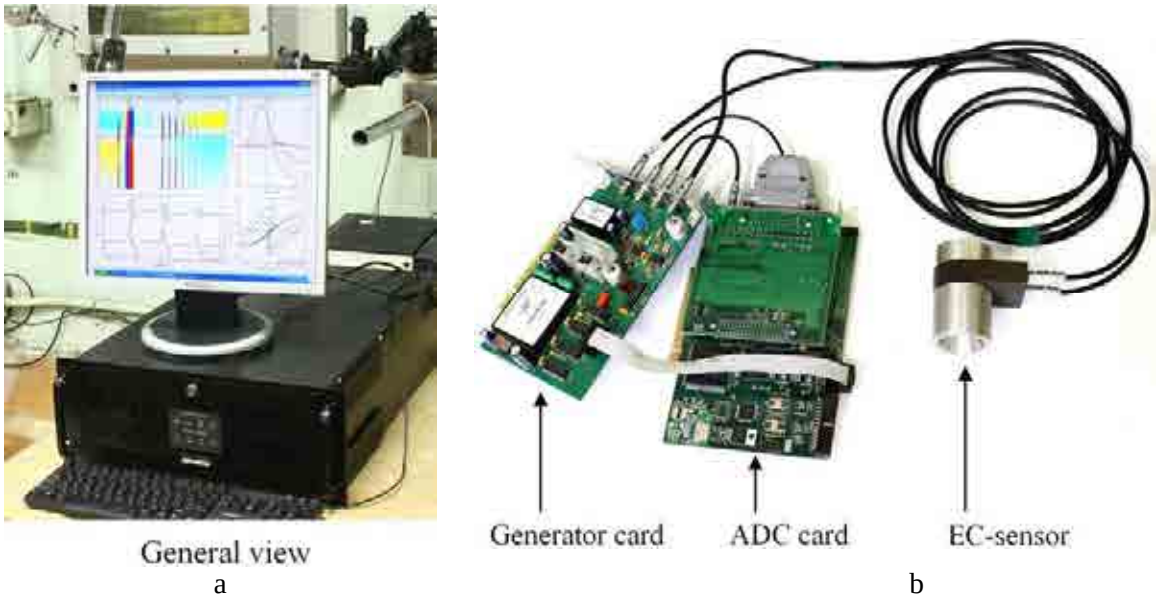

FIG. 3.1. EC equipment for defectoscopy of irradiated fuel rods.

With pulse excitation of eddy currents, identification of defects is based on the evaluation of parameters of A-scan that reflects a variation with time of the amplitude of signal of the inductive EC sensor at the place of defect location (Fig. 3.2) [3]. Response from the defect digitized at N points (strobes) at regular intervals Δt is incorporated in the defectoscope memory and further analysed. Definite moment of time $t_i = i\Delta t$ (i = 1, N) corresponds to a strobe with number i. Duration of the response under analysis is 7 μs, time strobing pitch Δt is 33 ns. Zero-crossing time t_{ZC} is used as an identification feature of the defect.

Figure 3.3 illustrates A-scans for various local defects of the cladding. The A-scans presented differ not only in the value of t_{ZC}, but also in their polarity. For super positions of defects, more complicated A-scan is typical, as well as a great number of zero-crossing points within the set time interval (Fig. 3.3(b)).

Type and relative dimensions of anomalies revealed during the fuel rod scanning are determined using an amplitude–time plane (Fig. 3.4). Values t_{ZC} are plotted as abscissas and values A_m (amplitude of response from defect) as ordinates. Sign of the half-plane corresponds to polarity of the first half-wave of the signal of the defect. Position of regions corresponding to this or that defect type at the amplitude–time plane is identified based on the scanning results of specimens with artificial anomalies of various type and size (for example, defects 1–6 — internal grooves 0.1; 0.2 … 0.6 mm deep).

Figure 3.5 presents the main window of the computer program used to analyse the results of the EC-control of fuel rods. For primary evaluation of the fuel rod state, D-scan is used (Fig. 3.5(a)). It allows rapid revealing of the cladding regions with minor defects [2]. D-scan shows the dependence of the probe response amplitude on the axial coordinate of the fuel rod and a strobing moment of the EC-pulse (strobe number). Amplitude is reflected in bright color shades: the greater the amplitude, the more intense the brightness of the color. Precise characteristics of specific anomalies are identified with A-scans (Fig. 3.5(b)). Envelope curve obtained for a specific strobe number (Fig. 3.5(c)) enables express evaluation of the presence of a certain type of defects for the entire fuel rod. Two envelope curves are used for plotting hodograph curves (Fig. 3.5(d)) the shape of which allows to differentiate a very deep defect from a through one [4]. The envelope curves are selected so that an angle between hodograph curves of internal and external shallow defects is equal to 90°.

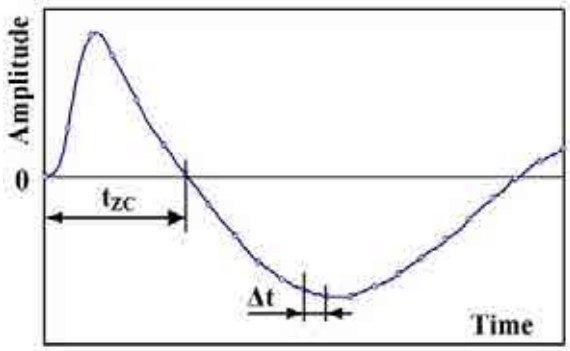

FIG. 3.2. Typical A-scan for the cladding defect.

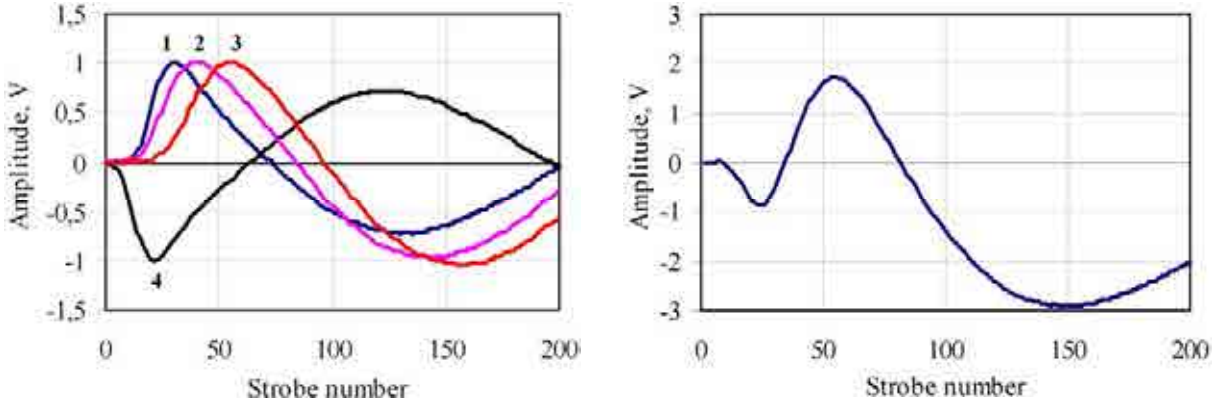

FIG. 3.3. A-scans for single defects (left): (a) 1, 2, 3 — external, through and internal defects of uniformity, 4 — "ridge"; (b) superposition of a "ridge" and through defect of the cladding (right).

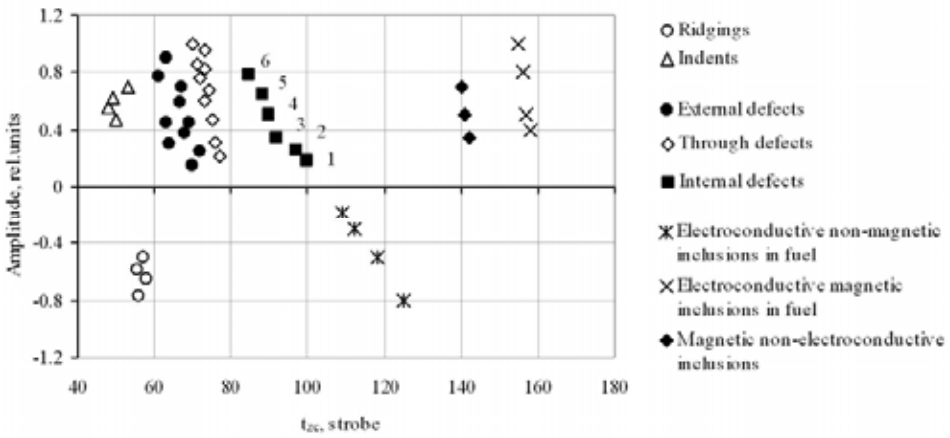

FIG. 3.4. Plane of identification of single defects for WWER fuel rods.

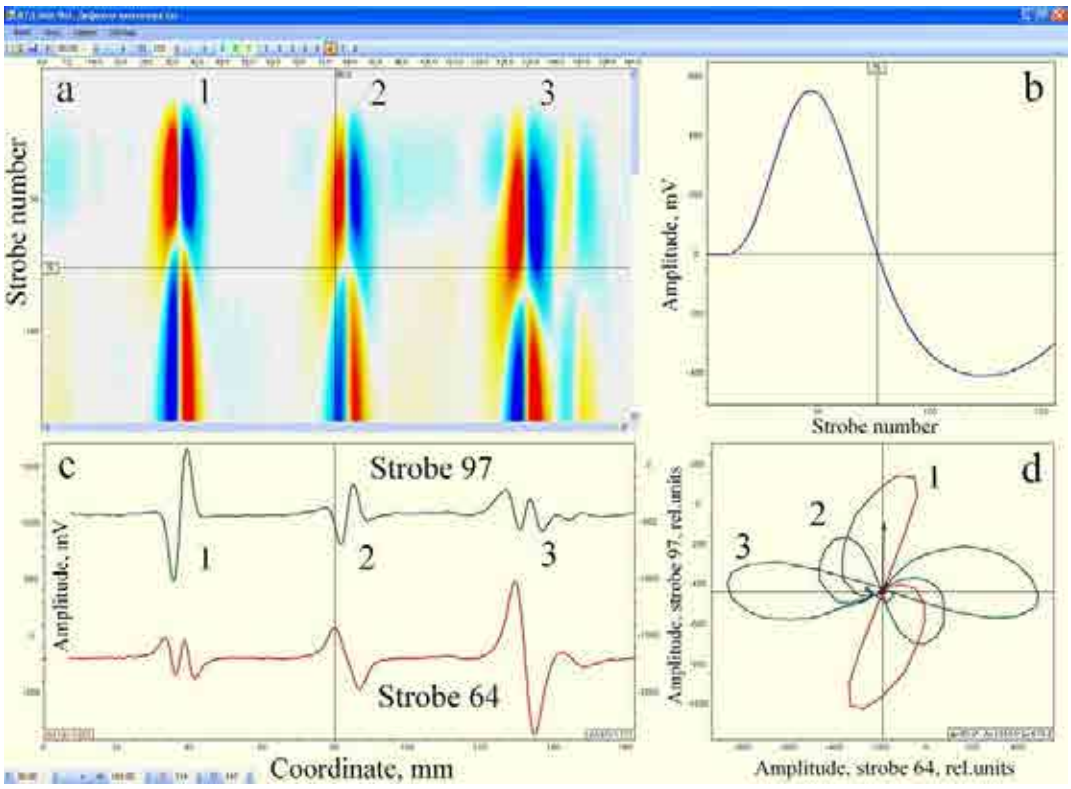

FIG. 3.5. Main window of the computer program showing the EC-control results for the imitator fragment with external (1), through (2) and internal (3) defects: (a) D-scan; (b) A-scan of the through defect; (c) envelope curves of EC-sensor signal; (d) hodograph curves.

4. EXAMPLE OF EC-DIAGNOSTICS OF FUEL ROD STATE

As an example illustrating the capabilities of the developed pulsed EC control system, let us consider a procedure for detecting a damaged fuel rod as a part of failed WWER-1000 FA and diagnostics of the state of its cladding. The EC-diagrams of 311 fuel rods in this FA are typical for leaktight fuel rods. Responses from a spring pin and lower plug were observed, background level was insignificant (Fig. 4.1(a)). Only one fuel rod was found to be abnormal as its EC-diagram had non-typical signals considerably exceeding the background level in the amplitude (Fig. 4.1(b)).

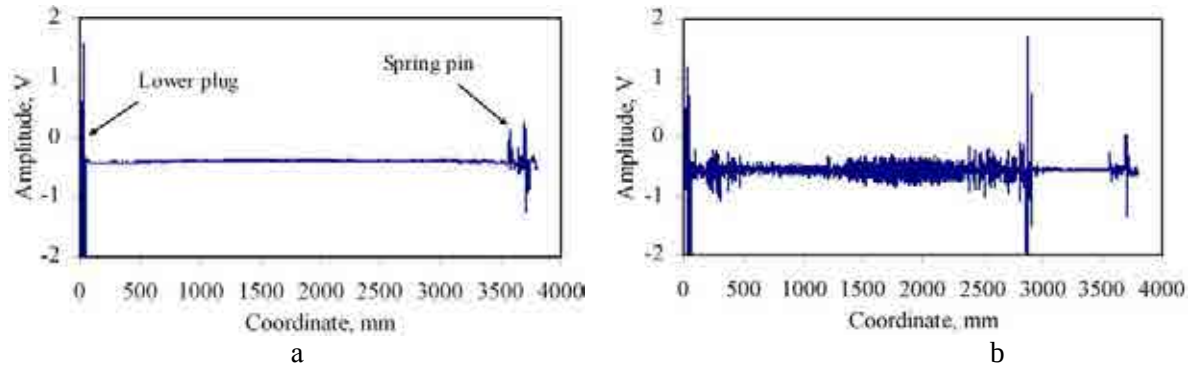

FIG. 4.1. Typical (a) and abnormal (b) EC diagrams of fuel rods.

The amplitude–time analysis of the EC scans of fuel rods showed the presence of a through defect (t_{ZC} = strobe 75) at the coordinate of 34 mm (Fig. 4.2(a)). Visual inspection of this region revealed a through debris-defect in the cladding (Fig. 4.2(b)).

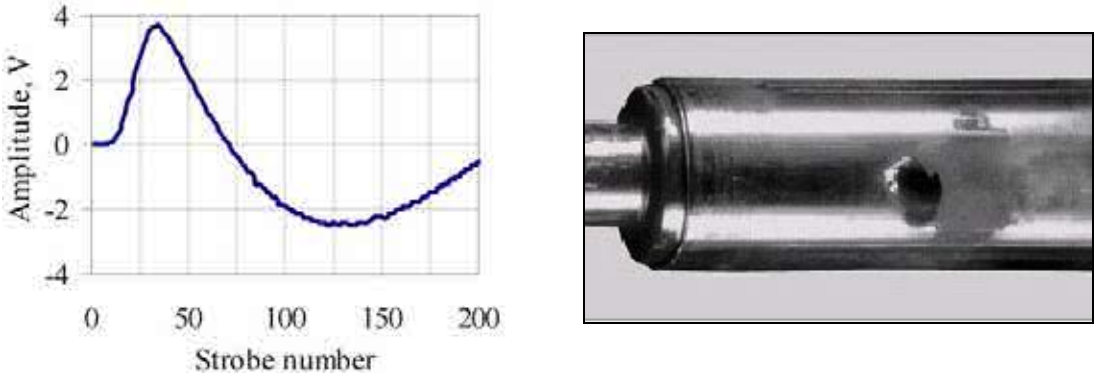

a b

FIG. 4.2. A-scan (a) and image of the through debris-defect (b).

Ingress of the water coolant inside the fuel rod though this defect leads to oxidation and hydrogenation of the inner surface of the cladding. Responses from numerous internal defects of various depth (t_{ZC} = strobe 95–103) were registered in the regions at the coordinates of 34–2400 mm. Metallography of one of such regions showed the presence of corrosion pits 40–50 μm thick on the inner surface of the cladding (Fig. 4.3(a)). The regions at 2400–2900 mm were found to have signals of the superposition of internal defects with local increase in the fuel rod diameter (t_{ZC1} = strobe 30–33, t_{ZC2} = strobe 101–105). Metallography of one of such regions showed significant hydrogenation of the cladding material together with internal non-uniformities, including formation of "sunburst" type hydride layers (Fig. 4.3(b)). As known, such hydrogenation induces the change in the WWER fuel rod cladding diameter due to the difference of molar volumes of zirconium and its hydride [5].

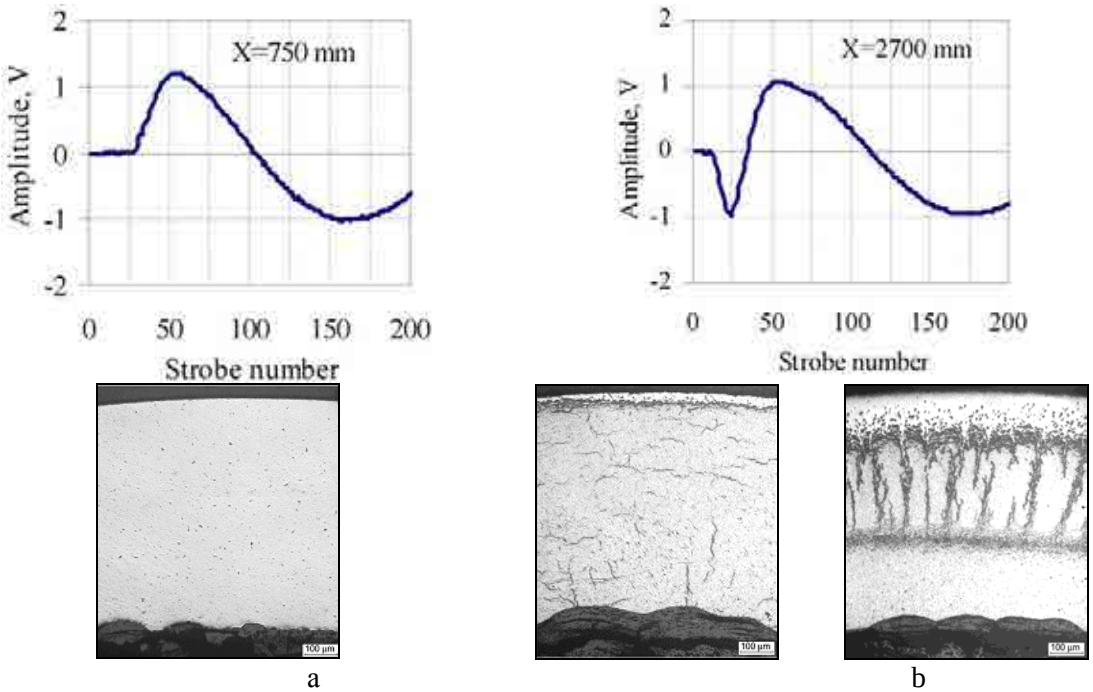

a b

FIG. 4.3. A-scans and images of abnormal regions at 750 mm (a) and 2700 mm (b).

The analysis of A-scans (Fig. 4.3) shows that the pulse EC method can reveal local diameter variations for a failed fuel rod in the regions with maximum hydrogenation. For this purpose, the envelope curve

corresponding to strobe 24 should be used. This strobe demonstrates no EC-sensor reaction to inner non-uniformities. Sensitivity to variation of diameter is maximum (Fig. 4.4(a)). Profilogram obtained by the contact method confirmed the results of the EC-control and showed the presence of the local increase in diameter up to 9.23 mm in the region with the coordinates of 2400–2900 (Fig. 4.4(b)).

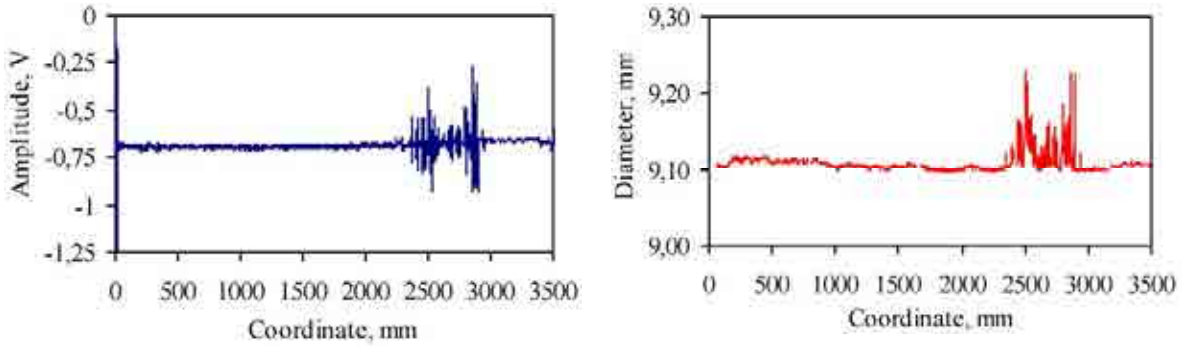

a b

FIG. 4.4. Envelope curve of sensor signal for strobe 24 (a) and profilogram (b) of failed fuel rod.

At 2860 mm, a signal with two zero-crossing points (one corresponds to the local change in diameter, while the other one corresponds to the through-defect of the cladding) was registered (Fig. 3.3(b)). Visual inspection revealed a crack at the coordinate of the EC signal (Fig. 4.3). The through character of the crack was confirmed by the metallography results.

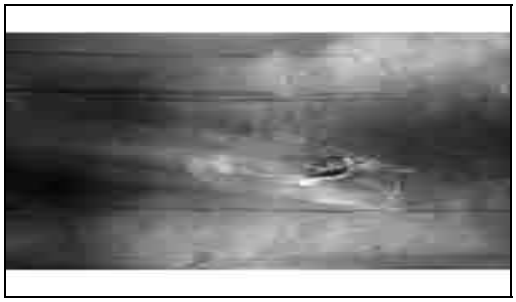

FIG. 4.5. Secondary through defect.

The time period from appearance of the primary through defect to considerable hydride damage of the cladding as a function of specific thermal load is one of the most important characteristics of the WWER fuel. For example, for LWR fuel rods with zircaloy claddings, this characteristic is determined by Loche curve [6].

5. CONCLUSION

The developed pulsed eddy current defectoscope is used for on-line control of the state of irradiated fuel rods in the hot cells of the RIAR Material Testing Complex. Examinations of 49 WWER FAs, including 18 failed FAs, were performed using this equipment. Its capabilities enable us to detect uniformity defects and change in form of the cladding, as well as to identify location of primary and secondary anomalies in failed fuel rods. The analog of this equipment is currently installed in the inspection stand of the cooling pond at the Kalinin NPP [7].

REFERENCES

[1] SUKHIKH, A.V., SAGALOV S.S., PAVLOV S.V., MARKOV, D.V., Application of pulsed eddy current control method for defectoscopy of irradiated WWER Fuel Rods, Atomnaya Energiya, Vol. 107, Issue 2 (2009) 115–118.

[2] PAVLOV, S.V., SUKHIKH, A.V., SAGALOV, S.S., Eddy current control methods in reactor material science, JSC "SSC RIAR" Dimitrovgrad (2010).

[3] GIGUERE, S., LEPINE, B.A., DUBOIS, J.M.S., Pulsed eddy current technology: characterizing material loss with gap and lift-off variations, Research in non-destructive evaluation **13** (2001) 119–129.

[4] SAGALOV, S.S., SUKHIKH, A.V., Pulsed Eddy Current Control Method, PATENT 2377554 RF, МПК[8] G01N27/90, Bulletin of Inventions **36** (2009).

[5] PEREPELKIN, S.O., MARKOV, D.V., POLENOK, V.S., et al., Results of PIEs of failed WWER fuel rods, Proceedings, Issue 4, Dimitrovgrad (2007) 12–21.

[6] LOCHE, D.N., "Mechanisms of deterioration of defected LWR fuel", IWGFPT-6, IAEA Specialists Meeting on Behavior of Defected Zirconium Alloy Clad Ceramic Fuel in Water Cooled Reactors, Chalk River (1980) 101–103.

[7] PAVLOV S.V., SAGALOV S.S., AMOSOV S.V., System of non-destructive control of irradiated fuel rods for inspection stand of WWER Fas, Bulletin of Universities, Nuclear Power Engineering **3** (2010) 5–11.

POSSIBILITIES AND FEATURES OF ELECTRON BACKSCATTER DIFFRACTION FOR REACTOR MATERIALS INVESTIGATION

Y.D. GONCHARENKO, L.A. EVSEEV, V.K. SHAMARDIN, T.M. BULANOVA
State Scientific Center
Research Institute of Atomic Reactors
Dimitrovgrad, Russian Federation
Email: bond@niiar.ru

Abstract

As a result of tightening safety and economic efficiency requirements imposed on operating and newly developed nuclear power reactors, their active cores have been recently fitted with or proposed to be fitted with elements made from different materials with modified structure (Zr-based alloys with specially developed texture; steels the crystal lattice of which is strengthened by nano-particles; various nano-structured materials) allowing either lifetime extension or improvement of performance of these elements, all other parameters being equal. Therefore, it is necessary to study properties of such materials with complicated structure both before their use in nuclear reactors and after reactor irradiation. In so doing, new research methods which allow the investigation into material structure and composition in small nano-size regions of materials should be used. One of such methods is recording and analysis of electron backscattered diffraction (EBSD). It allows the identification of crystallographic structure and its orientation in regions up to 25 nm in size. When applying this method together with X ray spectrum microanalysis, it also becomes possible to identify elemental composition in the same local regions of materials. Combination of these two methods is widely used when studying "standard" non-irradiated materials, however, only X ray spectrum microanalysis is still extensively applied in reactor material testing, what can not be stated for the EBSD method. RIAR has purchased the Zeiss SUPRA55VP, Carl Zeiss AG field emission scanning electron microscope of super high resolution equipped with X ray microanalysis system (wave and energy spectrometer) and HKL EBSD Premium System. Some examples of reactor material studies using EBSD system only or together with energy dispersed X ray spectrometer are presented.

1. INTRODUCTION

As a result of tightened safety and economic efficiency requirements imposed on operating and newly developed nuclear power reactors, their cores have been recently fitted with or proposed to be fitted with components made from different materials with modified structure allowing either lifetime extension or improvement of performance of these components, all other parameters being equal. Therefore, it is necessary to study properties of such materials with complicated structure both before their use in nuclear reactors and after irradiation. In so doing, new research methods should be used, which allow the investigation into material structure and composition in minor nano-size regions. One of such methods is recording and analysis of electron backscattered diffraction (EBSD).

There is a potential possibility to apply this technique for research of structural materials, which structure is strengthened by nano-particles, for example by yttrium oxide particles. This paper presents one more possibility of this method application that is to study the structure of high strained materials deformed in special way to have nano-structural components.

2. SAMPLES DETAILS

The backscattering electrons diffraction registration and the analysis system HKL EBSD Premium System was used to study the steel AISI321 structure after intensive plastic deformation by the method of equal channel angular pressing. This steel in this condition may be proposed to be used in core internal as bolts and pins for PWR type reactors.

The structure of the same steel after low plastic deformation was studied by sing the same method for comparison.

3. RESULTS

Figure 3.1 presents an image of a sample surface prepared for investigation by the secondary electrons method.

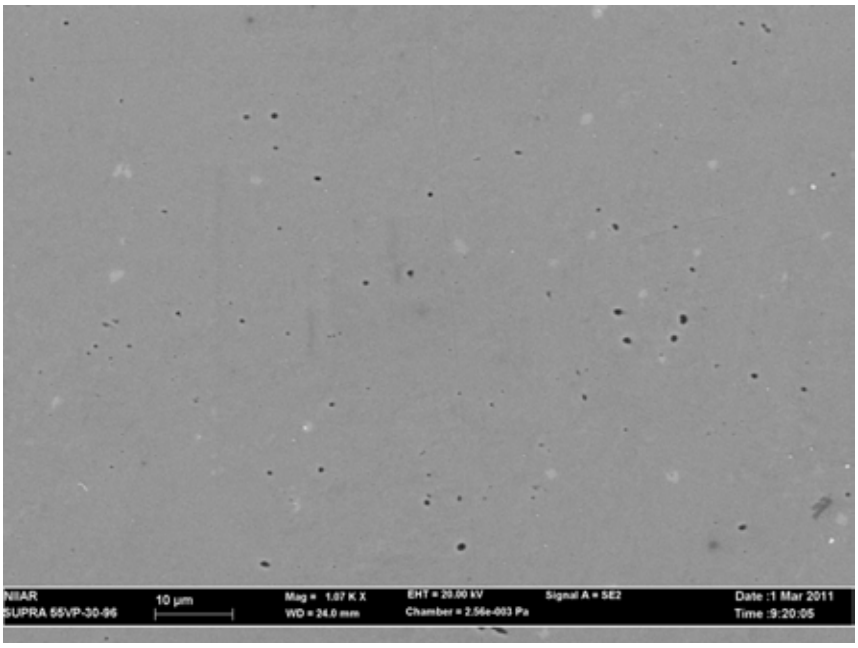

FIG. 3.1. Surface of a sample prepared for investigation.

An important point is that in this case it is difficult to distinguish any peculiarities in the image received in secondary electrons.

Figure 3.2 (top and bottom) present band contrast maps of the slightly deformed sample (Fig. 3.2 (top)) and that one after intensive plastic deformation (Fig. 3.2 (bottom)). When comparing the Figures, one can see a significant difference between the diffraction maps.

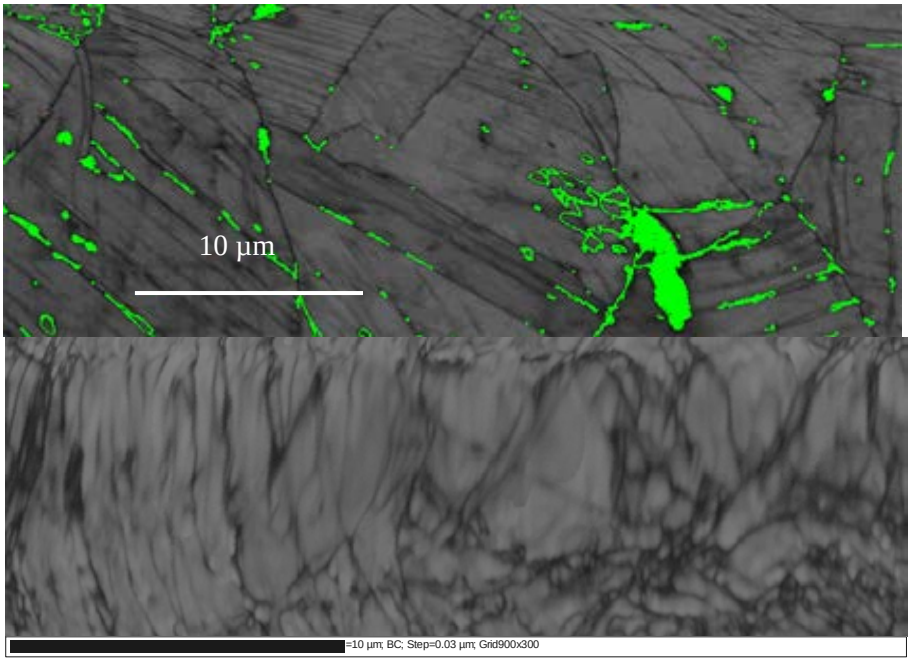

FIG. 3.2. Band contrast map of slightly deformed steel (top). In green, there are areas with zero decisions related to low quality of the slightly deformed sample surface preparation. Band contrast map of steel after intensive plastic deformation by the equal channel angular pressing method (bottom).

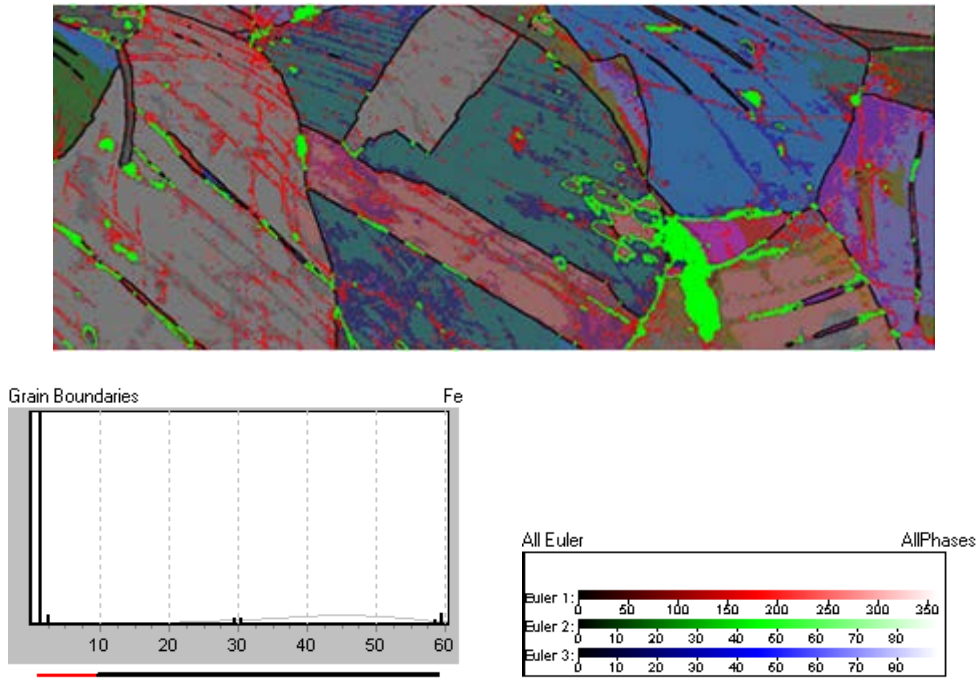

FIG. 3.3. Orientation map of the slightly deformed steel (Euler angles). Black lines: grain boundaries (>10°), red lines: sub-boundaries (>1°), shades of separate surface areas coloring: intra-granular misorientation (<1°).

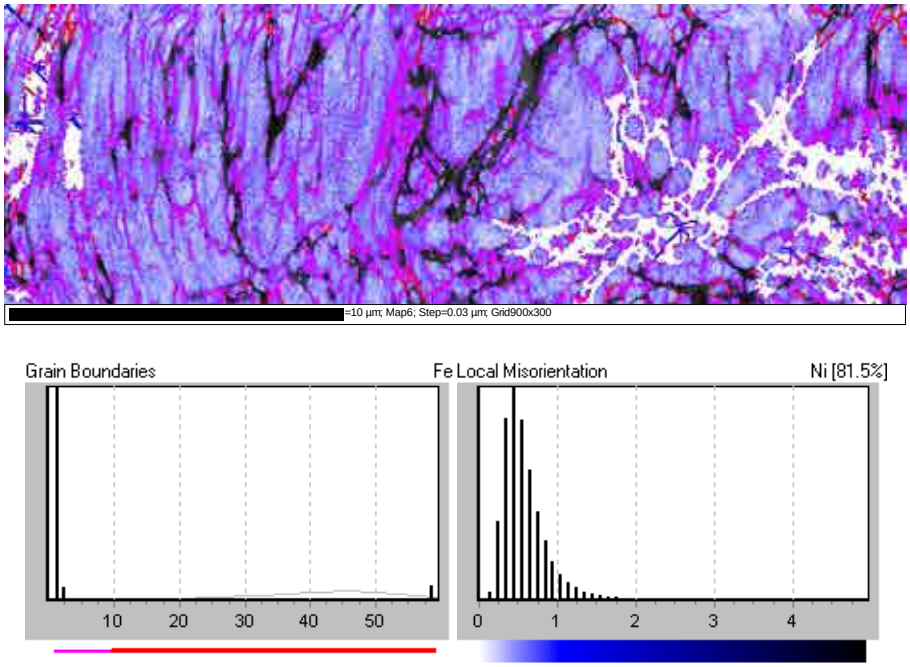

FIG. 3.4. Grain boundary map (red lines), sub-boundaries (purple lines) and intra-granular misorientation (lines colored from white to lilac) for an AISI321 steel sample after intensive plastic deformation by the equal channel angular pressing method. Non-indexed regions are colored black.

Figure 3.3 shows an orientation map of the slightly deformed sample surface areas, grain boundaries, sub-boundaries and intra-granular misorientation. Figure 3.4 presents a map of grain boundaries, sub-boundaries and intra-granular misorientation for an AISI321 steel sample after intensive plastic deformation by the equal channel angular pressing method.

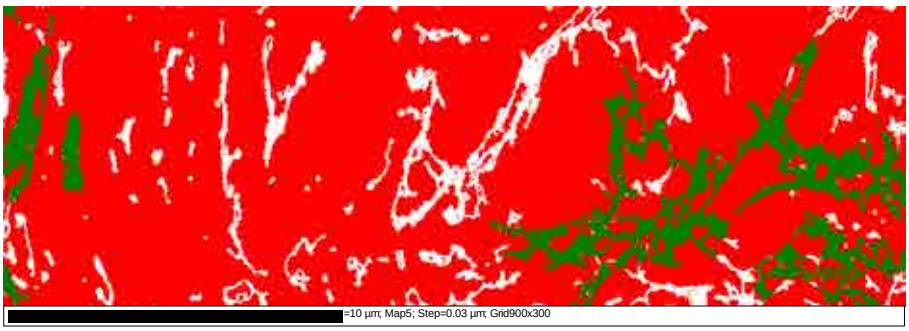

FIG. 3.5. Phase map from the steel after intensive plastic deformation by the method of equal channel angular pressing. Face centered cubic (FCC) lattices – red color, body centered cubic (BCC) lattices – green color. Non-indexed regions are colored white.

Figure 3.5 presents a distribution of regions with FCC and BCC lattices on the surface of a sample after intensive plastic deformation by the equal channel angular pressing method.

When comparing Figs 3.4–3.5, one may contend that in the area of a phase with the FCC lattice, there is a misorientation of the neighboring crystalline lattice areas; the average misorientation value is about 0.4–0.6 degrees. At the same time, in the examined area, there are practically no grain boundaries with a misorientation more than 10 degrees and there are a lot of sub-boundaries with a misorientation of 1.5–2 degrees.

In the comparable area of a slightly deformed sample, one can observe both grain boundaries (misorientation is more that 10 degrees, Fig. 3.3, black lines) and sub-boundaries (Fig. 3.3, red lines). The average value of the local misorientation (inside sub-grains) achieves 0.25–0.3 degrees in the slightly deformed sample (Figs 3.6–3.7).

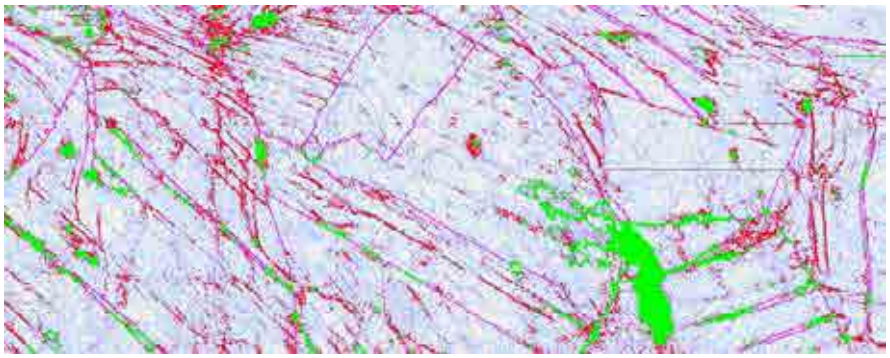

FIG. 3.6. Map of grain boundaries distribution (purple lines), sub-grain boundaries distribution (red lines) and local misorientation distribution (lilac shades) for a slightly deformed sample. Non-indexed regions are colored green. Straight black line is a place for local misorientations profile.

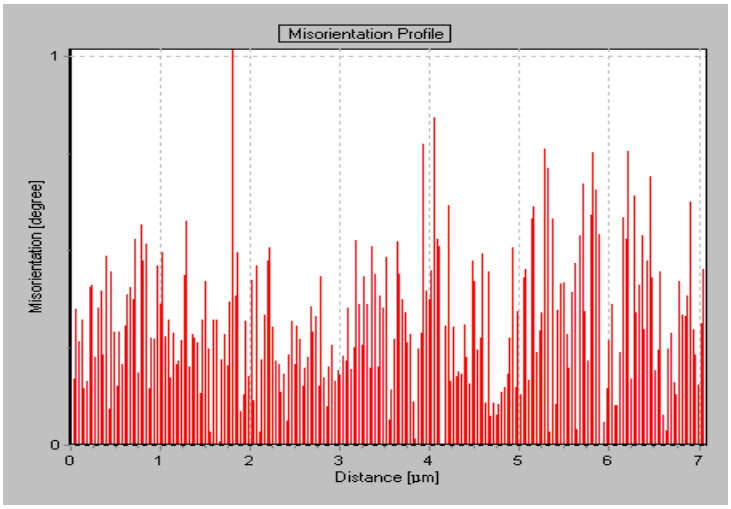

FIG. 3.7. Profile of local misorientations for a slightly deformed sample.

Figure 3.8 presents a profile of the local misorientations distribution for an area with the FCC lattice for a sample after intensive plastic deformation by the equal channel angular pressing method (straight line in Fig. 3.7). The average local misorientation achieves 0.4–0.6 degrees.

As for a sample after intensive plastic deformation by the equal channel angular pressing method, there are practically no local misorientations in the BCC lattice phase area (white area in Fig. 3.9).

The comparison of the appearance and distribution of non-indexed areas (a sample after intensive plastic deformation) and areas with FCC lattice allows au to suppose that non-indexed areas show the maximal local misorientation (maximal deformed areas with the FCC lattice), which state is a transition from an FCC to BCC lattice. An insignificant increase of the deformation level of these areas should result in the crystalline lattice conversion.

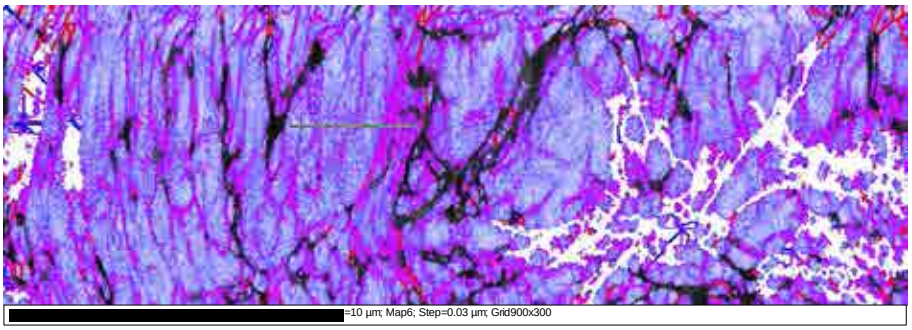

FIG. 3.8. Grain boundaries distribution map (red lines), sub-boundaries (purple lines), local misorientations (lilac shades) for a sample after intensive plastic deformation by the equal channel angular pressing method. Non-indexed regions are colored black. A straight line section is local misorientations profile (phase with FCC lattice).

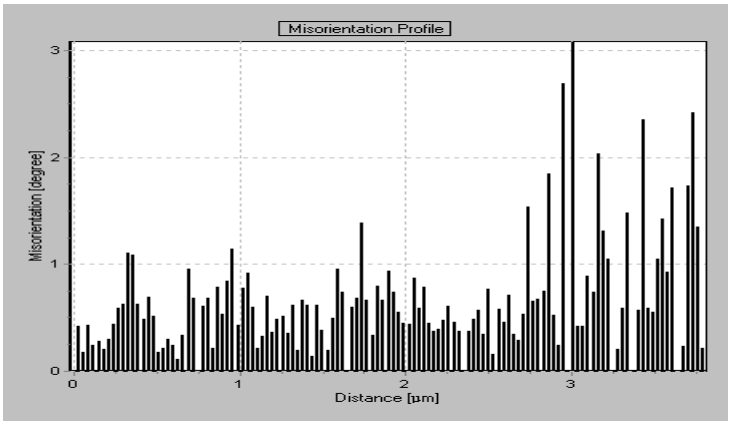

FIG. 3.9. Profile of local misorientations after intensive plastic deformation by the equal channel angular pressing method.

4. CONCLUSION

As a result of examinations of the AISI321 steel structure after intensive plastic deformation by the method of equal channel angular pressing using the electron backscattered diffraction registration and the analysis system HKL EBSD Premium System, it was determined that:

– the technique allows the detection and distribution of the secondary phase in space; the character of distribution of the secondary phase makes it possible to assume that highly deformed (highly stressed) areas of austenite, as well as areas with zero decisions (maximum deformed areas) are places of origin of the secondary phase;
– the technique provides a possibility to define misorientations in a condition of intensive plastic deformation; it is defined that the size of misorientations (stresses) in the secondary phase is significantly less than that of misorientations in the basic phase; in the examined material is found to have no misorientations in the secondary phase areas;
– the technique makes it possible to define the presence of large and small angle boundaries in the complex deformed condition; it is defined that after intensive plastic deformation by a method of equal channel angular pressing, the material is found to have practically no large angle (intergranular) boundaries, but the density of small angle boundaries (sub-boundaries) is very high.

The obtained results allow considering the EBSD technique as a highly effective procedure for examination of reactor materials in a condition of intensive plastic deformation.

PIE METHODS AND RESULTS (RESULTS)

(Session 5)

Chairpersons

J.Y. BLANC
CEA

Y. GONCHARENKO
SCC-RIAR

DEFECTIVE FUEL EXAMINATION USING COULOMETRIC TITRATION AND ANALYTICAL ELECTRON MICROSCOPY AT CHALK RIVER LABORATORIES

Z. HE, J. MOURIS, R. HAM-SU
Fuel Development Branch
AECL Chalk River Laboratories
Ontario, Canada
Email: hez@aecl.ca

Abstract

Although the fuel failure rate is very low in CANDU reactors, hot cell examination and characterization of representative defected fuels are performed on a continuing basis within fuel surveillance programs. The objectives are to fully understand defective fuel behaviour during irradiation and to further develop fuel behaviour models. This paper describes some techniques used at Chalk River Laboratories (CRL) for quantitative oxygen measurements on representative pellets from defected fuels, which were oxidized due to coolant ingress into the fuels during irradiation. When needed, quantitative O/M (i.e. oxygen to metal atom) ratio measurements are performed using a coulometric titration technique developed at CRL. This technique can determine the O/M ratio of fuel pellet samples taken by core drilling from an irradiated pellet. Further, electron probe analysis may be carried out using a shielded scanning electronic microscope to determine the extent of local oxidation in a fuel pellet. X ray wavelength dispersive spectrometry is used to determine the local oxygen and uranium concentration, thereby determining the local O/U ratio. The analysis can be performed in a very local region (e.g. close to a through wall sheath defect) owing to its spatial resolution of 2–3 microns. By using these techniques, and with known irradiation histories for defective fuel elements, detailed information required for fuel behaviour modelling is obtained.

1. INTRODUCTION

The change in oxidation state of UO_2 during irradiation alters its thermal conductivity, melting point and diffusion controlled processes such as fission gas release, creep and grain growth [1–3]. Quantitative knowledge of the oxidation state of irradiated fuel can provide significant insight into fuel structure and behaviour and aid the development of fuel performance models. Oxygen distribution varies within pellets inside a defected fuel element during irradiation [1–5]; however, detailed knowledge of its distribution is limited.

Although the defect rate of CANDU fuel is low, post-irradiation examination (PIE) of defective fuel elements is conducted at AECL Chalk River Laboratories (CRL) on a continuing basis within fuel surveillance programs. This ensures safe operation of CANDU fuels and facilitates further development of computer codes to simulate in-core defected fuel behaviour. Characterization of oxygen distribution in defected fuel has been ongoing at CRL for a number of years [6–7]. As a macroscopic analytical tool (millimetre scale), the coulometric titration technique developed at CRL provides a general picture with respect to the extent of pellet oxidation inside a defective fuel element. Using optical microscopy, scanning electron microscopy (SEM) and electron micro probe analysis (EPMA), pellet oxidation can be further characterized (micro meter scale) and related information (for example, the associated grain growth and condition of fission gas release) can be revealed. With the combination of these macro- and micro-analytical techniques, the oxidation condition of a defective fuel element can be systematically quantified and the results can be used to develop defective fuel models [3].

This paper primarily focuses on describing techniques used at CRL for characterization of UO_2 pellet specimens from defective fuel elements. Results of these characterizations are also provided.

2. COULOMETRIC TITRATION TECHNIQUE

2.1. Working principle

Figure 2.1 is a schematic diagram of the coulometric titration apparatus. Ar gas containing 2000 ppm H_2 is passed over the sample in the furnace at room temperature — no reaction between the sample and gas occurs. Downstream, the gas is passed through the ceramic coulometric titration cell, which measures the quantity of oxygen (O/M ratio) required to convert all the H_2 to H_2O (further described in the next paragraph). Next, the sample in the furnace is heated to 1000°C, nominally at a heating rate of 5°C per minute. When the temperature is sufficiently high, the gas and sample begin to react. Consequently, the H_2 in the gas flow converts UO_{2+x} to stoichiometric UO_2. Because the temperature only rises to 1000°C, the sample cannot become substoichiometric. This process continues until no further oxygen is released from the sample, rendering it stoichiometric. The decrease in the amount of H_2 in the gas, delivered to the downstream coulometric titration cell, is integrated; thereby, the amount of oxygen being released from the sample, x, is calculated.

A schematic diagram of the ceramic coulometric titration cell is shown in Fig. 2.2. The gas flows through a tube composed of zirconia (ZrO_2) doped with 8 mol% yttria (Y_2O_3). During operation, the coulometric titration cell is maintained at 750°C. At this temperature, this material readily conducts oxygen ions through the lattice, but will not conduct free electrons as metals do. Thus, when an electrical voltage is applied, oxygen ions are free to move, but free electrons are not. Therefore, any electrical current measured is an indication of oxygen ion transport. At the gas inlet, a voltage is created through the tube wall and current flows, in the form of oxygen ions. The air surrounding the tube allows oxygen ions to form at the outer surface of the tube. They pass through the wall where they recombine with other oxygen ions at the inner surface and desorb from the cell surface as O_2 (or combine directly with the H_2 in the gas to form H_2O). In this way, O_2 is passed from atmospheric air through the cell wall to the gas stream in the coulometric titration tube. At the coulometric titration gas outlet, the voltage between the inner surface and outer surface is measured. This voltage can be used to directly measure the O_2 partial pressure in the tube relative to the O_2 partial pressure in the air atmosphere. A feedback loop from this voltage controls the oxygen current inflow at the inlet end of the tube. In this way, only enough O_2 is provided to convert all H_2 to H_2O. (In fact, the O_2 content in the tube is always brought to a small fixed quantity of O_2 — about 40 ppm — this ensures that the H_2 quantity is extremely low).

To verify and calibrate the coulometric titration equipment, U_3O_8 is used to measure the change in stoichiometry to convert it to UO_2. The error in these tests is required to be below 1% of the change in O/U ratio. For UO_{2+x} samples with lower O/U ratios — about 2.10 — the uncertainty is about 5% of the change in stoichiometry (i.e. 0.005). Another source of uncertainty results from grinding the fuel samples into fine particles where some oxidation of the powder occurs prior to coulometric titration measurement. This can lead to an uncertainty of 0.01 in the stoichiometry change. For dense, non-friable fuel samples, this is the major source of error.

Figure 2.3 shows the result of an O/M-ratio measurement of an irradiated fuel sample from a fuel element with a through-wall sheath defect. The titration current represents the amount of oxygen ions required in the coulometric titration cell to exactly convert all H_2 to H_2O. Assuming that all oxygen released from the sample during the measurement came from altering the stoichiometry of the UO_2 (not from other phases that may have been present), the fuel sample is determined to have had an initial stoichiometry of $UO_{2.072}$ in this case. However, this is an upper limit because other phases in the fuel sample (e.g. oxidized fission-product phases) might also have released oxygen. Due to the low burnup of this fuel, the amount of the other oxidized phases is expected to be small.

2.2. Sample preparation for coulometric titration measurement

In a hot cell, 50–200 mg fuel samples were obtained from specific radial and longitudinal pellet-stack locations in an irradiated fuel element with a through-wall sheath defect. This was accomplished by

cutting approximately 10 mm pellet sections from the element and drilling them at precise positions with a 1.8 mm diamond drill, parallel to the element axis. Samples were then loaded into a glove box and placed in the coulometric titration furnace.

2.3. Example of coulometric titration results

Figure 2.4 shows how the extent of pellet oxidation inside a defected fuel element is quantified. As shown, all samples exhibited oxidation; the O/M values varied from 2.02–2.10. The centre cross-section (Section 6) exhibited slightly lower O/M values than the end sections because sheath defects occurred at both ends of the fuel element.

Ceramographic analysis indicated the presence of higher oxide phases and enhanced grain growth in the element, as described below.

2.3.1. Primary defect

The primary defect, caused by fretting damage, was small and no UO_2 loss was observed. UO_2 oxidation was observed along the exterior of the pellet and at a major radial crack (Fig. 2.5). Also, the grain boundaries in this vicinity were oxidized (Fig. 2.6). Moreover, at the centre of this region, the grain size was about 17 μm, compared with 6 μm at the periphery (the as manufactured grain size was 6 μm). This, and the observed intergranular gas bubbles and tunnels are unexpected at this power (29 $kW \cdot m^{-1}$) and burnup (3.4 $MW \cdot d \cdot kg^{-1}$ U) for intact fuel elements. Their presence is consistent with the observed pellet oxidation in this region, since pellet oxidation reduces thermal conductivity (increasing temperature), thereby enhancing UO_2 grain growth and fission-gas release [1].

2.3.2. Secondary defect

The secondary defect of the element was relatively large (about 13 mm^2, see Fig. 2.7) and UO_2 loss near the defect was observed.

In the mid-radius of this region, fuel oxidation was observed at cracks (Fig. 2.8). Islands of grains appeared throughout the oxidation phase, indicating preferential grain boundary oxidation. In the central region (not shown), oxidation along radial cracks was also observed, but the extent of oxidation was not as great as that in the mid-radius region.

Besides oxidation, UO_2 grain growth was observed in the mid-radius (14 μm; Fig. 2.9), and the central regions (30 μm) — the as fabricated grain size was 6 μm. Gas bubbles and tunnels were observed at the grain boundaries in both regions. These observations are indicative of decreased thermal conductivity.

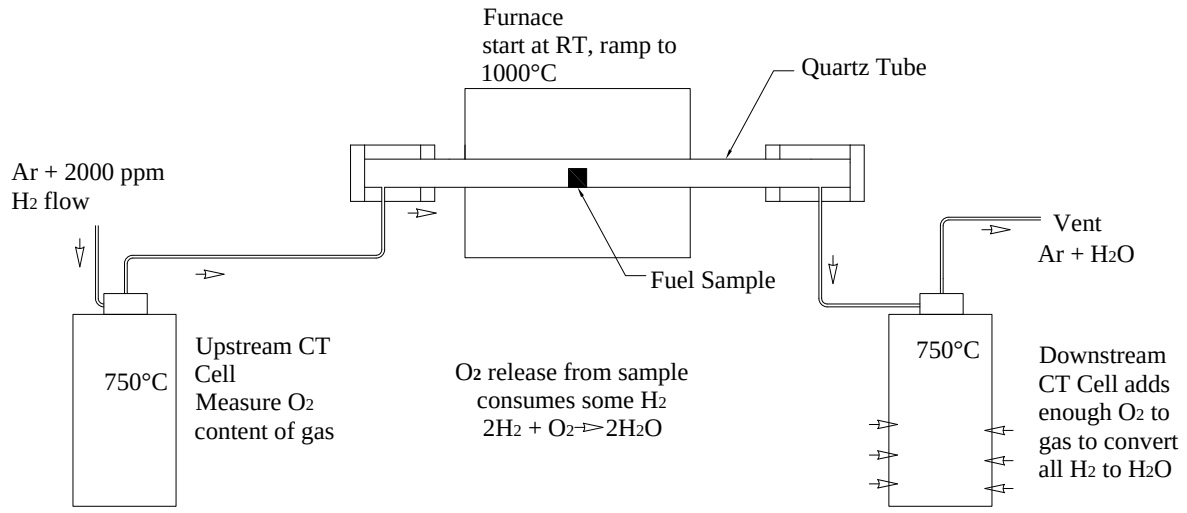

FIG. 2.1. Schematic diagram of coulometric titration apparatus.

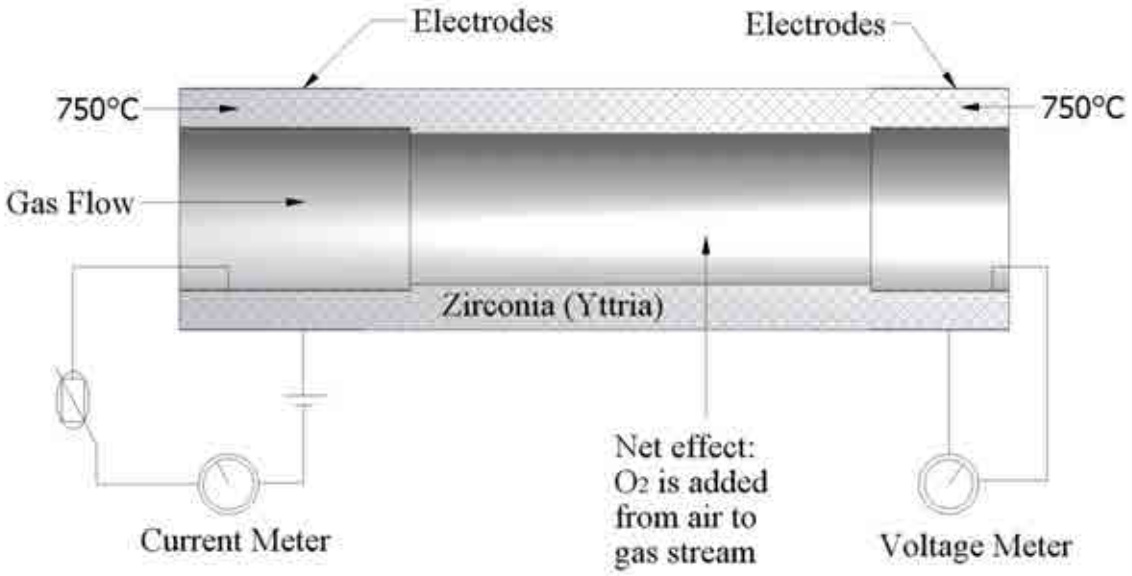

FIG. 2.2. Rough schematic diagram of a coulometric titration cell. Doping ZrO_2 with Y_2O_3 increases the O^{2-} vacancy concentration, thus enhancing the O^{2-} diffusion rate. Measuring the electric current (I) gives the O^{2-} diffusion rate. Measuring the voltage (U) gives the O_2 partial pressure inside the tube relative to the value outside the tube.

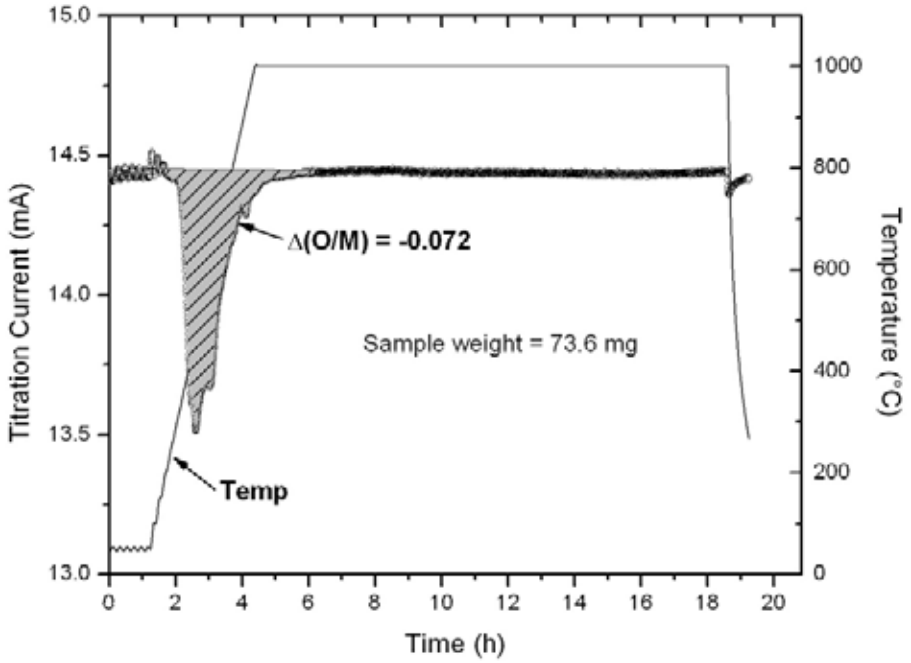

FIG. 2.3. Reduction of an irradiated sample of fuel with a through wall clad-defect.

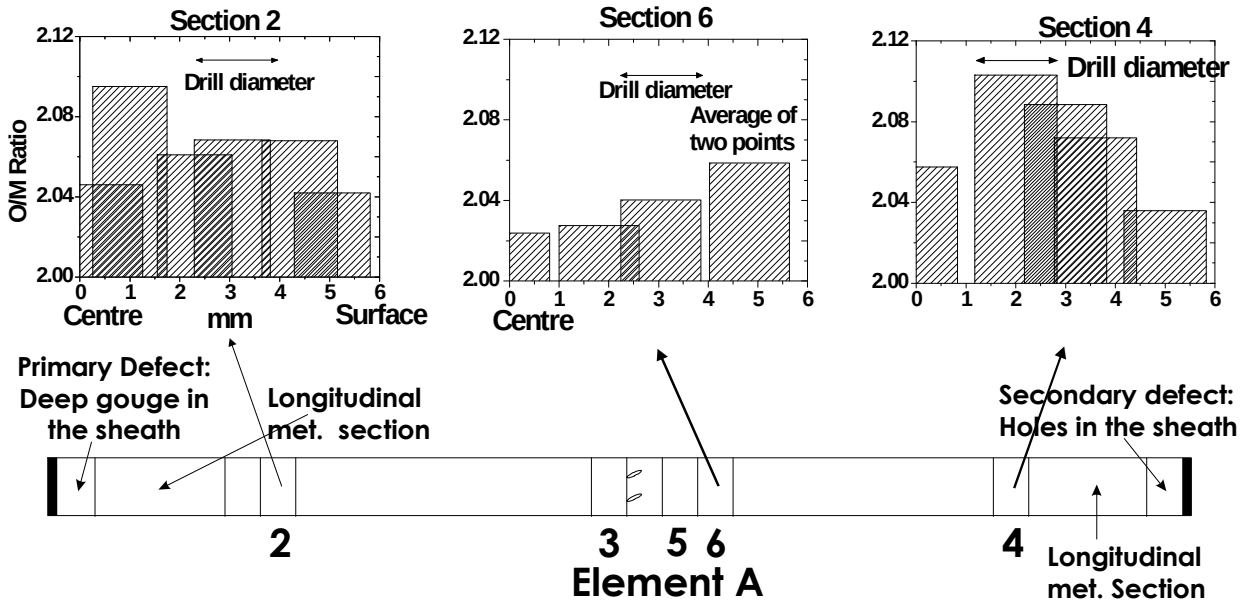

FIG. 2.4. O/M measurements on a defective fuel element.

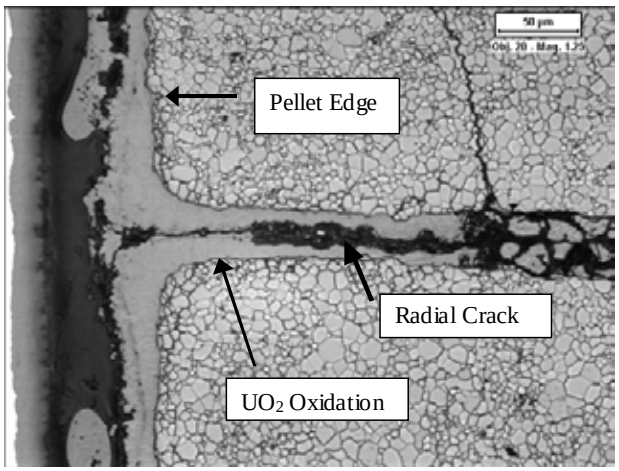

FIG. 2.5. Primary (fretting) defect, showing fuel oxidation on the pellet edge and radial crack.

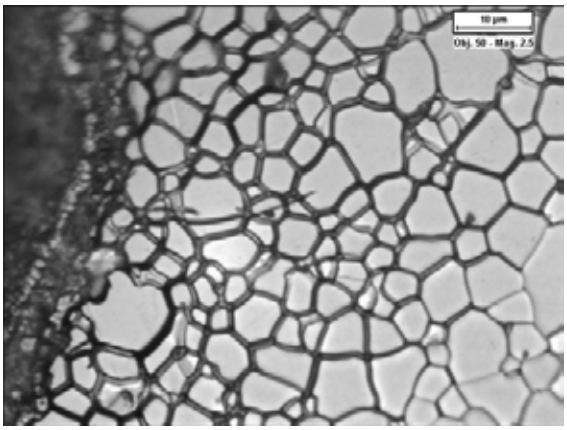

FIG. 2.6. Primary (fretting) defect: higher magnification than Fig. 3.5, showing fuel grain boundary oxidation near a radial crack.

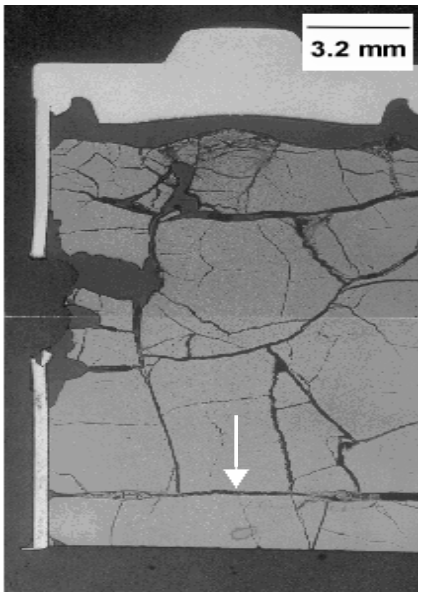

FIG. 2.7. At the secondary defect (a hole), low magnification: shows fuel local loss from hole, cracks and pellet–pellet interface (arrow).

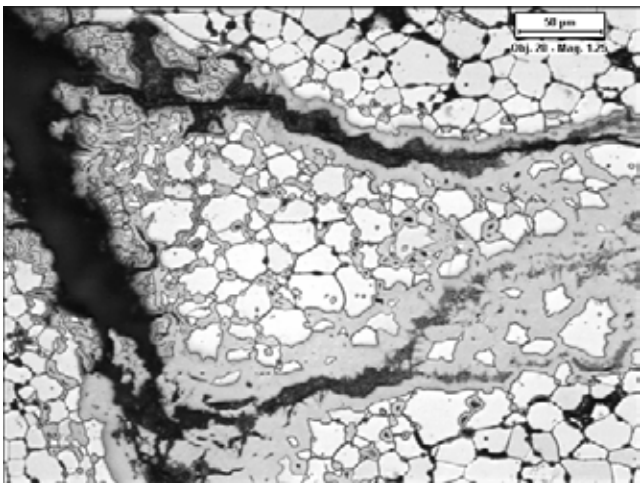

FIG. 2.8. At secondary defect mid-radius (i.e. 3.5 mm from the centre) along a radial crack: shows isolated grains embedded in darker fuel oxidation.

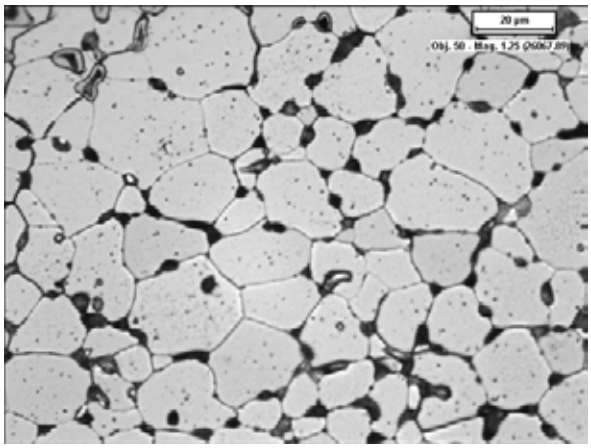

FIG. 2.9. At secondary defect mid-radius (i.e. 3 mm from centre): shows grain growth (average grain size 14 μm), and fission gas bubbles in grain boundaries and tunnels.

3. SEM/WDS QUANTIFICATION OF FUEL PELLET OXIDATION

3.1. Wavelength dispersive X ray spectroscopy (WDS)

X rays emitted from a specimen bombarded with a focused electron beam in a scanning electron microscope (SEM) can be used to identify which elements are present (qualitative analysis). With an optimized experimental set-up and data-analysis procedures, the measured X rays can also be used to quantitatively evaluate the chemical composition of the sample.

WDS is an electron probe micro-analytical (EPMA) technique with a spatial resolution of the order of 10 μm^3, and high spectral resolution of the order of 10 eV [8]. It detects elemental constituents in a surface layer of about 1–2 microns [9]. Quantitative WDS analysis is performed in relation to a known standard. If the standard is of composition, structure and density similar to the sample analysed, its fractional amount in the unknown with respect to the standard is given by:

$$\frac{C}{C_o} = \frac{I}{I_o} \tag{1}$$

Where C and C_o are the weight percentages of the probed element in the sample and the standard, I and I_o, are the peak intensities measured in the sample and the standard.

WDS requires the selection of a characteristic X ray wavelength from the element analysed. The X rays from the sample are selected by wavelength using diffracting crystals. Different types of crystals are used depending on the wavelength to be analysed and each crystal may detect only one element. As a consequence, WDS analysis is highly accurate but relatively time consuming.

3.2. Specimen preparation

An irradiated fuel pellet sample from a defected element and a sample of unirradiated UO_2 (to be used as a standard) were positioned together in a conductive metallographic mount. The metallographic sample was ground to 600 grit using SiC paper. This was followed by a two stage polish, first with aqueous 0.05 μm Al_2O_3 suspension and secondly with colloidal silica (average particle size of 40 nm). The sample was then slightly etched with a solution of H_2O_2/H_2SO_4 (90/10) to reveal the grain boundaries. The sample was re-polished and lightly etched using the same process in preparation for the present work. A secondary electron image of the overall sample is shown in Fig. 3.1. For analysis, the sample was divided into four regions: centre, mid-radius, periphery and edge.

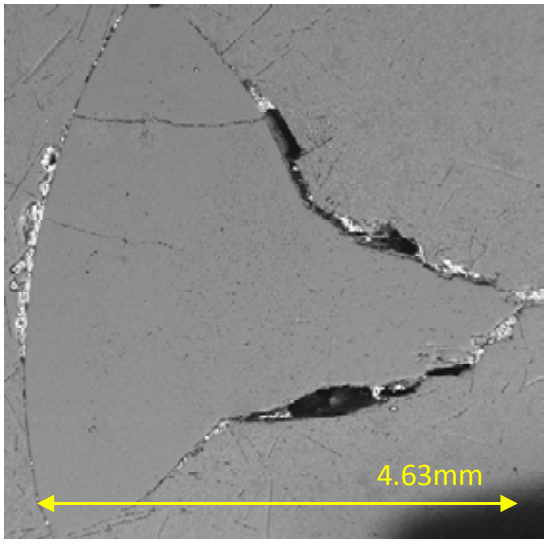

FIG. 3.1. Secondary electron image (SEI) of the pellet sample.

3.3. SEM and WDS analysis

Analytical scanning electron microscopy (SEM) was performed using a radiation shielded instrument. Secondary electron images (SEI) of the sample surface were taken at an acceleration voltage of 25 kV.

The WDS system used was equipped with Geller MicroAnalytical dQant software. The acceleration voltage applied for this study was 20 kV, which was recommended by the manufacturer for oxygen analysis. Two crystals were utilized during the analysis: pentaerythritol, to detect uranium (Mα peak, wavelength = 0.391 nm) and a synthetic layered dispersive element for oxygen (Kα peak, wavelength = 2.362 nm). An example of the uranium and oxygen peaks is given in Fig. 3.2.

Four different locations were measured in the sample (Table 3.1). For each location, point analysis along a line close to the tangential direction was performed. Each analysis set was composed of 30–60 points and each point was measured 5 times, for 30 seconds. Each point-intensity, I, was calculated from the average of the five (30 second) readings:

$$I_{oxygen} = \frac{\sum_5 I_{sample.oxygen}}{5} \quad (2)$$

$$I_{uranium} = \frac{\sum_5 I_{sample.uranium}}{5} \quad (3)$$

WDS analysis requires a reference-intensity value for quantitative analysis. The results presented here used the average of 11 standard readings to calculate an average reference intensity I_o:

$$I_{o-oxygen} = \frac{\sum_{11} I_{std.oxygen}}{11} \quad (4)$$

$$I_{o-uranium} = \frac{\sum_{11} I_{std.uranium}}{11} \quad (5)$$

The intensities measured in the sample were then normalized with respect to the standard:

$$I_{norm} = \frac{I}{I_o} \quad (6)$$

TABLE 3.1. FOUR DIFFERENT MEASUREMENT LOCATIONS

Different measurement locations	
Central region	$r/r_o = 0$
Mid-radius	$r/r_o = 0.5$
Periphery	$r/r_o = 0.8$
Edge	$r/r_o = 1$

3.3.1. WDS point analysis along a line

A micrograph of the central area where WDS was performed is shown in Fig. 3.3. The yellow line indicates the site of the analyses. The spacing between the points forming the analysis line was 5 μm for the centre and mid-radius regions, and 3 μm for the periphery and the edge regions. The SEM image of Fig. 3.3 shows that the sample surface is not featureless. There are fine cracks observable on the surface; lenticular pores and dimples are visible (likely the result of the creation of fission gas); line scratches resulting from the initial stages of ceramographic preparation, are also evident. These features will have an effect on the WDS analysis results. For example, the presence of voids and micro cracks will result in lower U and O peak intensities.

The normalized (with respect to the standard) oxygen and uranium intensities (as a function of position for the central region line scan) are shown in Fig. 3.4. The uncertainty associated with each point is expressed as the standard deviation (σ) attained and shown through the error bars. Variations in intensity occur in both the uranium and oxygen peaks. For the most part, the variation is small and peak intensities are relatively uniform within each region. Nevertheless, relatively large intensity variations can be observed sporadically in the graphs, as in the first 15 μm of the central region line scan (Fig. 3.4).

The WDS results showed that oxygen and uranium peak intensities are consistent from grain to grain within a region. In general, the large variations in intensity observed can be attributed to microstructural features such as pores and grain boundaries.

Ideally, the variations in intensity between sample and standard are only due to differences in composition. The underlying assumption, in Equations 1, 6 and the WDS analysis performed so far, is that the measured X ray intensity difference between sample and standard is due to their basic compositional difference.

In some cases, the intensity variations cannot be easily correlated with height variations on the surface. For example, the first three points measured in the central region (Fig. 3.4) show a decreased intensity. In the absence of topographical features, these variations are a result of the presence of microvoids, or other elements and compounds. The data analysis software calculates the percentage of uranium and oxygen in a spot (using the standard as a reference). If the percentage of uranium added to the percentage of oxygen is not approximately 100%, this is a strong indication of the presence of microvoids or other elements in the spot analysed. Hence, for further data analysis, the points acquired where the sum of the oxygen and uranium percentages was not close to 100% were removed.

Oxygen and Uranium Distribution

The average oxygen and uranium normalized intensities as a function of radial position are shown in Fig. 3.4. The amount of oxygen increases towards the edge. However, the oxygen intensities can be normalized with respect to the uranium intensities to attain a relative O/U concentration ratio. Calculated this way, the UO_2 standard would have an O/U concentration ratio of 1. The results and their uncertainty, calculated from the standard deviations, are shown in Fig. 3.6. These results indicate an increased O/U concentration ratio in the mid-radius, which agrees with previous coulometric titration measurements and modelling predictions [3]. The cause of the irregular uranium distribution shown in Fig. 3.5 (i.e. lower uranium intensity readings in the central and mid-radius regions) is uncertain, but likely related to temperature- and irradiation-dependent changes in pellet structure and density occurring during operation.

From the results shown in Fig. 3.5, the U content in the irradiated fuel sample is lower than in the standard. This is expected due to fissioning of U. In addition, microstructural/density changes (e.g. creation of fission-gas bubbles) will also affect the intensity of the U X ray signal. Separating these effects may be possible by analysing a non-defected fuel where only temperature and radiation effects are present. The structural and density changes that occur during operation may then be discerned from the oxidation related to the presence of defects.

Standard

In this work, an unirradiated UO_2 pellet was used as the standard; however, as mentioned previously, structural changes that occurred in the sample may affect the interaction and absorption of X rays. Therefore, the assumption that the standard and sample are essentially equal except for composition (Equations 1 and 6) may not be exactly valid. It is being considered to use a non-defected fuel with similar burnup as a standard. This will enable a relative measure of oxidation in the defected fuel.

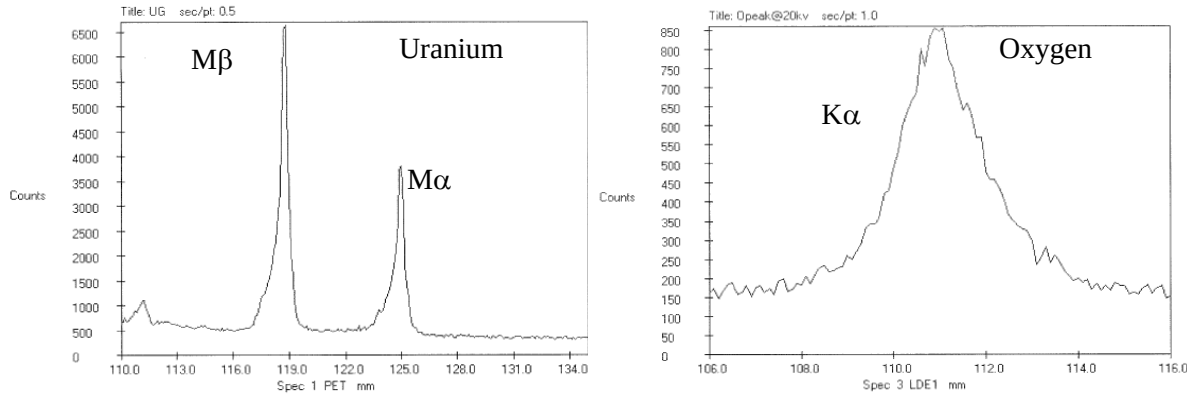

FIG. 3.2. WDS uranium and oxygen peaks at 20 kV; Note: The horizontal axis indicates the distance from the X ray source to the analysing crystal.

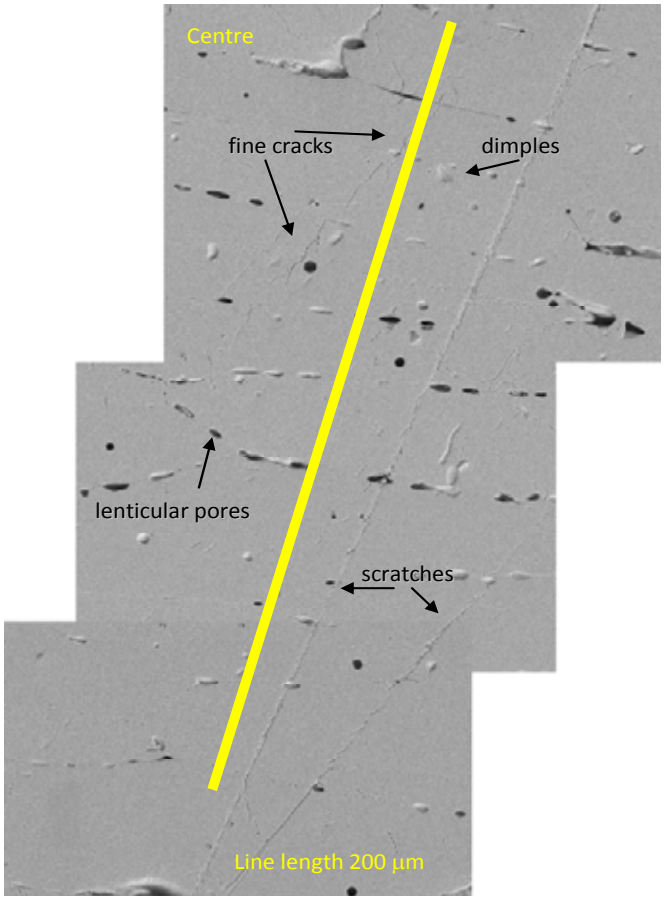

FIG. 3.3. WDS: central region.

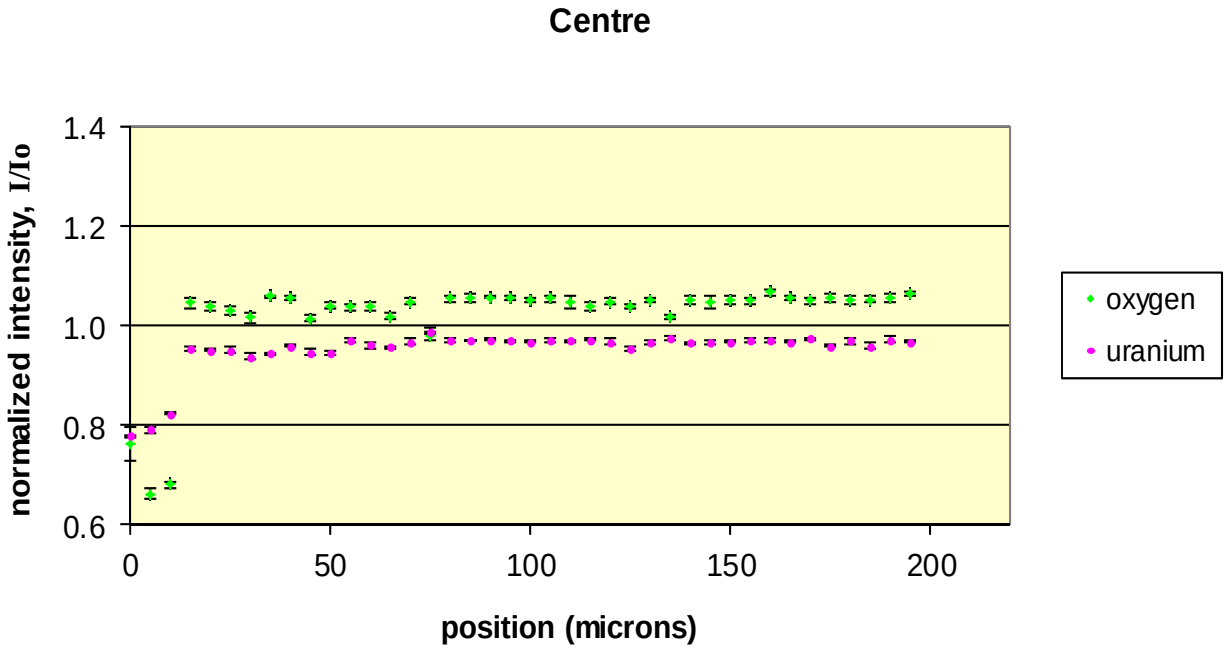

FIG. 3.4. Normalized oxygen and uranium intensities: central region; the error bars indicate the precision (σ) of the measurements.

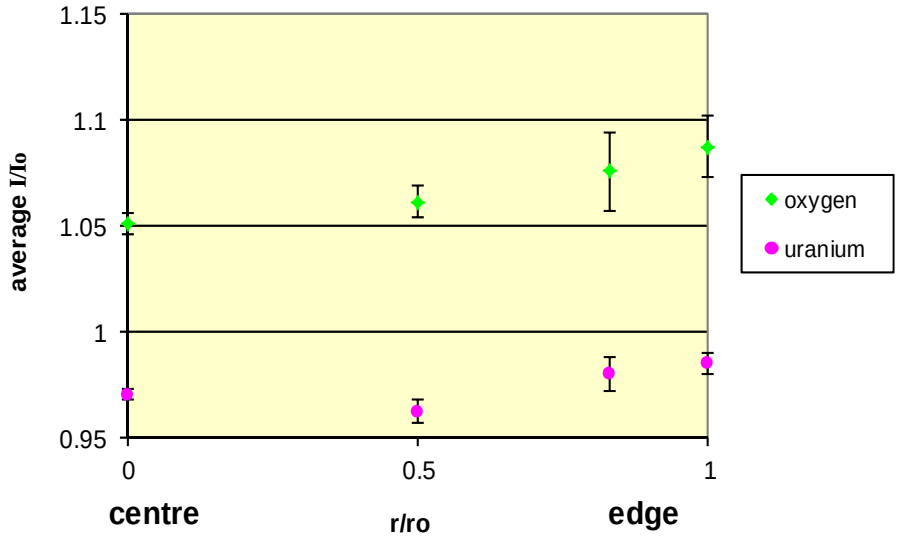

FIG. 3.5. Average oxygen and uranium normalized intensities (error bars denote the standard deviation of each point).

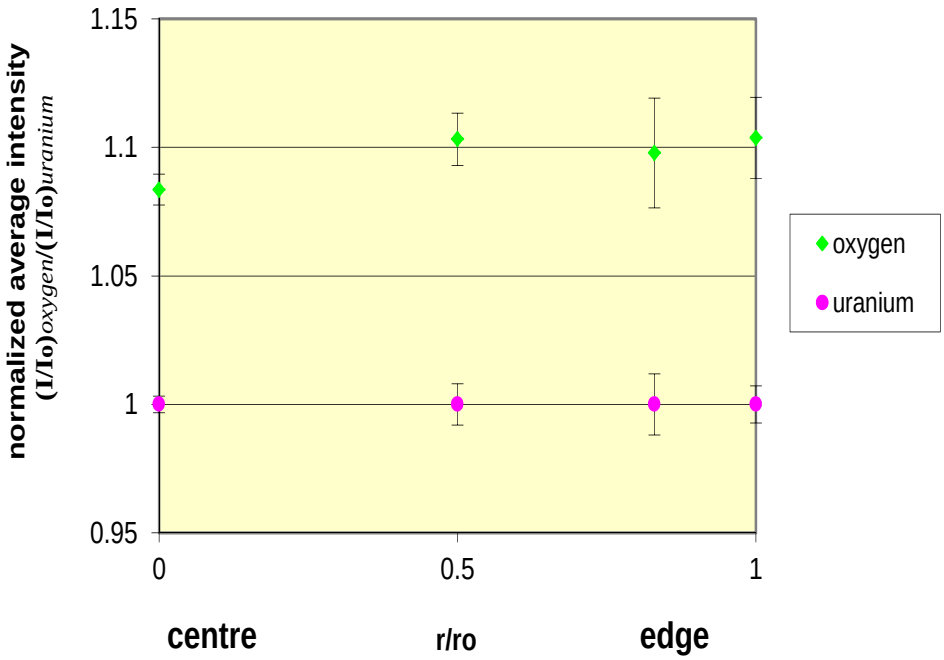

FIG. 3.6. Normalized intensities with respect to uranium intensity (error bars denote the calculated uncertainty).

4. SUMMARY

Characterization of oxygen distribution at macro- and microscopic levels in defected fuel has been ongoing at CRL for a number of years. The coulometric titration technique provides a macroscopic measurement of the extent of pellet oxidation inside a defective fuel element. Pellet oxidation can be further characterized using optical microscopy, SEM and EPMA techniques. With the combination of these macro- and micro-analytical techniques, the oxidation condition of a defective fuel element can be systematically quantified, and the information and data can be used to develop defective fuel models. The work described in this paper demonstrates that CT-based O/M measurements, optical microscopy and SEM/WDS analyses produce converging results.

The accuracy of WDS measurements is expected to be improved by taking the following precautions:

(a) The specimen should be polished in such a way that it is as flat and scratch free as possible.
(b) Using diamond based, water soluble polishing pastes will reduce oxygen, aluminium and silicon contamination in cracks and crevices.
(c) Using an irradiated pellet from an intact fuel element as a standard (with similar burnup to the sample) will facilitate the relative measure of oxidation in the defected fuel.

5. ACKNOWLEDGEMENTS

The authors would like to thank Craig Buchanan and Pam Ryan at CRL for optical examination and SEM/WDS analyses, respectively.

The work reported in this paper was funded by the CANDU Owners Group R&D, Safety and Licensing Program**,** under the joint participation of Atomic Energy of Canada Limited, Hydro-Québec, New Brunswick Power Nuclear, Ontario Power Generation, Bruce Power, and Societatea Nationala Nuclearelectrica (Romania).

REFERENCES

[1] WALKER, C.T., RONDINELLA, V.Z.V., PAIOANNOU, D., VAN WINCKEL, S., GOLL, W., MANZEL, R., On the oxidation state of UO_2 nuclear fuel at a burnup of around 100 $MW \cdot d \cdot kg^{-1}$ HM, Journal of Nuclear Materials **345** (2005) 192–205.

[2] VERRALL, R.A., MOURIS, J.F., O/M ratio measurement techniques, 8th International Conference on CANDU Fuel (2003) 65–73.

[3] HIGGS, J., LEWIS, B.J., THOMPSON, W.T., HE, Z., A conceptual model for the fuel oxidation of defective fuel, Journal of Nuclear Materials **366** (2007) 99–128.

[4] LEWIS, B.J., IGLESIAS, F.C., COX, D.S., GHEORGHIU, E., A model for fission gas release and fuel oxidation behaviour for defected UO_2 fuel elements, Nuclear Technology **92** (1990) 353–362.

[5] LEWIS, B.J., MACDONALD, R.D., IVANOFF, N.V., IGLESIAS, F.C., Fuel performance and fission product release studies for defected fuel elements, Nuclear Technology **103** (1993) 220–245.

[6] VERRALL, R.A., HE, Z., MOURIS, J.F., Characterization of fuel oxidation in rods with clad-holes, Journal of Nuclear Materials **344** (2005) 240–245.

[7] HAM-SU, R., HE, Z., RYAN, P., Wavelength dispersive X-ray spectroscopy (WDS) on defected fuel, Proceedings of the 10th CNS International Conference on CANDU Fuel (2008).

[8] BARKER, W., FOURNELLE, J., X-ray compositional microanalysis, Department of Geology and Geophysics, University of Wisconsin-Madison (1995).

[9] GOLDSTEIN, I., NEWBURY, D.E., ECHLIN, P., JOY, D.C., ROMIG, Jr. A.D., LYMAN, C.E., FIORI, C., LIFSHIN, E., Scanning electron microscopy and X-ray microanalysis, Second Edition, Plenum Press, New York (1992).

BIBLIOGRAPHY

[1] EXNER, H.E., WEINBRUCH, S., Scanning electron microscopy, Metallography and Microstructures, Vol. 9, ASM Handbook, ASM International (2004) 355–367.

[10] ASTM INTERNATIONAL, Standard test methods for determining average grain size, ASTM E112-96 (1996).

POST-IRRADIATION EXAMINATION OF THORIA–PLUTONIA MIXED OXIDE FUEL IN INDIAN HOT CELLS

J.L. SINGH, P. MISHRA, E. RAMADASAN, K.S. BALAKRISHNAN, S. KUMAR,
G.K. MALLIK, J.S. DUBEY, H.N. SINGH, P.M. OUSEPH, V.D. ALUR,
P.B. KONDEJKAR, P.K. SHAH, V.P. JATHAR, A. BHANDEKAR, K.M. PANDIT,
R.S. SHRIWASTAW, A. SHARMA, P.M. SATHEESH, N. KUMAWAT, S. ANANTHARAMAN
Post-irradiation Examination Division
Nuclear Fuels Group
Bhabha Atomic Research Center
Mumbai, India
Email: jlsss@barc.gov.in

Abstract

Mixed oxide (MOX) fuel clusters containing ThO_2+4%PuO_2, and ThO_2+6.75%PuO_2 fuel pins were irradiated in the pressurized water loop of the Indian research reactor CIRUS, to burnup in the range of 20 $GW{\cdot}d{\cdot}t^{-1}$ (HM). The ThO_2+4%PuO_2 fuel elements had free standing cladding made of zircaloy-2 and the ThO_2+6.75%PuO_2 had collapsible zircaloy-2 cladding. The fuel clusters had performed well during irradiation with no apparent indications of failure. The techniques used for the post-irradiation examination (PIE) of these fuels in the hot cells included visual examination, fuel pin diameter measurements, leak testing, gamma scanning, gamma spectrometry, ultrasonic testing, eddy current testing, ceramography, metallography, beta gamma autoradiography and measurement of released fission gases. Micro hardness measurement of cladding and evaluation of mechanical properties using ring tension test were also carried out. This paper elaborates on the techniques and the results of the PIE carried out on ThO_2+4%PuO_2 fuel.

1. INTRODUCTION

India has about four times more thorium resources than uranium. Utilization of thorium for large scale energy production is a major goal in the three stage nuclear power programme [1].

Hence, research and development in fabrication, characterization and irradiation testing of thoria based fuels is necessary. A six pin cluster, consisting of ThO_2-4% PuO_2 fuel pellets, had undergone irradiation testing in the pressurized water loop (PWL) of CIRUS thermal reactor up to a burnup of 18.5 $GW{\cdot}d{\cdot}t^{-1}$. Post-irradiation examination (PIE) of the fuel pins from the cluster was carried out at BARC hot cells facility. Non-destructive examination of the fuel pins from the cluster has been carried out by visual examination, fuel pin diameter measurements, leak testing, gamma scanning, gamma spectrometry, ultrasonic testing, eddy current testing. Micro structural characterization on two fuel pins, TH-5 and TH-2 from the cluster, has been done using optical microscopy, scanning electron microscopy, β–γ autoradiography and α autoradiography techniques. This paper presents the salient observations of the examinations carried out on the irradiated fuel pins.

2. FABRICATION DETAILS

The experimental six pin cluster (AC-6) consisting of ThO_2-4% PuO_2 fuel pellets, encapsulated in a free standing zircaloy-2 cladding, was fabricated at the Radio Metallurgy Division (RMD). The cluster consisted of short-length fuel pins of about 0.5m length and the sketch of a typical experimental MOX fuel pin is shown in Fig 2.1. Table 2.1 gives the details of the fabricated fuel pins.

3. IRRADIATION HISTORY

The AC-6 experimental cluster was irradiated in the PWL of CIRUS research reactor. The thermal neutron flux in the loop was 5×10^{13} $n{\cdot}cm^{-2}s^{-1}$ and the temperature and pressure of the coolant in the loop was 240°C and 105 $kg{\cdot}cm^{-2}$ respectively. Peak linear heat rating and peak burnup in the fuel pins was 40 $kW{\cdot}m^{-1}$ and 18.5 $GW{\cdot}d{\cdot}t^{-1}$ respectively.

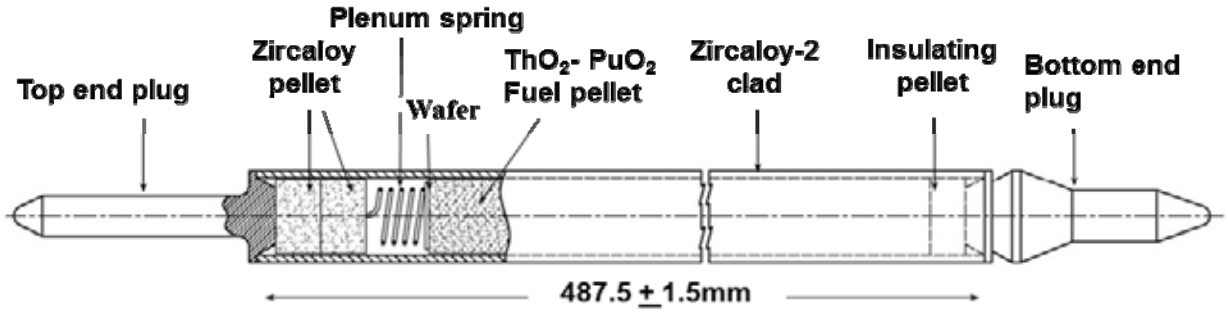

FIG. 2.1. A typical experimental MOX fuel pin.

TABLE 2.1. DETAILS OF THE THORIA BASED MOX FUEL PINS

Cluster	AC-6
Clad type	Free standing
Number of pins	6 (5 ThO_2-4% PuO_2 + 1 helium filled pin)
PuO_2 enrichment	4%
Pellet diameter	12.22 ± 0.01 mm
Pellet length	12.0 ± 1.0 mm
Pellet density	92–94% TD
Stack length	435 mm
Cladding outer wall diameter	14.3 mm
Cladding wall thickness	0.8 mm
Cold plenum length	20 mm

4. NON-DESTRUCTIVE TESTING

4.1. Visual examination

Visual examination was carried out on the individual pins using a wall mounted periscope. All the fuel pins were found with deposit of loose white powder which may have come from the storage water pool containing aluminum cladded research reactor fuel assemblies. The fuel pins were cleaned by cotton damped with alcohol. No abnormality was visible on the surface (Fig. 4.1).

4.2. Diameter measurement

A diameter measuring set-up was made to be suitable to keep the fuel pin straight on the platform. The diameter was read from the dial gauge display through the periscope. The diameter of the irradiated fuel pins was found to be within the manufacturing tolerances.

4.3. Leak testing

Leak testing was carried out in the hot cell using liquid nitrogen and alcohol leak test. During the test each pin was immersed in liquid nitrogen for 5–7 minutes. Subsequently the fuel pin was transferred to get immersed in a tank filled with alcohol. There was no leak observed in the fuel pins.

4.4. Ultrasonic testing

Two 10 MHz line focused immersion probes were fitted at an angle in the probe carriage for detection of axial and circumferential defects. Multi-channel ultrasonic flaw detector was used for slow helical scan combining axial probe translation and rotation of fuel pin. Surface roughness signals were predominant making interpretation difficult (Fig. 4.2).

FIG. 4.1. Loading of fuel pin to ultrasonic scanner using master slave manipulator.

FIG. 4.2. Two channels of ultrasonic flaw detector showing surface signals.

4.5. Eddy current testing

Eddy current testing (ECT) was carried out on 4 fuel pins except pin TH-5, which could not pass through the eddy current testing coil. Defect signals were obtained from the cladding of pin TH-2 as shown in Fig. 4.3. The fuel pin is pulled up slowly and signals are recorded by the computer.

4.6. Gamma scanning

Gamma spectroscopy and scanning using the HPGe detector and multi channel analyser/scaler (MCA/MCS) were carried out on these elements inside the hot cell. Co-60 and Cs-137 sources were used for calibration. The spectra obtained from these elements revealed the presence of Cs-137, Cs-134, Eu-154 and Tl-208. Figure 4.4 shows a typical gamma ray spectrum.

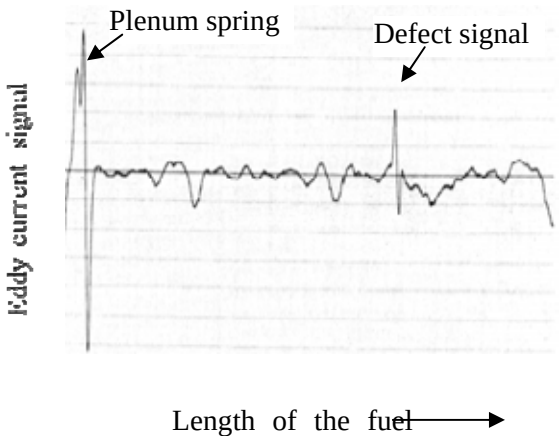

FIG. 4.3. ECT set-up inside the hot cell (left), ECT signal from defect location of TH-2 (right).

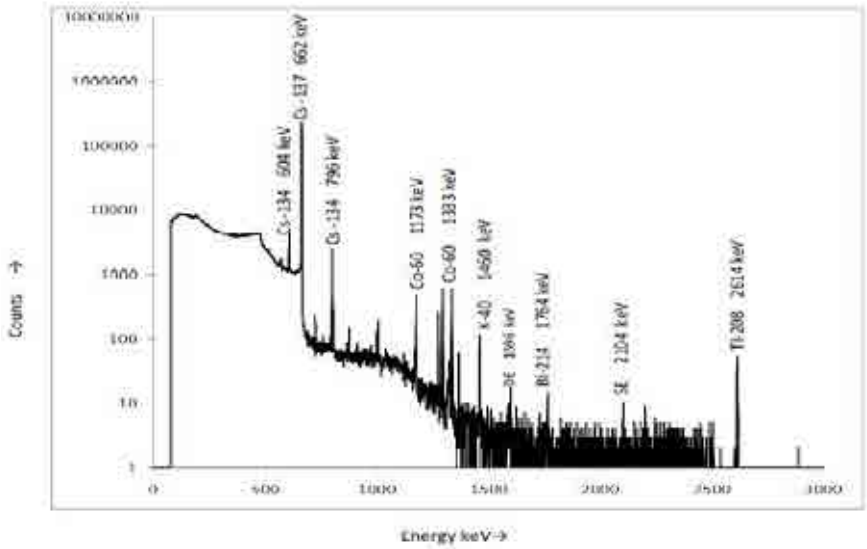

FIG. 4.4. Gamma ray spectrum of (Th-4%Pu)O_2 fuel pin.

4.7. Neutron radiography

The fuel pin TH-4 suspected to be defective during eddy current testing was subjected to neutron radiography in the test reactor Circus. The bottom and top end plugs were found in Insulation pellet cracks in the pellet were observed in the neutron radiograph shown in Fig. 4.5. The plenum spring was also observed to be free from any distortion.

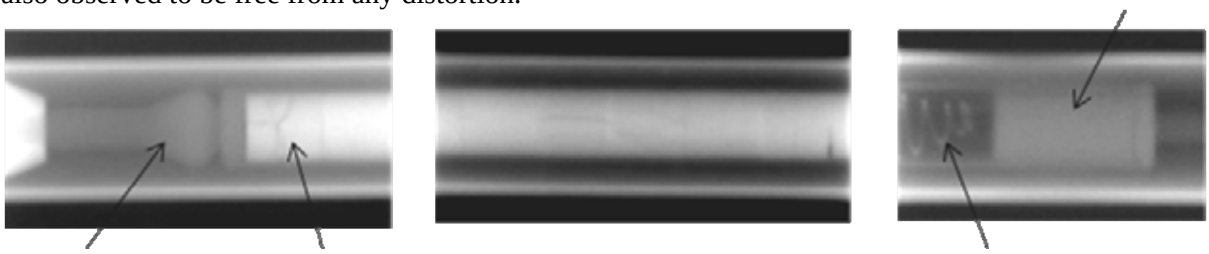

Bottom plug Multi-axial pellet cracks Plenum spring

FIG. 4.5. The neutron radiograph of fuel pin TH-4 shows no abnormality after irradiation.

5. DESTRUCTIVE TESTING

5.1. Fission gas analysis

Fuel pins were punctured for the measurement of the amount of released fission gases. The volume of the released fission gas and the void volume in the fuel pin were measured to arrive at the pressure of the gas inside the fuel pin. A dual column gas chromatograph and a quadrupole mass spectrometer were used to analyse the chemical composition and isotopic composition respectively of the collected gases. Fission gas analysis was carried out on the fuel pins TH-2, TH-4 and TH-5. The fission gas pressure in the pin TH-4 and TH-5 was 4.4 and 3 atmosphere respectively and the gases were He, Xe and Kr. The fuel pin TH-2 did not show fission gas, indicating it to be a leaky pin which was also found defective by ECT.

5.2. Metallographic examination

Metallographic examination of two fuel pins, TH-5 and TH-2 has been carried out to study the fuel restructuring, cladding oxidation and hydriding. β–γ autoradiography of the metallographic samples was carried out to study the distribution of the fission products (mainly Cs-137) across the cross-

section. α autoradiography was carried out to analyse the distribution of plutonium in the fuel [2]. Radiographs are shown in Figs 5.1–5.3.

FIG. 5.1. Photo macrograph.

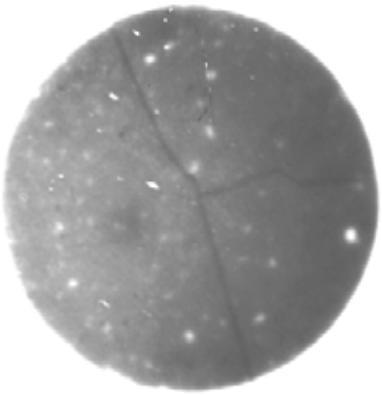

FIG. 5.2. β–γ autoradiograph.

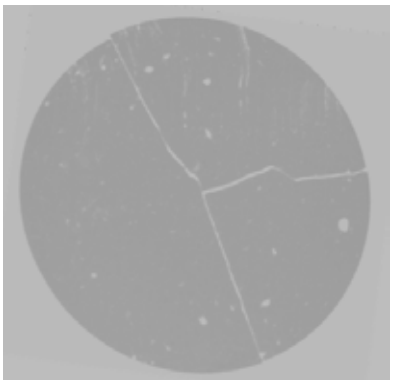

FIG. 5.3. α autoradiograph.

The white spots are the region of low activity, probably PuO_2 agglomerate created local high temperature and cesium migrated to other location. This observation is still under investigation. Radial cracks were observed in the fuel. No columnar grain formation or grain growth was observed in the fuel. The β–γ autoradiographs revealed asymmetric distribution β–γ activity across the fuel cross-section. Higher activity was observed in the cracks in the fuel. The α autoradiograph of the fuel sections revealed a uniform Pu-activity along the cross-section. Uniform oxide layer was observed on the outer surface of the cladding, whereas a discontinuous oxide layer was noticed on the inner surface. Average oxide layer thickness on the outer and inner surface of the cladding was 1.3 μm and 0.9 μm respectively.

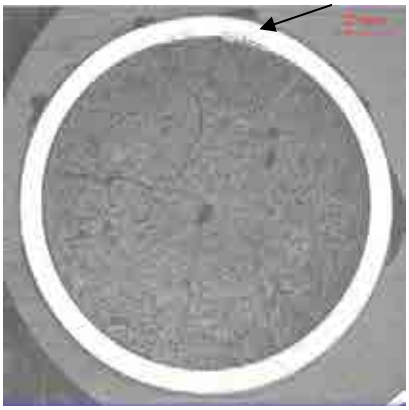

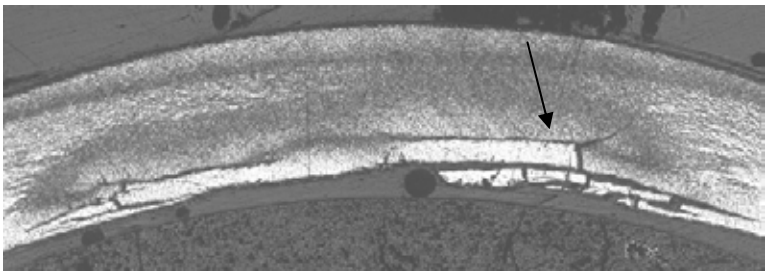

FIG. 5.4. Photo macrograph of the TH-2 fuel pin cross section. Massive hydride blister in the clad and subsequent cracking of clad.

5.2.1. Clad metallography at defect location

Metallographic samples were taken from fuel pin, TH-2, in which a defect location was identified during eddy current testing and no fission gas was obtained during fission gas measurement. Examination of the cladding revealed a massive hydride blister. Figure 5.4 shows the photo macrograph of a section from the pin with a defect region in the cladding. View of the hydride blister at high magnification is shown in Fig. 5.4 too.

5.2.2. Scanning electron microscopy (SEM)

The cellulose acetate replica prepared from the fractured surface of the fuel from pin TH-5 was examined under SEM. The grain size was measured from the impression of the grains on the replicating tape. Figure 5.5 (left) reveals the grain morphology observed in the fuel. The average grain size was found to be 14 µm. A bimodal grain size distribution with grains up to 30 µm in size and cluster of fine grains of 2–3 µm size were also observed among the larger grains as, shown in Fig. 5.5 (right).

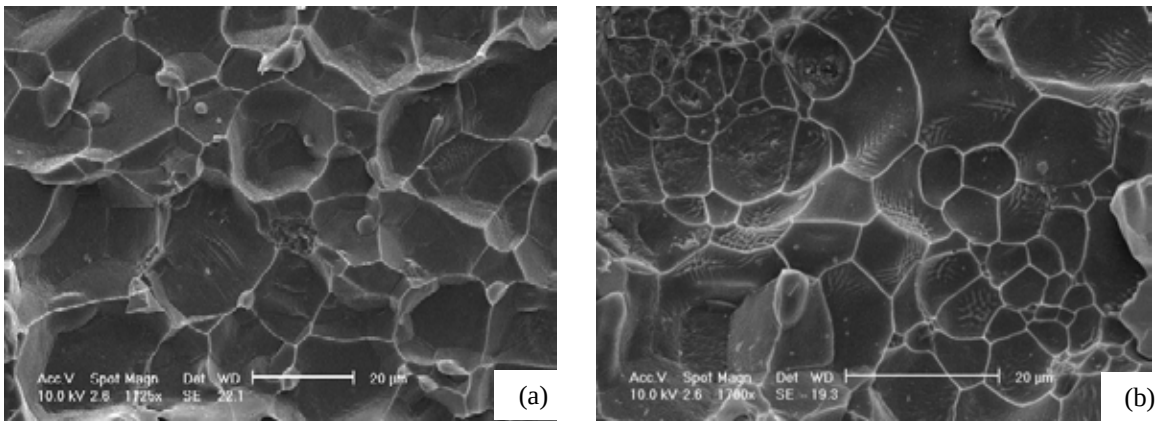

FIG. 5.5. SEM photograph showing grain morphology (left) and bimodal grain size distribution (right).

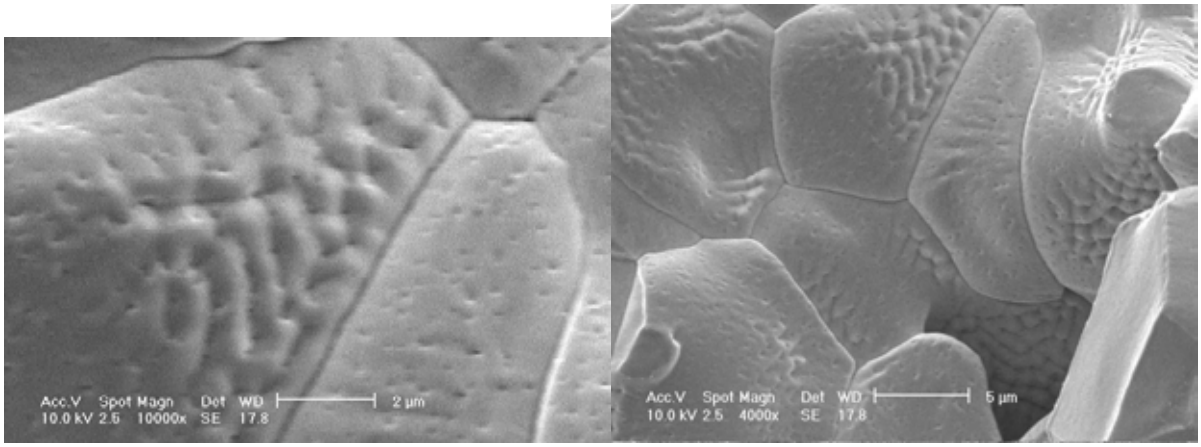

FIG. 5.6. Presence of fine bubbles on the grain faces (left) and magnified image shows interlinking of fission gas bubbles in TH-5 (right).

Examination of the fractured fuel surfaces revealed grains with as fabricated pores at the grain edges and corners. At a few locations, very fine fission gas bubbles were observed on grain faces and there was evidence of interlinking of the fine bubbles as shown in Fig. 5.6 (left). A magnified image of the interlinked features present on the grain face is shown in Fig. 5.6 (right).

6. CONCLUSIONS

1. Absence of visible grain growth or columnar grain formation was absent.
2. Radial cracks were present in the fuel pellet cross-section.

3. Measured grain size and grain morphology was similar to the as fabricated fuel with an average grain size of 14 μm. A few grains up to 30 μm in size and at some locations were observed. Clusters of fine grains of 2–3 μm were also observed. Bimodal grain size distribution occurred in some regions of the fuel.
4. Reduced porosity was seen in the central portion of the fuel.
5. Submicron size fission gas bubbles on the fuel grain surfaces in the central region and inter linkage was also observed.

REFERENCES

[1] ANANTHARAMAN, K., SHIVAKUMAR, V., SAHA, D., Utilization of thorium in reactors, Journal of Nuclear Materials **383**, Issues 1–2 (2008) 119–121.

[2] KARAM, M., DIMAYUGA, F.C., MONTIN, J., Post-irradiation examination of CANDU fuel bundles fuelled with (Th, Pu)O_2, Proceedings of 11th International Conference On CANDU Fuel, Niagara Falls, (2010).

DESTRUCTIVE EXAMINATION OF EXPERIMENTAL CANDU FUEL ELEMENTS IRRADIATED IN TRIGA-SSR REACTOR

S. IONESCU, O. UTA, C. GENTEA, M. MINCU, M. PARVAN, L. DINU
Institute of Nuclear Research,
Pitesti, Romania
Email: silviu.ionescu@nuclear.ro

Abstract

The object of this work is the behaviour of CANDU fuel elements under power cycling conditions. The tests were run in the 14 MW(th) TRIGA-SSR (Steady State Reactor) reactor from Institute for Nuclear Research (INR) Pitesti. zircaloy-4 is the material used for CANDU fuel sheath. The importance of studying its behaviour results from the fact that the mechanical properties of the CANDU fuel sheath suffer modifications during normal and abnormal operation. In the nuclear reactor the fuel elements endure dimensional and structural changes as well as cladding oxidation, hydriding and corrosion. These changes can lead to defects and even to the loss of integrity of the cladding. This paper presents the results of examinations performed in the Post-irradiation Examination Laboratory (PIEL) from INR Pitesti, on samples from a fuel element irradiated in TRIGA-SSR reactor: (i) Dimensional and macrostructural characterization; (ii) Microstructural characterization by metallographic analyses; (iii) Determination of mechanical properties; (iv) Fracture surface analysis by scanning electron microscopy (SEM). The obtained data could be used to evaluate the security, reliability and nuclear fuel performance, and for CANDU fuel improvement.

1. INTRODUCTION

The facilities from INR Piteşti allow the testing, manipulation and examination of nuclear fuel and irradiated materials. The most important facilities are the TRIGA SSR research and material test Reactor and the Post-Irradiation Examination Laboratory (PIEL).

The purpose of this work is to determine by post-irradiation examination, the behaviour of CANDU fuel, irradiated in the 14 MW TRIGA reactor. The results of post-irradiation examination are:

- Visual inspection of the cladding;
- Profilometry (diameter, bending, ovalization) and length measuring;
- Determination of axial and radial distribution of the fission products activity by gamma scanning and tomography;
- Microstructural characterization by metallographic and ceramographic analyses;
- Mechanical properties determination;
- Fracture surface analysis by scanning electron microscopy.

The irradiation of a fuel element can lead to defects in the cladding. This is due mainly to a combination between a strain quite high and a low ductility of the cladding material. In CANDU reactors, the fuel elements are subjected to power ramps severe enough when reloaded during the functioning of the reactor.

The CANDU reactors from Cernavodă Nuclear Power Plant (NPP) are using as nuclear fuel bundles of 37 elements each, assembled by some edge grids. This bundle has a length of 495 mm, a diameter of 103 mm and weight of 24 kg. The CANDU fuel element contains cylindrical pellets of UO_2 syntherized, placed into a zircaloy-4 tube (also known as sheath or cladding), closed at both edges with endcaps. It has a length of 492 mm and a diameter of 13.08 mm.

In order to check and improve the quality of the Romanian CANDU fuel, power ramp tests on experimental fuel elements were performed in our TRIGA SSR reactor. The irradiated fuel elements were further subjected to examination in the PIEL laboratory. During the irradiation, the fuel elements suffer dimensional and structural changes, and also modifications of the cladding surface aspect, as

result of corrosion and mechanical processes. This can lead to defects and even the integrity of the fuel element can be affected.

The performance of the nuclear fuel is determined by the following elements:

- Status of cladding surface and the effects produced by corrosion;
- Cladding integrity;
- Dimensional modifications;
- Distribution of fission products in the fuel column;
- Pressure and volume of the fission gas;
- Structural modifications of the fuel and cladding;
- Cladding oxidation and hydration;
- Isotopic composition of the fuel;
- Mechanical properties of the cladding.

2. CANDU FUEL CHARACTERIZATION

2.1. The aspect of the cladding surface

After irradiation, the fuel rod was kept in the reactor pool for three months, for cooling. The fuel rod was then transferred to the INR hot cells where it was subjected to detailed examinations.

An image of the fuel element is given in Fig. 2.1. It was obtained using a periscope, coupled with an OLYMPUS digital camera. The aspect of the cladding surface indicates a normal behaviour of the fuel element.

FIG. 2.1. Fuel element CANDU tested in the power ramp.

2.2. Profilometry

The diametrical profile, diametrical increasing, ovality and the arrow of fuel element were determined. In Fig. 2.2 is presented the average diameter profile of the fuel element. The average diameter is 13.149 mm. The average diametrical increasing is 0.087 mm (0.67%), with respect to the diameter before irradiation.

Ovality profiles of the fuel element for two different positions on the vertical axis, Z=97 mm and Z=172 mm, are presented in Fig. 2.3. The graphic representation was made based on the measurements performed at these positions on three directions (0°, 120° and 240°). The profiles of bending are presented in Fig. 2.4.

2.3. Gamma scanning and tomography

The gamma scanning equipment consists of a vertical fuel rod positioning machine equipped with SLO-SYN step-by-step motors, a collimator, in the hot cell shielding wall, a PGT intrinsic Ge detector and a multi channel analyser.

For axial gamma scanning, the slit of the collimator was horizontal, having an aperture of 0.5 mm. The gamma acquisition along the fuel rod was performed at regular intervals of 0.5 mm; the acquisition time per step was 200; Fig. 2.5(a)) shows the fuel rod axial gross gamma activity profile. A prominent depression of count rate at fuel pellet interfaces is observed, which means there is no interaction between the pellets. This gamma activity profile highlights practically a symmetric loading of the fuel rod.

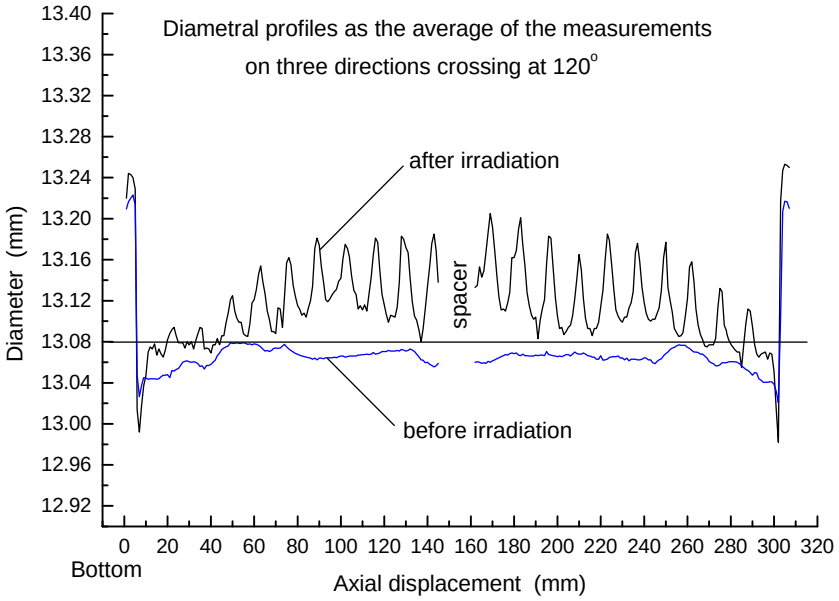

FIG. 2.2. Average diameter profile after irradiation.

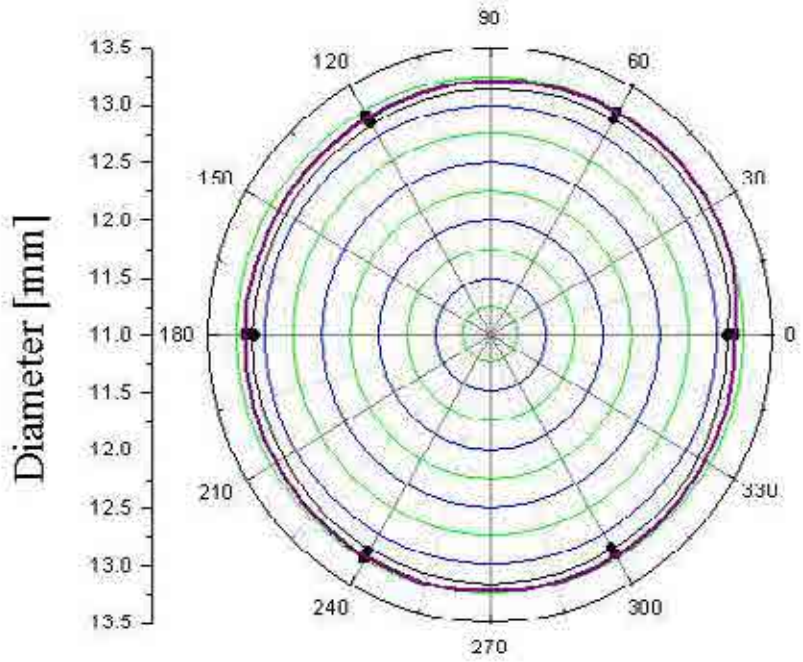

FIG. 2.3. Ovality profiles for Z = 97 mm and Z = 172 mm.

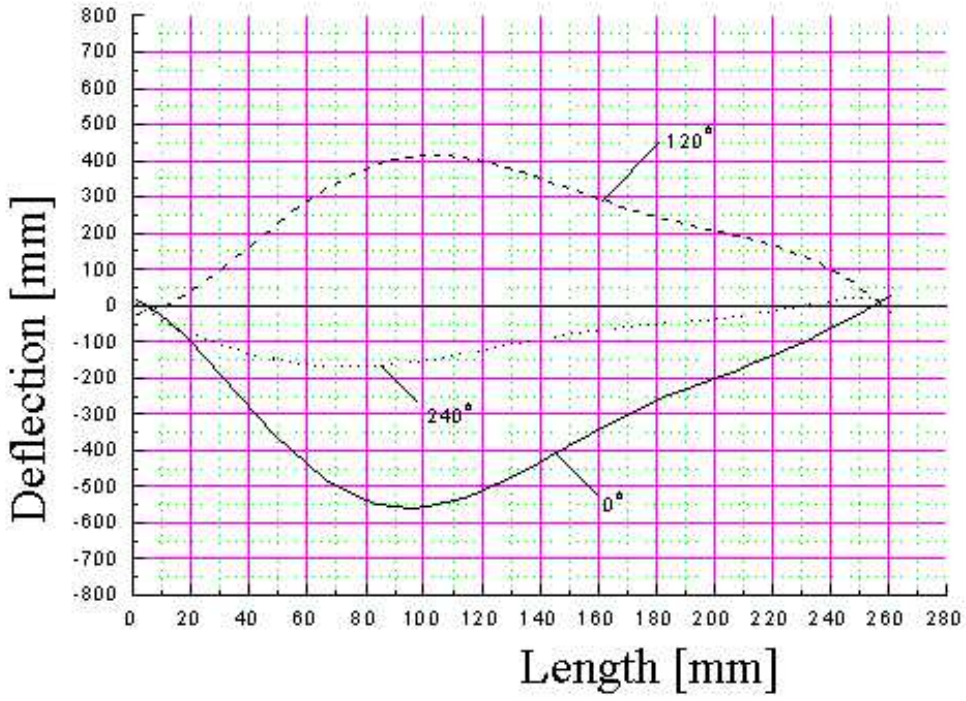

FIG. 2.4. Profiles of bending after irradiation.

A method of tomographic reconstruction based on a maximum entropy algorithm has been developed as described in [1–2]. The data acquisition was done while the fuel rod was moved transversally step-by-step at regular intervals of 0.25 mm after every 72º rotation in front of a vertical collimator slit (which is 50 mm high and has a 0.25 mm aperture). Figure 2.5(b) shows, qualitatively, the tomographic image of the radial distribution of ^{137}Cs gamma activity in the cross-section of the fuel rod, in the flux peaking area. This tomography indicates that the ^{137}Cs isotope migrated from the middle to the periphery of the fuel rod and was redistributed according to the temperature profile.

The ^{137}Cs isotope was used as burnup monitor. For an accurate determination of the burnup, the gamma self-absorption coefficient was calculated using the distribution of ^{137}Cs activity in the cross-section of the fuel rod. The burnup of the fuel rod is 8.77 MW·d·kg^{-1} U (for 192 MeV fission of U). The fuel rod burnup determined by mass spectrometry is 9 MW·d·kg^{-1} U (for 192 MeV fission of U). These results are in good agreement.

2.4. Metallographic and ceramographic examination

A LEICA TELATOM 4 optical microscope, with a magnification of up to 1000 times, was used for macrographic and microstructural analysis of the irradiated fuel rod. A computer-assisted analysis system is used for the quantitative determination of structural features, such as grain and pore size distribution.

The preparation of the samples includes precise cutting, vacuum resin impregnation, sample mounting with epoxy resin in an acrylic resin cup, mechanical grinding and polishing, chemical etching [3].

The analyses by optical microscopy provide information concerning:

- The aspect of pellet fissure (Fig. 2.6);
- The structural modifications of fuel and the sizes of the grains (Fig. 2.7);
- The thickness of the oxide layer and the cladding hydriding.

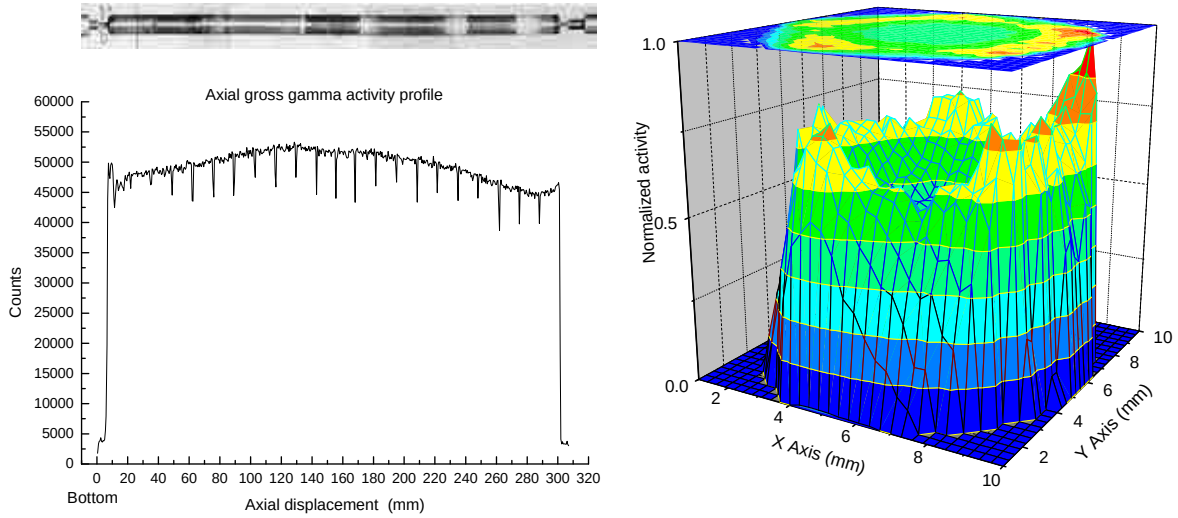

(a) (b)

FIG. 2.5. Axial gamma scanning (a) and tomography (b) on a CANDU fuel rodirradiated in the INR TRIGA reactor in a power ramping test.

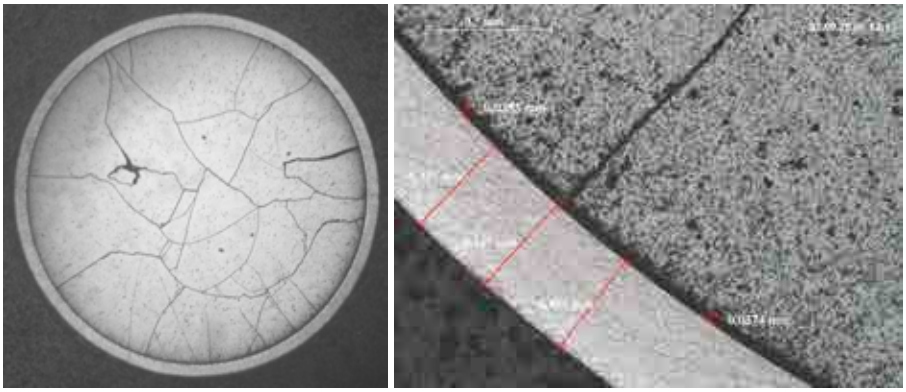

FIG. 2.6. The cross-section of the fuel pellet.

The cross-section of the fuel pellet (× 8) presents radial and circular fissures on the whole section. The cladding does not present nonconformities, the thickness of this being 0.431 mm. There are no visible effects on fuel sheath, due to mechanical or chemical interactions.

The hydride precipitates are orientated parallel to the cladding surface. A content of hydrogen of about 120 ppm was estimated by means of hydriding charts [4]. The fuel element presents on the outer side of the cladding a continuous and uniform zirconium oxide layer (Fig. 2.8). The thickness of the cladding oxide layer is 2.5 μm.

2.5. Determination of mechanical properties

After the preliminary tests, three ring samples (5 mm long each) were cut from the fuel rod, for further tensile tests (Fig. 2.9). The samples were prepared according to the shapes and dimensions given in [5–6].

The samples are tested in order to evaluate the changes of their mechanical properties as a consequence of irradiation. The tensile testing machine used is an INSTRON 5569 model. The machine uses the Merlin software for data acquisition and analysis.

The tests were done under the following conditions: constant testing temperature (300°C), 25N preload and constant tensile strain (v = 0.05 min^{-1}).

(a) Equiaxial grains (b) Unaffected grains

FIG. 2.7. The structural modifications in the fuel pellet.

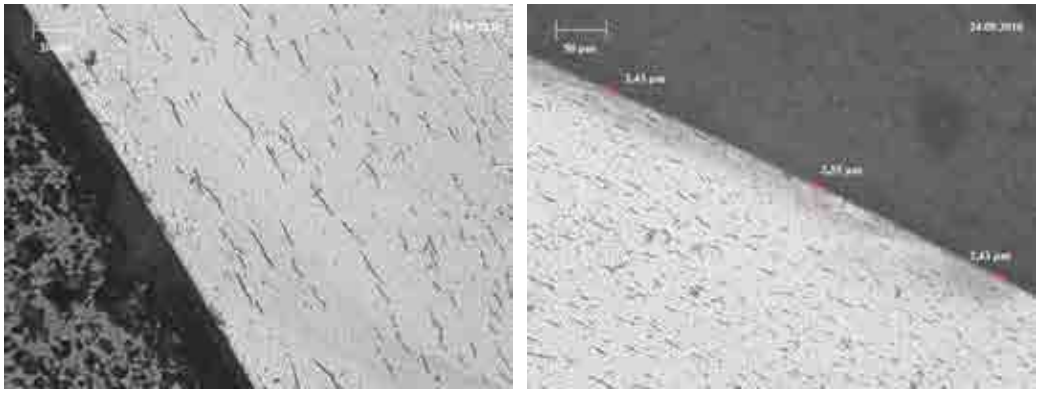

(a) Cladding hydrading (b) Outer oxide layer on cladding

FIG. 2.8. Cladding aspect.

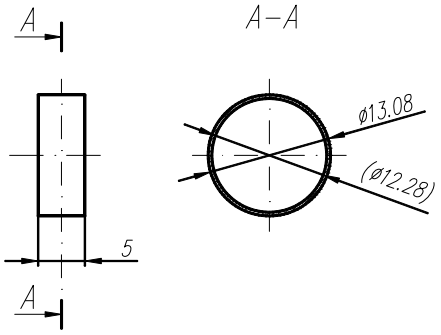

FIG. 2.9. Ring test sample.

The tests have been performed in order to record or evaluate the following mechanical characteristics:

- The strain–stress diagrams and load extension (Figs 2.10–2.11);
- The yield strengths (offset method at 0.2%);
- The elastic limit;
- The ultimate tensile strength of the samples.

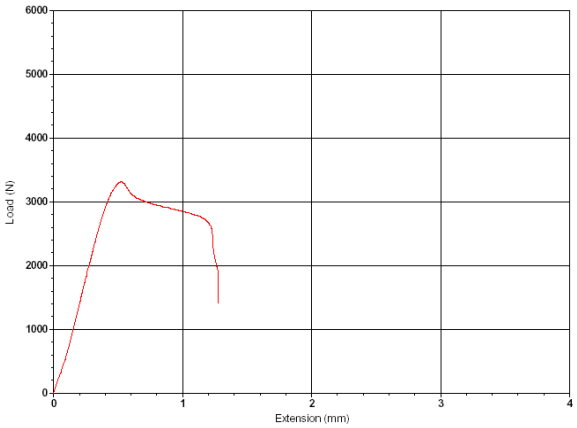

FIG. 2.10. Load–extension diagram.

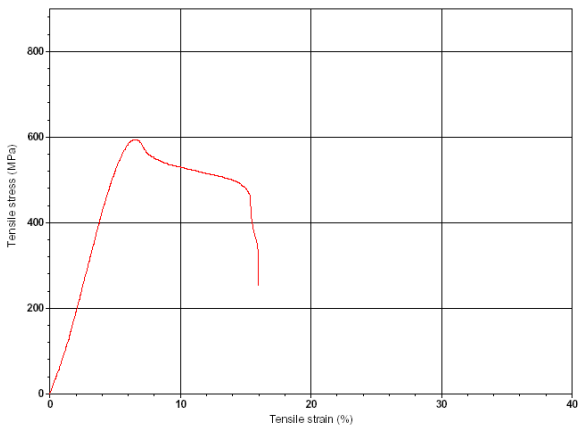

FIG. 2.11. Strain–stress diagram.

FIG. 2.12. Ring sample after test.

The tests were done according to the procedures and standards given in Ref. [7–8]. The aspect of the ring sample after the test is presented in Fig. 2.12.

2.6. Fracture surface analysis by scanning electron microscopy (SEM)

For sample analysis an electron microscop model TESCAN MIRA II LMU CS with Schottky field emission and variable pressure was used. The magnification range is × (4–1 000 000). An outstanding depth field, much higher than in the case of optical microscopy characterizes the scanning electron microscopy (SEM). This makes SEM very appropriate for analysing fracture surfaces of zircaloy 4 cladding resulted from tensile test.

Because of the ring shape of the sample, for rupture surface visualization, the sample was split in two parts, which were mounted in microscope chamber as in Fig. 2.13.

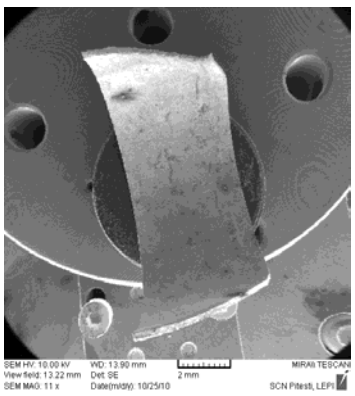

FIG. 2.13. Sample fixture on the electronic microscope table.

Both sides of the tensile fracture were analysed on each half of the ring. The dimples from the central zone are rather deep, whereas the ones on the outer side are tilted and smaller.

The central zone of the fracture presents equiaxial dimples (Fig. 2.14).

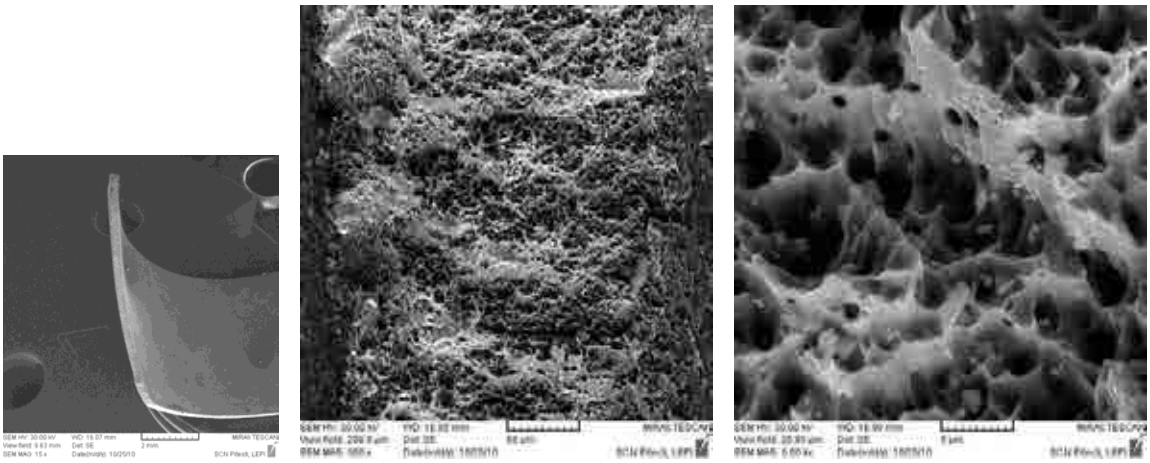

(a) general view × 15 (b) × 500 (c) × 2000

FIG. 2.14. The aspect of the central zone of the fracture.

3. CONCLUSION

After irradiation, the fuel rod was kept in the reactor pool, for cooling and then it was transferred to the INR-PIEL hot cells where it was subjected to detailed examinations.

- First of all, visual inspection of the cladding was done. The aspect of the cladding surface indicates a normal behaviour of the fuel element.
- The diametrical profile, diametrical increasing, ovality and the arrow of fuel element were determined.
- The tomography indicates that the 137Cs isotope migrated from middle to periphery of the fuel rod and was redistributed according to the temperature profile.
- By metallographic and ceramographic examination we determinated that the hydride precipitates are orientated parallel to the cladding surface. A content of hydrogen of about 120 ppm was estimated. The cladding does not present nonconformities. The fuel element presents on the outer side of the cladding a continuous and uniform zirconium oxide layer 2.5 μm thick.
- After the preliminary tests, three ring samples were cut from the fuel rod, and were subject of tensile test on an INSTRON 5569 model machine in order to evaluate the changes of their mechanical properties as a consequence of irradiation.
- Scanning electron microscopy was performed on a microscop model TESCAN MIRA II LMU CS with Schottky FE emitter and variable pressure. The analysis shows that the central zone has deeper dimples, whereas on the outer zone, the dimples are tilted and smaller.

A full set of non-destructive and destructive examinations concerning the integrity, dimensional changes, oxidation, hydriding and mechanical properties of the cladding was performed. The obtained results are typical for CANDU 6 type fuel.

REFERENCES

[1] ALEXA, A., CRĂCIUNESCU, T., MATEESCU, G., DOBRIN, R., The tomographic maximum entropy method in the 3-D analysis of nuclear fuel pins, Journal of Nuclear Materials **218** (1995) 139–142.

[2] CRĂCIUNESCU, T., DOBRIN, R., TUTURICI, I.L., The analysis of irradiated failed nuclear fuel rods by gamma computed tomography, Journal of Nuclear Materials **246** (1997) 37–42.

[3] ASTM INTERNATIONAL, Standard Practice for Preparation of Metallographic Specimens, ASTM E 3–95 (1995).

[4] HYATT, B.Z., Metallographic Standards for Estimating Hydrogen Content of Zircaloy-4 Tubing, Report WAPD-TM-1431 (1982);

[5] KITANO, K., Optimization of sample geometry in modified ring tensile test, The 23rd NSRR Technical Review Meeting, Japan Atomic Energy Research Institute, Tokyo (1998).

[6] DAUM, R., MAJUMDAR, S., TSAI, H., BRAY, T., BILLONE, M., KOSS, D., MOTTA, A., Mechanical property testing of irradiated zircaloy cladding under reactor transient conditions, 4th Symposium on Small Specimen Test Techniques, Reno (2001).

[7] ASTM INTERNATIONAL, Standard Methods for Tension Testing of Metallic Materials [Metric], ASTM E 8M– 96 (1996).

[8] ASTM INTERNATIONAL, Standard Recommended Practice for Elevated Temperature Tension Tests of Metallic Materials, ASTM E 21.

THE MAIN RESULTS OF INVESTIGATION OF MODIFIED DISPERSION LEU U–MO FUEL TESTED IN THE MIR REACTOR

V.V. IAKOVLEV, A.L. IZHUTOV, V.V. ALEXANDROV, A.E. NOVOSELOV,
V.A. STARKOV, A.A. SHELDYAKOV, V.YU. SHISHIN
Joint Stock Company State Scientific Center
Research Institute of Atomic Reactors
Dimitrovgrad
Email: adm@niiar.ru

I.V. DOBRIKOVA, A.V. VATULIN, V.B. SUPRUN, G.V. KULAKOV
A.A. Bochvar High-Technology Research Institute
of Inorganic Materials
Moscow

Russian Federation

Abstract

The report offers the results of the tests and of post-irradiation investigations of low-enriched U–Mo fuel tested in the MIR reactor under the RERTR program. The results of post-irradiation investigations of mini fuel elements with modified dispersion fuel containing 5%, 13% of silicon in the matrix and protective layers on fuel particles in the form of ZrN, tested up to the mean values of U-235 burnup ~60% and ~84%, have been drawn. Data proving the reduction of the process of interaction between U–Mo alloy and the aluminum matrix containing silicon additives is afforded. It is demonstrated that the interaction with the matrix does not happen until 84% of burnup when protective ZrN cladding is available on U–Mo particles. The impact of irradiation conditions on the interaction layer growth is discovered.

1. INTRODUCTION

Development of high density low enriched uranium fuel for research reactors is a worldwide tendency within the framework of mass-destruction weapons non-proliferation and anti-terrorism policy. Reactor conversion to a new fuel of reduced enrichment should be carried out provided specific requirements related to active core and fuel assemblies are observed:

- Reactor core design should be retained;
- Annual consumption of FAs with low enriched fuel should not exceed the number of FAs before conversion;
- Main operating parameters for research reactor should be retained.

Development of new low enriched fuel for low flux research reactors in the Russian Federation was initiated in 1978. Cooperation between Russian and foreign experts within the programme “Reduced Enrichment for Research and Test Reactors” (RERTR) started in the 1990s.

It should be noted that the Russian programme is the only one among national programs within the framework of which a new type of fuel composition is developed together with a new design of fuel elements. It is supposed to use currently developed unified dispersion fuel rods instead of standard FAs with tubular fuel elements.

Based on the examination results, the RERTR programme member countries came to the conclusion that U–Mo alloy is the best material for high density fuel of research reactors.

One of the main problems for low enriched dispersion U–Mo fuel is interaction of the U–Mo alloy particles with Al matrix. As a result of this interaction, fraction of the matrix material reduces with the fuel burnup, physical and mechanical properties of fuel meat significantly change, including considerable reduction of heat conduction, increase of fuel meat temperature and formation of gas bubbles. The paper [1] described gas bubbles formation and unpredicted fuel meat swelling caused by intensive interaction of U–Mo particles with Al matrix. Within the RERTR program, further comprehensive examinations were carried out in order to find a way to reduce this interaction. The authors of paper [2] showed possible reduction of interaction by adding silicon to Al matrix.

Within the Russian RERTR program, to solve this problem much attention was paid to the development of protective coatings on the U–Mo particles surface. Preliminary examinations showed that zirconium nitride coating on particles was determined as the most promising technology. It was decided to conduct comparative reactor tests of mini-rods with modified dispersion U–Mo fuel coated with ZrN and those with silicon additions in Al matrix.

This paper presents the results of fuel meat examinations using SEM and EPMA of non-irradiated mini-rods and those tested up to uranium-235 burnup of ~60% and ~84%. SEM and EPMA were used to obtain data on the fuel meat structure and composition.

2. BASIC CHARACTERISTICS AND TEST CONDITIONS OF MINI-RODS

Mini-rods with various U–Mo modifications were tested and examined in 2003–2006. Mini-rods with silicon additions in the matrix and protective coatings on fuel particles have been tested in 2008–2010. Basic characteristics and test conditions of mini-rods are given in Table 2.1. General view and cross-section of mini-rods are presented in TABLE 2.1.

TABLE 2.1. BASIC CHARACTERISTICS AND TEST CONDITIONS OF MINI-RODS

Parameter	Mini-rods with dispersed fuel meat, irradiation rig 1	Mini-rods with dispersed fuel meat, irradiation rig 2
Cross-section shape	Square with ribs at angles	Square with ribs at angles
Fuel	U-9.4%Mo	U-9.4%Mo
Type and size of U-Mo particles	Granules, ~100–140 μm	Granules, ~100–140 μm
Matrix material	Al; Al+2%Si; Al+5%Si; Al+13%Si	Al; Al+2%Si; Al+5%Si; Al+13%Si
Uranium density of fuel meat, [$g \cdot cm^{-3}$]	~6.0	~6.0
Clad material	SAV-6, alloy 99	SAV-6, alloy 99
Heat flux density, [$MW \cdot m^{-2}$]		
– aver. / max.	0.6/1.2	1.0/1.8
Temperature of outer surface, [ºC]		
– aver. / max.	90/140	120/180
Burnup U-235, [%]		
– aver. / max.	~84/93.0	~60/67.5
Fission rate in particles, [10^{14} $cm^{-3}s^{-1}$]		
– aver. / max.	~2.3/~4.6	~3.6/~6.8
Fission density in particles, [10^{21} cm^{-3}]		
– aver. / max.	~5.6/~6.2	~4.0/~4.5
Duration of tests, [days]	285	130

3. PREPARATION OF SPECIMENS

For SEM and EPMA examinations, full cross-sections of mini-rods were prepared. Preliminary examination of specimens using optical microscopy showed that the width of the interaction layer (IL) between U–Mo particles and matrix is significantly scattered. Therefore, it was impossible to evaluate an extent of the fuel-matrix interaction based on the IL width for separate particles. It was necessary to get SEM images of the entire cross-section of mini-rods and determine volume fraction of the IL.

Specimens were prepared in the specially equipped hot cells. The cross-section was made by fixing a specimen in the holder and its polishing to get a surface of the required quality. The specimen was fixed in the holder by wood alloy. Upon completion of preparations, specimens were transported using an inter-cell transporter to a hot cell with microscope Philips XL 30 ESEM-TMP. Specimens were installed in the microscope working chamber by means of manipulators. The SEM area at RIAR (Dimitrovgrad, Russian Federation) allows the examination of radioactive specimens with high level background ionizing radiation. This area is arranged so that the microscope column is placed on a separate base inside the hot cell (Fig. 3.1) and controlled remotely from the operator's room. This area and its SEM and EPMA capabilities were described in details at the HOTLAB conference in 2004 [3].

FIG. 3.1. View of the microscope from the operator's room through the hot cell window.

4. RESULTS OF EXAMINATIONS

4.1. State of fuel meat of non-irradiated mini-rods

The examination of unirradiated fuel compositions showed no interaction between fuel particles and matrix during manufacturing of mini-rods of all types.

For mini-rods with 5% Si matrix, silicon interacts with U-9%Mo alloy. A silicon saturated layer is formed on the surface of fuel particles. It does not form a continuous coating of particles, its size differs for various particles and is not uniform along the perimeter of one and the same particle.

Distribution maps of silicon, uranium, molybdenum and aluminum were plotted using EPMA (Fig. 4.1). The grain boundaries of the U–Mo alloy have reduced amount of Mo and increased amount of U, as it was mentioned in [4]. The distribution map analysis makes it possible to identify that Si diffuses inside U–Mo particles along the grain boundaries. No traces of Al penetration into U–Mo alloy were found. For 13% Si in the matrix, no qualitative change in the interaction between silicon and fuel particles is observed as compared to its 5% content in the matrix. Silicon penetrates deeper

into U-9%Mo alloy diffusing along the grain boundaries. The silicon-saturated layer becomes thicker on the surface of fuel particles. It covers larger surface of fuel particles without forming a continuous film.

For fuel elements with ZrN coating on fuel particles, the coating layer thickness makes up 2–3 μm (Fig. 4.2). For some U–Mo particles, ZrN coating layer is observed partially or not observed at all.

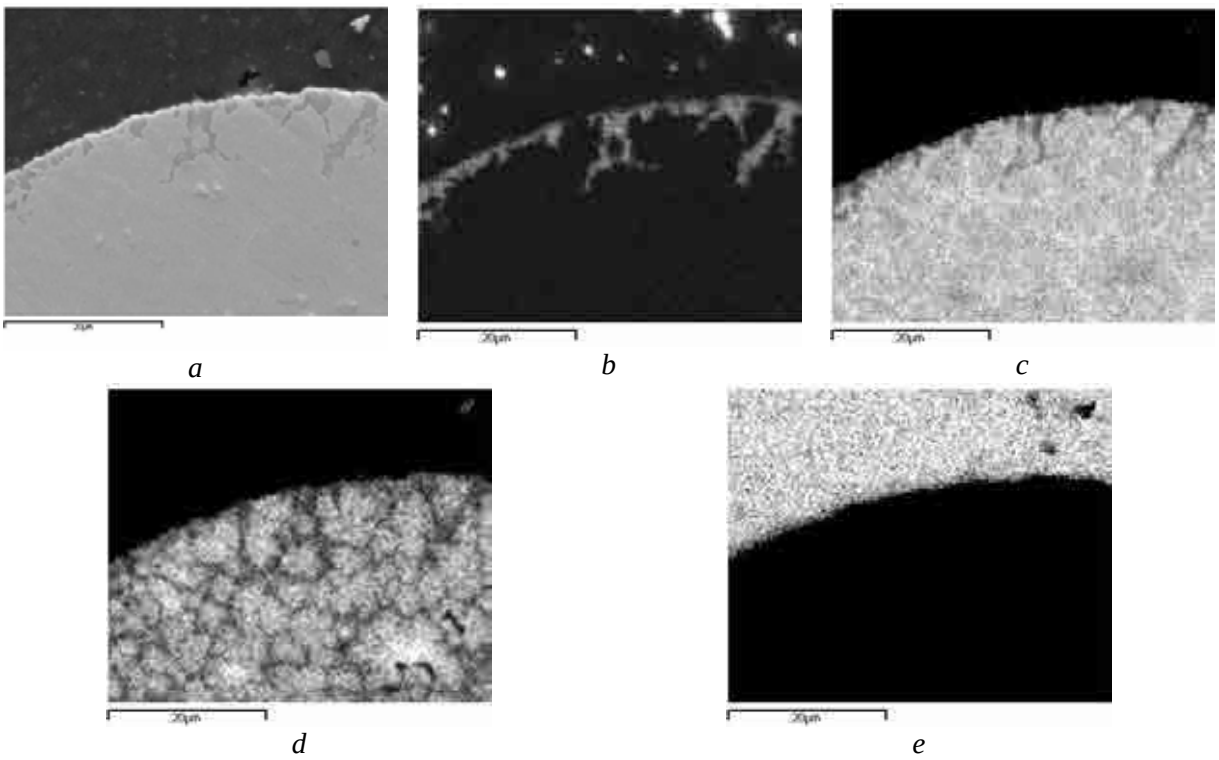

a *b* *c*

d *e*

FIG. 4.1. Image of the fuel meat region with 5% Si matrix (a) on which distribution maps of Si (b), U (c), Mo (d) and Al (e) were obtained.

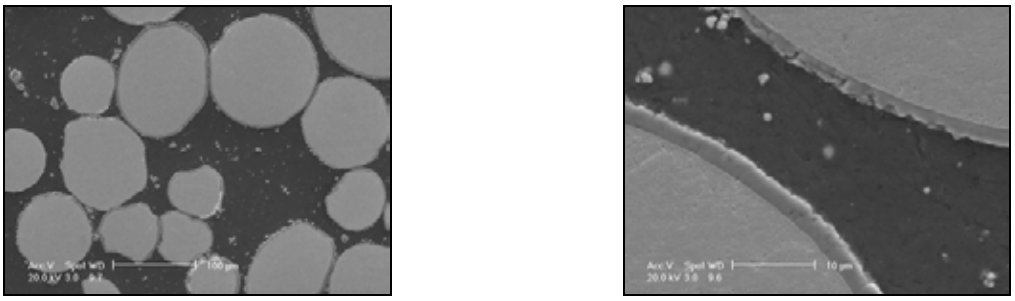

a *b*

FIG. 4.2. (a) Fragment of the fuel meat of the mini-rod with ZrN coating of U-9%Mo alloy particles ; (b) SE image of ZrN coating .

4.2. State of fuel meat after irradiation

The U–Mo alloy interacts with Al under irradiation. The degree of interaction between the U-9%Mo particles and matrix from aluminum powder PA-4, 5% Si and 13% Si and ZrN coating was evaluated based on the volume fraction of the interaction layer. The results are presented in Table 4.1.

Table 4.1 shows that with addition of silicon in the matrix, the IL significantly reduces. Increase of silicon concentration from 5% up to 13% considerably reduces the IL volume fraction.

For mini-rods with ZrN coating on fuel particles, the IL volume fraction remains at 6% for the above mentioned irradiation conditions. Microstructure of irradiated fuel compositions in examined mini-rods is presented in Fig. 4.3.

Analysis of the fuel meat state shows that the IL thickness is similar for all U–Mo particles of the U-9%Mo/Al (without Si) composition and makes up 25–30 μm. With addition of 5% Si to the matrix, the IL thickness becomes very non-uniform along the perimeter of fuel particles. Its values range from 2 μm to ~30 μm for high fission rate and a burnup of ~60%, and from 2 μm to ~20 μm for low fission rate and a burnup of ~84%. For 13% Si added matrix the major area of the U–Mo particles surface has IL ~(1–2) μm thick. At a high fission rate, this layer achieves its maximum thickness of 15 μm, while at low fission rate it is equal to 10 μm.

Protective ZrN coating completely prevents the interaction of U–Mo alloy with the Al matrix. The interaction layer is formed in the fuel meat of such mini-rods where there is no protective coating on the fuel particle surface, both for a burnup of ~60% and ~84%.

TABLE 4.1. RESULTS OF MEASURING THE IL VOLUME FRACTION IN MINI-RODS AFTER IRRADIATION UP TO THE AVERAGE BURNUPS OF ~60% AND ~84%

Fuel meat material	Rig No.2		Rig No.1	
	Burn-up, [%]	IL volume fraction, [%]	Burn-up, [%]	IL volume fraction, [%]
Si<0.4%	~60	40±4	~84	40±4
A1+5%Si	~60	25±3	~84	10±2
A1+13%Si	~60	10±2	~84	6±1
ZrN coating Si<0.4%	~60	6±1	~84	6±1

EPMA was used to determine silicon effect on the IL thickness. Silicon distribution maps were plotted. They demonstrate that with high amount of silicon in the IL, its thickness is equal to 2–3 μm (Fig. 4.4) irrespective of irradiation conditions for this experiment. Quantitative EPMA shows that the silicon content in such IL ranges within 7–15 at.%.

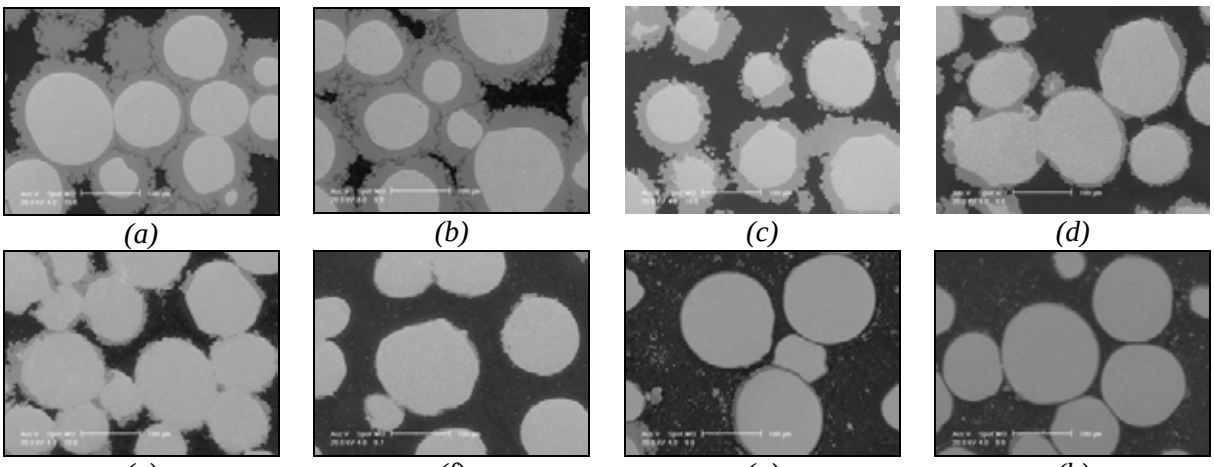

FIG. 4.3. SEM images of fuel meat microstructure: U-9%Mo particles in Al matrix. Burnup ~60% (a) and ~84% (b); U-9%Mo particles with addition of 5% Si in the matrix. Burnup ~60% (c) and ~84% (d); U-9%Mo particles with addition of 13% Si in the matrix. Burnup ~60% (e) and ~84% (f); U-9%Mo particles with ZrN coating. Burnup ~60% (g) and ~84% (h).

No silicon was revealed in the wide interaction layer. It concentrates at the boundary of wide IL with the matrix.

Summary of the EPMA results shows that the IL grows before contact with silicon particles. At that moment it stops to grow and further interaction is observed at adjacent silicon-free regions. With a great quantity of silicon particles, the IL growth stops in all directions. It is clearly seen in Fig. 4.5, where silicon particles prevent the IL growth in each direction.

No cases of silicon particles presence inside the IL were observed. Therefore, silicon particles effectively prevent the IL propagation.

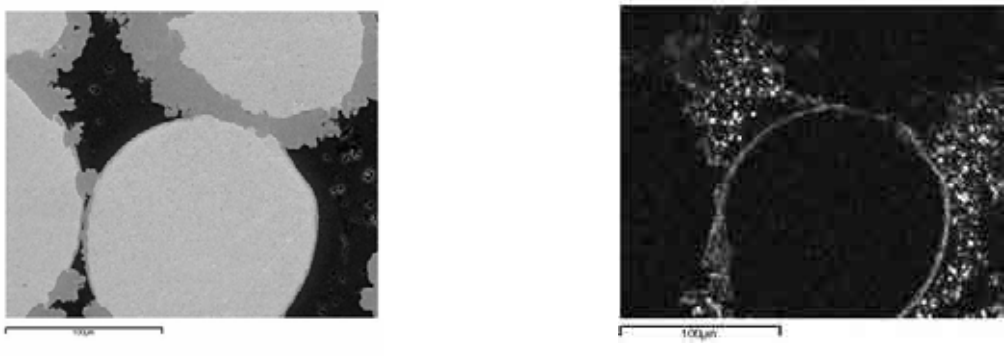

(a) *(b)*

FIG. 4.4. Non-uniform interaction layer in 5% silicon matrix. Burnup of U-235 is ~60%. Silicon distribution around fuel particles. No silicon is found in the wide IL.

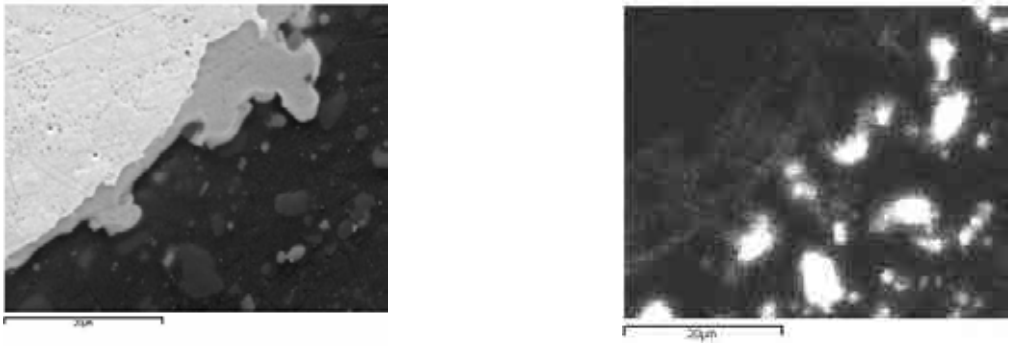

(a) *(b)*

FIG. 4.5. IL image. 13% Si matrix, U-235 burnup is ~60%. The IL propagation is stopped by silicon particles in all directions (b).

5. DISCUSSION

Results of examinations of mini-rods from two irradiation rigs where the testing conditions differed by thermal power (fission rate) are evident of significant effect of irradiation conditions on the IL formation intensity. For the first irradiation rig, an average burnup of U-235 of ~84% (average fission density in fuel particle is ~5.6×10^{21} cm^{-3}) was achieved at full power operation of 285 days, average fission rate of 2.3×10^{14} $cm^{-3}s^{-1}$. For the second irradiation rig, an average burnup of U-235 of ~60% (average fission density in fuel particles is ~4.0×10^{21} cm^{-3}) was achieved at full power operation of 130 days and an average fission rate of 3.6×10^{14} $cm^{-3}s^{-1}$. The following results were obtained (Table 4.1):

– For silicon-free matrix, nearly the same volume fractions of the fuel-matrix interaction layer were obtained;
– For mini-rods with the 5% silicon in the matrix, the IL volume fraction is 2.5 times higher than that for mini-rods with the 13% silicon in the matrix during irradiation in the second irradiation rig up to a burnup of ~60% at fission rate of $3.6 \times 10_{14}$ cm-3s-1;

– For mini-rods with the 5% silicon in the matrix, the IL volume fraction is 1.7 times higher than that for mini-rods with the 13% silicon in the matrix during irradiation in the first irradiation rig up to a burnup of ~84% at fission rate of 2.3×10^{14} $cm^{-3}s^{-1}$.

Therefore, with silicon addition to the matrix, interaction suppression effect of silicon concentration in the matrix is greater at relatively high fission rate (3.6×10^{14} $cm^{-3}s^{-1}$).

The above mentioned effects can be significantly influenced by fuel meat temperature.

In the production of mini-rods with silicon additions in the matrix, dissolution of silicon near the surface of U–Mo particles is not completed. As a result, fuel particles or some regions of the fuel particle surface are not saturated with silicon. In this case, when on the surface of U–Mo particles a silicon saturated layer is formed, it slows down the diffusion of uranium and molybdenum atoms from one hand and Al atoms from the other hand. The IL becomes 1–3 μm wide under irradiation. It was determined that to prevent intensive growth of the IL under irradiation in reactor MIR, 7 at.% silicon concentration is sufficient. If in the initial state silicon concentration on the fuel particle surface is not sufficient, formation of a wide interaction layer occurs during irradiation.

There is no silicon inside the wide IL. It is displaced to the IL boundary with matrix. With movement of the boundary inside the matrix the silicon concentration on it increases resulting in slowdown of the IL growth. If large silicon particles appear on the way of the IL boundary with matrix, the IL stops to grow in this area, while the interaction in regions free from silicon continues. It explains non-uniformity of the IL width in the fuel meat in the matrix of which there are silicon additions. Therefore, silicon particles form an effective barrier against U–Mo alloy interaction with Al. Increase of fuel meat temperature contributes to more intensive diffusion. It results in the increase of the IL volume fraction with increase of fission rate.

The most effective measure to stop the U–Mo alloy interaction with Al is application of ZrN coating on the surface of U–Mo particles. If the coating layer is 2–3 μm wide, interaction with the Al matrix under the above mentioned irradiation conditions up to a burnup of ~84% is not observed.

6. CONCLUSION

Post-irradiation examinations of mini-rods with modified dispersion U–Mo fuel tested in the MIR reactor up to average burnups of 60% and 84% of U-235 showed the following results:

– Protective coating on U–Mo particles with ZrN layer 2–3 μm thick almost completely prevents their interaction with the Al matrix without using any additions up to high burnups at fission rates of $3.6 \times 10_{14}$ cm-3s-1;
– Silicon added into the matrix decreases significantly the interaction between U–Mo particles and the matrix, both silicon content and fission rate being effective;
– Effect of interaction suppression with increase of silicon concentration in the matrix is higher at relatively high fission rate.

REFERENCES

[1] HOFMAN, G.L., FINLAY, M.R., KIM, Y.S., Post-irradiation analysis of low enriched U-Mo/Al dispersion fuel miniplate tests, RERTR 4 and 5, Proceedings of the 26th international meeting on reduced enrichment for research and test reactors, Vienna (2004).

[2] KIM, Y.S., RYU, H.J., HOFMAN, G.L., HAYES, S.L., FINLAY, M.R., WACHS, D.M., CHANG, G.S., Interaction layer growth correlations for (U-Mo)/Al and Si-added (U-Mo)/Al dispersion fuels, Proceedings of the 28th International Meeting on Reduced Enrichment for Research and Test Reactors, Cape Town (2006).

[3] GOLOVANOV, V.N., NOVOSELOV, A.E., KUZMIN, S.V., YAKOVLEV, V.V., Possibilities and prospects of investigation of irradiated structural and fuel materials using scanning electron microscope PHILLIPS XL 30 ESEM-TMP located in the hot cell, HOTLAB: European Hot Laboratories Research Capacities and Needs, Halden (2004).
[4] KEISER, D.D., Jr., JUE, J.F., ROBINSON, A.B., MEDVEDEV, P.G., FINLAY, M.R., SEM characterization of unirradiated dispersion fuel plate with U-10Mo particles and 6061 Al matrix, The 2009 International Meeting on Reduced Enrichment for Research and Test Reactor, Beijing (2009).

BIBLIOGRAPHY

[1] IZHUTOV, A.L., ALEXANDROV, V.V., NOVOSYOLOV, A.E., et al., Results of PIE pin type LEU U-Mo fuel elements tested in the MIR reactor, The 2006 International Meeting on Reduced Enrichment for Research and Test Reactors, Cape Town (2006).
[2] IZHUTOV, A.L., STARKOV, V.A., PIMENOV, V.V., et al., The status of testing LEU U-Mo full-size IRT type fuel elements and mini-elements in the MIR reactor, The 2008 International Meeting on Reduced Enrichment for Research and Test Reactors, Washington, D.C. (2008).

EXAMINATION OF AN IRRADIATED FUEL PIN SEGMENT BY LASER SCANNING PROFILOMETRY, GAMMA SPECTROMETRY AND NEUTRON RADIOGRAPHY

H. WIESE
Paul Scherrer Institute
Department Nuclear Energy and Safety
Hot Laboratory Division
Email: holger.wiese@psi.ch

P. VONTOBEL
Paul Scherrer Institute
Department of Research with Neutrons and Muons
Spallation Neutron Source Division

Villigen, Switzerland

Abstract

Paul Scherrer Institute (PSI) conducts post-irradiation examinations (PIE) on fuel pins irradiated in nuclear power plants. During poolside inspections of the nuclear fuel at one of these plants, an intact fuel pin showed a small deviation in diameter along several mm of the axial elevation. The pin was added to the fuel delivery transport to PSI in the frame of a surveillance program. To detect the exact dimensions of the pin section, a laser scanning profilometer was adapted for hot cell use by mirroring the laser beam. The examined length of the found clad necking matched the nominal length of one fuel pellet, indicating a missing or diameter reduced pellet. Axial gamma spectrometry confirmed the match of the neckings's length with the pellet gaps indicated by higher cesium count rates. The azimuthal variation in cladding diameter was confirmed by gamma spectrometry angle dependent mappings. To investigate the pellet integrity without destructive methods, a neutron radiography was decided for. After cutting a segment of the pin, the radiography at the PSI neutron irradiation facility SINQ revealed one pellet with variations in diameter, but without abnormal structural defects. This paper outlines the combination of the three non-destructive methods as well as technical descriptions of the methods and some results of the examinations.

1. MOTIVATION

To improve the economy of nuclear fuel assemblies, further development of cladding alloys and assembly designs is aimed for by utilities, suppliers and vendors. To confirm the effectivity of the developments as well as the compliance with safety margins, Paul Scherrer Institut (PSI) HOTLAB conducts a post-irradiation examination (PIE) program, where fuel pins irradiated at swiss commercial plants are characterized on a regular basis since 25 years. The fuel pin positions are chosen based on fuel assembly design changes and heat generation or burnup criteria and PSI offers the complete range of non-destructive and destructive analyses. During poolside inspections of the nuclear fuel at one of these plants, an intact fuel pin showed a small deviation in diameter along several mm of the axial elevation. This paper describes a set of three non-destructive tests delivering the basic information to choose the position for destructive analysing in case of this fuel imperfection.

2. CONDITIONS

The non-destructive testing is performed in the 1st cell of a hot cell chain built in the beginning of the 1960s and refurbished 1985–87 to conduct PIE of fuel pins irradiated in commercial power plants.

Equipped with 90 cm of steel encased concrete shielding and remote handlers „Wälischmiller A100“, the gamma dose rate at the different measurement systems can reach up to several $kGy \cdot h^{-1}$. As the dose rate and accumulated dose in the cell is steadily increasing due to higher burnup and earlier delivery of pins after their end of life, modern measurement systems with integrated electronics installed inside the cell required additional shielding. They replace the older systems based on mechanical principles or more robust, conventional electronics. Regarding the limitations of criticality and geometry for Hotcell 1, 37 UO_2 or 23 MOX fuel rods with a maximum enrichment of 5% and 7%, respectively and a rod length up to 4300 mm can be handled. The fuel pin movement is automated and programmable, allowing smallest stepwidths of 0.1 mm in axial and 1° in azimuthal direction.

3. EXAMINATION

An intact rod, examined in the frame of the regular PIE programme 2010 showed a very small azimuthal necking in diameter, hardly to be detected by visual inspection. The fuel manufacturer and the plant operator decided to investigate the cause. A non-destructive examination was chosen to avoid any impact to the material and to define the axial level of metallo-ceramography.

3.1. Profilometry

The exact dimensions of the necking were determined by laser scanning profilometry. The method detects the amount of light received from an oscillating laser beam after shadowed by the measured sample.

Properties and abilities of the method:

- Deviation from the calibrated diameter with accuracy and reproducability of 0.3 µm;
- Minimum axial step width of 0.3 mm;
- Measuring time for an axial rod profile of about 4 m length in approximately two hours;
- Rotational profiles, indicating the surface contour of the cladding.

This unique adaptation of an industrial system (Mitutoyo LSM) to highly radioactive ambience was achieved by mirroring of the laser beam. Therefore, shielding of emitter and receiver by ~10 half-value layers of lead was possible. The laser beam is distracted by a rotating polygonal mirror, thus oscillating along the position of the moving fuel pin. By exactly positioning of the additional mirrors, the accuracy of the encapsuled system was kept in the same order. Roughness and cleanliness of the mirrors are checked by the oscilloscope signal.

The system can be removed from the outer shielding for repairs or cleaning. Maintenance is negligible compared to the earlier used system with LVDTs as there is no mechanical wear.

The axial and azimuthal scanning of the fuel rod confirmed that the axial length of the necking matches the height of a single fuel pellet while the diameter was varying in circumferential direction with a pronounced minimum at one side of the rod (Fig. 3.1).

3.2. Gamma spectrometry

Knowing the length of the clad necking matches one pellet, gamma spectrometry was applied to confirm the positions and conditions of the fuel pellets. The method is an energy dispersive measurement of fission and activation products with positioning of the fuel pin equal to profilometry. Volatile and fixed species detected allow for conclusions regarding temperature and fission rate gradients in the fuel column, i.e. positions of the pellet gaps and possible fuel inhomogenities. The gamma beam is collimated with a slit width of 0.3 mm, the collimator itself is integrated within the hot cell shielding wall. The nitrogen cooled HPGe-Detector delivers a spectrum of 4096 energy channels, which correlates to a resolution of about 0.5 keV if used over the full energy range. Very high count rates up to 4×10^5 cps are accepted by the hardware due to digital amplification and loss free impulse

counting; the spectrum analysis software (Canberra Genie 2K) is remote controlled by a LabView based two-axis drive system moving the fuel pin.

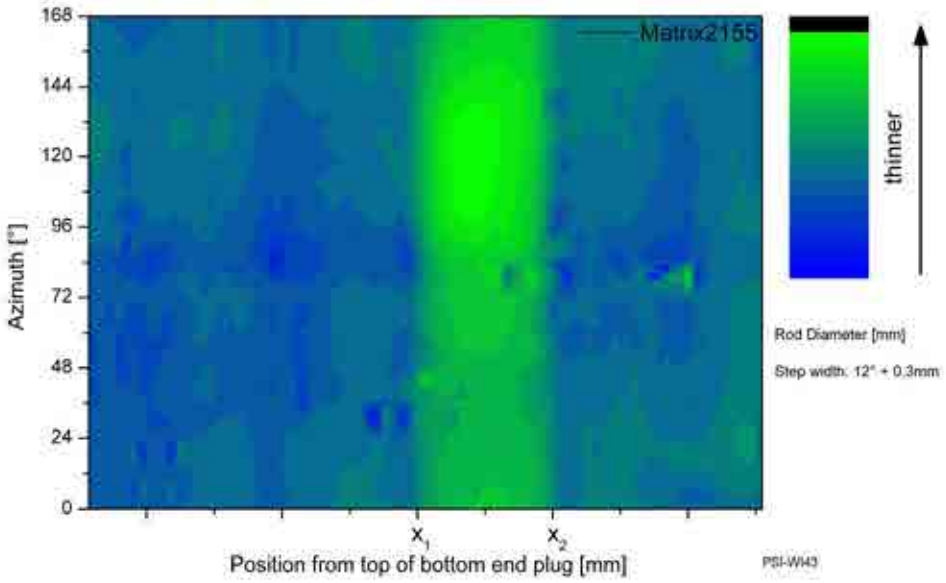

FIG. 3.1. Azimuthal diameter plot of the fuel rod necking; axial length determined to one pellet [x_1;x_2] and pronounced on one side of the rod.

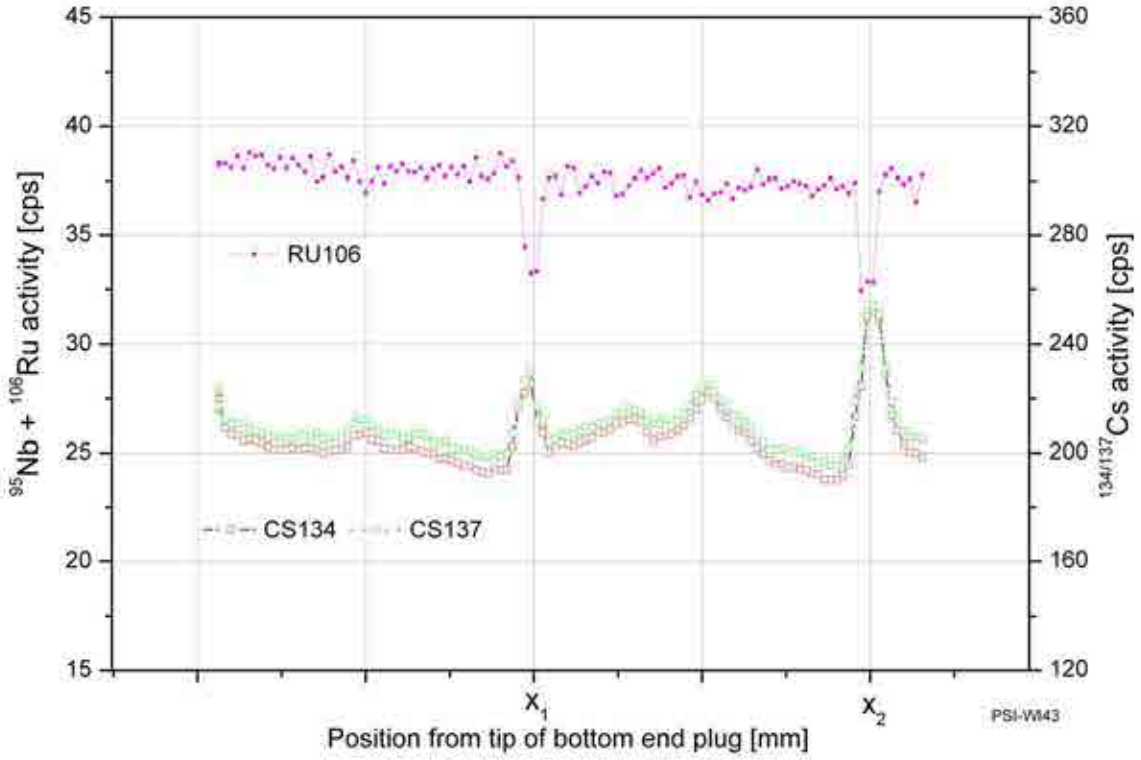

FIG. 3.2. Plot of axial count rate of caesium and ruthenium, indicating the gaps between the pellet matching the necking position.

As the volatile cesium accumulates at positions of lower temperature, pellet gaps and areas of better thermal conductivity or lower heat generation are indicated by higher count rates. As ruthenium is kept fixed in the fuel matrix, inhomogenities in the fuel are detected. The plots of count rate against fuel

rod elevation of these nuclides are compared in Fig. 3.2. The observed pellet gaps matched perfectly with the area of reduced diameter of the necking, and the higher count rates of ^{134}Cs and ^{137}Cs observed at mid pellet height can be attributed to positions of closer contact of pellet and cladding. On the other hand, the quite stable count rate of ^{106}Ru indicates no hint for fuel imperfection.

3.3. Neutron radiography

Now that the cause for the necking was identified in one certain fuel pellet, the obvious next step was ceramographic examination. But, proceeding directly with metallo-ceramography would imply a lot of grinding levels and possible influence of sample preparation on the defect. Decision was taken to "have a look first" by neutron radiography despite the effort and cost. The PSI Spallation Neutron Source is equipped with the station NEURAP, which allows non-destructive imaging of radioactive samples by 25 meV thermal neutrons at a flux of 1×10^{14} cm^{-2}.

After cutting the fuel pin, the 200 mm long segment to be examined was encased in an aluminum tube, referencing the azimuthal orientation by polyethylene markers. Said tube can be drawn into a shielded manipulation and transport cask which is connectable to both the cell at the hot laboratory and the beamline shielding at NEURAP. The relative attenuation of neutrons by the relevant materials zirconium, aluminum and polyethylene is given with ~0.01; ~0.1 and ~3.5, respectively. Thus, the neutron beam crossing the fuel segment is hardly hindered by the Zr and Al in contrast to the azimuthal mark made of PE. After passing the sample, the beam enters the detector slot, there exposing an imaging plate. The imaging plates contain a photoluminescent compound and a neutron absorber. While the plate is excited during exposure by gamma rays from the fuel, the absorber is activated by the attenuated neutron beam. After exposure, the plate is erased by light, followed by self-exposure through the activated absorber. Final readout is done by a laser scanner with 50 μm squared raster. This procedure was repeated 12 times, each time turning the fuel segment by 15°. Figure 3.3 shows as an example one aspect irradiated at 0–180°.

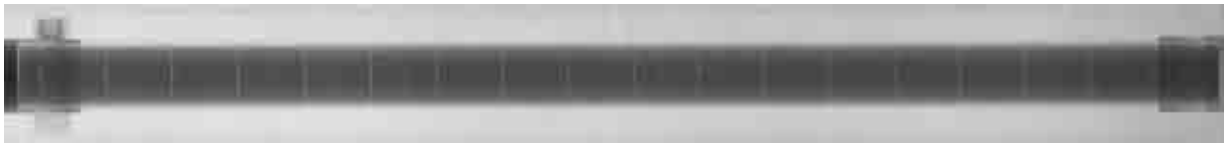

FIG. 3.3. Aspect of neutron radiography, total length of examinated segment.

Different image manipulation techniques like conversion to black/white and shifting the respective threshold values or enhancing the contrast and shifting the histogram values, showed no major defects inside the pellet. Consequently, the examination focused on the diameter of the pellet. The slight magnification of the images due to the collimation ratio of the neutron beam was accounted for by scaling against the known diameter of the segment end caps. Scaling was possible by counting the number of pixels of the diametral grayscale value, where the neutron beam was attenuated by solid material (Fig. 3.4). Regarding the examined pellet, the gray intensity of diametral lines was measured at different segment elevations comprising the neighbouring pellets (Fig. 3.5). Clear distinction was possible between cladding and fuel, allowing the determination of the pellet diameters. Although the resolution was restricted to 50 μm by the readout raster, a reduction of diameter at the considered pellet was confirmed. Through analysing the radiographs at different beam angles, a picture of the pellets outer shape and its position in the cladding was derived.

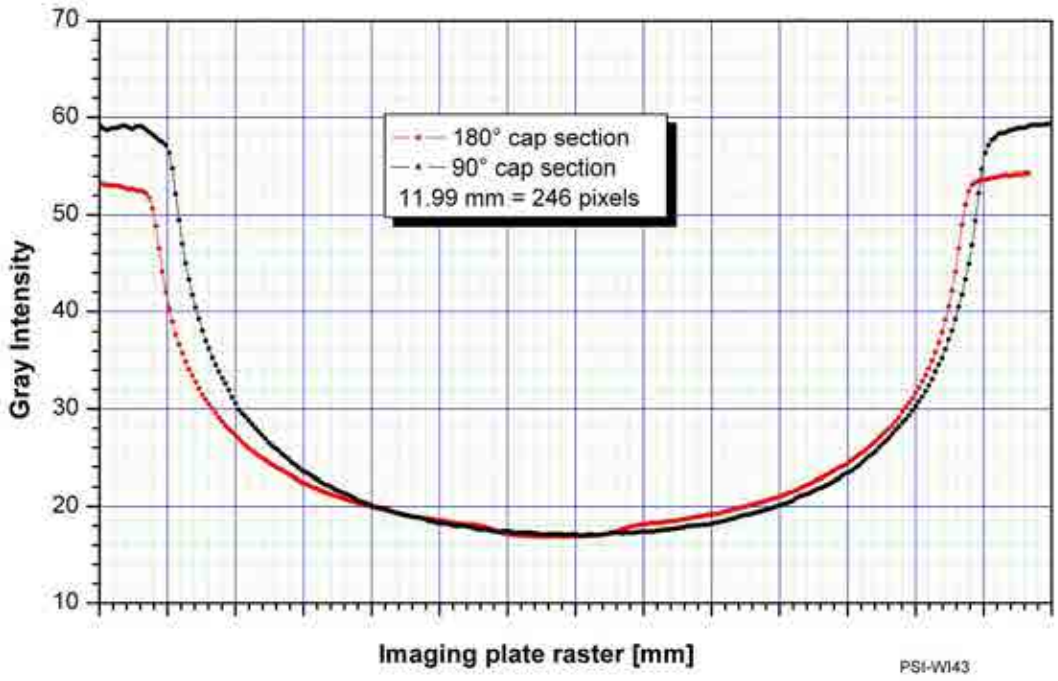

FIG. 3.4. Diametral grayscale intensity of segment end cap, used for scaling the neutron image.

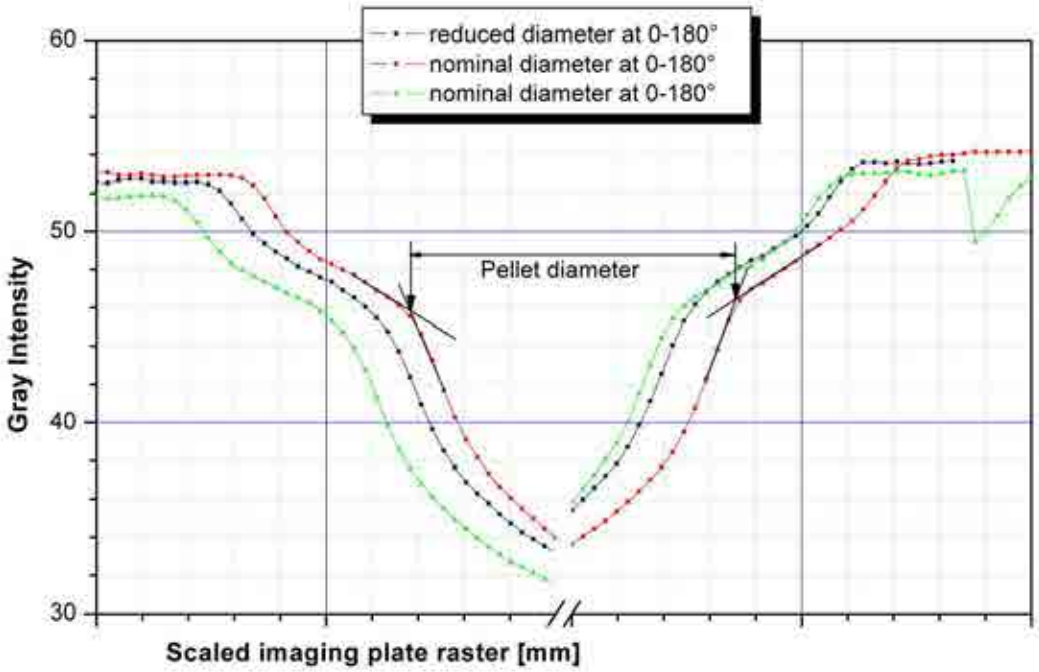

FIG. 3.5. Fuel pellet diameter determination by neutron radiography. Gray intensity levels of imaging plates exposed by the attenuated neutron beam allow the distinction between fuel and cladding.

4. RESULT AND CONCLUSIONS

The necking of diameter found at one elevation of an intact LWR fuel pin irradiated in a commercial power plant was explained by combination of three non-destructive methods:

– Laser profilometry and gamma spectrometry showed compliance of the position and length of the cladding constriction and one certain pellet;
– Neutron radiography imaging revealed no major flaw in the fuel but a slightly smaller and irregular diameter of the pellet;
– The combination of the three methods allowed the choice of a specific ceramography level followed by cutting of the segment without the possible influence on the cause of the defect.

Comparison of the results of the three non-destructive methods reveals a minimum diameter of the pellet at a certain rod elevation. The cladding tube has creeped down to the fuel surface with closest contact at positions of higher cesium count rates (Fig. 4.1). Neighbouring areas of the imperfect pellet are confirmed to be in a state as expected regarding the rod's burnup. The elevation of highest deviation in diameter was chosen as level for ceramography, and the ongoing investigations indicate an irregularity of the manufacturing process.

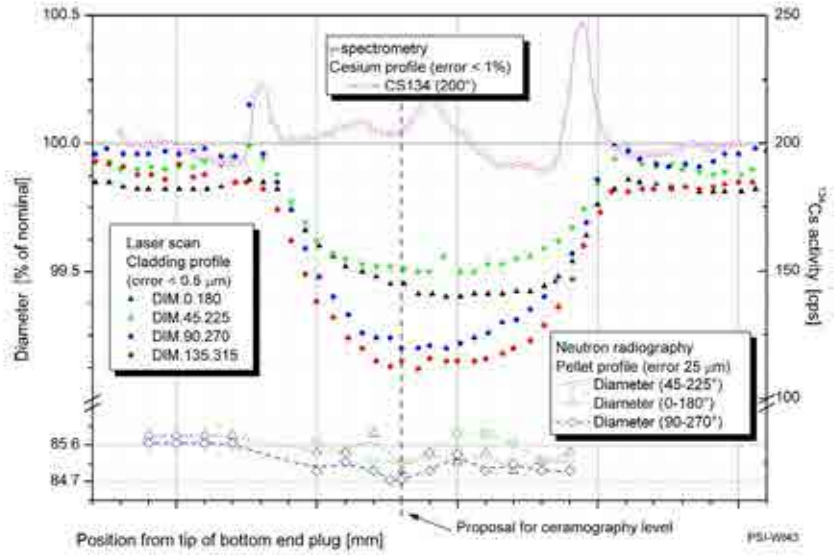

FIG. 4.1. Combined laser profilometry, gamma spectrometry and neutron radiography measurements.

POST-IRRADIATION EXAMINATION OF THE FUEL RODS OPERATED IN WWER-1000 MIXED CORES

V.S. KRASNORUTSKYY, V.I. KUZNETSOV, D.A. SOKOLOV, V.M. GRYTSYNA,
A.M. ABDULLAYEV, M.V. TRETYAKOV
National Science Center "Kharkov Institute of Physics and Technology"
"Nuclear Fuel Cycle" Science and Technology Establishment
Kharkov, Ukraine
Email: tretyakov_mv@kipt.kharkov.ua

Abstract

Ukraine has been implementing Ukraine Nuclear Fuel Qualification Project (UNFQP), within the frame of which SU NPP has been pilot operating mixed cores of nuclear fuel supplied by different vendors — OJSC TVEL and Westinghouse. The first stage of the project witnessed six Westinghouse LTAs loaded into the SU NPP unit 3 core for a four year operation fuel cycle. Westinghouse and TVEL fuel assemblies differ in some structural components and structural materials. It is, therefore, of interest to monitor not only compatibility and performance of various FA designs, but also mutual influence of various materials on their corrosion behaviour in the WWER-1000 water chemistry. Inspections were held after each year of operation: visual examination of fuel rods and FAs, measurement of FA top nozzle axial positions, FA drag force measurements during core loading, FA leakage tests. Due to certain design features associated with fixing fuel rods in Westinghouse FAs (fuel rods are kept in place by grids only), in some cases fuel rods slipped to the bottom nozzle and contacted the adaptor plate. After each year of operation, fuel assembly leakage test was performed. No loss of fuel cladding integrity was observed. The Russian fuel assemblies were examined on the faces adjacent to the Westinghouse FAs. The new core structural materials have not been observed to impact the corrosion behaviour of the fuel rod cladding and top and bottom nozzles of either TVEL or Westinghouse fuel. Visual inspection of the fuel rods and FAs revealed no visible defects (pitting, cracks, etc.), which confirms reliability of this weld under WWER-1000 operating conditions. Pilot operation of the Westinghouse LTAs allowed a conclusion that they can be operated in the WWER-1000 mixed core at the thermal loads provided for by the reactor operating specifications and RCS parameters corresponding to GND 95.1.06.02.001-07. Positive results of the LTA operation allowed loading of a reload batch of 42 fuel assemblies in the SU NPP unit 3 core and concluding a contract between NNEGC Energoatom and Westinghouse for delivery of nuclear fuel for three WWER-100 units.

1. INTRODUCTION

Ukraine has been implementing Ukraine Nuclear Fuel Qualification Project (UNFQP), within the frame of which SUNPP has been pilot operating mixed cores of nuclear fuel supplied by different vendors — OJSC TVEL and Westinghouse. The first stage of the project witnessed six Westinghouse LTAs loaded into the SU NPP unit 3 core for a four year operation fuel cycle. Westinghouse and TVEL fuel assemblies differ in some structural components and structural materials (ZIRLO^{TM} as fuel cladding, Zr-1%Nb and A718 as spacer grid materials). It is, therefore, of interest to monitor not only compatibility and performance of various FA designs, but also mutual influence of various materials on their corrosion behaviour in the WWER-1000 water chemistry. Besides, it was a first time application of Zr-1%Nb material for spacer grids in a Westinghouse fuel design. Inspections were held after each year of operation: visual examination of fuel rods and FAs, measurement of FA top nozzle axial positions, FA drag force measurements during core loading, FA leakage tests.

Design of 6 Westinghouse Lead Test Assemblies (WLTA) provides maximum compatibility with resident fuel (i.e. Russian fuel that operated at the time in the SUNPP unit 3. Basic design features a given below:

- Fifteen spacer grids located to match the axial locations of the resident fuel grids;
- Bottom additional grid for trapping fine particles;
- WLTA has dismountable design (top and bottom nozzles are detachable for substitution of leaking fuel rods);
- Top nozzle design provides compatibility with shipping and handling devices of power unit;

– Top and bottom nozzle designs assure adequate fit with upper core plate and bottom support tubes, as well as appropriate fuel assembly lateral alignment and support;
– Grid tabs and nozzle features are designed to preclude inadvertent hang up the WLTAs and the resident FAs;
– Grids are robustly connected to the guide thimbles;
– The grid loss coefficient is higher than for the resident fuel.

2. LOADING OF FUEL ASSEMBLIES INTO CORE

WLTAs were loaded into the SU NPP unit 3 core during 2005 outage. For loading WLTAs were used resident shipping and handling devices and procedures. Drag forces during installation in the core did not exceed 75 kgf [1].

After 4^{th} cycle of operation drag forces during unloading from the core did not exceed the design values and met the requirements of normative documents.

During unloading WLTAs from the core the data of changes in the weight of the refuelling machine mast were recorded on a strip chart. The measurement error was 2%. The data obtained were used to determine the FA drag force during their unloading from the core. The analysis of measurement data [2] demonstrated that:

– The maximum WLTA drag force during unloading from the core was as follows:
  • For WLTA AA01-03 ~60 kgf;
  • For WLTA AA02-03 ~42 kgf;
  • For WLTA AA03-03 ~58 kgf;
  • For WLTA AA04-03 ~56 kgf;
  • For WLTA AA05-03 ~55 kgf;
  • For WLTA AA06-03 ~50 kgf.

– The drag force of all WLTAs during their unloading from the core did not exceed the minimum set point of 75 kgf;
– The maximum WLTA drag force during installation into the storage pool rack was as follows:
  • For WLTA AA01-03 ~87 kgf;
  • For WLTA AA02-03 ~52 kgf;
  • For WLTA AA03-03 ~148 kgf;
  • For WLTA AA04-03 ~96 kgf;
  • For WLTA AA05-03 ~61 kgf;
  • For WLTA AA06-03 ~78 kgf.

– The drag force of all WLTAs during their installation into the storage pool rack did not exceed a set point of 150 kgf;
– The drag force during WFA unloading from the core did not exceed the design values and met the requirements of document [3];
– For purposes of comparison, below are the maximum drag forces of three TVS-Ms after their second operation cycle during installation into the storage pool rack:
  • TVS-M 02918 ~174 kgf;
  • TVS-M 02919 ~174 kgf;
  • TVS-M 02920 ~140 kgf.

3. AXIAL TOP NOZZLE POSITIONS

At the first load in 2005 the height difference of top nozzle positions did not exceed 2 mm (the maximum value according to the document TRBE is 5 mm).

Before the unloading from the core after 4th cycle of operation the height difference was 1 mm. This value corresponds to that obtained by the beginning of the 4th cycle.

4. WATER CHEMISTRY

During all cycles of WLTAs operation the core coolant chemistry was maintained within the RCS chemistry norms for different reactor power levels.

Coolant quality control was effected using plant control methods and with the frequency which meets the regulatory requirements for V-320. The data provided shows that:

- Coolant quality during all cycles was consistent with the regulatory parameters for RCS chemistry;
- No deviations in RCS chemistry from the regulatory requirements for reactors at power were observed;
- RCS boron concentration was maintained at the level which ensured reactor operation at the prescribed power level in accordance with the technical decision.

5. VISUAL INSPECTION

Visual inspection was carried out after each cycle during outages for all WLTAs. The inspection of the WLTAs was done in the storage pool using a special television system STS-PM-100V. Each LTA was inspected on all six faces for visible cladding defects, damaged LTA components, or other damages. During the inspection the Westinghouse LTAs were taken pictures of.

After the fourth cycle of operation the surface of WLTAs had oxide films of various shades. On the dark gray background of the clad in lower part of the fuel rod (between the 1st and 3rd spacer grids) had contrasting light grey spots, and the fuel rod surface showed good reflective properties. The size of gray spots increased towards the top of the WLTA. Starting with grid 5, the fuel rod clad surface was gray with observable light grey spots which increased in size towards the top of the WLTA. There were no spots in the plenum region, and the cladding surface was an even dim light grey color.

The visual inspection did not observe any visible mechanical damages of fuel rods. It should be noted that the bottom end plug of the corner rod between WLTA AA02-03 faces 4 and 5 showed marks visually resembling wear signs or a foreign particle (Fig. 5.1). The technical capabilities of the resident video and measuring equipment do not allow to unambiguously identify the nature and type of the marks.

Minor foreign objects were observed on the WLTA AA04-03 bottom nozzle and grids. Some of the particles observed on WLTA AA04-03 were flushed in the sipping test cask. WLTA AA04-03 requires further examination to identify the nature and type of the elements observed using the inspection stand to be supplied by Westinghouse under a separate contract.

Some grids on WLTAs had burnishes resulting from friction against the adjacent FAs during FA installation into and withdrawal from the core (Fig. 5.2).

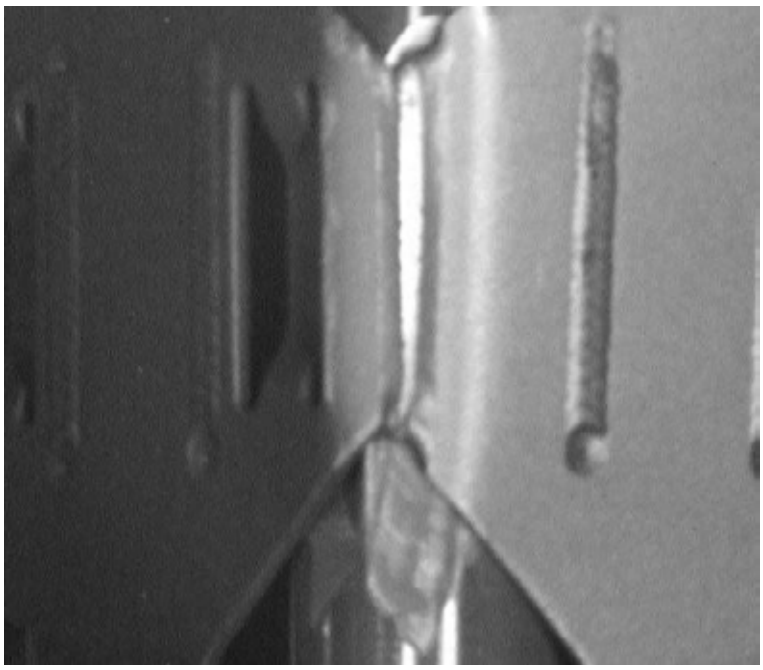

FIG. 5.1. Marks on the corner fuel rod bottom end plug, WLTA AA02-03, juncture of faces 4–5.

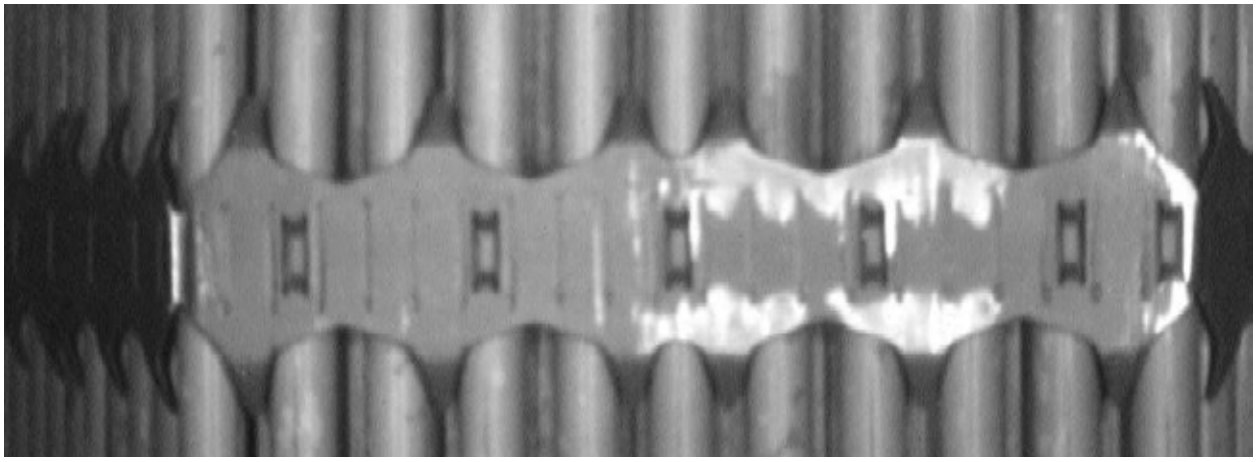

FIG. 5.2. Burnishes on Inconel grid 6 on WLTA AA03-03 face 3 after fourth operation cycle.

Visual inspection of the WLTAs on all faces demonstrated integrity of all spacer grids and absence of their axial displacement. The relative axial positions of the spacer grids were determined using the resident video system and selsyn readings during WLTA axial movement.

Fuel rod displacement (Figs 5.3–5.5) resulted in making contact between some bottom end plugs and the bottom nozzle plate. No fuel rod was observed, however, to have been displaced towards immediate proximity with the WLTA top nozzle.

Fuel rod downward displacement until making contact between the bottom end plugs and the WLTA bottom nozzle is a design feature and does not adversely affect nuclear, mechanical, and thermal hydraulic core parameters and does not result in violation of fuel rod and FA operability criteria.

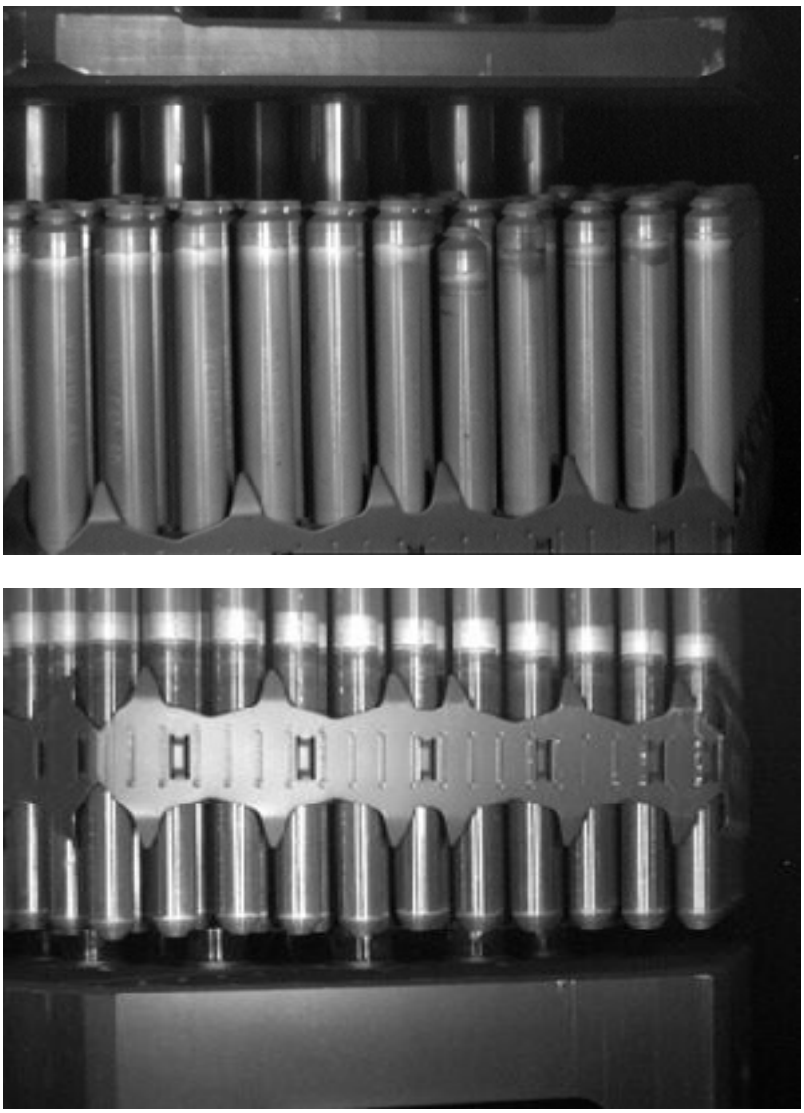

FIG. 5.3. Fuel rod displacement, WLTA AA02-03, face 4, inspection 2007.

The weld joints of the fuel rod top and bottom end plugs were uniformly light grey (Figs 5.6–5.7). Some fuel rods, however, were observed to have cladding dimness in the weld joint area of the top/bottom end plug. No damaged weld joints on the visible parts of the outer and inner strips of Zr1%Nb grids were observed [1–2, 4]. Along the weld joint on the outer side of the external Zr1%Nb grid straps, as well as on the surface of external strap surface there were light grey spots (see Figs 5.8–5.11), which evidence presence of oxide films on Zr1%Nb grid straps after the fourth operation cycle. The surface of zirconium grids had better reflecting properties than Inconel grids.

The inspection did not identify any visible damage to or non-design positions of individual WLTA components, which could result in the engagement with the adjacent core components, equipment or FA handling devices. None of the six WLTAs had any sings of damage, deformation or other defects preventing their handling.

It is necessary to mention that during all inspections were not observed visible changes of geometrical dimensions of fuel rods as a consequence of irradiation growth and irradiation induced swelling that can influence on decrease of operability [2,4].

Zirconium alloys Zr-1%Nb and ZIRLO^{TM} showed excellent corrosion resistance operability [2,4].

FIG. 5.4. Fuel, WLTA AA02-03, face 4, inspection 2008.

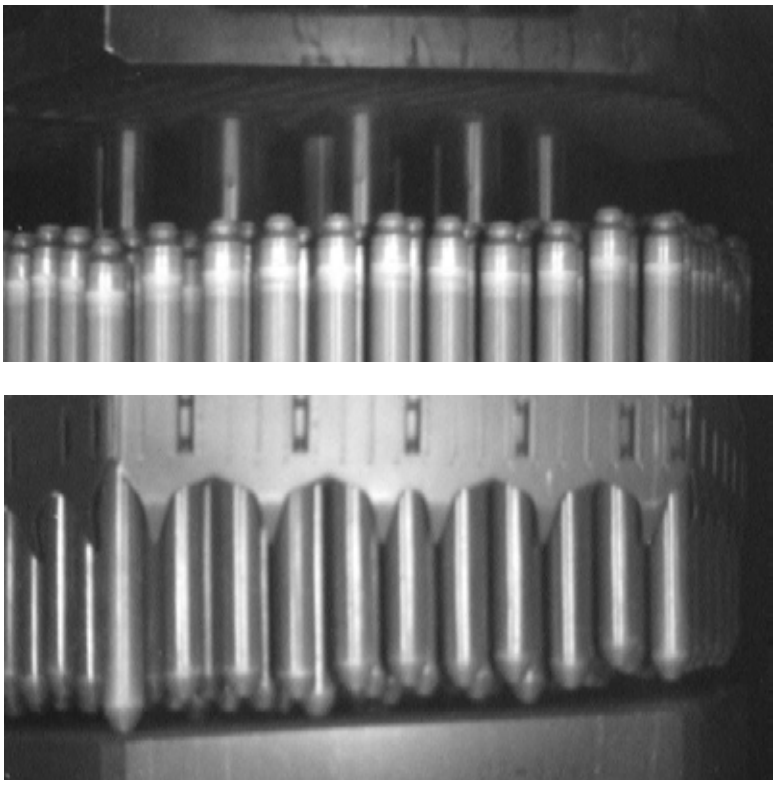

FIG. 5.5. Fuel rod displacement, WLTA AA02-03, face 4, inspection 2010.

FIG. 5.6. Weld joints of top end plugs, WLTA AA05-03, face 1, inspection 2010.

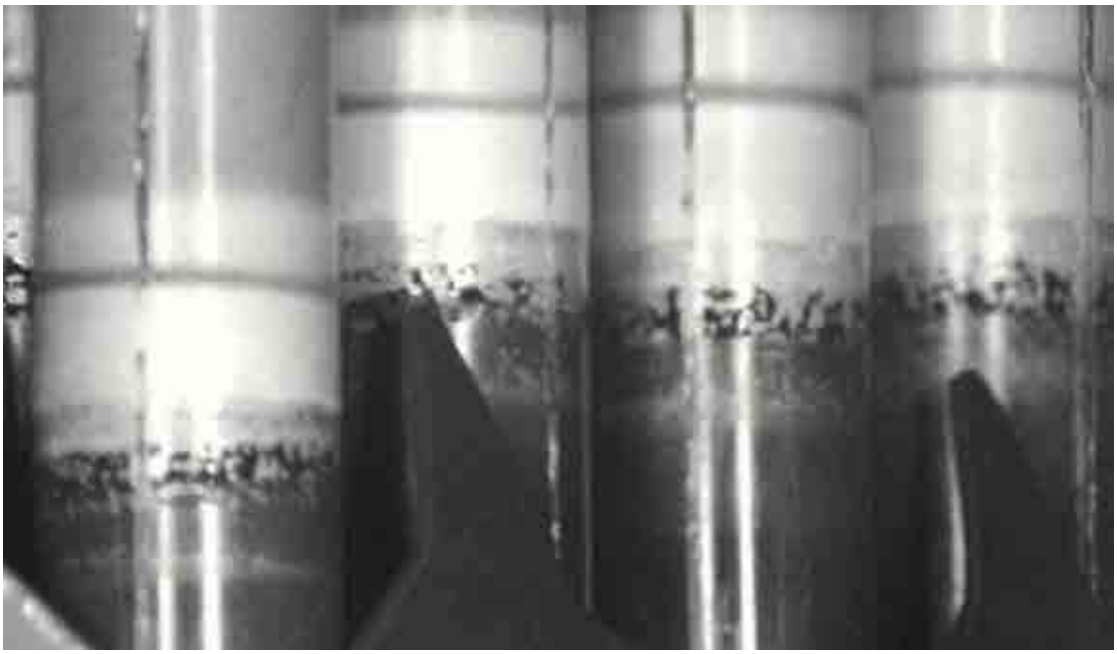

FIG. 5.7. Weld joints of bottom end plugs, WLTA AA02-03, face 4.

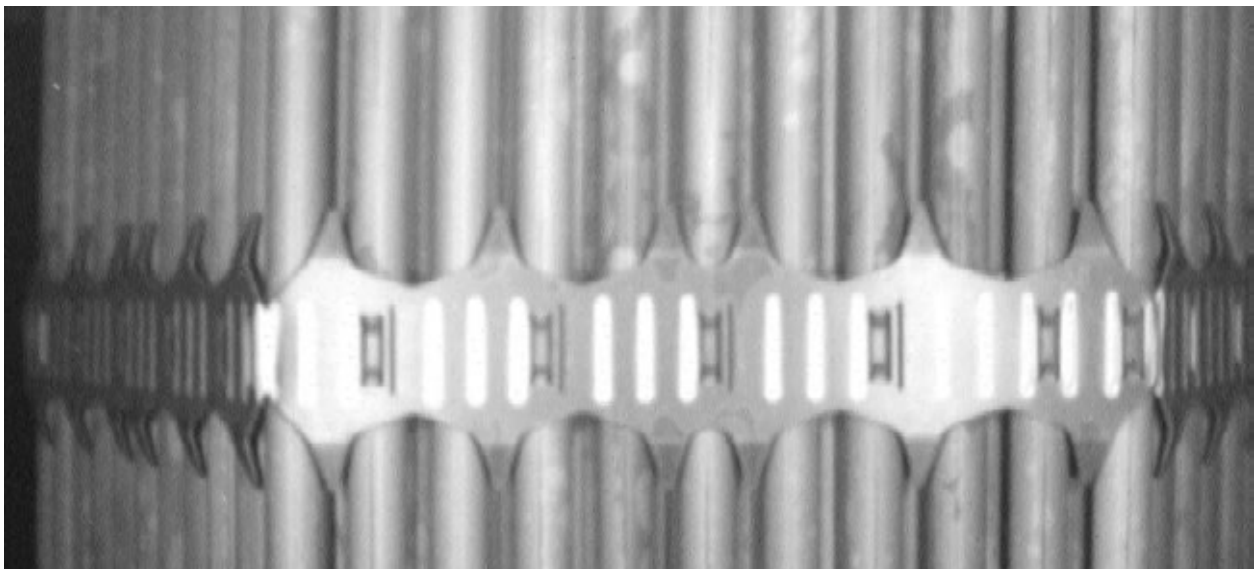

FIG. 5.8. Zr1%Nb grid 9, WLTA AA01-03, face 1, inspection 2010.

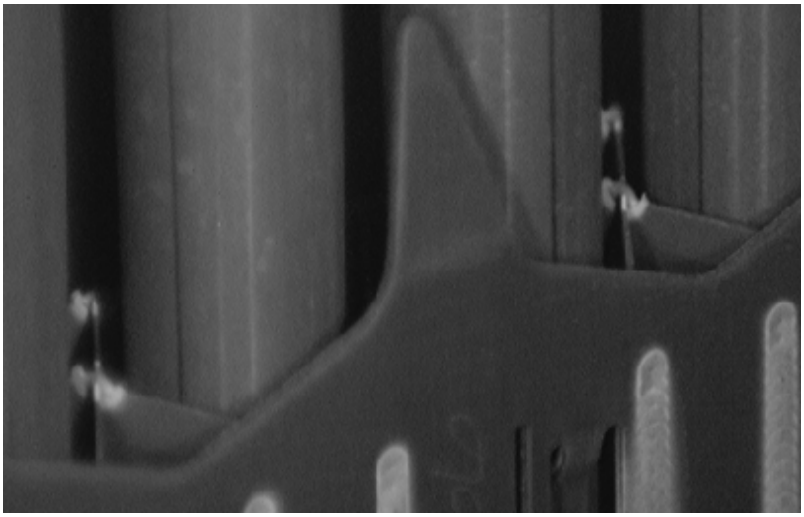

FIG. 5.9. Condition of Zr1%Nb grid 14 weld joints, WLTA AA03-03, face 1, inspection 2007.

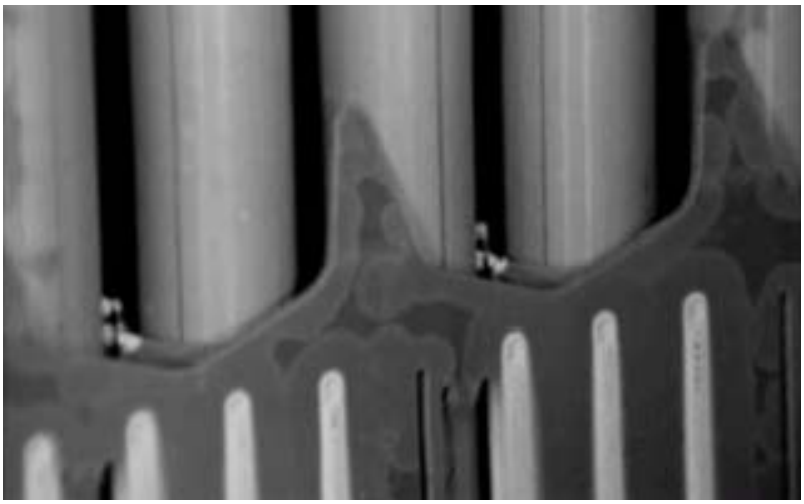

FIG. 5.10. Condition of Zr1%Nb grid 14 weld joints, WLTA AA03-03, face 1, inspection 2008.

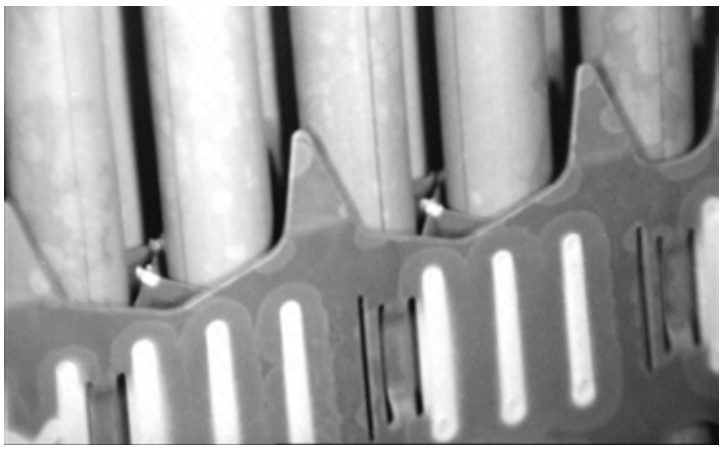

FIG. 5.11. Condition of Zr1%Nb grid 14 weld joints, WLTA AA03-03, face 1, inspection 2010.

Also the inspection of Russian fuel which faced WLTAs was done. Visual inspection has not revealed any appreciable impact of the new set of structural materials in the core on the corrosion behaviour of the fuel rod cladding, FA spacer grids, and FA top and bottom nozzles of either Russian or Westinghouse fuel.

During visual inspection were not observed any visible defects such as corrosion plaques, pittings or cracks in the area of weld joints. It gives the opportunity to state that this type of weld joint is operational in WWER-1000 conditions.

Also in mixed core conditions were not observed any mechanical mutual influence both Russian and Westinghouse fuel.

6. LEAKAGE TEST

Leakage test was done after each operation cycle using a standard SODS stand with further analysis of water samples in a gamma spectrometer. Statistical processing of the results thus obtained was done by I-131. The results obtained for Cs-134 and Cs-137 were also statistically treated.

After the 4^{th} cycle one WLTA had fuel rod non-tightness [2]. The defect was assumed to be minor "gas leakage" (in the leakage test sample the I-131 activity was 7.5×10^{-8} Ci·kg^{-1}; Xe-133 activity was 2.6×10^{-6} Ci·kg^{-1}; no activity of solid fission products, such as Ce-141,143 and Ru-103,106, was found in the leakage test sample).

The FA leakage test done in the operating reactor and during the outage found that after the 4^{th} operation cycle five WLTAs were leakage tight. It should be noted that FAs found to be leaking based on statistical analysis, but having I-131 activity in the leakage test samples below 1.0×10^{-6} Ci·kg^{-1}, can be further operated.

According to results of 4 cycles of operation it was concluded that Westinghouse fuel can be operated in mixed cores of WWER-1000 reactors at temperature loads corresponding to the regulatory basis and in primary water chemistry corresponding to [5].

7. SUMMARY

The post-irradiation examination of WLTAs after 4 cycles of operation did not reveal any visible damage to or non-design position of individual FA components, which could result in the engagement with the adjacent core components, equipment or FA handling devices. Neither were there observed visible changes of geometrical dimensions of fuel rods as a consequence of irradiation growth and irradiation induced swelling that could adversely affect operability. Further, PIE did not show any

mutual influence of different sets of structural materials of both WLTAs and the resident fuel on corrosion resistance.

Positive results of WLTAs operation allowed to install during 2010 outage 42 FAs produced by Westinghouse and enabled NNEGC Energoatom to enter into a contract with Westinghouse for delivery of fuel for three WWER-1000 units.

REFERENCES

[1] ABDULLAYEV, A., KOLOTILOV, A., MARYOKHIN, S., RIZNYCHENKO, A., SLYEPTSOV, A., SOLDATOV, S., Core Follow Report for Cycle 17 of South Ukraine NPP unit 3 with Westinghouse Lead Test Assemblies, 12-3-014, Revision 1 (2006).

[2] ABDULLAYEV, A., KOLOTILOV, A., MARYOKHIN, S., RIZNYCHENKO, A., SLYEPTSOV, A., SOLDATOV, S., Core Follow Report for Cycle 20 of South Ukraine NPP unit 3 with Westinghouse Lead Test Assemblies, 12-3-116, Revision 0 (2010).

[3] SOUTH UKRAINE NPP, ENERGOATOM, Technical Specifications for Safe Operation of SUNPP, unit 3 with VVER-1000 (V-320) [TRBE], RG.3.3810.0009.

[4] SHAH, H., LATORRE, R., RASPOPIN, G., SPARROW, J., Enhanced VVER-1000 fuel technology and performance, Proceedings of the 17th International Conference on Nuclear Engineering, Brussels (2009).

[5] ENERGOATOM, WWER-1000 primary coolant. Technical requirements. Ways of quality assurance, GND 95.1.06.02.001-07, Kiev, Ukraine (2007).

THE DEVELOPMENT OF XENON DIFFUSIVITY MEASUREMENT FOR IRRADIATED CERAMIC FUELS WITH LOW BURNUP

H.-M. KIM, M.S. CHO, K.H. KANG, S.H. NA, J.W. LEE, C.J. PARK, K.S. KIM
Korea Atomic Energy Research Institute
Daejon
Email: hkim1211@kaeri.re.kr

K.-H. PARK
Department of Nuclear Engineering
Kyunghee University
Kyunghee

Republic of Korea

Abstract

The fission gas diffusion coefficient is an important factor to study fission gas release, which is a common occurrence for fuel performance. Especially, Xe-133 is a good tracer and recommended in a post-irradiation annealing test. Annealing equipments for fuel was set up in IMEF in KAERI and several tests for various oxide fuels have been carried out. To obtain the atomic diffusivity of Xe-133, all fuel samples were irradiated with very low burnup (<0.1 $MW \cdot d \cdot t^{-1}$ U) to prohibit creation of fission bubbles. Therefore, these tests were not performed in a hot cell but a service area due to low radiation doses. The amount of production and release of Xe-133 were calculated by using ORIGEN-2 code. Based on the Booth theory, diffusion coefficients at each temperature were obtained. Diffusion coefficients of Xe-133 in all fuel samples were compared and analysed by a published data. Additionally, we consider installation of equipments in a hot cell for a high burnup fuel sample.

1. INTRODUCTION

Fission gas release occurs in nuclear fuel during reactor operation. Gaseous and volatile elements, fission products, are released from fuel pellets by temperature. It causes a fuel rod to have shorter lifespan due to higher internal pressure and pellet temperatures. Thus, the research of the fission gas release has been studied with diffusion mechanism. To set up a diffusion model, diffusion coefficient is important factor, which is obtained by experiments; one is an in-pile test and the other is a post-irradiation annealing (PIA) test. The former is effective in observing the apparent release behaviour (diffusion and mechanical release), while the latter is the thermal diffusion. The thermal diffusion in fuel pellets is considered as lattice diffusion, surface diffusion and grain boundary diffusion. The lattice diffusion was controlled by several factors, e.g. oxidation or reduction state in high temperature, valence of additives and burnup.

In this study, lattice diffusion of Xe-133 ($T_{1/2}$ = 5.2 d, 81 keV) has been observed by PIA test with various ceramic fuel samples and conditions. To observe atomic diffusion in lattice, the Booth model was adopted, thus, a very low burnup was decided to reduce traps which interrupt the atom mobility. Most samples were poly-crystal, accordingly grain boundary diffusion was considered.

2. EXPERIMENTAL

2.1. Sample preparations

Sixty samples were made, irradiated and annealed for the Xe-133 diffusion observation since 2000 as shown in Table 2.1. Most samples were made with 0.3 g and natural enrichment. Initially, UO_2 single grain powders were made and all following samples were poly-crystals. In Fig. 2.1, the cubic and disk shapes were available to calculate the volume.

A BET measurement was carried out in some samples but it was not reasonable. $(U,Th)O_2$ samples were made with 35% of ThO_2 and 65% of UO_2. SIMFUEL were made with natural elements based on the 27 500 MW•d•t-1 U as shown in Table 2.2. In 2008, Nitride fuel samples were made with disk type and high porosity to compare with oxide fuel. To observe the valence effect of additives, Nd_2O_3, CeO_2 and Nb_2O_5 were mixed with pure UO_2 in 2010. Moreover, two different grain sizes of UO_2 were made and, currently, two additional different grain sizes were added.

TABLE 2.1. CERAMIC SAMPLE SUMMARY FOR PIA TEST

Year	Samples	No.	Grain size [μm]	TD [%]	Enrichment
2000	UO_2 (powder)	1	23	N/A	Natural U
2001	UO_2 (powder)	4	23	N/A	
2002	[a]UO_2, [b]$(Th,U)O_2$ (powder, 3cubes)	13	[a]8.1±0.5 [b]7.5±0.5	95–97	
2003	SIMFUEL (3cubes)	1	10±2	95–97	
2004	SIMFUEL (3cubes)	12	10±2	95–97	
2006	SIMFUEL (3cubes)	2	10±2	95–97	
2007	SIMFUEL (3cubes)	4	10±2	95–97	
2008	UN (disk)	4	N/A	45.2	
	UO_2 (disk)	2	N/A	47.6	
2010	UO_2+additives (disk)	11	9–17	95–97	
2010	UO_2 (two grain size)	6	6, 13	95–97	

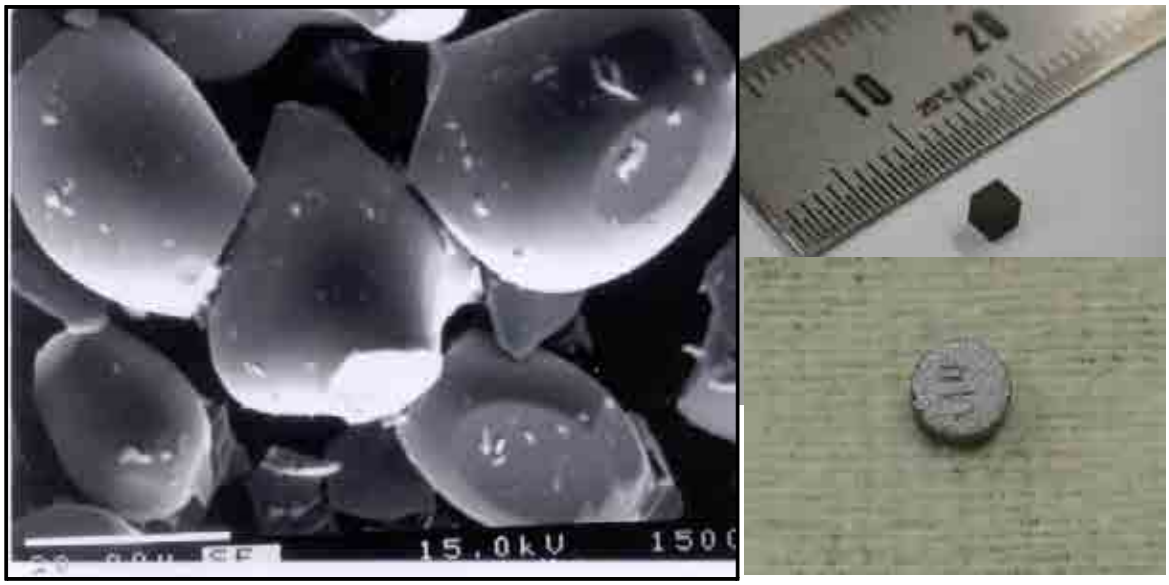

FIG. 2.1. Sample shapes (left: powder; right (top): cube; right (bottom): disk).

TABLE 2.2. CONTENTS OF SIMFUEL

Contents	mg	Contents	mg
Rb	0.095	PdO	0.34
SrO	0.171	TeO_2	0.126
Y_2O_3	0.12	$BaCO_3$	0.57
ZrO_2	1.04	La_2O_3	0.42
MoO_3	1.055	CeO_2	1.99
RuO_2	0.825	Nd_2O_3	1.46
Rh_2O_3	0.11	UO_2	300
Total	308.35		

2.2. Irradiation

Those samples were contained in a quarts tube at first, but was changed to a Zry-4 tube for safety. The container was filled with helium of 1.2 bar and inserted in 3 irradiation capsules as shown in Fig. 2.2. The capsules were placed in the IP4(C) hole in the HANARO research reactor for irradiation. Twenty minutes of irradiation time was available for 24 MW power of the reactor, but the irradiation time was reduced to 16 minutes for 30 MW of operation power, which was equivalent to same burnup. After irradiation and cooling time (7 days), the capsule was dismantled and contained in an alumina crucible at Irradiated Materials Examination Facility (IMEF).

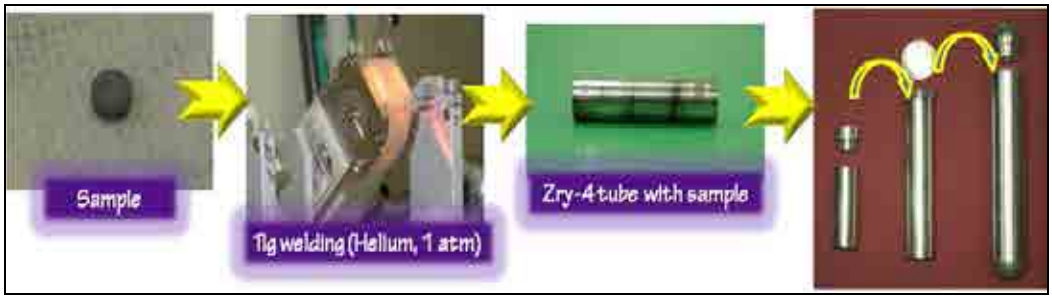

FIG. 2.2. Sample container (welding) for irradiation.

2.3. PIA system and procedures

For PIA test, the system was designed as shown in Fig. 2.3. It consisted of a furnace, filtration and gamma detection. The furnace was an electric resistance type (super kanthal) and withstand heat up to 1600°C. The chamber and internal structures were made of pure alumina. A B-type thermocouple was installed to measure the sample temperature. Oxygen sensor, ZrO_2 tube, measured the oxygen partial pressure in chamber. Helium gas was flowed with 100 ml·min^{-1} as carrier.

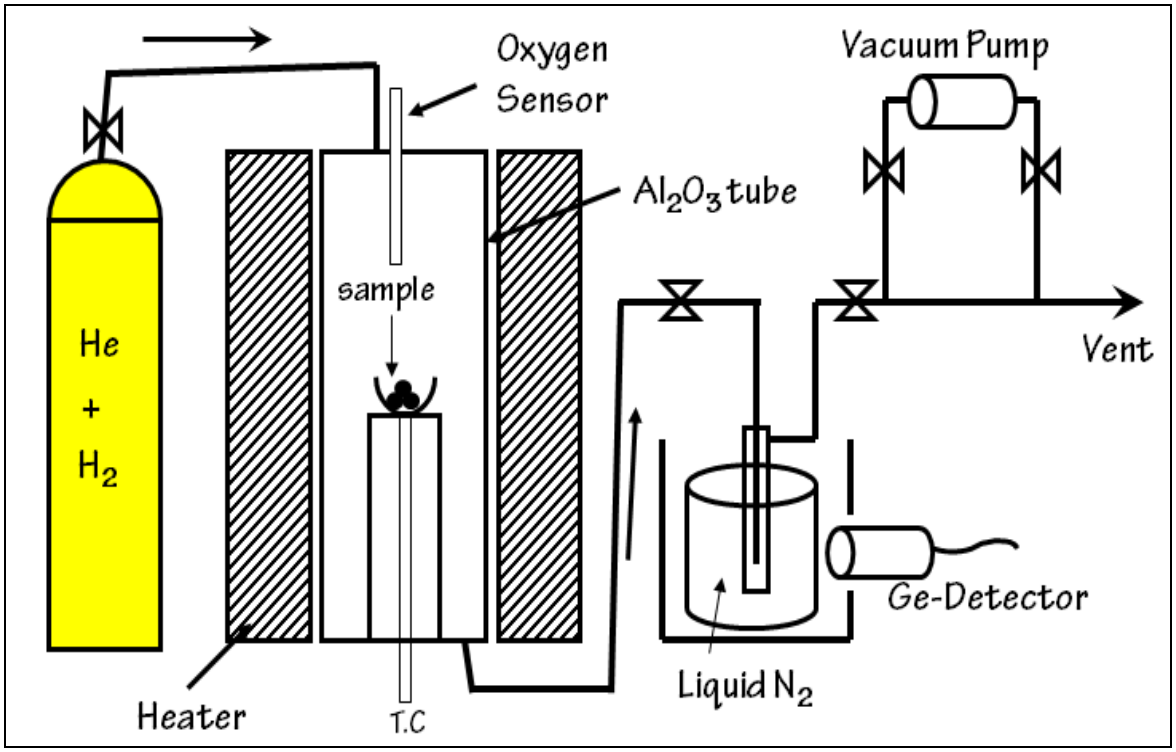

FIG. 2.3. Diagram of PIA system.

The filtration was designed as a cryogenic trap system to catch the gaseous xenon by solidification. The filter media was charcoal with a glass casing. It was placed into liquid nitrogen. The helium, as carrier, remained gas during filtration. The gamma detector was a semi-conductor type with high pure germanium crystal (HPGe). It was activated to obtain gamma rays of Xe-133 released from the sample.

The gamma scan for 3600 sec was carried out for the sample in crucible to obtain the radioactivity of Xe-133 generated before the annealing test. After the sample was loaded into the furnace chamber, the temperature was controlled incrementally at 1400°C, 1500°C and 1600°C for UO_2, $(Th,U)O_2$ and SIMFUEL at 1200°C, 1300°C and 1400°C for UN. The annealing time for each temperature was decided according to the amount of xenon release. Generally, a disk sample with 95% TD would be kept for 15 hours, 9 hours and 6 hours, respectively, but a shorter annealing time was applied in the case of oxidation atmosphere or low TD of sample. After annealing, a gamma scan was performed again before disposal.

3. RESULTS

Fractional release was obtained by means of Ba-133 of reference source which emit 81 keV of gamma ray equal to Xe-133. Plot of f^2 vs. t is valuable to obtain slope at each temperature range. The slope is compared to $(36D) \times (\pi a^2)^{-1}$. Therefore, if '$a$' value is decided, diffusion coefficient is obtained. ThO_2 and fission products effects show retardation of release as shown in Fig. 3.1. -370 kJ·mol^{-1}. of the oxygen potential is shown as 'x' value of UO_{2+x} was 0.0005 by means of oxygen sensor. Figure 3.2 showed Xe-133 release in uranium nitride and grain size effect of UO_2. A number of fractional release data were generated with various samples based on the same procedure.

Based on the plot of f^2 vs. t, the slope of each temperature range was calculated by a linear fitting. Finally, diffusion coefficients were obtained by means of slope. Figure 3.3 shows diffusion coefficients of Xe-133 in the single grained and the polycrystal UO_2 with different oxygen potential, and they were compared to SIMFUEL. Diffusion coefficients of all samples were higher in increased oxygen potential and ThO_2 showed a retardation of Xe-133 release. SIMFUEL showed a tri-valence effect due to lower diffusion coefficients.

Conversely, uranium nitride (UN) was showed in Fig. 3.4 as similar diffusion coefficients with UO_2 even though the structure was different, and a tri-, quad- and penta-valence effects show a difference of diffusivity. However, large grained samples were lower in diffusivity in the same valence samples even though higher contents (right graph on Fig. 3.4).

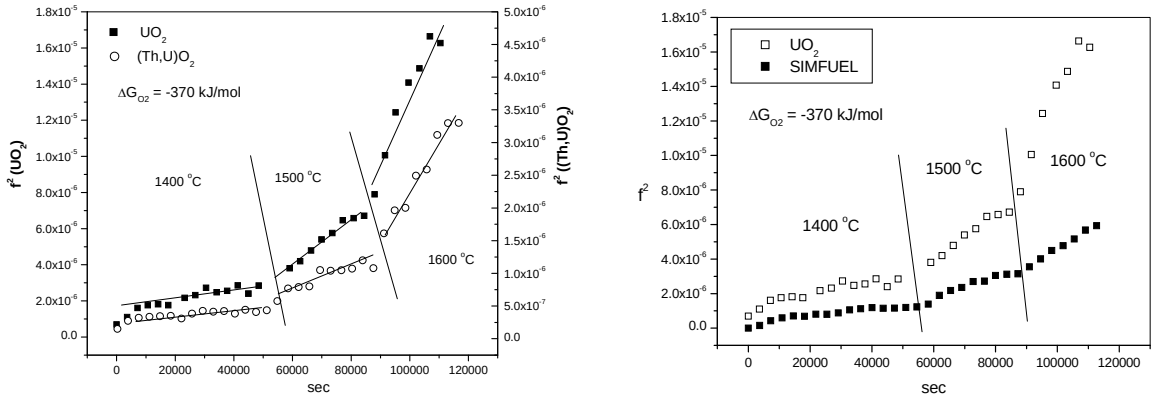

FIG. 3.1. Fractional release of UO_2, $(Th,U)O_2$ and SIMFUEL.

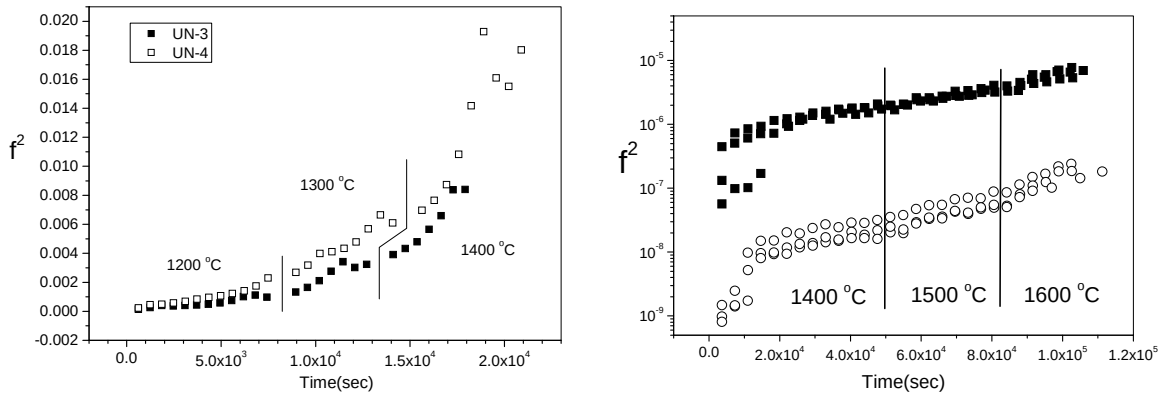

FIG. 3.2. Fractional release of UN and grain size effect of UO_2.

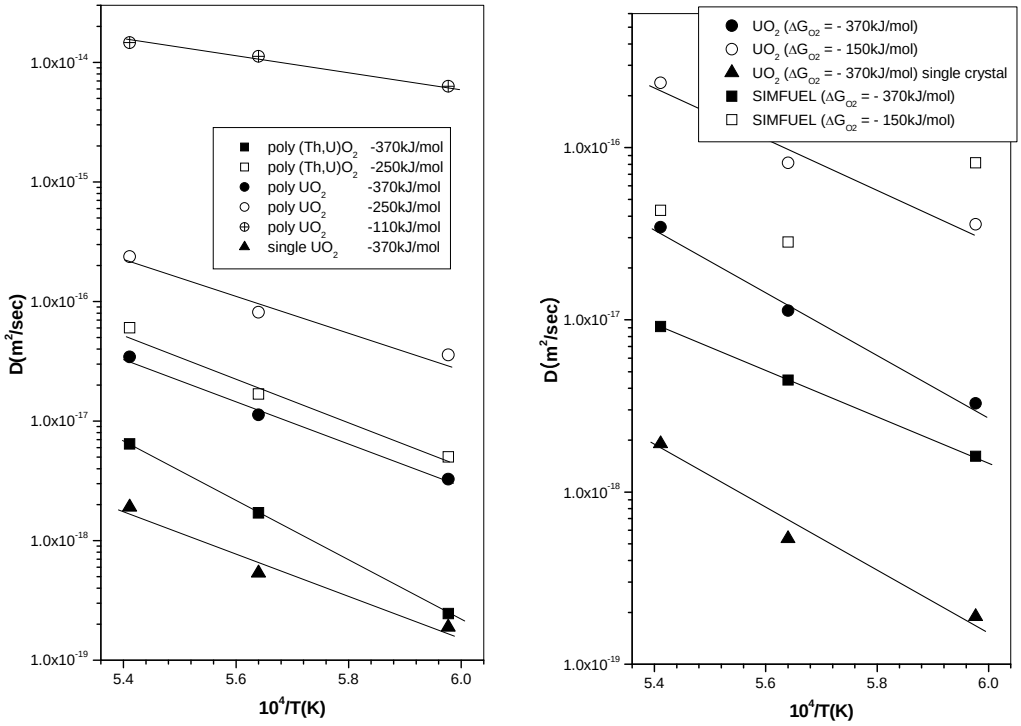

FIG. 3.3. Diffusion coefficients of UO_2(single and poly crystal) and $(Th,U)O_2$, and those of UO_2 were compared to SIMFUEL.

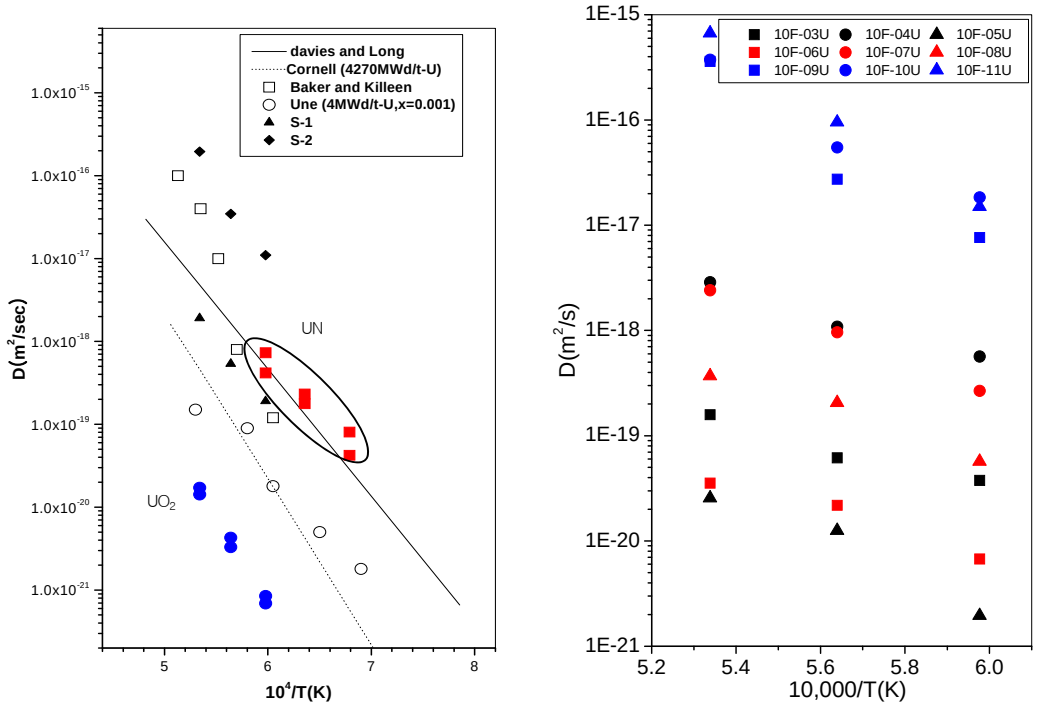

FIG. 3.4. Diffusion coefficients of UN with compared to UO_2 data and diffusion effects of doped UO_2 with different valence (10F-03U-10F-05U:Nd_2O_3; 10F-06U-10F-08U:CeO_2; 10F-09U-10F-11U:Nb_2O_5).

4. DISCUSSION

To measure diffusion coefficients of noble gases or volatile isotopes in fuel, a PIA and an in-pile test were used with each advantage [1]. To observe diffusion mechanism, a PIA test is useful with long lived tracer such as Xe-133.

PIA tests were performed based on the Booth theory [2] in this study as shown in Eq. (1):

$$f^2 = (36D) \times (\pi a^2)^{-1} \times t \quad (1)$$

Where

f is the fractional release;
D is the diffusion coefficient [$m^2 \cdot s^{-1}$];
a is the equivalent sphere radius [m];
t is the annealing time [s].

Equation (1) is available in the case of $f < 0.3$, and $(36D) \times (\pi a^2)^{-1}$ is almost linear. Fractional release was obtained by Xe-133 radioactivities of production and release using a standard source (Ba-133) and ORIGEN-2 code [3]. Based on the Ref. [4], the linear fitting on plots in Figs 3.1–3.2 were needed to obtain slope which is equal to that of Eq. (1). If '*a*' value was measured, finally, *D* can be obtained.

Diffusion coefficient of Xe-133 is controlled by temperature, oxidation condition, fission products and burnup. Lattice diffusion with no traps is carried out with low burnup to satisfy Booth theory, which was referred in Ref. [5]. Thus, 0.1 $MW \cdot d \cdot t^{-1}$ U of burnup was decided in this study. Matzke suggested xenon mobility via tri-vacancy cluster [6]. Some calculations showed xenon moved via uranium vacancy in hyper-stoichiometric UO_2. Both of them are related to uranium vacancy concentration. This concentration is controlled by an oxidation condition and valence effect of fission products.

Generally, fission gas release is higher in an oxidized sample, e,g, UO_{2+x}, and a higher valence of elements such as niobium (+5) which is one of fission products [7, 8]. Even though larger grains such as 10F-09U-10F-11U in Fig. 3.4, Nb_2O_5 enhanced the xenon release. The bonding energy of ThO_2 is stronger than UO_2, so it seems to disturb the xenon by causing it to jump to another site [9]. Therefore, diffusivity is lower than that of pure UO_2.

The xenon diffuses via tri-vacancy cluster in UO_2 based on ref. [4, 6]. However, it diffuses via uranium vacancy in non-stoichiometric UO_2. Thus, the uranium vacancy concentration is an important factor. Higher oxygen potential and valence elements are higher in uranium vacancy concentration, so it enhances the release of xenon.

On the other hand, uranium nitride (UN) has been studied as the fuel of a fast reactor. With the same condition of PIA test for UO_2, the results of UN were similar to UO_2 even though the structure was different. Mobility mechanism has not been found so far.

5. CONCLUSIONS

PIA tests for ceramic fuels were carried out by IMEF at Korea Atomic Energy Research Institute (KAERI). Sixty samples were used to obtain the diffusion coefficient of Xe-133 with various conditions. Lattice diffusion of xenon satisfying Booth theory have been studied since 2000. UO_2, $(Th,U)O_2$, SIMFUEL, doped UO_2, UN were used as a disk or cube type. Analyses of diffusion behaviours were performed and the data was accumulated. Even these data were useful to calculate fission gas release in fuel performance calculations. Diffusion coefficients of xenon in UO_2 were controlled by the oxygen potential, the valence of doped elements and the burnup as well as the annealing temperature. Xenon diffusion data in UN were similar to those in UO_2 to some extent of temperature despite the different structure. It is needed to be studied to observe the diffusion mechanism. Recently, U–Zr metallic fuels were prepared as PIA sample. To observe a high burnup effect, a PIA system is planned to be installed in a hot cell.

REFERENCES

[1] OLANDER, D.R., Fundamental Aspects of Nuclear Reactor Fuel Elements, TID-26711-P1, National Technical Information Services (1976).

[2] BOOTH, A.H., A method of calculating fission gas diffusion from UO_2 fuel and its application to the x-2-f loop test, Atomic Energy of Canada Limited, AECL-496, CRDC (1957) 721.

[3] CROFF, A.G., A user manual for the ORIGEN2 computer code, Oak Ridge National Laboratory, ORNL/TM-7175 (1980)

[4] MATZKE, H.J., Gas release mechanisms in UO_2-A critical review, Radiation Effects **53** (1980) 219–242.

[5] MACEWAN, J.R., STEVENS, W.H., Xenon diffusion in UO_2, J. Nucl. Mater. **11** (1964) 77.

[6] MATZKE, H.J., Diffusion in doped UO2, Nuclear Applications **2** (1966) 131.

[7] MIEKELEY, W., FELIX, F.W., Effects of stoichiometry on diffusion of xenon in UO_2, J. Nucl. Mater. **16** (1965) 76.

[8] UNE, K., TANABE, I., OGUMA, M., Effects of additives and the oxygen potential on the fission gas diffusion in UO_2 fuel, J. Nucl. Mater. **150** (1987) 93.

[9] KIM, H., et al., Xenon diffusivity in thoria-urania fuel, Nucl. Technol. **147** (2004) 149.

IRRADIATED FUEL AND RADWASTE MANAGEMENT

(Session 6)

Chairpersons

A. BEVILACQUA
IAEA

P. MARTY
CEA

ESTIMATION OF HYDROGEN PRODUCTION RATES FROM RADIOLYSABLE MATERIAL IN CONTACT WITH VARIOUS IRRADIATED FUELS

D. BOTTOMLEY, P. VAN BELLE, D. PAPAIOANNOU, R. NASYROV, V.V. RONDINELLA
European Commission, DG — Joint Research Centre,
Institute for Transuranium Elements (ITU)
Karlsruhe, Germany
Email: paul.bottomley@ec.europa.eu

Abstract

The storage of irradiated fuel is increasing as many installations are approaching their end of- ife and fuel or fuel-containing remnants from waste or samples are being placed in storage. Often these smaller experimental samples are mounted in epoxide resins or are placed containers with bitumen. It is particularly in combination with these radiolysable materials where the irradiation generates hydrogen that problems arise in longer term storage. The hydrogen generation results in either pressure buildup (with container bloating and eventual failure) or in case of gas release and mixture with air, a detonation. Previous work has examined the Phébus FPT1 bundle encased in resin where it was necessary for both transport and intermediate storage at Cadarache to assess this risk. This work is a first estimation of the radiolysis rates to be expected from various fuels and to assess the range of H_2 production from radiolysable material based on the results of the FPT1 Phébus bundle. The first step is to make a correlation of the total activity with the burnup of UO_2 fuel. Then using the H_2 production rates measured for the Phébus fuel, an estimate of its dependence on fuel burn–up will be made and so help define the necessary design for the foreseen storage time.

1. INTRODUCTION

The Phébus FPT1 test was carried out in 1993 [1–3] and the bundle was embedded in epoxy resin and transported to ITU Karlsruhe for post-irradiation sectioning, examination and analysis. The return transport was now due but the licences for the available transport containers did not permit the casque's use for material that could radiolyse or thermolyse.

Therefore it was necessary to measure the radiolytic production of H_2 by the bundle segments by gas mass spectroscopy to support the safety case for the return transport (this was financed by the CEA). The intention of this paper is to model the dose rates and energy deposition in resin surrounding a bundle geometry with increasing burnup and to combine this with the H_2 evolution measurements from the bundle to estimate resin radiolysis rates for resin embedded irradiated fuel. This measurement could be used to support licensing of other such transports as well as the design considerations for storage of radioysable materials.

2. DESCRIPTION OF PHÉBUS FPT1 BUNDLE RADIOLYSIS ESTIMATES

2.1. Gas mass spectroscopy of the specimens

An estimate of the radiolysis of Phébus FPT1 bundle was required. A series of 5 discs that were not used in the post–irradiation examination and were therefore intact were chosen for testing. The position of the selected discs on the vertical tomography of the degraded bundle made directly after the FPT1 test is shown in Fig. 2.1 along with the cross-sectional tomographies of each of the remnant discs. The selected discs, that come from representative sections of the degraded bundle, were placed in an airtight stainless steel container. Any hydrogen gas release resulting from degradation of the embedding resin would be measured by gas mass spectroscopy. The container was closed and then evacuated and backfilled with inert gas (Ar (5.0 purity — Air Liquide). A sample was taken and then the steel container was left for 69 days before a second sample of its atmosphere was taken. The 2 samples were then taken for analysis by gas mass spectroscopy.

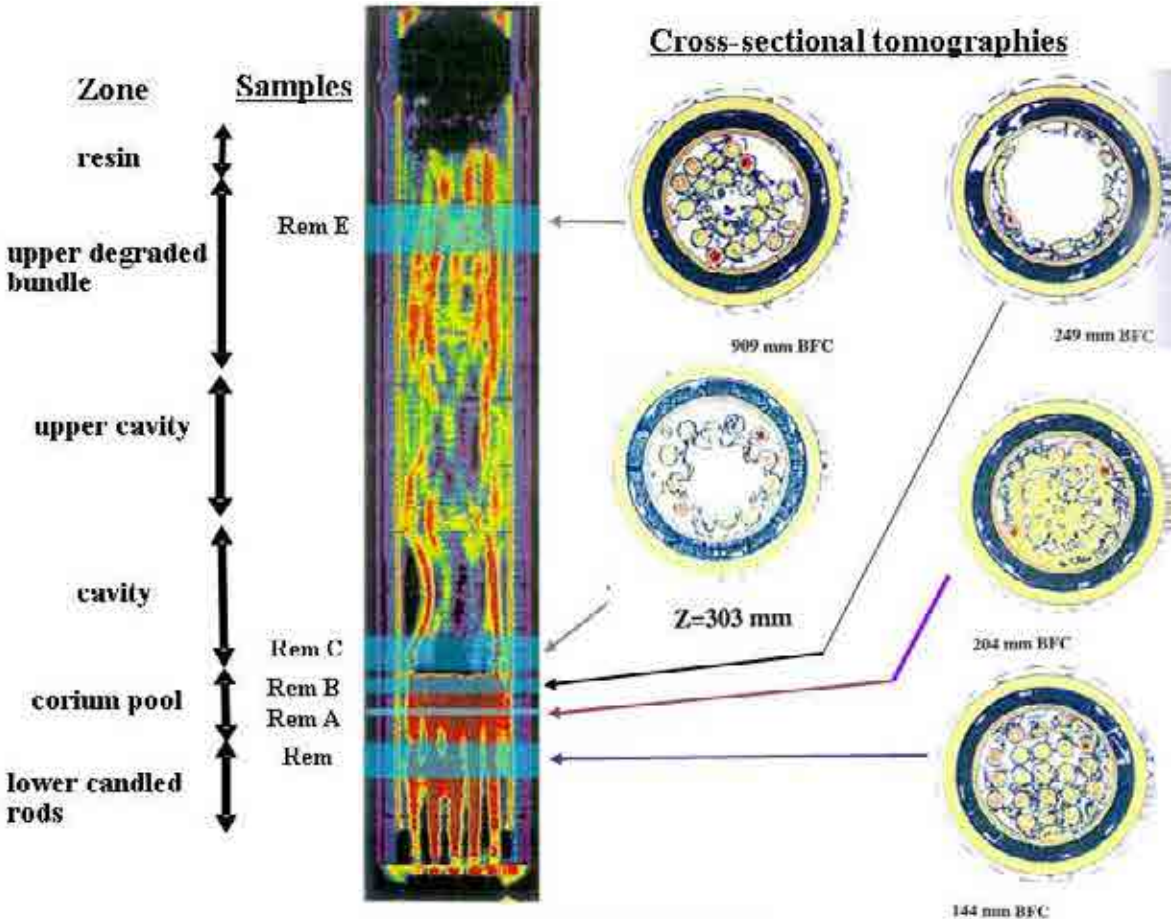

FIG. 2.1. The positions of the 5 remnant discs used for gas analysis are shown on the sectional tomography of the degraded FPT1 bundle. On the left, the sections of the degraded bundle are indicated; on the right cross-sectional tomographies corresponding to the positions of the remnant discs are shown. These were used to estimate the cross-sectional area of the fuel and the resin at these heights of the bundle.

The gas mass spectrograph was then calibrated with three certified Ar–H_2 mixtures with 1 ppm, 100 ppm and 1% H_2 content. The gas mass spectrographs (Balzers Omnistar MS) for the 2 gas samples (for the start and the end of the period) are shown in Fig. 2.2. The hydrogen content in the second sample taken from the container was then measured at 19 200 ppm +20% (from all sources of error). Therefore a value of (2±0.4)% (absolute) was determined. No fission gas (Kr and Xe) were observed in the spectrum, so that the fuel appears to be stable. Further details are given in Ref. [4].

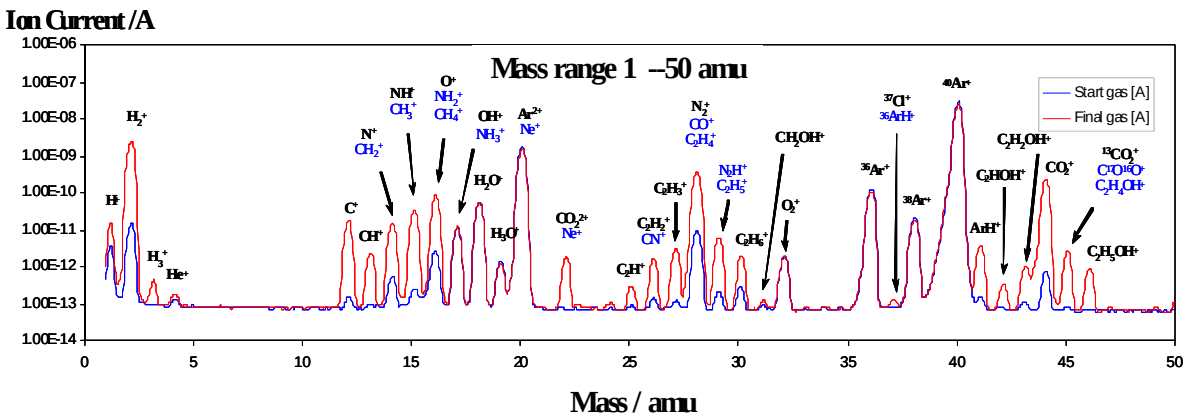

FIG. 2.2. The initial gas mass spectrograph (in blue) and the final spectrum (in red) taken after 69 days. In addition to the Ar peak, some hydrocarbon residues, N_2, O_2 and H_2 are seen.

2.2. Estimation of fuel and resin masses

It was next necessary to estimate the mass of fuel and reactor structural materials. This was done by using the linear density derived from tomograpic scans of the Phébus FPT1 bundle.

This linear mass graph is shown along with the tomography of the bundle after the FPT1 test in Fig. 2.3. The blue bars on the tomograph on the left show the positions of remnant discs used for the gas analysis. They are seen to have examples from a range of different bundle conditions: the upper degraded bundle (Rem E), cavity (Rem C), the corium pool and lower corium pool (Rem B and Rem A)) and finally the lower candled rods (Rem). On the right the discs are listed along with their average linear mass for the section they represent and an arrow showing the point on the graph. This is summarised in Table 2.1, and these values are used along with the thicknesses of the remnant discs to calculate the value for the mass of fuel and structural elements for the gas analysis samples (2872 g). In the final line the value for the whole bundle obtained by cross-multiplying all the discs thicknesses by the corresponding linear mass for that bundle section is given (14 366 g).

TABLE 2.1. POSITIONS, THICKNESSES AND FUEL MASSES OF ALL REMNANT DISCS ANALYSED BY GAS ANALYSIS FOR H_2 RADIOLYSIS AS WELL AS THE TOTAL BUNDLE MASS

Remnant and height above bottom of fuel	Area of bundle	Thickness of disc [mm]	Linear mass [g·mm^{-1}]	Mass of fuel in remnant [g]
Rem E @ 909 mm	Upper degraded bundle	52.5	15	787.5
Rem C @ 303 mm	Cavity	62	8.5	527
Rem B @ 249 mm	Corium pool	20.1	17	341.7
Rem A @ 204 mm	Lower corium pool	13.5	26	351
Rem @ 144 mm	Lower candling rods	42.2	20.5	865.1
Total estimated fuel and structural elements for sample				2872.3
Total estimated fuel and structural elements for FPT1 bundle				14366

2.2.1. Volume of resin per remnant disc

The calculations for the resin volume and the melt (fused fuel, cladding and structural material) for each disc are based on the cross-section of the 20 rod FPT1 bundle with a central Ag–In–Cd control rod combined with the thicknesses of the discs. Estimates are based on original fuel rod geometry and cross-sections and then adapted for swelling of rods and missing rods in upper part, and for resin – filled cavities, corium and rod cross-sections in the lower part. The various estimates were assessed using the cross-sectional tomographs given in Fig. 2.3.

Thus Rem C as part of the central cavity was estimated as having only an 8 mm wide thick outer ring of material with 10% porosity in order to calculate the percentage of cross-section as melt and that of free volume filled with resin. By contrast Rem E from the upper bundle was calculated as having a cross-section equivalent to having one rod extra in cross-section for half its height. More details are given in Ref. [4]. This enabled the volume of resin for the remnants used for gas analysis to be estimated and then the total volume of the resin in the FPT1 bundle; this was found to be 449 cm³ volume of resin for the remnants and 2872 cm³ for the FPT1 bundle. The free volume in the autoclave containing the segments was 920 cm³. The concentration of H_2 in the container was 2% (±0.4%) after 69 days. From this the H_2 release rate for the resin in the remnants calculated and hence releases could be estimated for the whole FPT1 bundle as 1.65±0.33 cm³ of H_2 per day. This gives 0.000594 cm³ H_2/day/cm³ resin (or 9.89×10^{-5} cm³ H_2/day/g UO_2 fuel of 23.4 GW·d·t^{-1}UO_2 BU). The current

estimates of the FPT1 bundle activity (total Cs-137 activity ~4.10^{12} Bq) show that it is at a steady level. Therefore radiation doses will not be expected to change much with time (Table 2.2).

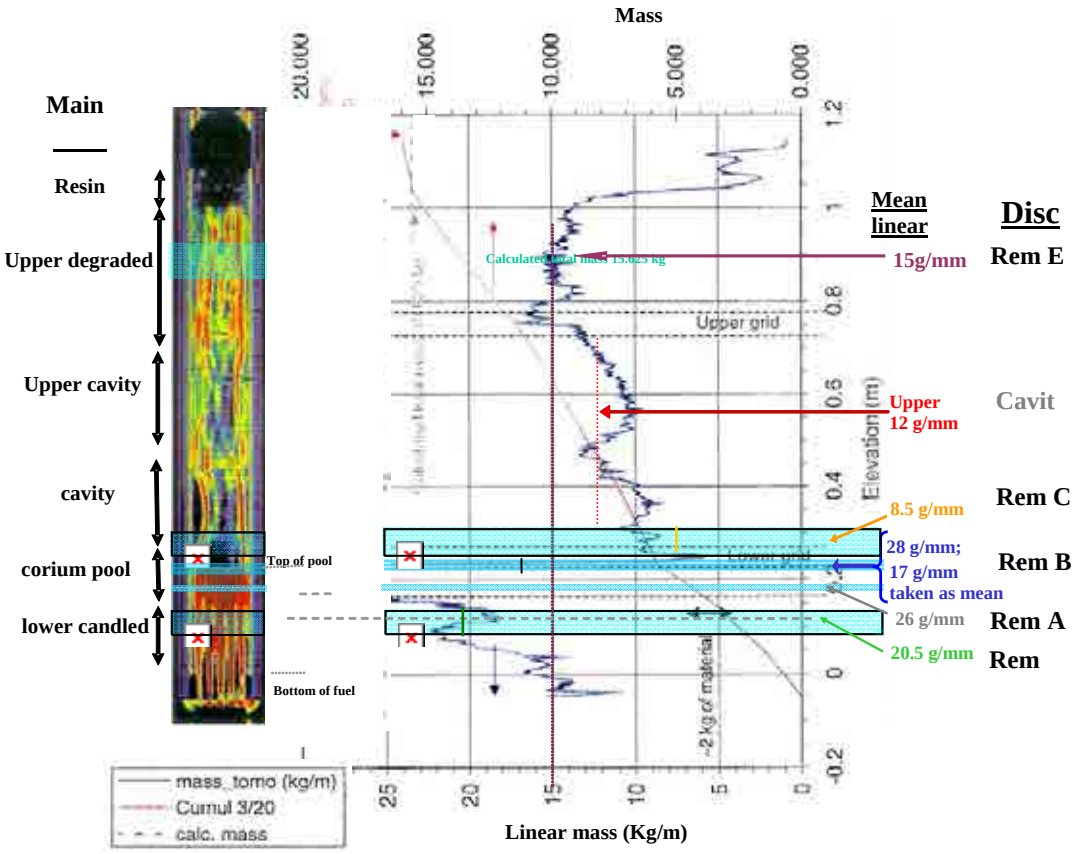

FIG. 2.3. Diagram giving the linear masses of the various remnants of the FPT1 bundle that have been selected for analysis of H_2 gas evolution along with their position in the bundle.

TABLE 2.2. ESTIMATED PARTITION BETWEEN RESIN AND FUEL FOR EACH OF THE DISCS USED IN THE TEST, ALONG WITH NOTES OF THE BUNDLE AND FUEL ROD'S DIMENSIONS

Zone	Remnants	Partition		Linear mass (see Fig. 2.2)
		Fuel [%]	Resin [%]	[g·mm^{-1}]
Lower candled rods	Rem	40	60	20.5
Corium pool	Rem-A	95	5	26
Cavity/corium pool	Rem-B	65	35	17
Cavity		36	64	8.5
Upper cavity	Rem-C	20	80	12
Upper bundle	Rem-E	34	66	15
Resin		20	80	2

Notes: (1) Thoria sheath: 73 mm int. dia., fuel cladding ~9.5 mm ext. dia.
(2) Bundle configuration: 20 rods, 1 control rod and guide tube (ext. dia. 12.1 mm) and 2 ultrasonic thermometers (ext. dia. 6 mm).
(3) 'Free' cross-section calculation: ThO_2 cross-section = $\pi(73/2)^2$ mm^2 = 41.854 cm². Rods cross-section = $[20.\pi(9.5/2)^2 + \pi(12.1/2)^2 + 2.\pi(6/2)^2]$ mm^2 =15.891cm². The difference is 25.96 cm² or 62.0% of the cross-section will be filled with resin for a bundle in its initial condition.

3. RADIOLYSABLE MATERIAL TRANSPORT AND STORAGE CONSIDERATIONS

3.1. Transport

Assuming that the container is filled with an inert atmosphere (eg. N_2) directly after loading then this will greatly reduce risk and power of any deflagation (typically Type B containers are airtight and capable of being inerted).

In addition to backfilling the transport container with inert atmosphere, one can ensure a large free volume to take up the releases, or to have a catalytic recombiner system in the container to getter the evolved H_2 or have an inert gas in the inner sealed container.

3.2. Storage — additional requirements

This problem also applies to all irradiated fuel due for storage where it is not possible to separate all the radiolysable material from the fuel. There are additional requirements that the inner containers are capable of atmosphere evacuation and backfilling with inert gas as well as the transport container. The licence for the Phébus FPT1 bundle storage at CEA (being applied for at the same time as the transport licence) required that there would be no pressure buildup in the inner containers. Hence, outer containers were constructed with open apertures and inner containers with poral filter apertures in order to avoid any pressure buildup while minimising contamination through the filters. Hence avoiding pressure buildup was the first priority.

4. ESTIMATION OF RADIATION

4.1. Data format

The modelling was performed with ORIGEN for a 17 × 17 Westinghouse PWR bundle. The neutron data was given in neutrons per sec per metric tonne U metal (Mt U). This was subdivided into:

(1) α, n neutrons;
(2) Spontaneous fission neutrons;
(3) Delayed neutrons (which were zero when fission had ceased).

The total neutron (in neutrons per sec per Mt U) was also given for various energy ranges and each class could be cross-multiplied with its mean energy and the total neutron energy estimated in MeV per sec per Mt U.

The gamma information was given as the gamma energy release rates in MeV per sec per Mt U for each energy range as well as for the total gamma energy range.

In addition the total power (Watt per Mt U) from all sources — neutrons, alpha, beta and gamma — was also given. The alpha and beta is not given directly, so an estimate of this is made by deduction of neutron and gamma energy from the total power. Finally a conversion from MeV per sec per Mt U to Watt per Mt U (equals J per sec per Mt U) was performed multiplying by 1.602×10^{-13}, while a conversion from tonne U metal to tonne of UO_2 was made by dividing by 0.88.

5. ESTIMATION OF RADIOLYSIS RATES

5.1. Density assumptions

It was assumed that 10 tonnes of U are embedded in 1 tonne of resin. Estimates needed to be made concerning the porosity; here the density of the epoxide resin is taken as 1.20 $g \cdot cm^{-3}$ [5].

The value of ρUO_2 ~9.90 $g \cdot cm^{-3}$ was assumed. This corresponds to the full theoretical density of UO_2

of 10.8 g·cm^{-3} at 92.5% density. This value yields the following volume ratios: 45.2 vol.% resin and 54.8 vol.% UO_2. This does not vary greatly as can be seen in Table 5.1 below: there is only a variation of 2% in 45% (or ~4% relative for a 3 times increase in porosity).

TABLE 5.1. UO_2 DENSITY AND VOLUME RATIOS FOR FUEL AND RESIN WITH VARIATION OF FUEL POROSITY

Fuel porosity [%]	Rel. fuel density [%]	Effective density UO_2 fuel(*) [g·cm^{-3}]	Volume resin [%]	Volume fuel [%]
5	95	10.00	45.4	54.6
7.5	92.5	9.90	45.2	54.8
15	85	9.18	43.3	56.7

(*) theoretical ρ_{UO2} (@ 100% density) = 10.8 g·cm^{-3}

5.1.1. Geometry

The fuel rod geometry assumed that 4 quarter rods (of each 10 mm dia.) were sited on each corner of a 15 × 15 mm square. This geometry corresponds to that of the rods in FPT1 bundle at the start of the experiment. However tomographic sections of FPT1 in Figs. 2.1–2.2 show that there is considerable deformation; the upper bundle has lost rods or they have swollen and/or have slumped together. The pool is a quite different geometry and the lower bundle also has additional rivulets of molten material candling down the rods. Therefore this geometry serves only as a rough estimate.

5.1.2. Deposition of power in the total mass

Given the high stopping power of the polymeric material for neutrons compared to the heavy metal present in the fuel, a division for the power deposition for neutrons was taken as 10% for fuel and 90% for resin.

For the power deposition for gamma it was assumed that was twice as much gamma being absorbed by the fuel compared to neutron radiation). This resulted in a division of 20% deposited in the fuel and 80% in the resin.

The deposition of power for alphas and beta between the fuel and the resin assumed an α penetration 40 μm into resin (as with water). However the problem was what to allow for beta given that it can penetrate thin steel or several centimeters of water or resin. As alpha radiation is estimated to cause 1000 times more ionisation than betas it was proposed to increase the ‘effective range’ of the alpha radiation to 50 μm to allow for this. This 10 μm increase would roughly compensate for 1 cm of beta radiation penetration. Using the starting rod geometry indicated in the previous section, this would give a ratio of cross-sectional area of resin compared to the total area in the bundle that would be penetrated by alpha and beta radiation as, $0.50025 \times \pi/25(9\text{-}\pi) = 0.010733$; thus it would penetrate approximately 1% by volume of the resin. However as the interface is likely to be the site of stresses and pre-existing cracks and hence accelerate the degradation, it was proposed to multiply this by a factor 10 to allow for this. Thus an estimate of 10% alpha and beta energy deposition in the resin was adopted. These values are summarised in Table 5.2 below.

TABLE 5.2. SUMMARY OF THE RATIOS OF POWER DEPOSITION BETWEEN FUEL AND RESIN FOR THE VARIOUS RADIATION SOURCES

Fuel–resin power division	Radiation	Fuel	Resin
1/10 & 9/10	neutron	0.1	0.9
2/11 & 9/11	gamma	0.2	0.8
See Sect. 5.1.1 & 5.1.2	α, β	0.9	0.1

5.2. Initial comments

Initially it was noted that the total power (gamma + beta + alpha + neutron power) per Mt U immediately after reactor shutdown, ie. with no cooling period, is insensitive to burnup as most of the power immediately after shutdown comes from the very short lived nuclides and their concentration will quickly reach equilibrium when a reactors runs for a few days; at higher burnups their concentration does not significantly increase because they decay as fast as they are created. By contrast, the total power after a five year cooling period does increase. Now there are only long lived nuclides remaining and their concentration builds up with rising burnup. No great differences between PWR and BWR conditions were anticipated.

5.3. Proportion of power deposited in resin and fuel

5.3.1. Total power distribution in resin

Figure 5.1 shows the total power deposition in the resin and fuel and it is seen that the resin receives close to 30% of the total power. There is a slow exponential growth that could be locally interpolated with a linear function.

5.3.2. Neutron power distribution

As can be seen in Fig. 5.2, the majority (91%) of the power from neutrons is deposited in resin as was assumed earlier. It is also seen that it is very small compared to gamma but that it is growing exponentially with burnup; it increase by 104 times in going to 60 $GW \cdot d \cdot t^{-1}$ UO_2, but still represents less than 1 in 106 of the total power deposition (~0.001 $W \cdot t^{-1}$ UO_2 vs. 10^3 $W \cdot t^{-1}$ UO_2).

5.3.3. Gamma power distribution

The gamma power distribution between can be seen in Fig. 5.3. However very large total powers (~1 $kW \cdot t^{-1}$ UO_2) are seen and there is a slow exponential growth of this source of deposited power with burnup. If a line is extrapolated from about 23 $GW \cdot d \cdot t^{-1}$ UO_2 then it is seen that there is an underestimate of about 18% for gamma power deposition in resin at 60 $GW \cdot d \cdot t^{-1}$ UO_2.

5.3.4. Alpha and beta power distribution

The estimate was that 10% of the alpha and beta power was deposited in the resin and it is calculated approximately by deduction of gamma and neutron power from the total power. Again as a consequence of the overall exponential growth of the total power this is reflected in a slow exponential (practically linear) growth of estimated alpha and beta power deposited in the resin with burnup in Fig. 5.4.

However the power deposition from alpha and beta in resin is ~300 $W \cdot t^{-1}$ UO_2 at a burnup of 60 $GW \cdot d \cdot t^{-1}$ UO_2 is lower than that from gamma and represents about a quarter of the gamma power deposited.

5.4. Effect of varying the neutron power deposition in resin

Since the gamma power is the major source of power deposited in the resin. The variation of the assumed gamma repartition between fuel and resin was also examined. Here the division of the gamma power deposition between fuel and resin was varied between 5% in fuel and 95% in resin to 30% in fuel and 70% in resin. The results are shown in Fig. 5.5 for low burn–up (5 $GW \cdot d \cdot t^{-1}$ UO_2) and high burnup fuel (60 $GW \cdot d \cdot t^{-1}$ UO_2).

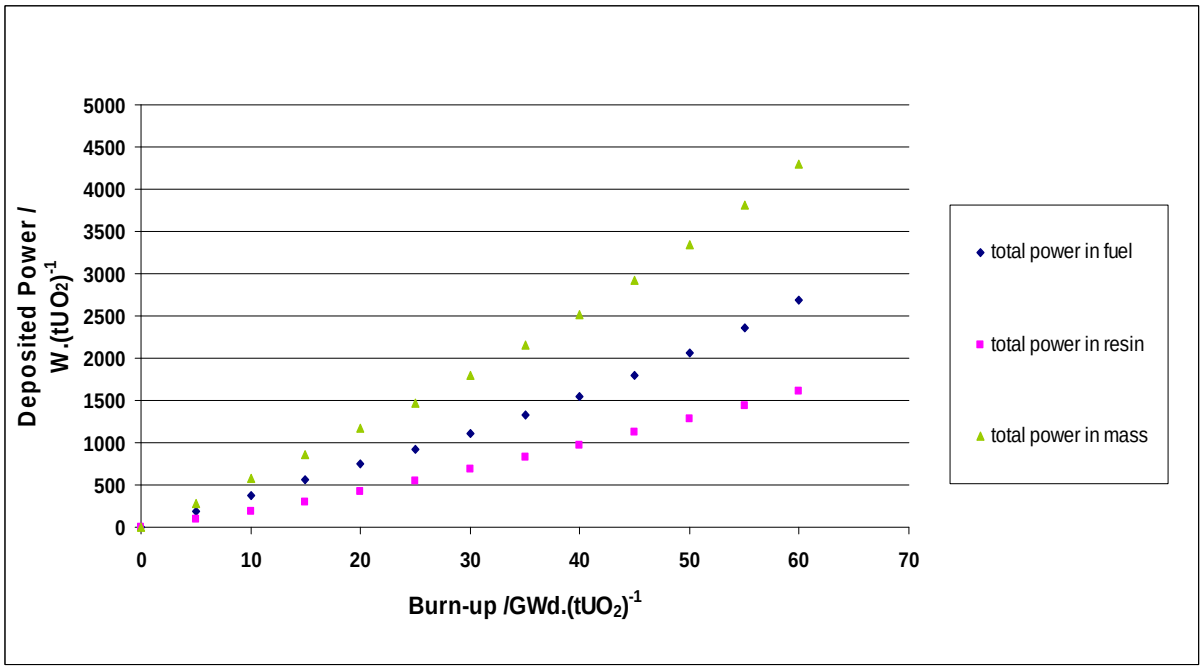

FIG. 5.1. Total power deposition in resin and fuel with burnup after a 5 year cooling time.

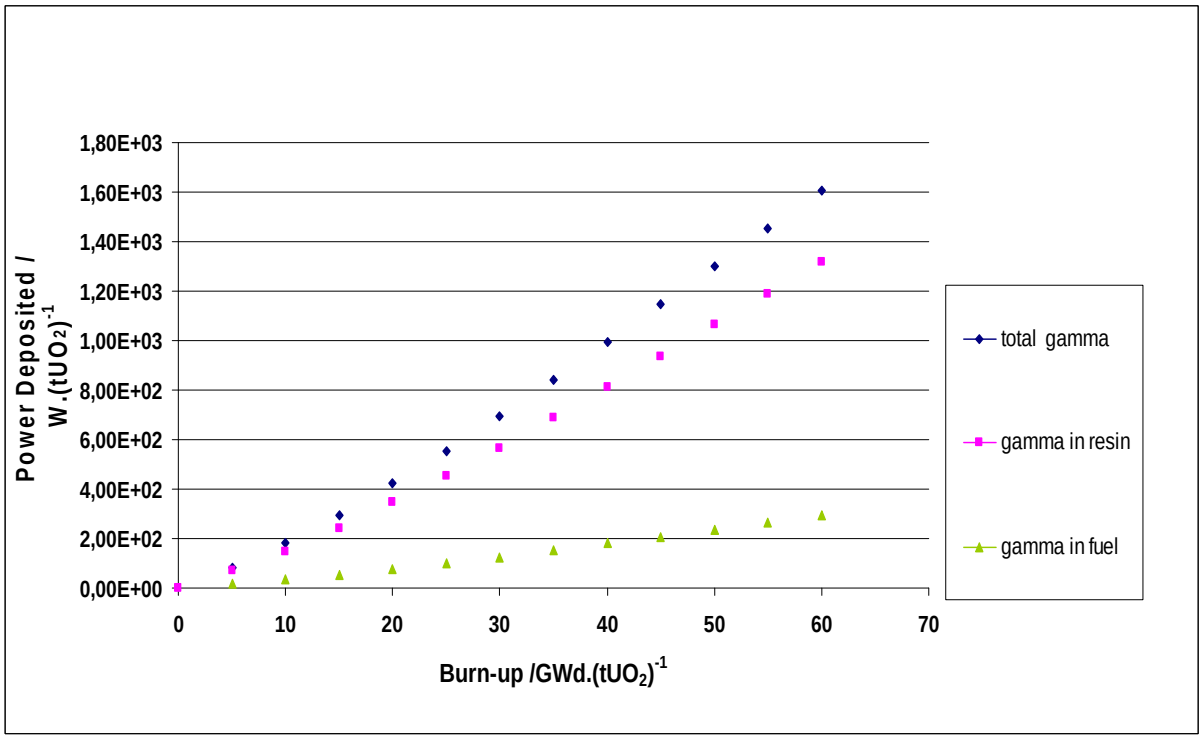

FIG. 5.2. Neutron power distribution in resin and fuel with burnup after a 5 year cooling time.

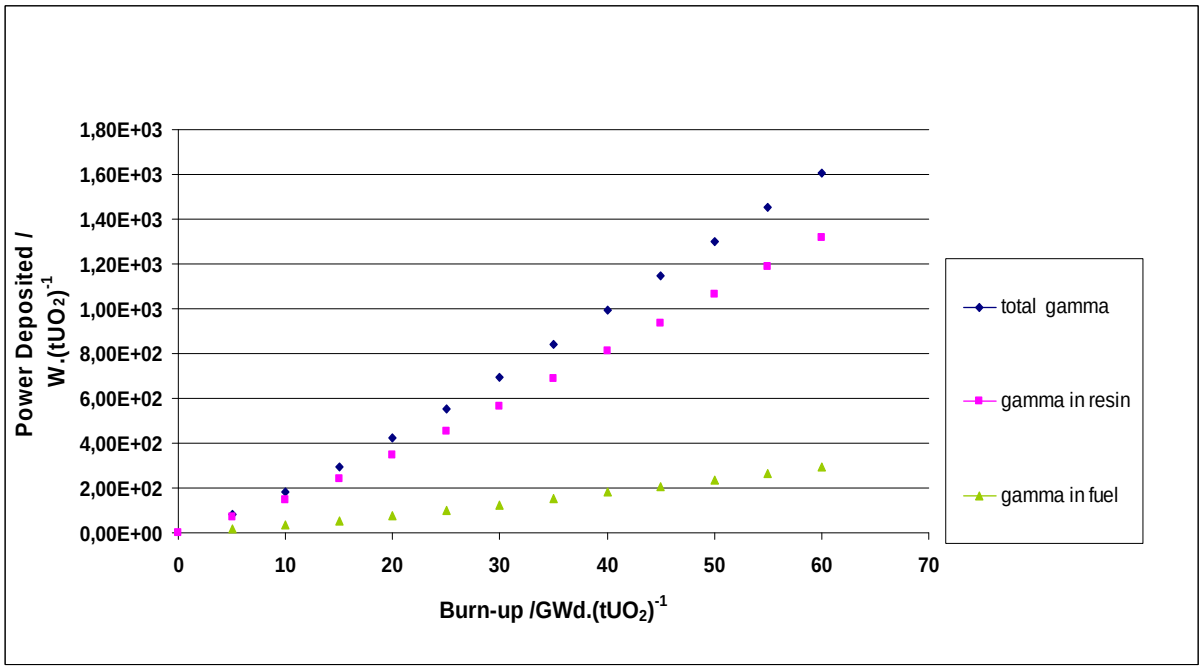

FIG. 5.3. Gamma power deposition in resin and fuel with burnup after a 5 year cooling time.

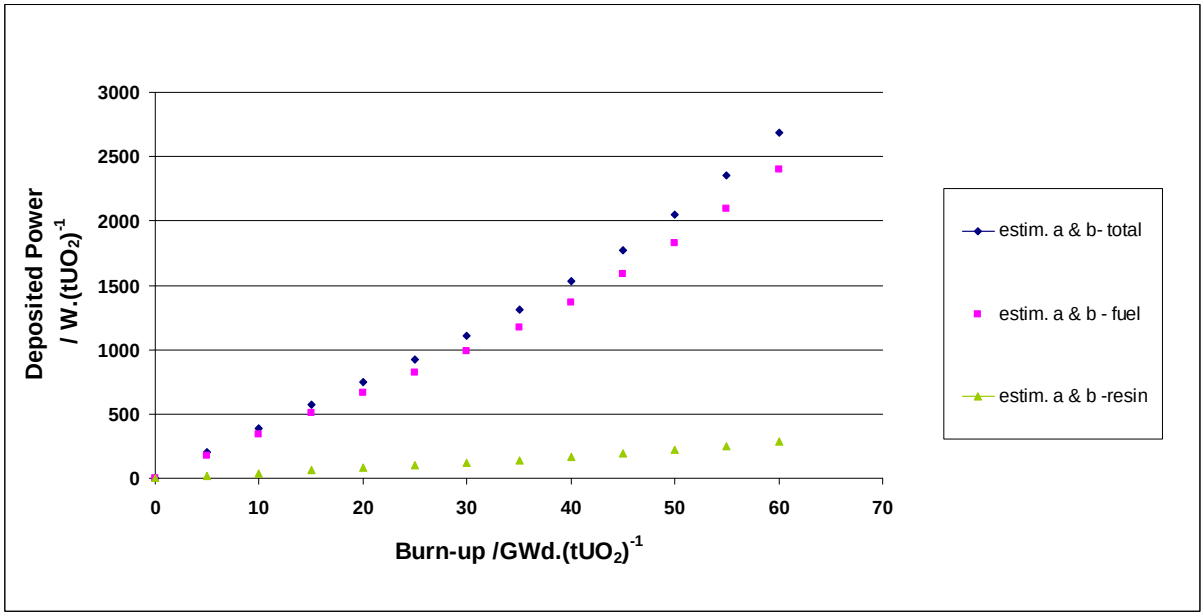

FIG. 5.4. Alpha and beta power deposition in resin and fuel with burnup after a 5 year cooling time.

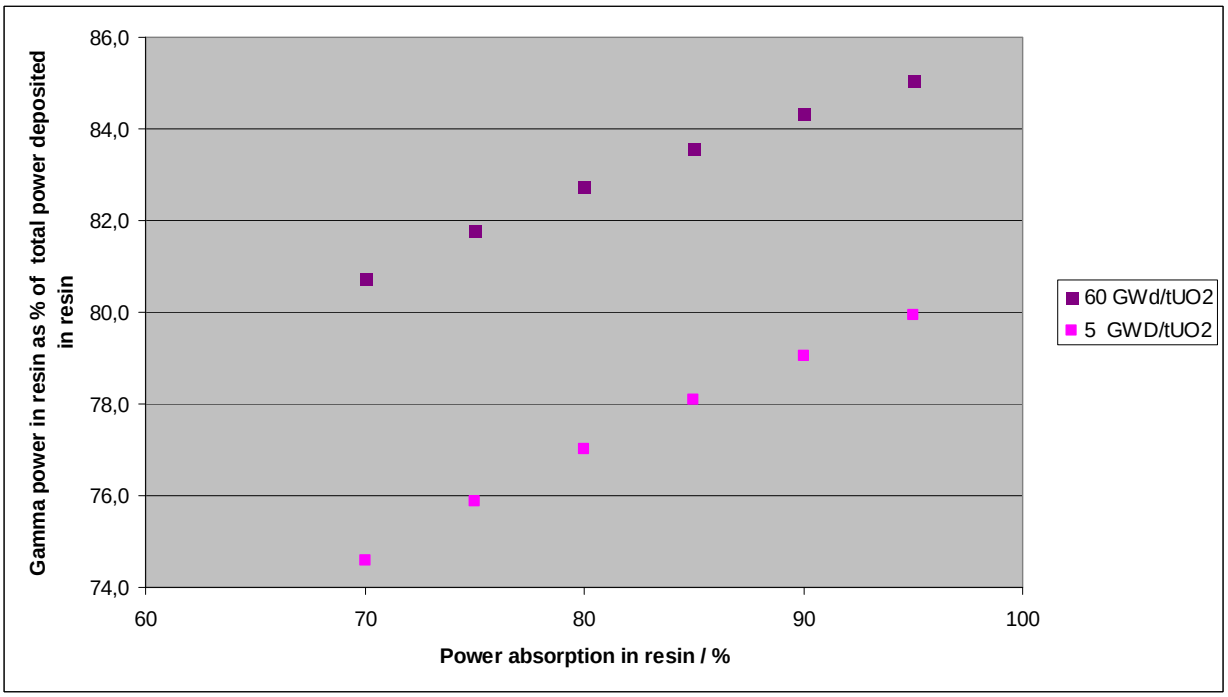

FIG. 5.5. Variation of gamma power deposited in resin as a percentage of total deposited power in resin with division of gamma power deposition from 30% fuel -70% resin to 5% fuel and 95% resin for a high and low burnup fuel after a 5 year cooling time.

They show that the total power deposited increases with burnup and that the variation in total gamma power deposited in resin (as percentage of the total deposited power) is quite small. Thus at the low burnup 5 GW·d·t^{-1} UO_2 (the most sensitive case) the gamma power deposited in resin is 75% of the total deposited power in resin when only 70% of gamma is deposited in resin but rises to 80% of the total deposited power in resin when 95% of the gamma is deposited in resin. For high BU 60 GW·d·t^{-1} UO_2 fuel the corresponding statistics are 81% of the total power is deposited in resin from gamma at 70% of gamma deposition in resin; this rises to gamma being 85% of the total deposited power in resin when a division of the gamma power of 95% in resin and 5% in fuel is used. Both these figures represent a variation of ~5% of total power over the range of deposition ratios. A slow reduction in this variation is seen with burnup — presumably because the total power deposited is rising steadily.

5.5. Calculation of hydrogen releases

This is based on the geometrical values of the Phébus FPT1bundle and the proportions selected for the power deposition between resin and fuel. The experimental value of the Phébus FPT1 bundle discs was given as 2.0% H_2 ± 0.4% H_2 (absolute) concentration in 69 days. This leads to an estimate of 1.65 (±0,33) cm³ of H_2 per day for the entire FPT1 bundle; (i.e. from 1.32–1.98 cm³·d^{-1}). This gives 0.000594 cm³ H_2 per day per cm³ resin, or (or 9.89 × 10^{-5} cm³ H_2 per day per g UO_2 fuel of 23.4 GW·d·t^{-1} UO_2 BU). The major contribution after a 5 year cooling period is gamma radiation at approximately 75–80% (see Sect. 5.4).

For transport and for intermediate storage conditions, the profile for gamma power deposition in resin is considered to be the best estimate of the radiolysis rates for resin in an irradiated fuel bundle. Therefore a linear extrapolation with a percentage addition has been taken. This linear percentage addition is based on the radiolysis value obtained for the Phébus FPT1 embedded bundle at 23.4 GW·d·t^{-1} UO_2. As stated earlier this excess over the linear extrapolation was 18% at 60 GW·d·t^{-1} UO_2 therefore a rounded value of 20% excess at 60 GW·d·t^{-1} UO_2 in addition to the linear extrapolation was chosen. Thus the estimate for radiolysis rates of resin-embedded irradiated fuel of 40–60 GW·d·t^{-1} UO_2 burnup was estimated as follows:

– A factor of (40/23.4) × 1.10 for a 40 GW·d·t-1 UO2 = 1.88;
– A factor of (50/23.4) × 1.15 for a 50 GW·d·t-1 UO2 = 2.46;
– A factor of (60/23.4) × 1.20 for a 60 GW·d·t^{-1} UO_2 = 3.08.

This yields radiolysis rates for resin surrounding UO2 fuel in a bundle geometry as given in Table 5.3 below:

TABLE 5.3. RADIOLYSIS ESTIMATES FOR UO_2 IRRADIATED FUELS FOR A RANGE OF BURNUPS FROM 23–60 GW·d·t^{-1} UO_2

Fuel BU [GW·d·t^{-1} UO_2]	Factor for increase	Radiolysis rate [cm^3 H_2/day/cm^3 resin]	Error (±30%)(*)
23.4	1	0.000594	±0.000178
40	(40/23.4) × 1.10 = 1.88	0.00112	±0.000335
50	(50/23.4) × 1.15 = 2.46	0.00146	±0.000438
60	(60/23.4)× 1.20 = 3.08	0.00183	±0.000548

(*) Accuracy is ±30% (20% on experimental value and 10% on modelling), assuming other factors are similar (i.e. accuracy under optimum conditions).

The accuracy of the radiolysis measurement was given as 20% relative [1], it was proposed to add an additional error of 10% for the extrapolation as the best possible. This estimate must be seen in the context that many estimated parameters relating the fuel–resin geometry and exact volumes of resin incorporated in the fuel are not well known and that individual assessments are made in each case. Here the main sources of errors can be established and specific calculations made to check the error levels or scoping calculations to verify the sensitivity of key parameters.

6. CONCLUSIONS

(1) Gamma power appears to be the main source deposited in resin at about 80% and shows a slow exponential growth with burnup at a cooling period of 5 years.
(2) Alpha and beta radiation are then the next major source at ~20%, but are the most poorly characterized.
(3) Neutron deposited energy appears to increase the most with increasing burnup but remains after a 5 years cooling period only a minor source at 10–7%. Its contribution could become more important in longer time frames which would need further studies.
MOX fuel would not be expected to very different in a similar study but the larger role of the neutron power could be significant for long term cooling times (or repository studies).
(4) Estimates of hydrogen generation have been made for fuel from 40–60 GW·d·t-1 UO2 burnup on the basis of the modelling of gamma power deposition in resin. These rates vary from 0.00059–0.002 cm^3 H2/day/cm^3 resin in going from 23.4–60 GW·d·t-1 UO2 burnup. Accuracy is expected to be ±30% under the most similar (i.e. optimum) cases.
(5) Varying the proportion of gamma power deposited in resin (as the major source) between 70–95% of gamma power being deposited in resin showed a slight variation of total power deposited in resin and indicates that it is not a critical parameter.
(6) These sorts of calculations can assist in transport licensing and design considerations of storage for irradiated radiolysable material.

REFERENCES

[1] VON DER HARDT, P., JONES, A.V., LECOMTE, C., TATTEGRAIN, A., Nuclear safety research. The Phebus FP severe accident experimental program, Nuclear Safety **35** (2) (1994) 187–205.

[2] SCHEURER, H., CLEMENT, B., PHEBUS FP Data Book FPT1, Document PH-PF IS/92/49, (1997).

[3] JACQUEMAIN, D., BOURDON, S., DE BRAEMECKER, A., BARRACHIN, M., Phébus PF — FPT1 Final Report, IPSN Tech. Report No. IP/00/479, (2000).

[4] BOTTOMLEY, D., PAPAIOANNOU, D., NEU, J.-M., UHLIG, M., GLATZ, J.-P., WEGEN, D, CARBOL, P., FORS, P., RONDINELLA, V.V., SIMONDI-TEISSEIRE, B., JOUDON, A., Obtaining a licence for transporting radiolysable material, 47th Annual Workshop of the Working Group 'Hot Laboratories & Remote Handling', RIIAR, Dimitrovgrad (2010).

[5] PANG, K.T., GILLHAM, J.K., Anomalous Behaviour of Cured Epoxy Resins: Density at Room Temperature vs. Time and Temperature of Cure, Tech. Rep. No. 15, (contr No. N00014-84-K-0021), Polymer Materials Program, Dept of Chemical Engineering, Princeton University, Princeton (1988).

CEA STRATEGY FOR CIVIL SPENT FUELS

J.-Y. BLANC, M.-H. LACIRE
Commissariat à l'énergie atomique et aux énergies alternatives
Gif-Sur-Yvette Cedex, France
Email: jean-yves.blanc@cea.fr

Abstract

As a heritage of CEA history, the Nuclear Energy Division has to manage different types of spent fuels issued from its experimental reactors or from post-irradiation examinations in its hot laboratories. For significant quantities such as Osiris MTR and Orphée fuels assemblies, the priority solution is reprocessing to value their energetic content. Further contracts should be negotiated with AREVA for Phénix FBR and Phébus. However specific spent fuels are not easily reprocessed, because quantities are too small for an economic treatment, or because they are embedded in epoxy. CEA manages interim storage facilities for spent fuels, such as PEGASE and CASCAD in Cadarache and other facilities (ISAI, STAR) for putting spent fuels inside welded canisters. But underwater storage in Pegase does not comply with current seismic standards. So these spent fuels are sent to STAR for new containerization before interim storage in dry wells at Cascad or under water in RES canal. Other old fuels are stored in INB 72 Saclay facility. Phénix fuels should be sent to La Hague inside canisters to be welded in ISAI in Marcoule. Retrieving old canisters of spent fuels requires safety demonstrations and sometimes R&D. One problem is to demonstrate that no water has penetrated inside the canister. Another is to find a way to remove the epoxy embedding of former metallographic samples or to deal with potential hydrogen due to radiolysis of epoxy. A stabilization treatment should be performed on metallic fuels from graphite reactors, to avoid a pyrophoric reaction. For very old fuels, surveillance of canisters inside dry wells or finding all necessary data before a new containerization is not easy. Sending small quantities of PWR fuel remnants to La Hague has been investigated recently. If this way is opened, it can be enlarged to other laboratory spent fuels.

1. INTRODUCTION

During its history, CEA has produced a relatively large quantity of spent fuels. It has also received fuels from Nuclear Power Plants for R&D purposes, and performed post-irradiation examinations (PIEs) in its hot laboratories. The present stockpile represents more than a hundred tons of heavy metal. This amount of spent fuels has been and has to be managed, either through reprocessing, or through containerization and interim storage. This induces a need for dedicated facilities and in some cases for the development of in-cell processes to perform the containerization.

2. SPENT FUELS TO MANAGE

The spent fuels to be managed are coming from:

- Old fuels coming from heavy water and natural uranium, graphite, gas 1st generation of reactors;
- Material testing reactors, like Siloe dismantled in Grenoble, Osiris running in Saclay and in the future from Jules Horowitz reactor in Cadarache;
- Prototype fast breeder reactors, namely Rapsodie and Phénix, both of them shutdown;
- Safety test reactors: Phébus, Scarabée both shutdown and later Cabri;
- Critical mock-ups and teaching mock-up, e.g. Ulysse decommissioned in Saclay and later Masurca, Eole, Minerve;
- PWR fuels coming mainly from the PIE on EDF rods and similar reactors (irradiation in the BR3 reactor in Belgium, for instance);

As a consequence, the physical and chemical forms of all these fuels are very different.

3. GENERAL STRATEGY

The reference strategy is based on sending spent fuels to La Hague reprocessing plants. This enables to recuperate the energetic value of the fissile materials, instead of considering spent fuels as a waste. However, this strategy has some restrictions:

– Technical difficulties for reprocessing due to the chemical or physical form of the spent fuel;
– Technical difficulties for La Hague to handle fuels whose geometrical forms are quite different from standard PWR or BWR fuels;
– Lack of economic and strategic interest to reprocess low quantities of spent fuels.

So it is possible to distinguish 3 cases:

– Fuels which could be sent, as soon as possible, to La Hague reprocessing plants;
– Fuels which cannot be reprocessed now, but can be later when the corresponding processes will be available;
– Fuels waiting for final underground storage, due to the above enumerated restrictions.

4. REPROCESSING

4.1. The 1993–1997 period

Due to a common funding agreement between CEA, EDF and COGEMA, more than 20 tons of various types of spent fuels were reprocessed in the UP1 plant located in Marcoule. Half of this quantity was constituted by old fuels from heavy water reactors and natural uranium graphite gas (UNGG in French), irradiated in the 1st generation of reactors. Rapsodie fast breeder upper blankets were also treated. For several tons of PWR type fuels, plate type fuels from Osiris reactor and other various MTR fuels e.g. the Orphée reactor, a preliminary cutting of the fuel was performed in other facilities, and in some cases, the dissolution itself was performed in the APM facility, before reprocessing of the chemical solutions in UP1. But the UP1 plant was closed in 1997.

4.2. From 1997 to the present

After closure of UP1, and waiting for new reprocessing agreements with La Hague plants and for the opening a national underground storage facility, CEA has gathered its spent fuels in some facilities in Cadarache: the PEGASE pool received most of PIE residues from hot laboratories, whereas the CASCAD dry storage received in its wells spent fuels from the EL4 heavy water power plant (Brennilis).

From 2001, new contracts were settled to reprocess UAl type MTR fuels from Scarabée (Cadarache), Siloe and Siloette (Grenoble) and Orphée, as well as Ulysse (totally transferred in 2008) and silicide type MTR fuels from Osiris. Regular shipments are organized for the operational reactors Orphée and Osiris. In 2003, it was decided to reprocess as well all Phénix fast breeder fuel elements and so to avoid the construction of a dedicated interim storage.

FIG. 4.1. 26 U–Al spent fuel assemblies from Osiris MTR have been placed inside the TN-MTR cask (left), and shipped from Saclay (right) to La Hague.

4.3. The near future

New reprocessing agreements are under negotiation with AREVA NC in order to:

– Continue to evacuate the fuels irradiated in both reactors in operation Orphée and Osiris;
– Evacuate all the Phénix fuel pins after some preparatory work in CEA facilities (dismantling of fuel assemblies, gathering pins inside canisters);
– Evacuate the Phébus assemblies and a few PWR rods from the 1st French PWR (SENA) under interim storage in a pool in Saclay.

In the case of Phébus assemblies, for instance, treatment at La Hague creates two issues: the small assemblies are not directly compatible with the first step of the process and the adaptation will be very costly, and they have been submitted to a very low irradiation thus a treatment together with other CEA fuels should be managed. The technical solution is first to dismantle the assemblies and then prepare special containers compatible with La Hague process and the dissolution could be performed during Phénix fuel pins dissolution campaigns.

Some discussions are also under way to evacuate small quantities of PWR segments issued from the R&D, directly from hot cells of LECI in Saclay to La Hague. A special campaign has already been performed successfully some years ago. This requires cutting the segments in hot cells before shipment to go directly to dissolution (Fig 4.1).

For the oxide, plate type fuels burnt in Osiris until 1997, the strategy is not completely defined, either a reprocessing (it has already been performed on a few tons, but after cutting the plates in ISAI) or an underground storage as a waste.

5. UNDERGROUND STORAGE

Geological storage, hopefully available after 2025, is the chosen solution for the remaining fuels from heavy water and UNGG reactors, for some experimental fuels and PIE samples. The largest quantity is constituted by the spent fuel from the EL4 heavy water EDF reactor.

6. CONTAINERISATION FACILITIES AND INTERIM STORAGES

6.1. Containerisation

Before sending the spent fuels to interim storage, there is always containerization inside stainless steels canisters. This can mainly be performed in two facilities: STAR and ISAI. Both facilities will be needed for many years: so refurbishment programs have been launched in order to upgrade both of them according to their latest safety reassessments.

FIG. 6.1. STAR working area.

Among other goals, STAR has been built in Cadarache to deal with spent fuels from natural uranium, graphite gas reactors. As these fuels are pyrophoric, they need a stabilization treatment (controlled oxidization) before containerization. So STAR was equipped with a stabilization furnace and reconditioning equipments for this purpose. During this campaign, between 1995 and 2004, about 2000 fuel elements of this type were stabilized and put into containers (Fig. 6.1).

STAR is also used for containerization of other spent fuels as well, mainly PWR fuels after post-irradiation examination.

ISAI is located in Marcoule. At first, this large facility was designed mainly to work on fast breeder fuel pins. In the case of the Phénix reactor, the spent fuel assemblies are dismantled after irradiation in Phénix hot cells and fuel pins are placed inside welded containers, waiting for a shipment to La Hague reprocessing plant. The shipment will be performed by the TN 17.2 cask, which is very heavy (78.8 tons) and can be charged in ISAI (Fig. 6.2).

ISAI has also been used for other campaigns, such as the preparation of Osiris spent fuels for reprocessing before 1997, by cutting the fuel plates and putting the chips inside aluminium canisters ready for dissolution.

6.2. Interim storages

CEA has mainly three interim storage facilities for spent fuels, all of them located in Cadarache. Two are pool type: PEGASE and a canal of the RES reactor (CARES), whereas PEGASE consists of dry wells.

PEGASE is an old reactor facility, in which the pool has been converted into an interim storage (Fig. 6.3). As the pool is not complying with new seismic regulations, it has been decided to evacuate all the fuels from the pool. This is a complicated and time consuming task. The fuel canisters are sent to STAR for reconditioning and then transferred to CASCAD. Part of the fuel segments are embedded in epoxy, because they are issued of metallographic examinations: in this case, the PEGASE canisters will be transferred to CARES.

FIG. 6.2. ISAI is equipped to handle very heavy casks such as the TN 17.2 (at right on the picture on the left), which can be then shipped by railway (picture on the right).

FIG. 6.3. The PEGASE pool, used for under water interim storage.

CASCAD is a more recent facility, consisting of a series of dry wells. It is used to store mainly heavy water reactor fuel elements (EL4 reactor), natural uranium graphite gas reactor fuels, Phénix fuels, and few others such as Rapsodie fast breeder, Osiris or PWR fuels. Fuels canisters are leaktight welded and some have been filled by an argon–helium gas mixture and some have been previously dried out to limit the water presence (criticality issue). CASCAD is ventilated through a natural ventilation scheme (see Fig. 6.4). A peculiar attention is given to the balance between the quantities of canisters to be received to CASCAD (or CARES) or sent to La Hague, in order to avoid a saturation of all the wells. No extension of CASCAD is foreseen.

The CARES pool is only used for some oxide type fuels from Osiris and as a backup facility for PEGASE (mainly for epoxy embedded samples) or for the Phébus assemblies if the agreement for reprocessing is too long to obtain. It is not foreseen to use it after 2024.

6.3. Evolutions

Basically, the final choices are either reprocessing in La Hague or interim storage inside CASCAD waiting for final disposal when the underground repository will be opened by 2025. There are other spent fuels stored in other facilities (for instance, in a pool in the INB 72 at Saclay), but sooner or later they will be transferred to CASCAD, if not reprocessed.

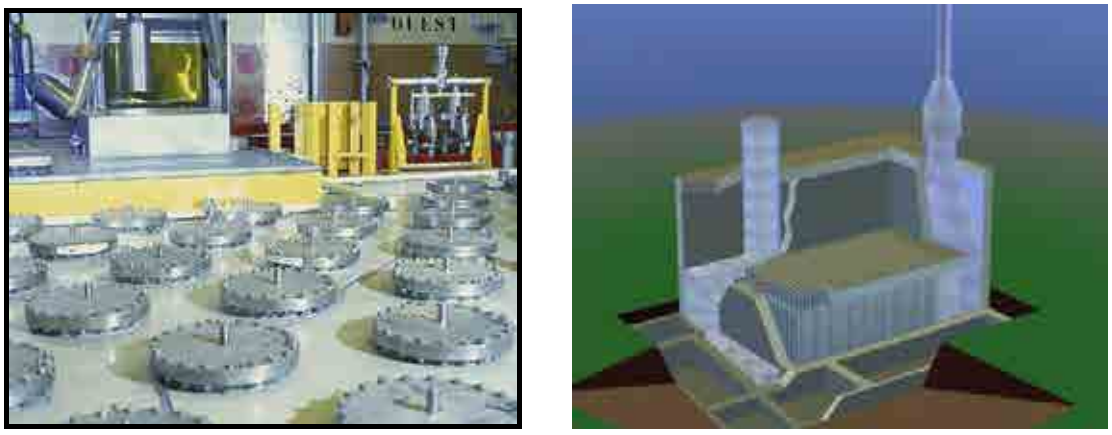

FIG. 6.4. CASCAD facility with the top of the dry wells (left) and a scheme of the building (right).

7. HOT CELLS PROCESSES

All these spent fuels need dedicated hot cell or in-pool equipments during the preparation for interim storage or prior to reprocessing.

7.1. Welding

The more classical equipment is welding the container. Such equipments are available in STAR and ISAI. They need very stringent quality insurance requirements, because the containers should be leak proof on a long term period (Fig. 7.1).

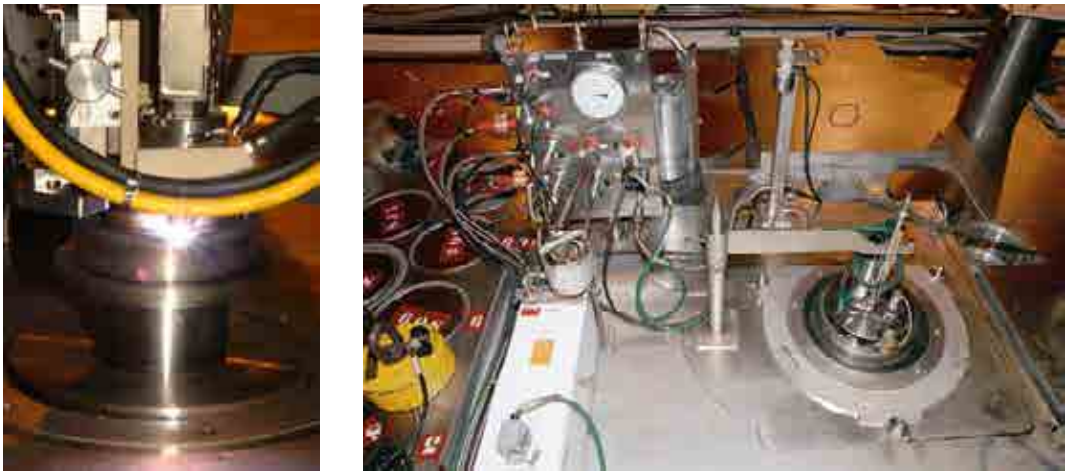

FIG. 7.1. TIG welding equipment for containerization in ISAI.

7.2. Checking the absence of water in the container

To avoid criticality concerns, STAR and CASCAD accepts only containers for which the absence of water inside has been demonstrated. For this reason, an under water X rays equipment is being developed to check any ingress of water in the canisters directly inside the PEGASE pool. This checking will be performed for some highly enriched spent fuels before shipment to STAR. If this technique is efficient, it can be also applied to the PWR type fuel elements stored inside the INB 72 pool in Saclay.

STAR is also equipped with a device for drying the canisters. The drying is obtained by vacuum pumping and inert gas filling. The absence of water is checked before closing the canister (Fig. 7.2).

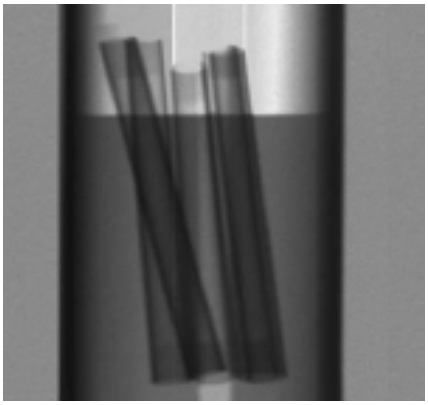

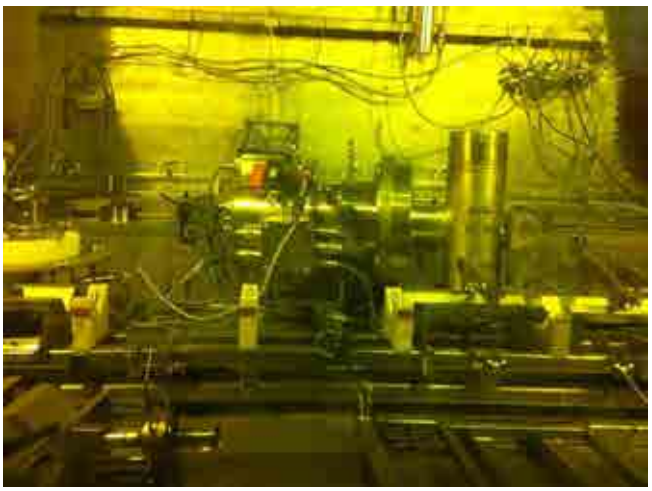

FIG. 7.2. Test of X ray detection of water (left) – puncturing and drying equipment for containers in STAR (right).

7.3. Stabilization

As mentioned above, the old natural uranium fuels from UNGG are pyrophoric. For this reason, one of the STAR hot cells was placed under inert atmosphere, and all the UNGG fuel cartridges were submitted to a stabilization treatment consisting in a controlled oxidization. Then the stabilized fuels were containerized.

Some HTR fuels should also be treated before interim storage.

7.4. Epoxy removing

At the moment, this is the most difficult problem. For long term storage, it is considered necessary to remove the epoxy from the metallographic fuel segments. It is considered that epoxy can release hydrogen, thus inducing explosion hazard. Several thermal or chemical treatments have been investigated, but the final process has not yet been chosen. One of the difficulties is that there are different types of epoxy. It is then recommended to PIE hot laboratories to use metal embedding, but this is not always the case. The preferred option is a systematic mechanical removal of the epoxy, followed by a pyrolytic treatment above 550°C under inert atmosphere without post combustion. It is envisaged that the stabilization furnace for UNGG fuels in STAR could be compatible with the pyrolysis temperature for epoxy.

8. CONCLUSIONS

The CEA has to manage quite a large quantity of spent fuels under many different physicochemical shapes. The general strategy is to send them to reprocessing when it is possible, and to store them waiting for final underground storage when it is not realistic. This needs several facilities for interim storage and reconditioning, and also a few developments in hot cells to be able to stabilize, weld and control the containers. A careful optimization is required to minimize the costs of the reprocessing, storages, reconditioning and minimize transportations.

BEFAST AND SPAR FROM 1981 TO PRESENT: THIRTY YEARS OF SPENT FUEL BEHAVIOUR, PERFORMANCE AND RESEARCH

A. BEVILACQUA
International Atomic Energy Agency
Nuclear Fuel Cycle and Materials Section
Vienna, Austria
Email: a.bevilacqua@iaea.org

Abstract

Spent fuel integrity and performance during storage have been investigated since 1981 through five completed Coordinated Research Projects and are currently being investigated in the framework of the third cycle of the Coordinated Research Project on Spent Fuel Performance Assessment and Research started in 2010. Concurrently since 1981, post-irradiation examination and inspection techniques — required for the research and the assessment of the performance of spent fuel — have been the topics of an IAEA Technical Meeting's series which holds its seventh edition this week. The need for continuous work on spent fuel integrity and performance as well as on post-irradiation examination and inspection techniques during wet and dry storage is stressed by the higher burnups being achieved, the likely longer storage periods being foreseen and the spent fuel wet storage incidents recently happened at Fukushima Daiichi site in Japan.

1. INTRODUCTION

In the late Seventies the interim storage of spent fuel (SF) storage had already been recognized as an important independent step in the nuclear fuel cycle. Furthermore, due to the delay in commercial reprocessing it was envisaged that SF in some cases should be stored for up to 30–50 years or more before reprocessing or disposal [1]. At that time *extended storage* was considered to be about 40 years.

Currently, some 30 years after, the SF storage period defined as *conventional or short term storage* could last up to approximately 50 years, and SF storage beyond approximately 50 years, defined as *long term storage*, is not expected to last more than approximately one hundred years and has a defined end point [2].

Because of the extension of the storage periods, SF integrity and performance under wet and dry storage have been investigated since 1981 in five completed IAEA Coordinated Research Projects or, as so called in the early years, Programs (CRPs): three cycles of the CRP on Behaviour of Fuel Assemblies in Extended Storage (BEFAST-I, II and III) as well as two cycles of the CRP on Spent Fuel Performance Assessment and Research (SPAR-I and II) [1, 3–6]. The third cycle of the CRP on SPAR begun in 2009 and will last until December 2013 [7].

Along these thirty years, the need for continuous work on SF behaviour, performance and research was driven by the achievement of longer storage periods as well as steadily higher burnups.

The recent incidents [8] at the Fukushima Daiichi site in Japan involving its wet storage facilities provide a further driving force as long this spent fuel undergoes unprecedented storage conditions: elevated water temperatures lasting up to weeks, additions (among others: sea water, hydrazine and concrete dust) to the hot water as well as the mechanical impact of debris from the fallout resulting after the explosions at the units 1, 3 and 4. A summary of these incidents directly related to the wet storage facilities at Fukushima Daiichi were summarized (available at the IAEA webpage of this publication's technical meeting: http://www-pub.iaea.org/mtcd/meetings/Announcements.asp ?ConfID=41211 or the HOTLAB webpage of this TM http://hotlab.sckcen.be/) by selecting the information provided in the Fukushima Nuclear Accident Update Log (from 11 March 2011 to 20 May 2011) available at http://www.iaea.org/newscenter/news/2011/fukushimafull.html.

2. BEFAST (BEHAVIOUR OF FUEL ASSEMBLIES IN EXTENDED STORAGE)

2.1. BEFAST-I (1981–1986)

In late 1977 the discussion on the first IAEA CRP on "Behaviour of fuel assemblies in extended storage", from now on BEFAST, was initiated within the framework of OECD/IEA. The first BEFAST proposal was discussed by participants from Austria, Italy, Sweden and the USA in February 1978.

After mostly political discussions BEFAST was transferred within OECD from IEA to NEA, and concurrently a joint IAEA–OECD/NEA programme was established for avoiding duplication of efforts. In 1979 and 1980 three meetings were held and a forum was established. Thirteen countries were represented, with Austria providing the chairman. A questionnaire issued by the IAEA to summarize the existing experience with SF wet storage was responded to by about 85% of the world's reactor operators and away from reactor (AFR) storage operators. In November 1980, NEA decided not to set up a specific working group on BEFAST and in recognition of the need for surveillance agreed to support an IAEA CRP. The need for continuing and encouraging international activities in monitoring the safe storage of SF was evidenced from international meetings. Austria, the lead Member State of the BEFAST meetings, collaborated to initiate the CRP and volunteered to lead it. The IAEA CRP on BEFAST was established in 1981 and research agreements were signed with 11 institutes from 10 Member States. Since the first review meeting in October 1983, Finland has been responsible for the chairmanship of the CRP. The final CRP meeting was held in May 1986.

The general aim of BEFAST was to provide a significant database on the SF cladding integrity after extended storage periods covering SF wet and dry storage.

In the context of this aim the CRP objectives were: to survey the existing experience in SF storage, to investigate SF by destructive techniques (DT) before and after extended storage periods, to investigate potential cladding degradation mechanisms, to evaluate suitable non-destructive techniques (NDT) for surveillance, and to investigate the behaviour of SF storage pool equipment.

The survey data on the existing experience in SF wet storage were reported in "Storage of Water Reactor Fuel in Water Pools, Survey of World Experience" in 1982 [9].

The research and development (R&D) areas to be covered by this first phase of BEFAST lately extended to cover potential problems in dry storage were:

- Spent fuel;
- Spent fuel — undamaged;
- Clad/water interface (oxidation, stress corrosion cracking, pitting, crevice corrosion, hydriding and galvanic effects);
- Clad/fuel interface (fission products attack, water logging and internal hydriding);
- Spent fuel — failed (leaching, canning and defect behaviour);
- Surveillance (visual, radiation monitoring, NDT and DT);
- Pool components (stress corrosion cracking, uniform, pitting, crevice and galvanic corrosion);
- Basic studies (effect of crud, cladding stress, galvanic hydriding, radiolysis, pellet–clad interactions and simulated defects);
- SF wet and dry storage systems data were reported in "Guide Book on Spent Fuel Storage" in 1984 [10].

The R&D matrix of the BEFAST CRP included:

- Wet storage;
- Spent fuel — undamaged (Austria, Canada, USA and former USSR);
- Spent fuel — failed (Canada, Sweden, USA and USSR);

– Pool water and pool components (Austria, former Czechoslovak Socialist Republic (CSSR), Finland, Hungary, Japan, USA and former USSR);
– Basic studies (CSSR and Hungary (Note: aluminium));
– Surveillance (Canada, CSSR, Finland, Hungary, USA and former USSR);
– Dry storage;
– Spent fuel (Canada, Japan (Note: Al-clad RR fuel) and USA);
– Basic studies (Canada, former German Democratic Republic (GDR) and Japan).

Most reports were devoted to the following fundamental problems in the development of SF storage facility design:

– Corrosion resistance of nuclear fuel materials, fuel cladding and constructional components in contact with the cooling medium (water or gases);
– Maximum fuel temperature and residual heat removal conditions during the extended storage;
– Potential degradation mechanisms of nuclear materials and cladding as well as the critical factors causing such degradation;
– Coolant chemistry in storage facilities (coolant purification from radioactive and non-radioactive impurities);
– Spent fuel burnups ranged from 6.5 GW·d·t-1 U (UnatO2/Zry-4, CANDU, Canada) to 40 GW·d·t^{-1} U ($U_{enr}O_2$/Zr-1%Nb, WWER-1000, former USSR).

Despite much work was done on improvement of the extended wet storage conditions, international design requirements and criteria had not been developed at that time. Some of the countries used national design parameters: thus, the design pool water temperature was 50°C in the USSR, 40–43°C in Finland, K_{eff} = 0.93 in Belgium and K_{eff} = 0.95 in the USA, former USSR, etc.

For the dry storage facilities the questions to be solved were related to the optimum gas composition (helium, argon, air) and the maximum fuel temperature. In the USA, the accepted recommendations for dry storage of SF with zirconium cladding, in closed canisters backfilled with helium were: maximum design temperature of the fuel cladding 370–400°C. For the Castor cask the maximum cladding temperature in the helium atmosphere was 400°C.

It was quite evident that the most important parameters related to the safe and reliable operation of the SF storage facility to be established and unified were:

– The maximum allowable Keff (≤ 0.95 in most cases);
– The maximum allowable cladding temperature for the dry storage (370–400°C);
– The cooling water chemistry (total salt content, chloride concentration and pH-value).

In criticality calculations the burnup was usually not considered, though some calculation programs showed the possibility to significantly increase the storage capacity (up to 30%) if this parameter was accounted.

Diverse pool water chemistries existing at the time were the result of the lack of uniform specifications for them as well as methods of calculating the flow capacity of water purification systems on the basis of controlled engineering parameters.

The conclusions of BEFAST-I can be summarized as follows:

– Wet storage: it was operated in a routine manner; there were no serious events in any of the participating countries and none of the reported events caused serious consequences; all known failure mechanisms could be excluded in proper conditions; SF and its environment was monitored at the time (method development work was ongoing).
– Dry storage: development programs showed no fundamental problems; specifically no problem was found in inert gas at temperatures limited to 450°C; only SF environment was monitored at the time (SF was retrieved, Kr-85 was measured in demonstration programs).

The results of the CRP compared with its general objectives are summarized below:

– First general objective “Survey the existing experience in SF storage”: a world survey was done and the results were published in 1982 [1]. An update based on a subsequent survey done in 1985 was planned to be published in 1987.
– Second general objective “Investigate SF by destructive examinations before and after extended storage periods”: DT results were reported both before and after storage on shipping port SF (USA) in wet storage for some 25 years and other programs were under way where after storage examinations were planned.
– Third general objective “Investigate potential cladding degradation mechanisms”: many contributions done on theoretical calculations, laboratory experiments, pilot tests and full scale storage experience produced a remarkable database indicating that all the known degradation mechanisms could be excluded in proper storage conditions.
– Fourth general objective “Evaluate suitable NDT methods for surveillance”: this was done and permanently continued gaining a lot of experience on the conventional NDT methods and allowing development work on new methods.
– Fifth general objective “Investigate the behaviour of spent fuel pool equipment”: research result on pool liner, rack and absorber materials were reported by many participants.

The main recommendations after completion the first cycle of the BEFAST CRP were the following:

– Further routine surveillance of SF wet storage seemed justified to assure that no substantial problems were developing in what had become a major worldwide SF storage technology;
– The suggestion that crud may have been loosening at least on some LWR SF in extended wet storage deserved additional definition though it was not likely to result in major impacts during subsequent SF handling;
– Rod consolidation appeared to offer more efficient use of SF wet and dry storage space, however, efficient and economical methods to conduct large scale SF consolidations as well as methods to store and dispose of SF hardware needed to be demonstrated;
– In SF wet storage, further research aimed at improving the technology and reducing both the capital and operational costs of SF storage facilities was needed: to further refine water chemistry and to improve the means of maintaining it; to study the selection of structural materials for SF storage pools, partly with a view to identify materials which were less expensive and more readily available; and to study the behaviour of SF in prolonged storage, especially SF with damaged cladding.

Continuation of the research cooperation on spent SF storage area was considered very important among the BEFAST participants and also other leading nuclear countries; therefore, a continuation program, BEFAST-II, was planned for the years 1986–1991 on eight different areas of interest that were identified:

(i) Further collection of data on SF dry and wet storage experience to confirm the safety of available storage concepts (including also experience on consolidated fuel);
(ii) SF monitoring (monitoring/ inspection methods for SF, SF storage components and SF storage environment);
(iii) Decontamination and cleaning of SF storage, transport and handling facilities (effects on SF assemblies and SF storage materials);
(iv) Handling and transport of SF after *interim* — currently defined as *conventional or short term* — storage (experience, effects on SF assemblies);
(v) Storage of defected SF (growth of defects, impacts on safety);
(vi) Super long term — currently defined as long term — SF storage (100 years) in wet and dry storage facilities (extrapolation of present experience, validity of extrapolated data, accelerated tests, etc.);
(vii) Development of predictive models for the behaviour of SF during and after interim — i.e. conventional or short term — storage (material aspects, failure mechanisms);
(viii) Crud impact on SF integrity.

The final report on BEFAST-I entitled “Behaviour of spent fuel assemblies during extended storage” was published as IAEA-TECDOC-414 in April 1987 [1] and presents the results on SF wet and dry storage technologies obtained from 11 institutes from 10 countries (Austria, Canada, the CSSR, Finland, the GDR, Hungary, Japan, Sweden, the USA and the former USSR) participating in the CRP from 1981–1986.

This first phase or cycle of the BEFAST CRP was evaluated by all its participants and observers as very important and helpful for the nuclear community and for that reason it was decided to continue it further from 1986–1991 as BEFAST phase II (BEFAST-II).

2.2. BEFAST-II (1986–1991)

By mid-Eighties considerable quantities of SF were continuously arisen and accumulated though some new reprocessing facilities were being constructed. In such context many countries were investigating the option of extended SF storage prior to reprocessing or fuel disposal. At the time SF wet storage continued to predominate as an established technology with the construction of additional AFR SF storage pools. SF dry storage, however, was increasingly used and most of the CRP participants were considering SF dry storage concepts for the longer term.

In 1986 the second cycle or phase of the BEFAST CRP entitled “Behaviour of Spent Fuel and Storage Facility Components during Long Term Storage” was initiated with the participation of 16 organizations representing 13 countries (Argentina, Canada, Finland, Germany (previously the GDR and the Federal Republic of Germany (FRG)), Hungary, Italy, Japan, the Republic of Korea, Sweden, the UK, the USA and the USSR) in September 1986. The first research coordination meeting (RCM) was held in April 1988 in Budapest, Hungary and the third — and final — meeting was held in March 1991 in Vienna, Austria.

The objectives of the BEFAST-II CRP were to issue a final report for updating the SF management technologies in the participating countries and to provide a forum for the exchange of information on SF storage between specialists from Member States.

Eight subjects were initially proposed to be covered by the BEFAST-II:

(i) Wet and dry storage experience;
(ii) Spent fuel monitoring;
(iii) Effects of decontamination on materials;
(iv) Handling and transport of spent fuel after storage;
(v) Storage of defected fuel;
(vi) Storage of fuel exceeding 50 years, extrapolation of present experience;
(vii) Predictive models: Failure mechanisms including material aspects;
(viii) Crud impact on spent fuel integrity during extended storage.

These subjects were later grouped under three major topics for both SF wet and dry storage:

(a) Long term behaviour;
(b) Surveillance;
(c) Facilities and operation.

The research subjects corresponding to each major topic were:

(a) Long term behaviour: materials, degradation mechanisms and models, validation (experiments or experience);
(b) Surveillance: monitoring wet/dry (environment, components, fuel assemblies, operational doses), fuel conditions (operation, fabrication, failed rod and assembly) and different reactor types;

(c) Facilities and operation: dose rate reduction, system performance, migration wet/dry and capacity enhancement (re-racking, doped coolant and rod consolidation).

The R&D matrix of the BEFAST-II CRP included:

(a) Long term behaviour:
   — Materials (Canada, Hungary (Note: also aluminium), UK and former USSR);
   — Mechanisms and models (Canada, Germany, USSR);
   — Validation (Canada, Finland, Germany, Republic of Korea, UK, USA and former USSR).
(b) Surveillance:
   — Wet (Argentina, Canada, Finland, Hungary, Republic of Korea, UK and former USSR);
   — Dry (Canada, USA and former USSR).
(c) Facilities and operations (Canada, Germany, Hungary, Italy (Note: Magnox SF), Sweden and former USSR).

The following topics on SF wet storage were addressed:

(a) Methods of monitoring and assessing ongoing SF integrity;
(b) Factors that affect intact and defective SF integrity;
(c) Factors important to maintaining water pool liner and structure longevity;
(d) Operational experience with SF wet storage and methods of enhancing water pool capacity;
(e) Experience with water pool SF handling and transfer of spent fuel from wet to dry storage.

Spent fuel burnups ranged from 4 $GW \cdot d \cdot t^{-1}$ U ($U_{enr}O_2$ / Zry-2, Shipping port, USA) to 55 $GW \cdot d \cdot t^{-1}$ U ($U_{enr}O_2$ / zircaloy, Zion, USA) and SF storage year of first pool exposure ranged from 1959 (Deionized water, Shipping port, USA) to 1982 (boric acid, Zion, USA). Stainless steel (from advanced gas reactor (AGR)) as well as magnesium alloy (Magnox) cladded SF was also investigated along the BEFAST-II CRP.

The major methods of surveillance in practice worldwide during SF wet storage at the time included the following:

– Pool inspections;
– Underwater visual and TV examination;
– Diameter measurements;
– Eddy current techniques (oxide thickness, crack detection, hydrides);
– Periodical analysis of pool water;
– Electrochemical potential and noise measurements;
– Gamma scanning of fuel assemblies;
– Ultrasonic tests;
– Crack detection by neutron interrogation;
– Out of pool inspections;
– NDT and DT examinations in hot cells.

Main conclusions on SF wet storage were:

– Extended wet storage of zirconium alloy clad SF with no loss of cladding or fuel pellet integrity was feasible even if the cladding has through-wall operational defects.
– Magnox and AGR SF storage times were relatively short because currently SF was or was to be reprocessed after a few years of wet storage and to maintain Magnox and AGR SF cladding integrity, close chemical control of pool water was necessary.
– Monitoring and surveillance had confirmed that adherence to the specified pool water chemistry was essential to prevent SF degradation during pool storage for all types of SF. Whereas near-

neutral pH conditions with low ion content were satisfactory for zirconium alloy clad SF, elevated pH was beneficial for Magnox and AGR SF. For aluminium clad SF, a pH of ~5.5 was in use.

– Adherence to specified pool water temperatures was required to maintain SF assembly (SFA) integrity, minimize water radioactivity levels and preserve the pool structural integrity.
– For extended — currently defined as long term — wet storage (over 50 years), certain water pool liner materials, such as non-stabilized stainless steel and epoxies, further investigation would be required.
– In addition to the standard pool inspection techniques and hot cell inspections, some advanced monitoring techniques such as gamma scanning, neutron interrogation, ultrasonic inspection and electrochemical noise analysis were being employed at the time.
– Wet storage would continue to be the main SF storage option in all participating countries.
– For the long term, most participating countries were investigating SF dry storage options.
– Enhancement of SF wet storage capacity would remain an important activity: SF rod consolidation to increase wet storage capacity would continue in the UK, was being evaluated for LWR fuel in the USA and could start in some other countries; high density storage racks had been successfully introduced in many existing pools and were planned for future facilities.
– For extremely long — currently defined as long term — SF wet storage (>50 years), there was a need to continue work on fuel integrity investigations and LWR fuel performance modelling; it was suggested that pool component performance in some cases could be more limiting than the SFA storage performance; it was desirable to make concerted efforts in the field of corrosion monitoring and prediction of SF cladding and pool component behaviour in order to maintain good experience of wet storage.

The following topics on SF dry storage were addressed:

(a) Performance;
(b) Surveillance;
(c) Facilities and operation.

Spent fuel burnups ranged from 2.225 $GW \cdot d \cdot t^{-1}$ U ($U_{nat}O_2$ / Zry-2, CANDU, Canada) to 40 $GW \cdot d \cdot t^{-1}$ U ((U–Pu)O_2/stainless steel, FBR, France).

Main conclusions on SF dry storage by type of cladding material were:

– Zircaloy clad SF:
  • Dry storage in an inert atmosphere was licensed in Germany and the USA, and in air in Canada;
  • Maximum SF cladding temperature was licensed in the USA (380°C) and in Germany (410°C);
  • Various design approaches were used: higher SF storage temperatures required an inert gas atmosphere (e.g. Germany, USA) while low storage temperatures allowed SF storage in air (e.g. Canada);
  • In all operational applications, no significant SF degradation in storage had been observed; a few indications of krypton release had been observed indicating possible individual SF rod failures, however, these suspected SFA had not been examined to confirm the failures.
– Zr-l%Nb clad SF:
  • Inert gas SF storage was feasible;
  • Maximum SF cladding temperature of 350°C was licensed for inert gas;
  • Dual purpose SF casks constituted the preferred design approach in the USSR;
  • One successful demonstration using intact SF with the cladding temperature of 340°C had already been performed.
– Stainless steel clad (water reactor) SF:
  • No systematic SF storage experience was available.
– Stainless steel/oxide (gas cooled reactor) SF:
  • Dry storage was being investigated for AGR SF.

– Magnox SF:
  • Dry storage of Magnox SF had been licensed in the UK (CO_2 or air depending on SF temperature) and in Italy (nitrogen).
– Aluminium clad SF:
  • Limited experience existed of inert gas storage for aluminium clad SF at ambient temperature.

Dry storage was becoming widely used as a supplement to wet storage for zirconium alloy clad oxide SF. SF storage periods as long as under wet conditions appeared to be feasible. Dry storage would also continue to be used for aluminium clad and Magnox type SF.

The final report on BEFAST-II entitled "Extended storage of spent fuel" was published as IAEA-TECDOC-673 in October 1992 [3] and presents the results on SF wet and dry storage technologies obtained from 16 institutes from 13 countries (Argentina, Canada, Finland, Germany, Hungary, Italy, Japan, the Republic of Korea, Sweden, the UK, the USA and the USSR) participating in the CRP from 1986–1991.

On completion of the BEFAST-II CRP it was appropriate to consider future activities in the field of extended SF storage. A note was prepared during the final RCM in March 1991 suggesting the formation of a new five year CRP BEFAST-III (1992–1996).

2.3. BEFAST-III (1991–1996)

At the beginning of the nineties, with essentially the same context as in the mid-Eighties, considerable quantities of SF were continuously be produced and accumulated. Although some new reprocessing facilities had been constructed, many countries were investigating the option of extended SF storage prior to reprocessing or disposal. At the time SF wet storage continued to predominate as an established technology, however, SF dry storage was increasingly used and many countries were considering SF dry storage for the longer term.

In 1991 the third and final cycle or phase of the IAEA CRP on the Behaviour of Spent Fuel Assemblies during Extended Storage, BEFAST-III, was initiated with the participation of 16 organizations representing 13 countries (Canada, Finland, France, Germany, Hungary, Japan, the Republic of Korea, the Russian Federation, Slovakia, Spain, Sweden, the UK and the USA). The first RCM was held in October 1992 in Toronto, Canada and the third (and final) meeting was held in October 1995 in Paris, France.

The objectives of BEFAST-III were to collect and exchange SF storage experience of participating countries to build a comprehensive international database and to carry out research work which would evaluate the storage of spent fuel for extremely long — currently defined as long term — periods of time (more than 50 years). The scope of this CRP included both wet and dry storage for all types of SF from power reactors.

The three major topics were, as in the case of BEFAST-II, (a) long term behaviour, (b) surveillance, and (c) facilities & operation, with the respective associated research subjects shown below:

(a) Long term behaviour: validation (experiments or experience);
(b) Surveillance: monitoring (environment, components, fuel assemblies, workers dose rate), fuel conditions (operational, fabrication, technology, defective fuel rods and assemblies), different reactor types;
(c) Facilities and operation: changing modes (wet–dry), handling of heavily damaged fuel, system performance.

For power reactor SF wet storage the burnup ranged from 4 $GW \cdot d \cdot t^{-1}$ U ($U_{nat}O_2$/zircaloy, CANDU, Canada and U_{nat}/magnesium alloy, Magnox, Japan) to 60 $GW \cdot d \cdot t^{-1}$ U ($(U,Pu)O_2$/stainless steel,

BN-600, Russian Federation) and SF wet storage residence time ranged from 1 year (U_{nat}/magnesium alloy, Magnox, Japan) to 32 years (UO_2/Zry-2, LWR/PHWR, Sweden).

For power reactor SF dry storage the burnup ranged from 4.5 GW·d·t^{-1} U (U_{nat}/magnesium alloy, Magnox, UK) to 35 GW·d·t^{-1} U ($U_{enr}O_2$/zircaloy, PWR, USA) and SF dry storage residence time ranged from less than 1–19 years ($U_{nat}O_2$/Zry-4, CANDU, Canada).

The conclusions of BEFAST-III were:

– The batch average bumup of PWR and BWR reloads was steadily increasing in the last decade from 40 GW·d·t-1 U towards 50 GW·d·t-1 U in most of the countries participating in the BEFAST CRPs. It was stated that "burnup increase results in: an increase in fuel rod internal pressure at the end of the service life; more zirconium alloy cladding corrosion due to longer in-service residence time; and an increase in the cladding hydrogen concentration resulting from the increased zircaloy corrosion".
– It was also stated that "Increased EOL pressure together with more corrosion results in increased stresses in the spent fuel rod cladding wall. It was concluded that this has no major consequences during wet storage. It has also been shown that under dry storage conditions for LWR fuel in an inert atmosphere, the increased burnup has had no major consequences for spent fuel storage performance so far".
– After 14 years cooperation under the IAEA umbrella, the fundamental R&D questions had been largely answered to the degree that licensing of both wet and dry storage was possible at the time in most countries requiring additional SF storage facilities.
– The key objectives of SF storage related R&D had changed over the years: less effort was required to solve the basic material science questions; work was at the time more focused on technological as well as on economical improvements in SF storage; these changes indicated that SF storage was a mature technology in the back end of fuel cycle.
– The effects of extended burnup on the behaviour of the SF in storage conditions needed to be assessed since there was a tendency in the Member States to achieve increasingly higher burnups.
– Although there was positive SF storage experience at the time, the extrapolation of those results for very long — currently defined as long term — storage times (>50 years, exceeding the periods covered by the CRP) had to be confirmed.

The final report on BEFAST-III entitled "Further Analysis of Extended Storage of Spent Fuel" was published as IAEA-TECDOC-944 in May 1997 [4] and contains analysis of SF wet and dry storage technologies obtained from 16 organizations representing 13 countries (Canada, Finland, France, Germany, Hungary, Japan, the Republic of Korea, the Russian Federation, Slovakia, Spain, Sweden, the UK and the USA) which contributed to the CRP as participants or observers.

3. SPAR (SPENT FUEL PERFORMANCE ASSESSMENT AND RESEARCH)

3.1. SPAR-I (1997–2001)

In 1997, twenty years after the initial discussions on BEFAST, the first cycle or phase of the IAEA CRP on "Spent fuel performance assessment and research", from now on SPAR, was initiated.

The SPAR CRP involved 11 organisations from 10 countries (Canada, France, Germany, Hungary, Japan, the Republic of Korea, the Russian Federation, Spain, Sweden, the UK and the USA). In addition Sweden participated in the CRP as an observer. The first RCM was held in April 1998 in Washington, D.C. and the third and final meeting was held in October 2001 in Córdoba, Spain.

The overall objectives of the SPAR CRP were:

(1) To carry out research work to evaluate the technical basis for storing SF for *extended* — currently defined as *long term* — periods of time, i.e. more than 50 years;
(2) To evaluate and exchange data on SF storage research and experience among the participating countries to build a comprehensive, international database supporting the licensing of present and future technologies;
(3) To assist in defining how the requirements for SF storage and the whole fuel cycle backend are connected;
(4) To exchange operating experience in SF storage.

Furthermore, the specific objective of the SPAR CRP was to identify materials issues in long term SF storage facilities.

The rapid evolution of dry storage technology, the increasing burnups, the new fuel materials and designs and the *extremely long* — currently defined as *long term* — periods of time (more than 50 years) were addressed along the progress of this CRP.

The results were not presented in the form used for BEFAST final reports because an approach of compliance of results and objectives by project was adopted, most project objectives were fulfilled and no general conclusions on the overall objectives were synthesized.

The final report on SPAR-I entitled "Spent Fuel Performance Assessment and Research" was published as IAEA-TECDOC-1343 in March 2003 [5].

3.2. SPAR-II (2004–2008)

As of the beginning of 2008 most of the SF discharged from nuclear power reactors was under water, but dry storage was becoming a widely used technology with more than 25 000 t HM stored in various countries. In the future, SF storage capacity needs would continue to increase and some of these fuels would have to be stored for 50 years or more, before their reprocessing or final disposal could takes place. As a result, interim storage for long periods of time would continue to be a key technology for all Member States.

At the beginning of the 21st century the rapid evolution of dry storage technology, new fuel and material design changes and steadily increased target burnups (60 GW·d·t^{-1} U, 33 GW·d·t^{-1} U and 10 GW·d·t^{-1} U in LWR, GCR and CANDU, respectively) had shown that some SF would have to be stored for extremely long — currently considered as very long term — periods of time (100 years and beyond).

The second cycle or phase of the IAEA Spent Fuel Performance Assessment and Research (SPAR-II) CRP (2004–2008) involved the European Commission as well as 13 other organizations from 12 countries (Argentina (joined later), Canada, France, Germany, Hungary, Japan, the Republic of Korea (only for a limited period), Slovakia, Spain, Sweden, the UK, and the USA). Sweden and the UK participated in the CRP as active observers. The first RCM was held in June 2005 in Karlsruhe, Germany and the third (and final) in June 2008 in Hungary. The overall objective of the SPAR-II CRP was to develop a technical knowledge base on long term storage of power reactor SF through evaluation of operating experience and research by participating Member States.

Specific research objectives included:

– Fuel and materials performance evaluation under wet and dry storage;
– Monitoring programs of spent fuel storage facilities;
– Collection and exchange of relevant spent fuel storage experience of the participating countries.

As it was the case for the SPAR-I final report the results were presented under an approach of compliance of results and objectives by project, most project objectives were fulfilled and no general conclusions on the overall objectives were synthesized. The final report on SPAR-II entitled "Spent

fuel performance assessment and research" was sent to the publication committee in December 2010 [6].

3.3. SPAR-III (2009–2013)

The third (and last) cycle of phase of the SPAR CRP deals with research of SF and storage materials behaviour over *long* — currently considered *very long* — term storage (100 years and potentially more). Programs carried out so far (BEFAST-I to -III and SPAR-I and -II) have identified some potential deterioration mechanisms of spent fuel elements that required detailed investigation. Investigations of these mechanisms indicate unlikely impact of most of them on spent fuel integrity over storage periods. There are still impacts of some deterioration mechanisms that have to be investigated over long time periods (i.e. hydrogen effects on fuel elements) and countries that participated in SPAR-II continue this research. In addition, behaviour and impact on these mechanisms under transportation and some extreme conditions need to be investigated. Surveillance and monitoring results of spent fuel in storage are important inputs in assessing spent fuel performance in storage. The long term objective of spent fuel integrity is to keep all future spent fuel management options open [7].

Dry storage technologies have rapidly evolved to technical maturity, new fuel and material design changes continue to be introduced and target burnups continue to rise albeit at a reduced rate, spent fuel will have to be stored for extremely long periods of time e.g. for up to 100 years and beyond

The two overall objectives of SPAR-III are:

– To develop a technical knowledge base on long term storage of spent fuel from nuclear power reactors through evaluation of operating experience and research;
– To extrapolate predictions of spent fuel behaviour over long periods of time.

The six specific objectives relate to:

(i) Fuel and materials performance evaluation under wet and dry storage and assessment of impact of interim storage on associated spent fuel management activities (like handling and transport);
(ii) Surveillance and monitoring programs of spent fuel storage facilities as one of the means to evaluate spent fuel performance during storage;
(iii) Collection and exchange of relevant experience of spent fuel storage and the impact on associated spent fuel management activities;
(iv) Facilitate transfer of knowledge by documenting technical basis for spent fuel storage;
(v) Creating a synergy among research projects within the CRP;
(vi) Developing capability to assess the impact of potential deterioration mechanisms on fuel.

The expected output is the final report to be published at the end of the CRP cycle.

The expected outcomes relate to:

(i) A survey of research activities accessible to stakeholders of spent fuel storage facilities (e.g. for reference, performing analyses or supporting licensing and re-licensing of spent fuel storage facilities);
(ii) Surveillance and monitoring results from wet and dry storage facilities;
(iii) Operating experience from wet and dry spent fuel storage;
(iv) Results from surveillance and monitoring programs;
(v) Updated assessment of spent fuel integrity during long term storage;
(vi) Country specific clarification of how the specifications for subsequent conditioning for reprocessing and/or disposal impact spent fuel storage requirements will be developed.

The first RCM was held in Tokyo, Japan in November 2010 to collect research results and national updates and to outline plans for future investigations. The meeting was attended by representatives of the nine countries (Argentina, France, Germany, Hungary, Japan, the Republic of Korea, Slovakia, Spain and the USA) and the international organization (European Commission) who participate in the CRP. It was tentatively decided to hold the second RCM in May 2012 in Charlotte, USA, hosted by the Electrical Power Research Institute (EPRI).

The third cycle or phase of the CRP Spent Fuel Performance Assessment and Research (SPAR-III), CRP code T13013, is active from November 2009 to November 2013.

REFERENCES

[1] INTERNATIONAL ATOMIC ENERGY AGENCY, Behaviour of Spent Fuel Assemblies During Extended Storage, IAEA-TECDOC-414, IAEA, Vienna (1987).

[2] INTERNATIONAL ATOMIC ENERGY AGENCY, Storage of Spent Fuel, IAEA Safety Standards Series SSG-15, IAEA, Vienna (2012).

[3] INTERNATIONAL ATOMIC ENERGY AGENCY, Extended Storage of Spent Fuel, IAEA-TECDOC-673, IAEA, Vienna (1992).

[4] INTERNATIONAL ATOMIC ENERGY AGENCY, Further Analysis of Extended Storage of Spent Fuel, IAEA-TECDOC-944, IAEA, Vienna (1997).

[5] INTERNATIONAL ATOMIC ENERGY AGENCY, Spent Fuel Performance Assessment and Research, IAEA-TECDOC-1343, IAEA, Vienna (2003).

[6] INTERNATIONAL ATOMIC ENERGY AGENCY, Spent Fuel Performance Assessment and Research, IAEA-TECDOC-1680, IAEA, Vienna (2012).

[7] INTERNATIONAL ATOMIC ENERGY AGENCY, INES The International Nuclear and Radiological Event Scale User's Manual, 2008 Edition, IAEA, Vienna (2009).

[9] INTERNATIONAL ATOMIC ENERGY AGENCY, Storage of Water Reactor Fuel in Water Pools: Survey of World Experience, Technical Reports Series No. 218, IAEA, Vienna (1982).

[10] INTERNATIONAL ATOMIC ENERGY AGENCY, Guidebook on Spent Fuel Storage, Technical Reports Series No. 240, IAEA, Vienna (1984).

DEVELOPMENT OF A SET-UP FOR THE DETECTION OF FAILED FUELS IN TAPS BWR SPENT FUEL STORAGE BAY

J.L. SINGH, N. KUMAWAT
Post-irradiation Examination Division
Nuclear Fuels Group
BARC
Email: jlsss@barc.gov.in

A.K. SINHA, S. BHAT
Centre for Design and Manufacture
Design Manufacture and Automation
BARC

K. JAYARAJAN, C. DEY
Division for Remote Handling and Robotics Design
Manufacture and Automation
BARC

Mumbai, India

Abstract

Detecting failed fuel elements in the leaky fuel assemblies during poolside examination is of great help in monitoring BWR fuel performance and selection of fuel elements for detailed post-irradiation examination. Water enters inside the fuel pin through the breach in the zircaloy clad. Presence of water inside a fuel pin confirms clad/weld failure. Detection of presence of water by non-destructive method helps in identifying the failed fuel pin without dismantling the fuel assembly. Ultrasonic testing technique using wafer probes in transmit and receive mode, has been developed to identify failed fuel pins by detecting presence of water inside the fuel rod.

1. INTRODUCTION

Failed fuel detection methods used in the early stages of the nuclear industry concentrated on the release of the fission products into the coolant. The continuous surveillance of coolant activity levels and effluent release rates were the means of detecting fuel failures. The off-gas system was used for gamma spectrometer monitoring to identify the quantities of Xe and Kr isotopes during reactor operation. Instead of water detection some researchers had tried to use the internal gas pressure in the rod as the measure of its integrity. The gas pressure is calculated from the gamma radiation emitted by Kr^{85}, one of the fission products accumulated inside the fuel rod. For boiling water reactors (BWRs), sipping is done at the reactor site to detect assembly having failed fuel rods.

Ultrasonic testing techniques have been used to detect presence of water inside the fuel pin world over from the late 1970s. It is based mainly on attenuation of ultrasonic wave energy due to water coupling available inside the fuel pin. The different working groups worldwide have tried either pulse-echo [1] or transmit/receive method and patented their technique. Both the techniques monitor attenuation suffered by ultrasonic beam due to water coupling on the internal diameter (ID) surface of the clad. Pulse-echo uses single transducer while pitch-catch has separate transmitter and receiver. It is difficult to maintain the same geometry of beam alignment which affects reliability during scanning [2]. In our laboratory we have tried both pulse-echo and pitch-catch techniques on individual pins. Two wafer thin probes in pitch catch mode have been developed to be used to identify the failed rod in the storage pool without dismantling the fuel assembly. This paper discusses the problems associated with the testing geometry, weak signal strength and various approaches to enhance the reliability of failed fuel detection technique.

2. DESCRIPTION OF FUEL ASSEMBLY

The nuclear power station at Tarapur, consists of two boiling water reactors of 200 MW(e) each. The fuel used in the reactors is enriched cylindrical UO_2 pellets, which is enclosed in zircaloy-2 cladding tube of 14.3 mm outer diameter and 0.89 mm wall thickness. The ends of the ~4 meter long fuel element is sealed by zircaloy-2 end plugs welded to the cladding tube by inert gas welding. A fission gas plenum is provided at the upper end of the element, the plenum being maintained with a wire spring. Helium is used as filler gas in the element.

Each TAPS fuel assembly consists of 36 fuel elements arranged in a 6 6 square array. The different fuel elements in the assembly are held together by two stainless steel tie plates, one on either end of the assembly. The fuel elements in the assembly are spaced from each other by seven spacer grids, the distance between two adjacent grids being 48.8 cm along the length of the assembly. The fuel assemblies are held vertically in the reactor core. There are 284 fuel assemblies in the reactor core.

3. CONCEPT OF ULTRASONIC TESTING

In case of a fuel rod failure, water enters inside through the breach in either the weld or clad wall. Water entering inside through the same leak finally settles down near the bottom plug in a vertically standing fuel pin. These fuel assemblies are kept under water inside storage pool where water may again penetrate through the site of clad breach. Presence of water inside a fuel rod confirms clad/weld failure and forms the basis to identifying the failed rod.

The presence of water in the gap between pellet and clad provides coupling for the ultrasonic waves to get transmitted to the pellets. Transmitted part of the ultrasonic energy gets absorbed in the pellets and does not reach the receiver probe. The lost ultrasonic energy is seen as the attenuation of the received beam from the clad ID surface in the ultrasonic signal. An intact fuel pin will have gases inside therefore, ultrasonic waves do not get transmitted to the pellets resulting in total reflection from the ID surface.

4. PULSE-ECHO METHOD OF TESTING

In pulse-echo mode an ultrasonic pulse is sent from outer diameter (OD) side to the cladding wall using a single transducer and a number of back wall echoes are obtained on the CRT. A single focused normal probe sends ultrasonic beam to the fuel pin OD surface to produce multiple back echo pattern from a sound fuel pin shown in Figs 4.1–4.2. An attenuated reflection pattern of back wall echoes is seen in case of a failed pin because of partial transmission of ultrasonic energy at ID surface. Transmission takes place through the water coupling in the gap between clad and pellet. A small fraction of ultrasonic energy (~1 dB) is transmitted to the pellets which does not come back to the probe. The attenuation ~1 dB per trip in the clad wall is too less compared to the attenuation arising due to misalignment of the probe.

5. PITCH-CATCH METHOD OF TESTING

Two wafer thin probes are placed opposite each other in pitch-catch method of testing. The wafer probes pair which can go inside the BWR fuel assembly to detect the failed rod is shown in Fig. 5.1. Three pairs of wafer probes fixed at the end of two stainless steel blades and three more pairs in staggered position are used for the testing of all the fuel pins in the assembly. The six pairs of probes are inserted inside the fuel assembly at a height nearly 25 mm from the bottom plug weld.

Water available in the pool couples the ultrasonic transducers from OD side of the fuel rod. The encoder based movement controller inserts the probe to the precalculated offset position on the first row of the fuel elements. The signal is shown in Fig. 5.2 for sound fuel rod. The amplitude of the

signal in the gate goes down below the threshold in case of failed rod. The pitch-catch technique provides higher reliability of detection of failed fuel rod as there is 8–10 dB difference in signal strength. A similar situation is obtained on the other side offset of the same fuel rod.

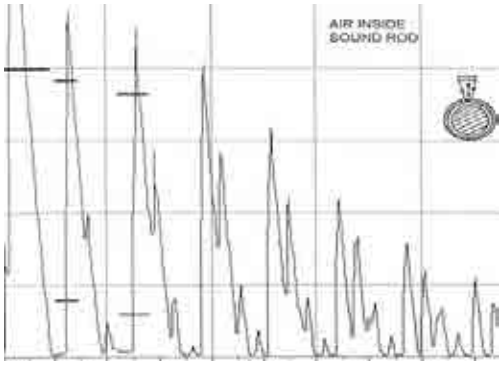

FIG. 4.1. Multiple pulse-echo back wall pattern.

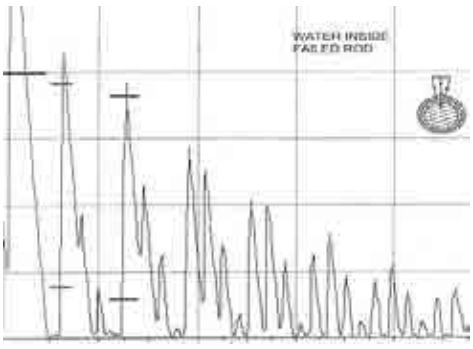

FIG. 4.2. Attenuated back wall decay pattern.

FIG. 5.1. 100% signal for sound fuel rod.

FIG. 5.2. Signal reduced for failed fuel rod.

All the fuel elements are examined in a fuel assembly till the defective rod is identified. The signal is rechecked while reversing the probe out of the fuel assembly.

6. CONCLUSION

Both pulse-echo and pitch-catch techniques were tried in our laboratory and the results were compared. The single probe pulse-echo technique was prone to misalignment problem.

It was found that the pitch-catch technique has higher signal to noise ratio. Trials have been taken to demonstrate the technical feasibility and reliability of pitch-catch mode of testing to detect failed fuel elements without dismantling the fuel assembly.

Remotely operable gadgets for reconstitution have been tried on a dummy fuel assembly.

REFERENCES

[1] MACHADO, J.C., THOMÉ, Z.D., XAVIER, A.J., SOARES, J.C.A.C.R., An ultrasonic probe for NDT inspection of fuel assembly used in nuclear power plant reactors, Proceedings of 15th World Conference on Non-Destructive Testing, Rome (2000) Paper idn007.

[2] PEREIRA, W.C.A., THOMÉ, Z.D., SEIXAS, J.M., BOSSAN, M.C., Ultrasonic pulse-echo method for failed rod detection based on neural network, Proceedings of 15th World Conference on Non-Destructive Testing, Rome (2000) Paper idn008.

ESTABLISHMENT OF THE DISASSEMBLING TECHNIQUE OF THE DRIVER FUEL ASSEMBLY IRRADIATED IN JOYO

S. ICHIKAWA, H. HAGA, K. KATSUYAMA, K. MAEDA, T. NAGAMINE
Japan Atomic Energy Agency
Ibaraki-ken, Japan
Email: ichikawa.shoichi@jaea.go.jp

Abstract

A disassembling technique for the JOYO driver fuel assembly has been established at the Fuel Monitoring Facility in JAEA. This technique made it possible to remove the fuel pins from the driver fuel assembly without fuel pin sectioning. After disassembling, some selected fuel pins can be reassembled into a new irradiation vehicle for continuous irradiation in JOYO. This technique allows the irradiation data of high burnup fuel and high neutron dose material to be obtained.

1. INTRODUCTION

In the fast reactor cycle technology development project (FaCT Project), development of fuel corresponding to high burnup is one of the important issues, and for this it is necessary to obtain the irradiation data of high burnup fuel and high neutron dose material. To obtain these irradiated data, it is very effective to irradiate the fuel pins irradiated in the experimental fast reactor JOYO again. But re-irradiation is very difficult due to the relationship between the structure of the driver fuel assembly and the conventional disassembling technique. Therefore, a new disassembling technique of the driver fuel assembly was established so that the re-irradiation of the fuel pins irradiated in JOYO might become possible.

2. CONSIDERATION OF DISASSEMBLING TECHNIQUE

2.1. Conventional disassembling technique

Figure 2.1 shows the fixation method of fuel pins and the conventional disassembling technique used in the Fuel Monitoring Facility (FMF). The JOYO driver fuel assembly is composed of 127 fuel pins, and these fuel pins are arranged in 13 rows. In the fuel pin structure, a piercing hole is opened in the end-plug of the fuel pin, and two knock-bars (upper knock-bar, lower knock-bar) are inserted in the piercing hole to fix each row in place. Both ends of the knock-bars are welded with the B side and F side or the C side and E side of the wrapper tube.

The conventional disassembling technique procedure used in the FMF is as follows. The six sides of the wrapper tube are cut in an end-mill, and the wrapper tube is pulled out. The row of fuel pins is separately cut by a band-saw. The cut is made 5mm from the upper knock-bar.

2.2. Irradiation vehicle

There are several kinds of irradiation vehicles in JOYO and the choice is made by considering the irradiation conditions and purpose, etc. The irradiation vehicle used for re-irradiation will be a capsule type, the uninstrumented fuel irradiation subassembly type-B (UNIS-B). The use of the capsule type UNIS-B is considered as a countermeasure for possible fuel failure during irradiation. Figure 2.2 shows the method of loading the fuel pins to the UNIS-B. The fuel pins are put in a three-part container consisting of a shroud tube, a capsule, and a compartment, and the container is loaded into the UNIS-B. When the fuel pin is loaded into the shroud tube, the fuel pin is fixed by the support spring through the piecing hole of the lower end-plug. Threfore, it is necessary to leave the lower end-plug of fuel pin in place when disassembling the driver fuel assembly if the irradiated fuel pin is to be irradiated again.

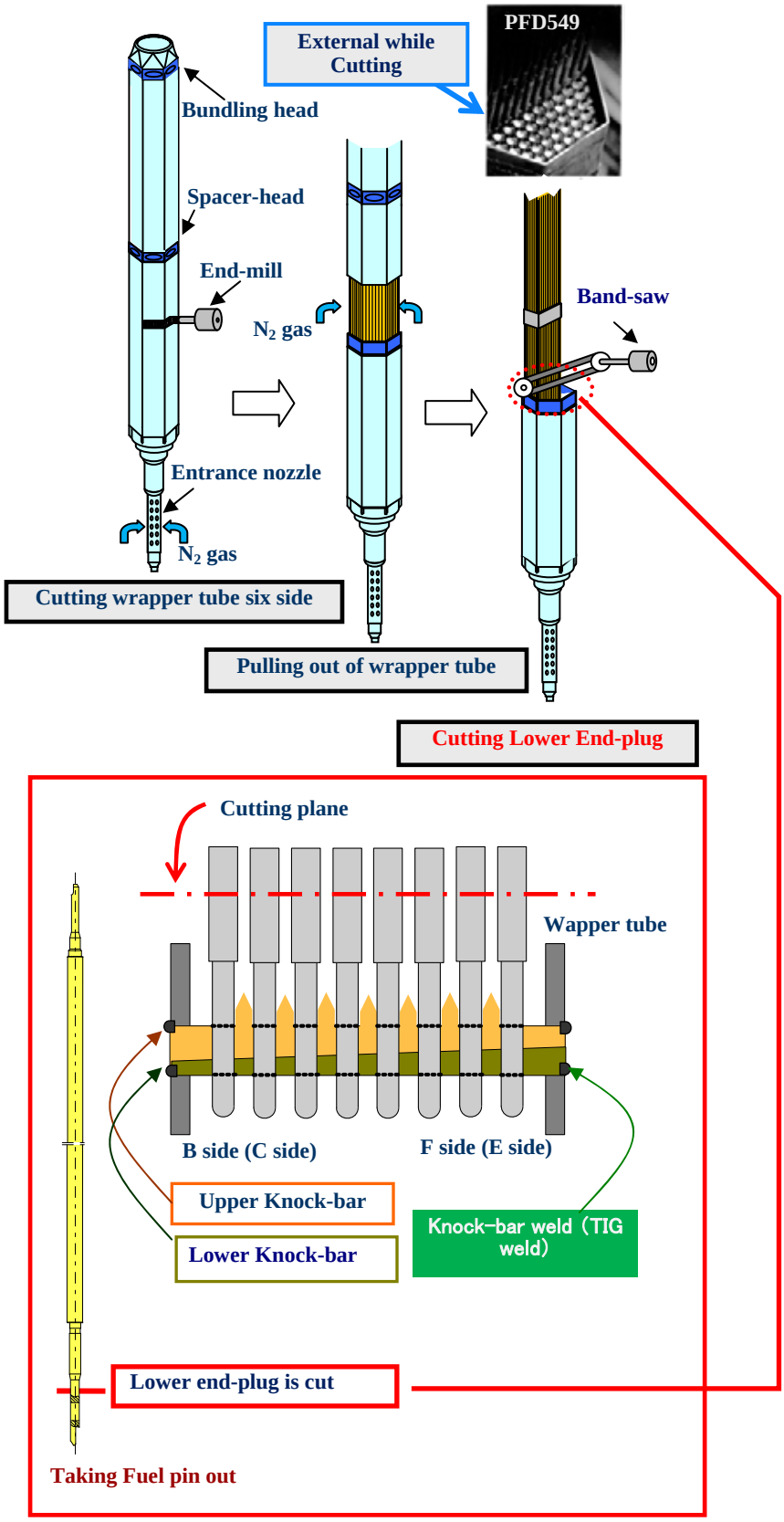

FIG. 2.1. Conventional disassembling technique.

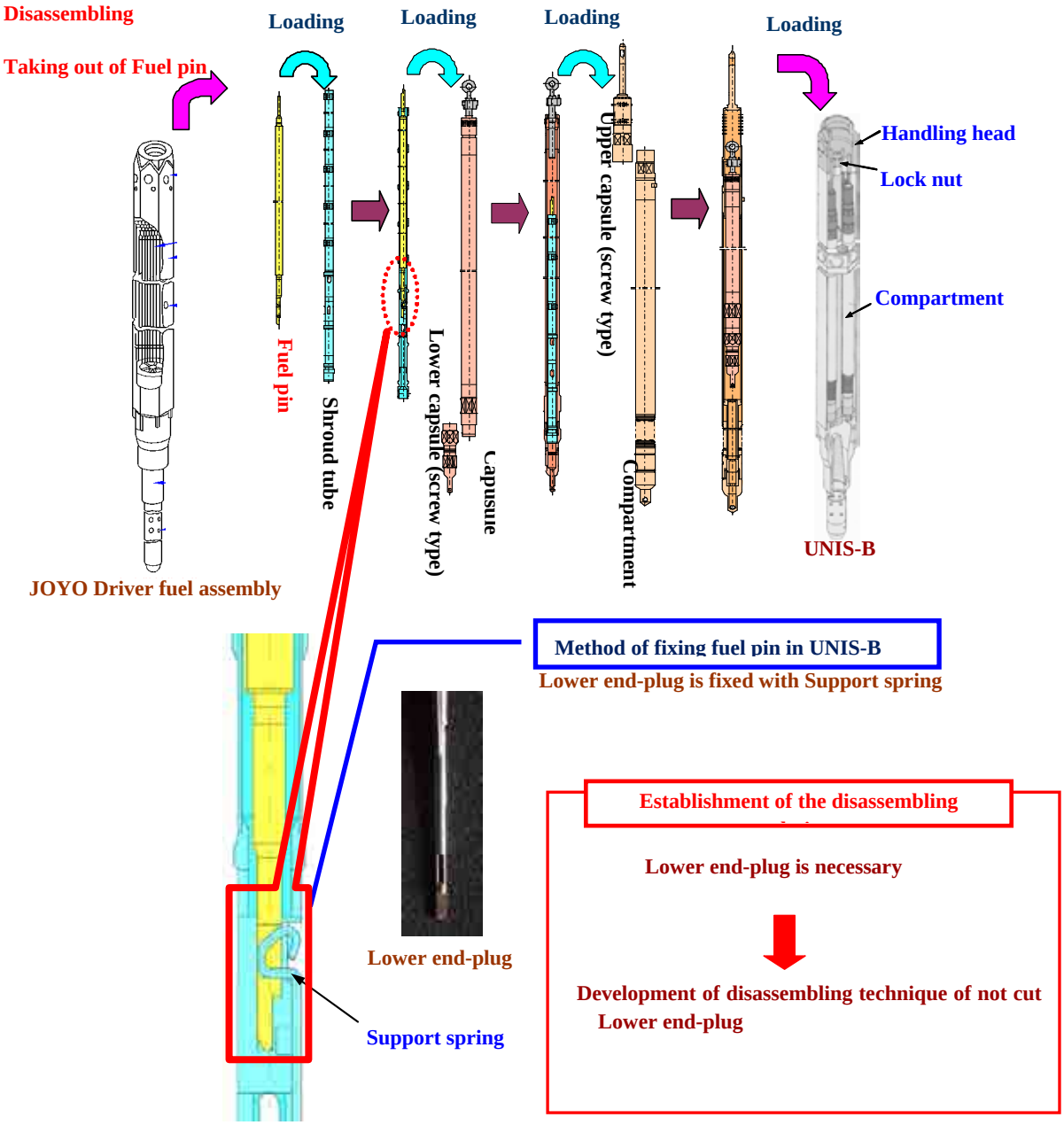

FIG. 2.2. Method for loading UNIS-B.

2.3. Establishment of the disassembling technique

The newly designed disassembling technique is shown in Fig. 2.3. The work consists of cutting knock-bar weld and taking out the knock-bar. The weld of the wrapper tube and the knock-bar to the fuel pin is cut by the end-mill separately. The knock-bar is taken out with a newly developed extrusion tool. This method does not cut the lower end-plugs of the fuel pins. Moreover, the shape, etc. of the extrusion tool was devised to allow for remote operability in all work.

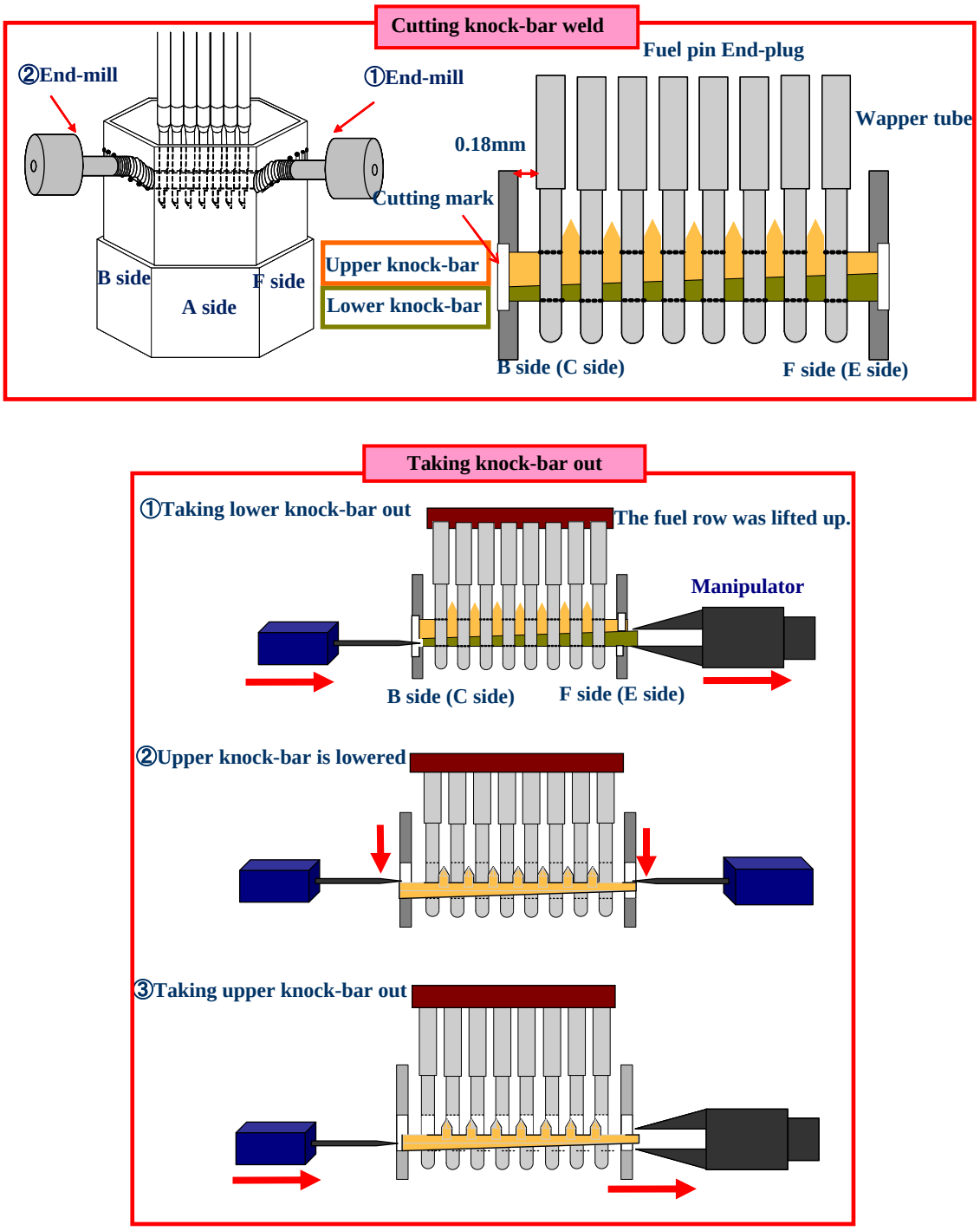

FIG. 2.3. Caption correction work procedure.

3. APPLICATION TO JOYO DRIVER FUEL ASSEMBLY

3.1. Outline of the JOYO driver fuel assembly

This disassembling technique was applied to the JOYO MK-Ⅱ driver fuel assembly. The irradiation conditions of this driver fuel assembly were as follows:

– Burnup:
  - Average: 6.09×10^4 MW·d·t^{-1}
  - Max: 9.49×10^4 MW·d·t^{-1}
– Fluence: 8.83×10^{22} n·cm^{-2} (E>0.1 MeV)

Moreover, this driver fuel assembly had been kept in water for about 17 years after irradiation. After disassembling, part of the fuel pins taken will be provided for the re-irradiation test and part for the post-irradiation examination (PIE).

3.2. X ray computer tomography observation

As for the structure of the driver fuel assembly, the space between the wrapper tube and the lower end-plug is very narrow. Therefore, it is necessary to know the internal situation. Then, the driver fuel assembly was observed by X ray computer tomography (XCT) before disassembling. Figs 3.1–3.2 show the XCT image of the driver fuel assembly. As a result, it was confirmed that neither the fuel pin lower end-plug nor the knock-bar were changed by the irradiation. Moreover, it was confirmed that there was a space (0.18 mm) between the wrapper tube and the fuel pin lower end-plug. It was judged to be possible to apply this disassembling technique to the driver fuel assembly.

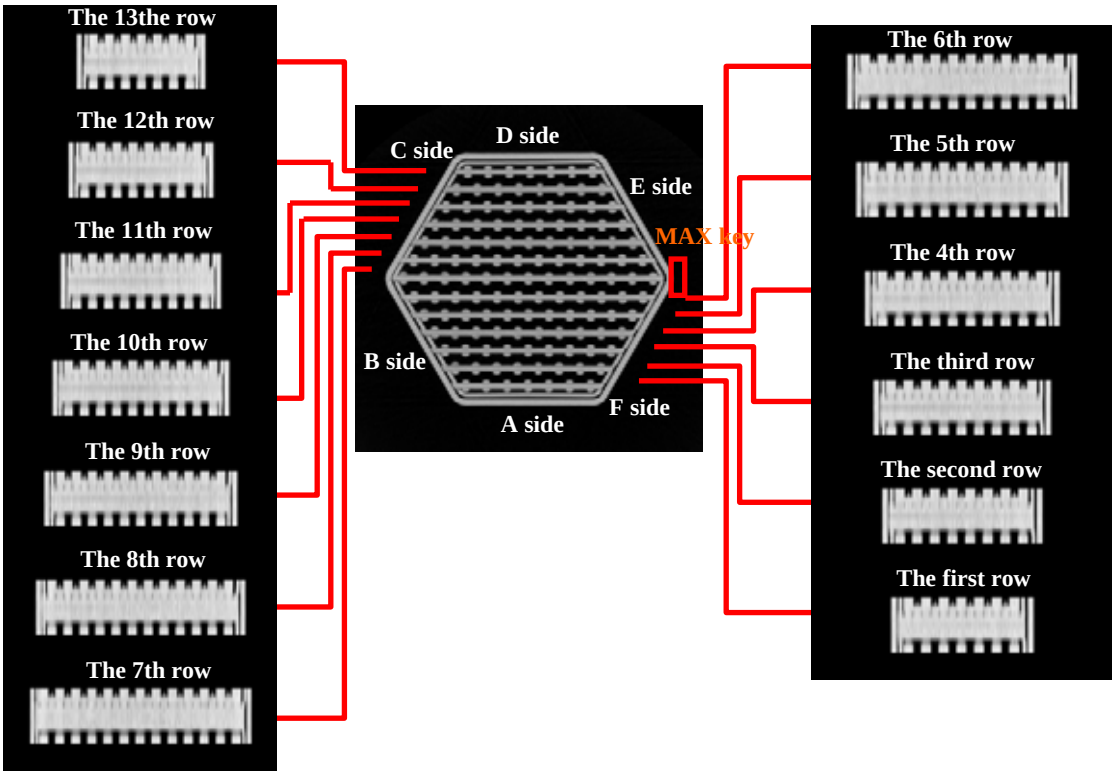

FIG. 3.1. Cross-section observation (range of taking picture: 1249.6–1267.6 mm from bottom of assembly).

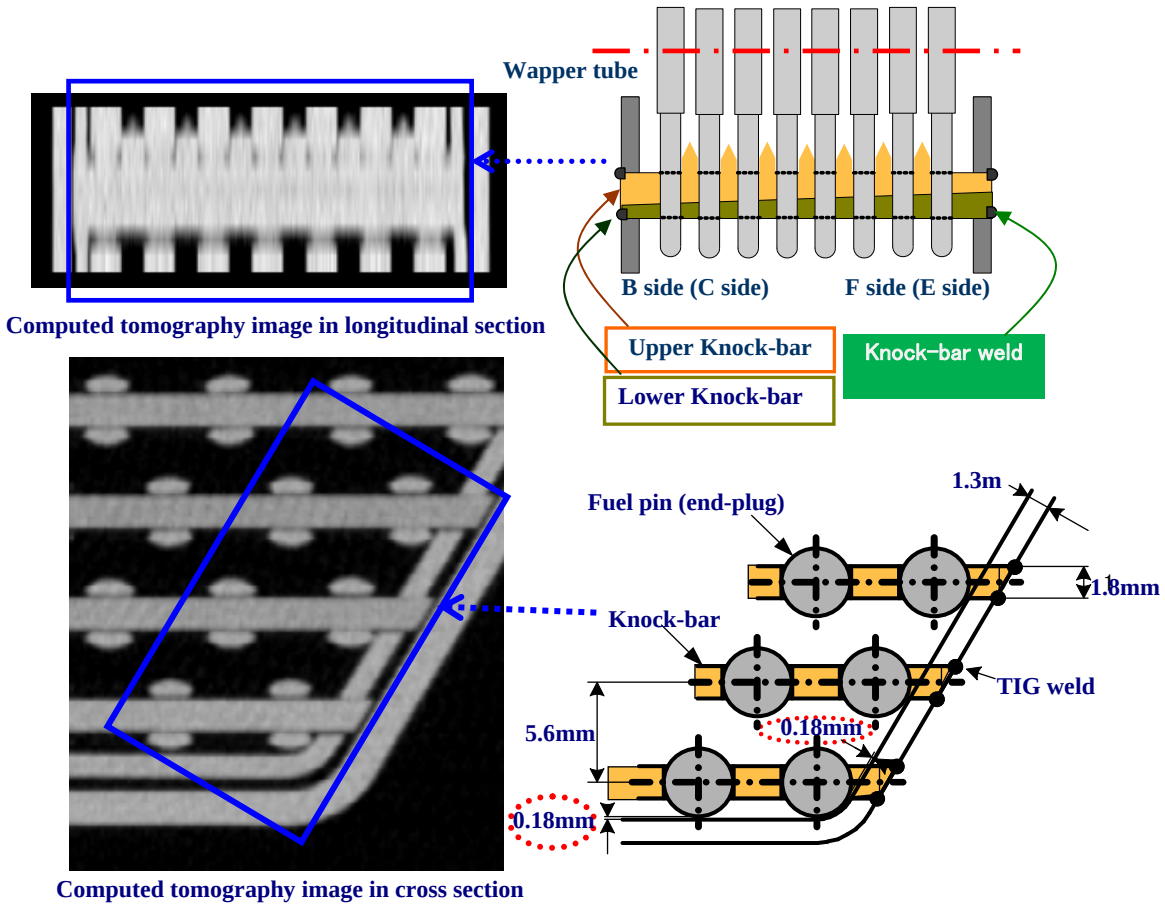

FIG. 3.2. State of the driver fuel assembly.

3.3. Cutting knock-bar weld

Figure 3.3 shows cutting of the knock-bar weld. The knock-bar weld on the wrapper tube (thickness: 1.3 mm) was cut by the end-mill. The cutting conditions of the end-mill were as follows. Max amount of cutting was 0.3 mm per one time, sending speed was 3 mm·s^{-1}, and cutting position was 1.2567 mm from the bottom of the driver fuel assembly. A row of fuel pin was cut separately for each row in order to take out the knock-bar out. Cutting the knock-bar was in the order of the F side and B side then the E side and C side. To avoid touching the fuel pin lower end-plug by the end-mill, the amount of cutting in the end-mill was controlled in detail.

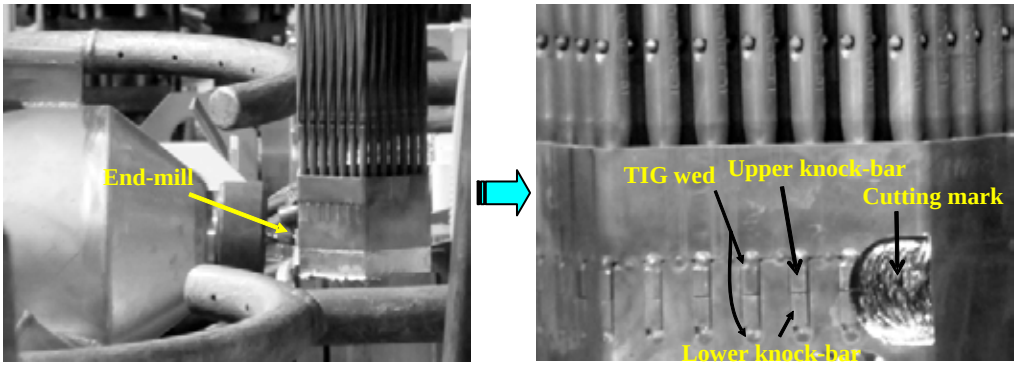

FIG. 3.3. Cutting knock-bar weld.

3.4. Taking the knock-bar out

Figure 3.4 shows taking the knock-bar out. The knock-bar is pushed out of the B side or C side by the extrusion tool, and taken out of the F side or E side by a manipulator. The knock-bar was taken out in the order of lower knock-bar then upper knock-bar. The upper knock-bar was pushed up by the lower knock-bar in a fuel pin row. Therefore, after the low knock-bar had been taken out, the upper knock-bar was lowered to the position of the piercing hole by using the extrusion tool.

Figure 3.5 shows the disassembling procedure of the first row. All fuel pins could be taken out without cutting the lower end plugs. Some of these fuel pins will be loaded to UNIS-B and re-irradiated in JOYO.

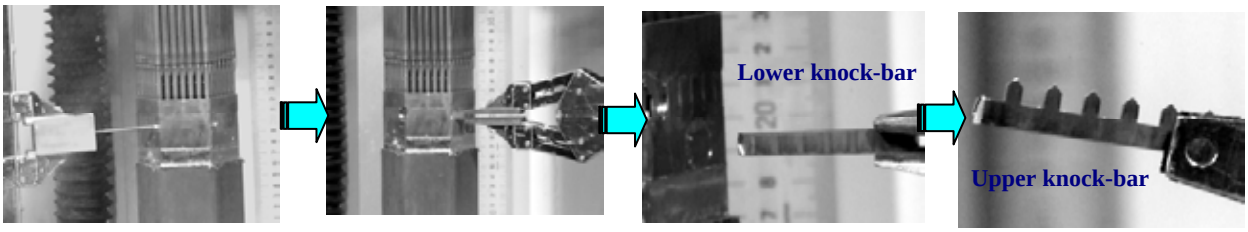

FIG. 3.4. Taking knock-bar out.

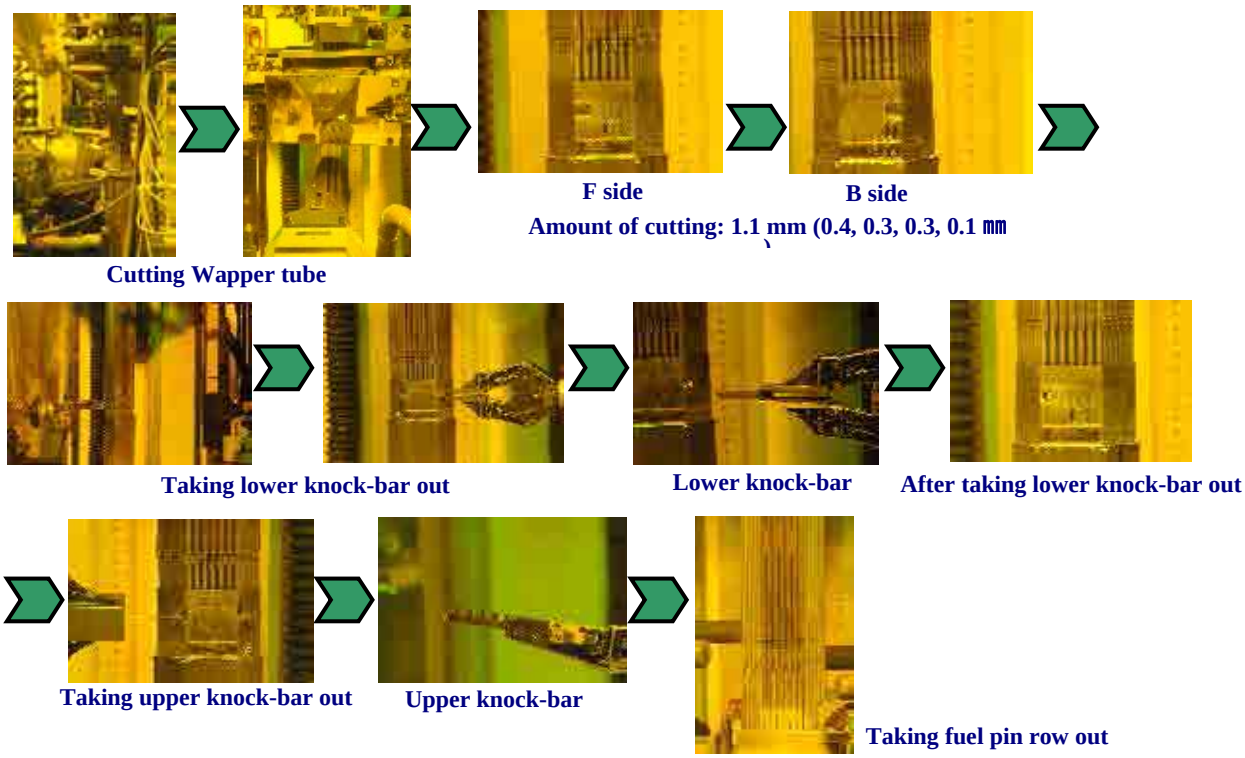

FIG. 3.5. Disassembling procedure of the first row.

4. APPLICATION OF THE DISASSEMBLING TECHNIQUE

This disassembling technique can also be applied to disassembling the uninstrumented fuel irradiation subassembly type-C (UNIS-C). UNIS-C is an irradiation vehicle similar to UNIS-B, and the method of fixing fuel pins in UNIS-C is the same “knock-bar fixation type” as the JOYO driver fuel assembly.

UNIS-C is a double wrapper tube structure, and continuous irradiation of the fuel pins is possible by exchange of the outside wrapper tubes. A further continuous irradiation using UNIS-B becomes possible by applying this disassembling technique after the continuous irradiation of UNIS-C ends.

5. CONCLUSION

The re-irradiation of the fuel pin of the driver fuel assembly (knock-bar fixation type) irradiated in JOYO has become possible. As a result, it will be possible to obtain high burnup fuel for the FaCT Project and to reuse irradiated fuel in JOYO. This disassembling technique can get many fuel pins for the continuous irradiation from the same driver fuel assembly. It will be possible to carry out important irradiation examinations such as the power tomelt (PTM) examination using the previously irradiated pins.

BIBLIOGRAPHY

[1] JAPAN ATOMIC ENERGY AGENCY, Irradiation Center User Guide, Japan Nuclear Cycle Development Institute (2000).

REASSEMBLING PROCEDURE OF THE FUEL ASSEMBLIES FOR THE NUCLEAR POWER SHIP “MUTSU”

H. MATSUI, N. KAMINAGA
Department of Hot Laboratories and Facilities
Japan Atomic Energy Agency
Tokai
Email: matsui.hiroki@jaea.go.jp

K. KITAHARA
Mutsu Office
Aomori Research and Development Center
Japan Atomic Energy Agency
Mutsu City

Japan

Abstract

Japan’s first voyage utilized by nuclear power was made by the nuclear powered ship "Mutsu" in 1990. After a research voyage in 1992, decommissioning work of the nuclear reactor for “Mutsu” was started to change it from the nuclear power ship to an ordinary power ship. Thirty-four irradiated fuel assemblies of “Mutsu” were removed from the reactor and transported to the Reactor Fuel Examination Facility (RFEF) in Nuclear Science Research Institute (NSRI) of Japan Atomic Energy Agency (JAEA). “Mutsu” fuel assemblies were loaded into a hot cell of RFEF using the roof gate as the top loading procedure. After the reliability confirmation tests, fuel assemblies were reassembled for reprocessing. To perform the reliability confirmation tests and reassembling, new devices were developed and installed in the hot cells, “Fuel assembly transportation device” for transporting the fuel assemblies between the hot cells, “Upper nozzle cutting device” for removing the upper nozzle from the fuel assembly, “Fuel rod drawing device” for drawing a fuel rod from the fuel assembly and so on. Thirty-four fuel assemblies were reassembled as six PWR type fuel assemblies in order to adjust the acceptable specifications of the reprocessing plant in JAEA: the shape of fuel assembly is the same as the PWR type commercial reactor fuel and the average enrichment of uranium in the assembly is under 4.0%. This paper reports the reassembling techniques of the “Mutsu” irradiated fuel assemblies for reprocessing.

1. INTRODUCTION

The “Mutsu” was built as the first nuclear power ship in Japan. However, the minor leak of neutrons and gamma rays from the reactor pressure vessel occurred during the first stage of the power raising test in the Pacific Ocean. The research voyage of about 82 000 km was made after the repairs of shielding [1]. The decontamination programme for “Mutsu” was started in 1992 after completing the nuclear power ship project. In the decontamination work, the “Mutsu” fuel assemblies were reassembled like power plant fuel assemblies for the reprocessing of the fuel. The reassembling work required for the fuel handling in the reprocessing plant was performed at the Reactor Fuel Examination Facility (RFEF) in Nuclear Science Research Institute (NSRI) of Japan Atomic Energy Agency (JAEA). “Mutsu” fuels were stored in the custom designed casks and transported three turns for thirty-four fuel assemblies by ship from Aomori prefecture to RFEF in Tokai village. Additionally, the handling device and in-cell transportation device were developed in RFEF for reassembling work. The reassembling of these fuels was performed in 2001–2007 and the reassembled fuels were stored in the storage pool in RFEF. After decontamination, the “Mutsu” was rebuilt from the nuclear power ship to an ordinary power ship “Mirai”.

2. SPECIFICATIONS OF “MUTSU” FUEL ASSEMBLY

A marine nuclear reactor was developed in Japan. The reactor type was pressurized water reactor (PWR) with 36 MW in thermal power. Two types of fuel assemblies having the different fuel enrichment, namely A-type: 3.24% and B-type: 4.44%, were loaded in “Mutsu” reactor. The cladding tube was made of stainless steel. The specifications of “Mutsu” fuel assembly are shown in Table 2.1.

TABLE 2.1. SPECIFICATIONS OF “MUTSU” FUEL ASSEMBLY

Total amount of assemblies	34
Total amount of rods	3808
^{235}U enrichment [%]	3.24 and 4.44
UO_2 [kg]	87
Length of assembly [mm]	1,431(L) × 167.7(W) × 167.7(W)
Alignment of rods	11 × 11
Total weight [kg]	Approx. 123

3. DEVELOPMENT OF REASSEMBLING DEVICES

To perform the reassembling work, the new devices were developed and installed in the hot cells. Details of specifications of these devices are described below.

3.1. In-cell transportation device

The aim of the device was to receive the loaded assembly and transport it between hot cells. The assembly was loaded into the cell through a roof gate and transported to the adjacent cell. The device is composed of a receiving basket for holding the assembly and a carrier unit for transportation of the assembly with basket to the adjacent cell, as shown in Fig. 3.1. The carrier unit can be moved by electric power when the other routines are performed in the cell. The carrier moving rollers and frames are made of stainless steel. The assembly can be transported safely and smoothly by this device.

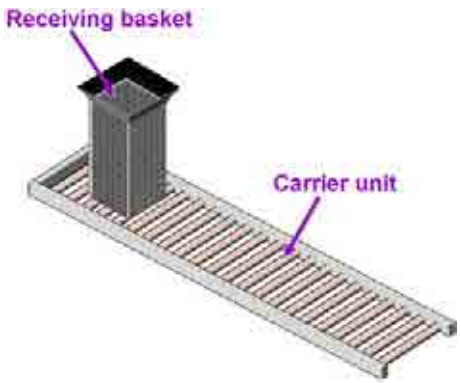

FIG. 3.1. A schematic drawing of the in-cell transportation device.

3.2. The cutting device for upper nozzle

For first step of reassembling procedure, the upper nozzle was unfixed from the assembly for drawing the fuel rods. The skeleton components of the fuel assembly such as the upper and lower nozzles and spacer grids were welded on the side plate of the fuel assembly. Therefore, the upper nozzle had to be

cut away from the side plate. However, the space between the upper nozzle and top of the fuel rods was only 7 mm in distance, which required adjusting the cutting position adequately to avoid doing damage to the fuel rods. The cutting device consists of a cutter head with a driving unit and a chucking device for the fuel assembly. A portable band saw was selected for the cutter head. A schematic drawing of the cutting device is shown in Fig. 3.2.

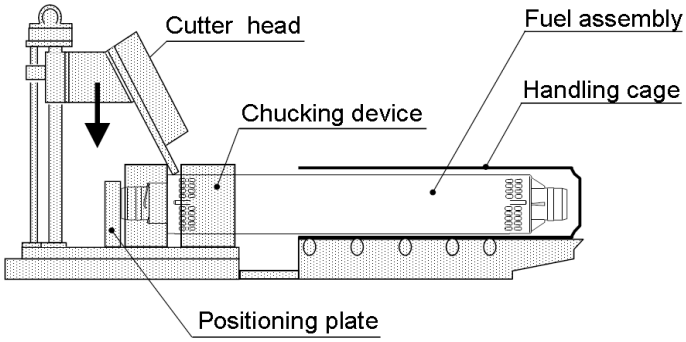

FIG. 3.2. A schematic drawing of the cutting device.

The fuel assembly, which was placed in the handling cage, was laid on the table of the cutting device. The cutting position was adjusted by bringing the top of upper nozzle into contact with the positioning plate which was set on the cutting device. These procedures can make the accurately cutting, because the fuel assemblies were manufactured with high dimensional accuracy. Then, the fuel assembly was clamped by the chucking device. The upper nozzle was cut with the cutter head moving down. After the cutting, the fuel assembly with handling cage was raised up and moved by in-cell crane. Therefore, the upper nozzle could be cut from the fuel assembly quickly and accurately by the cutting device.

3.3. Fuel rod drawing device

A collet chuck system was adopted for conventional drawing device, which could not be inserted between the side plate and fuel rod at the outermost row. The side plate was an obstacle to draw the fuel rod by using the conventional device. Additionally, the conventional drawing device required a manipulator operation to move the chucking device, which would spend a lot of time during the process. Consequently, the drawing device was improved for “Mutsu” fuel rod. The drawing device has a compact clamping head with compression air actuation unit. A schematic drawing of the drawing device is shown in Fig. 3.3.

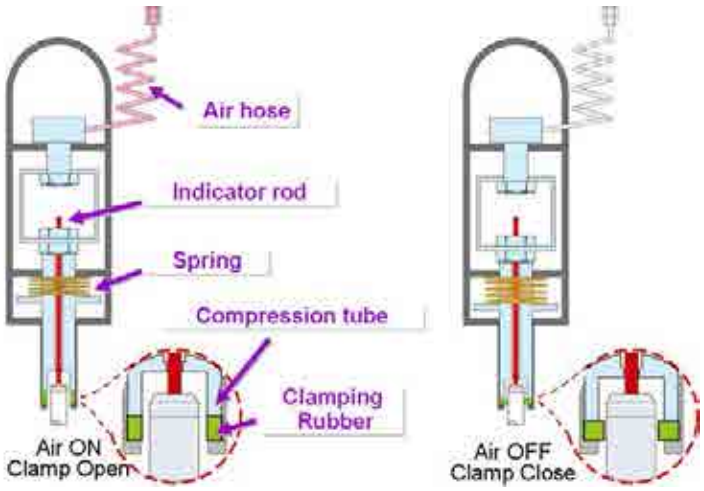

FIG. 3.3. A schematic drawing of the drawing device.

The clamping head has a ring shaped rubber, a compression tube and a spring. The compression tube moves up against the spring force to release the compressive force to the rubber when the compressed air is injected into the clamping head. Without the injection of the air, the spring in the clamping head would compress the rubber to clamp the top of fuel rod by the friction force of over 300 N. To select the rubber compression system, diameter of clamping head had to be smaller than the conventional drawing device. The improved clamping head can be inserted in the gap between side plate and outer side of fuel rods of the "Mutsu" fuel assembly. The operation of this device, chuck opening and closing, was controlled from operation area using air valve. Furthermore, fuel rod clamping condition was indicated by indicator rod attached in the clumping head.

4. PROCEDURE OF REASSEMBLING

Approximately six assemblies of "Mutsu" fuel were reassembled to one PWR type like assembly for reprocessing. The surface cleaning of the "Mutsu" assemblies using an ultrasonic water bath and the external observation test of the assemblies were performed as the first process of reassembling work, and then cutting of the upper nozzle, drawing of the fuel rods, the visual inspection of the fuel rods and reassembling process were preformed in series. Detailed procedures of each process are described below.

4.1. Upper nozzle cutting

The upper nozzle was cut by the cutting device with the cutting accuracy of ±1mm. There was no additional damage of the fuel rod in this procedure.

4.2. Fuel rod drawing

The fuel rods were drawn from the fuel assembly using the in-cell crane and the fuel rod drawing device. In this procedure, deformation of the fuel rod was confirmed to measure the pull-out force by a load cell unit which is attached between the in-cell crane and the drawing device. The fuel rods drawn from the assemblies were placed in the temporary storage rack by each assembly.

4.3. Visual inspection of fuel rods

After the drawing of all fuel rods, the confirmation test was performed by the periscope in the cell to search the defect at the surface of the fuel rods and deformation during irradiation.

4.4. Fuel rods insertion and assembling

The length of "Mutsu" fuel rod was approximately one third of the commercial reactor fuel rod (1123 mm as Mutsu, approx. 3900 mm as commercial reactor). Therefore, three rods of "Mutsu" fuel were inserted in the same grid cell of the PWR type skeleton vertically as three tiers. To improve the efficiency of the insertion, twenty-four rods were inserted in the thimble tube because the reassembling fuel will not be loaded in a reactor. However, it was necessary to adjust the average enrichment of a fuel assembly less than 4.0% for the acceptable specifications of the reprocessing plant. The "Mutsu" fuel assembly was comprised of two enrichment types of fuel rods; A-type is 3.24% and B-type is 4.44%. The identifying mark of the enrichment, namely "A" or "B", was carved at the bottom side of fuel rods. In order to adjust the average enrichment of reassembled fuel assembly to less than 4.0%, arrangements of the insertion position for the fuel rods were needed. The fuel rods were inserted into the PWR skeleton in accordance with the predetermined arrangement pattern. The typical arrangement pattern is shown in Fig. 4.1. To insert the fuel rod adequately to the arrangement pattern, the identifying mark of enrichment (A or B) was confirmed using check sheets in every insertion process. After that, portal films of insertion patterns were taken to confirm the inserted fuel rods. Finally, thirty-four fuel assemblies were reassembled as six PWR type-like fuel assemblies in order to adjust the acceptable specifications of the reprocessing plant. The photograph of reassembled assembly is shown in Fig. 4.2.

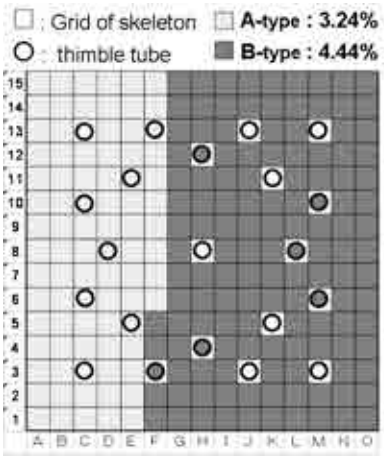

FIG. 4.1. The typical arrangement pattern of fuel rods.

FIG. 4.2. Reassembled PWR type fuel assembly.

5. SUMMARY

The new devices and systems were developed in RFEF to perform the reprocessing work of “Mutsu” fuel, and reassembling work for 34 “Mutsu” fuel assemblies was performed in 2007.

The reassembled fuels will be transported to the reprocessing plant in JAEA, near future.

6. ACKNOWLEDGMENT

The authors acknowledge to K. Minato, director of Department of Hot Laboratories and Facilities at JAEA. The authors would like to express their thanks to the staffs of Department of Hot Laboratories and Facilities.

REFERENCES

[1] YAMAJI, A., SAKAMOTO, Y., Comparison between measured and design dose rate equivalents on board of nuclear ship MUTSU, J. Nucl. Sci. Technol. **30** (9) (1993).

PAPERS TO THE POSTER SESSION

STATUS OF THE JOINT IAEA–HOTLAB POST-IRRADIATION EXAMINATION FACILITIES DATABASE (PIEDB)

A. AQRAWI, V. INOZEMTSEV, H. TULSIDAS
International Atomic Energy Agency
Vienna, Austria
Email: a.aqrawi@iaea.org

H. JENSSEN
OECD Halden Reactor Project
Institutt for Energiteknikk
Halden, Norway

A. LEENAERS
HOTLAB, Studiecentrum voor Kernenergie/Centre d'Etude de l'Energie Nucleaire — Laboratories (SCK•CEN)
Mol, Belgium

Abstract

While the number of states with nuclear power programs are growing, the number of hot cells decreased during the last decades, creating problems with post-irradiation examination (PIE) for fuel surveillance, safety control and nuclear materials studies, including the development of new radiation resistant materials for advanced and innovative nuclear applications. Therefore, there is a permanent need for wider international exchange of information about existing PIE facilities to enable increased efficiency in their use. The Joint IAEA–HOTLAB Post-irradiation Examination Facilities Database (PIEDB) attempts to fill this requirement. In 2007–2008, following an agreement with the international HOTLAB Working Group (http://www.sckcen.be/hotlab), the IAEA PIE Database integrated the HOTLAB PIE Catalogue, including transport casks information. The merged data is available at the Integrated Nuclear Fuel Cycle Information Systems (iNFCIS) website (http://www-nfcis.iaea.org/PIE/PIEMain.asp) and jointly managed by the IAEA and HOTLAB, representing the only publicly accessible worldwide source of information on the subject. The database consists of six main areas describing PIE facilities (i.e. acceptance criteria for irradiated components, cell characteristics, PIE techniques, re-fabrication/instrumentation capabilities, storage and conditioning capabilities, and references) as well as major technical and licensing data of casks. The database can also be used to compare the PIE capabilities with current and future requirements, as well as to provide development incentives for laboratories with limited PIE techniques. An important advantage of the PIEDB is the procedure of the professional reviewing of all new inputs made on-line. The PIEDB is experiencing a growth in popularity, with an increasing number of users, which indicates its practical usefulness. Hence it is important to continuously update the information, to promote and advertise individual hot lab capabilities. The paper contains a portrayal of the history of the PIEDB, and presents a description of its content, the web form and its current status and development.

1. INTRODUCTION

The number of hot cells in the world in which post-irradiation examination (PIE) can be performed has decreased during the last few decades. This creates problems for countries that have nuclear power plants and require PIE for surveillance, safety and fuel development. With this in mind and according to the recommendation made by the IAEA's Technical Working Group on Fuel Performance and Technology (TWGFPT) (formerly Technical Working Group on Water Reactor Fuel Performance and Technology), the IAEA initiated the issue of a catalogue within the framework of a Coordinated Research Programme (CRP) (1992–1995), under the title of "Examination and Documentation Methodology for Water Reactor Fuel (ED-WARF-II)".

Within this program, a group of technical consultants prepared a questionnaire to be completed by relevant laboratories. From these questionnaires a catalogue was assembled that listed the hot laboratories and PIE possibilities worldwide in order to make it more convenient to arrange and perform contractual PIE on water reactor fuels and core components. The catalogue was published in 1996 as an IAEA Working Material [1].

The proposal to create an international database on PIE facilities/techniques was further discussed at the Technical Meeting (TM) on Advanced Post-irradiation Examination Techniques for Water Reactor Fuel held in Dimitrovgrad (2001), Russian Federation. The participants of this meeting agreed to convert the catalogue of PIE facilities into a database. It was stated, that common approaches in PIE techniques allow comparison of results obtained in different countries and different laboratories that improve the trustworthiness of data used for fuel performance assessment and licensing. The group of PIE specialists from the Dimitrovgrad TM agreed upon following basic principles of the database development:

– It should not interfere with commercial interests of participating organizations;
– The database should be regularly updated;
– All of the interested IAEA Member States should have access to the database.

All previous activities in the area (e.g. PIE facilities catalogue) should be taken into account and the PIE database should be seen in cooperation with other related programs and databases on nuclear fuel examinations. During 2002 and 2003, the catalogue was converted into a database and updated through questionnaires to the laboratories in the IAEA Member States.

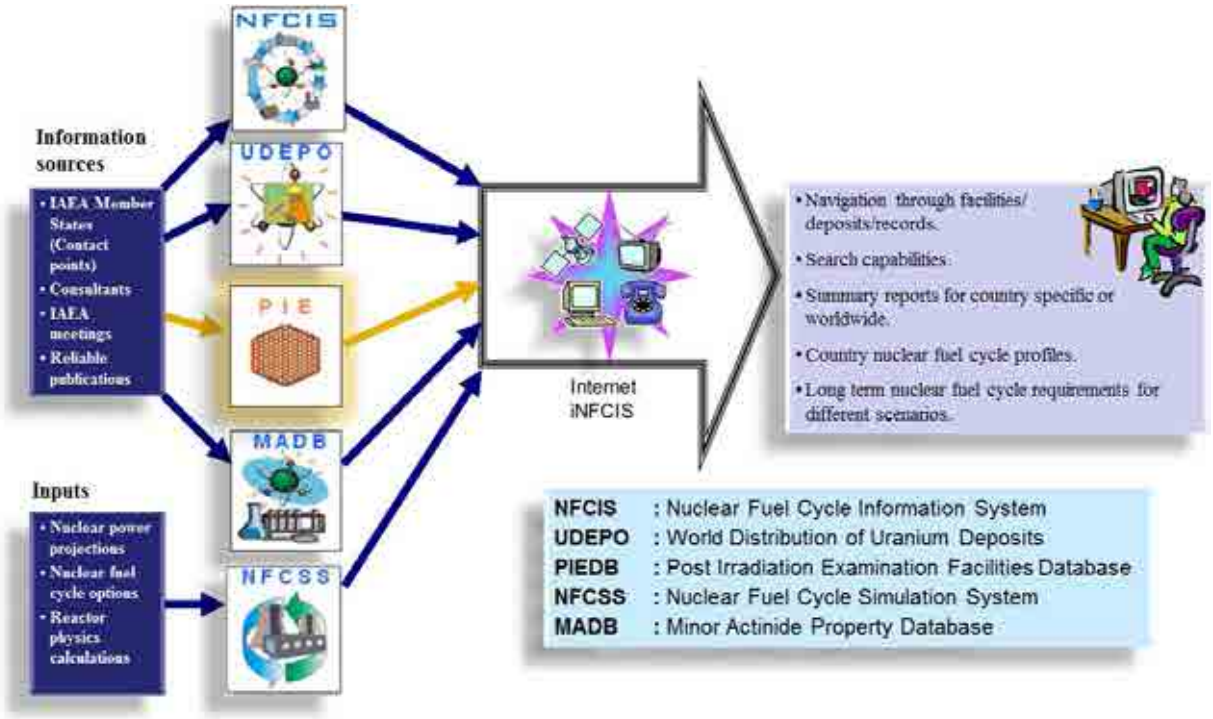

FIG. 1.1. Integrated Nuclear Fuel Cycle Information System (iNFCIS) of the IAEA.

In early 2004, the IAEA's Integrated Nuclear Fuel Cycle Information System (iNFCIS) became the home of the PIE database [2]. Figure 1.1 gives the general description of the iNFCIS database system. The database was further developed and improved during 2005. The most important improvement was the organization of interactive on-line access for registered hot lab managers to edit facility data records. New entries are checked by reviewers and only before being published in iNFCIS website. The administrators, reviewers and facility coordinators have different roles and functions to perform, that enable the desired interactive database levels of flexibility and reliability.

The 6th Framework Programme of the European Commission funded a "HOTLAB" project in 2004 and 2005. HOTLAB included 19 organizations from 13 countries and was concentrated around three tasks [3]:

– A public web catalogue to present capabilities of European hot laboratory facilities;
– Their post-irradiation examination techniques;
– To provide contact points.

In 2007–2008 the IAEA and the European Commission (EC) 'HOTLAB' project collaborated, by integrating the EC HOTLAB catalogue into the IAEA PIE database, creating the Joint IAEA–HOTLAB PIE Facilities Database (PIEDB). This merger also added the HOTLAB catalogue's casks information.

Since then, the PIEDB has been jointly managed by the IAEA and HOTLAB, making it the only publicly accessible worldwide source of the subject information. This demands an up-to-date picture of PIE capabilities of the individual facilities, so in 2010–2011 the PIEDB has undergone a large update process of its facility data, including a modification of its capabilities.

2. CONTENT OF THE PIEDB

The IAEA operates a number of nuclear fuel cycle related databases and simulation systems for long term projections of nuclear fuel cycle material and service requirements. Some of the databases and simulation systems are currently available at the iNFCIS web site at http://www-nfcis.iaea.org/ where the PIE database is located. Their purpose is to provide the IAEA Member States and public users with current, consistent, and readily accessible information for planning activities related to the nuclear fuel cycle. For accessing this database system the user must register in order to get a user-ID and a password. Necessary login information will be then sent to the user's email address and with that access to all iNFCIS databases will be possible, including the Joint IAEA–HOTLAB PIEDB.

The currently 45 facilities included in the database are listed in the opening page by country. The selection of facilities can also be sorted by an individual PIE technique or a technique topic. The general database user has the possibility to check the laboratories that perform for instance neutron radiography. The actual laboratories are listed if a search is performed on a specific technique. Listing of techniques linked to the specific laboratories is possible without extra navigations because the searching tools are always displayed in the upper part of the web page. The home and help buttons can also be reached without extra navigations, i.e. these links or "hand tool" buttons are always displayed in the title bar at the upper part of the web interface.

The database consists of six main areas or topics related to the PIE facilities, i.e. general/cell characteristics, acceptance criteria for irradiated components, available PIE techniques, refabrication and instrumentation capabilities, storage and conditioning capabilities and reference documents.

The general topic supplies facility name, the country where the facility is located, contact persons (1st and 2nd), phone and fax numbers, email address, and links to the company/laboratory web page. The cell characteristics give the main purpose of the facility, e.g. the specific materials that are examined in the laboratory, the number of cells and information of gamma activity limits for the concrete, steel and lead cells. The dimension of the largest cell and the maximum fuel rod length that the according laboratory can receive are also important information given under this topic. Figure 2.1 gives an example of the general cell characteristics page for the KINR (Ukraine) facility.

The acceptance topic gives information about acceptance type and condition, e.g. fuel rods, assemblies or structural components that could be received at the hot lab facility. Transfer mode, maximum cask length and weight are given to support information in relation to external transportation. Maximum fuel enrichment and fissile weight, failed rod acceptance, eventual protection packing and a general comment field are also included under this topic.

The techniques topic gives the type of technique (destructive (DT) or non-destructive (NDT)). The technique is then described by several fields, giving a detailed description of the technical capability of the according facility, see Fig. 2.2. One example of text in the description field under neutron

radiography examination can be that neutron radiography is applied on irradiated and non-irradiated fuel rod internal components and material test samples. The “Form of Data Presentation” field gives the format of the prepared data acquired under PIE, e.g. digital images and graphs. This is important information since it influences the dataflow between the facility and the customer, e.g. digital images are possible to exchange by email immediately after data acquisition while analogue images must be sent by traditional post. There are additional fields for general comments, references, equipment, standards and test parameters. The content of the “Comment” field is decided by the facility staff involved in the description of the techniques. The test parameters are normally related to the ambient conditions under which the PIE is executed, e.g. sample temperature, atmospheric pressure and amount and strength of HNO_3 + HCl acid. PIE details for type of specimen, measured and calculated parameters and features (e.g. measurement accuracy, microscope magnifications, etc.) are given in the respective fields of the various PIE techniques. Software tools and codes can be filled in mentioning “Software Tool” in the “Technique” field.

FIG. 2.1. An example (KINR, Ukraine) of the ‘General & Cell Characteristics’ page of the PIEDB. The selection of other topics, such as ’Acceptance Info.’, ‘Techniques’, ‘Refabrication & Instrumentation’, ‘Storage & Conditioning’ and ‘Reference Documents’, is located on top of the page.

Refabrication and instrumentation possibilities of irradiated fuel rods are a separate topic. The information included hereunder is for instance fuel centre-line thermocouple, de-fuelling, welding of instrumented end plugs and pressurization/leak testing, and other features.

The next topic included in the PIEDB is about “Storage & Conditioning” possibilities. Fields for description in relation to intermediate and long term storage and connection to reprocessing plants are implemented. There is a general reference field and also one for description of encapsulation purposes, e.g. in relation to reinsertion of fuel rod.

The last topic, “Reference Documents”, gives the facility coordinator the possibility to include further reference material that can be easily uploaded and made available to the interested user.

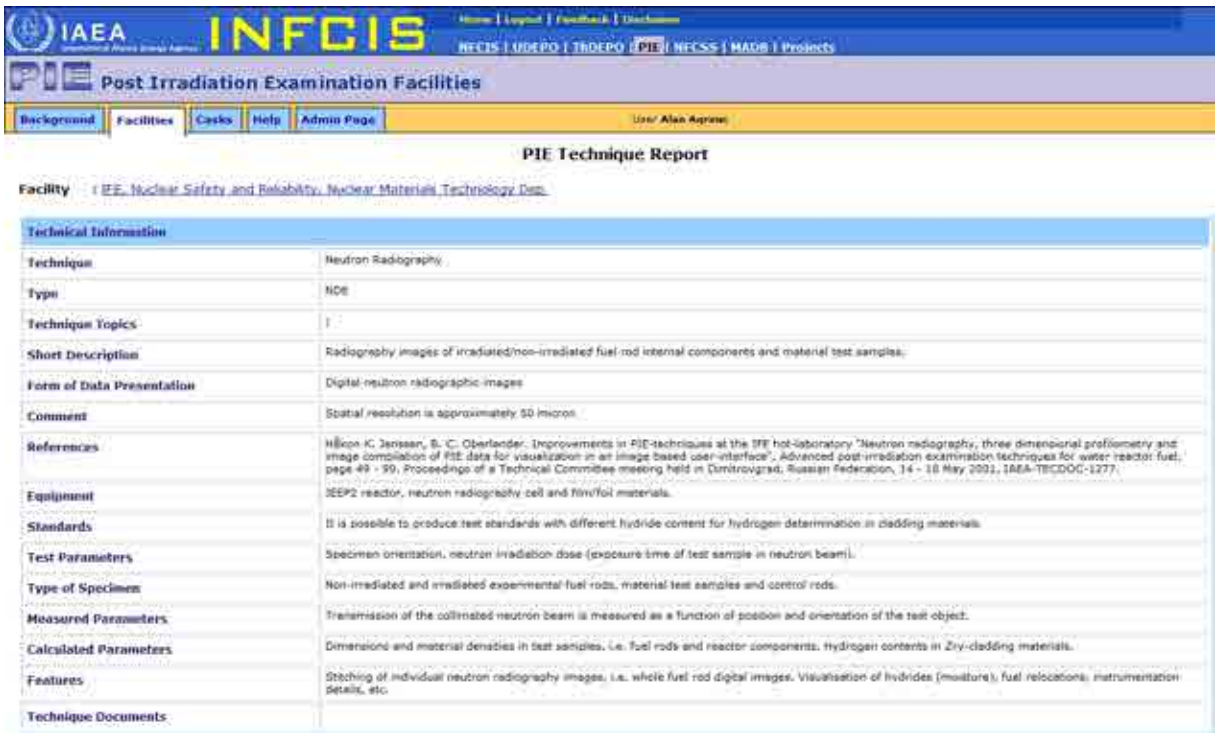

FIG. 2.2. An example of the technical information on neutron radiography capabilities (IFE, Norway).

The casks section of the PIEDB includes 19 casks, with detailed casks reports, including specifications on cask type, provider, purpose, classification, type of loads, licensing, accessories, packaging characteristics, content characteristics, specific characteristics, transportation mode, loading mode, technical support, reference and contact data (see Fig. 2.3).

3. ON-LINE ENTRY, REVIEW PROCESS AND REGISTRY WITH THE DB

The main advantage of the PIEDB is its open internet availability, simple interface, information volume, interactive on-line editing access for registered facility coordinators and the professional review and verification process. The data entered by the according facility coordinator of the facility, is then verified by DB reviewers, before it is released and integrated.

There are several predefined fields for detailed descriptions of the different PIE methods. The field layouts are similar for all different PIE methods to ensure a uniform structure of the database. With the adoption of a uniform database format for all laboratories and details of techniques, it is assured that the IAEA Member States are able to use the database to select laboratories most relevant to their particular needs.

Registering a new facility, hence registering as a facility coordinator, requires registering with the database and requesting an administrator log-in for the according new facility. In addition to this, an official letter of nomination by the Head, or Director of the facility nominating an official 1st and 2nd facility coordinator is required (an example letter can be found in the Appendix “Example Letter ‘Official Nomination of Contact Persons’”). Table 3.1 gives a detailed description of the procedure.

FIG. 2.3. An example of the technical report and contact details for a cask (AGNES cask, LA CALHENE, Belgium).

4. RECENT UPDATES AND MODIFICATIONS

The high importance of an up-to-date picture of PIE capabilities is a main goal of the PIEDB. In 2009, it was decided that the PIEDB should undergo a general update of its data, as some parts of it had been last updated in 2003. In addition to this, alongside with the update process, the PIEDB would undergo a modification process, as there were necessary improvements to its stability and innovations to be included. For example, did the PIEDB experience instabilities, due to data entries with unconformable symbols — these led to data loss.

In early 2010 facilities were requested to update their data. During this process, it became obvious that many facility contact points were outdated, and in some cases some effort was needed to establish the correct contact. The renewal phase of the technical and contact data in the PIEDB was succesfully completed with very positive results by late 2010 (see Fig. 4.1). Through 2010 the DB was constantly reviewed, tested to run stable, and further new requests from facilities were integrated. The admin manual for facility admins has been updated. After the update process, 9 new facilities have been included, leading to an overall number of 45 facilities from 23 different countries and 19 casks.

New modifications, such as improved stability of the PIEDB during operation, the possibility to export the full content of an individual facility as a PDF file have been accomplished.

By mid-2011, it is planned to begin with the migration of the PIEDB to the IAEA “Nucleus” platform (http://nucleus.iaea.org), IAEA’s common access to scientific, technical and regulatory information resources. Subsequently it will be a target, to adopt a common Nucleus ‘look and feel’.

TABLE 3.1. PIEDB REGISTRATION PROCEDURE

Registration procedure
1. Appoint someone from your organization to be the 1st and 2nd facility coordinator for the PIEDB.
2. Send an email to Victor Inozemtsev (DB Custodian) (V.Inozemtsev@iaea.org, cc: A.Aqrawi@iaea.org; piedb.contact-point@iaea.org) requesting registration as the official facility coordinator and contact person for the PIEDB. A corresponding facility page will be created in the database by the IAEA.
3. Next in the process, please provide an official letter of nomination for the 1st and 2nd official contact persons for the facility signed by your Head of Division, Department, or Director or equivalent and send it to Victor Inozemtsev (V.Inozemtsev@iaea.org, cc: A.Aqrawi@iaea.org; piedb.contact-point@iaea.org). An example letter can be found in the Appendix of this paper.
4. In the meantime you should register with the database and send your newly generated user-ID to Victor Inozemtsev (V.Inozemtsev@iaea.org, cc: A.Aqrawi@iaea.org; piedb.contact-point@iaea.org), in return your account will be activated as the admin for the facility page.
5. Fill in the database with the facility's infrastructure. An admin handbook is located in the PIEDB admin section for your convenience.

5. RECEPTION AND GROWING COLLABORATION

The PIEDB is experiencing a year-by-year growth in popularity and reception. The numbers of visits to the PIEDB were 10 810 in 2010, in comparison the whole IAEA iNFCIS website was visited 3350, 4887 and 7680 times in 2004, 2005 and 2006 respectively.

The excellent collaboration between the IAEA and HOTLAB (http://hotlab.sckcen.be/) regarding the PIEDB is ongoing and growing. Another good example of the close collaboration was the organization of the Technical Meeting on 'Hot Cell Post-Irradiation Examination and Pool-Side Inspection of Nuclear Fuel' in May 2011 in Smolenice'.

In 2010, involvement of the European NULIFE research network for plant life management (launched under the EURATOM framework program) was established. Instead of developing a new DB, the existing PIEDB is being used and NULIFE facilities are being included (http://www.vtt.fi/proj/nulife/index.jsp). A separate admin manual for NULIFE hot lab managers was written and provided.

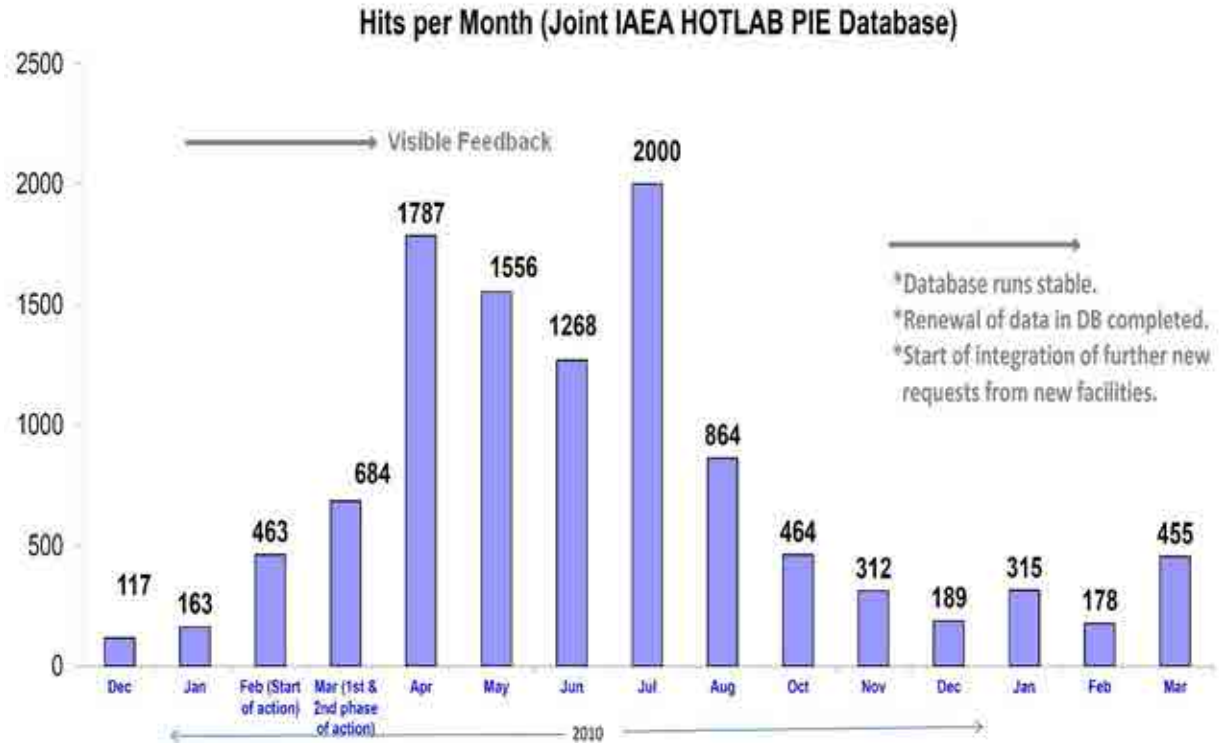

FIG. 4.1. Visible feedback during the renewal and update phase of the PIEDB, based on the 'hits per month'. The hits per month after the update process remain higher on average than previous months, due to a growth in advertency.

6. CONCLUSION

The PIEDB is used as an authoritative source of information about PIE facilities worldwide and for comparison of their capabilities with current and future requirements. It presents a special opportunity for facilities to promote their services. The DB plays an important role in giving an incentive for laboratories with limited PIE techniques to increase and improve their own capabilities, and it provides interested users with a tool to select the most appropriate facilities, casks and examination techniques.

The keyword in this regard is 'proactive'. The possibility for the facility coordinators to edit their PIE data on the webpage interactively is a well received advantage, but it requires being proactive about it. The success of the database depends mainly on the quality of the data that the IAEA receives from the hot laboratories, and on how frequent the updating is being performed. Therefore the data being up-to-date is crucial to the main goal of the database. This strongly depends on the individual facility coordinators being aware of this, and on regular initiatives by the IAEA and HOTLAB to uphold focus on up-to-date information. As it showed during the update process, facility coordinators might change, therefore timely informing the IAEA or HOTLAB is important for keeping the process going.

The recent update process has been successful and the feedback is positive. This revitalization of the database and its growing advertency lead to six new facilities being included, making it an overall number of 45 facilities from 23 different countries, and 19 casks.

Regarding the near future of the PIEDB it is planned to extend the number of included PIE facilities. As the database is growing, the role of the administrators and reviewers is to ensure that the review process continues to be effective and timely. In case of difficulties or problems, the IAEA and HOTLAB have and will provide an efficient and competent support.

REFERENCES

[1] INTERNATIONAL ATOMIC ENERGY AGENCY, Catalogue of PIE which can examine LWR fuel and structural components, Working Material IAEA-IWGFPT/46, IAEA, Vienna (1996) (limited distribution).

[2] JENSSEN, H.K., "Status of the iNFCIS IAEA PIE facilities database", Post-Irradiation Examination and In-Pile Measurement Techniques for Water Reactor Fuels, IAEA-TECDOC-CD-1635, IAEA, Vienna (2010) 176–179.

[3] SANNEN, L., et al., "The European HOTLAB project and its future, with emphasis on its internet catalogue", Post-Irradiation Examination and In-Pile Measurement Techniques for Water Reactor Fuels, IAEA-TECDOC-CD-1635, IAEA, Vienna (2010) 163–175.

Appendix: EXAMPLE LETTER 'OFFICIAL NOMINATION OF CONTACT PERSONS'

To be sent as email attachment to:

V.Inozemtsev@iaea.org
DB Custodian
Division of Nuclear Fuel Cycle and Waste Technology
IAEA

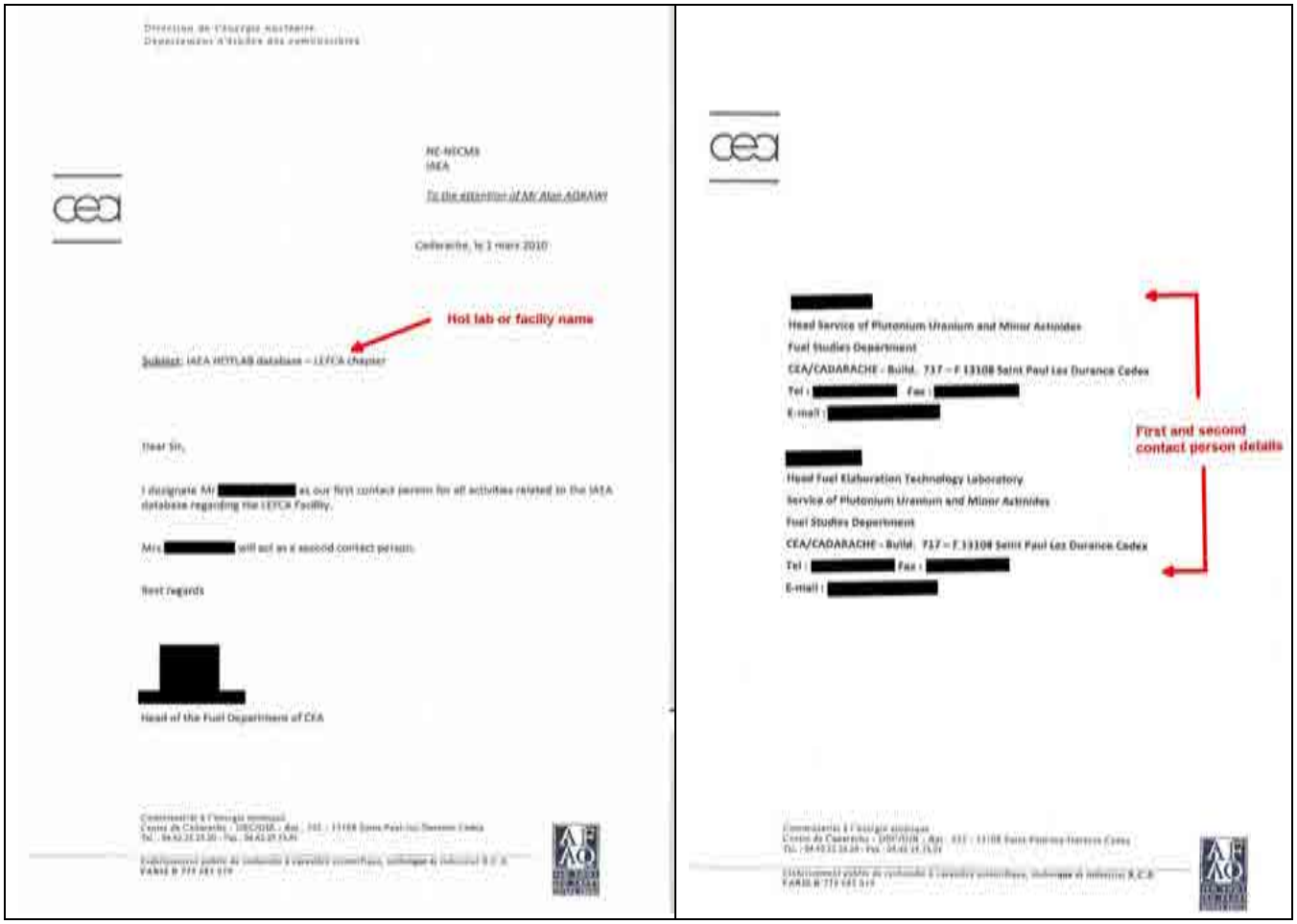

NEW IRRADIATION DEVICE AT THE BUDAPEST RESEARCH REACTOR

R. SZÉKELY, Á. HORVÁTH, F. GILLEMOT, G. URI, D. ANTOK, M. HORVÁTH
Hungarian Academy of Sciences KFKI
Atomic Energy Research Institute
Budapest, Hungary
Email: rszekely@aeki.kfki.hu

Abstract

In close cooperation with the Paul Scherer Institute (Switzerland) two new rigs called BAGIRA (Budapest Advanced Gas cooled Irradiation Rig with aluminium structure) have been built [1–2]. The irradiation volume of the largest rig is 360 × 20 × 30 mm and it can operate in the temperature range of 150–650°C. The heating is combined gamma and electrical heating; the temperature measurement is performed by 6 thermocouples, and controlled by a helium–nitrogen gas mix flow. The neutron flux within the rig is about $2–6 \times 10^{13}$ $n \cdot cm^{-2}s^{-1}$. Similar but smaller irradiation channel have been built for long term irradiations at lower temperature for testing the materials of the fusion reactor. Altogether 24 different irradiations have been performed until now studying the radiation resistance of RPV steels, model alloys, titanium and tungsten, aluminium alloys and ceramics. In 2010 the irradiation facilities of the BRR were under upgrade again. The purpose of the modernisation was to satisfy the requirements at the development and testing of materials for the third and fourth generation reactors, fusion devices and advanced testing of presently used materials. The new irradiation rig is: i) Shielded from the thermal neutrons by boron carbide shield (better fast/thermal neutron ratio, less gamma heat generation, less activation of the samples); ii) The temperature range of the operation is increased up to 600°C; iii) The minimum stable operation temperature is as low as 100°C; iv) The target can be rotated during irradiation to avoid self-shield; v) The temperature control became to electric resistance heating in 6 zones instead of the present 3 zones; vi) The sample removal after irradiation simplified and the personal dose during sample removal will be reduced; vii) The mass of the activated structure also reduced and also the preparation costs of a new irradiation reduced; viii) Further new feature of the design is the in-pile creep and low cycle fatigue test on small size specimens.

1. INTRODUCTION

Radiation embrittlement is one of the main ageing mechanisms of the materials of the fission and fusion reactors. In many cases it determines the lifetime of these devices.

The Budapest Research Reactor (VVR-SM type) was built in 1957, and after full reconstruction and power upgrade to 20 MW was restarted in 1993. The reconstructed reactor passed successfully the 1 year test period, and since January 1994 it is on normal operation with 10 MW power. Radiation embrittlement research is available since then. The Budapest Research Reactor and the BAGIRA 1 and 2 irradiation rigs are widely used for studying the irradiation effects on the structural materials to evaluate the safety and lifetime of the presently operating and future nuclear energy sources.

The institute participated in the IAEA coordinated research programs (CRP-3 to CRP-9) by performing irradiated material testing. Irradiations in the BAGIRA rigs have also been performed for many EU framework programme (FRAME, GRETE, COBRA, ATHENE, PERFECT, COVERS, NULIFE) and for the European Fusion Program. National irradiation programs supported the lifetime extension of the Paks NPP. Nowadays further development of the irradiation facilities is going on to widen the irradiation temperature range, to produce harder spectra (better rate of fast/thermal neutrons), and to study the effect of combined mechanical load and irradiation.

2. THE BAGIRA 1 AND 2 IRRADIATION RIG SYSTEMS

In close cooperation with the Paul Scherer Institute, Switzerland, two new rigs called BAGIRA (Budapest Advanced Gas-cooled Irradiation Rig with Aluminium Structure), Hungary, have been built during 1996–2003. [1–3]. The irradiation volume of the largest rig (BAGIRA 1) is 360 × 20 × 30 mm (see Fig. 2.1), and it can operate in the temperature range of 150–450°C. The heating is combined gamma and electrical heating; the temperature measurement is performed by 6 thermocouples, the temperature controlled by a helium–nitrogen gas mix flow. Foil dosimeter and fluence calculations are combined to support the evaluation of neutron flux, fluence and spectra. The fast fluence within the rig is about $2–6 \times 10^{13}$ n·cm^{-2}s^{-1}. Similar but smaller irradiation device (BAGIRA 2) has been built for low temperature long term irradiations for fusion materials testing.

2.1. Irradiations in the BAGIRA 1 and 2 rigs

2.1.1. RPV cladding tests

Most of the reactor pressure vessels (RPVs) are clad inside with a stainless steel layer. It is generally made by welding, and 3–10 mm thick. Previously at pressurized thermal shock (PTS) analysis the cladding was neglected; at present hypothetical cracks starting from the clad surface are considered. If the RPV cladding is ductile and free from defects, than the VERLIFE [4] and the IAEA PTS guide [5] does not requires the use hypothetical surface cracks during the PTS calculations. Without hypothetical surface cracks, the PTS calculations give 20–30% longer lifetime [6]. The irradiation damage of cladding is different from the ferritic and austenitic steels, which is an interesting topic to study, and important for long operational life. The result shows that the cladding ductility is the best around room temperature, and at 300°C the elongation of the unirradiated cladding is less than the elongation of EOL irradiated cladding at room temperature. At 300°C testing the irradiation only slightly affects the elongation [7].

2.1.2. Application Cr–Mo–V steel on high temperature

The Cr–Mo and Cr–Mo–V steels are the vessel materials of the PWRs. The irradiation resistance of these materials are widely studied at the operating temperature range of the present PWRs (250–320°C). To increase the efficiency of the future reactors, higher operating temperatures are required. First option is to increase the operating temperature into the 350–560°C range. The fossil plants are operating at this temperature and built from Cr–Mo and Cr–Mo–V steels. These materials are widely used by the industry; the nuclear application does not need too much technology development because the long term creep and thermal ageing properties of them are well known. They are candidate materials for the future fourth generation SCWR (supercritical water cooled) reactors. Irradiation of 15Ch2MFA steel performed in the BAGIRA 1 rig at 450°C and the results are promising [8].

2.1.3. Ti-alloys

Ti alloys have been irradiated and tested for ITER fusion device. In Tokomak type fusion devices the first wall and the vessel is connected with elastic elements. The high strengths and low Young modulus of Ti-alloys allow using them as spring elements. This part of the device suffers about 0.5 dpa irradiation. Ti-6l-4V alloy has been irradiated and the mechanical properties were tested.

2.1.4. Tungsten

Tungsten is resistant against high temperature. Divertors and other first wall elements of the fusion devices and some parts of the high temperature gas cooled reactors are planned to be prepared from tungsten alloys. The radiation embrittlement of tungsten alloys were studied on samples irradiated in the BAGIRA rig. The irradiation with 0.5 dpa reduced the conductivity, caused swelling and decreased the ductility of unalloyed tungsten rods.

2.1.5. 9% Cr steels

The 9% Cr containing ferritic-martensitic steels have high strengths at high temperature, are resistant against creep and can be applied at the 650–900°C temperature range. It consists of low half decay time elements, so after limited decay time it can be treated like low activity waste, and after 100 years decay it can be freely reused. In the power industry similar steels are regularly used and the production and machining technology is well known. The purpose of the study was how much the fracture toughness can be measured on small size irradiated Euroferr specimens, which are the limitations of the use of reconstituted specimens and the so called master curve method [9].

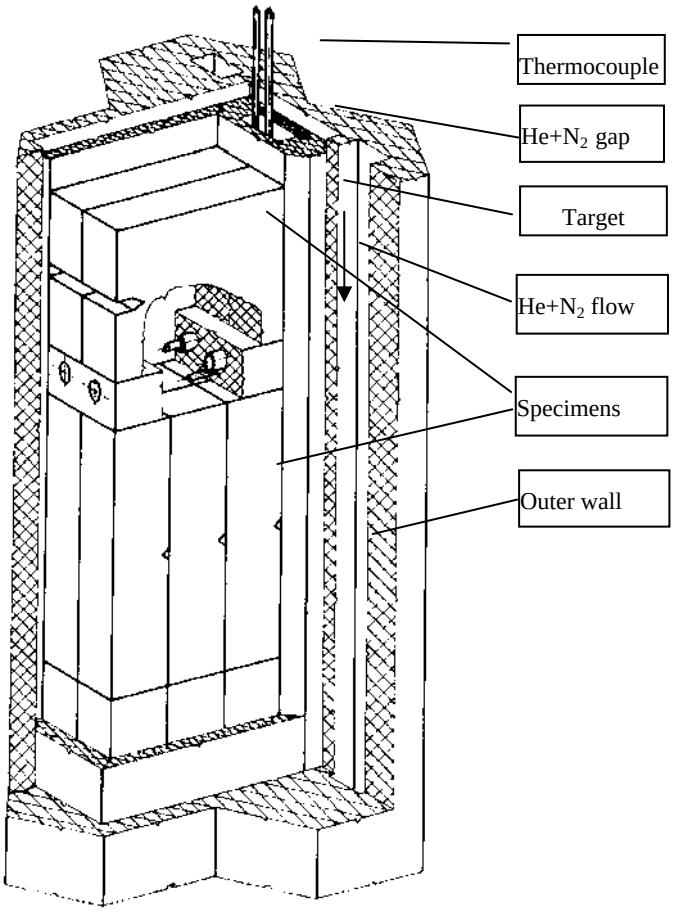

FIG. 2.1. Cross-section of BAGIRA-1 irradiation rig.

3. FUTURE OF IRRADIATIONS IN VVR-SM REACTOR

The nuclear industry is facing the challenge of the development of fusion and Gen IV fission reactors. To increase the efficiency and decrease the impact on the environment, high operation temperature will be used. Consequently high temperature irradiation combined with in-pile creep and fatigue testing are the future tasks of the irradiation devices.

The future recators will suffer very high fluences (50–100 dpa) during their lifetime. Presently the medium research reactors (like the VVR-SM) can produce only ≈1 dpa·y^{-1}. Although this fluence is not comparable to the expected target values, two facts support the future use of them:

– At very high fluxes the so called flux rate effect causes high bias in the material ageing results;
– Considerable part of the ageing occurs at low fluence levels.

The radiation embrittlement is the sum of at least five different ageing mechanisms: precipitations, radiation induced segregations, increase of the dislocation density, thermal ageing and annelaing at irradiation temperature [10]. The first two ageing mechanism occur at low fluence (generally much less than 1 dpa) and quickly saturate. The time dependent annealing and thermal ageing also cannot be studied in high flux devices. Large size specimens cannot be used in high flux irradiation devices due to the high heat generation in the middle section of the specimens. These facts require the combined use of the high flux devices (high flux reactors, spallation neutron sources, two and three beams accelerators) and the present research reactors.

3.1. Development of the BAGIRA 3 rig for future irradiations

The future energetic reactors (fusion and fission) will be operated at higher temperature, and irradiation assisted fatigue and creep became releveant ageing mechanism. To study them, the BAGIRA system is under upgrade development. The BAGIRA 3 rig will be located in a fast neutron irradiation channel where the thermal neutrons will be filtered out by a boron carbide layer. The reduction of the thermal neutrons will decrease the nuclear heating and the activation of the specimens, consequently the temperature control will be more effective, and the decay time will be shorter after irradiation. A step motor will turn the target around to eliminate the self shielding effect of the specimens. Finally the irradiation spectrum will be harder, simulating better the future fission and fusion reactor spectra. The inside structure (target holder) of the rig will be manufactured from titanium alloy to be able to operated up to 650°C. The cross-section of the target holder will be 48 mm in diammeter (instead 20 × 30 mm in the BAGIRA 1), allowing the use of bigger specimens if it is required. All of this development increases the operation window of the irradiation device.

3.2. Development compressed ring shape specimens

For in situ loading few irradiation devices have been built. Traditionally tensile specimens are used for creep and fatigue study. Within the irradiation rigs at high temperature and radiation the precise measurement of elongation in the function of time is very difficult. Due to this a different type of specimens is considered: small size compressed rings — 10–20 rings with a diameter of 10 mm designed in the loading grip (see Fig. 3.1).

The ring shape is selected because it is easy to produce; with a change in the lengths or wall thickness of it the stresses in the loaded ring can be increased or decreased when applying the same load. The deformation of the rings is relatively large even at small creep, and easy to measure.

The geometry of the irradiation channel permits us to place specimens on each other, therefore several rings can be tested simultaneously. The mechanical stability of the vertically pile up ring-system is essential. Consequently mechanical stabilizer elements (beds) are installed between the rings to ensure that the rings will hold their position during the experiment. The geometry of the beds determines the results. Horizontal plane sheets (Fig. 3.2(a)) would not be a good choice, because during the cycling loading the rings could move away in the horizontal direction. A bed with a cylindrical (Fig. 3.2(b)) or a V-shape (Fig. 3.2(c)) groove prohibits the horizontal displacement of the rings.

The most important parameters that describe the beds are Rb (Fig. 3.3(a)) and α (Fig. 3.3(b)).

Finite element model of the ring has been developed and the beds to design the details of the rig and to be able to simulate the future experiments. For this purpose we used the MSC.Marc2005r3 general-purpose nonlinear finite element software. The models are 2D, assuming plane strain deformation. The software applies the theory of large strain. A typical distribution of the total equivalent plastic strain in the ring is depicted in Fig. 3.4.

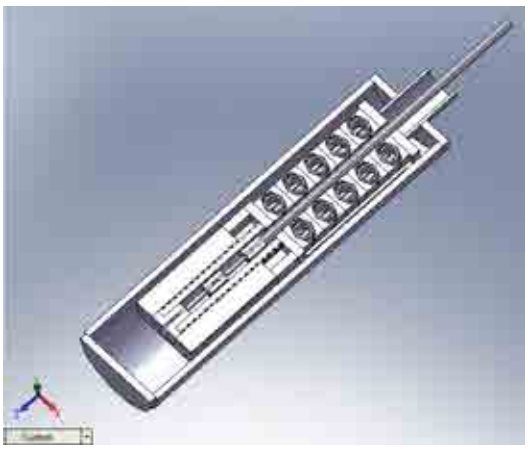

FIG. 3.1. Tensile specimens and compressed rings in the loading grip.

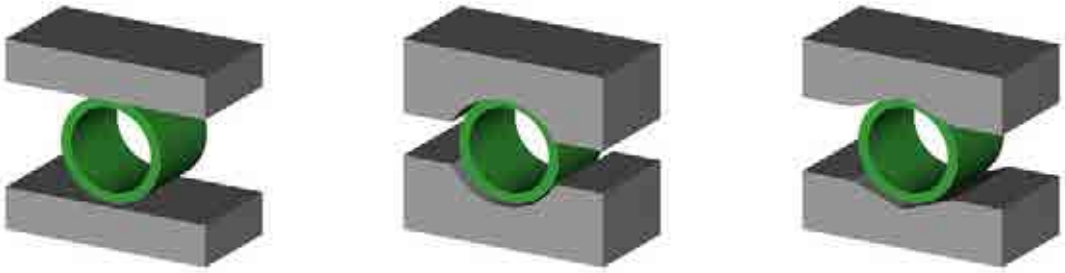

a. *b.* *c.*

FIG. 3.2. Different plane sheets of the tool. (a) shows a horizontal shape, (b) shows a cylindrical shape and the (c) shows a V-shape.

FIG. 3.3. (a) V-shape.

FIG. 3.3. (b) Cylindrical shape.

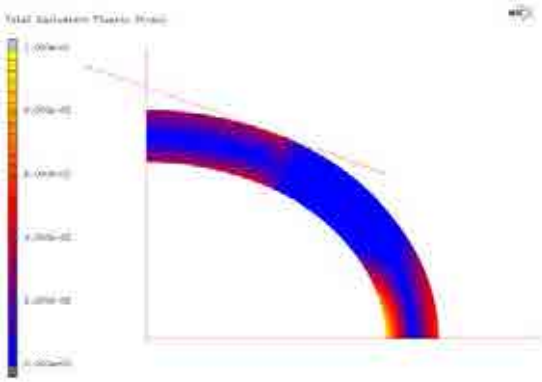

FIG. 3.4. Total equivalent plastic strain in ring.

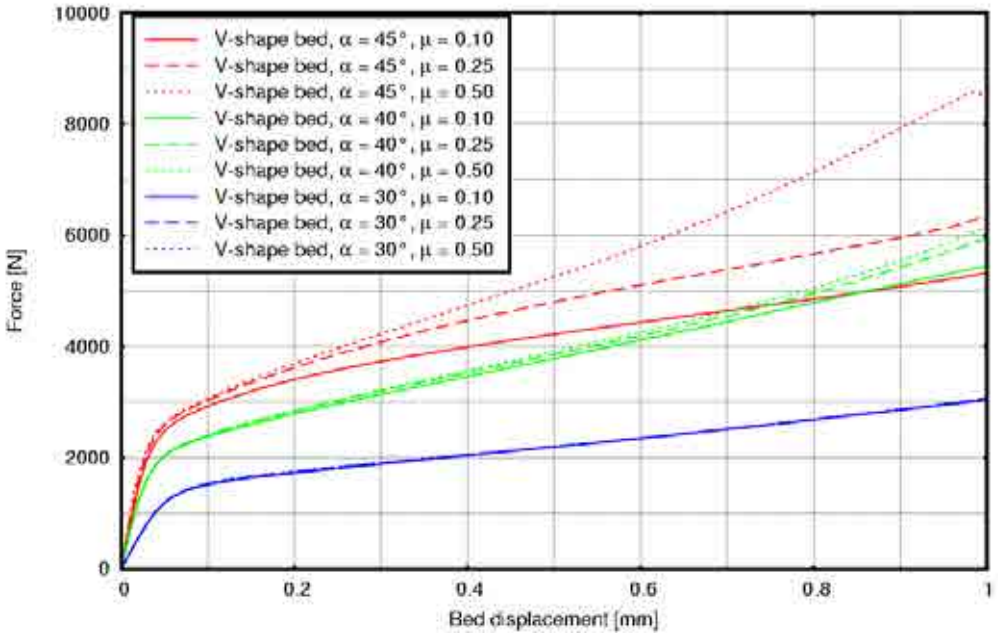

FIG. 3.5. Calculated results of the effect of different parameters.

In the simulations we calculated the role of the friction coefficient between the specimen and the bed. Coulomb friction model was applied with friction coefficients: μ = 0.10, 0.25 and 0.50. In Figs 3.5–3.6 the force–displacement results of the simulations are shown, where continuous lines represent μ = 0.10, the dashed lines μ = 0.25 and the dotted lines μ = 0.50. The force–displacement results are sensitive to the variation of μ if the bed is V-shaped and α is more then 30°. However with the decreasing α the required compression force is also getting smaller. At small displacements (δ<0.2 mm) the cylindrical bed acts like a horizontal plane sheet bed. At higher values of the displacement the ring gets jammed in the bed, a progressive geometrical hardening can be observed. The increase of Rb would delay the appearance of the jam, but it would also destabilize the ring system.

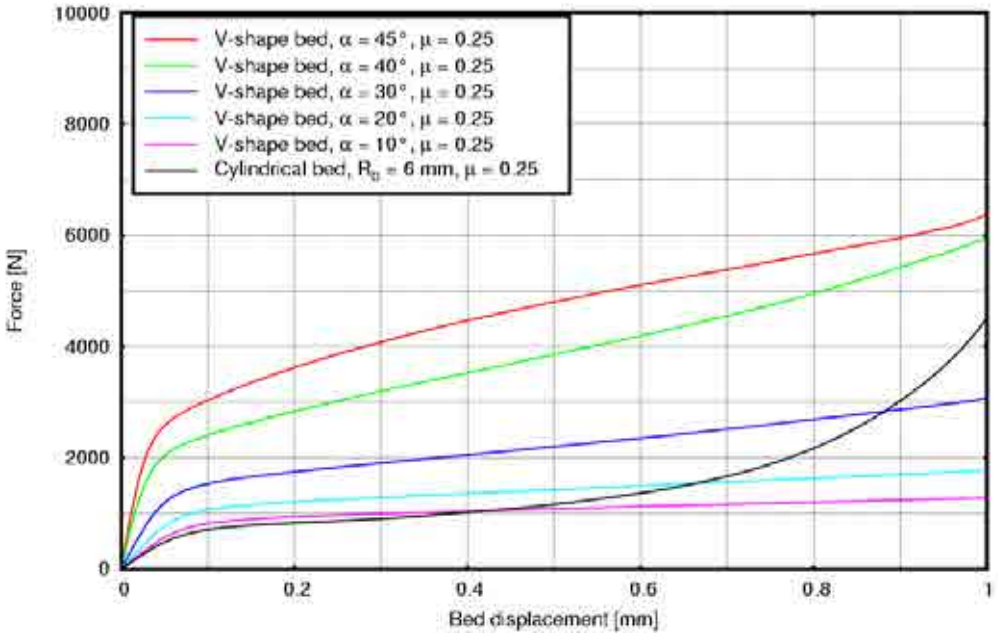

FIG. 3.6. Calculated results of the effect of different parameters.

Since it is expedient to avoid the geometrical hardening and the sensitivity to the friction coefficient, the V-shaped bed with a low value of α (e.g. 20°) would be an optimal choice.

A furnace has been manufactured with electric heating, and a set of rings has been tested at 550°C. The recently performed tests verified the calculations.

4. SUMMARY

The new BAGIRA 3 rig is designed either for conventional irradiations in wide temperature range on tensile, impact and fracture toughness specimens, either it will be prepared to be able to perform irradiation creep and irradiation low/cycle fatigue tests on compressed rings or tensile bars.

REFERENCES

[1] GILLEMOT, F., URI, G., FEKETE, T., GAJDOS, F., FRANKL, L., The new high temperature irradiation rig of the Budapest Research Reactor, Specialist Meeting on Irradiation Embrittlement and Mitigation, Espoo (1995).

[2] GILLEMOT, F., URI, G., Development of the BAGIA Irradiation rig, Yearly Report of the Budapest Neutron Centre (2000).

[3] GILLEMOT, F., Study of the Irradiation Effects at the Research Reactor, Strenghts of Materials **42** (1) (2010) 78–83.

[4] FEKETE, T., GILLEMOT, F., TATÁR, L., "Investigation of the cladding effect using elastic-plastic FE simulation of PTS phenomenon", IAEA Specialist Meeting on Methodology for Pressurized Thermal Shock Evaluation, IWG-LMNPP-00/1, Rockville (2000) 394–407.

[5] GILLEMOT, F., HORVATH, M., URI, G., FEKETE, T., HOUNDEFFO, E., ACOSTA, B., DEBARBERIS, L., VIEHRIG, H.-W., Radiation stability of WWER RPV cladding materials, International Journal of Pressure Vessels and Piping **84** (2007) 469–474.

[6] GILLEMOT, F., HORVATH, M., HORVÁTH, Á., Study of 15H2MFA steel properties for use in SCRW reactor, 4th International Symposium on Supercritical Water Cooled Reactors, Heidelberg (2009).

[7] VERLIFE, Unified Procedure for Lifetime Evaluation of Components and Piping in WWER NPPs (http://www.ist-world.org/ProjectDetails.aspx?ProjectId=5f13c9c6c78f42fe96dba3d7e68819a6&SourceDatabaseId=9cd97ac2e51045e39c2ad6b86dce1ac2).

[8] INTERNATIONAL ATOMIC ENERGY AGENCY, Guidelines on Pressurized Thermal Shock Analysis for WWER Nuclear Power Plants (Rev. 1), IAEA, Vienna (2006).

[9] GILLEMOT, F., HORVATH, M., TATÁR, L., URI, G., Mastercurve Application for Euroferr, TW5-TTMS-005, AEKI Yearbook (2006).

[10] DEBARBERIS, L., ACOSTA, B., ZEMAN, A., SEVINI, F., BALLESTEROS, A. KRYUKOV, A., GILLEMOT, F., BRUMOVSKY, M., Effect of Irradiation Temperature in PWR RPV Materials and its inclusion in semi mechanistic model, Scripta Materiala **53** (2005) 769–773.

ABBREVIATIONS

ADC	analog-to-digital converter
AEM	Auger electron microprobe
AFM	atomic force microscope
AL	Analytical Laboratory
AOA	axial offset
ATR	Advanced Test Reactor
ATR-SUF	Advanced Test Reactor-National Scientific User Facility
BARC	Bhabha Atomic Research Centre
BU	burnup
BWR	boiling water reactor
CAES	Center for Advanced Energy Studies
CANDU	Canada deuterium uranium reactor
CANS	Centre for Advanced Nuclear Systems
CC	coolant channels
CCD	corner-to-corner distance
CCL	Carbon Characterization Laboratory
CEA	Commissariat à l'énergie atomique
CEFR	Chinese Experimental Fast Reactor
CELCA	Ezeiza Atomic Center
CFBR	Commercial Fast Breeder Reactor
CJNF	China Jianzhong Nuclear Fuel Co., Ltd
CNSC	Canadian Nuclear Safety Commission
CP	construction permit
CRIEPI	Central Research Institute of Electric Power Industry
CRL	Chalk River Laboratories
CRP	Coordinated Research Project
CT	central tube (defined as such, only in Paper S1-P2)
CVR	Research Centre Řež Ltd
CW	cold-worked
DB	database
DOE	United States Department of Energy
DRC	dynamic reaction cell
DSC	differential scanning calorimeter
DT	destructive techniques
EBSD	electron backscattered diffraction
EC	European Commission
EDM	electron discharge machine
EFPD	effective full power days
EML	Electron Microscopy Laboratory
EOI	end of irradiation
EPMA	electron probe microanalysis
EPR	emergency protection rods
ET	eddy current testing
FA	fuel assembly
FASB	Fuels and Applied Science Building
FBTR	Fast Breeder Test Reactor
FCC	face centered cubic
FCCI	fuel cladding chemical interaction
FCMI	fuel clad mechanical interaction
FE	fuel element
FEG-TEM	field effect gun-scanning transmission electron microscope
FFD	flat-flat distance
FGR	fission gas release
FIB	focused ion beam
FMF	Fuel Monitoring Facility
FP	framework programme
FRIE	fuel repair and inspection equipment
HBRP	High Burnup Rim Project
HFEF	Hot Fuel Examination Facility
HFETR	High Flux Engineering Test Reactor

HFIR	High Flux Isotope Reactor
HTR	high temperature reactor
HT-XRD	high temperature X ray diffractometer
HVAC	heating, ventilation, and air conditioning
IAEA	International Atomic Energy Agency
IASCC	irradiation assisted stress corrosion cracking rig
ICP-AES	inductively coupled plasma atomic emission spectroscopy
ICP-MS	inductively coupled plasma mass spectrometry
ICVD	Cherenkov viewing device
ID	internal diameter
IFBA	in-fuel burnable absorber
IGCAR	Indira Gandhi Centre for Atomic Research
IL	interaction layer
IMCL	Irradiated Materials Characterization Laboratory
INL	Idaho National Laboratories
INR	Institute for Nuclear Research
IRI	incomplete rod insertion
ISFSF	Interim Spent Fuel Storage Facility
ITU	Institute for Transuranium Elements
JAEA	Japan Atomic Energy Agency
JRC-ITU	Joint Research Centre — Institute for Transuranium Elements
KAERI	Korea Atomic Energy Research Institute
KIPT	National Science Center – Kharkov Institute of Physics & Technology
LEU	low enriched uranium
LHR	linear heat rating
LIBS	laser induced breakdown spectroscopy
LRUS	laser resonant ultrasound spectrometer
LT	leakage testing
LWR	light water reactor
MCA/MCS	multi channel analyser/scaler
MFC	Materials and Fuels Complex
MFFES	Mechanistic Fuel Failure Evaluation System
MNR	McMaster Nuclear Reactor
MOX	mixed oxide
MPS	missing pellet surface
MPS	missing chips from the pellet surface
MSM	master-slave manipulator
MTA	material test assembly
MTR	materials testing reactor
MXRD	micro-X ray diffractometer
NDT	non-destructive testing
NE	nuclear energy
NFC	Nuclear Fuel Complex
NNL	National Nuclear Laboratory
NNSA	National Nuclear Safety Administration
NPIC	Nuclear Power Institute of China
NPP	nuclear power plant
NRG	Nuclear Research and Consultancy Group
NRI	Nuclear Research Institure
NSRI	Nuclear Science Research Institute
OD	outer diameter
OECD	Organisation for Economic Co-operation and Development
OM	optical microscopy
ORNL	Oak Ridge National Laboratory
PAS	positron annihilation spectrometer
PHWR	pressurised heavy water reactor
PIA	post-irradiation annealing
PIE	post-irradiation Examination
PIEDB	Post-irradiation Examination Facilities Database
PIEL	Post-Irradiation Examination Laboratory

PIIP	post-irradiation inspection programme
PRW	pressurized resistance welding
PSI	Paul Scherrer Institut
PT	penetration testing
PTM	power to melt
PWL	pressurized water loop
PWR	pressurized water reactor
QNPP	Qinshan NPP
R&D	research and development
RCM	Research Coordination Meeting
REC	Research and Education Campus
RERTR	Reduced Enrichment for Research and Test Reactors
RFEF	Reactor Fuel Examination Facility
RIAR	State Scientific Center— Research Institute of Atomic Reactors
RMD	Radio Metallurgy Division
RML	Radio Metallurgy Laboratory
RPV	reactor pressure vessel
RTN	removable top nozzle
RVI	remote visual inspection
SCK•CEN	Studiecentrum voor Kernenergie/Centre d'Etude de l'Energie Nucleaire
SE	secondary electron
SEM	scanning electron microscope
SEU	slightly enriched uranium
SF	spent fuel
SIMS	secondary ion mass spectrometry
STDM	scanning thermal diffusivity microscope
SUJB	Czech Nuclear Regulatory Body
TAB	Tandem Accelerator Building
TECDOC	technical document (IAEA publication type)
TEM	transmission electron microscopy
TIMS	thermal ionization mass spectrometry
TM	technical meeting
TREAT	Transient Reactor Experiment and Test
TWGFPT	Technical Working Group on Fuel Performance and Technology
UN	uranium nitride
UNFQP	Ukraine Nuclear Fuel Qualification Project
UT	ultrasonic thickness
UTS	ultimate tensile strength
VNIIM	A.A. Bochvar All-Russia Research Institute of Inorganic Materials
VT	visual inspection
WDS	wavelength dispersive spectrometry
WLTA	Westinghouse Lead Test Assemblies
XANES	X ray absorption near edge spectroscopy
XCT	X ray computer tomography
XGAR	X gamma autoradiography
XRD	X ray diffraction
YS	yield strength

LIST OF PARTICIPANTS

Almási, I.	Institute of Isotopes of Hungarian Academy of Sciences Konkoly Thege M. ut 29-33 PO Box 77 1525 Budapest, Hungary Email: almi.i@freemail.hu
Aqrawi, A.	International Atomic Energy Agency Nuclear Fuel Cycle and Materials Section PO Box 100 Wagramer Strasse 5 1400 Vienna, Austria Email: a.aqrawi@iaea.org
Armstrong, J.	Atomic Energy of Canada Limited 1 Plant Road (Chalk River Laboratories) Ontario K0J 1J0 Chalk River, Canada Email: armstrongj@aecl.ca
Beffort, O.	Eidgenössisches Nuklearsicherheitsinspektorat ENSI Sektion Beförderung und Abfalltechnik Industriestrasse 19 5200 Brugg, Switzerland Email: olivier.beffort@ensi.ch
Berdoula, F.	CEA Cadarache Center Sa3C/LEGEND 13108 St Paul Lez Durance, France Email: francis.berdoula@cea.fr
Bevilacqua, A.	International Atomic Energy Agency Nuclear Fuel Cycle and Materials Section PO Box 100 Wagramer Strasse 5 1400 Vienna, Austria Email: a.bevilacqua@iaea.org
Blanc, J-Y.	C.E.A. DEN/DADN Building 121, CEA Saclay 91191 Gif-Sur-Yvette Cedex, France Email: jean-yves.blanc@cea.fr
Bobák, T.	SE, a.s. NPP Mochovce Slovenske elektrarne, a.s. Atomove elektrarne Mochovce 93539 Mochovce, Slovakia Email: tomas.bobak@enel.com
Bottomley, P.W.D.	European Commission, DG Joint Research Centre Institute for Transuranium Elements (ITU) PO Box 2340 Hermann-von-Helmholtz Pl. 1 76125 Karlsruhe, Germany Email: paul.bottomley@ec.europa.eu

Brzobohaty, K.	Czech Power Company CEZ Duhova 2/1444 Prague, Czech Republic Email: karel.brzobohaty@cez.cz
Burján, T.	Paks Nuclear Power Plant Ltd. PO Box 71 7031 Paks, Hungary Email: burjan@npp.hu
Bychkov, A.	International Atomic Energy Agency Nuclear Fuel Cycle and Materials Section PO Box 100 Wagramer Strasse 5 1400 Vienna, Austria Email: a.bychkov@iaea.org
Chrapčiak, V.	VUJE a.s. Nuclear Design and Fuel Management Okruzna 5 918 64 Trnava, Slovakia Email: chrapciak@vuje.sk
De-Weerd, W.	European Commission Joint Research Centre Institute for Transuranium Elements (ITU) PO Box 2340 76125 Karlsruhe, Germany Email: wim.de-weerd@ec.europa.eu
Feng, M.	Nuclear Power Institute of China, NPIC PO Box 291-100 610005 Chengdu China Email: fengmq1@163.com
Flachet, F.	GDF SUEZ Electrabel. Synatom, Arianelaan 7 1200 Brussels, Belgium Email: femke.flachet@electrabel.com
Frediani, J.M.	Nucleoelectrica Argentina Central Nuclear Atucha I CC 20 Lima CP 2806, Argentina Email: fredianij@na-sa.com.ar, josema2003@hotmail.com
Gavillet, D.	Paul Scherrer Institut OHLA/130 CH-5232 Villigen-PSI, Switzerland Email: Didier Gavillet@psi.ch
Goncharenko, Y.	JSC State Scientific Center — Research Institute of Atomic Reactors Ulyanovsk Region 433510 Dimitrovgrad-10, Russian Federation Email: bond@niiar.ru
He, Z.	Atomic Energy of Canada Ltd. Chalk River Laboratories K0J 1J0 Ontario, Canada Email: hez@aecl.ca

Hlavathy, Z.	Institute of Isotopes of Hungarian Academy of Sciences Konkoly Thege M. ut 29-33 PO Box 77 1525 Budapest, Hungary Email: hlavathy@iki.kfki.hu
Iakovlev, V.	SCC-RIAR State Scientific Center Research Institute of Atomic Reactors Ulyanovsk Region 433510 Dimitrovgrad-10 Russian Federation Email: adm@niiar.ru
Ichikawa, S.	Japan Atomic Energy Agency (JAEA) 4002 Narita-cho, O-arai-machi, Higashi-ibaraki-gun 3111393 Ibaraki-ken, Japan Email: ichikawa.shoichi@jaea.go.jp
Inozemtsev, V.	International Atomic Energy Agency Nuclear Fuel Cycle and Materials Section PO Box 100 Wagramer Strasse 5 1400 Vienna, Austria Email: v.inozemtsev@iaea.org
Ionescu, S.	Institute for Nuclear Research PO Box 78 115400 Mioveni, Romania Email: silviu.ionescu@nuclear.ro
Jenssen, H.K.	Institute for Energy Technology PO Box 40 2027 Kjeller, Norway Email: haakonj@ife.no
Jussofie, A	Gesellschaft für Nuklear-Service mbH, GNS Hollestraße 7A 45127 Essen, Germany Email: astrid.jussofie@gns.de
Katsuyama, K.	Japan Atomic Energy Agency (JAEA) 4002, Narita-cho, O-arai-machi, Higashi-ibaraki-gun 311-1393 Ibaraki-ken, Japan Email: katsuyama.kozo@jaea.go.jp
Kim, H.	Korea Atomic Energy Research Institute 1045 Daedeok-daero, Yuseong-gu, 305-353 Daejeon, Republic of Korea Email: hkim1211@kaeri.re.kr
Kopriva, R.	Nuclear Research Institute Rez Husinec-Rez 130 25068 Rez, Czech Republic Email: kor@ujv.cz
Kytka, M.	Nuclear Research Institute Rez Husinec-Rez 130 25068 Rez, Czech Republic Email: kyt@ujv.cz

Laloy, V.	AREVA TN International 1 Rue Des Herons Montigny Le Bretonneux 78 180, France Email: vanessa.laloy@areva.com
Le Cocguen, A.	CEA Commissariat à l'Energie Atomique et aux énergies alternatives CE Cadarache SEEC/LECD Bât.326 13108 St Paul Lez Durance, France Email: alexandre.le-cocguen@cea.fr
Leenaers, A	SCK-CEN Boeretang 200 2400 Mol, Belgium Email: ann.leenaers@sckcen.be
Léorier, C.	CEA/DEN/SDTC/LEMA Bat 166 30207 Bagnols/Cèze, France Email: caroline.leorier@cea.fr
Li, G.	Nuclear Power Institute of China, NPIC PO Box 291-100 610005 Chengdu, China
Liu, L.	China Institute for Radiation Protection XueFu street 102 030006 Taiyuan, China Email: liye.liu@gmail.com
Luxat, J.	McMaster University Engineering Building, Room A326 L8S 4K1 Ontario, Canada Email: mailto:luxatj@mcmaster.ca
Marty, P.	Commissariat à l'Energie Atomique et aux énergies alternatives (CEA) CEA MARCOULE Atalante Bât. 166 30207 Bagnols Sur Cèze BP 17171, France Email: pierre.marty@cea.fr
Matsui, H.	Japan Atomic Energy Agency (JAEA) 2-4 Shirakatashirane, Tokai Villege, Naka-gun 319-1195 Ibaraki Prefecture, Japan Email: matsui.hiroki@jaea.go.jp
Mikloš, M.	Research Centre Řež Ltd. (CV Rez) Husinec - Řež, čp. 130 250 68 ŘEŽ, Czech Republic Email: mkl@cvrez.cz
Owen, G.	International Nuclear Services Ltd, Hinton House, Birchwood Park Avenue Risley WA3 6GR Warrington, United Kingdom of Great Britain and Northern Ireland Email: gco1@innuserv.com
Páleník, P.	Slovenské elektrárne a.s. ENEL NPP Mochovce 935 39 Mochovce, Slovakia Email: peter.palenik@enel.com

Papaioannou, D.	European Commission Joint Research Centre Institute for Transuranium Elements (ITU) PO Box 2340 76125 Karlsruhe, Germany Email: dimitrios.papaioannou@ec.europa.eu
Robinson, A.	Idaho National Laboratory PO Box 1625 83415-6188 Idaho Falls, The United States of America Email: laura.cox@inl.gov
Rondinella, V.V.	European Commission Joint Research Center Institute for Transuranium Elements (ITU) PO Box 2340 76125 Karlsruhe, Germany Email: vincenzo.rondinella@ec.europa.eu
Ru, F.	The 404 LTD. CNNC JIA 37 PO Box 508 Lanzhou City, China Email: cr741026@126.com
Ruggirello, G.	Ciclo Combustible Nuclear, Comisión Nacional Energía Atómica (CNEA) Av. Del Libertador 8250 (1429) Ciudad Autónoma de Buenos Aires, Argentina Email: ruggirel@cnea.gov.ar
Sagalov, S.	JSC “SSC RIIAR” Bratskaya, 19-46 433504 Dimitrovgrad, Russian Federation Email: adm@niiar.ru
Šajtlava, J.	Slovak University of Technology in Bratislava Hájska 654/52 92003 Hlohovec-Šulekovo, Slovakia Email: jurajsajtlava@gmail.com
Schneider-Eickhoff, R.	Gesellschaft für Nuklear-Service mbH, GNS Hollestraße 7A 45127 Essen, Germany Email: ralf.schneider-eickhoff@gns.de
Serrano-Ramirez, L.	Comisión Nacional de Seguridad Nuclear y Salvaguardias Dr Barragán 779, Narvarte, Benito Juárez, 03020 03020 México City, Mexico Email: mlserrano@cnsns.gob.mx
Singh, J.L.	Bhabha Atomic Research Centre PIED/RLG/BARC, Trombay 400085 Mumbai, Rep. of India Email: jlsss@barc.gov.in
Sipos, H.	Studsvik Nuclear AB 61182 Nykoping, Sweden Email: hakan.sipos@ studsvik.se

Székely, R.	Hungarian Academy of Sciences KFKI Atomic Energy Research Institute 1525 Budapest 114, PO Box 49 1121 Budapest, Hungary Email: rszekely@aeki.kfki.hu
Thijssen, P.	Nuclear Research and Consultancy Group Westerduinweg 3 1755 Petten, The Netherlands Email: thijssen@nrg.eu
Tretyakov, M.	Nuclear Fuel Cycle, Science and Technology Establishment National Science Center "Kharkov Institute of Physics and Technology" (NFC STE NSC KIPT) Akademicheskaya str.1 61108 Kharkov, Ukraine Email: tretyakov_mv@kipt.kharkov.ua
Urban, P.	Slovenské elektrárne a.s. ENEL NPP Mochovce 935 39 Mochovce, Slovakia Email: peter.urban@enel.com
Václav, J.	Nuclear Regulatory Authority of the Slovak Republic Okruzna 5 918 64 Trnava, Slovakia Email: juraj.vaclav@ujd.gov.sk
Venkiteswaran, C.N.	Indira Gandhi Centre for Atomic Research (IGCAR) 603102 Tamilnadu Kalpakkam, Rep. of India Email: cnv@igcar.gov.in
Vreeling, A.	Nuclear Research and Consultancy Group NRG Westerduinweg 3 Petten, The Netherlands Email: vreeling@nrg.eu
Wade, M.	Merrick & Company 1093 Commerce Park Drive, Suite 200 Oak Ridge, 37830 Tennessee The United States of America Email: mike.wade@merrick.com
Walker, V.	Merrick & Company 2450 S. Peoria Street Aurora, 80014-5472 Colorado The United States of America Email: valerie.walker@merrick.com
Wang, S.	Qinshan Nuclear Power Plant Hedianxincun 15-3-509 Zhejiang province, Jiaxing City 314300 Haiyan, China Email: wangsw@qnpc.cn

Wang, X.	China Institute of Atomic Energy, CIAE PO.Box 275(57) 102413 Beijing, China Email: wx082701@139.com; wx082701@ciae.ac.cn
Wiese, H	Paul Scherrer Institute OHLD/110 5232 Villigen, Switzerland Email: holger.wiese@psi.ch
Williams, M.	International Nuclear Services Ltd, Hinton House, Birchwood Park Avenue Risley WA3 6GR Warrington, United Kingdom of Great Britain and Northern Ireland Email: martin.z.williams@innuserv.com
Wright, D.	National Nuclear Laboratory B22 Sellafield Seascale CA20 1PG Cumbria, United Kingdom of Great Britain and Northern Ireland Email: des.wright@nnl.co.uk
Zajac, R.	VUJE a.s. Okruzna 5 918 64 Trnava, Slovakia Email: vladimir.chrapciak@vuje.sk
Zsoldos, J.	Hungarian Atomic Energy Authority Fényes Adolf utca 4 1036 Budapest, Hungary Email: zsoldos@haea.gov.hu
Zubler, R.	Paul Scherrer Institut Laboratory for Nuclear Materials OHLA/102 CH-5232 Villigen PSI, Switzerland Email: robert.zubler@psi.ch